NASA Technical Paper 1359

Engineering Handbook on the Atmospheric Environmental Guidelines for Use in Wind Turbine Generator Development

Walter Frost, B. H. Long,
and R. E. Turner

DECEMBER 1978

NASA

NASA Technical Paper 1359

Engineering Handbook on the Atmospheric Environmental Guidelines for Use in Wind Turbine Generator Development

Walter Frost and B. H. Long
The University of Tennessee Space Institute
Tullahoma, Tennessee

R. E. Turner
George C. Marshall Space Flight Center
Marshall Space Flight Center, Alabama

National Aeronautics
and Space Administration

**Scientific and Technical
Information Office**

1978

ACKNOWLEDGMENTS

The work was funded by the Department of Energy under NASA contract NAS8-32118. The authors have worked very closely with the personnel from NASA Lewis Research Center, Cleveland, Ohio, and have received from them many inputs and much sound advice. In particular, Bob Wolf, Harold Neustadter and Dave Spera have contributed immensely to the final documentation. Review of the work with Bill Cliff, Chuck Elderkin, Larry Wendly, Chris Doran, and others from Battelle PNL has added significantly to the handbook.

The initiation of the project by George Fichtl, NASA Marshall Space Flight Center, is also appreciated.

Finally, the authors wish to thank George Tennyson, Carl Aspliden, and Donald Teague, Wind Energy Conversion Branch, Division of Solar Energy, Department of Energy. Particular thanks is given to Donald Teague, Program Manager, whose guidance has set the tenor of the engineering philosophy contained throughout the handbook.

TABLE OF CONTENTS

TABLE OF CONTENTS (Continued)

TABLE OF CONTENTS (Continued)

TABLE OF CONTENTS (Continued)

TABLE OF CONTENTS (Continued)

TABLE OF CONTENTS (Continued)

TABLE OF CONTENTS (Continued)

TABLE OF CONTENTS (Concluded)

NOMENCLATURE

Symbol	Definition
A	Area
$A_{\alpha}(h, z_o, L)$	Function defined by equations (4.37), (4.38), and (4.39)
a	Rise time fraction of gust duration
a_{α}	Decay coefficient on coherence function
b	Sun' s altitude
C_D	Drag coefficient
C_F	Capacity factor
C_L	Lift coefficient
C_P	Pressure coefficient
C'_{α}	Empirical constant in turbulence intensity relationship
C_{α}	Empirical constant in cut-off frequency relationship
c	Scale factor in Weibull distribution
c	Effective height of undulating terrain
D	Rotor diameter
dN/ds	Number of times per unit time the wind speed crosses the line segment ds
F	Force
F_G	Gust factor
F_T	Total wind load

Symbol	Definition
G_o	Number of times the wind fluctuates about the mean component per unit time
$\hat{G}_o$	Dimensionless value of G_o defined as $hG_o/\eta_{o\alpha}\overline{W}_h$
$G(w_\alpha)$	Number of peaks in wind speed fluctuations above the value w_α per unit time
h	Height above the surface
h''	Wind turbine generator site reference height
h_H	Hub height
$H(\hat{n})$	Frequency response function
I	Horizontal solar radiation
I_{DH}	Diffuse sky radiation intensity
I_{DN}	Direct normal incident solar radiation
I_N	Intensity of solar radiation after absorption through N air masses
I_o	Solar spectral irradiance
I_{TH}	Hourly total of horizontal solar and sky radiation
I_{TN}	Total normal incident solar radiation intensity
$I_{1.00}$	Intensity of solar radiation after absorption through one air mass
K	Conversion factor
k	Shape factor in Weibull distribution

Symbol	Definition
L	Monin-Obukhov stability length multiplied by the ratio of momentum to thermal diffusivity
L'	Monin-Obukhov stability length
$\hat{L}$	Integral turbulence length scale
L_i	Ice load
L_p	Longitudinal isotropic turbulence integral scale
L_r	Effective length scale for structure response
L_s	Snow load
L_{w_x}	Characteristic length scale of longitudinal wind fluctuation
L_{w_y}	Characteristic length scale of lateral wind fluctuations
M	Atmospheric transmittance factor
M_N	New value of atmospheric transmittance
N	Number of years of expected useful life
N	Number of air masses
n	Wind speed power law exponent
$\hat{n}$	Frequency in cycles per second
$\hat{n}_{co}$	Cut-off frequency
$\hat{n}_G$	Frequency associated with gusts of spatial extent greater than Δx

Symbol	Definition
$N(\theta)$	Number of crossings of the angle θ per unit time
N_o	Number of crossing of the value of zero per unit time
N_x	Number of crossing of the value x per unit time
$\bar{P}$	Average power
$P(W)$	Power as a function of wind speed W
P_r	Rated power
$P(\geq r)$	Probability of at least one occurrence of ice $\geq$ r
$p(W)$	Frequency distribution of wind speeds
$p(w_x, w_y)$	Probability of w_x and w_y
q	Dynamic pressure
R	Rotor radius
R	Percent risk of exceedance
R_e	Extreme rainfall
Ri	Richardson' s number
R_s	Turbulence simulation scale factor
R_{w_x}	Longitudinal correlation
R_{w_y}	Lateral correlation
r	Separation distance in turbulence correlations

NOMENCLATURE (Continued)

Symbol	Definition
S	Scaling factor for ice thickness increase with elevation
$\hat{S}$	Complex frequency
s	Number of standard deviations
T_i	Ice thickness
T_{iE}	Ice thickness adjusted for elevation
T_R	Recurrence interval
t	Time
u_*	Friction velocity
u_{*s}/u_{*n}	Ratio of friction velocities for stable and neutral conditions with the same wind speed at a given height
u_{*o}	Friction velocity at the Earth's surface
v	Correlation between $\dot{w}_x$ and $\dot{w}_y$
W'	Fluctuation about the mean of the peak wind speed
$W(\tau)$	Wind speed centered arround the peak wind averaged over the period τ
W_G	Instantaneous gust wind speed
W_g	Peak wind speed
W_h	Wind speed at height h
W_i	Gust magnitude
W_P	Prescribed value of wind speed

Symbol	Definition
W_x	Longitudinal wind speed
w_x	Longitudinal wind speed fluctuation about the mean
W_y	Lateral wind speed
w_y	Lateral wind speed fluctuation about the mean
W_z	Vertical wind speed
w_z	Vertical wind speed fluctuation about the mean
$\dot{w}_x$	Time derivative of w_x
$\dot{w}_y$	Time derivative of w_y
z_o	Surface roughness
β	Correction factor for extreme gust magnitude
β_1, β_2	Parameters which characterize the aerodynamics and weight of a rotor correction factor for extreme gust magnitude
$\Gamma(\ )$	Gamma function
$\eta_{o\alpha}$	Characteristic dimensionless frequency
η	Reduced frequency, $nh/\overline{W}$
$\tilde{\eta}$	Dimensionless height
$\hat{\zeta}$	Ratio of η/η_o
ζ	Dimensionless time, t/τ

Symbol	Definition
$\bar{\xi}$	Dimensionless two-point spectrum, $2\phi(\sigma,\bar{\eta})_{w_\alpha} / \sigma^2_{w_\alpha}$
θ	Wind angle measured relative to mean longitudinal wind direction
ξ	Dimensionless rms value, $\sigma_{w_\alpha} / cA_\alpha(h, z_o, L)$
κ	Von Karman's constant assigned a value of 0.4
Λ	Dimensionless number $\eta_{o\alpha} \bar{W}_h / h\hat{n}_{co}$
λ	Average number of ice storms in any year
ρ_i	Ice density
σ_{w_α}	Standard deviations of the turbulence fluctuations where α represents x, y, or z, respectively
$\sigma_{\dot{\alpha}}$	Standard deviation of the time derivative fluctuations
τ	Gust duration
$\phi(h/L)$	Dimensionless wind shear
$\phi_{ij}(\hat{n})$	Two-point spectrum
$\phi_{w_\alpha}(\hat{n})$	Spectral density function for turbulence kinetic energy
$\hat{\phi}$	Ratio of rotor radius to hub height R/h_H
ν	Kinematic viscosity of the atmosphere
χ	Exponent on bivariate normal distribution function
$\bar{\omega}$	Mean angular rotation of rotor
$\omega'(t)$	Rotational fluctuations of the rotor about its mean angular rotation

Sybmol	Definition
Over Symbols	
$(\bar{})$	10 min average or greater
$(\hat{})$	Over wind speed denotes annual average
$(\tilde{})$	Extreme wind speed
Subscripts	
α	Designates either of three wind vector component directions, x, y, and z

ENGINEERING HANDBOOK ON THE ATMOSPHERIC ENVIRONMENTAL GUIDELINES FOR USE IN WIND TURBINE GENERATOR DEVELOPMENT

CHAPTER 1. INTRODUCTION

This report provides the environmental design criteria necessary to develop a wind turbine generator (WTG). All criteria are provided in a working engineering format. More specifically, the report provides inputs for structural and dynamic analysis such as data on wind loading, turbulence level, snow and ice loading, etc., but it does not directly address the general problem of siting wind turbine generators.

Since wind is the most important design parameter for WTG development, four chapters have been devoted to wind under the following classifications: Chapter 2, Wind Speed; Chapter 3, Wind Shear; Chapter 4, Turbulence; and Chapter 5, Wind Direction. A complete chapter, Chapter 6, has been devoted to ice and snow loadings because of their importance to the structural design of a wind turbine generator. Finally, Chapter 7 addresses climatological factors such as precipitation, temperature, and other environmental parameters which are of importance, but to a lesser degree, in the design of a WTG.

Each of the Chapters 2 through 6 starts with a summary section containing the specific design values recommended for design of a "general purpose WTG."[1] The next section provides an explanation of how these particular design values were determined, including presentation of detailed computational procedures based on working data given in the latter sections of the chapter. These latter sections contain design formulae, graphs and tables, plus detailed descriptions of how the WTG design engineer may apply these to compute design

1. A general purpose WTG is defined as an "off-the-shelf" type unit which has general applicability for all feasible sites in the continental United States.

values other than those given in the summary. Thus, in addition to the recommended general purpose design inputs given in the summary sections, the handbook supports the designer in developing criteria for a WTG requiring either specialized or specific site applications.

In several sections of Chapter 7, the available data relative to climatological and environmental design parameters are insufficient to make a summary section meaningful. For these sections (particularly Sections 7.2, 7.3, 7.4, and 7.5), it is recommended that the reader utilize the entire chapter in selecting design values.

The presentation of the detailed computational procedures and working data differs slightly from chapter to chapter. Design inputs which vary regionally, such as wind speed (Chapter 2), ice and snow loading (Chapter 6), and climatological parameters such as rain, hail, temperature and humidity (Chapter 7), are provided in the form of basic design value contour maps of the United States. Where maps are not available, data for as many regions as possible are tabulated. Procedures for adjusting the basic design value for influencing factors such as height, surface roughness, atmospheric stability, etc., are provided. Also, a method of estimating the risk of exceeding the selected design value for a given life expectancy of the system is specified. This is necessary, since meteorological quantities are random variables and there is always a degree of risk that the design of the WTG will be exceeded during its useful life.

Design parameters such as wind shear (Chapter 3), turbulence (Chapter 4), or wind direction (Chapter 5) vary regionally but only through their dependence on wind speed. Thus, contour maps or regional data are not given in these chapters since the regional variation is introduced through the mean wind speed. Factors are also provided for adjusting wind shear, turbulence and wind direction for height, surface roughness and atmospheric stability.

This report presents a collection from the literature of the more reliable data applicable to wind turbine generator design. In addition, the interpretation of the data to make them more directly applicable to WTG development has been carried out. Lengthy discussions and extensive mathematical developments of the theory associated with the cited design criteria have been omitted in favor of providing step-by-step application procedures. Considerable effort has been expended to assure that the data are meaningful and constitute the best source available to the authors. The reader who is interested in more details of the

data source and of the data reliability is directed to the references listed at the end of each chapter. Citations in the text to referenced material are indicated by the item reference number in square brackets.

In general, the data are verified only for homogeneous and uniform terrain. Lack of data relative to large-scale nonuniform terrain prohibits the development of basic design inputs which take these conditions into account. However, due to the localized nature of WTG' s relative to large-scale geomorphic features, it is reasonable that these data for homogeneous, uniform terrain be applied even to nonuniform terrain until more detailed data are available. Obviously, the designer must use caution and good judgment in applying this assumption, particularly when the scales of the WTG and the terrain features are of similar magnitude.

Two systems of units are used in this report. Either the engineering system of units is given with the cgs system in parentheses or vice versa. The units used first in each section are those consistent with the original contour maps as taken from the referenced literature. The cgs system of units, however, is given preference wherever possible. In practically all cases, both systems of units are provided in the text and, when useful, on the figures. In parts of Chapter 7 where the engineering system of units is unwieldy, only the cgs system has been used.

CHAPTER 2. WIND SPEED

Summary of Wind Speed

2.1 Introduction

Extreme wind speed and mean wind speed design values for a general purpose WTG[1] based on aerospace and building code design philosophies, respectively, are given in this section, Section 2.1. Sections 2.2, 2.3, and 2.4 provide the detailed computational procedures and data from which these recommended design values have been computed and from which the design engineer may compute his own values if desired.

Section 2.1.1 states the basic recommended extreme and mean wind speed design values and presents mathematical expressions for correcting these values for elevation, terrain roughness, and risk of exceedance. Also, procedures are recommended for adjusting the extreme wind speed to account for the response time of different size structures or structural components of the WTG. Section 2.1.2 describes how the basic wind speeds and correction factors are determined from the detailed computational procedures contained in Sections 2.2, 2.3, and 2.4.

2.1.1 Wind Speed Design Values

2.1.1.1 Extreme Wind Speed

2.1.1.1.1 Basic Design Value

Two design values of extreme wind speed specified at an elevation of 30 ft (10 m) are:

$$\tilde{W}_{h=30\ \text{ft}} = 163\ \text{mph};\quad \tilde{W}_{h=10\ \text{m}} = 262\ \text{km h}^{-1}$$

$$\tilde{W}_{h=30\ \text{ft}} = 115\ \text{mph};\quad \tilde{W}_{h=10\ \text{m}} = 185\ \text{km h}^{-1} \qquad (2.1)$$

1. A general purpose WTG is defined as an "off-the-shelf" type unit which has general applicability for all feasible sites in the continental United States.

where h is the height at which the wind speed is evaluated. The higher value is computed on the basis of aerospace design philosophy which specifies a 10-percent risk of exceedance during the expected life of the structure [2.1]. The lower value is computed on the basis of building code design philosophy which specifies 63-percent risk of exceedance during an expected 50-year life of the proposed structure [2.2]. Details of the procedure for computing these values are given in Section 2.1.2.1.

Figure 2.1 provides a plot of extreme wind speed versus risk of exceedance for a 25-year and a 50-year expected life. It is anticipated that the WTG design engineer will wish to select his own degree of risk which presumably will be somewhere between aerospace design procedures and standard building code practices.

2.1.1.1.2 Adjustment for Elevation

The recommended adjustment of extreme wind speed with height h is:

$$\tilde{W}_h = 0.90\, \tilde{W}_{h=30\ \mathrm{ft}}\, h^{0.03}; \quad h\ (\mathrm{ft})$$

$$\tilde{W}_h = 0.93\, \tilde{W}_{h=10\ \mathrm{m}}\, h^{0.03}; \quad h\ (\mathrm{m}) \qquad (2.2)$$

where $\tilde{W}_h$ has the same units as $\tilde{W}_{h=30\ \mathrm{ft}}$ ($\tilde{W}_{h=10\ \mathrm{m}}$). The height, h, is typically measured from level grade surrounding the WTG site; however, for sites near cliffs or escarpments, h should be determined as described in Section 2.3.4.

2.1.1.1.3 Adjustment of Basic Wind Speed for Structural Response Time

The basic design wind speed, $\tilde{W}_h$, is adjusted to $\tilde{W}_h(\tau)$ for structures or structual components of different response times, τ, with the following relationships:

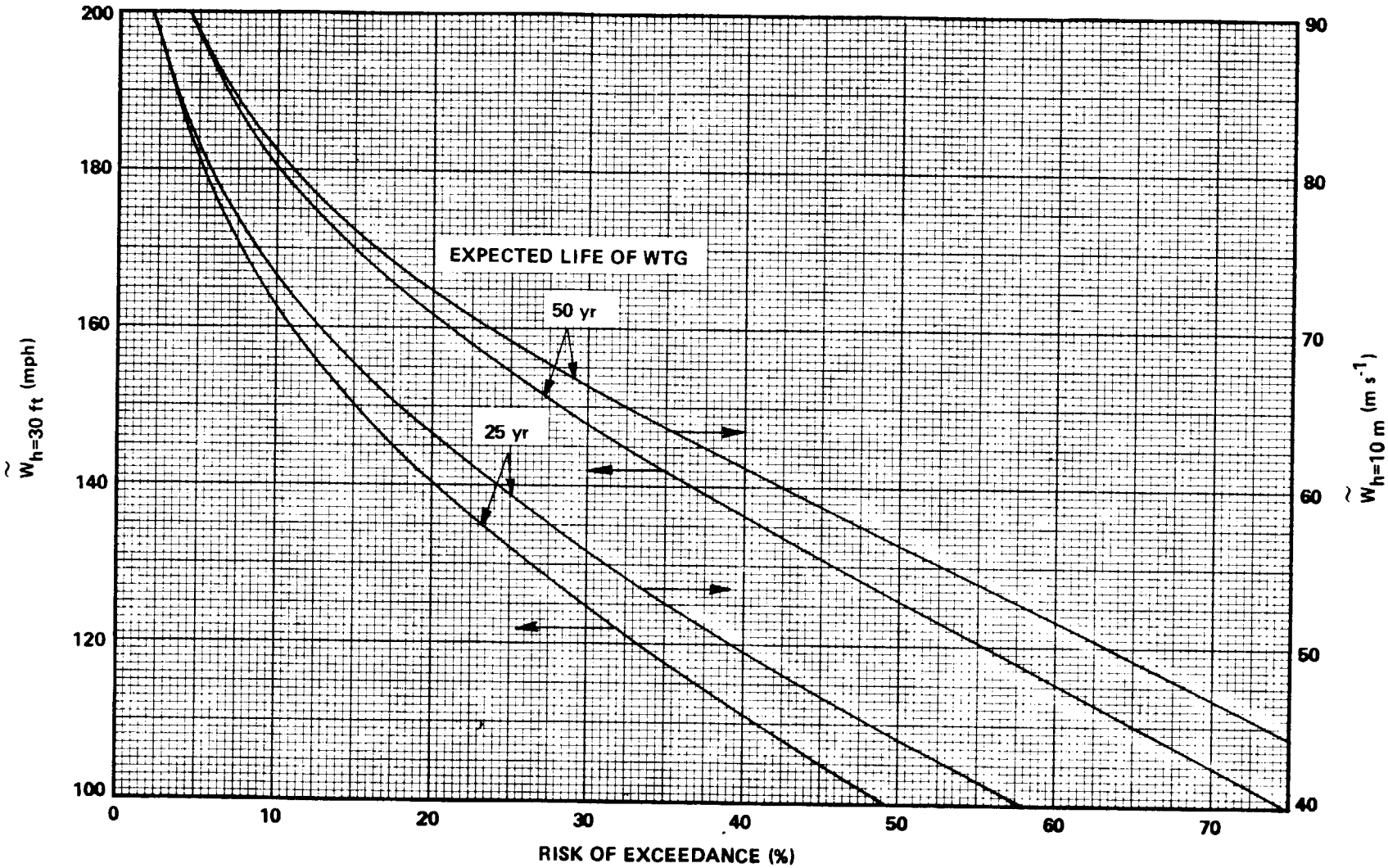

Figure 2.1 Risk of exceeding extreme wind speed.

Structures or structural components of 65 ft (20 m) or less in extent:

$$\tilde{W}_{h_\tau} = 1.85\ \tilde{W}_h^{0.91};\quad \tilde{W}_h\,(\text{mph})$$

$$\tilde{W}_{h_\tau} = 1.72\ \tilde{W}_h^{0.91};\quad \tilde{W}_h\,(\text{m s}^{-1}) \quad . \tag{2.3}$$

Structures or structural components larger than 65 ft (20 m) but for which neither the greatest horizontal nor vertical dimension exceeds 165 ft (50 m):

$$\tilde{W}_{h_\tau} = 1.80\ \tilde{W}_h^{0.91};\quad \tilde{W}_h\,(\text{mph})$$

$$\tilde{W}_{h_\tau} = 1.67\ \tilde{W}_h^{0.91};\quad \tilde{W}_h\,(\text{m s}^{-1}) \quad . \tag{2.4}$$

For all larger structures the basic design value from Section 2.1.1.1.1 remains unadjusted. The procedure for adjusting winds for response time is provided in Section 2.3.2.2.

2.1.1.2 Mean Wind Speed

2.1.1.2.1 Annual Mean Wind Speed

A recommended design value of the annual mean wind speed based on an area averaging technique for the mainland United States is as follows:

Percent Area of USA with Wind Speeds Above $\hat{W}$ (percent)	$\hat{W}_{h=30\text{ ft}}$ (mph)	$\hat{W}_{h=10\text{ m}}$ (m s^{-1})
10	11.9 ± 0.9	5.3 ± 0.4
20	11.6 ± 0.9	5.2 ± 0.4
40	10.7 ± 0.9	4.8 ± 0.4
60	9.8 ± 0.7	4.4 ± 0.3
80	8.9 ± 0.7	4.0 ± 0.3
90	8.5 ± 0.5	3.8 ± 0.2

2.1.1.2.2 Wind Speed Duration Curve

The probability of a wind speed, W, greater than or equal to a prescribed wind speed, W_P, can be estimated by a Rayleigh distribution [2.3]

$$p(W \geq W_P) = \exp[-\pi(W_P/2\hat{W})^2] \qquad (2.5)$$

where the units of W_P and $\hat{W}$ must be consistent.

A plot of the wind speed duration curve is given in Figure 2.2.

2.1.1.2.3 Adjustment for Elevation

The recommended adjustment with height of the mean wind speed, $\overline{W}$ (i.e., an averaging period of approximately 10 min to 1 h) for elevation greater than h = 30 ft (10 m) is:

$$\overline{W}_h = 0.62\, \overline{W}_{h=30\text{ ft}}\, h^{0.14}; \quad h\text{ (ft)}$$

$$h > 30\text{ ft (10 m)} \qquad (2.6)$$

$$\overline{W}_h = 0.72\, \overline{W}_{h=10\text{ m}}\, h^{0.14}; \quad h\text{ (m)}$$

and for elevations less than h = 30 ft (10 m) is:

$$\overline{W}_h = 0.26\, \overline{W}_{h=30\text{ ft}}\, h^{0.4}; \quad h\text{ (ft)}$$

$$h < 30\text{ ft (10 m)}$$

$$\overline{W}_h = 0.40\, \overline{W}_{h=10\text{ m}}\, h^{0.4}; \quad h\text{ (m)} \qquad (2.7)$$

where $\overline{W}_h$ has the same units as $\overline{W}_{h=30\text{ ft}}$ ($\overline{W}_{h=10\text{ m}}$). A plot of these correction curves is given in Figure 2.3.

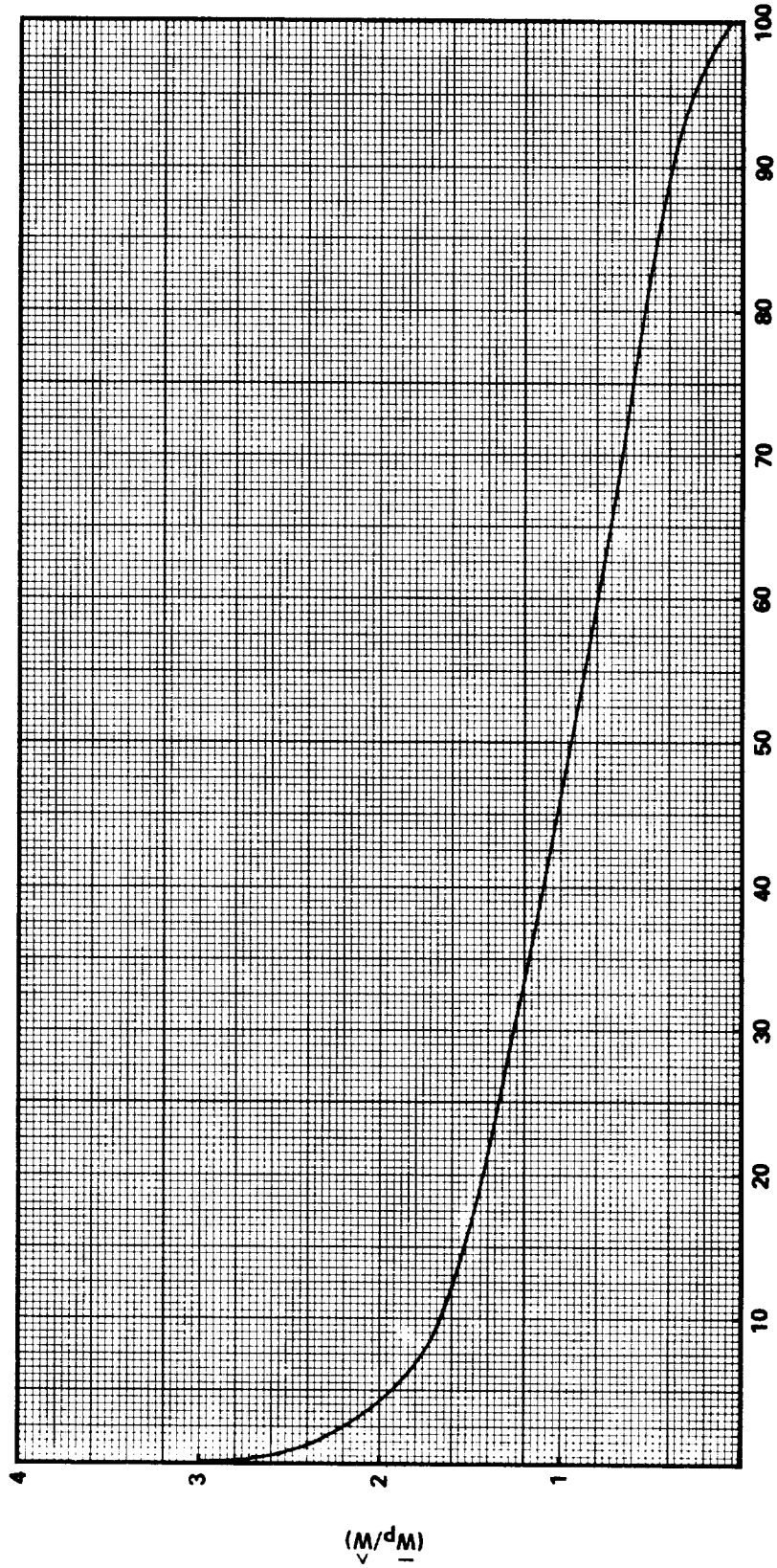

Figure 2.2 Rayleigh cumulative probability distribution of wind speed.

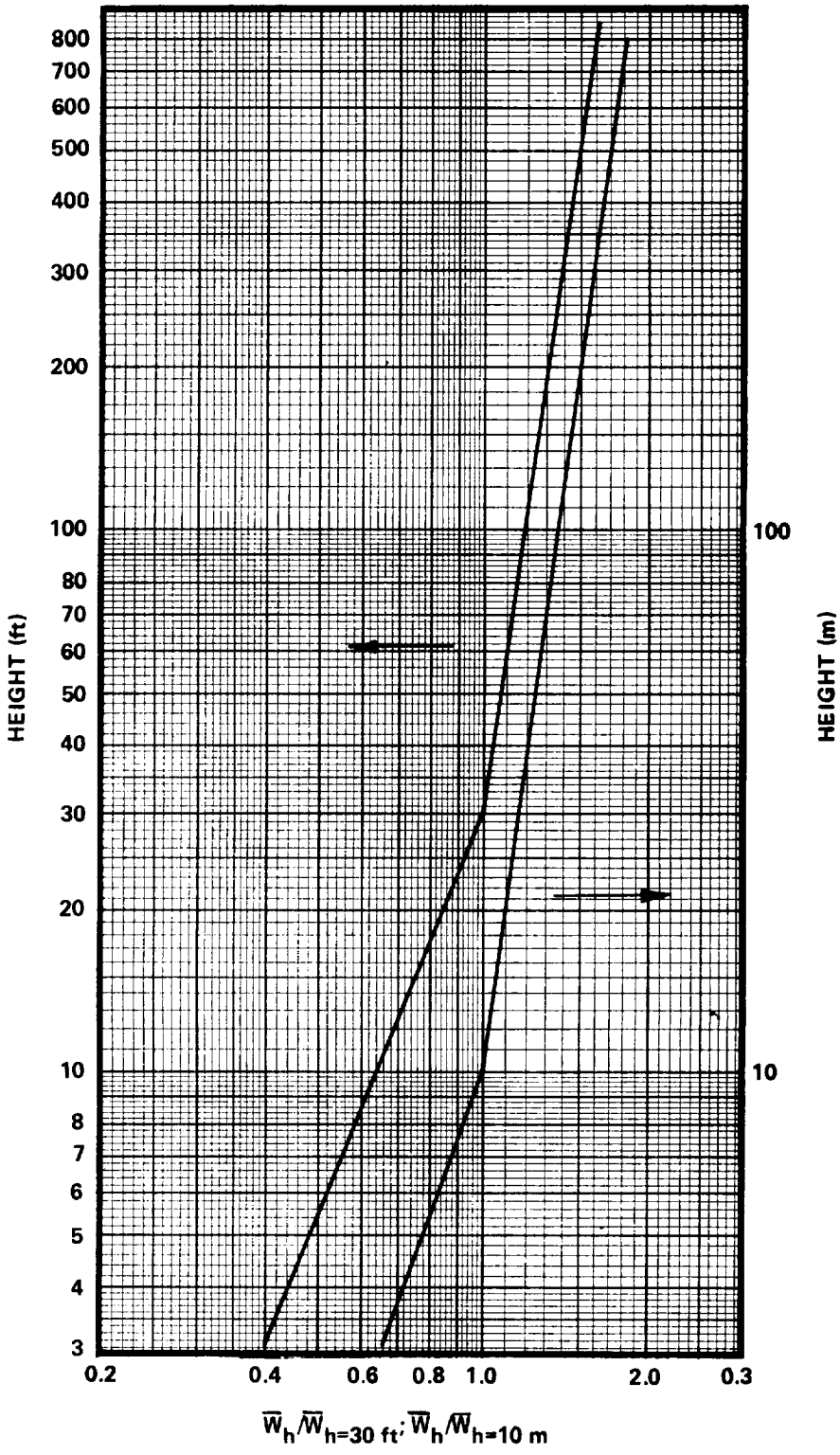

Figure 2.3 Adjustment of mean wind speed with height.

2.1.2 Description of Recommended Design Values

The computation of the specific design values given in the preceding sections, from information contained in Sections 2.2, 2.3, and 2.4 of this chapter, is described below.

2.1.2.1 Extreme Winds

The most extreme winds recorded on isotach maps of the United States occur on the tip of the Florida Peninsula and along the Atlantic coast near Cape Hatteras. These locations were therefore selected to represent the highest wind speed region in which a general service WTG is likely to be sited. A Fisher-Tippett probability distribution of the extreme winds for the Miami location (Cape Hatteras is essentially the same) is shown in Figure 2.4 (for details see Section 2.3.1.4.1). This figure gives the expected mean recurrence interval, T_R, of the extreme fastest mile wind speed. The recurrence interval at which the extreme value is to be selected for design is determined by application of Figure 2.5. This figure gives the recurrence interval associated with a given lifetime of the structure, N, for a prescribed risk of exceedance, R. Since wind speed is a statistically random quantity, the engineer must accept some risk that his design wind speed value may be exceeded at least once in the expected useful life of the structure.

Two design philosophies for selecting the basic design value for the extreme wind speed interval were considered. Both values are quoted to establish for the designer an order of magnitude estimate of extreme wind speed. One philosophy is based on aerospace vehicle design principles [2.1] which recommended that a 10-percent risk of exceedance for any given expected life period be used in determining the extreme wind. An alternate design philosophy was taken from the building code standards [2.2] which accepts a 63-percent risk for an expected life of 50 years.

The following describes the selection procedure for the basic extreme wind speed design value based on both philosophies. For further details, see Section 2.3.1.4.2.

Since the aerospace vehicle design philosophy gives no specific expected life, assume 25 years as the expected life of the WTG. Employing a 10-percent risk that the design wind will be exceeded no more than once in the lifetime of the structure, the recurrence interval T_R is found as follows. The value of

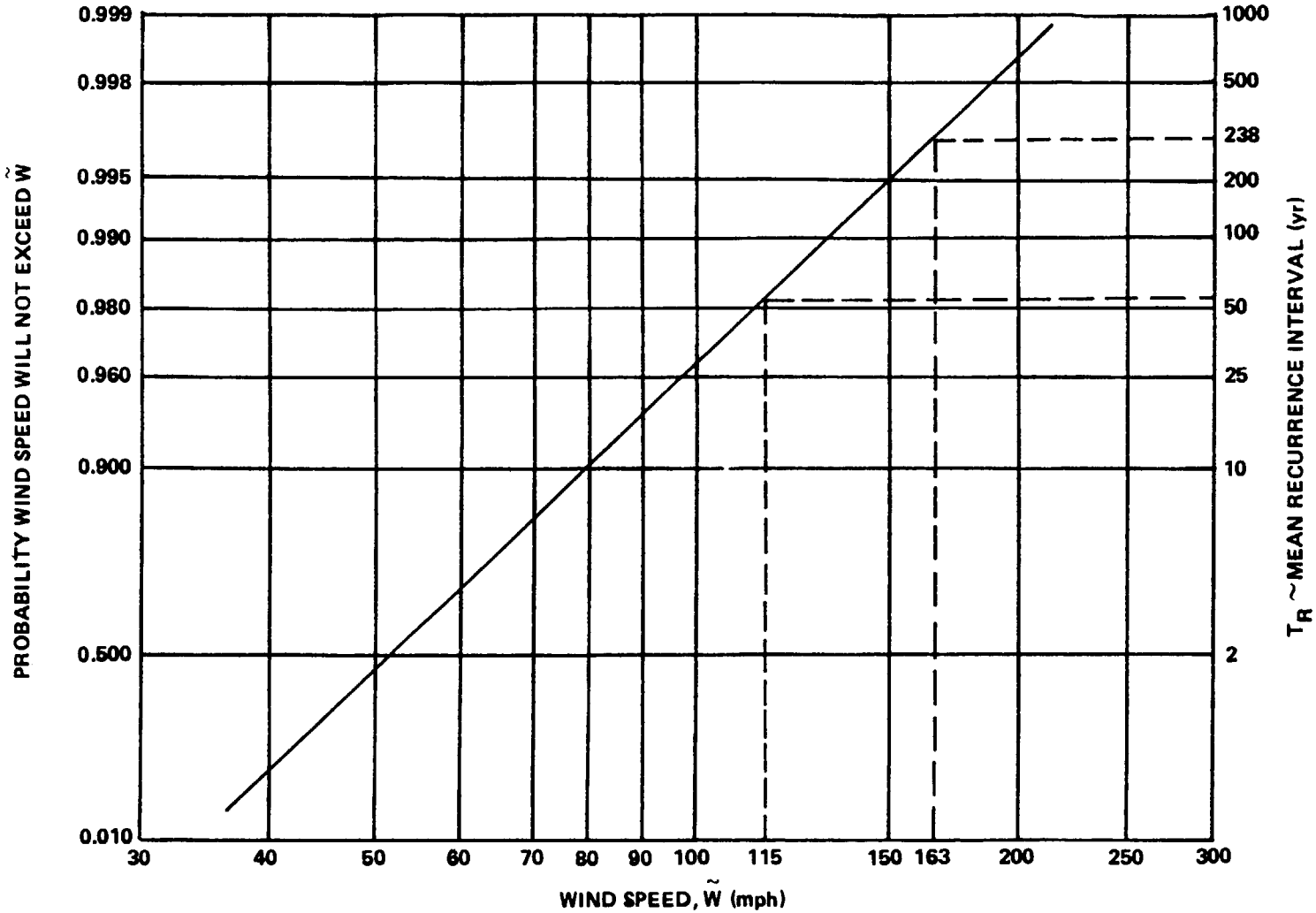

Figure 2.4 Extreme value wind speed distribution.

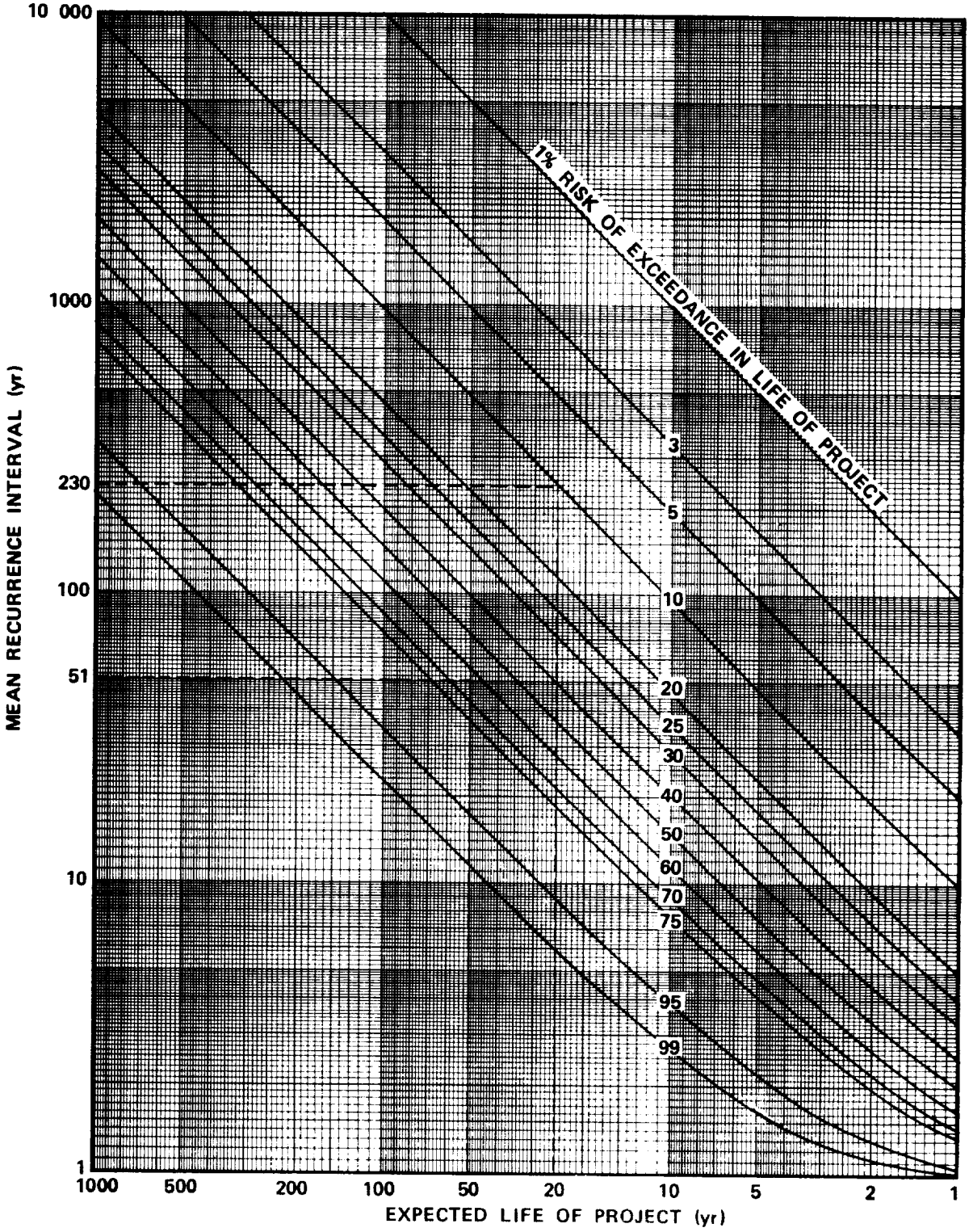

Figure 2.5 Mean recurrence interval for risk of occurrence within the expected life of the project.

N = 25 is found on the horizontal axis of Figure 2.5; a vertical line is projected upward to intersect with the R = 10 percent line. A horizontal projection to the vertical axis indicates T_R = 238 years. From Figure 2.4, a 238-year recurrence interval is associated with an extreme wind speed of 163 mph (262 km h^{-1}).

Alternately, utilizing an expected life of 50 years and accepting a 63-percent risk of exceedance, Figure 2.5 indicates a recurrence interval of 51 years. A horizontal projection from 51 years on Figure 2.4 indicates a design value for the extreme wind speed of 115 mph (185 km h^{-1}).

The WTG designer will probably accept an intermediate value between those previously computed because a WTG does not require the same fail-safe features required of a manned space vehicle. However, a WTG is deliberately exposed to high winds and hence requires a somewhat higher degree of reliability than a standard building design. Figure 2.1 provides a readily usable curve for selection of extreme wind speeds based on the two individual design philosophies.

The extreme wind speed design values selected in the preceding paragraphs are measured at a 30-ft (10-m) elevation. Adjustment of these values to the WTG hub height, h_H, or to the height of the structural component being designed is necessary. The recommended correction of extreme wind values for height is a power law relationship (Section 2.3.2.1.2). The variation of wind speed with height (i.e., the value of the exponent, n, of the power-law relationship) is a strong function of surface roughness, atmospheric stability, and wind speed. The power-law relationship and the functional form of the exponent n are discussed in detail in Section 3.3.4. For high wind speeds of short averaging times the value of n is predicted from Reference 2.1:

$$n = 1.02(\tilde{W}_{h=30\ ft})^{-3/4};\quad \tilde{W}_{h=30\ ft}(mph)$$

$$n = 0.56(\tilde{W}_{h=10\ m})^{-3/4};\quad \tilde{W}_{h=10\ m}(m\ s^{-1}) \qquad . \qquad (2.8)$$

Based on an average wind speed between 163 and 115 mph of 140 mph (225 km h^{-1}), the value of n is 0.025. A conservative value of n = 0.03 is selected for general design purposes.

The value of the basic design wind speed must also be corrected to account for the time response associated with WTG components of different sizes or different structural components of a given WTG. The British building code suggests that a structural component of size 65 ft (20 m) or less will respond to a 3-s gust and that a structural component larger than this but less than 165 ft (50 m) will respond to a 5-s gust. The recommended power-law correction for response time is

$$\tilde{W}_{h_\tau} = C\tilde{W}_h^{0.91} \tag{2.9}$$

where C = 1.85 and 1.72 for a 3-s gust and C = 1.80 and 1.67 for a 5-s gust for $\tilde{W}$ in mph and for $\tilde{W}$ in m s^{-1}, respectively. Equation (2.9) is a curve fit established by computing $\tilde{W}_{h_\tau}$ as described in the following paragraphs.

To adjust the magnitude of the wind speed to that associated with, e.g., a 3-s gust, the mean wind speed, $\overline{W}_h$ (averaging period of approximately 10 min to 1 h) corresponding to the extreme fastest mile wind speed is determined. The mean wind speed, $\overline{W}_h$, associated with 163 mph (262 km h^{-1}) is determined from Figure 2.6.

On the vertical axis, the basic design value of the extreme wind speed 163 mph (262 km h^{-1}) is found and projected horizontally to intersect with the "fastest mile" curve. This intersection point is projected downward and the mean wind speed $\overline{W}$ = 120 mph (193 km h^{-1}) is read on the horizontal axis. Next the gust factor for a 3-s gust is determined to have a value of 1.59 from Figure 2.7, which is reproduced from Section 2.3.2.2. The extreme value wind speed associated with a 3-s gust is the gust factor times the mean wind speed. The adjusted design wind speed is 191 mph (307 km h^{-1}). This procedure was carried out for several values of $\tilde{W}$, and the curve-fit relationship [equation (2.9)] was established.

2.1.2.2 Mean Wind Speed

The recommended mean wind speed design values are determined from the information contained in Section 2.4. Annual mean wind speeds and annual wind speed distribution functions for 138 locations in the United States have been

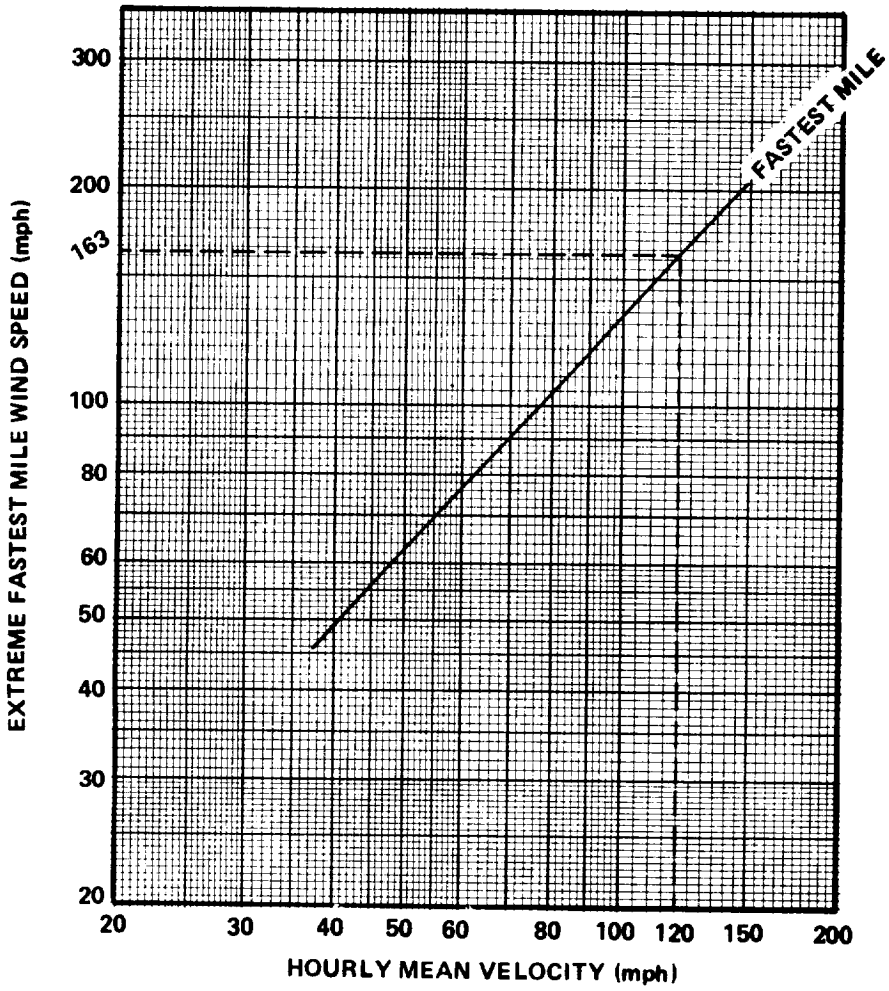

Figure 2.6 Relationship between extreme fastest mile wind speed and mean wind speed.

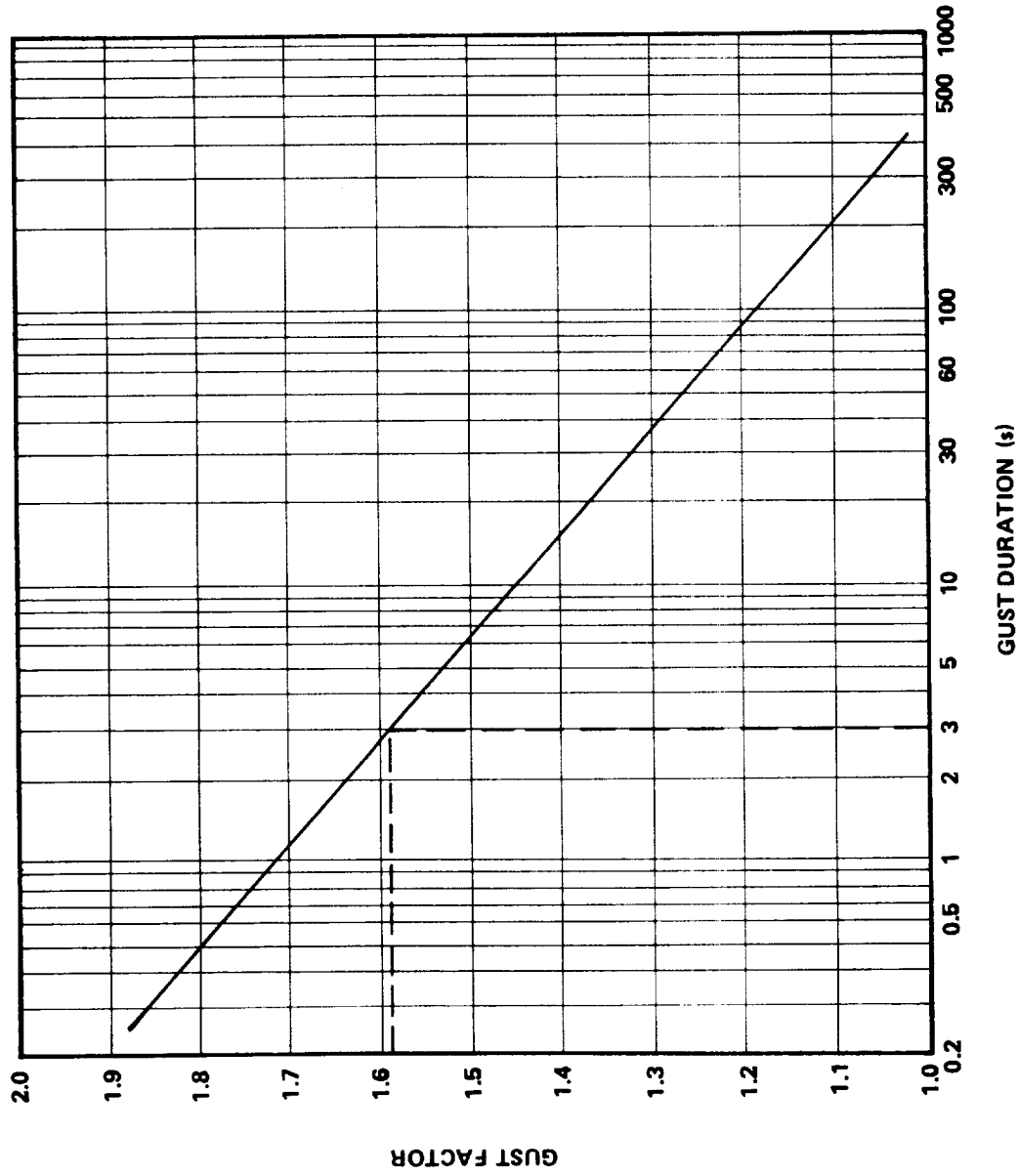

Figure 2.7 Ratio of wind speed average over τ to mean wind speed.

compiled by Justus, et al. [2.4]. These data are presented in Section 2.4 for computation of mean wind speed at specific sites. Mean wind speeds for designing a general purpose WTG are discussed below.

A recent report by Elliot [2.5] has synthesized all recent wind data and has developed maps of the mean annual wind power above exposed area over the contiguous United States. Figure 2.8a presents contour lines of the annual wind power and Figure 2.8b presents the computed approximate percentage of area with wind power above a given value. Along the coast a region 10 miles on either side of the coastline was used; a similar procedure was used for the Great Lakes region. The following results were obtained:

Mean Annual Power Equal to or Greater Than the Power (W/m^2)	Percent of Area of Contiguous United States (percent)
500	5.5
400	22.2
300	50.8
250	56.6
200	84.0
150	91.8

The mean wind speed relative to these levels of power was determined based on the assumption of a Weibull wind speed distribution; i.e.,

$$P = \rho\langle W^3\rangle = \rho \hat{W}^3 \Gamma\left(1 + \frac{3}{k}\right) / \Gamma^3\left(1 + \frac{1}{k}\right) \quad . \tag{2.10}$$

A standard atmospheric density ($\rho = 1.255$ kg m^{-3}) and a Rayleigh distribution (for which the shape factor $k = 2$) was assumed. The annual mean wind speeds given in Section 2.1.1.2.1 result from this calculation. These wind speeds are adjusted to the 10-m level using the same 0.2 power law utilized in Reference 2.5. The plus or minus limits specified are computed by assuming that the value of k can range between 1.6 and 2.4.

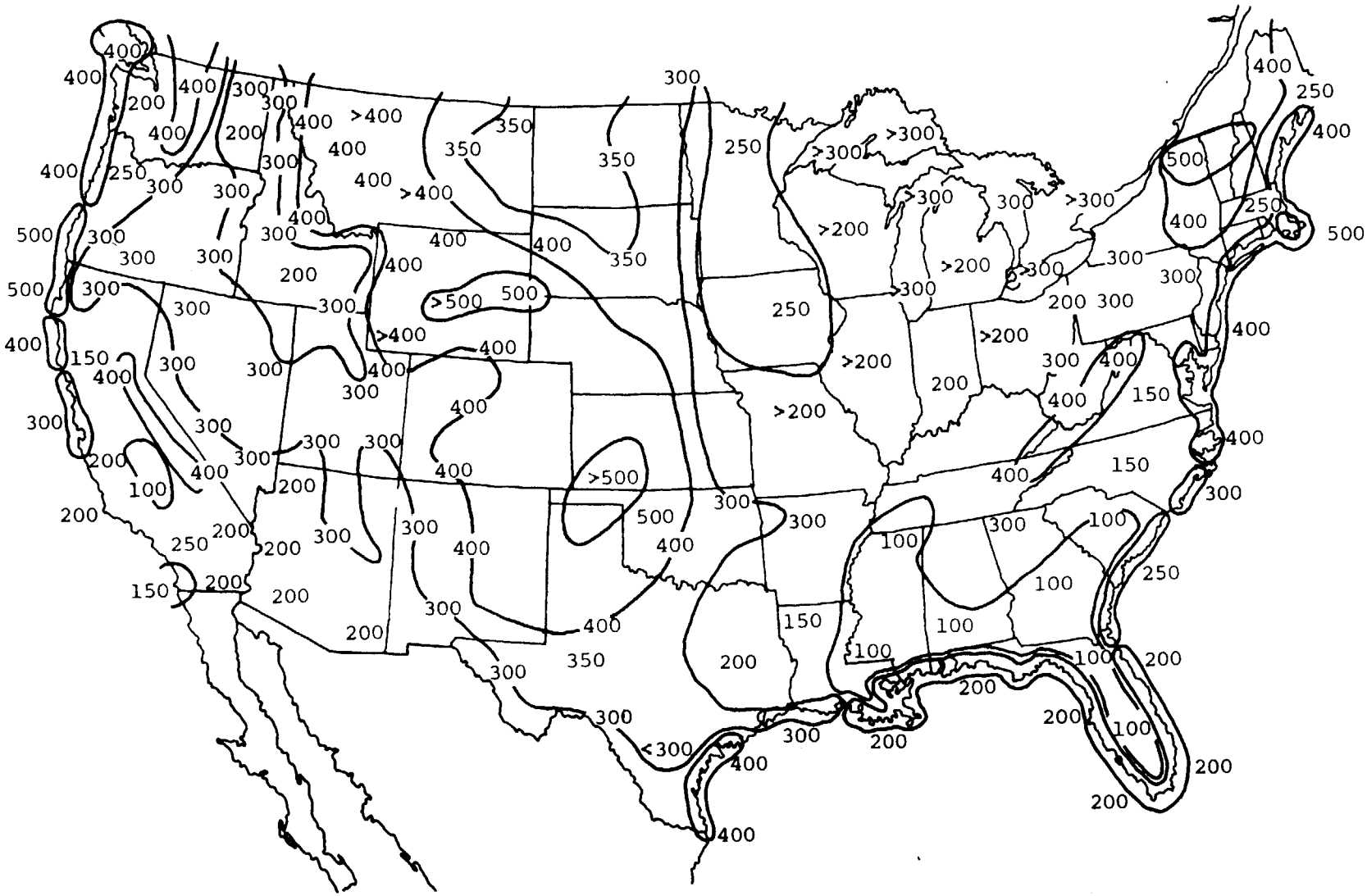

Figure 2.8a Mean annual wind power (W/m^2) estimated at 50 m above exposed areas [2.5] (contour lines by authors).

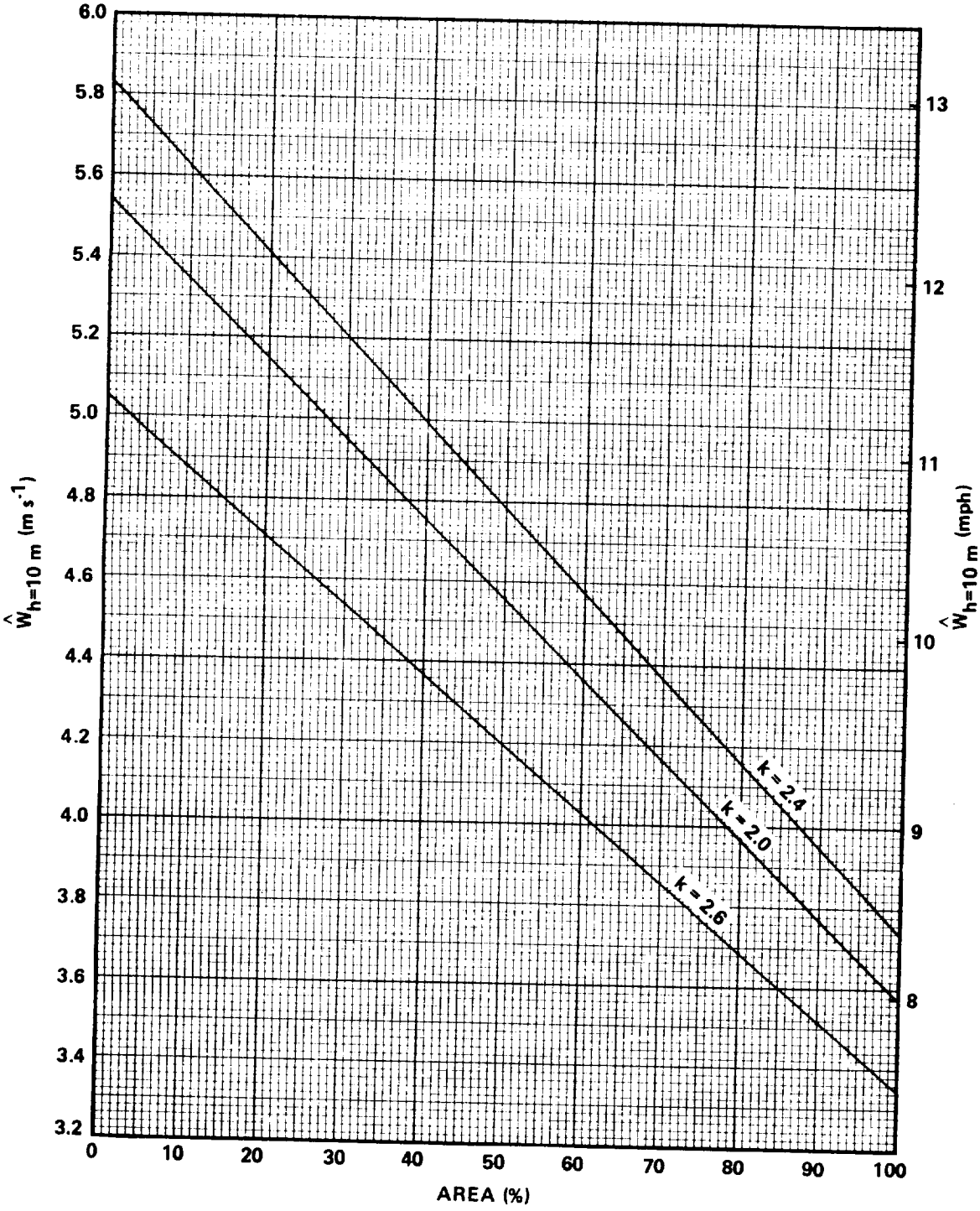

Figure 2.8b Percent area of the United States with annual mean wind speeds greater than $\hat{W}$.

The variation of mean wind speed with height for general design purposes is given by a power law with a recommended exponent, $n = 0.14$, above $h = 30$ ft (10 m); and $n = 0.40$, below $h = 30$ ft (10 m). Although n varies over a wide range ($0.50 < n < 0.08$) due to surface roughness and atmospheric stability effects, the selected values and height range of n are considered conservative from a design point of view. The justification of this is that for wind turbine generators with hub heights greater than $h = 30$ ft (10 m) an exponent of 0.14 gives the smallest correction to the reference wind speed with height. Power predictions based on this adjusted wind speed represent the lower value of power which can be expected. The performance of a WTG designed at the lower wind speed will provide more power than rated if located at a site of rougher terrain with a corresponding larger value of n and equivalent reference wind speed.

For hub heights less than $h = 30$ ft (10 m), the reverse situation is true; i.e., large values of n give lower power predictions. Therefore, a value of $n = 0.4$, which corresponds to a surface roughness typical of high woods or residential suburban areas, is recommended for elevations less than 30 ft (10 m).

Detailed Computational Procedures and Working Data

2.2 Introduction

The preceding sections were intended to give a concise overview of characteristic wind speeds for general purpose design of a WTG to operate in most any region of the United States. The following sections provide detailed information for WTG design for a specific site or region and give data to substantiate the previously quoted values.

Wind speed influences the structural strength and the performance of the WTG. Structural strength depends on extreme values of the wind; whereas, performance relies upon mean speed and its frequency distribution.

Design of the WTG for structural integrity requires that the support structure and the rotor and generator assembly be of sufficient strength to withstand the maximum or most extreme wind loading which the WTG encounters over the period of its useful life. Section 2.3 describes prediction and application of extreme wind speeds for design purposes. It is anticipated that for extreme winds the rotor will be feathered and dynamic loading of the rotor due to its rotation is not a factor in extreme wind cases. Thus, the comments in this section pertain to stationary loading.

Section 2.4 presents information on mean wind speeds and on the general characteristics of frequency distribution curves. These data permit performance estimates for preliminary design purposes, but more precise data are needed for final performance design where small errors in wind speed are critical. These data are being developed under other Department of Energy (DOE) sponsored research efforts and are not included herein.

2.3 Extreme Winds

The assessment of extreme wind loads is made as follows:

1) The basic extreme wind speed $\tilde{W}$ appropriate to the district where the structure is to be erected is determined on the basis of the expected life of the structure and the degree of risk the engineer is willing to accept that his prescribed design load will be exceeded during that life time. This procedure is described in Section 2.3.1.

2) The basic extreme wind speed is corrected for topographic features, terrain roughness, and structure size and height above ground. The correction procedure is described in Section 2.3.2.

3) The corrected design wind speed $\tilde{W}_h(\tau)$ is converted to dynamic pressure q using the relationship

$$q = K\tilde{W}_h(\tau) \quad . \tag{2.11}$$

Figure 2.9 is a conversion chart of wind speed to dynamic pressure.

4) The dynamic pressure q is then multiplied by an appropriate pressure coefficient C_p to give the pressure p exerted at any point on the surface of the structure,

$$p = C_p q \quad . \tag{2.12}$$

If the value of the pressure coefficient is less than zero, this indicates a negative p, i.e., suction, as distinct from a positive pressure. For the rotor blades, the

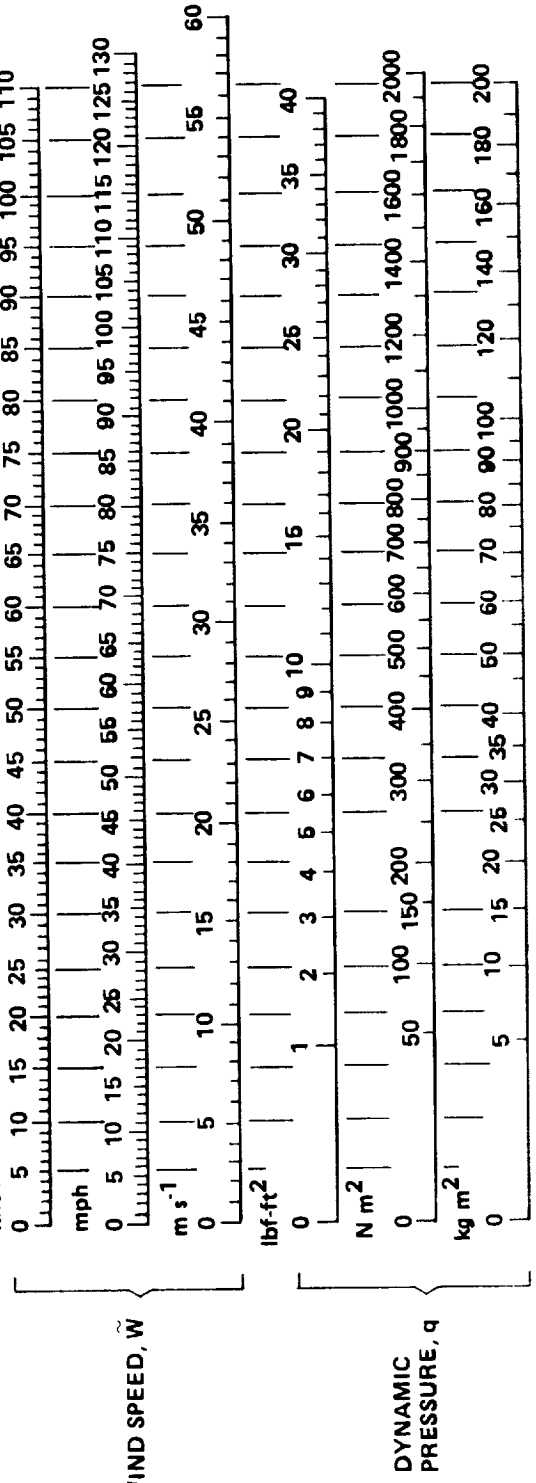

Figure 2.9 Conversion chart showing wind speed $\tilde{W}$ and the equivalent dynamic pressure q in various units. (Density equals 0.0772 lb ft^{-3}; 1.225 kg m^{-3}.)

bending loads and required braking loads to maintain a stationary rotor will be dependent on the lift coefficient C_L and the drag coefficient C_D. The design force F on any element of area A is then given by either

$$F = C_p qA, \quad F = C_L qA, \quad \text{or} \quad F = C_D qA \quad . \tag{2.13}$$

The total wind load F_T on the WTG may be obtained by vectorial summation of the loads on all the surface elements.

Typical pressure coefficients for girdered towers may be found in References 2.2, 2.4, 2.6, and 2.7, and lift and drag coefficients for a variety of rotor airfoil shapes may be found in [2.8].

2.3.1 Basic Design Extreme Wind Speed

2.3.1.1 Introduction

This section deals with computing wind speeds which would typically be employed in maximum strength analysis. Preferred features of three somewhat different approaches reported in References 2.1, 2.8, and 2.9 are incorporated into the recommended computational procedure. The general concept of determining a design wind is to select the most extreme value of the wind that the structure will experience in a given number of years' exposure.

There is always a certain probability, however, that the actual wind will exceed the design value, and the design engineer must select the degree of risk he is willing to accept that this might happen at some time during the useful life expected of the structure.

Extreme wind values are therefore tabulated according to percent probability of occurring at least once in a given recurrence interval. These values reported at a given reference level over smooth, uniform terrain must be corrected for surface roughness, for elevation, and to account for the response time of the structure to wind fluctuations. The procedure for approximately evaluating these factors and the selection of a realistic design wind for loading analyses of structures are described in the following sections.

2.3.1.2 Extreme Wind Definition

Two extreme wind speed values are currently used in wind engineering — the "extreme wind speed," or "fastest mile," and the "peak gust."

2.3.1.2.1 Extreme Wind Speed

Anemometers which make electrical contact and record a transverse mark on a rotating drum at the completion of each respective whole mile of wind movement past the anemometer are called "1-mile contact anemometers." The shortest time interval between consecutive pairs of transverse marks in any given wind record corresponds to the "fastest mile." On this basis the "fastest single-mile wind speed" is the quotient of 1 mile and the minimum time interval (in hours) elapsed during the passage of 1 mile of wind movement. Figure 2.10a illustrates this concept.

2.3.1.2.2 Peak Gust

An example of a peak wind is given in Figure 2.10b. Peak wind statistics have two advantages over mean wind statistics. First, peak wind statistics do not depend upon an averaging operation by the observer as do mean wind statistics. Second, to construct a mean wind sample, a chart reader or weather observer must perform an "eyeball" average of the wind data, causing the averaging process to vary from day to day, according to the skill of the observer, and from observer to observer. Hourly peak wind speed readings avoid this subjective averaging process.

The time duration of a peak wind speed is an important factor in wind loading design, and this duration is a function of the wind anemometer response. Standard weather service anemometers measure approximately a 3-s gust; whereas research type anemometers such as used in the research reported in Reference 2.10 can be resolved to 0.1 s.

2.3.1.3 Occurrence of the Extreme Fastest Mile

Thom [2.11] has published isotach maps of the extreme mile wind speed in miles per hour for 48 states. Maps for quantile values of 0.50, 0.10, 0.04, 0.02, and 0.01 which have corresponding mean recurrence intervals of 2, 10, 25, 50, and 100 years, respectively, are given in Figures 2.11 through 2.15. These data are based on Weather Bureau measurements for a 21-year period and are adjusted to a common elevation of 30 ft above the ground by the one-seventh power law. The accuracy of these maps is given as approximately 15 percent.

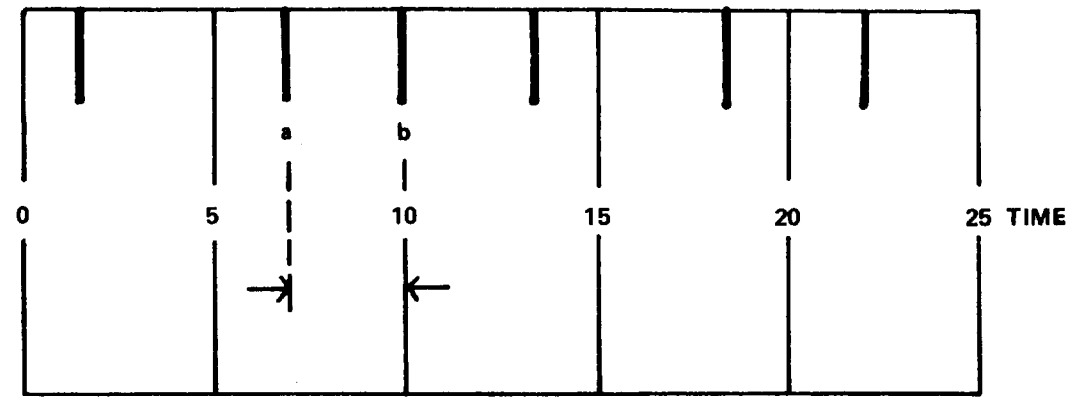

(a)

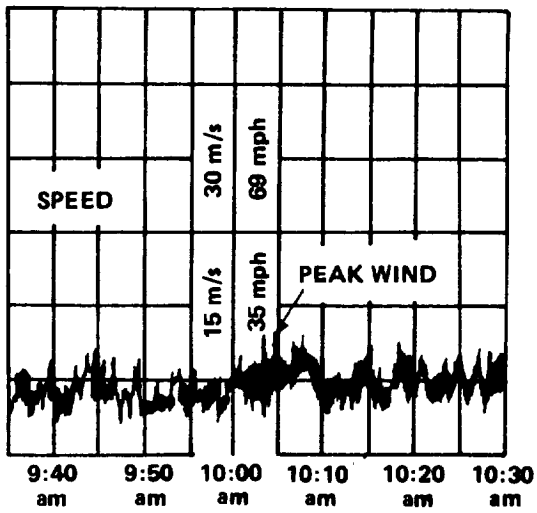

(b)

Figure 2.10 Illustration of extreme fastest mile (a) and of peak gust (b).

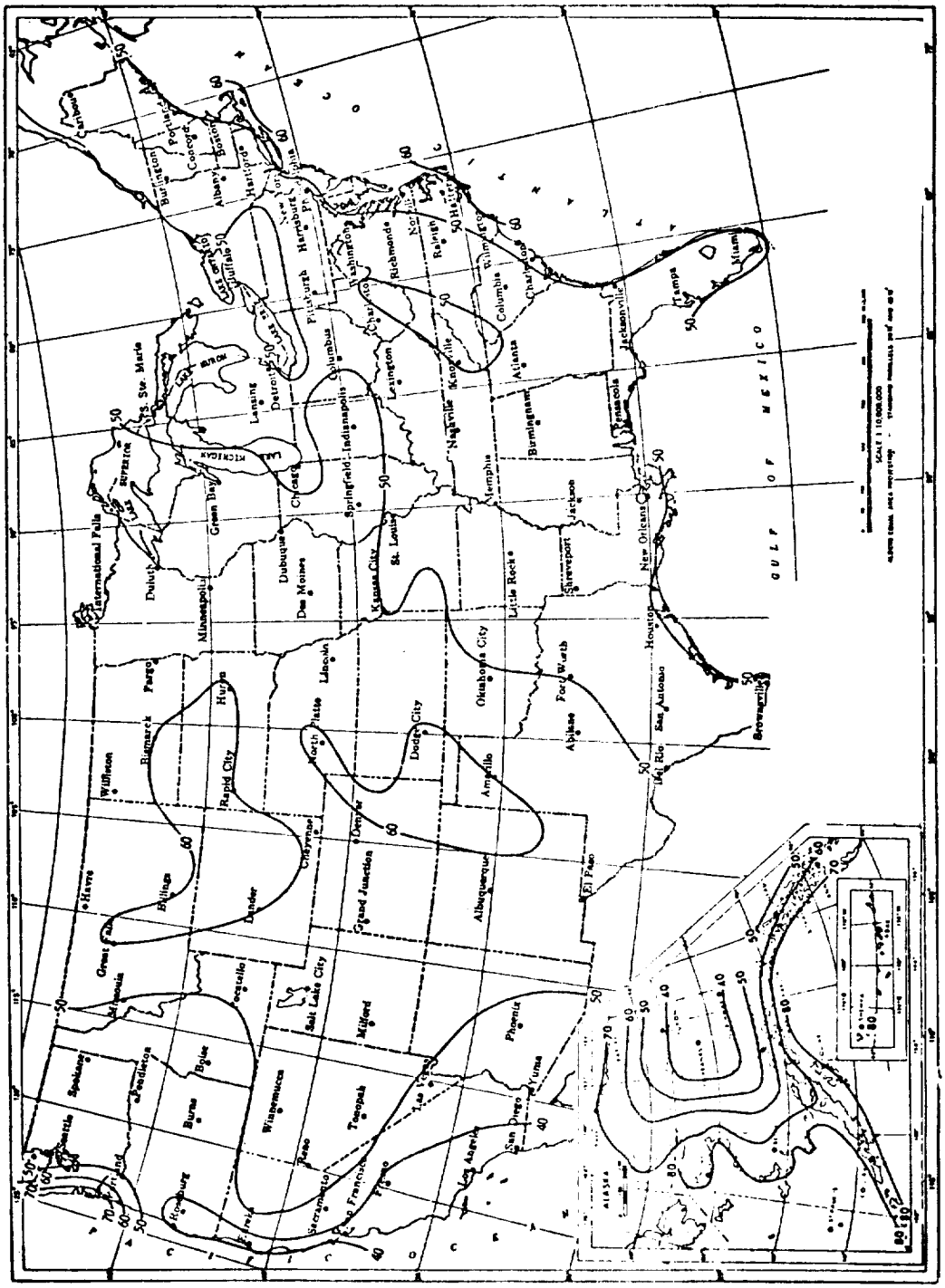

Figure 2.11 Isotach 0.50 quantiles, in miles per hour, annual extreme-mile 30 ft above ground, 2-year mean recurrence interval [2.11].

Figure 2.12 Isotach 0.10 quantiles, in miles per hour, annual extreme-mile 30 ft above ground, 10-year mean recurrence interval [2.11].

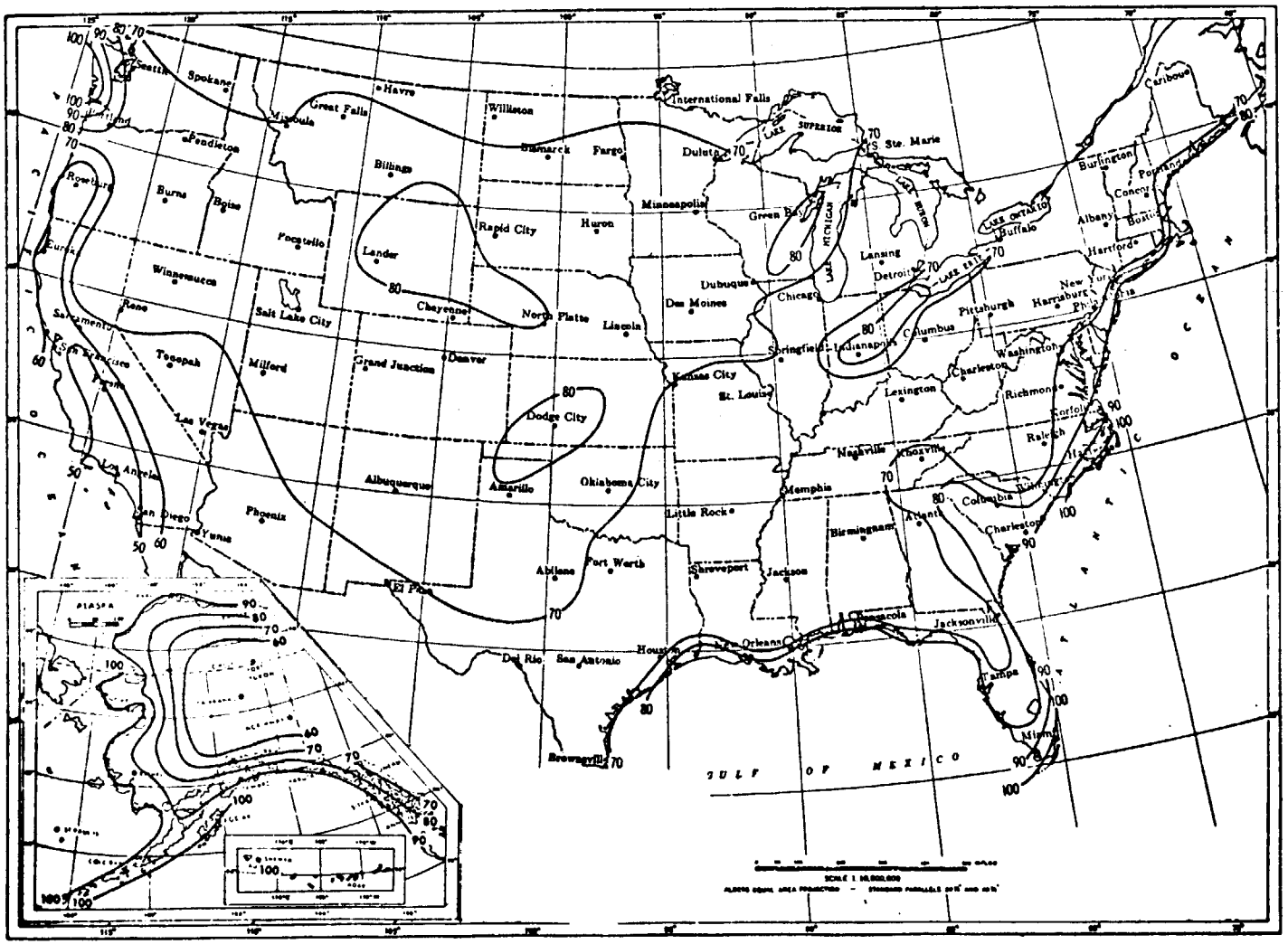

Figure 2.13 Isotach 0.04 quantiles, in miles per hour, annual extreme-mile 30 ft above ground, 25-year mean recurrence interval [2.11].

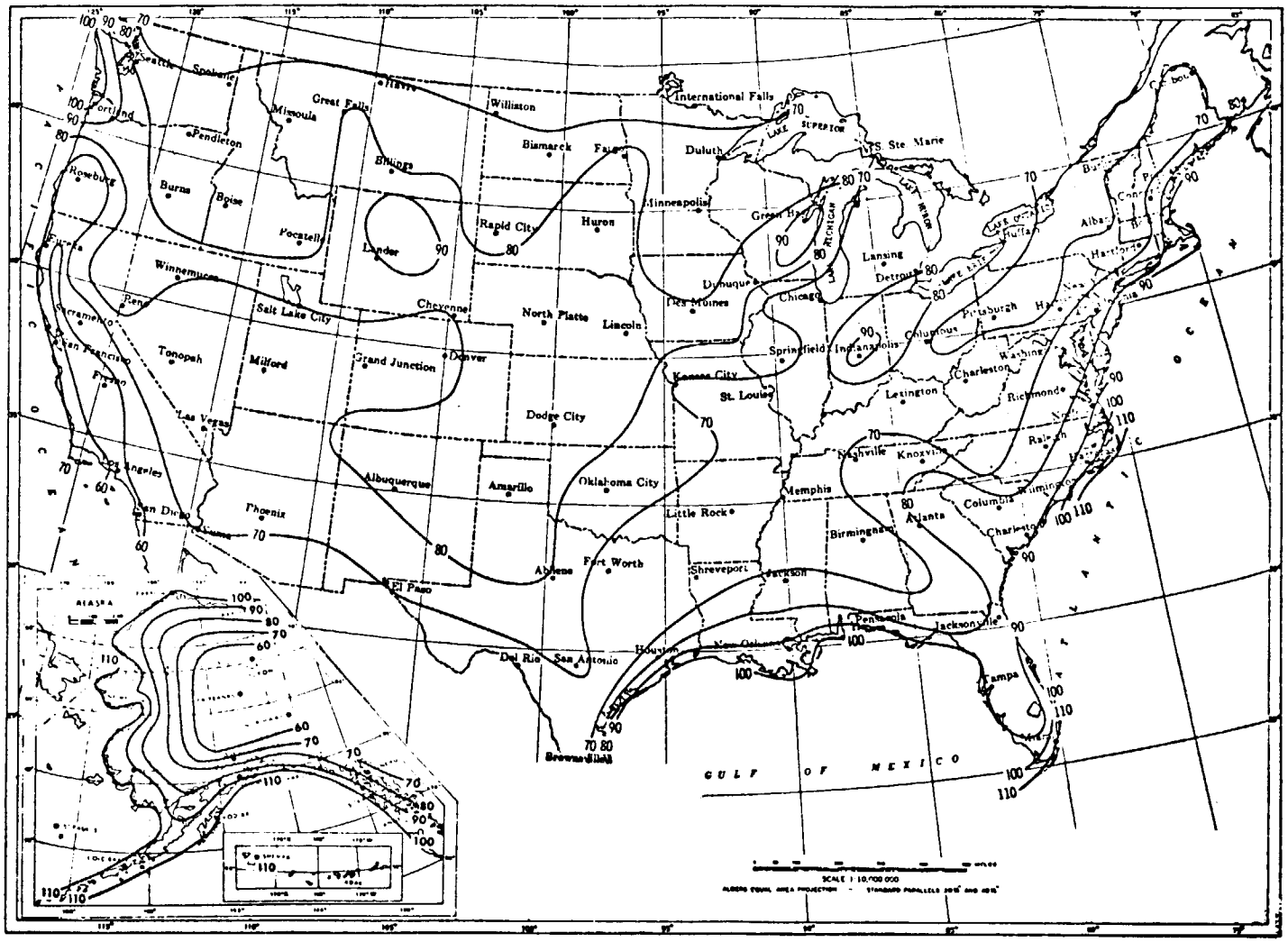

Figure 2.14 Isotach 0.02 quantiles, in miles per hour, annual extreme-mile 30 ft above ground, 50-year mean recurrence interval [2.11].

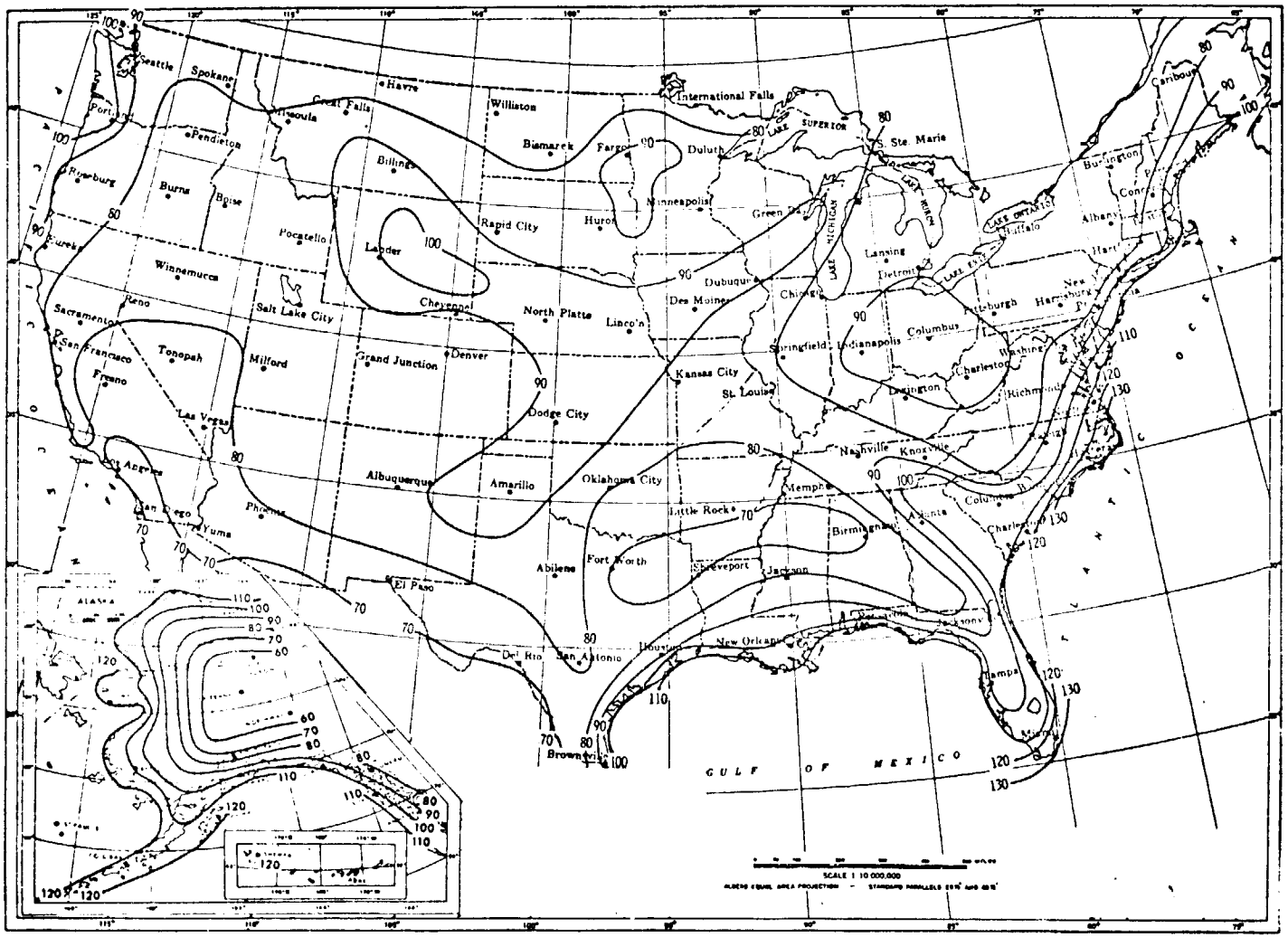

Figure 2.15 Isotach 0.01 quantiles, in miles per hour, annual extreme-mile 30 ft above ground, 100-year mean recurrence interval [2.11].

2.3.1.4 Selection of Basic Design Wind Speed

2.3.1.4.1 Extreme Fastest Mile Winds for Given Recurrence Intervals

The basic design wind speed is selected as follows:

1) The site of the WTG is located on the maps shown in Figures 2.11 through 2.15.

2) The values of the extreme fastest mile wind speed are interpolated from the isotachs for each mean recurrence interval.

3) The selected wind values are plotted on extreme value probability plotting paper, Fisher-Tippett Type II distribution, given in Figure 2.16.

4) A straight line is drawn through the plotted values.

The resulting curve gives the wind speed that may be expected to occur at least once in the given recurrence interval in the region of the United States from which the datum points were selected. If the designer prefers to work with probabilities, the curve also provides the probability of winds equal to or less than the given value.

Example 2.1: The extreme value wind speed probability for the city of Chicago has been plotted in Figure 2.16. This plot shows that an extreme-mile wind speed of 67 mph (108 km h^{-1}) may be expected at least once in 25 years and of 101 mph (163 km h^{-1}) at least once in 1000 years. In terms of probabilities, the figure shows a 4 percent chance of exceeding a 67 mph (108 km h^{-1}) fastest mile of wind and a 0.1-percent chance of exceeding a 101 mph (163 km h^{-1}) fastest mile of wind.

2.3.1.4.2 Risk of Exceeding Design Wind Speed During Expected Life of Structure

With a knowledge of the probable recurrence of the extreme fastest mile wind speed, it is necessary to establish the percent risk of the design wind speed being exceeded in the expected life of the structure. Figure 2.17 shows the risk of occurrence of wind speeds of various mean recurrence interval within the expected life of the project.

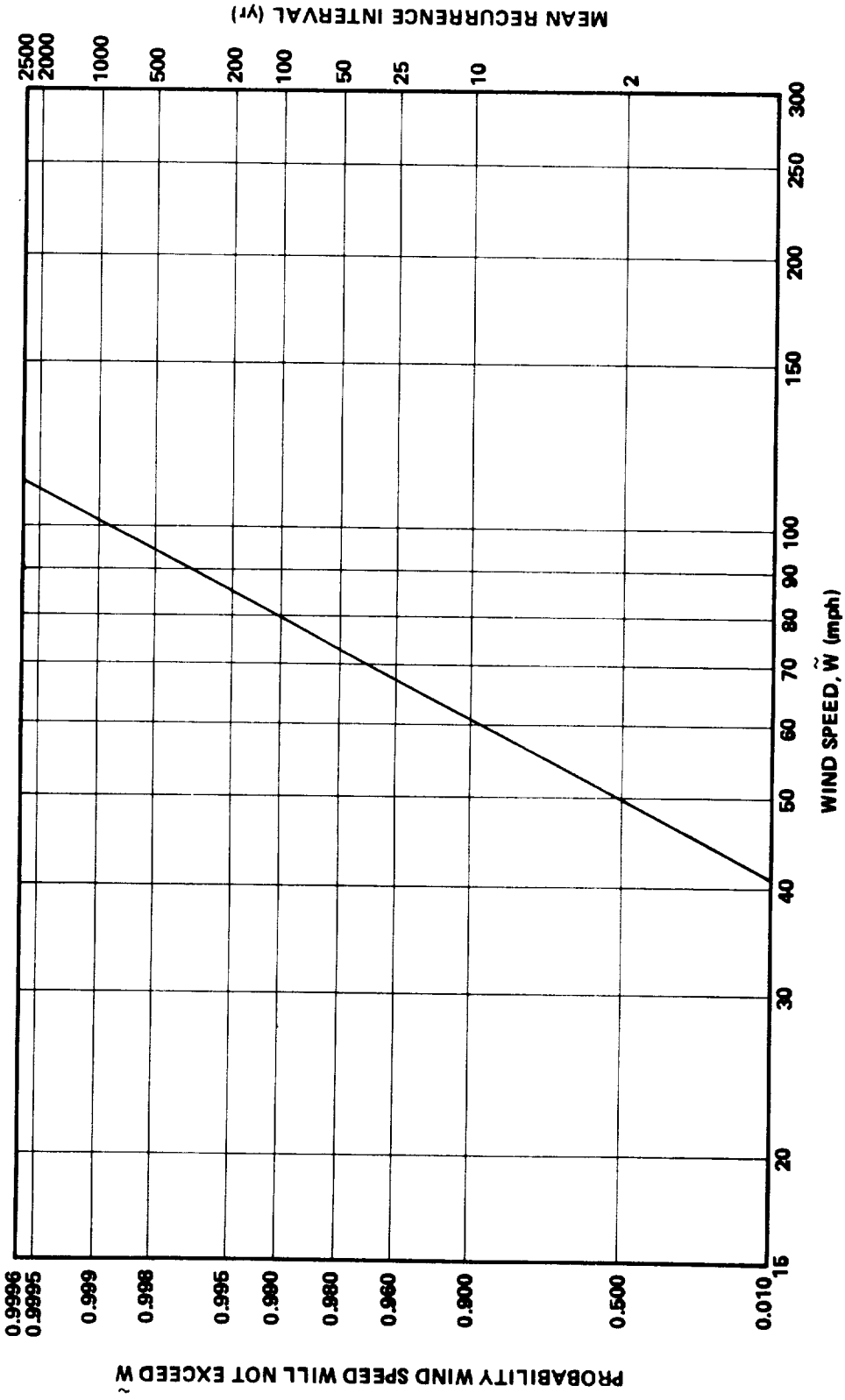

Figure 2.16 Extreme value probability plotting paper, Fisher-Tippet Type II distribution.

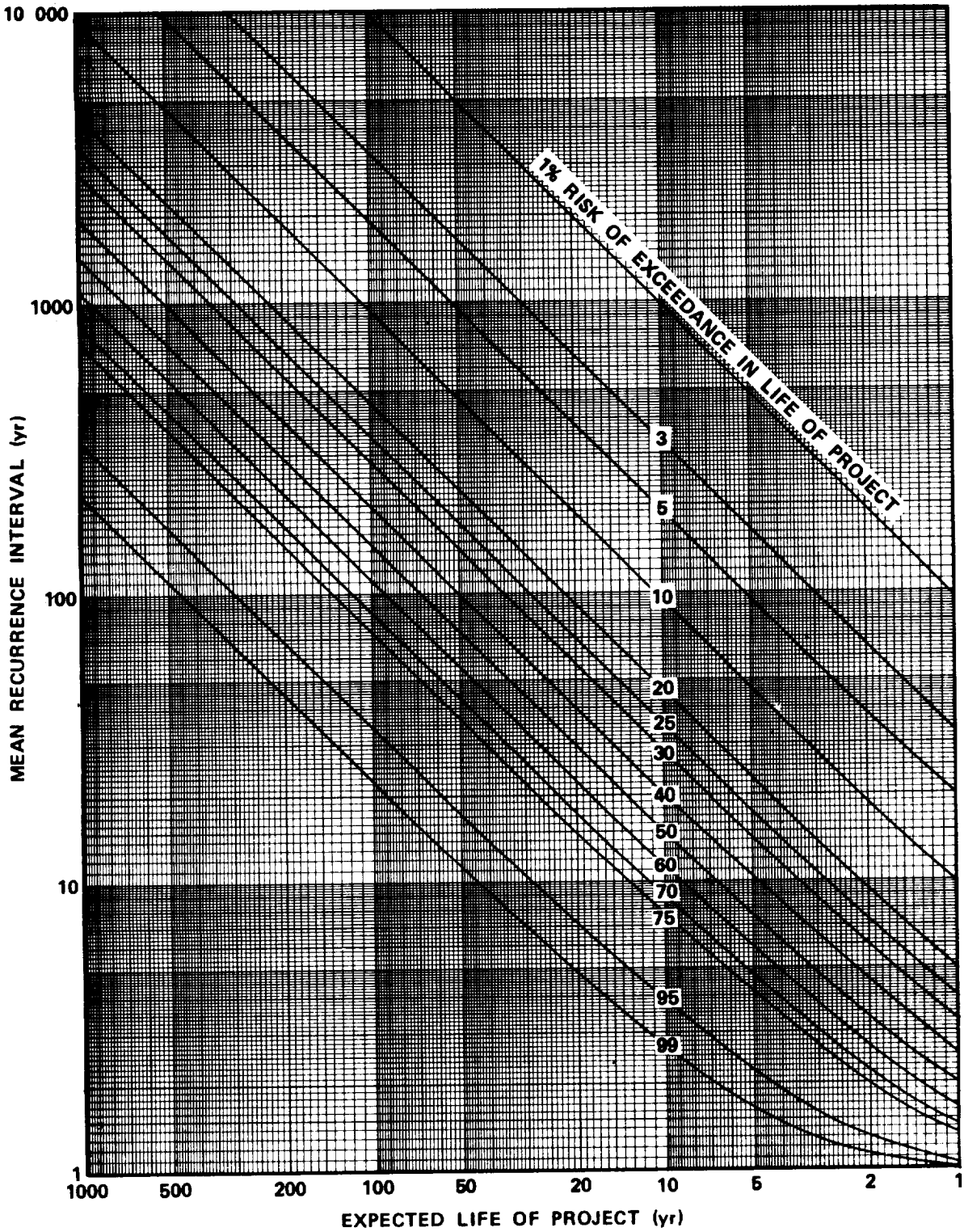

Figure 2.17 Risk of occurrence of winds of various mean recurrence intervals within the expected life of the project.

To use Figure 2.17:

1) Select the expected life of the structure under design.

2) Determine the risk that you are willing to accept that the wind might exceed the value for which you have designed. For normal buildings, Reference 2.9 suggests that an acceptable risk for design purposes is a 63-percent chance that in 50 years (expected life period) the wind speed will not exceed the 50-year (mean recurrence interval) wind speed. When greater than normal safety or operational reliability is required, the acceptable risk should be lower.

3) From Figure 2.17 find the mean recurrence interval corresponding to the values of risk and of expected life selected in items 1) and 2).

4) From Figure 2.16 find the basic design wind speed corresponding to the mean recurrence interval.

5) Correct the basic design wind speed for elevation and roughness and for structure response time as described in Section 2.3.2.

Example 2.2: An example of the procedure involved in steps 1) through 4) is as follows: A structure having a useful life of 25 years is to be designed for the Chicago area. Since wind data are statistical in nature, it is not possible to categorically state that a given value of wind will not be exceeded. The engineer is willing, however, to take a 10-percent chance that the structure may encounter winds greater than those for which it is designed and, consequently, it may fail structurally.

From Figure 2.17 the mean recurrence interval for a 25-year expected life at a 10-percent risk of exceedance is 240 years. From Figure 2.16, the basic design wind speed is found to be 89 mph (143 km h^{-1}).

2.3.2 Correction of Basic Design Wind Speed for Elevation, Terrain Roughness, and Structure Response Characteristics

2.3.2.1 Variation of Wind Velocity with Elevation

2.3.2.1.1 Introduction

The basic design extreme wind speed determined from Section 2.2.1 is the value at 30 ft (10 m) above the ground at a site typical of an airport where the surface terrain features are smooth. To adjust the velocity for a different elevation or terrain roughness, the relationship

$$\tilde{W} = \tilde{W}_{ref}(h/h_{ref})^{n} \quad , \tag{2.14}$$

where W_{ref} is the basic design wind speed at the reference height h_{ref} = 30 ft (10 m), is used. The exponent n is dependent on the surface roughness of the surrounding terrain (see Section 3.3.4 for additional information on n).

Extrapolating extreme-mile wind speed distributions from the 30-ft (10-m) level to other levels with the power-law relationship, equation (2.14) is justified by Huss as reported by Thom [2.12]. A more rigorous extrapolation procedure of peak gust statistics is described by Fichtl, et al. [2.10]. This procedure is based on several years of wind profile data measured at Kennedy Space Center, Florida; its general applicability to other regions where such extensive data are not available has not been confirmed. Therefore, a simpler method of adjusting the basic design wind speed for variations in elevation based on the power-law relationship as recommended by Hollister [2.8] is employed herein. A discussion of the value of n for extreme winds is given in Section 3.3.4.

2.3.2.1.2 Adjustment of Wind Speed for Elevation

Figure 2.18 illustrates the procedure of Hollister [2.8] for adjusting wind speed for elevation. There is no apparent scientific justification of this procedure; thus it must be considered a "rule of thumb" until a more accurate method is determined. The wind speed is adjusted according to the concept that the wind speed magnitude and profile slope, α, at 1200 ft (365 m) over flat smooth terrain are displaced a height 4c where c is the effective thickness of the undulating terrain with trees, buildings, etc. The value of c may be estimated from topographical maps and inspection of the site.

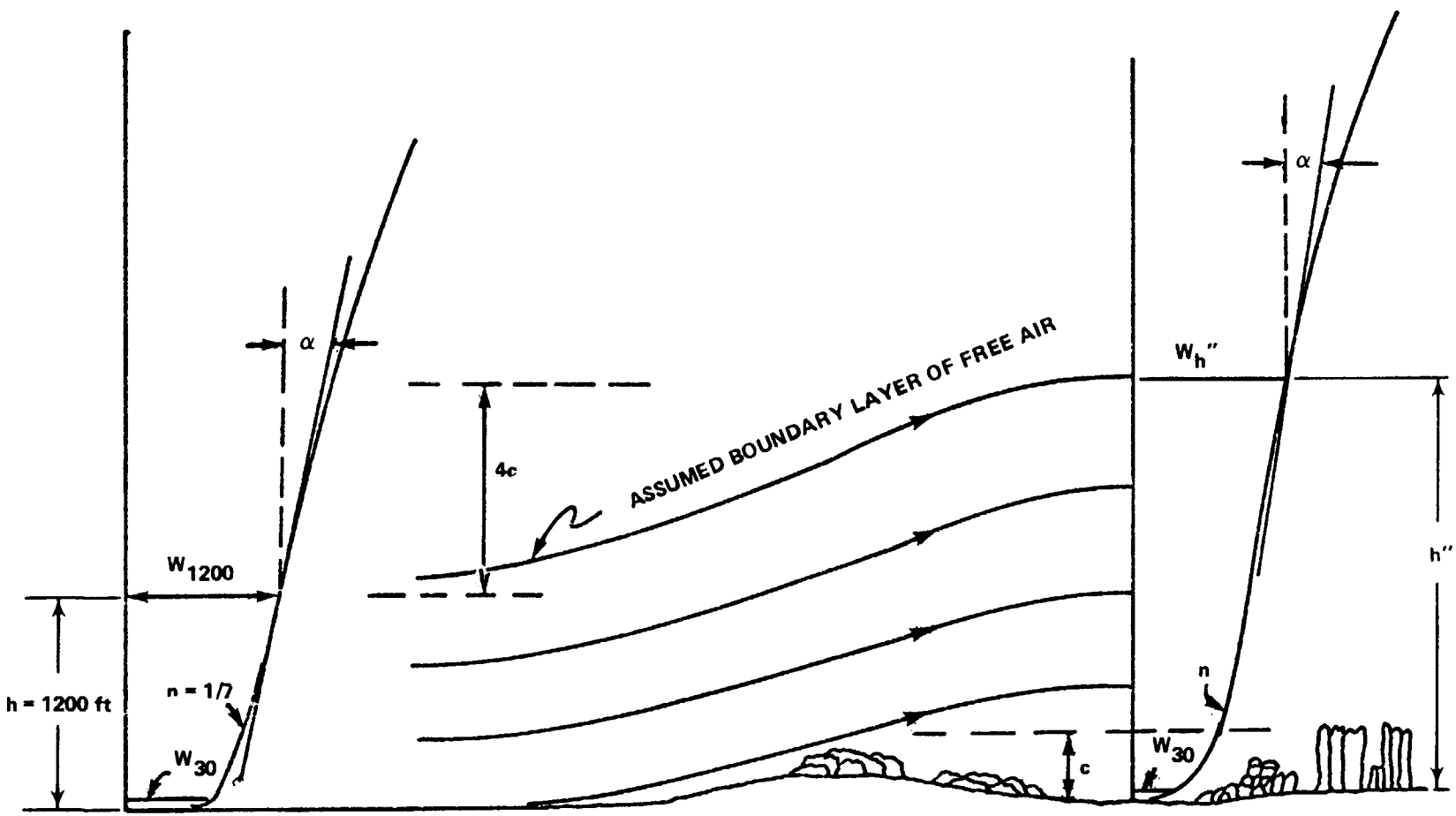

Figure 2.18 Schematic effect of surface roughnesses on atmospheric boundary layer flow.

The steps involved in adjusting the extreme-mile wind speed for terrain other than flat, smooth terrain (typically an airport) are as follows:

1) The basic design extreme wind speed $\tilde{W}$ found in Section 2.3.1 is extrapolated to 1200 ft by

$$\tilde{W}_{h=1200\ ft} = \tilde{W}_{h=30\ ft}(1200/30)^{1/7} \qquad (2.15a)$$

or

$$\tilde{W}_{h=1200\ ft} = 1.69\ \tilde{W}_{h=30\ ft} \qquad (2.15b)$$

2) The approximate thickness c for the WTG site is estimated from contour maps and surrounding surface features such as tree height, building height, etc.

3) The height h'' at which the wind speed magnitude and slope over the airport at 1200 ft have the same value over the WTG site is estimated from

$$h'' = 1200 + 4c; \quad c\ (ft)$$

$$h'' = 365 + 4c; \quad c\ (m) \qquad (2.16)$$

4) Equating the slopes α gives the exponent

$$n = h''/8400; \quad h''\ (ft)$$

$$n = h''/2560; \quad h''\ (m) \qquad (2.17)$$

5) The height-adjusted extreme wind speed $\tilde{W}_h$ over the WTG site at the required design elevation h is given by

$$\tilde{W}_h = 1.69\ \tilde{W}_{h=30\ ft}(h/h'')^{h''/8400};\quad h''\ (ft)$$

$$\tilde{W}_h = 1.69\ \tilde{W}_{h=10\ m}(h/h'')^{h''/2560};\quad h''\ (m) \quad , \qquad (2.18)$$

where

$\tilde{W}_{h=30\ ft}$ ~ Basic design wind speed from Section 2.3.1.

h'' ~ WTG site reference height from equation (2.16).

Equation (2.18) is plotted in Figure 2.19 for quick engineering reference.

Example 2.3: An example application of Figure 2.19 is as follows. Assume the extreme wind speed at 30 ft (10 m) over an airport type terrain is 90 mph (145 km h^{-1}). A WTG of hub height h_H = 200 ft (61 m) is located in a region where c is on the order of 100 ft (30 m). From equation (2.16), h'' is 1600 ft (488 m). Locating the curve h'' = 1600 ft (488 m) in Figure 2.18, find h_H/h'' = 0.13 on the vertical scale. A vertical projection from where h_H/h'' = 0.13 and the line h'' = 1680 ft (approximately 1600 m) intersect gives $\tilde{W}_h/\tilde{W}_{h=30\ ft}$ = 1.25. Thus, the design extreme wind speed is 112 mph (181 km h^{-1}).

2.3.2.2 Adjustment of Gust for Structure Response Time

Wind gusts or fastest-mile winds have a certain interval of duration. For example, an extreme-fastest-mile gust of 60 mph (97 km h^{-1}) would have a duration of (1 mile · 3600 s h^{-1}/60 mph) = 60 s.

The response of a structure to a gust of wind cannot fully develop unless the gust duration is sufficient to establish the particular regime of the response. In turn, a wind record averaged over a given interval, e.g., 60 s, will have

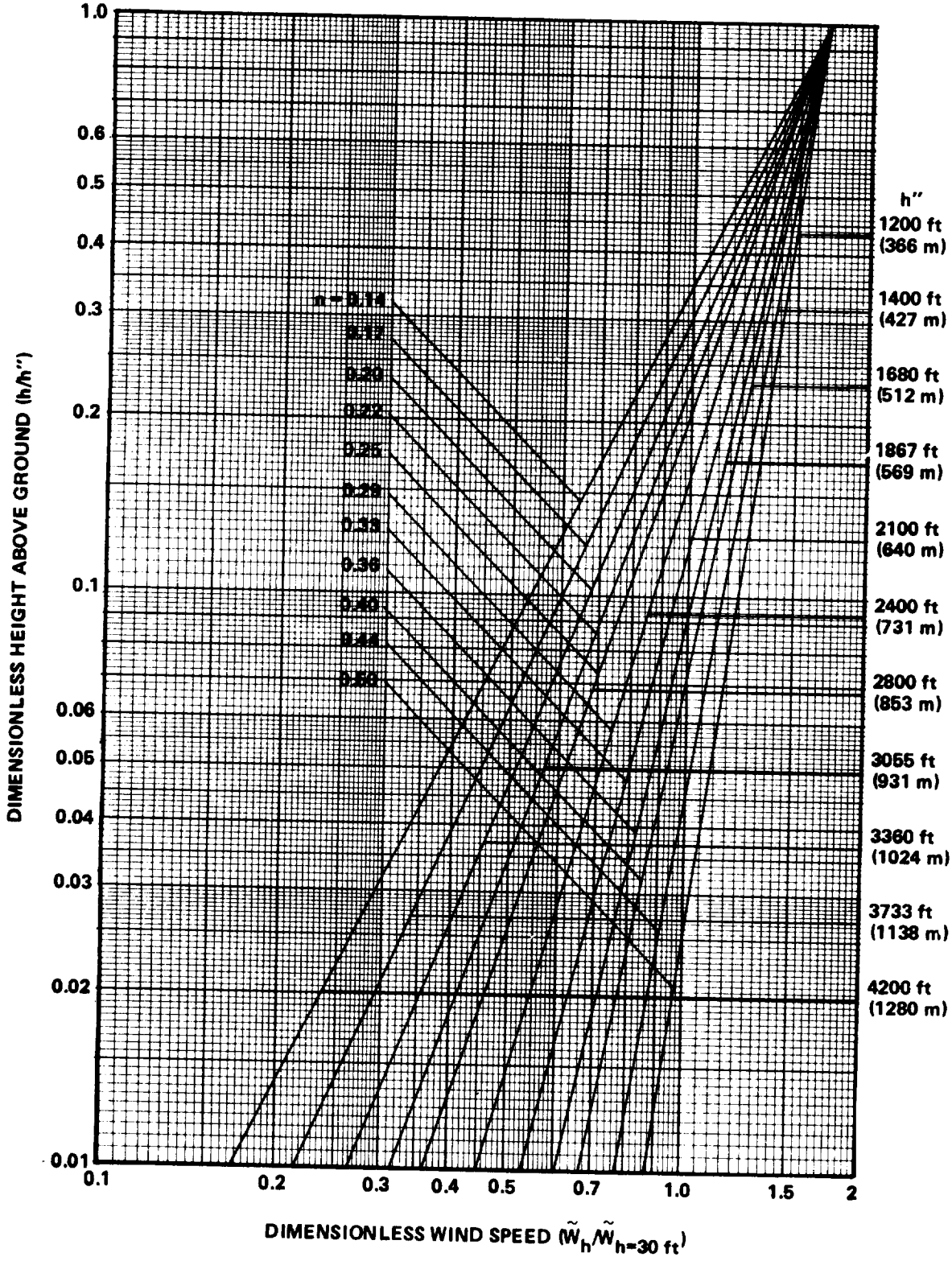

Figure 2.19 Correction for wind speed with height.

within the 60-s period, shorter period gusts, e.g., 3-s gusts, which may have a considerably higher wind speed than the wind speed averaged over the complete 60 s. If the response of a structure or of a component of the structure is 3 s, then a design wind speed based on a 60-s average will be too low, and the higher wind speed associated with the 3-s gust should be employed.

For this purpose, a gust factor, F_G, has been defined as the ratio of the mean velocity over a short period to the hourly mean. A plot of gust intensity versus gust duration is shown in Figure 2.20. In general, F_G becomes unity for periods longer than 10 min (i.e., the 10-min mean and hourly mean are essentially equivalent). This gust factor relationship, Figure 2.20, is given by Hollister [2.8] where it is reported that the intensity of gusts is found to be independent of height at least up to approximately 500 ft. More recent data [2.1] of which a complete discussion is given in Section 4.4 show the gust factor to be height dependent, particularly for small-duration gusts. However, Figure 2.20 is consistent with data used throughout this section and is recommended for use in the extreme wind speed design analysis.

The procedure for adjusting the design wind speed for the structure response time is as follows:

1) The response time, t_r, of the structure is estimated. In general, the design engineer will know the approximate response time of the structure under design. However, a rough estimate of the time required to establish the response regime of a structure is given by Farren [2.13] from research conducted on airplanes. He found the time required to achieve the response regime was that needed by the windstream to pass through a distance equal to eight times the greatest width of the structure. Also, the Building Research Establishment in Great Britian [2.2] provides the following guidelines for response time estimates:

a) Three seconds for structures or components of 65 ft (20 m) or less in extent (e.g., all cladding and roofing).

b) Five seconds for structures where neither the greatest horizontal dimension nor the greatest vertical dimension exceeds 165 ft (50 m).

c) Fifteen seconds for all larger structures.

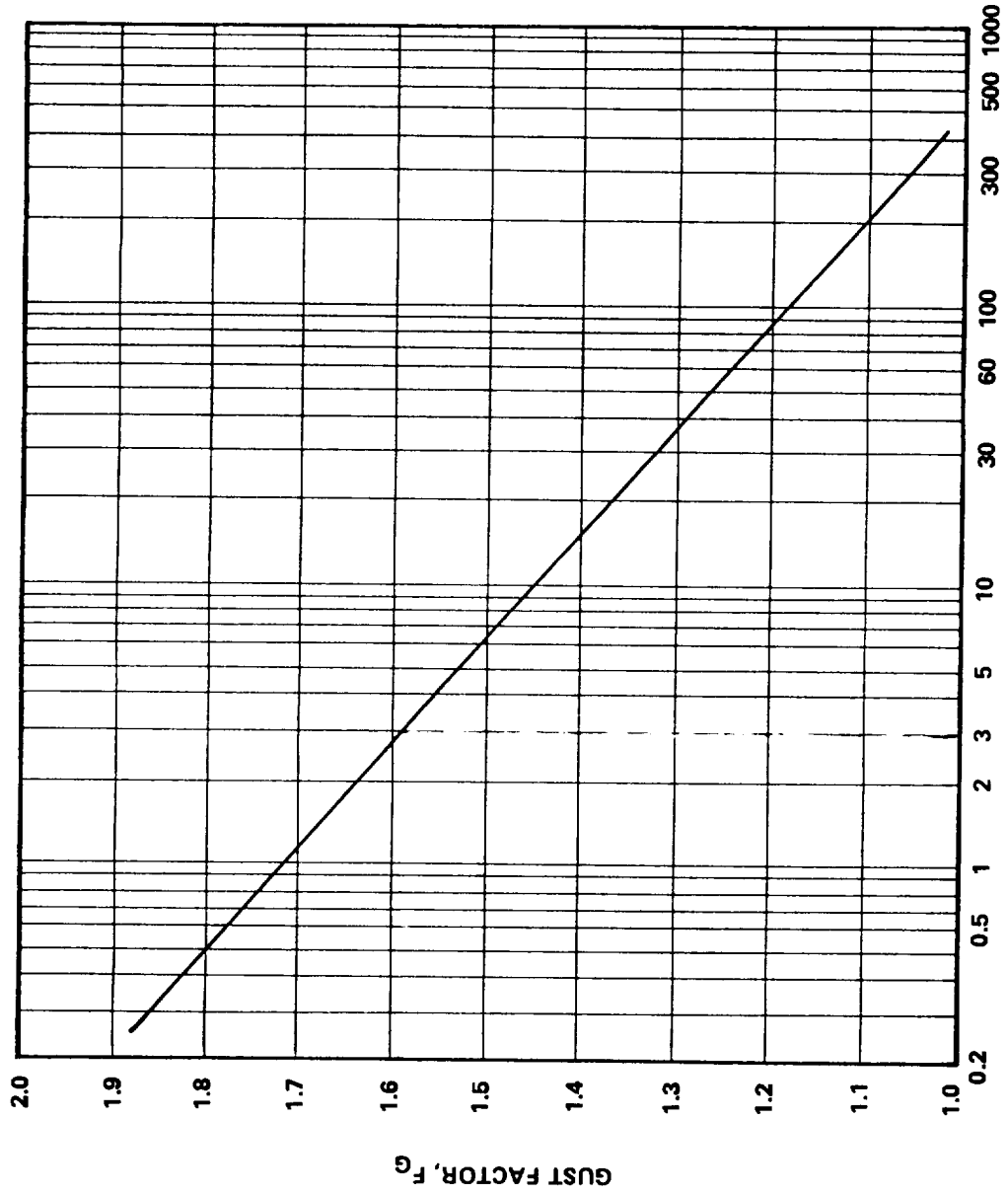

Figure 2.20 Relation between gust intensity and gust duration.

Two procedures follow depending on whether Farren's approach or the British Building Code method is employed.

Farren's estimate [2.13] of the response is in terms of a length scale, L_r (i.e., eight times greatest width); thus the following steps are taken after step 1):

2) $\tilde{W}_h$ determined from the preceding sections is found on the vertical scale of Figure 2.21, and a horizontal projection to the fastest-mile curve is made.

3) The intersection with the fastest-mile curve gives the hourly mean wind speed $\overline{W}_h$ on the horizontal scale.

4) The value of $\overline{W}_h$ is projected vertically to the curve corresponding to the value of the response length scale, L_r.

5) The adjusted design wind speed $\tilde{W}_h(\tau)$ is then found from the vertical scale.

For the british Code, the following steps are taken after step 1):

2) The extreme fastest-mile wind speed $\tilde{W}_h$ obtained from Section 2.3.2.1 is converted to an hourly mean velocity, $\overline{W}_h$, from Figure 2.21.

3) The gust factor F_G for the required response time is found from Figure 2.20 by equating t_r to gust duration, τ.

4) The design wind speed is then computed from

$$\tilde{W}_h = \overline{W}_h F_G \quad . \tag{2.19}$$

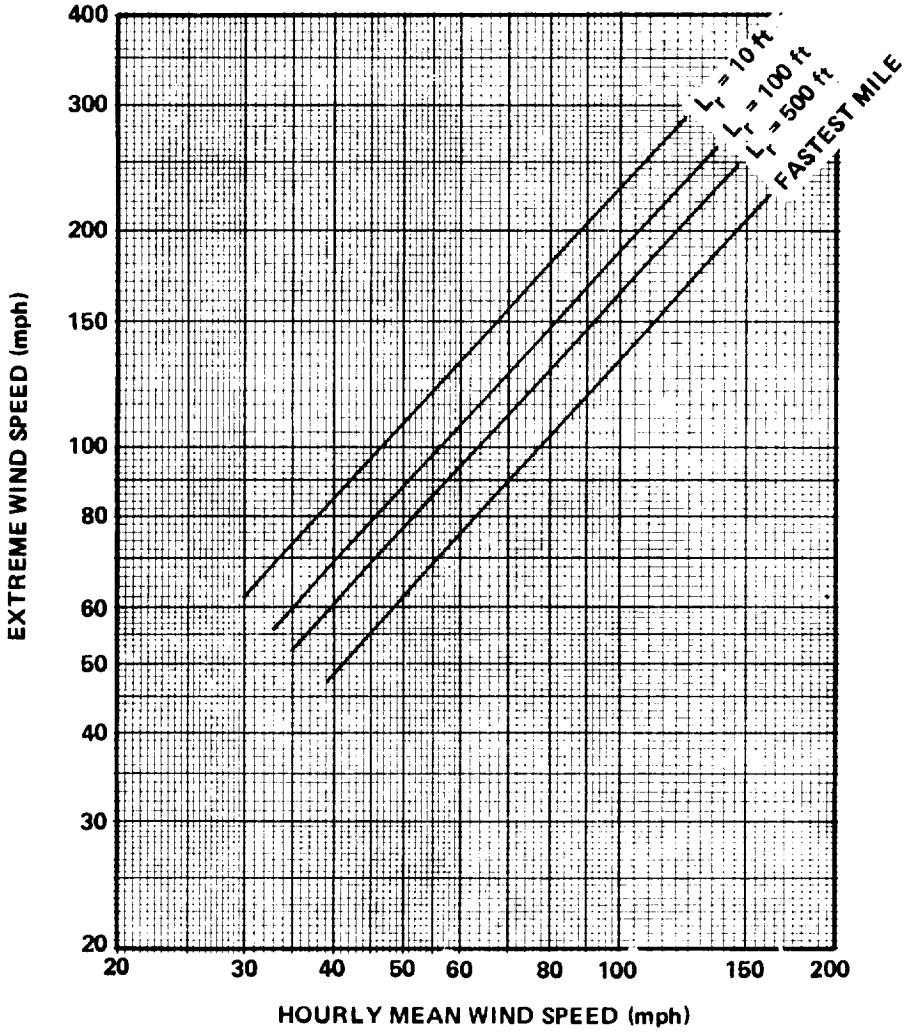

Figure 2.21 Relation between hourly mean wind speed and extreme wind speed for fastest-mile, fastest 500 ft, fastest 100 ft and fastest 10 ft of wind.

Example 2.4: Suppose we have determined the design wind speed $\tilde{W}_h$ from the preceding sections to be 80 mph (129 km h^{-1}). Since this is a fastest-mile value, the gust duration is (1 mile • 3600 s h^{-1}/ 80 mph) = 45 s. The structural component under design has a largest dimension of 20 ft (6 m). By Farren's [2.13] method, the response time is the time required for the windstream to pass eight times the greatest width of the structure which is 20 ft (6 m); hence, L_r = 160 ft (48 m). From Figure 2.21 this corresponds to a design wind speed of 108 mph (174 km h^{-1}).

Alternatively, the British Code calls for a 3-s gust for any structure of largest dimension less than 65 ft (20 m). Hence, from Figure 2.20, F_G = 1.59 at τ = 3 s. From Figure 2.21, $\bar{W}_h$ corresponding to $\tilde{W}_h$ = 80 mph (129 km h^{-1}) for the fastest mile is 62 mph (100 km h^{-1}). Thus, the adjusted $\tilde{W}_h(\tau)$ = 98 mph (km h^{-1}).

2.3.3 Application of Design Wind Speed

The design wind speed as computed in Sections 2.3.1 and 2.3.2 is converted to dynamic pressure and coupled with an appropriate pressure coefficient to compute the static loading on the structure under design. The height used in computing $\tilde{W}_h$ should be taken to the top of the structure or, alternatively, the height of the structure may be divided into convenient parts and the wind load on each part calculated using a design wind adjusted to the height of the top of the part. The load should be applied at the mid-height of the structure or part, respectively.

For a site where the ground roughness is different from different directions, the most severe grading (i.e., the smoothest) should be used, or appropriate gradings may be used for different wind directions.

In the previous paragraphs, height above ground means the dimension above the general level of the ground in the vicinity of the structure assuming that there are no unusual conditions. Allowances should, however, be made for special conditions. For example, in some cases the height above ground of the

WTG on a cliff top or a steeply sloped escarpment should be determined as described in the following section.

2.3.4 Effective Height for WTG on Cliffs or Escarpments

A method for estimating the effective height to which the wind speed should be correct for sites near sharp edge cliffs is proposed in Reference 2.2 as follows. To account for the effect of a cliff or escarpment on the height above ground h, consider three cases as shown in Figures 2.22, 2.23, and 2.24. In the figures, Z_1 is the general level of the ground at the foot of the escarpment and Z_2 is the general level of the top of the escarpment. The difference in levels is $\Delta h = Z_2 - Z_1$ and the artificial base from which h, for use in the wind speed profile [equation (2.14)] is measured, is Z_c. θ is the inclination of the mean slope of the cliff to the horizontal.

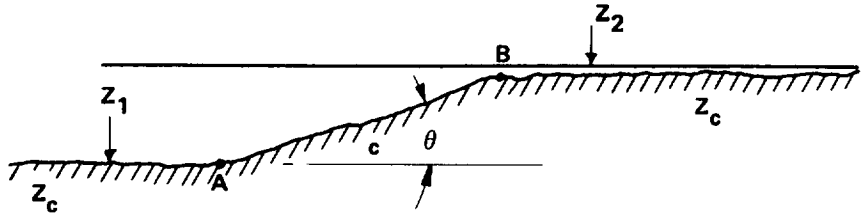

Figure 2.22 Slope of escarpment is $\tan \theta \leq 0.3$.

For Case 1 in which the average slope θ of the escarpment is $\tan \theta \leq 0.3$, the artificial base Z_c is that of the ground immediately around the structure.

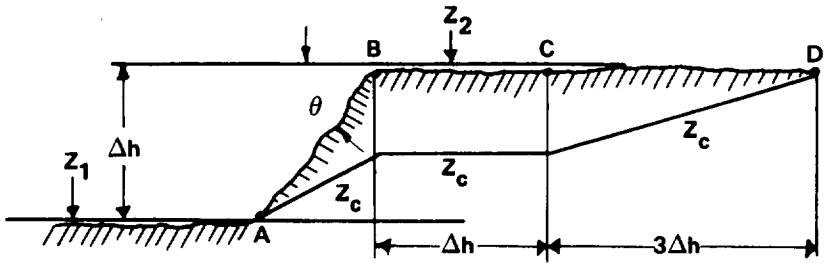

Figure 2.23 Slope of escarpment is $0.3 < \tan \theta \leq 2$.

For Case 2 in which the average slope θ of the escarpment is $0.3 < \tan\theta < 2$, the following points serve for reference:

1) A is the point of intersection of the level Z_1 and the mean slope of the escarpment

2) B is the point of intersection of the level Z_2 and the mean slope of the escarpment

3) C is such that $BC = \Delta h$

4) D is such that $CD = 3\Delta h$.

The value of Z_c is then taken such that in front of A, $Z_c = Z_1$. From B to C, $Z_o = Z_1 + [(2 - \tan\theta)/1.7]\Delta h$; and beyond D, $Z_c = Z_2$. Between A and B and between C and D, Z_c is obtained by linear interpolation.

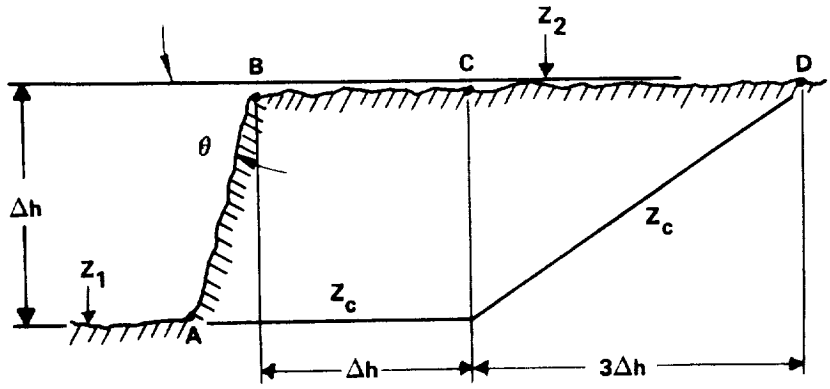

Figure 2.24 Slope of escarpment is $\tan\theta > 2$.

For Case 3 in which the average slope θ of the escarpment is $\tan\theta > 2$, A, B, C, and D are defined as in Case 2 whereas in front of A, $Z_c = Z_1$; from A to C, $Z_c = Z_1$; and beyond D, $Z_c = Z_2$. Between C and D, Z_c is obtained by linear interpolation.

Example 2.5: As a comparison of the computed influence of terrain effects on the extreme wind speed, consider the measured wind speeds for Rattle Snake Mountain near Richland, Washington.[2] The maximum wind speed measured at the foot of Rattle Snake Mountain at an elevation of approximately 50 ft (15 m) above the ground is 72 mph (116 km h^{-1}). This value was the maximum recorded in a period of approximately 30 years. At the top of the mountain, approximately 2500 ft (762 m) measured from the base of the mountain, the maximum speed recorded over the same 30-year period was 120 mph (193 km h^{-1}) at which time the anemometer blew away. The corresponding design value of extreme wind speed would be computed from this manual as follows. From the isotach maps, for a 30-year recurrence interval, a velocity at Richland, Washington, of approximately 69 mph (111 km h^{-1}) is found. Adjusting this according to Figure 2.24 requires that the reference altitude in this case be the full 2500 ft (762 m). Thus, the ratio of 2500:30 raised to a power of n of approximately 1/7 gives an adjusted velocity for a 30-year recurrence interval at the top of the mountain of 130 mph. This value seems most reasonable in view of the fact that the anemometer blew away at approximately 120 mph.

Example 2.6: The application of the design wind speed is now illustrated with an example calculation. Suppose a WTG, 100-ft (30-m) high, is to be constructed in Boston and is expected to have a useful life of 50 years.

From Figures 2.11 through 2.15 the extreme-mile wind speeds are:

Mean Recurrence Interval (yr)	Extreme-Mile (mph)
100	94
50	86
25	73
10	70
2	50

2. Personal communication with Atmospheric Sciences Department Personnel at Battelle, PNL.

A plot of these values on the Fisher-Tippett Type II paper is shown in Figure 2.25.

Accepting a 30-percent risk that the design wind might be exceeded at least once in the 50 years of the project life, the engineer finds from Figure 2.17 a mean recurrence interval of 140 years. Thus, from Figure 2.25, the basic design wind, $\tilde{W}$, is 98 mph (158 km h^{-1}).

This is the velocity at 30 ft (10 m). The WTG site is in an area where the undulations of the terrain together with the envelope of average terrain features are 50 ft (15 m). From equation (2.16), h'' = 1400 ft (427 m). From equation (2.17), n = 0.17 and from equation (2.18),

$$\tilde{W}_h = 1.69\ \tilde{W}(h/1400)^{0.17} \quad .$$

(Note: $\tilde{W}_h$ can be selected from Figure 2.19 for any given height ratio h/h'' and n = 0.17.)

Thus, at the top of the 100-ft structure, $\tilde{W}$, corrected for height from equation (2.18) or Figure 2.19, is $\tilde{W}_h$ = 106 mph (170 km h^{-1}).

To determine the structure response factor, we use Farren's rule of eight times the largest dimension, i.e., L_r = 800 ft (244 m) of windstream. From Figure 2.21, $\overline{W}_h$ corresponding to a fastest mile of 106 mph (170 km h^{-1}) is 80 mph (129 km h^{-1}), and $\tilde{W}_h(\tau)$ is then read by interpolating to L_r = 800 ft as 120 mph (193 km h^{-1}).

The pressure produced by this velocity in standard air, q, is from Figure 2.8, 40 psf (1900 N m^{-2}). To convert this to a load, the engineer must have available the C_p value for his structure [2.2, 2.4].

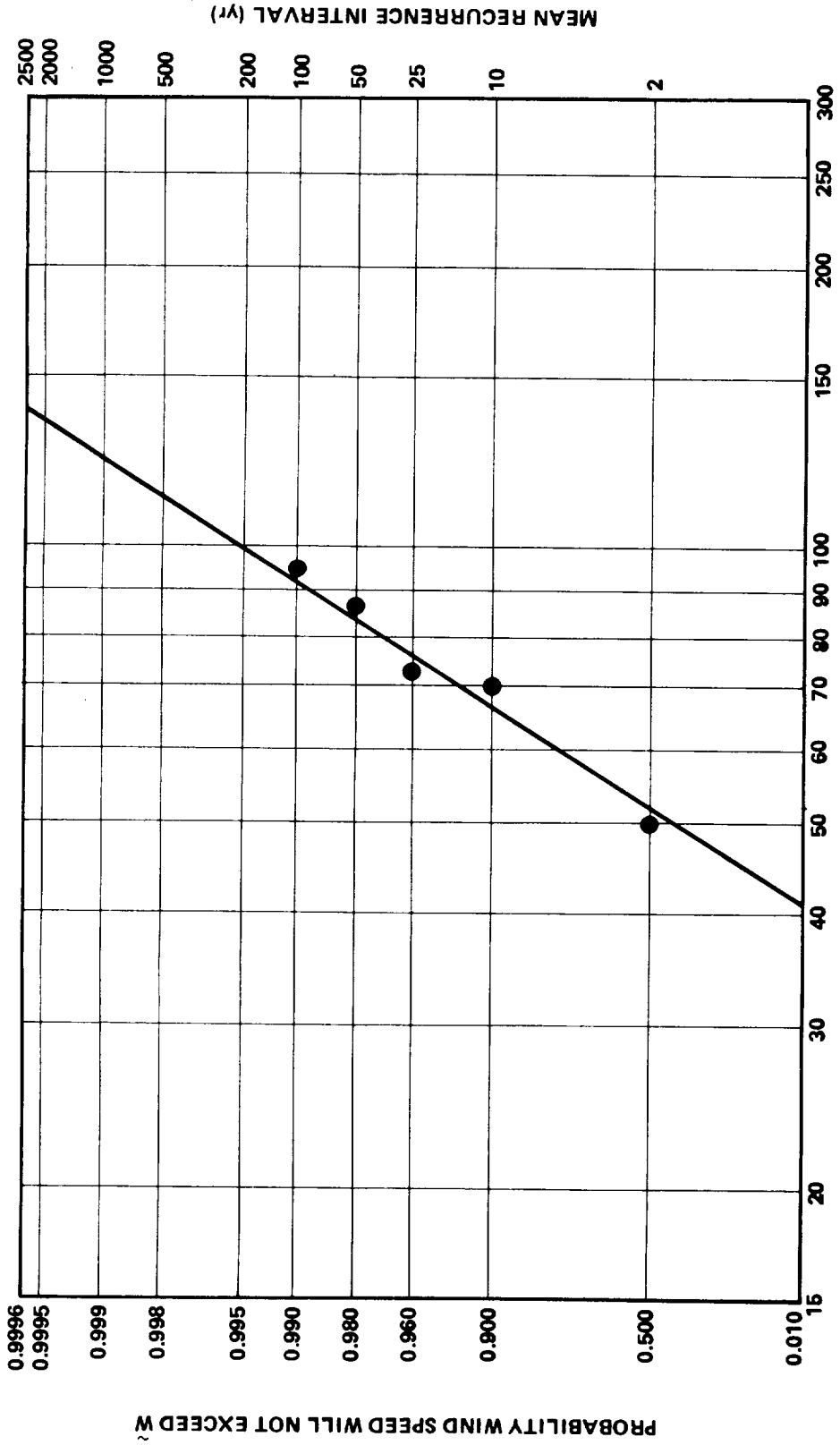

Figure 2.25 Distribution of extreme value wind speed for the Boston area.

2.4 Mean Wind Speed

The magnitude and duration of the mean wind speed is an important factor in the design of the wind turbine generator. The actual power that can be achieved from a wind turbine of rated power P_r is dependent upon the frequency distribution of the wind and on the cut-in and cut-out wind speeds which are in turn dependent upon the cumulative distribution of wind speeds. The wind speed duration curve also becomes a significant factor in evaluating the fatigue of a wind energy machine due to continuous operation in turbulence. The turbulence level is a function of mean wind speed and consequently varies throughout the lifetime of the rotor. The application of the mean wind speed distribution to the analysis of turbulence input for fatigue computation is described in Section 4.3.3.

Justus, et al. [2.4] have analyzed mean wind speeds at 138 geographical locations throughout the United States. They have presented these data in terms of a Weibull statistical distribution which shows good agreement with experimental results. The parameters of the Weibull distribution are height dependent and show a statistical distribution about their mean value. Thus, the wind speed distribution curves computed from the methodology of Justus, et al. [2.4] are adjustable for height effects and can be specified in terms of the probability of exceedance.

Cliff [2.3] has suggested that the higher wind speeds tend to have a Rayleigh frequency distribution. The Rayleigh distribution, as noted earlier, is a special case of the Weibull distribution. In the Rayleigh distribution, the shape parameter of the Weibull distribution is fixed at a value equal to 2.0. Thus, the distribution becomes a single parameter distribution depending only on the annual mean wind speed. Cliff suggests if a long-term frequency distribution of the wind speed for a particular site is known, the designer should use a Weibull distribution for estimating expected power output of a WTG. When frequency distribution of the wind speed is not known and the annual mean wind speed is greater than 4.5 m s^{-1} (10 mph), it is recommended that the Rayleigh distribution be used to estimate the wind speed frequency.

The results of Reference 2.4 have been incorporated into this section in a graphical and analytical format which provides for a rapid evaluation of a mean wind speed duration curve for given geographic locations throughout the

United States. It must be borne in mind, however, that wind speed duration curves are quite sensitive to location and the present data are valid essentially for relatively flat terrain and encompass a wide range of surface roughness conditions.

The mean wind speed data include the influence of atmospheric stability (Section 3.3) and terrain features peculiar to the site at which they are measured. These factors influence the wind speed distribution but are normally small enough under high wind conditions that the data presented herein are considered to be a good representation of the wind for design purposes. If a more rigorous design is required for a very specific site, wind data must be acquired over a period of several years.

2.4.1 Magnitude of the Mean Wind Speed

The annual mean wind speed based on the Weibull distributions is given by a Gamma function distribution [2.4]:

$$\hat{W} = c\Gamma(1 + 1/k) \quad , \tag{2.20}$$

where values of c and k, adjusted to the 10-m (30-ft) level for 138 geographical locations, are tabulated in Table 2.1. $\hat{W}$ represents the annual mean wind and $\Gamma(1 + 1/k)$ represents the Gamma function of the argument $1 + 1/k$. Equation (2.20) is plotted for easy reference in Figure 2.26.

> Example 2.7: As an example calculation of the annual mean wind speed at Seattle, Washington, one selects k and c from Table 2.1 as 1.67 and 3.81, respectively. From Figure 2.26 the value of $\hat{W}/c = 0.893$ is found corresponding to $k = 1.67$. Multiplying by c gives $\hat{W} = 3.40$ m s^{-1} (7.6 mph).

Table 2.2 provides seasonal values of k, c, and $\hat{W}$ adjusted to the 10-m (30-ft) level. These values are of interest to WTG design where the application may be seasonal.

TABLE 2.1 WEIBULL c AND k ANNUAL VALUES ADJUSTED TO 10-m (30-ft) REFERENCE ELEVATION, AND COMPUTED VALUES OF ANNUAL MEAN WIND SPEED, $\hat{W}$ [EQUATION (2.10)]

City	c ($m\ s^{-1}$)	c (mph)	k	$\hat{W}$ ($m\ s^{-1}$)	$\hat{W}$ (mph)
ALABAMA					
Birmingham	3.45	7.72	1.61	3.09	6.91
Mobile	4.07	9.10	1.72	3.63	8.12
ARIZONA					
Phoenix	3.04	6.80	1.36	2.78	6.22
Tucson	4.28	9.57	1.52	3.86	8.64
Yuma	4.04	9.04	1.52	3.64	8.14
ARKANSAS					
Ft. Smith	3.96	8.86	1.92	3.51	7.85
Little Rock	4.19	9.37	1.96	3.71	8.30
CALIFORNIA					
Bakersfield	1.45	3.24	1.16	1.38	3.09
Fresno	2.50	5.59	1.39	2.28	5.10
Los Angeles	4.41	9.87	2.00	3.91	8.75
Oakland	3.47	7.76	1.57	3.12	6.98
Sacramento	4.03	9.02	1.67	3.60	8.05
COLORADO					
Colorado Springs	4.77	10.67	1.45	4.33	9.69
Denver	3.80	8.50	1.54	3.42	7.65
Pueblo	4.21	9.42	1.25	3.92	8.77

Note: Where two values are given for a particular city, wind speeds have been measured at two locations within the city.

TABLE 2.1 (Continued)

City	c ($m\ s^{-1}$)	c (mph)	k	$\hat{W}$ ($m\ s^{-1}$)	$\hat{W}$ (mph)
CONNECTICUT					
Bridgeport	4.21	9.42	1.78	3.75	8.39
Hartford	3.69	8.25	1.81	3.28	7.34
FLORIDA					
Kennedy SC	3.93	8.79	2.03	3.48	7.78
Daytona	4.70	10.51	2.09	4.16	9.31
Jacksonville	4.88	10.92	2.15	4.32	9.66
Miami	3.78	8.46	1.70	3.37	7.54
Orlando	3.69	8.25	1.70	3.29	7.36
Tallahassee	3.42	7.65	1.74	3.05	6.82
Tampa	4.07	9.10	1.79	3.62	8.10
GEORGIA					
Atlanta	3.82	8.55	1.69	3.41	7.63
	4.01	8.97	1.94	3.56	7.96
Augusta	3.32	7.43	1.52	2.99	6.69
	3.35	7.49	1.57	3.01	6.73
Columbus	3.98	8.90	1.98	3.53	7.90
Macon	3.73	8.34	1.83	3.31	7.40
Savannah	3.24	7.25	1.56	2.91	6.51
	3.90	8.72	1.76	3.47	7.76
IDAHO					
Pocatello	4.76	10.65	1.38	4.35	9.73
ILLINOIS					
Chicago	5.59	12.51	2.05	4.95	11.07
	4.61	10.31	1.79	4.10	9.17
Rockford	5.52	12.35	2.25	4.89	10.94
Springfield	5.35	11.97	1.87	4.75	10.63
	5.85	13.09	2.07	5.18	11.59

TABLE 2.1 (Continued)

City	c ($m\ s^{-1}$)	c (mph)	k	$\hat{W}$ ($m\ s^{-1}$)	$\hat{W}$ (mph)
INDIANA					
Evansville	3.92	8.77	1.77	3.49	7.81
	4.47	10.00	1.95	3.96	8.86
Indianapolis	4.39	9.82	1.81	3.90	8.72
South Bend	4.72	10.56	2.09	4.18	9.35
IOWA					
Burlington	4.91	10.90	1.91	4.36	9.75
Des Moines	4.86	10.87	1.85	4.32	9.66
KANSAS					
Wichita	6.81	15.23	2.20	6.03	13.49
KENTUCKY					
Lexington	4.09	9.15	1.77	3.64	8.14
Louisville	3.57	7.99	1.72	3.18	7.11
	4.48	10.02	2.06	3.97	8.88
LOUISIANA					
New Orleans	3.93	8.79	1.66	3.51	7.85
	4.40	9.84	1.81	3.91	8.75
Shreveport	3.98	8.90	1.79	3.54	7.92
	3.94	8.81	1.77	3.51	7.85
MAINE					
Portland	3.98	8.90	1.65	3.56	7.96
MARYLAND					
Baltimore	3.29	7.36	1.50	2.97	6.64

TABLE 2.1 (Continued)

City	c ($m\ s^{-1}$)	c (mph)	k	$\hat{W}$ ($m\ s^{-1}$)	$\hat{W}$ (mph)
MASSACHUSETTS					
Boston	6.71	15.01	2.38	5.95	13.31
MICHIGAN					
Detroit	4.00	8.95	1.81	3.56	7.96
Flint	5.33	11.92	2.09	4.72	10.56
Grand Rapids	4.18	9.35	1.88	3.71	8.30
Lansing	5.57	12.46	2.04	4.93	11.03
Muskegon					
MINNESOTA					
Duluth	5.46	12.21	2.12	4.84	10.83
Minneapolis	5.42	12.12	2.17	4.80	10.74
MISSISSIPPI					
Jackson	4.06	9.08	1.79	3.61	8.08
MISSOURI					
Columbia	5.72	12.80	2.72	5.09	11.39
Springfield	5.45	12.19	2.06	4.83	10.80
	5.14	11.50	2.17	4.55	10.18
St. Louis	3.45	7.72	1.68	3.08	6.89
	4.79	10.72	1.86	4.25	9.51
MONTANA					
Billings	5.16	11.54	1.72	4.60	10.29
	5.48	12.26	1.99	4.80	10.74
Glasgow	5.86	13.11	1.85	5.20	11.63
Hayre	5.62	12.57	1.74	5.01	11.21
Helena	3.30	7.38	1.35	3.03	6.78
Kalispell	3.69	8.25	1.42	3.36	7.52
Miles City	4.35	9.73	1.56	3.91	8.75

TABLE 2.1 (Continued)

City	c ($m\ s^{-1}$)	c (mph)	k	$\hat{W}$ ($m\ s^{-1}$)	$\hat{W}$ (mph)
NEBRASKA					
Scottsbluff	5.37	12.01	1.86	4.77	10.67
NEVADA					
Ely	4.79	10.72	1.64	4.29	9.60
NEW JERSEY					
Atlantic City	5.48	12.26	1.81	4.87	10.89
Newark	5.50	12.30	2.05	4.87	10.89
NEW MEXICO					
Albuquerque	3.40	7.61	1.24	3.17	7.09
NEW YORK					
Albany	4.29	9.60	1.84	3.81	8.52
	4.08	0.13	1.72	3.64	8.14
Buffalo	5.73	12.82	1.85	5.09	11.39
New York City	6.05	13.53	2.06	5.36	11.99
	6.02	13.47	2.22	5.33	11.92
Syracuse	3.92	8.77	1.73	3.49	7.81
NORTH CAROLINA					
Asheville	2.08	4.65	1.09	0.97	2.17
	4.16	9.31	1.51	3.75	8.39
Cape Hatteras	5.69	12.73	2.19	5.04	11.27
Charlotte	3.38	7.56	1.61	3.03	6.78
Greensboro	3.23	7.23	1.52	2.91	6.51
	3.59	8.03	1.71	3.20	7.16
Raleigh	4.24	9.49	1.75	3.78	8.46

TABLE 2.1 (Continued)

City	c ($m\ s^{-1}$)	c (mph)	k	$\hat{W}$ ($m\ s^{-1}$)	$\hat{W}$ (mph)
NORTH DAKOTA					
Bismark	5.25	11.74	1.76	4.67	10.45
	5.64	12.62	1.81	5.01	11.21
Williston	5.28	11.81	1.84	4.69	10.49
OHIO					
Akron	4.84	10.83	1.94	4.29	9.60
Cincinnati	3.88	8.68	1.78	3.45	7.72
Cleveland	5.26	11.77	1.98	4.66	10.42
Dayton	4.25	9.51	1.67	3.80	8.50
	5.03	11.25	2.03	4.46	9.98
Toledo	4.92	11.01	1.83	4.37	9.78
Youngstown	4.20	9.40	1.83	3.73	8.34
	5.07	11.34	2.12	4.49	10.04
OKLAHOMA					
Tulsa	5.82	13.02	2.05	5.16	11.54
Oklahoma City	4.62	10.34	1.80	4.11	9.19
OREGON					
Eugene	3.80	8.50	1.61	3.41	7.63
Portland	3.95	8.84	1.55	3.55	7.94
Salem	3.95	8.84	1.53	3.56	7.96
PENNSYLVANIA					
Allentown	4.83	10.80	1.59	4.32	9.66
Harrisburg	3.23	7.23	1.42	2.94	6.58
	3.96	8.86	1.45	3.59	8.03
Philadelphia	5.12	11.45	1.46	4.64	10.38
Pittsburg	4.90	10.96	1.89	4.35	9.73
Scranton	3.15	7.05	1.83	2.80	6.26

TABLE 2.1 (Continued)

City	c ($m\ s^{-1}$)	c (mph)	k	$\hat{W}$ ($m\ s^{-1}$)	$\hat{W}$ (mph)
RHODE ISLAND					
Providence	5.28	11.81	1.80	4.55	10.18
SOUTH CAROLINA					
Charleston	4.27	9.55	1.85	3.79	8.48
Columbia	3.33	7.45	1.50	3.01	6.73
	3.56	7.90	1.68	3.16	7.07
Greenville	3.96	8.86	1.89	3.51	7.85
SOUTH DAKOTA					
Huron	5.53	12.37	1.91	4.91	10.98
Rapid City	5.21	11.66	2.14	4.61	10.31
	5.58	12.48	1.41	5.08	11.36
Sioux Falls	2.59	5.79	2.26	2.29	5.12
TENNESSEE					
Bristol	3.17	7.09	1.55	2.85	6.38
Chattanooga	2.90	6.49	1.52	2.61	5.84
	3.59	8.03	1.76	3.20	7.16
Knoxville	3.15	7.05	1.48	2.85	6.38
Memphis	4.59	10.27	1.94	4.07	9.10
Nashville	4.26	9.53	1.79	4.08	9.13
TEXAS					
Abilene	6.07	13.58	2.30	5.38	12.04
Amarillo	6.19	13.85	2.12	5.38	12.04
Austin	4.81	10.76	2.04	4.26	9.53
	4.92	11.01	1.92	4.36	9.75
Brownsville	5.52	12.35	2.03	4.89	10.94
Dallas	5.64	12.62	2.31	5.00	11.19
El Paso	4.16	9.31	1.47	3.77	8.43

TABLE 2.1 (Continued)

City	c ($m\ s^{-1}$)	c (mph)	k	$\hat{W}$ ($m\ s^{-1}$)	$\hat{W}$ (mph)
TEXAS (Cont'd)					
Fort Worth	4.86	10.87	2.10	4.30	9.62
	4.91	10.98	1.80	4.10	9.17
Galveston	5.06	11.32	2.28	4.48	10.02
Houston	4.66	10.42	1.91	4.13	9.24
	5.44	12.17	2.11	4.82	10.78
Lubbock	5.58	12.48	2.01	4.94	11.05
Port Arthur	5.43	12.15	2.25	4.81	10.76
Waco	4.92	11.01	2.11	4.36	9.75
Wichita Falls	5.07	11.34	2.15	4.49	10.04
UTAH					
Salt Lake City	3.67	8.21	1.31	3.38	7.56
VERMONT					
Burlington	4.69	10.49	2.00	4.16	9.31
VIRGINIA					
Lynchburg	3.82	8.55	1.78	3.40	7.61
Richmond	2.71	6.06	1.49	3.45	7.72
Roanoke	3.84	8.59	1.47	3.48	7.78
Wallops	5.01	11.21	1.82	4.45	9.95
WASHINGTON					
Seattle	3.81	8.52	1.67	3.40	7.61
Spokane	4.63	10.36	1.64	4.14	9.26
Hanford	3.02	6.76	1.19	2.85	6.38
WEST VIRGINIA					
Charleston	3.00	6.71	1.54	2.70	6.04
Huntington	3.10	6.93	1.47	2.81	6.29

TABLE 2.1 (Concluded)

City	c ($m\ s^{-1}$)	c (mph)	k	$\hat{W}$ ($m\ s^{-1}$)	$\hat{W}$ (mph)
WISCONSIN					
Green Bay	5.04	11.27	1.91	4.47	10.00
	5.34	11.95	2.06	4.73	10.58
LaCrosse	4.57	10.22	1.93	4.05	9.06
Madison	5.11	11.43	2.06	4.53	10.13
Milwaukee	6.40	14.32	2.19	5.67	12.68
	5.43	12.15	2.30	4.81	10.76
WYOMING					
Casper	6.56	14.68	1.77	5.84	13.06
Cheyenne	5.86	13.11	1.52	5.28	11.81
	6.04	13.51	1.71	5.39	12.06

2.4.2 Mean Wind Speed Frequency

The frequency of a wind speed having a value between W and W + dW is given by

$$p(W)dW = (k/c)(W/c)^{k-1} \exp[-(W/c)^{k}]\ dW \quad . \qquad (2\text{-}21)$$

Figure 2.27 shows a plot of the frequency distribution of W/c for a range of k values. The wind speed W is a mean value, but the data from which the statistics have been developed are for a wide range of averaging times.

Justus, et al. [2.4] effectively used 1-min averages while Doran, et al. [2.14] utilized a 2-min averaging period. Since the averaging period for W can be less than 10 min, it is not identified with an overbar.

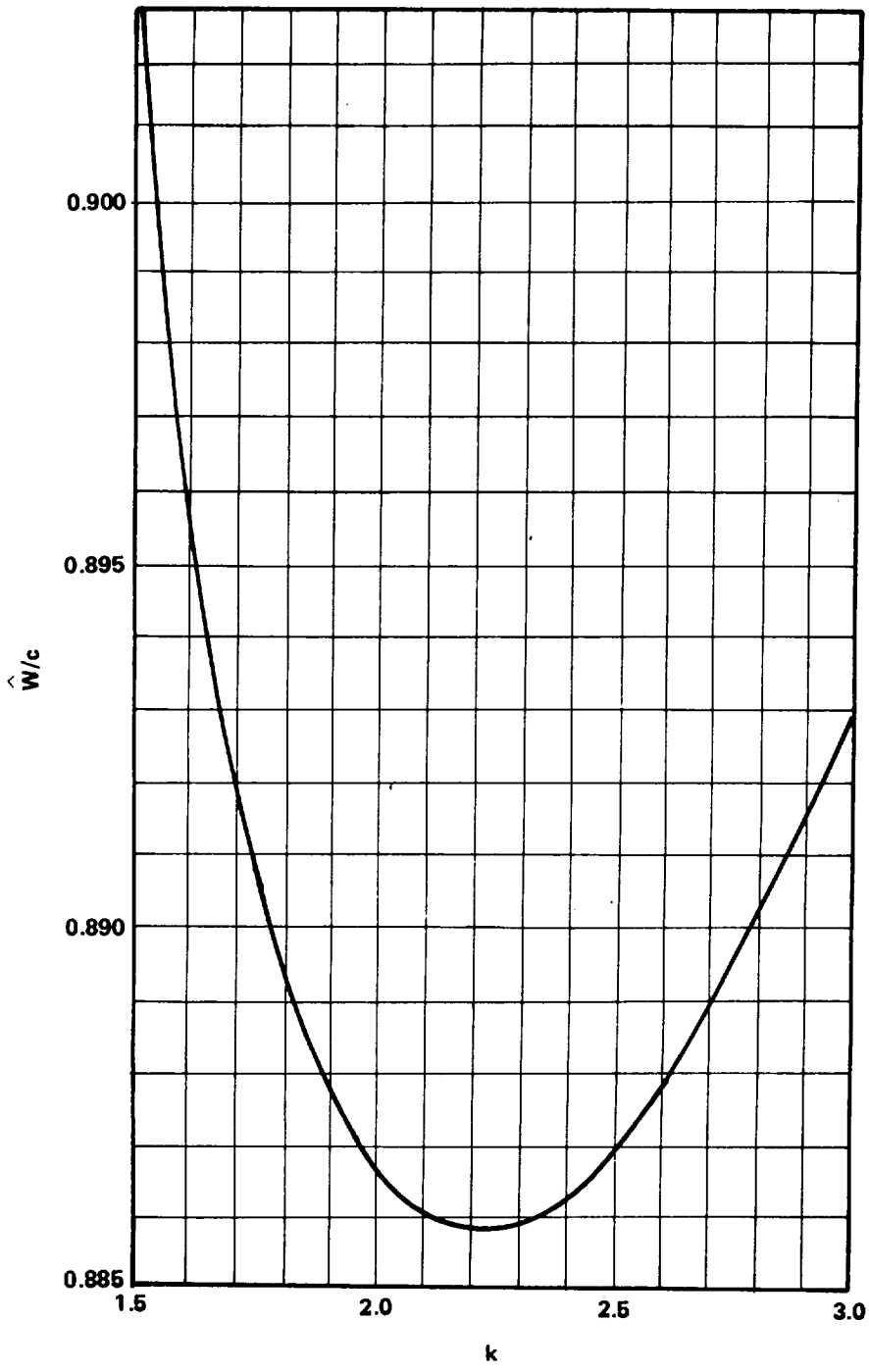

Figure 2.26 Annual mean wind speed as determined from the Weibull statistical distribution.

TABLE 2.2 WEIBULL c AND k VALUES ADJUSTED TO 10-m (30-ft) HEIGHT [2.4]

City	Winter		Spring		Summer		Fall	
	c ($m\ s^{-1}$)	k	c ($m\ s^{-1}$)	k	c ($m\ s^{-1}$)	k	c ($m\ s^{-1}$)	k
ALABAMA								
Birmingham	4.03	1.80	3.90	1.72	2.46	1.43	3.28	1.63
Mobile	4.83	1.86	4.59	1.96	2.91	1.47	3.86	1.72
	5.03	2.22	4.93	2.02	2.72	1.36	3.93	1.83
ARIZONA								
Phoenix	2.33	1.15	3.40	1.48	3.24	1.39	3.08	1.42
Tucson	3.88	1.37	4.62	1.60	4.36	1.64	4.21	1.48
Yuma	3.67	1.54	4.35	1.88	4.48	1.87	3.57	1.53
ARKANSAS								
Ft. Smith	4.36	1.99	4.47	2.16	-	-	-	-
Little Rock	4.64	2.10	4.75	2.16	-	-	-	-
CALIFORNIA								
Bakersfield	2.24	1.16	3.32	1.48	-	-	2.38	1.18
Fresno	2.13	1.24	3.24	1.68	2.84	1.68	2.13	1.43
Los Angeles	3.51	1.59	4.78	2.00	-	-	4.21	1.98
Oakland	2.45	1.08	4.12	1.84	4.11	2.09	2.82	1.40
Sacramento	3.65	1.41	4.54	1.87	4.30	2.01	3.61	1.51

TABLE 2.2 (Continued)

City	Winter		Spring		Summer		Fall	
	c ($m\ s^{-1}$)	k	c ($m\ s^{-1}$)	k	c ($m\ s^{-1}$)	k	c ($m\ s^{-1}$)	k
COLORADO								
Colorado Springs	4.37	1.31	5.62	1.56	4.56	1.57	4.55	1.44
Denver	3.95	1.59	4.22	1.51	3.65	1.63	3.46	1.55
Pueblo	3.43	1.07	5.01	1.35	4.70	1.48	3.55	1.15
CONNECTICUT								
Bridgeport	5.59	1.87	5.04	1.89	3.91	2.03	4.68	1.77
Hartford	4.05	1.77	4.17	1.90	3.17	1.83	3.43	1.81
FLORIDA								
Kennedy SC	4.25	2.11	4.35	2.46	2.95	1.90	4.16	2.04
Daytona	4.66	2.04	5.23	2.34	-	-	4.77	2.21
Jacksonville	3.50	1.61	3.87	1.92	3.35	1.89	3.64	1.78
Miami	5.05	2.17	5.43	2.41	4.05	1.92	4.75	2.16
Orlando	4.12	1.75	4.13	1.86	3.50	1.69	3.71	1.70
Tallahassee	3.05	1.83	3.36	2.22	3.16	1.70	3.49	1.68
	3.89	1.93	-	-	2.36	1.27	-	-
Tampa	4.26	1.81	4.84	2.34	2.88	1.29	3.94	1.76

TABLE 2.2 (Continued)

City	Winter		Spring		Summer		Fall	
	c ($m\ s^{-1}$)	k	c ($m\ s^{-1}$)	k	c ($m\ s^{-1}$)	k	c ($m\ s^{-1}$)	k
GEORGIA								
Atlanta	4.58	1.91	4.22	1.81	2.79	1.55	3.62	1.31
	4.74	2.23	4.32	2.02	-	-	-	-
Augusta	3.80	1.66	3.71	1.55	3.23	1.82	2.90	1.42
	4.04	1.88	3.45	1.63	-	-	2.71	1.44
Columbus	4.32	2.11	4.32	2.06	-	-	-	-
Macon	4.08	1.91	4.18	1.92	-	-	-	-
Savannah	3.70	1.71	3.61	1.74	2.72	1.57	3.28	1.77
	4.15	1.74	4.57	1.97	-	-	-	-
IDAHO								
Pocatello	5.43	1.41	5.27	1.42	4.35	1.46	4.13	1.32
ILLINOIS								
Chicago	6.07	2.14	6.26	2.23	4.72	2.05	5.36	2.05
	5.21	1.94	5.43	1.99	-	-	4.43	2.00
Rockford	5.89	2.39	6.09	2.41	4.84	2.30	5.36	2.22
Springfield	6.16	2.21	6.12	2.04	3.95	1.77	5.15	1.85
	6.59	2.19	6.73	2.40	4.57	2.01	5.53	2.16

TABLE 2.2 (Continued)

City	Winter		Spring		Summer		Fall	
	c ($m\ s^{-1}$)	k	c ($m\ s^{-1}$)	k	c ($m\ s^{-1}$)	k	c ($m\ s^{-1}$)	k
INDIANA								
Evansville	4.51	2.04	4.50	1.86	2.79	1.51	3.68	1.74
	5.08	2.13	5.03	2.18	-	-	4.30	1.94
Indianapolis	5.06	1.92	5.05	2.07	-	-	3.98	1.76
South Bend	5.17	2.50	5.23	2.16	3.87	2.01	4.59	1.99
IOWA								
Burlington	5.59	2.14	5.59	2.14	3.50	1.60	4.76	1.99
Des Moines	5.11	1.94	5.63	2.03	4.04	1.92	4.72	1.76
KANSAS								
Wichita	6.75	2.10	7.44	2.21	6.46	2.30	6.66	2.31
KENTUCKY								
Lexington	4.86	2.08	4.59	1.91	3.29	1.83	3.70	1.64
Louisville	4.13	1.99	4.08	1.85	2.77	1.65	3.37	1.74
	5.01	2.21	4.97	2.21	-	-	-	-

TABLE 2.2 (Continued)

City	Winter		Spring		Summer		Fall	
	c ($m\ s^{-1}$)	k	c ($m\ s^{-1}$)	k	c ($m\ s^{-1}$)	k	c ($m\ s^{-1}$)	k
LOUISIANA								
New Orleans	4.53	1.76	4.34	1.79	3.13	1.91	3.99	1.77
	5.03	2.14	5.05	2.06	3.01	1.46	4.09	1.81
Shreveport	4.56	1.97	4.47	1.97	3.24	1.71	3.65	1.76
	4.38	1.85	4.54	2.07	2.89	1.48	3.62	1.70
MAINE								
Portland	4.26	1.63	4.55	1.83	3.46	1.75	3.74	1.58
MARYLAND								
Baltimore	3.54	1.44	3.90	1.82	2.76	1.61	3.04	1.53
MASSACHUSETTS								
Boston	7.41	2.39	7.26	2.49	6.02	2.81	6.25	2.42
MICHIGAN								
Detroit	4.52	2.02	4.18	1.91	3.09	1.64	3.90	1.78
Flint	5.95	2.27	5.72	2.19	4.39	2.00	5.27	2.15
Grand Rapids	4.53	2.06	4.73	1.99	3.40	1.81	4.03	1.79
Lansing	6.47	2.44	6.28	2.18	4.05	1.85	5.44	2.19
Muskegon	6.58	2.30	6.15	2.31	5.00	2.27	5.76	2.22

TABLE 2.2 (Continued)

City	Winter		Spring		Summer		Fall	
	c ($m\ s^{-1}$)	k	c ($m\ s^{-1}$)	k	c ($m\ s^{-1}$)	k	c ($m\ s^{-1}$)	k
MINNESOTA								
Duluth	5.82	2.26	5.92	2.23	4.90	1.99	5.18	2.09
Minneapolis	5.43	2.19	5.98	2.31	4.94	2.10	5.33	2.18
MISSISSIPPI								
Jackson	4.80	1.99	4.63	2.12	2.61	1.39	3.65	1.67
MISSOURI								
Columbia	3.23	1.71	3.40	1.72	-	-	-	-
Springfield	5.97	2.24	6.12	2.16	4.61	2.10	5.19	2.08
	5.71	2.43	5.74	2.34	-	-	4.88	2.16
St. Louis	3.90	1.92	4.14	1.84	2.70	1.74	3.24	1.77
	5.50	2.00	5.41	2.03	3.73	1.77	4.53	1.96
MONTANA								
Billings	5.89	2.12	5.31	1.63	4.37	1.51	4.95	1.70
	6.35	2.19	5.43	2.01	4.24	1.73	5.78	2.19
Glasgow	5.71	1.81	6.42	1.90	5.65	1.86	5.70	1.86
Hayre	5.50	1.63	6.08	1.84	5.29	1.81	5.65	1.75

TABLE 2.2 (Continued)

City	Winter		Spring		Summer		Fall	
	c ($m\ s^{-1}$)	k	c ($m\ s^{-1}$)	k	c ($m\ s^{-1}$)	k	c ($m\ s^{-1}$)	k
MONTANA (Cont' d)								
Helena	2.99	1.09	3.86	1.50	3.28	1.33	3.15	1.46
Kalispell	3.63	1.20	4.39	1.74	3.69	1.64	3.28	1.42
Miles City	4.26	1.62	5.00	1.71	3.92	1.51	4.24	1.44
NEBRASKA								
Scottsbluff	5.98	1.77	6.21	1.87	4.46	1.73	4.92	1.59
NEVADA								
Ely	5.12	1.65	4.97	1.59	4.49	1.76	4.75	1.72
NEW JERSEY								
Atlantic City	6.23	1.78	6.30	2.09	4.68	1.98	4.89	1.85
Newark	6.18	2.23	5.99	2.16	4.71	2.22	5.53	2.12
NEW MEXICO								
Albuquerque	2.78	1.06	4.31	1.43	3.41	1.34	2.97	1.15

TABLE 2.2 (Continued)

City	Winter		Spring		Summer		Fall	
	c ($m\ s^{-1}$)	k	c ($m\ s^{-1}$)	k	c ($m\ s^{-1}$)	k	c ($m\ s^{-1}$)	k
NEW YORK								
Albany	4.72	1.86	4.76	1.97	3.78	1.94	4.05	1.89
	6.36	2.05	4.52	1.78	-	-	-	-
Buffalo	6.75	2.00	6.03	1.94	4.99	1.83	5.27	1.87
New York City	6.87	2.17	6.49	2.23	5.31	2.31	5.70	1.97
	6.97	2.49	6.32	2.47	5.11	2.43	5.66	2.27
Syracuse	4.25	1.28	4.21	1.76	3.39	1.69	3.87	1.75
NORTH CAROLINA								
Asheville	2.98	1.43	3.21	1.68	1.77	1.34	2.20	1.25
	5.40	1.77	4.60	1.64	2.80	1.47	3.88	1.54
Cape Hatteras	6.36	2.22	5.85	2.32	5.01	2.37	5.63	2.20
Charlotte	3.71	1.64	4.04	1.81	-	-	-	-
Greensboro	3.52	1.57	3.78	1.72	2.54	1.39	3.11	1.54
	4.15	1.82	4.16	1.95	-	-	-	-
Raleigh	4.88	1.93	4.84	1.86	-	-	-	-
NORTH DAKOTA								
Bismark	4.72	1.64	5.91	1.90	5.12	1.93	5.25	1.63
	5.53	1.71	6.19	1.90	5.35	1.99	5.52	1.74
Williston	5.15	1.79	5.73	1.92	4.94	1.84	5.31	1.85

TABLE 2.2 (Continued)

City	Winter		Spring		Summer		Fall	
	c ($m\ s^{-1}$)	k	c ($m\ s^{-1}$)	k	c ($m\ s^{-1}$)	k	c ($m\ s^{-1}$)	k
OHIO								
Akron	5.73	2.32	5.29	2.05	3.64	1.77	4.61	1.92
Cincinnati	4.44	1.99	4.40	1.90	2.94	1.67	3.80	1.88
Cleveland	6.41	2.33	5.54	2.10	-	-	4.94	1.98
Dayton	5.19	2.06	4.77	1.79	3.11	1.58	3.89	1.59
	5.72	2.23	5.42	2.14	4.00	1.89	4.88	2.11
Toledo	5.68	2.13	5.77	2.02	3.70	1.64	4.61	1.82
Youngstown	5.06	2.25	4.46	1.84	3.15	1.67	4.05	1.82
	6.10	2.55	5.48	2.22	3.64	1.82	4.78	2.19
OKLAHOMA								
Tulsa	5.43	1.95	6.25	2.18	4.96	2.07	5.11	1.96
OREGON								
Eugene	4.15	1.64	3.78	1.58	-	-	3.59	1.54
Portland	5.21	1.86	3.60	1.50	-	-	3.85	1.51
Salem	4.79	1.60	3.89	1.59	-	-	4.12	1.71

TABLE 2.2 (Continued)

City	Winter		Spring		Summer		Fall	
	c ($m\ s^{-1}$)	k	c ($m\ s^{-1}$)	k	c ($m\ s^{-1}$)	k	c ($m\ s^{-1}$)	k
PENNSYLVANIA								
Allentown	5.76	1.65	5.53	1.84	3.84	1.65	3.94	1.58
Harrisburg	3.82	1.49	3.98	1.72	2.31	1.33	2.87	1.41
	4.95	1.56	4.52	1.66	3.01	1.57	3.58	1.44
Philadelphia	5.83	2.06	6.90	2.24	3.97	1.85	4.74	1.96
Pittsburgh	5.72	2.15	5.24	1.93	-	-	4.71	1.89
Scranton	3.64	1.97	3.50	1.90	2.77	1.86	3.10	1.86
RHODE ISLAND								
Providence	6.06	1.86	6.08	2.14	4.67	2.24	4.65	1.84
SOUTH CAROLINA								
Charleston	4.48	1.82	4.82	2.00	-	-	3.88	1.85
Columbia	3.72	1.68	3.99	1.69	3.01	1.62	3.09	1.60
	4.08	1.86	4.29	1.84	-	-	3.08	1.51
Greenville	-	-	3.96	1.89	-	-	-	-
SOUTH DAKOTA								
Huron	5.29	1.87	6.17	2.04	5.11	1.99	5.56	1.87
Rapid City	4.82	1.29	5.85	1.70	5.06	1.79	5.40	1.47
	5.31	1.27	6.54	1.53	5.02	1.69	5.61	1.38
Sioux Falls	6.31	2.08	7.16	2.50	5.88	2.41	6.19	2.50

TABLE 2.2 (Continued)

City	Winter		Spring		Summer		Fall	
	c ($m\ s^{-1}$)	k	c ($m\ s^{-1}$)	k	c ($m\ s^{-1}$)	k	c ($m\ s^{-1}$)	k
TENNESSEE								
Bristol	3.72	1.69	3.91	1.84	-	-	-	-
Chattanooga	3.40	1.72	3.42	1.67	1.97	1.27	2.87	1.74
	3.88	1.83	4.17	1.96	2.16	1.23	-	-
Knoxville	3.48	1.55	3.81	1.61	-	-	-	-
Memphis	5.19	2.00	5.29	2.35	3.51	1.73	4.33	2.00
Nashville	4.85	1.93	4.98	2.06	-	-	3.87	1.72
TEXAS								
Abilene	6.10	2.18	6.69	2.53	5.66	2.47	5.86	2.23
Amarillo	6.11	1.96	6.95	2.24	5.84	2.34	5.87	2.14
Austin	5.05	2.06	5.43	2.27	4.59	2.27	4.19	1.74
	5.28	1.92	5.56	2.16	-	-	4.46	1.77
Brownsville	5.42	2.02	6.37	2.29	5.41	2.47	4.70	1.99
Dallas	5.78	2.24	6.43	2.69	5.03	2.36	5.26	2.17
El Paso	4.00	1.30	5.09	1.56	3.99	1.66	3.69	1.50
Fort Worth	5.00	2.08	5.44	2.15	4.52	2.24	4.50	1.96
	5.28	1.84	5.69	2.00	4.17	1.79	9.81	1.83
Galveston	4.46	1.82	4.39	2.16	3.77	2.18	3.75	1.62

TABLE 2.2 (Continued)

City	Winter		Spring		Summer		Fall	
	c ($m\ s^{-1}$)	k	c ($m\ s^{-1}$)	k	c ($m\ s^{-1}$)	k	c ($m\ s^{-1}$)	k
TEXAS (Cont'd)								
Houston	4.91	2.04	5.27	2.02	3.61	1.79	4.10	1.94
	6.00	2.27	6.30	2.44	4.62	2.05	4.75	1.89
Lubbock	5.68	1.90	6.45	2.19	5.14	2.20	5.11	2.02
Port Arthur	5.80	2.32	6.27	2.69	4.76	2.33	4.81	2.00
Waco	5.06	2.07	5.43	2.23	4.80	2.39	4.38	1.90
Wichita Falls	5.01	2.13	5.74	2.29	4.79	2.30	4.72	2.01
UTAH								
Salt Lake City	3.26	1.13	4.11	1.39	3.77	1.51	3.56	1.30
VERMONT								
Burlington	4.97	2.11	4.91	2.03	-	-	4.68	1.96
VIRGINIA								
Lynchburg	4.14	1.82	4.60	2.05	-	-	-	-
Richmond	3.10	1.73	3.37	1.86	2.14	1.37	2.51	1.47
Roanoke	4.68	1.56	4.56	1.75	-	-	3.43	1.46
Wallops	5.37	1.73	5.57	1.96	4.17	1.80	4.89	1.94

TABLE 2.2 (Concluded)

City	Winter		Spring		Summer		Fall	
	c ($m\ s^{-1}$)	k	c ($m\ s^{-1}$)	k	c ($m\ s^{-1}$)	k	c ($m\ s^{-1}$)	k
WASHINGTON								
Seattle	4.97	1.86	4.16	1.71	-	-	4.06	1.69
Spokane	4.89	1.50	4.95	1.83	4.41	1.88	4.50	1.62
Hanford	2.54	1.07	3.49	1.30	3.40	1.29	2.65	1.14
WEST VIRGINIA								
Charleston	3.94	2.19	3.40	1.64	2.14	1.31	2.94	1.69
Huntington	3.76	1.60	3.57	1.60	-	-	-	-
WISCONSIN								
Green Bay	5.44	2.14	5.37	2.02	4.11	1.77	5.21	1.86
	5.88	2.19	5.75	2.26	4.43	1.84	5.21	2.06
LaCrosse	4.67	1.92	4.94	2.02	4.15	1.95	4.57	1.97
Madison	5.53	2.15	5.58	2.14	4.44	2.11	5.09	2.15
Milwaukee	6.52	2.42	6.13	2.15	5.08	2.13	5.78	2.32
	5.88	2.35	5.76	2.46	4.72	2.20	5.37	2.35
WYOMING								
Casper	8.26	2.03	6.70	1.97	4.79	1.61	6.53	1.88
Cheyenne	7.40	1.60	6.49	1.61	4.66	1.71	5.36	1.61
	7.27	1.76	6.47	1.84	4.75	1.85	5.93	1.81

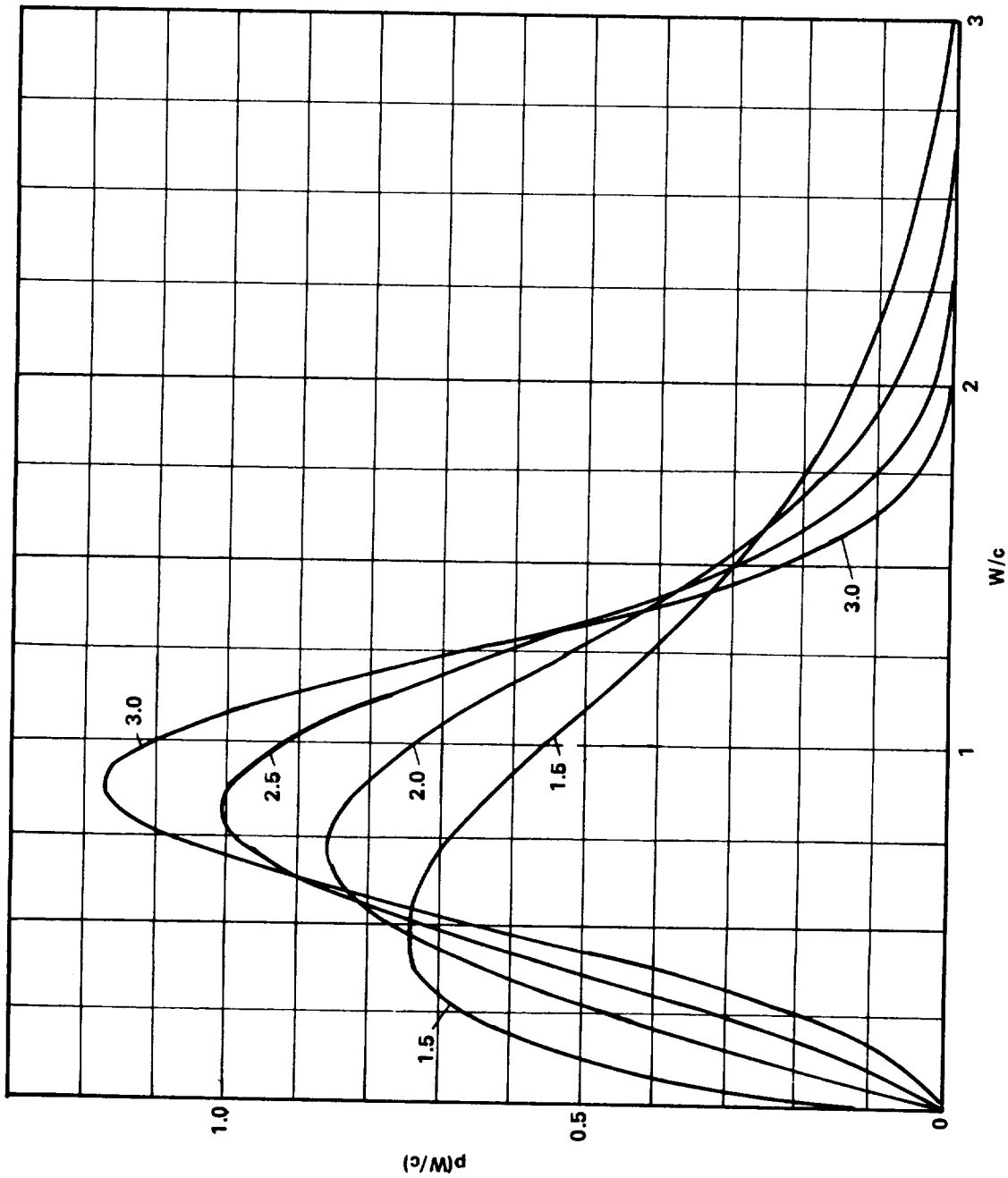

Figure 2.27 Standard Weibull probability distribution (wind speed frequency) curves for standard Weibull k values.

The wind speed frequency distribution curve is useful for computing performance factors for WTG. One measure of performance is the capacity factor, C_f, which is the ratio of actual average power output to the rated power of the wind turbine, $\bar{P}/P_r$. This ratio is given by

$$C_f = \int P(W)/P_r p(W)\, dW \tag{2.22}$$

where P(W) is the frequency distribution of the wind speed at the geographic location of interest adjusted to the wind turbine hub height.

Example 2.8: To illustrate this with an example, consider a WTG of 10-m (30-ft) hub height designed for an output power as a function of wind speed given by

$$p(W) = \begin{cases} 0; & W \le W_i \\ P_r(A + BW + CW^2); & W_i < W \le W_r \\ P_r; & W_r < W \le W_o \\ 0; & W > W_o \end{cases} \tag{2.23}$$

where

W_i = cut-in wind speed

W_o = cut-out wind speed

W_r = rated wind speed

P_r = rated power of the wind turbine.

The coefficients A, B, and C are given by

$$B = [(W_m^2 - W_i^2) - (W_m/W_r)^3 (W_r^2 - W_i^2)]/D \tag{2.24a}$$

$$C = [(W_m/W_r)^3 (W_r - W_i) - (W_m - W_i)]/D \qquad (2.24b)$$

$$A = -BW_i - CW_i^2 \qquad (2.24c)$$

and

$$D = (W_r - W_m)(W_m^2 - W_i^2) - (W_m - W_i)(W_r^2 - W_i^2) \qquad (2.24d)$$

and

$$W_m = (W_i + W_r)/2 \quad . \qquad (2.24e)$$

Consider the WTG to be located near Providence, Rhode Island, for which c and k at the 10-m (30-ft) level from Table 2.1 are 5.28 and 1.80, respectively.

Substituting equation (2.23) into equation (2.22) results in

$$C_f = \int_{W_i}^{W_r} (A + BW + CW^2)p(W)\, dW + \int_{W_r}^{W_o} p(W)\, dW \quad . \qquad (2.25)$$

Nondimensionalizing the wind speed with c and introducing p(W) dW from equation (2.21) gives

$$C_f = Ap_{ir} + Bc \int_{x_i}^{x_r} x^{1/k} e^{-x}\, dx + Cc^2 \int_{x_i}^{x_r} x^{2/k} e^{-x}\, dx + p_{ro} \qquad (2.26)$$

where $x = (W/c)^k$.

The terms p_{ir} and p_{ro} are the cumulative probabilities

$$p_{ir} = p(W \leq W_r) - p(W \leq W_i) = e^{-x_i} - e^{-x_r} \tag{2.27}$$

and

$$p_{ro} = p(W \leq W_o) - p(W \leq W_r) = e^{-x_r} - e^{-x_o} \quad . \tag{2.28}$$

Numerical integration of the integrals and evaluation of the cumulative probabilities for $W_i = 1.8$ m s^{-1} (4 mph), $W_r = 4.5$ m s^{-1} (10 mph), and $W_o = 26.8$ m s^{-1} (60 mph) give $C_f = 30$ percent.

Justus, et al. [2.4] discuss several other features of the application of the Weibull wind speed distributions to wind turbine performance.

2.4.3 Mean Wind Speed Duration Curve

The wind speed distribution curve is given by

$$p(W \geq W_P) = \exp[-(W_P/c)^k] \tag{2.29}$$

where $p(W \geq W_P)$ is the probability that the wind speed W will be greater than or equal to a prescribed value W_P. Equation (2.29) is converted to a wind speed duration curve in hours per year $H(W \geq W_P)$ by multiplying it by 8760 hours per year. Thus,

$$H(W \geq W_P) = 8760 \exp[-(W_P/c)^k] \quad . \tag{2.30}$$

Plots of $H(W \geq W_P)$ for various k values are given in Figure 2.28.

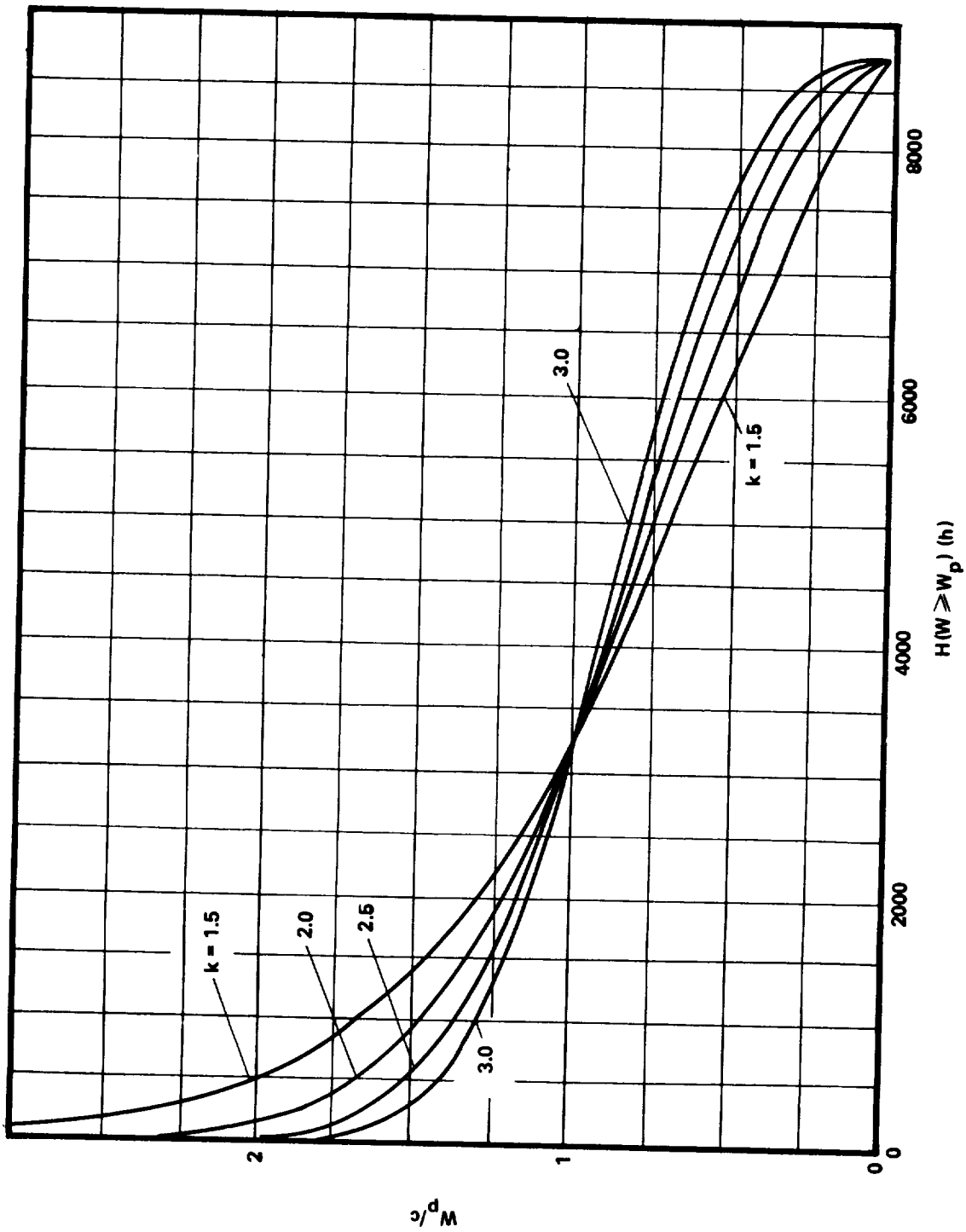

Figure 2.28 Cumulative probability (wind speed duration) curves for various Weibull k values.

Example 2.9: An example application of the wind speed duration curve is to estimate the number of hours per year of downtime because of low wind speed for a WTG of 10-m hub height located near Chicago if the cut-in wind speed is 1.8 m s^{-1} (4 mph). Values of k = 2.05 and c = 5.59 m s^{-1} (12.5 mph) at the 10-m (30-ft) level are found in Table 2.1. From equation (2.30) or Figure 2.28, the number of hours for which the wind exceeds 1.8 m s^{-1} (4 mph) is 7942 h. Thus, the number of hours of downtime is (8760 - 7942) = 818 h.

2.4.4 Adjustment of Mean Wind Speed for Height

Adjustment of the mean wind speed for height is achieved by adjusting the k and c values through a power law relationship:

$$c = c_{ref}(h/h_{ref})^{n} \tag{2.31}$$

$$k = k_{ref}[1 - 0.088\,\ell n(h_{ref}/10)]/[1 - 0.088\,\ell n(h/10)] \quad , \tag{2.32}$$

where h and h_{ref} are in meters and n is given by

$$n = [0.37 - 0.088\,\ell n(c_{ref})]/[1 - 0.088\,\ell n(h_{ref}/10)] \quad . \tag{2.33}$$

The reference values of c and k can be taken from Table 2.1 at a reference height of 10 m. These equations are valid for height corrections over a fairly wide range of surface roughnesses provided the terrain is relatively flat, and are plotted in Figure 2.29 for convenient use. It is shown in Reference 2.4 that the adjusted wind speed distribution $p(W \leq W_{adj})$ can be transformed such that

$$p(W \leq W_{adj}) = p(W \leq W_{ref})$$

or

$$p(W \leq W_{adj}) = 1 - \exp[-(W_{ref}/c_{ref})^{k_{ref}}] \quad . \tag{2.34}$$

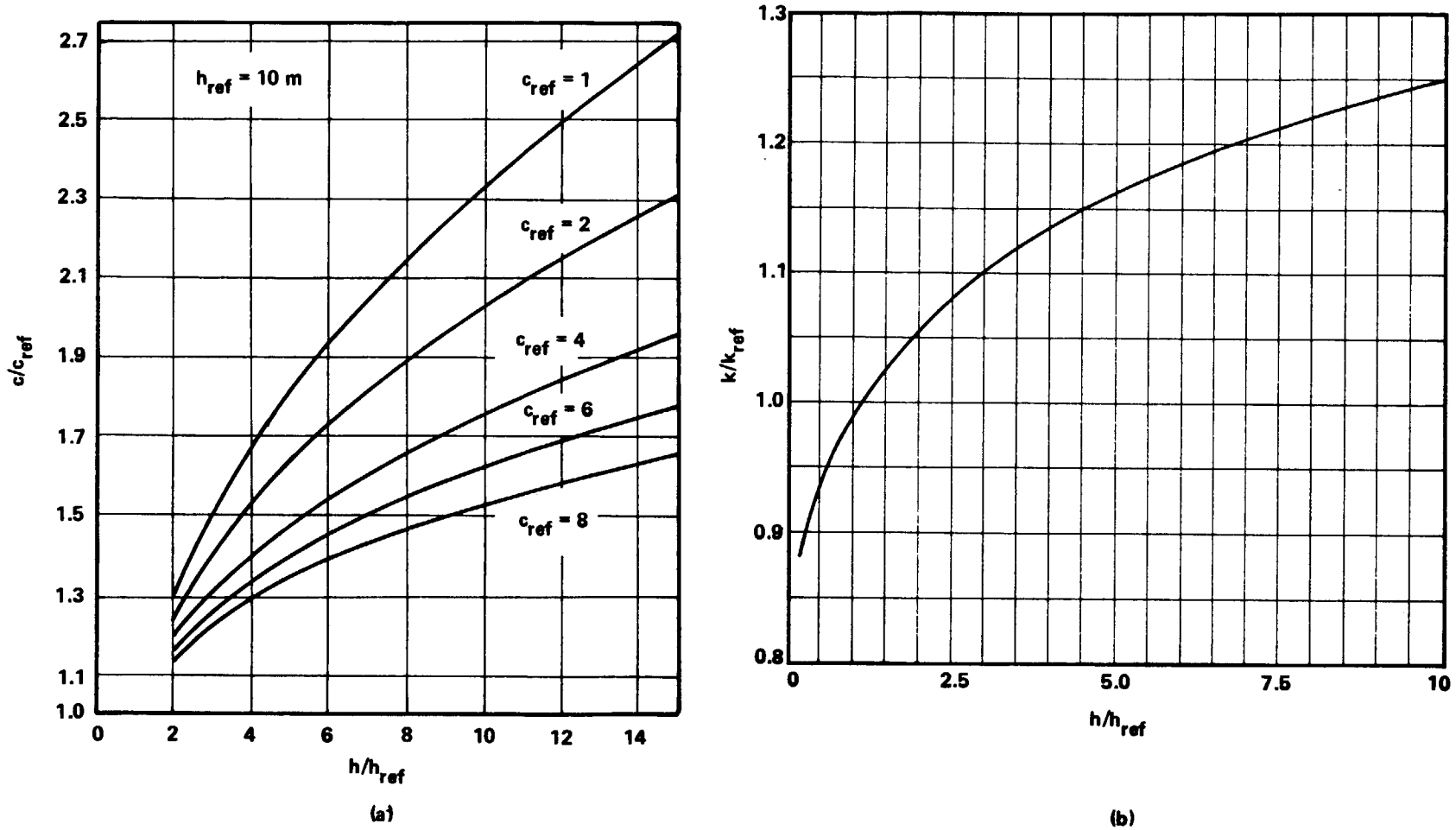

Figure 2.29 Variation of the Weibull distribution c and k parameters with height h.

Example 2.10: The correction of the wind speed duration curve to a height of $h_1 = 90$ m (295 ft) for the Phoenix area is straightforward.

From Table 2.1, c and k are found to be 3.04 m s^{-1} (6.8 mph) and 1.36, respectively. Thus, from equation (2.29) the duration curve is

$$p(W \geq W_P) = \exp[-(W_P/3.04)^{1.36}] \quad . \tag{2.35}$$

The mean annual wind speed at the two different levels, however, is different. That is,

$$\hat{W}(h_1) = c_1\Gamma(1 + 1/k_1) \quad , \tag{2.36}$$

where $c_1 = 5.53$ m s^{-1} (12.4 mph) and $k_1 = 1.69$ are evaluated from equations (2.31) and (2.32) or from Figure 2.29 based on $c_{ref} = 3.04$ and $k_{ref} = 1.36$, respectively. Thus, the mean annual wind speed is, from Figure 2.26, $\hat{W}/c_1 = 0.892$ and $\hat{W} = 4.93$ m s^{-1} (11.0 mph).

2.4.5 Probability of Exceeding Design Mean Wind Speed

Figure 2.30 is a plot of the variation of k with annual mean wind speeds for various percentile levels. Low values of k correspond to high variance; hence, one observes from Figure 2.30 that at $\hat{W} = 4$ m s^{-1} there is a 10-percent chance that k will be less than 1.47 and a 90-percent chance that it will be less than 2.10. This information can be utilized to establish the degree of risk associated with a selected design value of the annual mean wind speed and corresponding duration curve. To compute the risk associated with these values, proceed as follows:

1) Determine the average annual mean wind speed for which the wind turbine is to be designed.

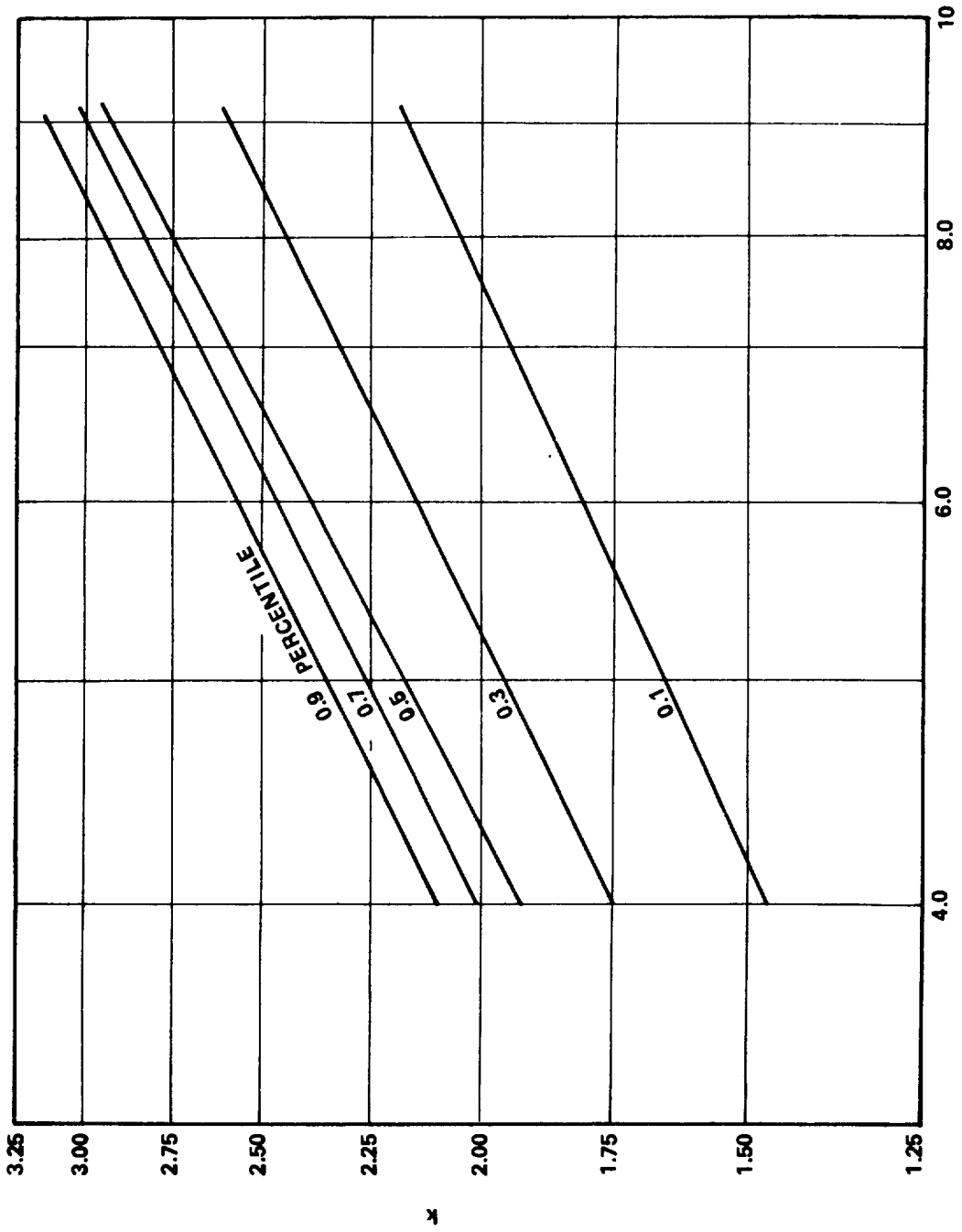

Figure 2.30 Variation of Weibull k value with annual mean wind speed for various percentile levels.

2) From Figure 2.30 determine k at the annual mean wind speed determined in Step 1) and for the percentile value of interest.

3) Determine the value of c corresponding to k in Step 2) from

$$c = 1.12\,\hat{W} \quad . \tag{2.37}$$

4) Correct the values of c and k for the height of interest as described in Section 2.4.4.

5) The velocity corresponding to a given percentile value on the duration curve can then be determined from

$$W_P = c[-\ell n\, p(W \geq W_P)]^{1/k} \quad . \tag{2.38}$$

Example 2.11: Consider a wind turbine under design for the Daytona, Florida, area. Assume a 10-m (30-ft) hub height from Table 2.1, c = 4.70 m s^{-1} (10.5 mph) and k = 2.09. The annual mean wind speed from Figure 2.26 is $\hat{W}/c = 0.886$ and $\hat{W} = 4.16$ m s^{-1} (9.3 mph). The designer specifies the cut-in speed to be 2 m s^{-1} (4.5 mph). From Figure 2.28, he finds there is a 15 percent chance that the WTG will not operate 1352 h of the year. However, there is a further 10 percent chance that if the turbine were to be located elsewhere k may be as low as 1.50 [from Figure 2.30 at $\hat{W} = 4.16$ m s^{-1} (9.3 mph)] in which case for 15 percent of the time the wind speed will not exceed 1.36 m s^{-1} (3.0 mph) rather than the designed for value of 2 m s^{-1} (4.5 mph). Determining the hours the rotor will not turn during a year when k = 1.5 for a cut-in speed of 2 m s^{-1} (4.5 mph) gives 2147 h. A graphical illustration of this calculation is given in Figure 2.31.

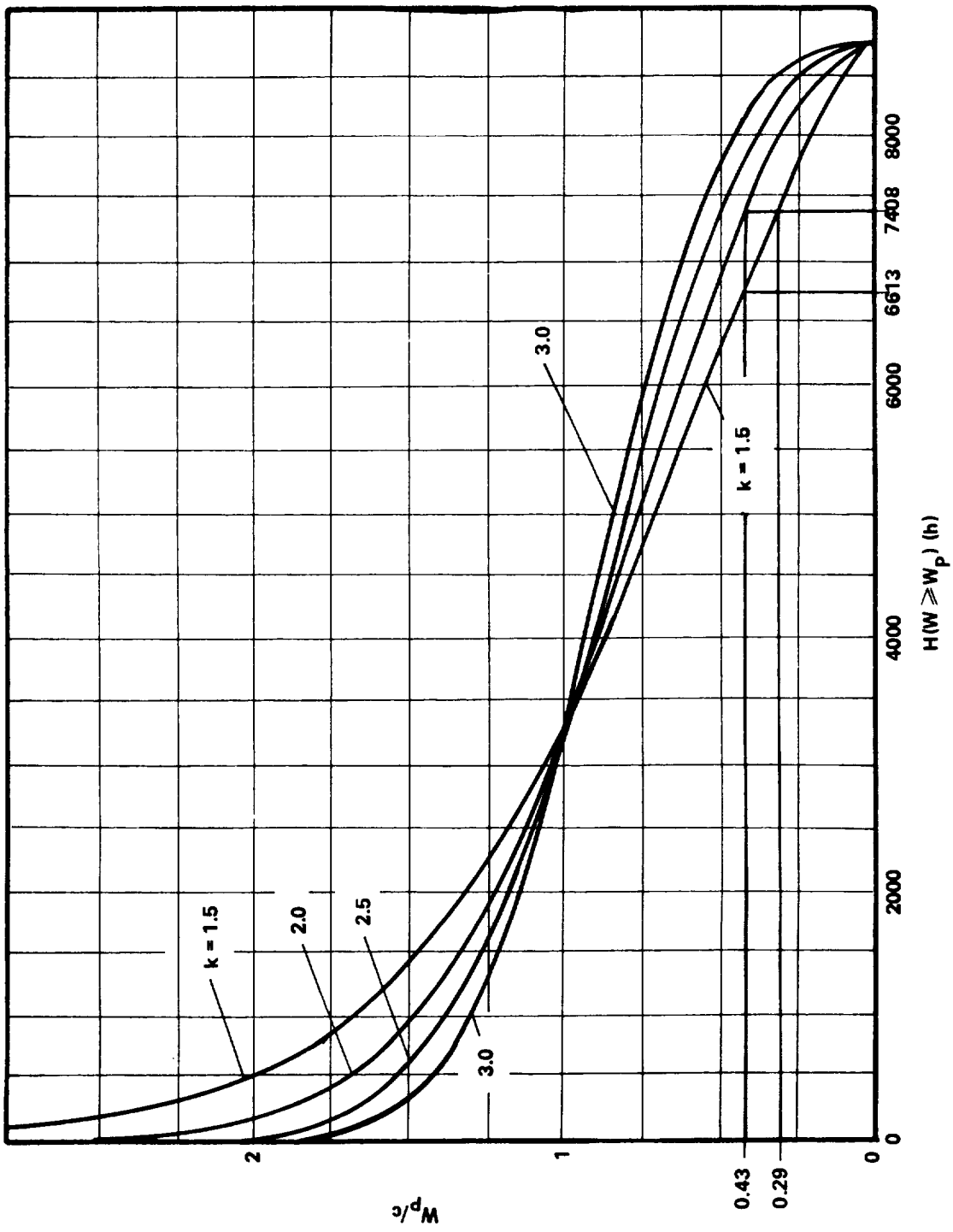

Figure 2.31 Graphical illustration of Example 2.11.

REFERENCES

2.1 Kaufman, J. W. (editor): Terrestrial Environment (Climatic) Criteria Guidelines for Use in Aerospace Vehicle Development, 1977 Revision. NASA TM X-78118, 1977.

2.2 Code of Basic Data for the Design of Buildings. British Standards Institution. Chapter 5, Part 2, 1972.

2.3 Cliff, W. C.: The Effect of Generalized Wind Characteristics on Annual Power Estimates from Wind Turbine Generators. PNL-2436 UC-60, Battelle PNL, October 1977.

2.4 Justus, C. G., Hargraves, W. R., and Mikhail, Amir: Reference Wind Speed Distributions and Height Profiles for Wind Turbine Design and Performance Evaluation Applications. ORO/5108-76/4 UC 60, August 1976.

2.5 Elliot, D. L.: Synthesis of National Wind Energy Assessments, BNWL-2220 Wind-5 UC-60, Battelle PNL, July 1977.

2.6 Sachs, P.: Wind Forces in Engineering. Pergamon Press, 1972.

2.7 Hollister, S. C.: The Engineering Interpretation of Weather Bureau Records for Wind Loading on Structures. Building Science Series 30, U.S. Department of Commerce, 1970.

2.8 Jacobs, E. N. and Ward, K. E.: The Characteristics of 78 Related Airfoil Sections from Tests in the Variable-Density Wind Tunnel. TR No. 460, NACA, 1932.

2.9 Newberry, C. W. and Eaton, K. J.: Wind Loading Handbook, Building Research Establishment Report, Her Majesty's Stationery Office, 1974.

2.10 Fichtl, G. H., Kaufman, John K., and Vaughan, William W.: The Characteristics of Atmospheric Turbulence as related to Wind Loads on Tall Structures. Building Science Series 30, U.S. Department of Commerce, 1970.

2.11 Thom, H. C. S.: New Distributions of Extreme Winds in the United States. Jour. Struct. Div., Proc. ASCF, Paper No. 6038, July 1968.

2.12 Thom, H. C. S.: Distributions of Extreme Winds in the United States. ASCE Trans., Vol. 126, 1961.

2.13 Farren, W. S.: Apparatus for Measurement of Two-Dimensional Flow at High Reynolds Numbers with Application to Growth of Circulation Around Wing Started Impulsively From Test. Proc. 3rd. Atmos. Conf. Appl. Mech., 1930.

2.14 Doran, J. C., et al.: Accuracy of Wind Power Estimates. PNL-2442 UC-60, Battelle PNL, October 1977.

CHAPTER 3. WIND SHEAR

Summary of Wind Shear

3.1 Introduction

In this section, the magnitude of wind shear to which a general purpose WTG (see footnote, page 1) is exposed during routine daily operations is given as a function of mean wind speed, height, and surface roughness. Values of maximum wind shear reported in thunderstorms are given as estimates of extreme wind shear values. Wind shear in this chapter refers to vertical spatial variation of the mean wind speed (generally a 10-min average or greater is taken as mean wind speed, but for thunderstorms 10-s averages are given).

Sections 3.2 through 3.4 present the detailed computational procedures and data from which additional values of wind shear can be computed if desired. Section 3.1.3 describes how the expressions for wind shear quoted in Section 3.1.1 were determined from the procedures and data given in Sections 3.2 through 3.4. Only shear in the wind speed is considered in this chapter. Directional wind shear is discussed in Chapter 5.

3.1.1 Wind Shear Design Values

3.1.1.1 Routine Daily Wind Shear

A linear variation of wind speed across the rotor of

$$\frac{\Delta \overline{W}}{\Delta h} = \frac{\overline{W}_{h=10\ m}}{(h + z_o)\, \ell n(10/z_o + 1)} \qquad (h \text{ and } z_o \text{ in meters})$$

$$\frac{\Delta \overline{W}}{\Delta h} = \frac{\overline{W}_{h=30\ ft}}{(h + z_o)\, \ell n(30/z_o + 1)} \qquad (h \text{ and } z_o \text{ in feet}) \qquad (3.1)$$

is recommended for general design. Typically, the surface roughness, z_o, varies between 1 m and 10^{-3} m, with the larger values giving the highest shear.

A value of 1 m is characteristic of forest terrain or of suburban areas and gives approximately the largest shear value a WTG would experience at reasonable operating sites. Thus z_o = 1 m is the suggested value for use in equation (3.1) when designing a WTG for all possible sites.

3.1.1.2 Thunderstorm Wind Shear (Extreme Values)

Table 3.3 in Section 3.4 gives values of wind shear potential encounterable during thunderstorm activity. These data are the maximum values measured in 13 thunderstorms and do not necessarily represent the most extreme wind shear which could be experienced during thunderstorm passage.

3.1.2 Description of Recommended Design Values

This section discusses the method of computing the previously given wind shear magnitudes from the information contained in Sections 3.2 through 3.4.

Predictions of wind shear given in the summary assume a neutral atmosphere and are based on a logarithmic velocity profile; i.e.,

$$\overline{W} = \frac{u_{*_o}}{\kappa} \ell n \frac{h + z_o}{z_o} \quad . \tag{3.2}$$

Differentiation of this velocity profile with respect to h gives

$$\frac{\partial \overline{W}}{\partial h} = \frac{u_{*_o}}{\kappa} \frac{1}{(h + z_o)} \quad . \tag{3.3}$$

Thus, vertical wind shear is seen to be a function of the friction velocity, u_{*_o}, surface roughness, z_o, and the height, h. The friction velocity at the Earth's surface, u_{*_o}, can be related to reference wind speed by

$$\frac{u_{*_o}}{\overline{W}_{ref}} = \frac{\kappa}{\ell n[(h_{ref} + z_o)/z_o]} \quad . \tag{3.4}$$

Thus, wind shear is indirectly a function of the mean wind speed at the reference elevation. Combining equations (3.3) and (3.4) gives the recommended expression for vertical wind shear at any given height, h.

For additional details of wind shear computations and for a description of the thunderstorm wind shear data, see Sections 3.3 and 3.4, respectively.

Detailed Computational Procedures and Working Data

3.2 Introduction

The influence of wind shear on a wind turbine generator can be threefold. The fatigue strength of the rotor will be influenced by the continuous rotation through a wind field that varies in the vertical direction; the structural integrity of the system can be exceeded under extreme wind shear; and the power output may show an effect due to vertical variation of the wind. Lateral variations in wind also create shear; however, the mean wind generally does not vary significantly in the lateral direction and is neglected herein. Gust gradients across the rotor are discussed in Chapter 4.

The design of a rotor for fatigue strength requires knowledge of the variations in the wind to which the rotor is daily exposed throughout its useful life. Mean wind shear depends on both surface roughness and a reference mean wind speed. Thus, the frequency distribution of mean wind speed given in Section 2.4 must be employed to compute the cumulative wind shear experienced by the rotor. Mean wind shear data are described in Section 3.4.

Since the stability of the atmosphere can strongly influence the magnitude of the wind speed gradient, consideration of the neutral, stable, and unstable conditions is required. Wind speed profiles in the atmospheric boundary layer employ either a power-law variation or a logarithmic law variation of wind speed in the vertical direction. The former is empirical while the latter is supported by physical arguments as well as experiments. Thus, the logarithmic law more readily allows stability effects to be incorporated and is discussed first in this section. Following this discussion, it is shown that the power law and logarithmic law can be related through the surface roughness parameter, z_o, and the power-law exponent, n.

Under extreme weather conditions wind shear may, in addition to fatigue, have a pronounced effect on the structural strength of the rotor. Even though the rotor may be feathered during severe storms, the magnitude of the wind shear across the rotor conceivably can be large enough to create damage even in the static position. Thus, a design of the rotor requires an estimate of the magnitude of the extreme wind shears that the rotor may encounter throughout its useful application. Some information is available on the extremes of wind shear in thunderstorms. It is difficult to separate wind shear from turbulence in these situations, however, and the frequency content which classifies turbulence is simply a matter of definition. Section 3.4 discusses this definition and provides some limited data as to wind shear relative to thunderstorms.

It should be noted that the distribution of wind speeds across the rotor due to two-dimensional turbulence effects also generates wind shear. This chapter, however, deals with mean wind shears whereas consideration of the effects of instantaneous wind shears associated with turbulent gusts is given in Chapter 4.

Finally, the performance or output of the wind turbine is possibly influenced by the mean wind shear. Plaks[1] carried out some analyses and found that power output depends slightly on the exponent, n, of the power-law wind profile. Spera and Neustadter[2] report negligible effect of wind shear on performance. No other information was found relative to the influence of wind shear on the power output of a WTG. Simple analyses in this section show a small influence.

Data are provided in the next section which allow the design engineer to analyze the influence of wind variation in the vertical direction on wind energy conversion systems.

3.3 Continuous Wind Shear

All wind fields must go to zero at the ground, and, consequently, the rotor of a WTG is continuously exposed to a wind variation in the vertical direction which creates fatigue throughout the life of the rotor. A common way of

1. Personal communication with A. Plaks (Kaman Aerospace, Inc.), The Wind Characteristic Workshop, Boston Massachusetts, June 1976.

2. Personal communication with D. Spera and H. F. Neustadter (NASA, Lewis Research Center), Cleveland, Ohio, October 1977.

expressing wind shear mathematically is in nondimensional form [3.1, 3.2] as described in Section 3.3.2. Because wind shear is strongly influenced by atmospheric stability, however, this subject will be discussed first.

3.3.1 Atmospheric Stability

Two measures of atmospheric stability are h/L and Ri. The former is the ratio of height to a scaling length defined as the Monin-Obukhov stability length multiplied by the ratio of thermal to momentum diffusivity; the latter is the gradient Richardson's number. The relationship between h/L and Ri is given by

$$h/L = \phi(h/L)\ Ri$$

where $\phi(h/L)$ is a universal function of h/L defining nondimensional wind shear. A complete discussion of this relationship is given in References 3.1 and 3.2, and only a brief description is given here. Both parameters are a measure of the influence of mechanical turbulence relative to buoyance-induced turbulence.

The atmosphere is said to be unstable if $L < 0$, $Ri < 0$; neutral if $L = \infty$, $Ri = 0$; stable if $L > 0$, $Ri > 0$; and highly stable if $Ri > 0.18$.

Based on the stability of the atmosphere, the two parameters h/L and Ri are related by

$$h/L = Ri/(1 - 18\ Ri)^{1/4} \quad ; \quad h/L < 0 \qquad (3.5a)$$

$$h/L = Ri/(1 - 4.5\ Ri) \quad ; \quad h/L > 0 \qquad (3.5b)$$

$$h/L = 5.5\ Ri \quad ; \quad h/L > 1.0 \ . \qquad (3.5c)$$

A plot of equation (3.5) is provided in Figure 3.1 to facilitate conversion.

Barr, et al. [3.1] have estimated the cumulative probability of the Richardson's number at a reference height of 6 m (20 ft) as shown in Figure 3.2. These curves are based on data from only two sites, however, and should be

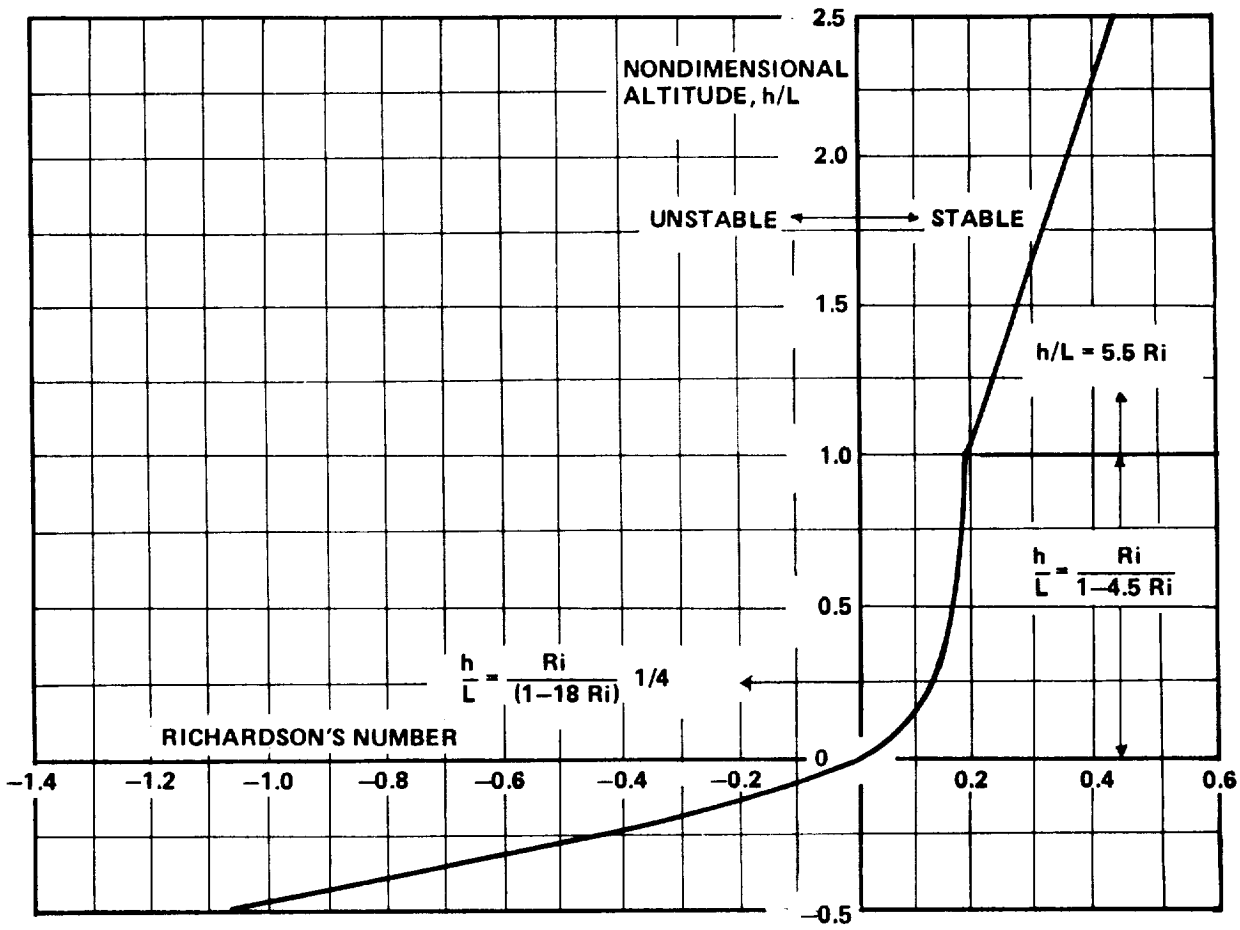

Figure 3.1 Richardson's number profile.

generalized with great caution. One observes from these data that for high wind speeds the probability of a Richardson's number near zero is very large. This indicates that at high values of wind speed most useful for power generation, a condition of neutral stability generally can be assumed for the atmosphere.

Example 3.1: Consider a WTG site with a mean wind speed of 6 m s^{-1} (14 mph) at a 6-m (20-ft) elevation. Since the logarithmic law or power-law wind speed profile without correction for stability is valid for a neutral atmosphere for which $Ri_{h=6\ m\ (20\ ft)}$ is approximately in the range of ±0.05, one observes from Figure 3.2(a) a cumulative frequency of Ri ≤ 0.05 of 54 percent and of

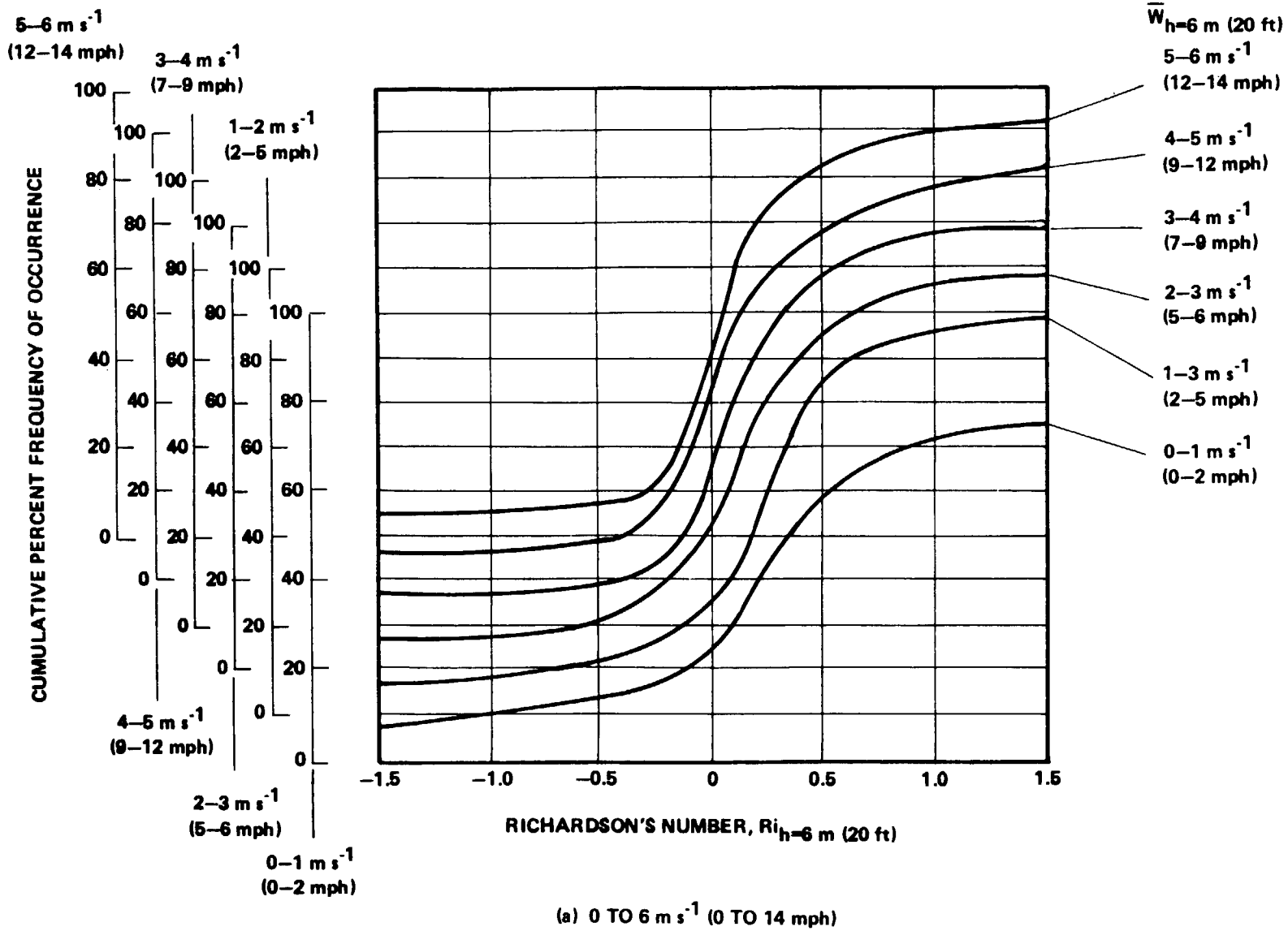

Figure 3.2 Cumulative percent frequency of occurrence of Ri at given wind speeds.

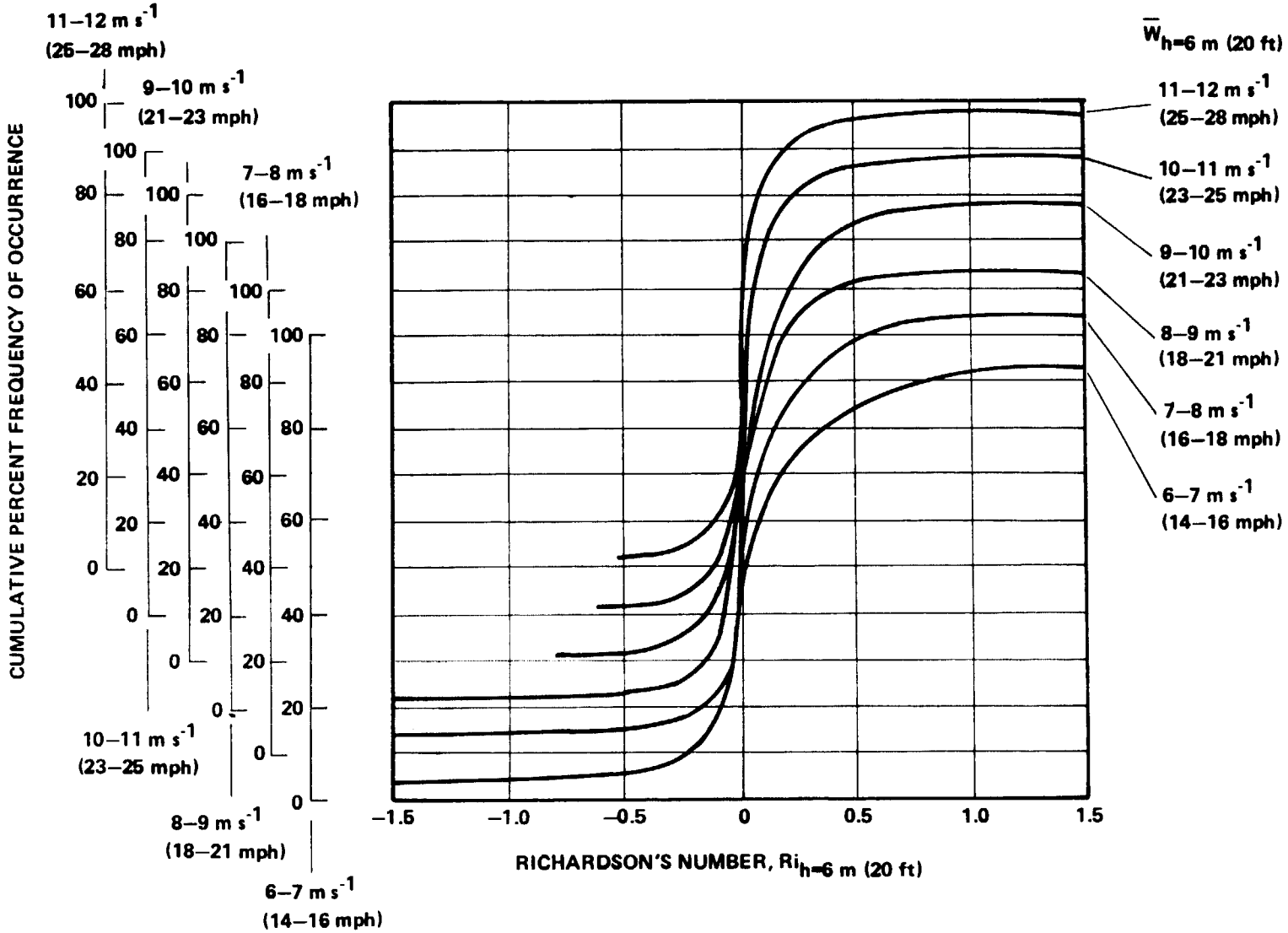

(b) 6 TO 12 m s^{-1} (14 TO 28 mph)

Figure 3.2 (Continued).

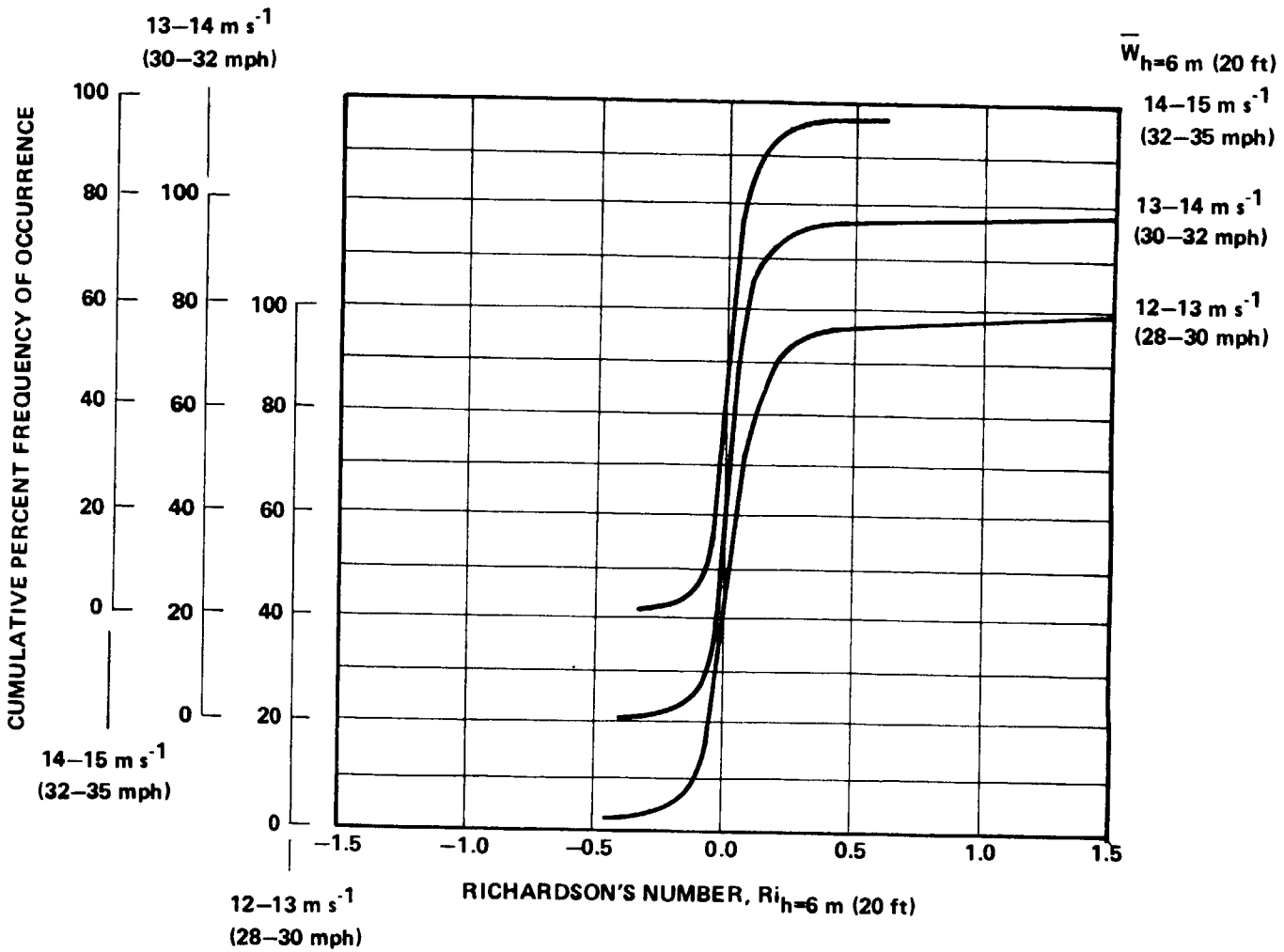

(c) 12 TO 15 m s^{-1} (28 TO 32 mph)

Figure 3.2 (Concluded).

$Ri \leq -0.05$ of 34 percent. Thus, the probability of a neutral atmosphere is only 20 percent at 6 m s^{-1} (14 mph). However, at 15 m s^{-1} (35 mph) the same graphical analysis shows a (80 - 12) = 68 percent probability of neutral conditions.

Nondimensional mean wind shear as a function of atmospheric stability is discussed in the following section.

3.3.2 Nondimensional Vertical Wind Shear

Figure 3.3 shows nondimensional wind shear as a function of the height, h, divided by the stability parameter, L. Wind shear $\partial \overline{W}/\partial h$ is nondimensionalized with $u_{*_o}/\kappa h$ where κ is the Von Karman constant (the value of κ is taken as 0.4) and u_{*_o} is the friction velocity at the ground. The value of u_{*_o} depends on the reference mean wind speed, $\overline{W}_{ref}$, and on the surface roughness of the surrounding terrain, z_o. Values of u_{*_o} are determined through the relationship

$$\frac{u_{*_o}}{\overline{W}_{ref}} = \frac{\kappa}{\ell n\left(\frac{h_{ref} + z_o}{z_o}\right) + \psi(h_{ref}/L)} \quad . \tag{3.6}$$

A plot of $u_{*_o}/\overline{W}_{ref}$ is given in Figure 3.4. The function $\psi(h_{ref}/L)$ is an empirically determined function which accounts for the stability conditions of the atmosphere and is described in Section 3.3.3. The value of the friction velocity, u_*, is assumed to vary with altitude according to the relationship [3.1]

$$u_* = u_{*_o}(1 - h/\delta) \tag{3.7}$$

where δ is the thickness of the atmospheric boundary layer defined as:

$$\delta = u_{*_o}/5.35\, f \tag{3.8}$$

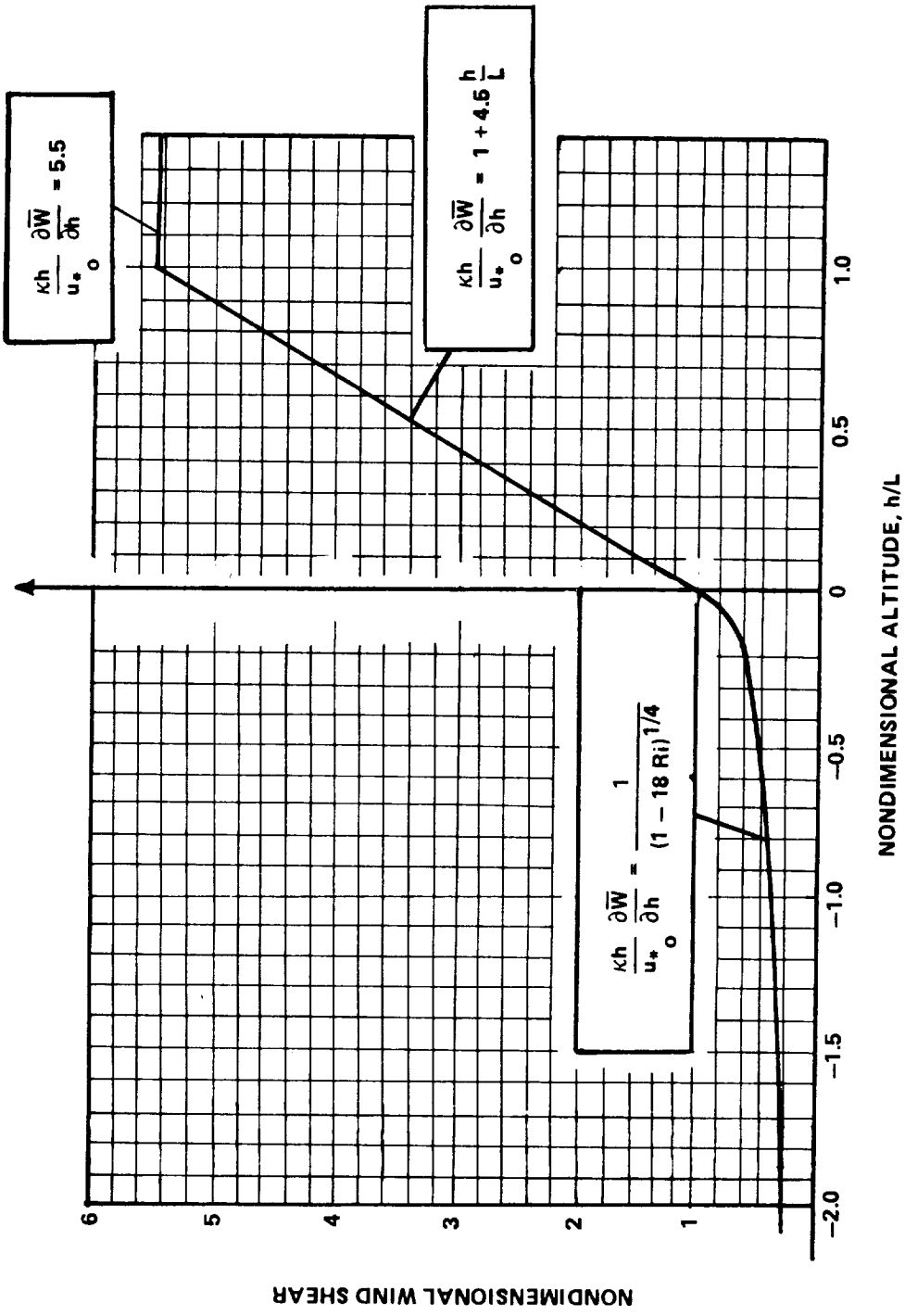

Figure 3.3 Nondimensional vertical wind shear.

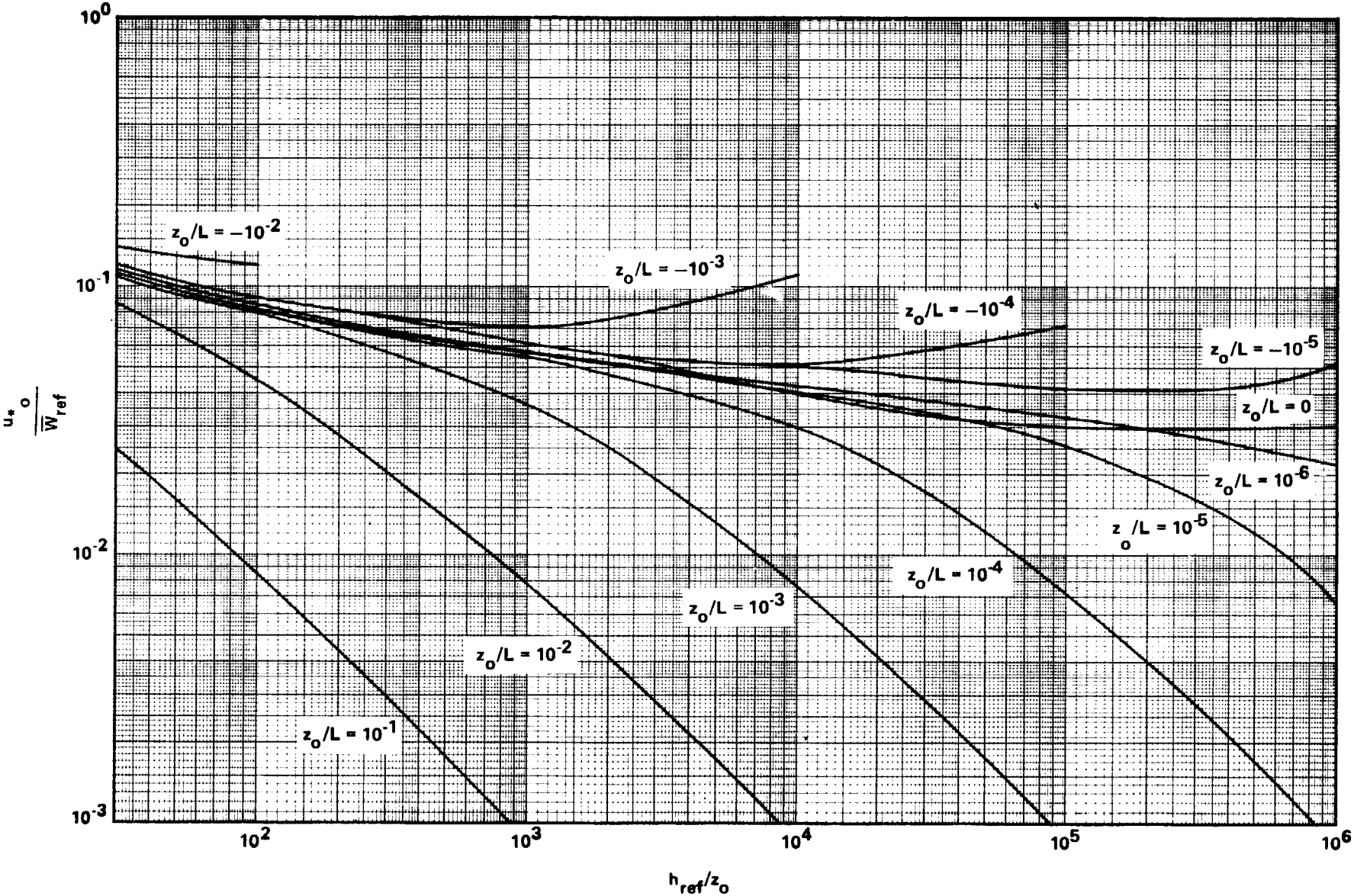

Figure 3.4 Variation of surface friction velocity with height.

where f is the Coriolis parameter. The Coriolis parameter is given by the angular velocity of the Earth, ω_E, times the trigonometric sine of latitude, λ; i.e., $f = 2\omega_E \sin\lambda$. Since most of the United States lies between 30 and 50 deg latitude, δ is adequately represented by:

$$\delta = 2000\, u_{*_o} \quad . \tag{3.9}$$

In Alaska this value would change to approximately $1420\, u_{*_o}$. Although the variation of u_* with altitude is generally negligible (particularly below 100 m) the correction with altitude as given in equation (3.7) is plotted in Figure 3.5 for computations where very tall WTG are to be designed. In this figure the parameter

$$\mu = 5.35\, f\, z_o / u_{*_o}$$

is a dimensionless parameter which results from making h dimensionless with respect to z_o in equation (3.7).

The surface roughness, z_o, is an empirically determined parameter which characterizes the influence of small-scale surface roughness on the wind speed profile. Without recourse to experiment, the engineer must select z_o from visual inspection of the surrounding terrain and from reference to tables or plots such as those given in Table 3.1 and Figure 3.6, respectively. Figure 3.6 also gives the exponent of the power-law wind speed profile as a function of surface roughness. Further details of this relationship are given in Section 3.3.4.

Having discussed the variables involved in the expression for the non-dimensional wind shear, attention is returned to Figure 3.3. The curve plotted in this figure is determined empirically [3.2] and is given by the relationships

$$\phi(h/L) = 1 \quad ; \quad h/L = 0 \tag{3.10a}$$

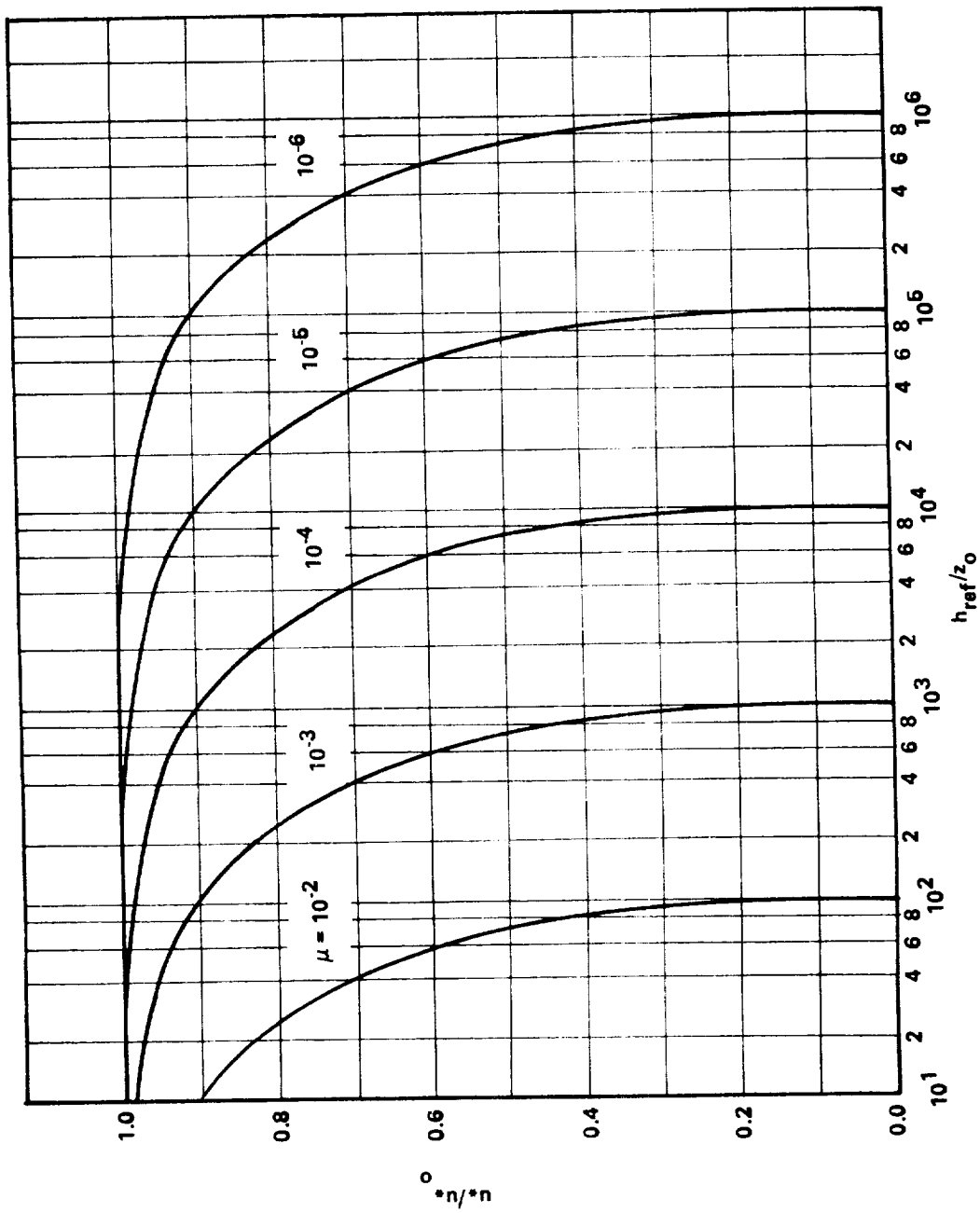

Figure 3.5 Variation of friction velocity with altitude, $\mu = 5.35\ fz_o / u_{*_o}$.

TABLE 3.1 TYPICAL VALUES OF SURFACE ROUGHNESS LENGTH, z_o, FOR VARIOUS TYPES OF SURFACES

Type of Surface	z_o (m)	z_o (ft)
Mud Flats, Ice	$10^{-5} - 3 \cdot 10^{-5}$	$3 \cdot 10^{-5} - 10^{-4}$
Smooth Sea	$2 \cdot 10^{-4} - 3 \cdot 10^{-4}$	$7 \cdot 10^{4} - 10^{-3}$
Sand	$10^{-4} - 10^{-3}$	$3 \cdot 10^{-4} - 3 \cdot 10^{-3}$
Snow Surface	$10^{-3} - 6 \cdot 10^{-3}$	$3 \cdot 10^{-4} - 2 \cdot 10^{-2}$
Mown Grass (0.01 m)	$10^{-3} - 10^{-2}$	$3 \cdot 10^{-3} - 3 \cdot 10^{-3}$
Low Grass, Steppe	$10^{-2} - 4 \cdot 10^{-2}$	$3 \cdot 10^{-2} - 10^{-1}$
Fallow Field	$2 \cdot 10^{-2} - 3 \cdot 10^{-2}$	$6 \cdot 10^{-2} - 10^{-1}$
High Grass	$4 \cdot 10^{-2} - 10^{-1}$	$10^{-1} - 3 \cdot 10^{-1}$
Palmetto	$10^{-1} - 3 \cdot 10^{-1}$	$3 \cdot 10^{-1} - 1$
Forest and Woodland	$10^{-1} - 1$	$3 \cdot 10^{-1} - 3$
Suburbia	1 - 2	3 - 6
City	1 - 4	3 - 13

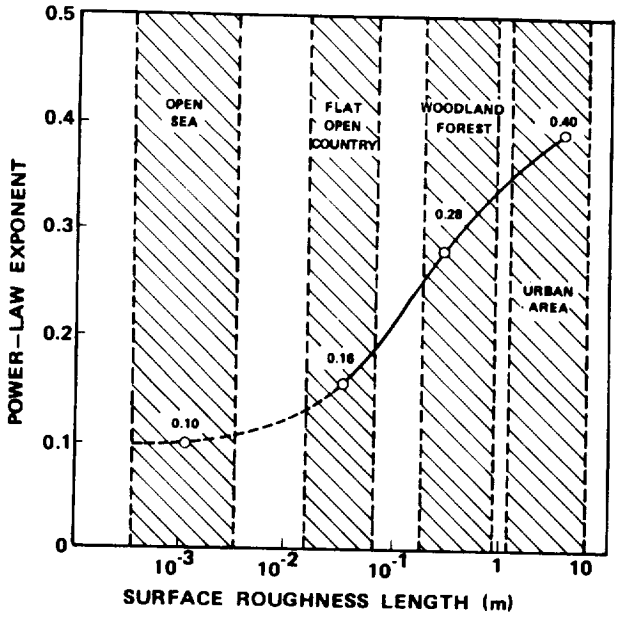

Figure 3.6 Surface roughness length z_o, versus the power-law exponent, n, where $\overline{W}/\overline{W}_{ref} = (h/h_{ref})^n$.

$$\phi(h/L) = 1 + 4.5\, h/L \;\; ; \;\; 1.0 \geq h/L > 0 \qquad (3.10b)$$

$$\phi(h/L) = (1 - 18\, Ri)^{-1/4} \;\; ; \;\; h/L < 0 \qquad (3.10c)$$

where the relationship between Ri and h/L needed for utilization of equation (3.10c) is given in Figure 3.1.

A fourth regime, called the very stable atmosphere, is not well understood physically, and no reliable mathematical formulation of the wind shear is available. Barr, et al. [3.1], however, suggest

$$\phi(h/L) = 5.5 \;\; ; \;\; h/L > 1.0 \qquad (3.11)$$

which is proposed for design in this report. Fortunately, very stable conditions do not occur frequently nor generally at an elevation critical to WTG operations. It should be noted in this regard that close to the ground, since h/L is very small or zero, the wind speed profile behaves as in a neutral atmospheric boundary layer.

Example 3.2: An application of Figure 3.3 to design is to evaluate the wind shear at hub height and assume it constant over the rotor. As an example, consider neutrally stable atmospheric conditions at a site in Denver, Colorado, for WTG of $h_H = 30$ m (100 ft). From Section 2.4, $k = 1.54$ and $c = 3.80$ m s^{-1} (8.5 mph) for Denver, and thus the annual mean wind speed is 3.42 m s^{-1} (7.7 mph). The surface friction velocity u_{*_o} is found from equation (3.6) or Figure 3.4 where $h/L = 0$ and $\psi(h/L) = 0$ for the neutral case. For a surface roughness of 0.1 m (typical of a wood area), u_{*_o} becomes

$$u_{*_o} = 3.42 \text{ m s}^{-1} \frac{0.4}{\ell n\left(\frac{10 + 0.1}{0.1}\right)}$$

$$= 0.30 \text{ m s}^{-1} \text{ (0.67 mph)} \quad . \qquad (3.12)$$

Introducing u_{*_o} into the relationship

$$\partial \overline{W}/\partial h = u_* (\kappa h)^{-1} \phi (h/L)$$

where $\phi (h/L)$ is obtained from equation (3.10) or Figure 3.3, the wind shear is

$$\frac{\partial \overline{W}}{\partial h} = \frac{0.3 \text{ m s}^{-1}}{(30 \text{ m})(0.4)} = 0.03 \text{ s}^{-1} \quad .$$

If one assumes this value to be constant across the rotor, the error associated with this assumption can be estimated as follows. Consider the effects of wind shear on the effective wind power or energy content of the wind over a 40-m (130-ft) diameter rotor:

$$P_{eff} = \int_{10m}^{50m} 2\overline{W} (h)^3 \sqrt{R^2 - (h - h_H)^2}\, dh \quad . \qquad (3.13)$$

Assume two conditions: constant shear or linear variation of wind speed with height referenced to h_H:

$$\overline{W}_h = 0.03(h - 30) + 4.28 \text{ m s}^{-1} \quad ; \text{ h in meters}$$

[(the wind speed corrected to h_H = 30 m (100 ft) is 4.28 m s^{-1} (14 mph)], and on variable shear with logarithmic variation of wind speed with altitude.

$$\overline{W}_h = \frac{u_{*_o}}{\kappa} \ell n \left(\frac{h + 0.1}{0.1} \right) . \qquad (3.14)$$

Numerically integrating for both cases gives the potential power for constant shear as 19.90×10^4 m^5 s^{-3} and for the variable shear as 19.22×10^4 m^5 s^{-3}. The difference in the computed energy content of the wind over the rotor area is approximately 3.5 percent. Neglecting shear altogether gives

$$(\overline{W}_{h=30\ m})^3 \pi R^2 = 19.70 \times 10^4\ m^5\ s^{-3}$$

which is only approximately 2.5 percent difference. This result suggests that the effects of wind shear on power computations is negligible in concurrence with the previously cited personal communications with A. Plaks and D. Spera and H. E. Neustadter.

3.3.3 Vertical Profiles of the Mean Wind

Mathematical profiles of the mean wind speed as a function of height are useful for integrating over the extent of the rotor to determine design conditions such as bending moments or available wind energy, although these influences of mean wind shear appear to be small.

Wind speed variations in the vertical direction are achieved by integrating

$$\frac{\partial \overline{W}}{\partial h} = \frac{u_{*_o}}{\kappa h} \phi(h/L) \qquad (3.15)$$

where $\phi(h/L)$ is given by equation (3.10). The mean wind speed as a function of height, h, becomes

$$\overline{W} = \frac{u_{*_o}}{\kappa} \left(\ell n \frac{h + z_o}{z_o} + \psi(h/L) \right) \qquad (3.16)$$

where for the neutral case

$$\psi(h/L) = 0 \quad , \qquad (3.17a)$$

for the stable case

$$\psi(h/L) = 4.5\, h/L \quad , \tag{3.17b}$$

and for the unstable case

$$\psi(h/L) = -\{ 2\,\ell n[(1 + x)/2] + \ell n[(1 + x^2)/2] - 2\tan^{-1}(x) + \pi/2 \} \tag{3.17c}$$

where

$$x = (1 - 18\, h/L)^{1/4} \quad .$$

Equation (3.16) can thus be used with the appropriate expression for $\psi(h/L)$ to determine the variation in mean wind over the rotor.

Example 3.3: To illustrate the influence of atmospheric stability on the potential wind energy at a site and the application of equation (3.16), consider the following example. A wind turbine has a hub height of $h_H = 10$ m (30 ft) and a rotor of 10 m (30 ft) in diameter. The surface roughness at the site is 0.1 m. The influence of wind speed variations due to atmospheric stability on the available energy can be determined from equation (3.16).

The energy potential is evaluated by integrating the cube of wind speed over the area of the rotor, i.e.,

$$P_{eff} = \int_{h_H - R}^{h_H + R} 2W(h)^3 \sqrt{R^2 - (h - h_H)^2}\, dh \quad . \tag{3.18}$$

Making the variables dimensionless with hub height gives

$$P_{eff} = \frac{2u_*^3\, h_H^3}{\kappa^3} \int_{1-\phi}^{1+\phi} W'(\tilde{\eta})^3 \sqrt{\hat{\phi}^2 - (\tilde{\eta} - 1)^2}\, d\eta \tag{3.19}$$

where

$$\hat{\phi} = R/h_H$$

$$\tilde{\eta} = h/h_H$$

$$W'(\eta) = \ell n \frac{\tilde{\eta} + \tilde{\eta}_o}{\tilde{\eta}_o} + \psi(\tilde{\eta} h_H/L) \quad . \tag{3.20}$$

Substituting equations (3.20) and (3.17) appropriately nondimensionalized into equation (3.19) and numerically integrating for the ratio $\hat{P} = P_{\text{eff stable}}/P_{\text{eff neutral}}$ results in Table 3.2. The assumption is made that the wind speed at the hub height is the same for all wind profiles. Thus, the friction velocity will be different for the different stability conditions. The second column of the table provides the ratio of the friction velocities.

TABLE 3.2 INFLUENCE OF STABILITY ON POTENTIAL WIND ENERGY; $\hat{\phi} = 0.5$, $\tilde{\eta}_o = 0.01$

h_H/L	$\left(u_{*_s}/u_{*_n}\right)^3$	$\hat{P}$
-0.75	2.35	0.99
-0.50	1.90	0.99
-0.25	1.50	1.00
0	1.00	1.00
0.25	0.52	1.02
0.50	0.30	1.04
0.75	0.19	1.05
0.95	0.14	1.06

The table clearly indicates that, for the same wind speed at hub height, slightly more wind energy is available in a stable atmosphere but that the effect appears sufficiently small to be negligible in design procedures.

3.3.4 Power Law Versus Logarithmic Law

It was mentioned earlier that the power-law relationship for the wind speed profile

$$\overline{W}(h) = \overline{W}_{ref}(h/h_{ref})^{n} \tag{3.21}$$

was frequently used in place of the logarithmic law

$$\overline{W}(h) = \frac{u_{*_o}}{\kappa}\left(\ell n \frac{h + z_o}{z_o} + \psi(h/L)\right) \quad . \tag{3.22}$$

In general, for neutral atmospheric conditions the two can be used interchangeably if n is expressed as

$$n = \left(\left(\ell n \frac{h_{ref} + z_o}{z_o}\right)(1 + z_o/h_{ref})\right)^{-1} \quad . \tag{3.23}$$

This relationship is achieved by equating the slopes of the profiles at h_{ref}, i.e.,

$$\left.\frac{\partial \overline{W}}{\partial h}\right|_{power} = \left.\frac{\partial \overline{W}}{\partial h}\right|_{logarithmic} \tag{3.24}$$

$$n\overline{W}_{ref}\left(\frac{h_{ref}}{h_{ref}}\right)^{n}\frac{1}{h_{ref}} = \frac{u_{*_o}}{\kappa}\frac{1}{h_{ref} + z_o} \quad . \tag{3.25}$$

Equation (3.23) follows directly from this expression when $u_{*_o}/\overline{W}_{ref}$ is substituted in the form of equation (3.4).

The power-law relationship does not, however, take account of stability effects in the atmosphere. Justus, et al. [3.3] suggest that the exponent n be expressed as a function of wind speed

$$n = (0.37 - 0.088 \ell n \overline{W}_{ref})/[1 - 0.088 \ell n(h_{ref}/10)] \quad (3.26)$$

where $\overline{W}_{ref}$ is in meters per second and h_{ref} is in meters. This relationship partially accounts for stability effects since low wind speeds are most frequently associated with stable or unstable conditions. Surface roughness which is known to strongly influence the value of n does not directly enter equation (3.26), however.

The profiles of wind speeds averaged over shorter periods than the mean wind speed (averaging period on the order of 10 min to 1 h) are also of interest. Equation (3.26) is actually valid for 1-min averages whereas Kaufman [3.4] recommends for peak wind speeds (effective averaging period of 1/10 s):

$$W_g/W_{g_{ref}} = (h/h_{ref})^n \quad (3.27)$$

where $h_{ref} = 18.3$ m (60 ft), $W_{g_{ref}}$ is evaluated at h_{ref}, and

$$n = 0.52\left(W_{g_{ref}}\right)^{-3/4} \quad . \quad (3.28)$$

Reference [3.4] also provides gust factors which allow peak wind speeds to be corrected to longer averaging periods, τ, i.e.,

$$W_g(\tau) = W_g/G\left(\tau, h, W_{g_{ref}}\right) \quad . \quad (3.29)$$

The gust factors depend on height, h, reference peak wind speed, $W_{g_{ref}}$, and the averaging period, τ. A detailed discussion of gust factors is given in Section 4.4.

Figure 3.7 has been prepared from the gust factor data and provides the relationship between the shear for wind speeds averaged over different time periods, i.e.,

$$\frac{W(\tau,h)}{W(\tau,h_{ref})} = (h/h_{ref})^{n} \quad . \tag{3.30}$$

where $h_{ref} = 10$ m. Thus for analyzing structural components having response times faster than 10 min, the influence of wind shear can be assessed utilizing equation (3.30) and Figure 3.7.

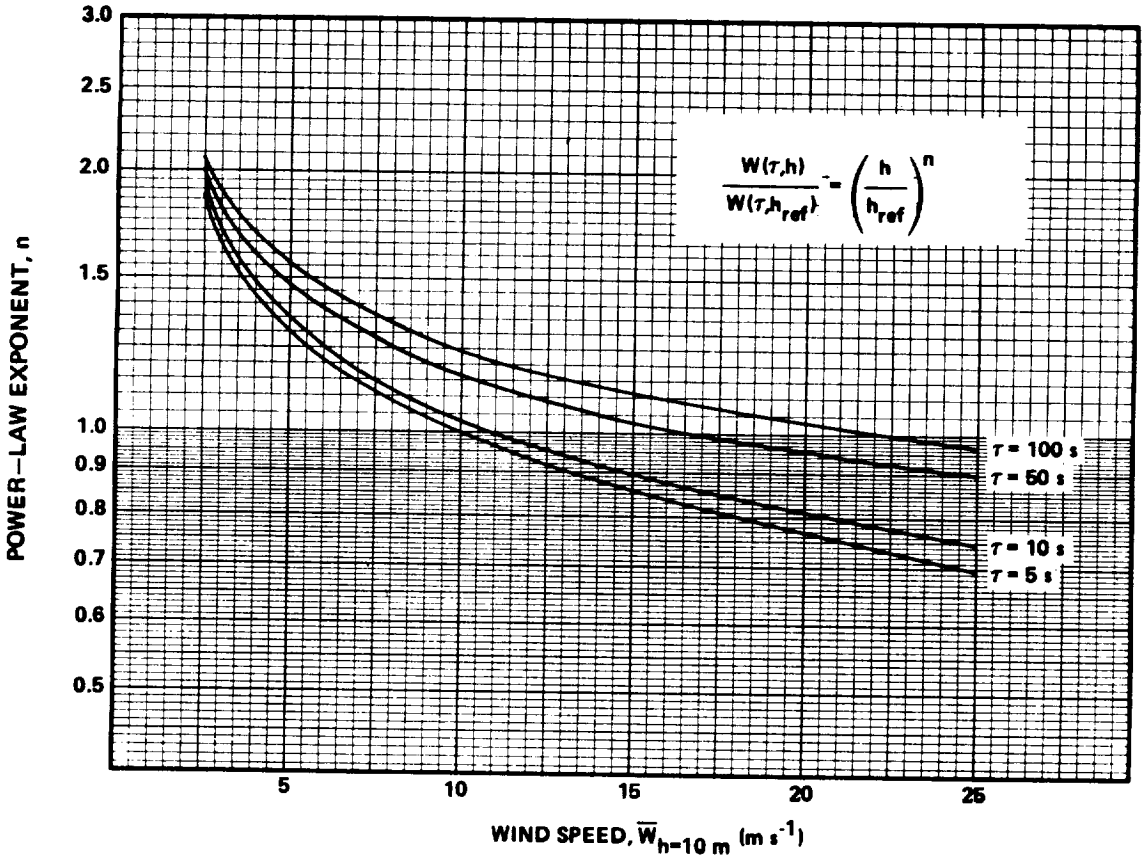

Figure 3.7 Power-law exponent variation with averaging time and mean wind speed.

3.4 Wind Shear in Thunderstorms

Certain areas of the United States have a high average number of thunderstorms per year, as illustrated by Figure 3.8. Only limited data are available on the wind fields associated with a thunderstorm; however, Goff [3.5] has measured 20 storms with a 500-m tower in Norman, Oklahoma. The data were averaged over 10-s periods and typical velocity profiles through the thunderstorm at various times of its development are illustrated in Figure 3.9. Maximum wind shear values computed by Goff are tabulated in Table 3.3. The wind shear data are given in terms of meters per second per 100 meters and thus represent the wind shear which would be experienced across a 100-m rotor. The nomenclature W_x, W_y, and W_z denote the wind vector components in the direction of the storm, x, the direction perpendicular to x, y, and the vertical direction, z. Although these do not necessarily represent the most extreme wind shears that may be encountered in a thunderstorm, they do represent the maximum recorded in 13 different thunderstorms and may be used by the design engineer as a guide to the magnitude of wind shear which can be encountered by a wind turbine generator during the passage of a thunderstorm.

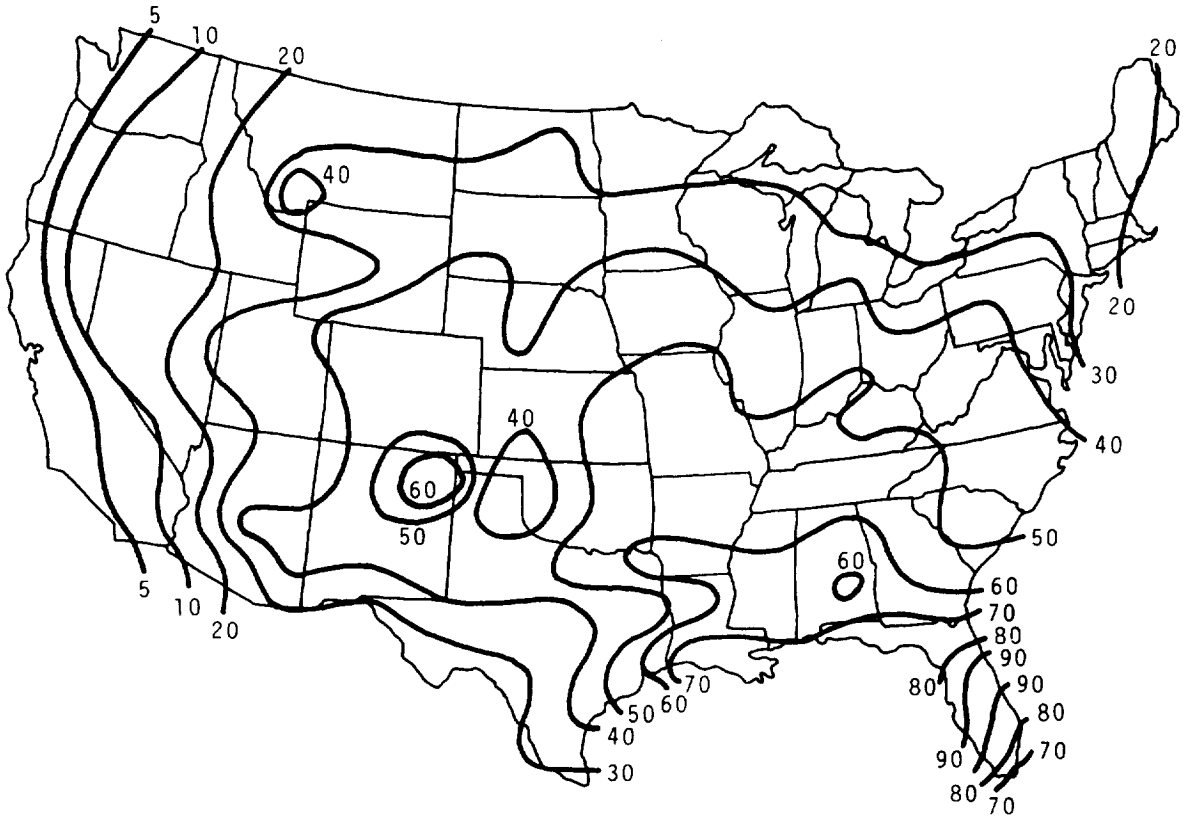

Figure 3.8 The average number of thunderstorms per year.

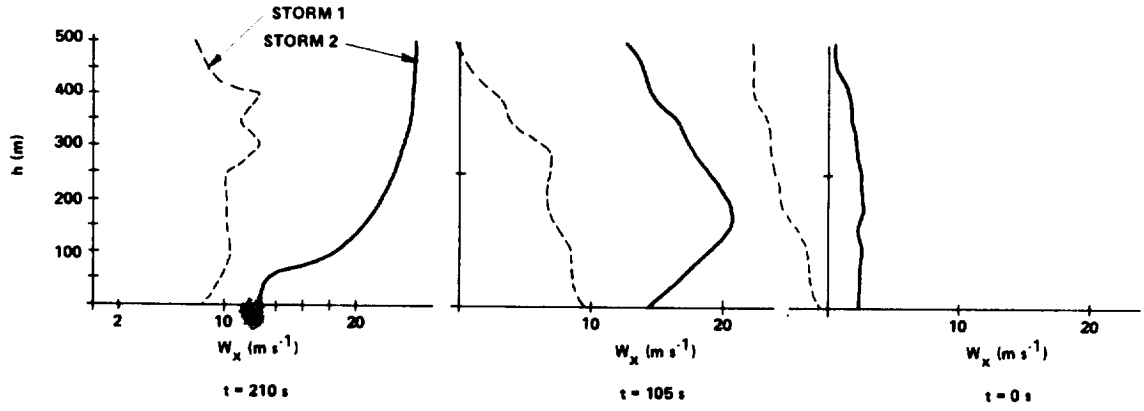

Figure 3.9 Typical profiles of wind speed in direction of storm motion for two thunderstorms selected at random from a set of 20.

TABLE 3.3 MAXIMUM ABSOLUTE SHEAR FROM 13 THUNDERSTORMS [m s^{-1} (100 m)$^{-1}$]

	50 m	100 m	150 m	200 m	250 m	300 m	350 m	400 m	450 m
$\Delta W_x/\Delta h$	16.2	8.4	8.7	9.6	9.4	8.6	10.8	6.5	10.6
$\Delta W_y/\Delta h$	26.1	10.4	6.9	5.6	8.2	6.4	6.4	6.3	9.7
$\Delta W_z/\Delta h$	3.8	2.1	2.3	2.0	2.6	3.1	3.1	3.1	3.1

REFERENCES

3.1 Barr, N. M., Dagfinn, Gangas, and Schaeffer, D. R.: Wind Models for Flight Simulator Certification of Landing and Approach Guidance and Control Systems. Report No. FAA-RD-74-206, December 1974.

3.2 Haugen, D. A.: Workshop on Micrometeorology. American Meteorological Society, 1973.

3.3 Justus, C. G., Hargraves, W. R., and Mikhail, Amir: Reference Wind Speed Distributions and Height Profiles for Wind Turbine Design and Performance Evaluation Applications. ORO/5108-76/4 UC 60, August 1976.

3.4 Kaufman, J. W. (editor): Terrestrial Environment (Climatic) Criteria Guidelines for Use in Aerospace Vehicle Development, 1977 Revision. NASA Technical Memorandum, NASA TM 78118, 1977.

3.5 Goff, R. Craig: Thunderstorm Outflow Kinematics and Dynamics. NOAA Technical Memorandum ERL NSSL-75, December 1975.

CHAPTER 4. TURBULENCE

Summary of Turbulence

4.1 Introduction

Turbulence is presented in spectral form and in discrete gust form in this chapter. The spectral data are recommended for continuous load analysis (for example, fatigue) and the discrete gust data for extreme load analysis. Both models depend on height and mean wind speed. The spectral model is also a function of surface roughness.

Section 4.1.1 provides generalized mathematical expressions for a spectral model and for a gust model, respectively. These formulae are applicable to the design of general purpose WTG's (see footnote, page 1). Detailed computational procedures and working data are given in Sections 4.2 through 4.6. Section 4.1.2 describes how the generalized formulas in Section 4.1.1 are developed from the detailed information contained in Sections 4.2 through 4.6.

4.1.1 General Purpose Design Values

4.1.1.1 Spectral Model

4.1.1.1.1 Spectra

The recommended turbulence spectra for design, which have units of $m^2\ s^{-2}/s$ when h is expressed in meters and $\overline{W}_{h=10\ m}$ is in meters per second, are

Longitudinal:

$$\phi_{w_x}(\hat{n}) = \frac{12.3\,\overline{W}_{h=10\ m}\ h\,[\ell n(10/z_o + 1)\ \ \ell n(h/z_o + 1)]^{-1}}{1 + 192\ [h\,\hat{n}\,\ell n(10/z_o + 1)/W_{h=10\ m}\ \ \ell n(h/z_o + 1)]^{5/3}} \qquad (4.1)$$

Lateral:

$$\phi_{w_y}(\hat{n}) = \frac{4.0\,\overline{W}_{h=10\ m}\ h\,[\ell n(10/z_o + 1)\quad \ell n(h/z_o + 1)\,]^{-1}}{1 + 70\ [h\,\hat{n}\,\ell n(10/z_o + 1)/\overline{W}_{h=10\ m}\quad \ell n(h/z_o + 1)\,]^{5/3}} \tag{4.2}$$

Vertical:

$$\phi_{w_z}(\hat{n}) = \frac{0.5\,\overline{W}_{h=10\ m}\ h\,[\ell n(10/z_o + 1)\quad \ell n(h/z_o + 1)\,]^{-1}}{1 + 8\ [h\,\hat{n}\,\ell n(10/z_o + 1)/\overline{W}_{h=10\ m}\quad \ell n(h/z_o + 1)\,]^{5/3}} \tag{4.3}$$

4.1.1.1.2 Turbulence Intensity, σ

The recommended values of turbulence intensity where $\overline{W}_{h=10\ m}$ and z_o are in meters per second and meters, respectively, are

Longitudinal:

$$\sigma_{w_x} = 1.0\,\overline{W}_{h=10\ m}/\ell n(10/z_o + 1)$$

Lateral:

$$\sigma_{w_y} = 0.8\,\overline{W}_{h=10\ m}/\ell n(10/z_o + 1) \tag{4.4}$$

Vertical:

$$\sigma_{w_z} = 0.5\,\overline{W}_{h=10\ m}/\ell n(10/z_o + 1)$$

4.2

The term z_o is the surface roughness length. The value of z_o ranges from rural terrain, $0.01 \leq z_o(m) \leq 0.15$; suburban and forest terrain, $1 \leq z_o(m) \leq 2$; and urban terrain, $2 \leq z_o(m) \leq 4$. (also see Table 3.1).

4.1.1.2 Discrete Longitudinal Gust Model

4.1.1.2.1 Discrete Gust Shape

The gust shape recommended for design is:

$$W_G(\zeta) = 1.8\, W_i\{1 - \exp[-(\sin(\pi\zeta/2a))^{1/3}]\} \quad ; \quad 0 \leq \zeta \leq a$$

$$W_G(\zeta) = 1.8\, W_i\{1 - \exp[-(\sin(\pi(1-\zeta)/2(1-a)))^{1/3}]\} \quad ; \quad a \leq \zeta \leq 1 \qquad (4.5)$$

where

$$a = 0.12 + 0.05\, \ell n\, h \quad ; \quad \zeta = t/\tau \quad ; \quad h \text{ in meters} \qquad (4.6)$$

and $W_G(\zeta)$ is the amplitude of the instantaneous wind speed above the mean, i.e., $W_G(\zeta) = W(\zeta) - \overline{W}$, and W_i is an effective average discrete gust magnitude, i.e., $W_i = W(\tau) - \overline{W}$ where $W(\tau)$ is the average wind speed over the time period, τ, centered around the peak wind speed.

4.1.1.2.2 Discrete Gust Magnitude

The horizontal scalar discrete gust magnitude of interest to design is that associated with the response time of the structure. For structures or components of an approximately 5-s time response and for a wind speed $\overline{W}_{h=10\ m} = 5\ m\ s^{-1}$

$$W_i = 2.05\, h^{-0.037} \quad ; \quad h \text{ in meters} \quad . \qquad (4.7)$$

For structure or components of an approximately 50-s time response the gust magnitude is:

$$W_i = 1.14\, h^{-0.019} \quad ; \quad h \text{ in meters} \quad . \tag{4.8}$$

For structures or components of an approximately 300-s time response the gust magnitude is:

$$W_i = 0.295 \quad . \tag{4.9}$$

These values of W_i are based on several approximations (see Section 4.1.2.2); hence, for more specific gust magnitudes and other time responses of interest, Section 4.4 should be consulted.

4.1.2 Description of Recommended Design Values

The development of the specific design values given in the preceding section from information contained in Sections 4.2 and 4.3 of this report is described in the following sections.

4.1.2.1 Turbulence Spectra

The turbulence spectra recommended for design use is developed from:

$$\frac{\hat{n}\phi_{w_\alpha}(\hat{n})}{\sigma_{w_\alpha}^2} = \frac{0.164(\eta/\eta_{o\alpha})}{1 + 0.164(\eta/\eta_{o\alpha})^{5/3}} \tag{4.10}$$

where η is the reduced frequency, $\eta = \hat{n}h/\overline{W}_h$, and the subscript α represents the wind speed fluctuation component of interest, i.e., w_x, w_y, or w_z. This equation describes the turbulence spectra in stable and neutral boundary layers. The reduced frequency $\eta_{o\alpha}$ is a function of the stability parameter Ri and thus accounts for atmospheric variability; however, equations (4.1, 4.2, and 4.3) have been reduced to neutrally stable conditions by neglecting Ri effects and introducing $\eta_{o\alpha}$ as:

$$\eta_{o\alpha} = 0.0144 \quad ; \quad \alpha = w_x$$

$$\eta_{o\alpha} = 0.0265 \quad ; \quad \alpha = w_y \tag{4.11}$$

$$\eta_{o\alpha} = 0.0962 \quad ; \quad \alpha = w_z \quad .$$

These values of reduced frequencies specifically pertain to the neutral atmospheric boundary layer and are described in greater detail in Section 4.3.2.

The turbulence intensity, σ_{w_α}, for the neutrally stable atmosphere is related to u_{*_o} at the 10-m level by the following relationships:

$$\sigma_{w_x} = 2.5\, u_{*_o} \quad ; \quad \sigma_{w_y} = 1.6\, u_{*_o} \quad ; \quad \sigma_{w_z} = 1.3\, u_{*_o} \quad . \tag{4.12}$$

Utilizing the expression for u_{*_o} given in Section 3.3.2,

$$\frac{u_{*_o}}{\overline{W}_{h_{ref}}} = \frac{\kappa}{\ell n\left(\frac{h_{ref} + z_o}{z_o}\right) + \psi\left(\frac{h_{ref}}{L}\right)} \quad , \tag{4.13}$$

the turbulence intensity for the longitudinal, lateral, and vertical turbulent fluctuations in a neutral atmosphere [i.e., $\psi(h_{ref}/L) = 0$] can be reduced to

$$\sigma_{w_\alpha} = C'_\alpha \frac{\kappa\, \overline{W}_{h_{ref}}}{\ell n\left(\frac{h_{ref} + z_o}{z_o}\right)} \quad . \tag{4.14}$$

where C'_α is the empirically determined constant in equation (4.12).

The turbulence intensities can therefore be described in terms of the mean wind speed at the prescribed reference height [which is generally chosen as 10 m (30 ft) throughout this report] and for the surface roughness, z_o, which is specific to the site. Expressing W_h in terms of $\overline{W}_{h=10\ m}$ by

$$W_h = W_{h=10\ m}\ \ell(h/z_o + 1)/\ell n(10/z_o + 1) \quad , \tag{4.15}$$

introducing this expression together with equation (4.14) into equation (4.10), and carrying out the appropriate algebra gives equations (4.1), (4.2), and (4.3), respectively. The recommended value of z_o to be used in equation (4.14) is $z_o = 1$ m. Higher values of z_o create higher turbulence fluctuations and, since $z_o = 1$ m is a relatively high value, this assumption is considered conservative for design. It should be noted that $z_o = 1$ m is characteristic of suburban and forest-like terrain, which some design philosophies may consider too large. However, it is recommended here to compensate for nonflat terrain effects and for the likelihood that suburban growth around large WTG's is a very real possibility.

Section 4.3 gives additional details from which turbulence spectra for other than neutrally stable atmospheric conditions can be determined. Also, the influence of height and surface roughness on the turbulence spectra, and the application of turbulence spectra to WTG design are described and examples given.

4.1.2.2 Discrete Gust Model

The discrete gust shapes given by equation (4.5) were determined by fitting a curve to the statistical gusts given by Camp [4.1]. Figure 4.1 illustrates the curve fit through a gust of 18-s duration. The figure represents the percentage of gusts of 14- to 18-s duration which at the given time on the horizontal axis have the magnitudes given on the vertical axis. For example, at 4-s, of all 14- to 18-s gusts, 50 percent have a magnitude of approximately 1.9 m s^{-1}, or less. Ninety percent have a magnitude of approximately 3.9 m s^{-1} or less, etc. The parameter, a, in equation (4.5) represents the fraction of time that the gust is increasing in magnitude (rise time) and 1-a represents the fraction of time in which the gust is decaying. The parameter ζ, is the

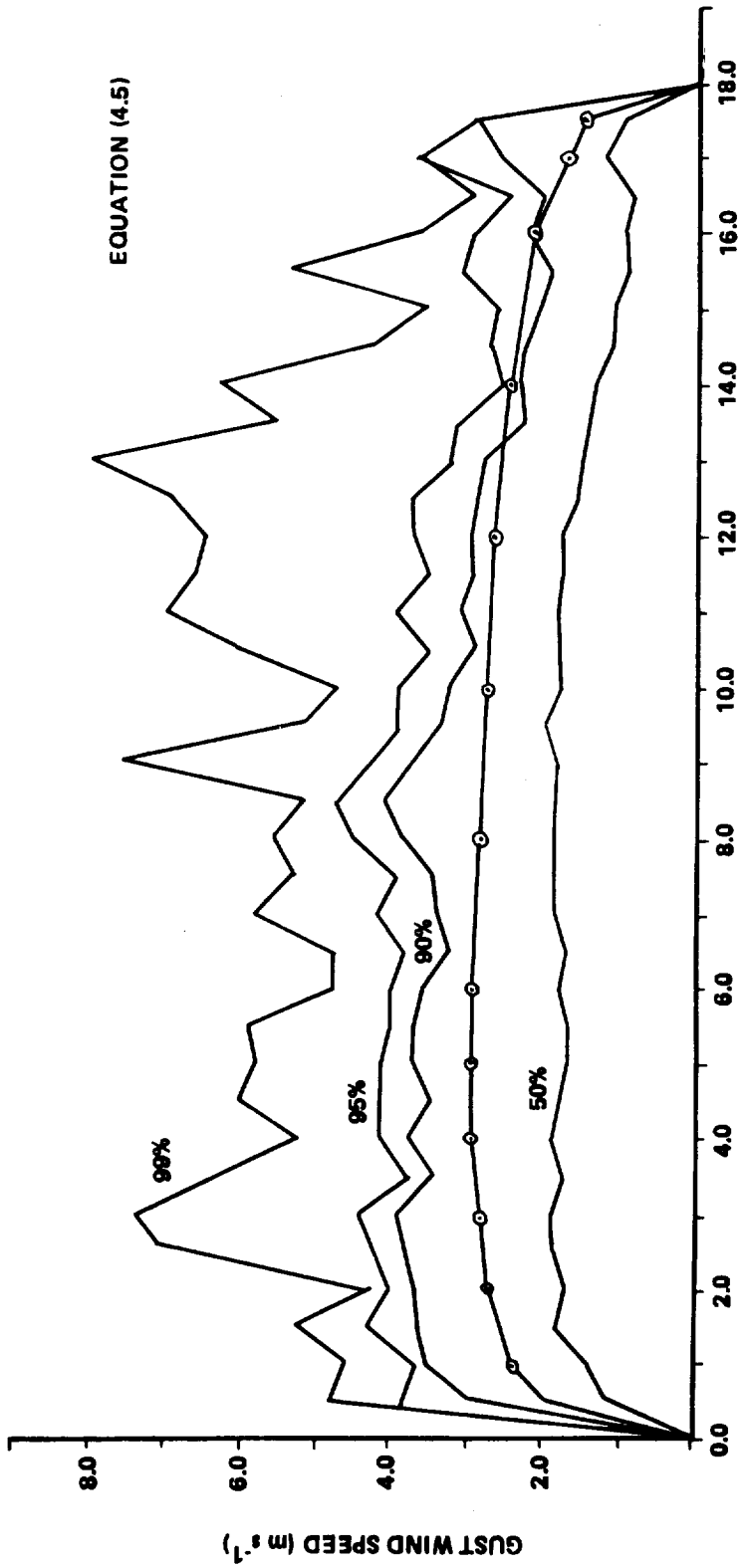

Figure 4.1 Comparison of gust shape with statistical gust based on 88 gusts having a time duration of 14 to 18 s occurring at the 18-m level.

ratio of time measured from the start of the gust, t, to the total duration or lifetime of the gust, τ. The parameter, W_i, is defined as the wind speed average over the period, τ, minus the mean wind speed, $W_i = W(\tau) - \overline{W}$. Its value is determined from the data given in Section 4.4. The gust magnitude is a function of the duration of the gust, τ, and of the height at which the gust is measured. The gust is also dependent upon mean wind speed. Figures are given in Section 4.4.1.2 from which W_i can be computed for general conditions of design interest. The representative values of W_i prescribed by equations (4.7), (4.8), and (4.9) were determined from figures in Section 4.4.1.2.

To describe how W_i in equation (4.7) is determined, Figure 4.2 is reproduced from Section 4.4 for illustrative purposes. From this curve the value of $\hat{F}_G$ which is equal to the gust factor, F_G, minus unity ($F_G - 1$) is determined for a number of elevations, h (see Table 4.1). The gust factor, F_G, is the ratio of the wind speed average over the period, τ, to the mean wind speed, $\overline{W}_h$, at the height, h. The factor, $\hat{F}_G$, is therefore equal to $(W(\tau) - \overline{W}_h)/\overline{W}_h$ and, hence, $W_i = \hat{F}_G \overline{W}_h$. The value of W_i at the height, h, is determined by correcting the mean wind speed given on the curve in Figure 4.2 to the appropriate height. Note the data in Figure 4.2 is for a specific mean wind speed of $\overline{W}_{h=10\ m} = 5\ m\ s^{-1}$, and, therefore, equation (4.7) is only valid for that wind speed. Other wind speed conditions can be determined from the complete set of gust factor curves given in Section 4.4.1.2. The standard power-law relationship recommended in Chapter 2 for correcting mean wind speed for height variations is used. However, in adjusting $W_{h=10\ m}$ to the height, h, the exponent $n = 0.14$ is used for values of h below 10 m, rather than 0.4, because Figure 4.2 was constructed on this basis. A curve fit of the tabulated data results in equation (4.7).

The preceding discrete gust model values are selected as described for general design purposes. However, it is recommended that the WTG designer become familiar with the procedures of computing gusts given in Section 4.4 which can be used for more detailed design purposes. The response of a structure to a discrete gust is highly dependent upon the rigidity of the structure and its response time. Moreover, the gusts' magnitudes specified in the summary section are effectively an average of the extremes and for structural

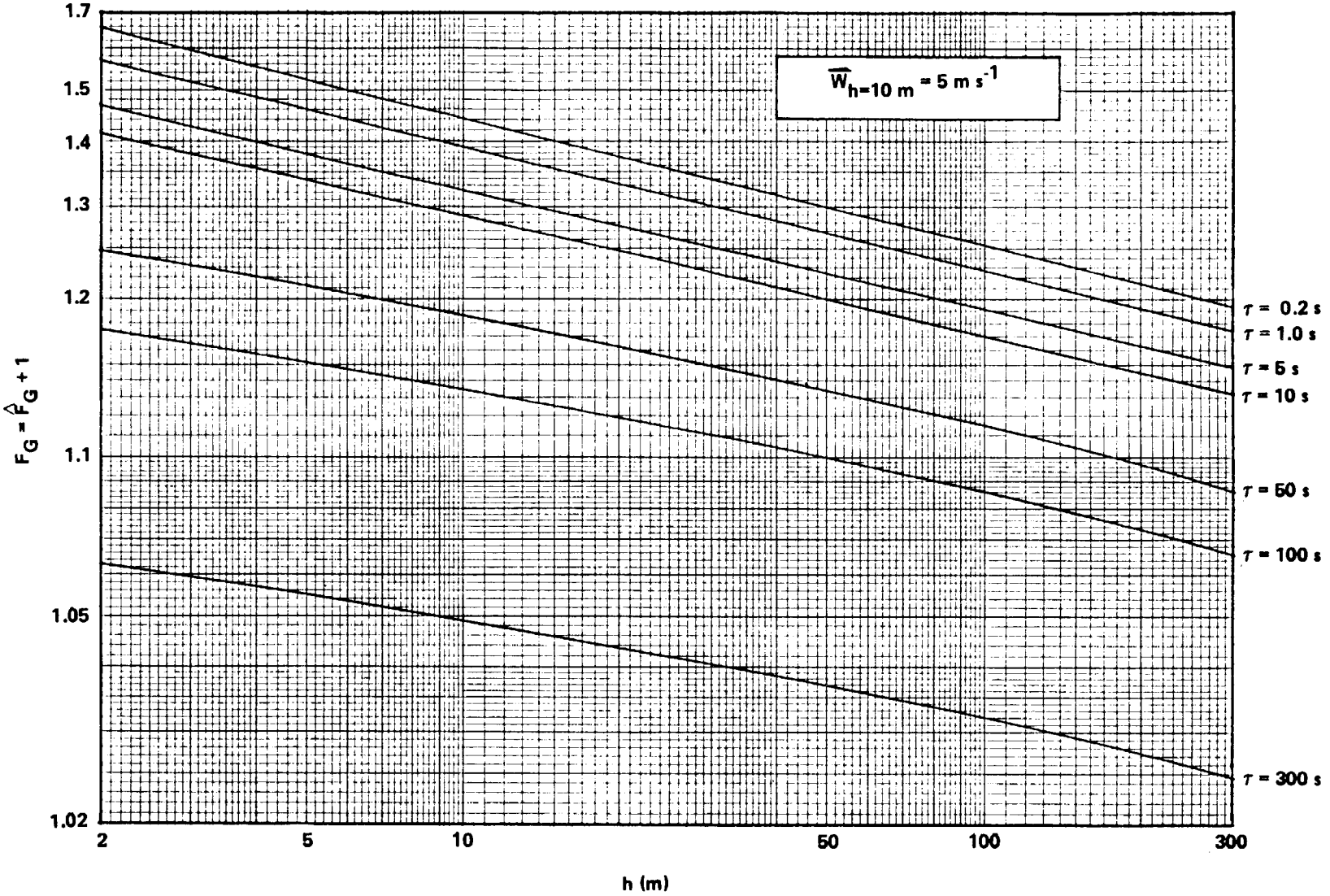

Figure 4.2 Gust factor: $F_G = W_h(\tau)/\overline{W}_h$.

TABLE 4.1 DATA FOR EVALUATION OF EQUATION (4.7)

h (m)	$\hat{F}_G$ (τ = 5 s)	$\overline{W}_h/\overline{W}_{h=10\ m}$ $(h/10\ m)^{0.14}$	$W_i/\overline{W}_{h=10\ m}$ ($W_{h=10\ m}$ = 5 m s^{-1})
2	0.497	0.798	0.397
5	0.428	0.908	0.388
20	0.337	1.102	0.371
60	0.276	1.285	0.355
300	0.205	1.610	0.330

design purposes where strength is a factor, a correction factor should be applied to the gust magnitudes to account for the extreme of the extremes. These correction factors are described with a step-by-step computational procedure outlined in Section 4.4.1.4. The preceding summary section is provided for quick reference to general design values. More detailed information pertaining to turbulence and gusts in the atmosphere is presented in Sections 4.2 through 4.6.

Detailed Computational Procedure and Working Data

4.2 Introduction

4.2.1 Influence of Turbulence

Turbulence will affect both the fatigue strength and the structural strength of a wind turbine generator. Fatigue strength is a function of routine or daily turbulence inputs which provide a continuous dynamic loading of the rotor and the structure itself. Methods of analyzing continuous turbulence input generally rely upon the spectral model. The spectral model, however, is applicable only to a system of equations which can be linearized. Section 4.3 of this chapter describes the spectral method of analyzing turbulence.

Spectral models require information on the spectral properties of the atmospheric turbulence which for engineering evaluation generally require mean wind speed and surface roughness at the site. Thus, in addition to the spectrum of the wind, one requires the temporal distribution of mean wind speeds given in

Section 2.4. Generally, it is sufficient to carry out turbulence analyses only for neutral atmospheric conditions. However, if a large part of the turbulence analysis is to be carried out for stable or unstable atmospheric conditions, one requires a distribution of a representative stability parameter as described in Section 3.3.2.

The structural strength of a wind turbine generator is influenced by extreme values which occur in the turbulence. For analysis of extreme values, one generally resorts to a gust model. The analysis in this case is carried out by analyzing the response of the system to the largest gust that the system is likely to encounter in its useful lifetime. The input to the system is therefore discrete rather than continuous and provides a transient response. The required gust information for carrying out such an analysis is the duration of the gust, its magnitude, and its buildup and decay rate which are expressed in terms of the shape of the gust. Section 4.4 provides data on discrete gusts.

A third method of analyzing a machine's interaction with the turbulent atmosphere is turbulence simulation. In this method an actual wind record is produced by either analog or digital filtering of a gaussian white noise input. The response of the system is then calculated in real time by solving the equations of motion with the random signal as the wind input. This method incorporates the best features of both the spectral and the gust models previously described. The output from this analysis is a simulation of the actual dynamic response of the system. The drawback to the turbulence simulation approach is that it requires an elaborate computer code and hence a lengthy computational procedure.

It is therefore recommended in designing a system for both fatigue and structural strength in the turbulent atmosphere that quick initial design be carried out with the spectral and gust models, respectively, and that the final design be evaluated using the turbulence simulation technique.

In addition to influencing fatigue and structural strength, turbulence will also have an input to the design of the system controls. Both gust and spectral models will have application for certain control features. Shutdown and safety controls will be influenced by the extremes occurring in the wind field such as peak gusts and their buildup rate; whereas, directional and pitch rate controls will be influenced by continuous turbulence.

The power output of the wind turbine generator conceivably may be influenced by continuous turbulence inputs. However, the authors are unaware of any analysis of the sensitivity of a wind turbine generator output to fluctuations in the wind input.

4.2.2 Models of Turbulence

Turbulence models can be classified as one-, two-, or three-dimensional models. One-dimensional models assume that the typical length scale of the turbulent fluctuations is sufficiently large that the rotor is entirely engulfed by the gusts and thus the components of the turbulent wind are uniform across the entire expanse of rotor or supporting structure. This is illustrated in Figure 4.3. In this manual the definition "one-dimensional" does not reflect the number of components of wind speed that are included in the analysis. For example, the longitudinal and the lateral velocity component which both can contribute to the drag and life on the rotor will be considered one-dimensional turbulence, providing that the fluctuations are uniform over the entire span of the system. Two- and three-dimensional turbulence are therefore defined as turbulence of sufficiently small length scale that variations in fluctuations of the wind across the wind energy conversion machine must be taken into account. Figure 4.4 illustrates three-dimensional turbulence.

Nonuniform gusts across the span of the structure cause antisymmetric and higher frequency modes to become excited which are not excited with uniform spanwise gusts. Analyses of these gusts call for multirandom inputs rather than single inputs and require that cross spectra between individual inputs as well as the individual spectra be taken into account. Section 4.6 briefly describes two- and three-dimensional turbulence inputs.

As noted, turbulence models can also be classified as spectral models, discrete gust models, or turbulence simulation models. The spectral model requires as input the spectrum of the turbulence $\phi_{W_\alpha}(\hat{n})$ and the frequency response function of the system under analysis, $H(\hat{n})$. As outputs, the spectral model provides the root mean square value, σ_x, of the quantity, x, under investigation; i.e., x can be a bending moment, a rotation, power, etc. Additionally, the number of times per unit time, N_x, a fluctuation in the quantity, x, exceeds a prescribed value, x_p, is provided by this model and can be used for fatigue analysis.

The discrete gust model requires as input, gust magnitude, duration, and shape. As output, the gust model provides a transient response to a discrete input from which the maximum magnitude of the response and the rate at which the load is applied can be determined.

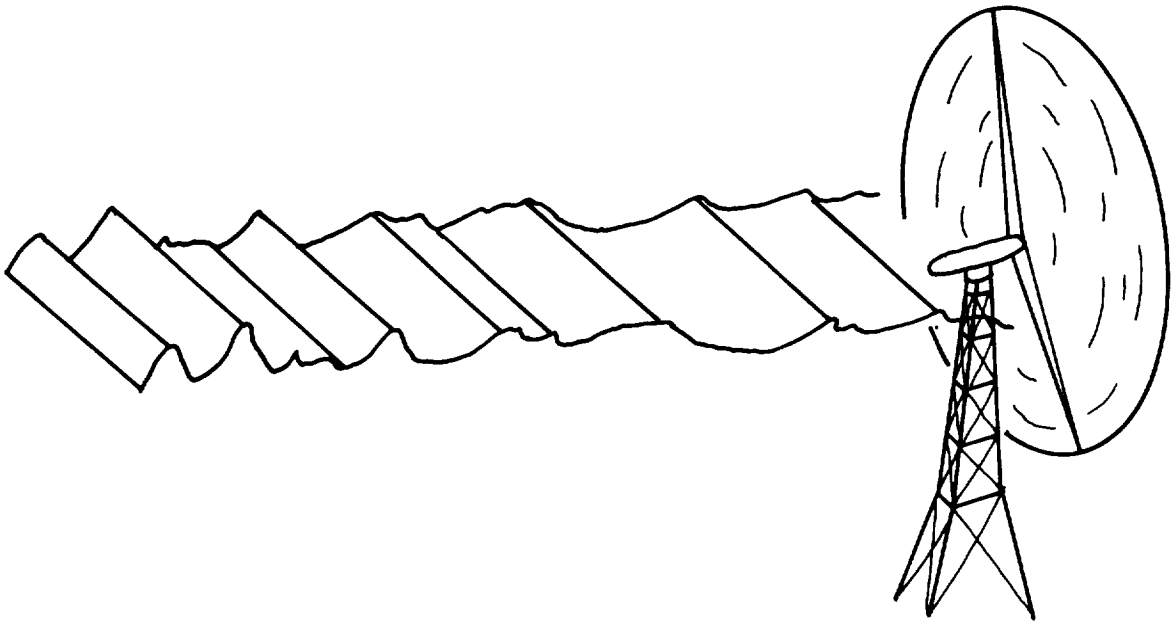

Figure 4.3 One-dimensional turbulence.

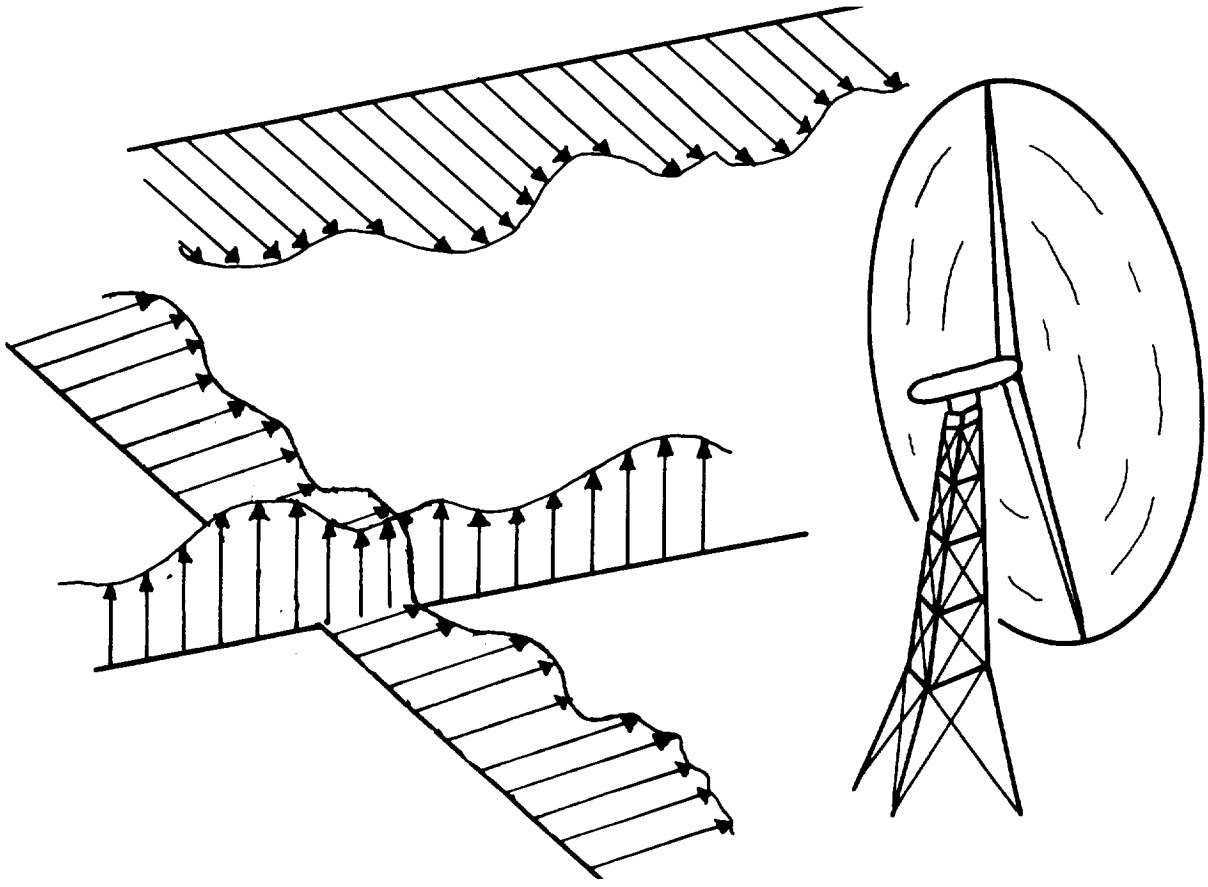

Figure 4.4 Three-dimensional turbulence.

The sophisticated turbulence simulation scheme requires as inputs the spectrum of the turbulence and, depending on the model, the distribution of wind speed fluctuations in the atmosphere. As outputs, one obtains the fluctuating transient response of the system from which all of the quantities computed by the other two models can be determined. For example, the time history output of the system is a simulation of an actual wind speed time history for which the number of crossings of the signal of a prescribed value of wind speed can be statistically evaluated, the peak response which corresponds to the magnitude of the extremes in the system output can be found, and many other output features of importance to design can be determined.

The spectral model is described in Section 4.3, the gust model is described in Section 4.4, and turbulence simulation schemes are described in Section 4.5. All of these descriptions pertain initially to the one-dimensional analysis. Section 4.6 provides information on two- and three-dimensional turbulence analyses.

4.3 Spectral Models

4.3.1 Basic Relationships

The basic relationships between spectra of atmospheric turbulence and the spectra of structure or rotor response such as motions, deformations, loads, etc., are contained in the following relationship, which is general for one velocity component. (Note: This expression is easily extended to three components of velocity.)

$$\phi_x(\hat{n}) = \phi_{11}(\hat{n})H_1(\hat{n})H_1^*(\hat{n}) + \phi_{22}(\hat{n})H_2(\hat{n})H_2^*(\hat{n}) + \ldots$$

$$+ 2\,\mathrm{Re}[\phi_{12}(\hat{n})H_1^*(\hat{n})H_2(\hat{n}) + \phi_{13}(\hat{n})H_1^*(\hat{n})H_3(\hat{n})$$

$$+ \phi_{23}(\hat{n})H_2^*(\hat{n})H_3(\hat{n}) + \ldots] \qquad (4.16)$$

where

$\phi_x(\hat{n})$ = power spectrum of the system response of the quantity x

$\phi_{ij}(\hat{n})$ = two-point spectrum of turbulence velocities at center of the ith and the jth segmented areas of the system

$H_i(\hat{n})$ = frequency-response function of x due to a unit sinusoidal gust velocity over the segment of the surface associated with the ith point

$H_i^*(\hat{n})$ = complex conjugate of $H_i(\hat{n})$

Re = the real part.

Equation (4.16) is general within linear theory. It can be reduced to a simpler form depending on whether the assumed turbulence model is two-dimensional (nonuniform gust variation across the span) or one-dimensional (uniform gust velocities spanwise).

For one-dimensional, isotropic turbulence, the equation reduces even further (i.e., when the scale of turbulence is larger relative to the scale of the structure or rotor and independent of direction). For this case

$$\phi_x(\hat{n}) = |H(\hat{n})|^2 \phi_{\substack{w \\ \alpha}}(\hat{n}) \quad . \tag{4.17}$$

The basic assumptions contained in equation (4.17) are:

1) A linear system

2) One-dimensional homogeneous turbulence.

Figure 4.5 is a schematic illustration of equation (4.17). The upper figure illustrates a typical spectrum for the turbulent atmosphere, the middle figure illustrates a typical response function for a fictitious system, and the lower figure illustrates the product of the upper curve and the middle curve. This lower figure represents the spectrum of the output, $\phi_x(\hat{n})$, and describes how the average squared value of x is distributed with frequency. The peak in $\phi_x(\hat{n})$ occurs where the product of the spectrum of the wind and the frequency response function squared, $H(\hat{n})^2$, has maxima. This illustrates that it is not meaningful to discuss turbulent inputs without reference to the frequency

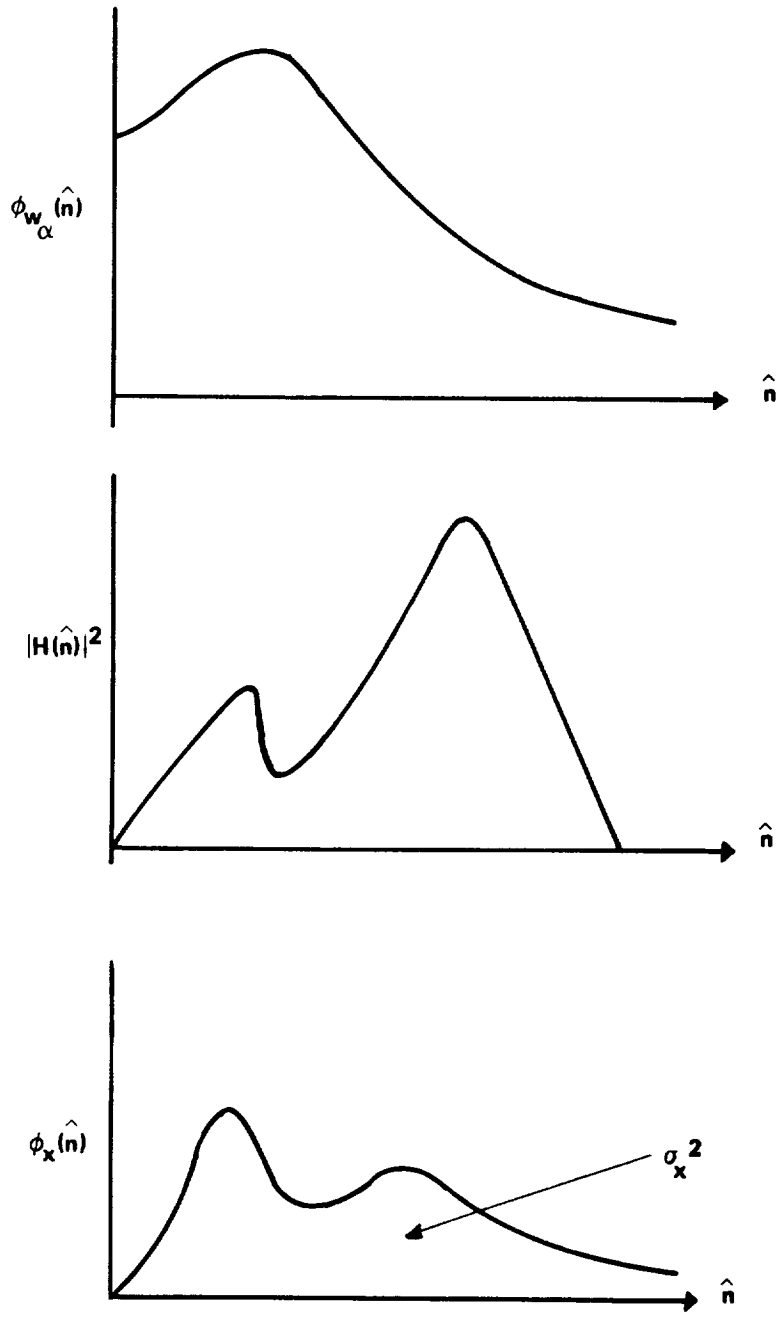

Figure 4.5 Power spectrum of WTG response quantity, x.

response function of the system. If, for example, the system is responsive at a frequency where the atmospheric turbulence has little or no energy, then the system will be insensitive to fluctuations in the wind. However, if the system has its maximum response at a frequency which corresponds with the peak or is close to the peak in the turbulence energy spectrum, then the system will be highly responsive to turbulence and must be designed accordingly.

Integrating under the lower curve, $\phi_x(\hat{n})$, of Figure 4.5 provides the variance σ_x^2 of the quantity x about its mean value. The square root of the variance provides the root mean square or one standard deviation of the system response. Thus, the design load of the system can be specified as to the mean, plus or minus the desired number of standard deviations.

The number of times the system exceeds a prescribed value, x_p, is given by

$$N_x = N_o e^{-x_p^2/2\sigma_x^2} \tag{4.18}$$

and can be computed once σ_x is known. N_o appearing in equation (4.18) is the average number of times per unit time that the system response x(t) crosses the value zero with positive slope. The value of N_o is given by

$$N_o = \frac{1}{\sigma_x}\left[\int_o^\infty \hat{n}^2 \phi_x(\hat{n})\, d\hat{n}\right]^{1/2} . \tag{4.19}$$

Thus from the results of a spectral analysis, the statistical design strength is given in terms of σ_x and the fatigue strength of the system can be computed from N_x, the number of times the system exceeds a prescribed fatigue value, x_p.

The following section describes the turbulence input required to carry out a spectral analysis as outlined in the foregoing. It must be stressed again, however, that a meaningful design analysis can only be carried out when the system response function, $H(\hat{n})$, is known along with the data provided in Section 4.3.2.

4.3.2 Turbulence Spectra

4.3.2.1 Neutral Atmosphere

Analytical models for spectra of the longitudinal, lateral, and vertical components of turbulence are given in References 4.2 and 4.3. Kaimal [4.3] proposes

$$\frac{\hat{n}\phi_{w_\alpha}(\hat{n})}{\sigma^2_{w_\alpha}} = \frac{0.164\,\eta/\eta_{o\alpha}}{1 + 0.164(\eta/\eta_{o\alpha})^{5/3}} \tag{4.20}$$

where

$$\eta = \frac{\hat{n}h}{\overline{W}_h} \quad . \tag{4.21}$$

These equations were developed from measurements only to a height of 23 m. However, comparison of the equation with data measured at 40, 60, 80, and 150 m [4.4,4.5] shows good results. In equation (4.20) $\overline{W}(h)$ is the quasi-steady wind speed at height, h, and α refers to the component of fluctuating velocity which may be either w_x, the longitudinal component, w_y, the lateral component, or w_z, the vertical component, all measured relative to the direction of the mean wind.

For conditions of neutral stability, the following values of $\eta_{o\alpha}$ are recommended:

$$\eta_{o\alpha} = 0.0144 \quad ; \quad \alpha = w_x$$

$$\eta_{o\alpha} = 0.0265 \quad ; \quad \alpha = w_y$$

$$\eta_{o\alpha} = 0.0962 \quad ; \quad \alpha = w_z \tag{4.22}$$

where σ_{w_α} is called the intensity, the standard deviation or the rms value of the turbulence fluctuation of the α component. A method of predicting σ_{w_α} is given in Section 4.3.2.2.

4.3.2.2 Intensity of the Turbulent Fluctuation

Figure 4.6, taken from Reference 4.6, shows σ_{w_z}, the turbulence intensity of the vertical wind speed component nondimensionalized with u_*, plotted as a function of nondimensional altitude, h/L. For neutral conditions, h/L = 0, the ratio of vertical turbulence intensity to the friction velocity u_* is 1.3. At h/L = 1.22, the turbulence intensity vanishes [4.6] as the atmospheric boundary layer becomes so stable that essentially laminar flow is achieved. In general, σ_{w_z}/u_* increases with decreasing stability.

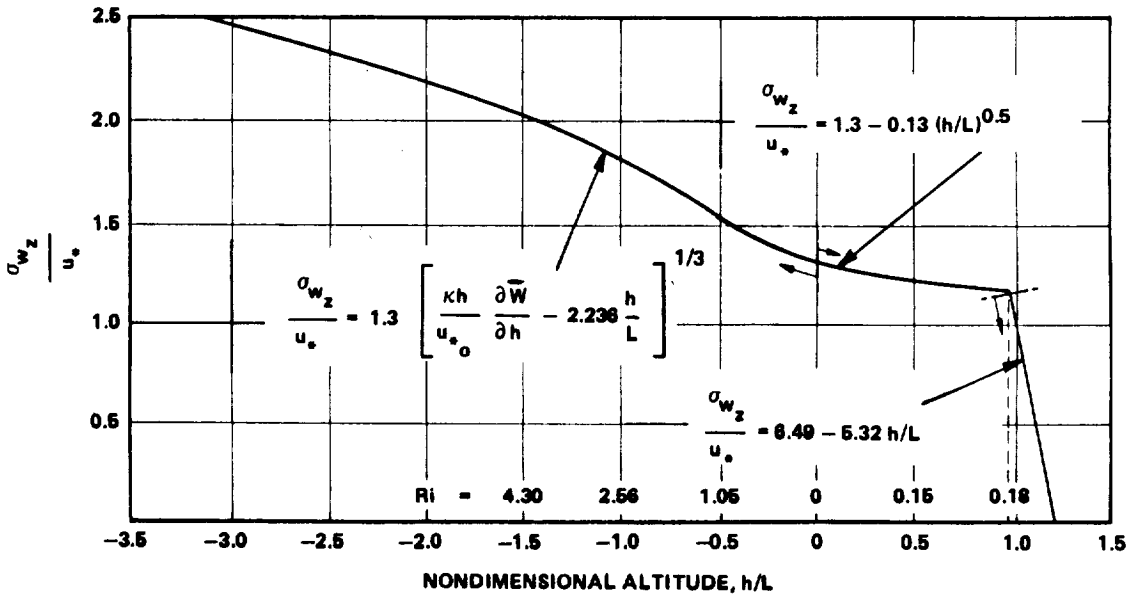

Figure 4.6 Vertical turbulence intensity.

From Figure 4.6 which is a plot of

$$\sigma_{w_z}/u_* = 1.3[(\kappa h/u_{*_o})\,\partial\overline{W}_x/\partial h - 2.236\,h/L]^{1/3} \quad ; \quad h/L < 0$$

$$\sigma_{w_z}/u_* = 1.3 - 0.13(h/L)^{0.5} \quad ; \quad 0 \le h/L < 0.95 \qquad (4.23)$$

$$\sigma_{w_z}/u_* = 6.49 - 5.32\,h/L \quad ; \quad 0.95 \le h/L < 1.22$$

the value of σ_{w_z}/u_* can be selected for an atmospheric stability condition and σ_{w_z} evaluated from equation (4.23) by multiplying by u_*. The value of u_* is found as described in Section 3.3.2.

It is observed from the above that under neutral conditions σ_{w_z} is dependent upon the mean wind speed, $\overline{W}_{h_{ref}}$, and terrain conditions through the surface roughness parameter, z_o. Experimental results indicate that the vertical gust component is primarily a function of small-scale roughness features; whereas the lateral and longitudinal components are influenced by large-scale surface features.

No satisfactory mathematical description of how σ_{w_x} and σ_{w_y} vary with large-scale features nor how they vary with atmospheric stability is available. Barr, et al. [4.6] propose that the ratio $\sigma_{w_x}/\sigma_{w_z}$ be treated as a function of altitude only, according to the following relationship:

$$\sigma_{w_x}/\sigma_{w_z} = \begin{cases} [0.177 + 0.832\,h/h_i]^{-0.4} & ; \quad h < h_i \\ 1.0 & ; \quad h > h_i \end{cases} \qquad (4.24)$$

h_i = 600 m (2000 ft) .

Reference 4.6 also proposes that $\sigma_{w_y}/\sigma_{w_z} = \sigma_{w_x}/\sigma_{w_z}$. This relationship does not result in satisfactory agreement with equation (4.20), however, and the relationship

$$\sigma_{w_y}/\sigma_{w_z} = \begin{cases} [0.583 + 0.417\, h/h_i]^{-0.8} & ;\quad h < h_i \\ 1.0 & +\quad h > h_i \end{cases} \tag{4.25}$$

is proposed herein. Equation (4.25) is developed identically to equation (4.24) but assumes that σ_{w_y} is less than σ_{w_x} near the ground. The assumption is that for neutral conditions $\sigma_{w_x}/\sigma_{w_y}/\sigma_{w_z} = 2.6/2.0/1.3$, which is consistent with a number of reported results.

Values of $\sigma_{w_x}/\sigma_{w_z}$ and $\sigma_{w_y}/\sigma_{w_z}$ are plotted in Figure 4.7 as a function of dimensionless height to facilitate computation of these values. Inspection of equations (4.23), (4.24), and (4.25) shows that for the neutral atmosphere at the 10-m level (where u_* is essentially u_{*_o}):

$$\sigma_{w_x} = 2.5\, u_{*_o} \quad ; \quad \sigma_{w_y} = 1.6\, u_{*_o} \quad ; \quad \sigma_{w_z} = 1.3\, u_{*_o} \quad . \tag{4.26}$$

Example 4.1: The values of σ give a measure of the standard deviation of the wind from the mean value. In Figure 4.8, obtained through personal communication with D. Spera, measurements of the stress in the Mod 1 rotor blade are compared with theory. The theoretical model assumes a constant wind speed. To estimate the one standard deviation error bands in the bending moment shown on the figure, one simply compares the results with the theoretical model based on a wind speed of $\overline{W} \pm \sigma_{w_x}$.

Consider $\overline{W}$ = 30 mph (13.4 m s^{-1}) at h_H = 100 ft (30 m).

From equation (4.13), u_{*_o} = 2.10 mph (0.94 m s^{-1}) assuming

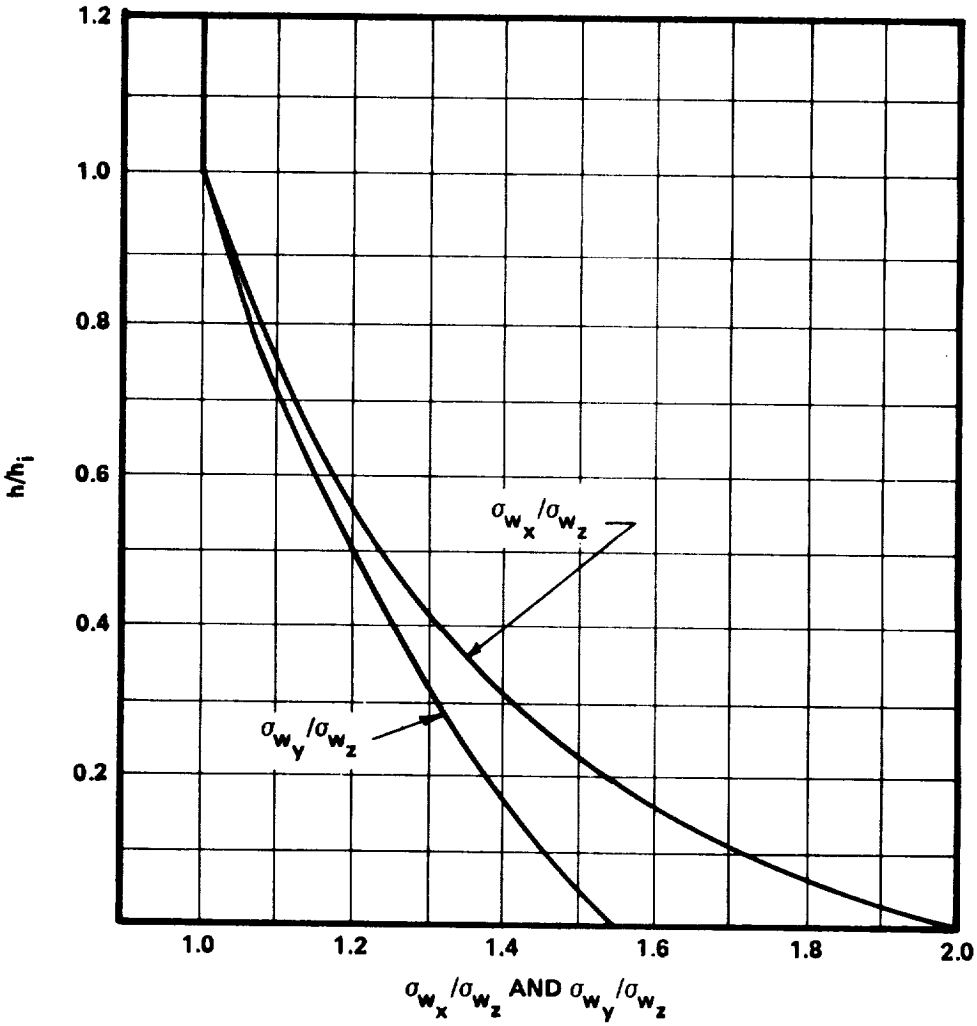

Figure 4.7 Longitudinal and lateral turbulence intensity.

z_o = 0.22 ft (0.1 m). Substituting u_{*_o} into equation (4.26) gives σ_{w_x} = 4.8 mph (2.1 m s^{-1}). The wind speed which should give one positive standard deviation of the stress is thus 34.8 mph (15.5 m s^{-1}). Projecting that wind speed back to the 30 mph (13.4 m s^{-1}) value on the horizontal axes as shown in Figure 4.8 shows good agreement with the measured data.

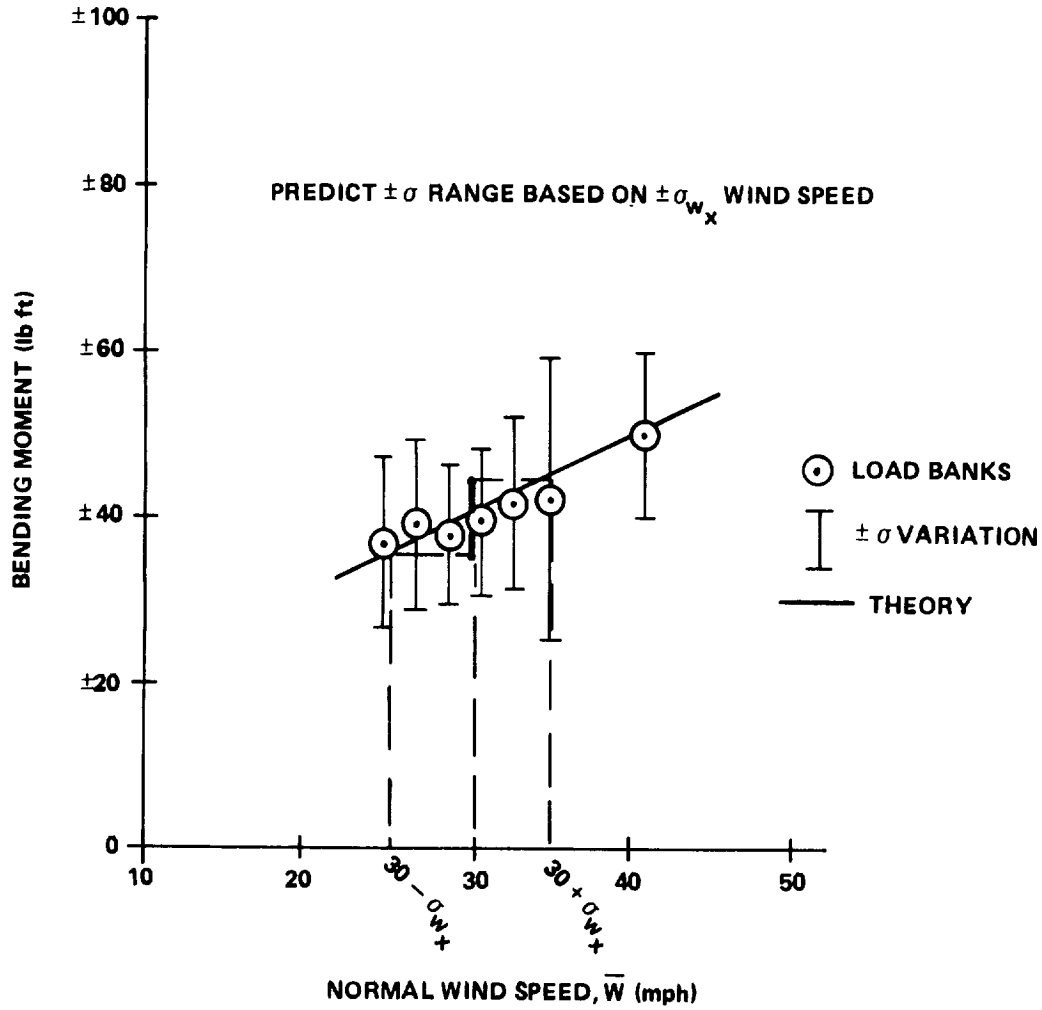

Figure 4.8 Bending moments compared with theory based on mean wind speed plus or minus one standard deviation, i.e., $\overline{W} \pm \sigma_{w_x}$.

4.3.2.3 Evaluation of Turbulence Spectra for the Neutral Atmosphere

The procedure for evaluating the turbulence energy spectra for the neutral atmosphere is as follows:

1) Select the value of $\eta_{o\alpha}$ corresponding to the longitudinal, lateral, or vertical turbulence component of interest, equation (4.22).

2) Introduce the value of $\eta_{o\alpha}$ into equation (4.20).

3) From equation (4.26) find the relationship between the turbulence intensity and u_* for the wind component under investigation.

4) From Figure 3.4, Section 3.3, determine the u_{*_o} at the mean wind speed and surface roughness conditions for the given site.

5) Determine u_* from Figure 3.5, Section 3.3.

6) Compute the turbulence intensity from equation (4.26) and determine the turbulence spectrum of wind as a function of $\hat{\zeta} = \eta/\eta_{o\alpha}$.

The spectrum of the turbulence thus computed can be multiplied by the square of the absolute value of the frequency response function for the system being analyzed. The spectral form of the system output is then defined as described in Section 4.3. Sections 4.3.2.4 and 4.3.2.5 which follow illustrate computation of the wind spectrum and the application of the spectral model.

Example 4.2: As an example computation of a turbulence spectrum, consider a wind turbine of hub height $h_H = 20$ m (65 ft), located near Amarillo, Texas, on a site of surface roughness $z_o = 0.05$ m (0.16 ft). It is desired to determine the turbulence spectrum based on annual mean wind speed. The annual mean wind speed at 10 m (33 ft) for $k = 2.26$ which has been adjusted to 20 m (65 ft) with Figure 2.29 is from Figure 2.26, Section 2.4, $\overline{W}/c = 0.89$. The value of $c = 6.20$ m s^{-1} (13.9 mph) adjusted to 20 m (65 ft) is 7.17 m s^{-1} (16.0 mph) and $\overline{W} = 6.38$ m s^{-1} (14.3 mph).

The value $\eta_{o\alpha}$ for neutral conditions is given by equation (4.22) as $\eta_{ox} = 0.0144$. Thus,

$$\frac{\hat{n}\phi(\hat{n})}{\sigma_{w_x}^2} = \frac{11.4\,\eta}{1.0 + 192.4\,\eta^{5/3}} \qquad (4.27)$$

where $\sigma_{w_x} = 2.6\, u_*$. The value of u_{*_o} from Figure 3.3 is 0.43, and the adjusted value of u_* from Figure 3.4 becomes 0.42. Finally, substituting η as $h\hat{n}/\overline{W}_h$ into equation (2.25) and carrying out the algebra gives

$$\phi_{w_x}(\hat{n}) = \frac{42.6}{1.0 + 1291.9\,\hat{n}^{5/3}} \quad . \tag{4.28}$$

Example 4.3: As an example application of the spectral model, consider the rotational fluctuation $\omega'(t)$ about the mean rotation of a simple unloaded rotor having constant lift and drag. Assume that only the longitudinal wind speed influences the rotor. The frequency transfer function for this rotor, $H(\hat{n})$, is given in Reference 4.7 as

$$H(\hat{n}) = \left[RI_2\left(1 + (M_2 I_1 \hat{n}/I_2)^2\right)^{1/2} \right]^{-1} \quad . \tag{4.29}$$

The power density spectrum for $\omega'(t)$ is thus given by

$$\phi_{\omega'}(\hat{n}) = \left[RI_2^2\left(1 + (M_2 I_1 \hat{n}/I_2)^2\right) \right]^{-1} \phi_{w_x}(\hat{n}) \quad . \tag{4.30}$$

Utilizing $\phi_{w_x}(\hat{n})$ from equation (4.20) for the longitudinal turbulence component gives the power density spectrum for $\omega'(t)$ as

$$\hat{n}\phi_{\omega'}(\hat{n}) = \frac{\psi_1 \zeta}{[1 + (\psi_2 \zeta)^2][1 + \psi_3 \zeta^{5/3}]} \tag{4.31}$$

where

$$\zeta = \eta/\eta_{o\alpha} \tag{4.32}$$

$$\psi_1 = \frac{0.164\ \sigma_{w_x}^2}{(RI_2)^2} \tag{4.33}$$

$$\psi_2 = \frac{M_2 I_1 \eta_{o\alpha}\ \overline{W}_h}{I_2 h} \tag{4.34}$$

$$\psi_3 = 0.164 \quad . \tag{4.35}$$

A plot of $\hat{n}\phi_{\omega'}(\hat{n})/\psi_1$ is given in Figure 4.9 for a range of values of ψ_2. This figure shows how the rotational fluctuations $\omega'(t)$ increase and also become more sensitive to higher frequencies as ψ_2 decreases. The value of ψ_2 increases with rotor mass, the characteristic frequency, η_{ox}, of $\phi_{w_x}(\hat{n})$, the mean wind speed, and the ratio of mean wind speed to rotor tip speed; and decreases with the mean lift force on the rotor. Thus, assessment of these design parameters is possible.

The value of $\sigma_{\omega'}$, is determined from the area under the curve, i.e.,

$$\sigma_{\omega'} = \int_0^\infty \phi_{\omega'}(\hat{n})\, d\hat{n} \quad . \tag{4.36}$$

Table 4.2 provides values of $\sigma_{\omega'}$, for selected values of ψ_2, where

$$\psi_1' = \sqrt{\psi_1 \overline{W}_h \eta_{ox}/h} \quad .$$

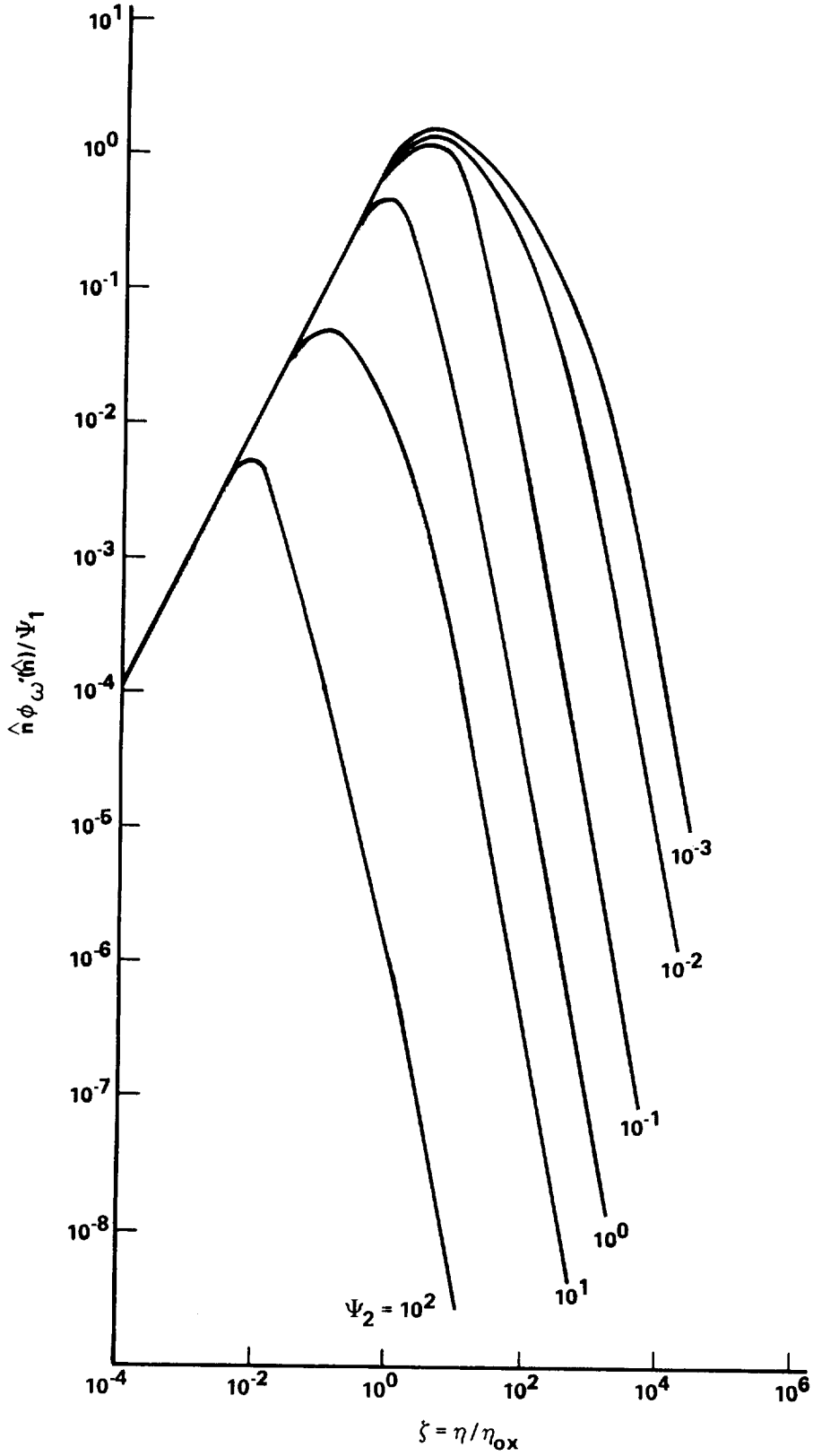

Figure 4.9 Power spectral density function for rotational fluctuations $\omega'(\hat{n})$.

TABLE 4.2 RMS VALUES OF $\omega'(t)$

ψ_2	$\sigma_{\omega'}/\psi_1'$
10^{-3}	2.41
10^{-2}	2.33
10^{-1}	1.95
10^{0}	1.09
10^{1}	0.39
10^{2}	0.13

The tabulated values of $\sigma_{\omega'}$ represent the magnitude of the rotational fluctuations which $\omega'(t)$ can be expected to exceed 32 percent of the time.

Interpretation of the results shown in Figure 4.9 as they relate to the influence of rotor mass on the fluctuations in rotational speed due to turbulence is as follows. ψ_2 is a function of mass and is larger for heavier rotors. One sees from the figure that for the largest value of ψ_2, the peak in the spectrum of the rotational fluctuations is shifted to the left, indicating that the system is becoming responsive at lower frequencies. The peak for the lowest value of ψ_2, however, is the farthest to the right, indicating that a light rotor responds at higher frequencies.

One can also compare the areas under the two curves which are proportional to the variance or square of the rms value of rotor speed about the mean value. The area under the curve for small ψ_2 is larger than the area under the curve for large values of ψ_2. This illustrates that the heavy rotor has smaller deviations from the mean rotational speed and is less responsive to fluctuations in the wind. That is, due to high inertia, a heavy rotor does not respond to small gusts but has sufficient angular momentum to carry it through a typical wind disturbance, unless the disturbance occurs at very low frequencies. The lightweight rotor, however, responds significantly to fluctuations of a higher frequency which are more common in the wind and, therefore, shows more sensitivity to wind disturbances.

A complete discussion and interpretation of the results of the preceding example computation are given by Frost [4.7].

4.3.3 Influence of Mean Wind Speed Distribution

4.3.3.1 Continuous and Composite Turbulence Parameters

The turbulence intensity depends on the mean wind speed and, consequently, has some frequency distribution of its own. The wind turbine generator therefore is exposed to turbulence of various intensities for different periods of operation throughout its useful life, as illustrated in Figure 4.10. Thus, it "sees" effective periods of turbulence of different mean square intensity which in the limit become a continuously variable distribution of rms gust velocity. It is understood that the periods of different turbulence intensity are encountered in random fashion and not in succession, as illustrated.

A continuous distribution of σ_{w_α} can be obtained from the relationship of σ_{w_α} to the reference wind speed, $\overline{W}_{ref}$, and from the known Weibull mean wind speed distribution given in Section 2.4. The theory of functional transformations of random variables [4.8] is applied to arrive at the frequency distribution of σ_{w_α} given by

$$p(\sigma_{w_\alpha}) = \frac{1}{|A_\alpha|}\left\{\frac{k}{c}\left(\frac{\sigma_{w_\alpha}}{A_\alpha c}\right)^{k-1}\exp\left[-\left(\frac{\sigma_{w_\alpha}}{A_\alpha c}\right)^{k}\right]\right\} . \qquad (4.37)$$

The symbol A_α represents a function of h_{ref}, z_o, and L and is given by

$$A_z(h_{ref}, z_o, L) = \frac{\sigma_{w_z}/u_*}{\frac{1}{\kappa}\ell n\left(\frac{h_{ref}+z_o}{z_o}\right)} \qquad (4.38)$$

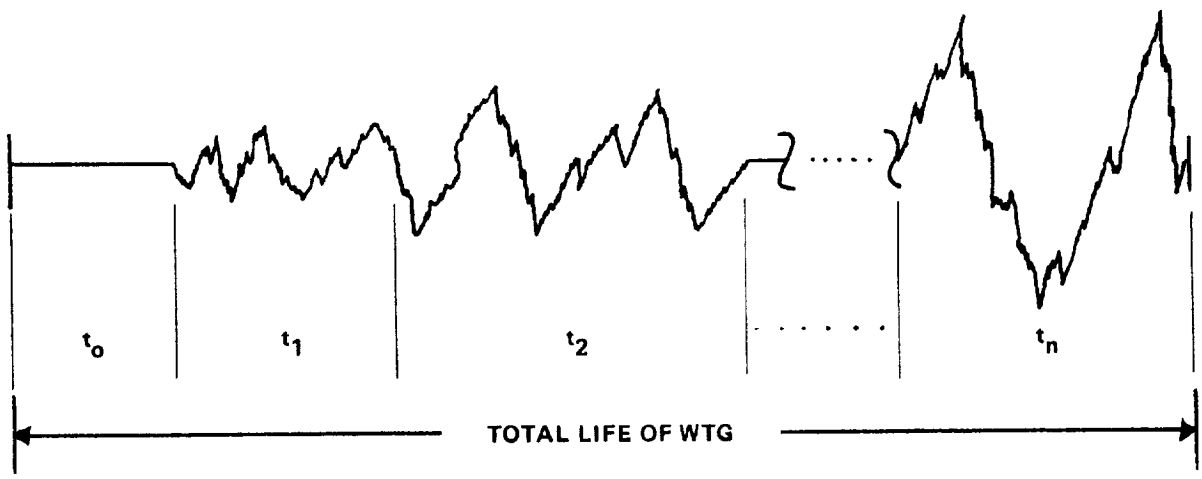

Figure 4.10 Different turbulence levels encountered for varying periods of lifetime of a WTG.

where σ_{w_z}/u_* is given by equation (4.23),

$$A_x(h_{ref}, z_o, L) = A_z(h_{ref}, z_o, L)\,[0.177 + 0.832\ h/h_i]^{-0.4} \quad , \qquad (4.39)$$

and

$$A_y(h_{ref}, z_o, L) = A_z(h_{ref}, z_o, L)\,[0.583 + 0.417\ h/h_i]^{-0.8} \quad . \qquad (4.40)$$

The utility of $p(\sigma_{w_\alpha})$ for fatigue analysis is to provide a design input for the number of times the wind exceeds a peak value or a dynamic system exceeds a particular peak load level due to turbulent gusts. For example, the average number of peaks in velocity fluctuation above w_{α_p} per unit time for a given value of σ_{w_α} is given by Houbolt, et al. [4.9] as

$$G(w_{\alpha_p}) = G_o \exp\left[-\left(w_{\alpha_p}^{\ 2}/2\ \sigma_{w_\alpha}^{\ 2}\right)\right] \qquad (4.41)$$

Note: For larger values of w_{α_p}, most, but not all, local maxima are immediately preceded by a positive crossing of the value w_{α_p}; thus, equation (4.41) can be interpreted as a good approximation to the number of peaks per unit time that are greater than w_{α_p} [4.10].

where α takes on x, y, z, and G_o is the average number of crossings with positive slope per unit time of the zero value of w_α. The value of G_o depends only on the turbulence spectrum shape and thus is the same for all turbulence intensities, i.e.,

$$G_o = \left[\frac{\int_o^\infty \hat{n}^2 \phi_{w_\alpha}(\hat{n})\, d\hat{n}}{\int_o^\infty \phi_{w_\alpha}(\hat{n})\, d\hat{n}} \right]^{1/2} . \qquad (4.42)$$

The total number of crossings of w_{α_p} is thus found by introducing $p(\sigma_{w_\alpha})$ and integrating over the probability distribution,

$$G\left(w_{\alpha_p}\right) = \int_o^\infty G_o\, p\left(\sigma_{w_\alpha}\right) \exp\left[-\left(w_{\alpha_p}^2 / 2\, \sigma_{w_\alpha}^2 \right) \right] d\sigma_{w_\alpha} . \qquad (4.43)$$

The above analysis assumes that turbulence has a Gaussian distribution which is a reasonable assumption in this case. Introducing $p(\sigma_{w_\alpha})$ into equation (4.43) and defining

$$\xi = \sigma_{w_\alpha} / cA_\alpha(h, z_o, L)$$

and

$$\hat{w}_{\alpha_p} = w_{\alpha_p} / cA(h, z_o, L)$$

gives

$$G(\hat{w}_{\alpha_p})/G_o = k \int_o^\infty \xi^{k-1} \exp\left[- (\xi^k + \hat{w}_{\alpha_p}{}^2/2\xi^2) \right] d\xi \quad . \qquad (4.44)$$

A plot of equation (4.44) is given in Figure 4.11.

In the development of equation (4.44), G_o has been taken as independent of mean wind speed. From equation (4.42), it appears that G_o is directly proportional to wind speed. However, the integration of equation (4.42) requires a definition of cutoff frequency, $\hat{n}_{co}$, which varies with wind speed such that G_o is effectively independent of the mean wind. This is discussed in detail by Frost [4.11] and shown experimentally by Ramsdell [4.12]. Figure 4.12 shows dimensionless values of the number of zero crossings with positive slope,

$$\hat{G}_o(\Lambda) = hG_o(\Lambda)/\eta_{o\alpha}\overline{W}_h \quad ,$$

as a function of the parameter

$$\Lambda = \overline{W}_h \eta_{o\alpha}/h\hat{n}_{co} \quad .$$

A slight dependence on wind speed is indicated, but this is sufficiently small that treating G_o as constant in the development of equation (4.44) is believed justifiable. Values of G_o[1] can be directly determined from Figure 4.12, although a representative value of $G_o = 0.30\ s^{-1}$ can be used as a good approximation.

The value of $\hat{n}_{co}$ is the cutoff frequency and is related to the characteristic frequency of the Kolmogoroff equilibrium range. Frost [4.11] express the relationship as

1. In evaluating G_o from Figure 4.12 an average wind speed over the period of interest should be used, i.e., for a yearly period use the annual mean wind speed.

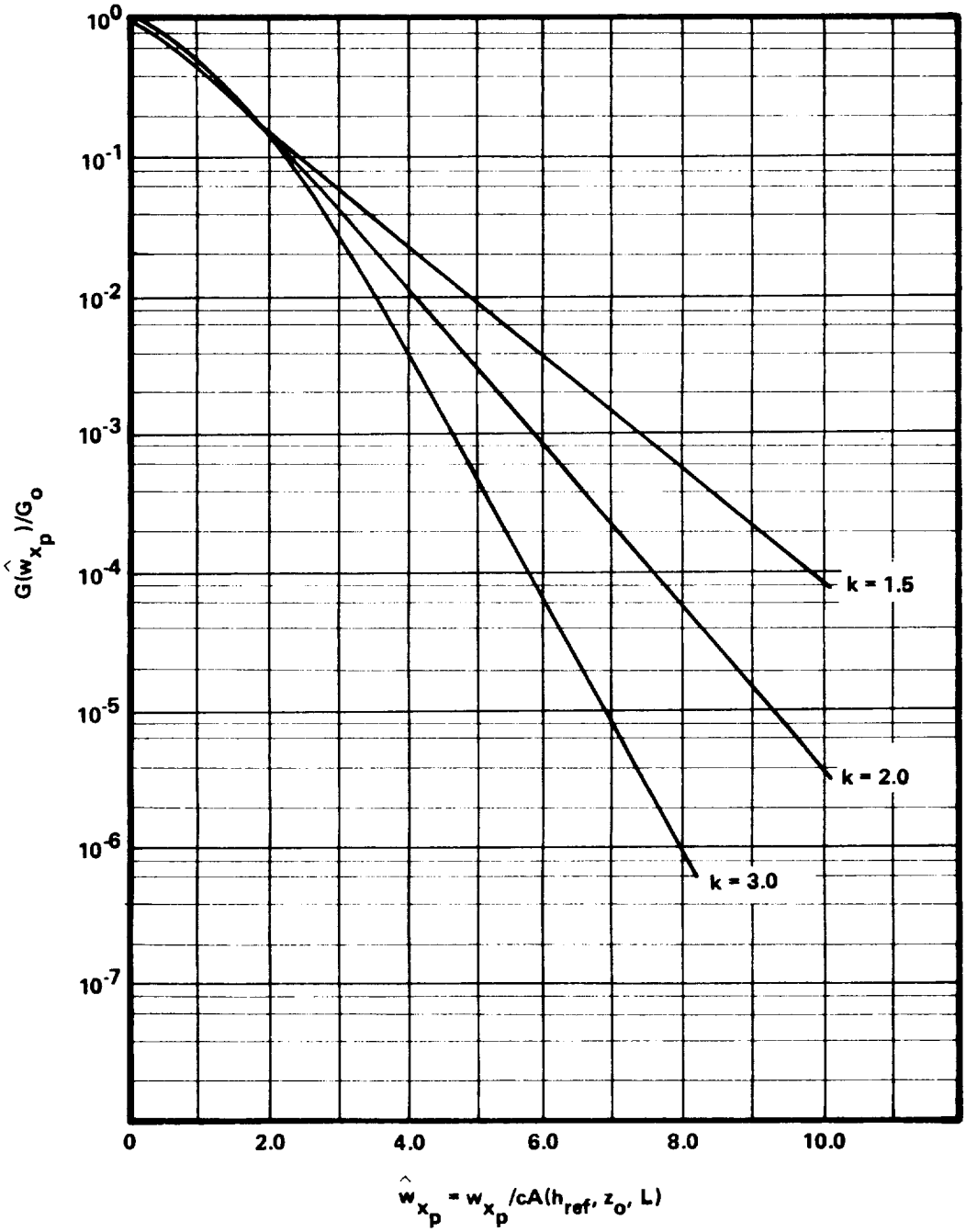

Figure 4.11 Ratio of number of longitudinal gust exceeding the value w_x per unit time to the number crossing zero with positive slope per unit time (assumes G_o independent of mean wind speed).

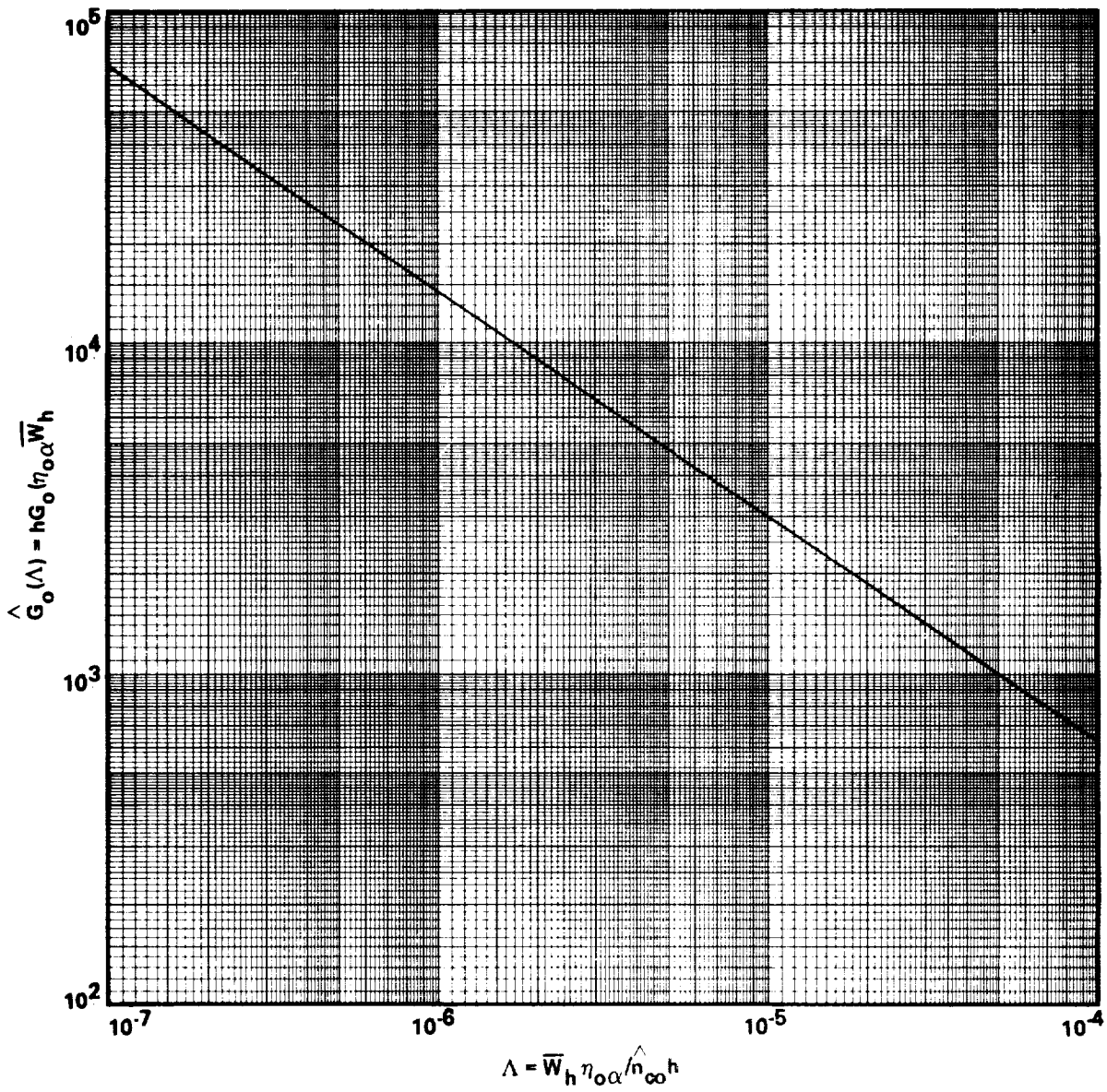

(a) VALUES OF ZERO CROSSINGS FOR Λ RANGE $10^{-7} - 10^{-4}$.

Figure 4.12 Values of zero crossings for selected Λ ranges.

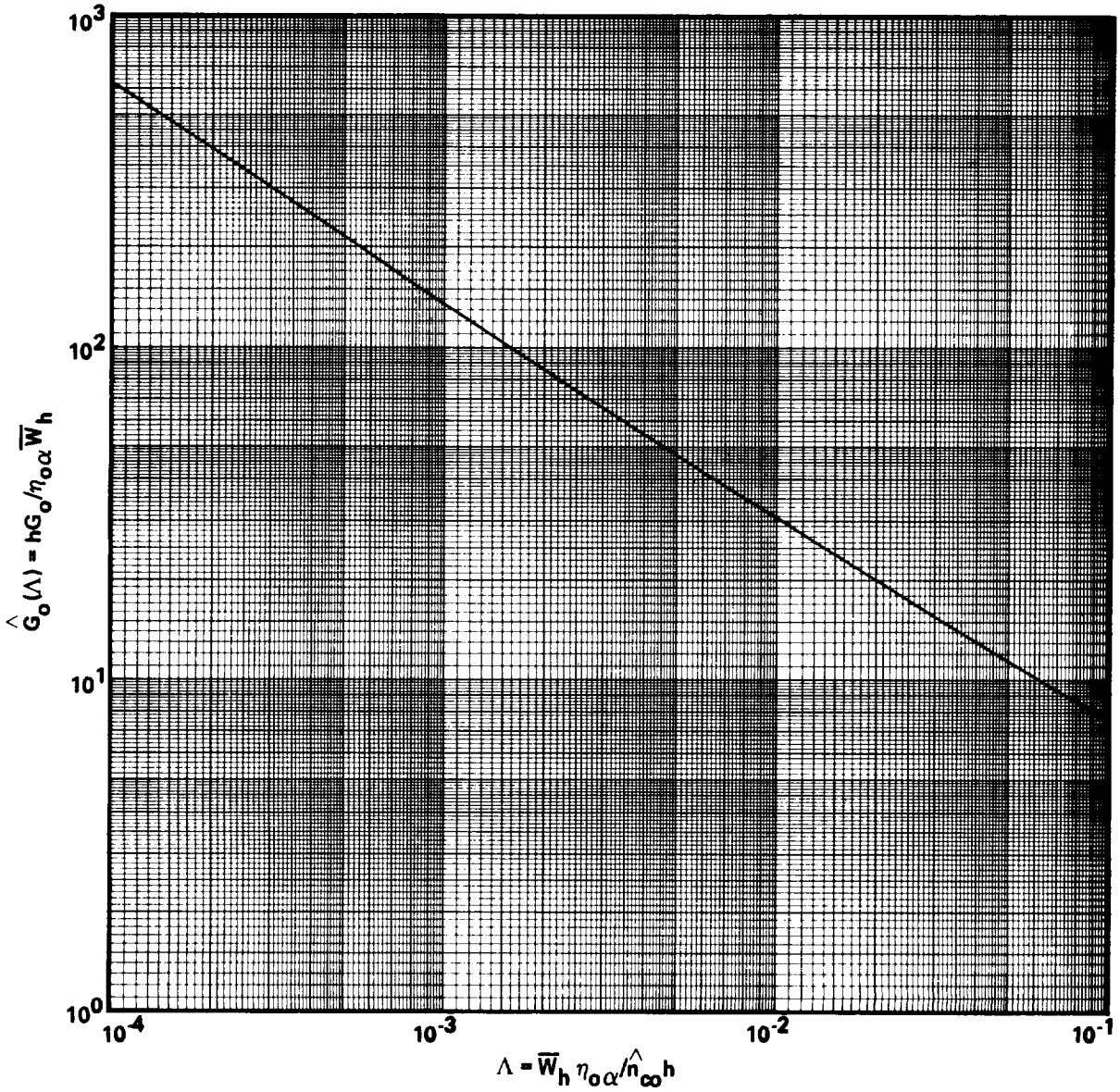

(b) VALUES OF ZERO CROSSINGS FOR Λ RANGE $10^{-4} - 10^{-1}$.

Figure 4.12 (Continued).

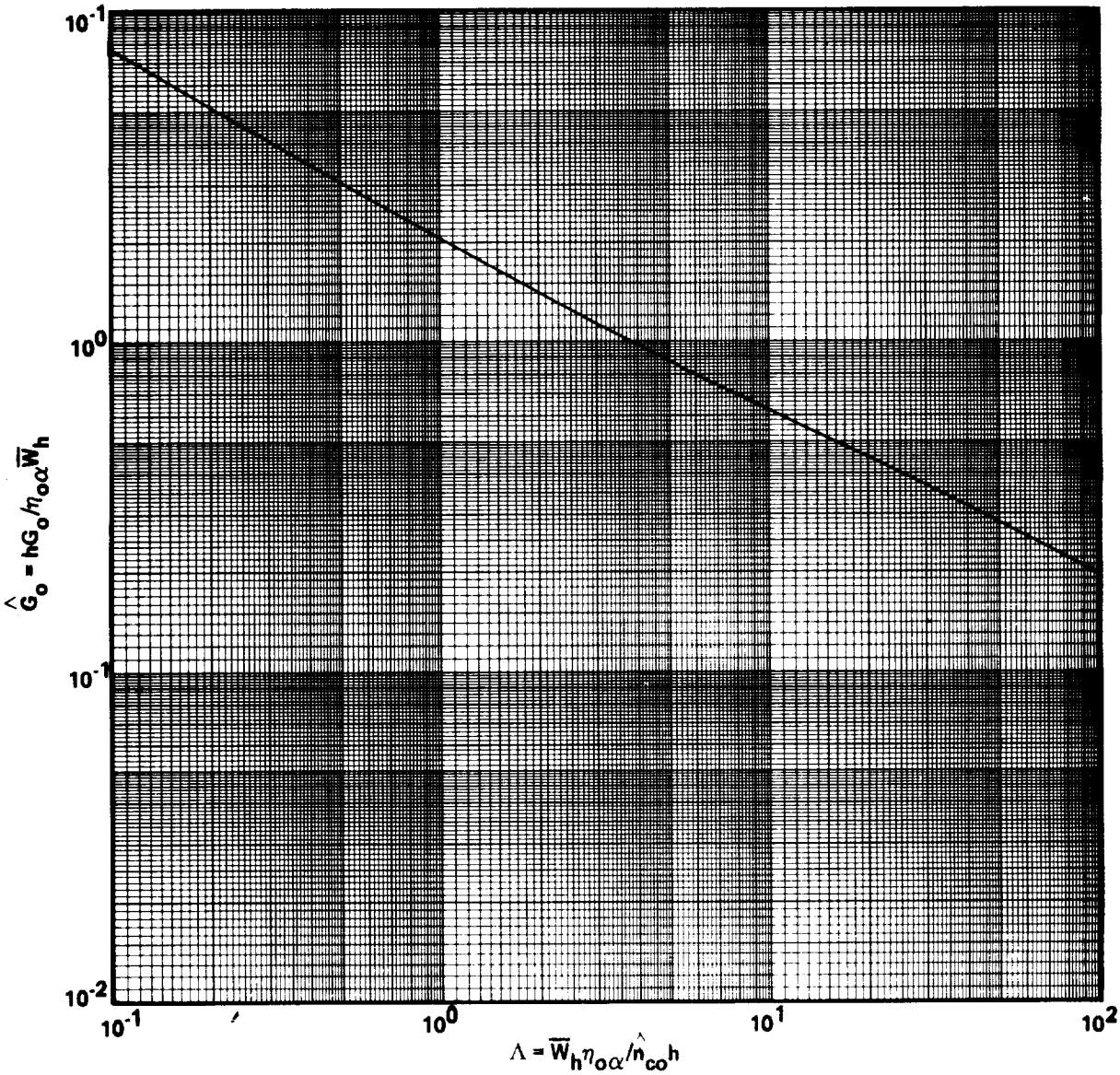

(c) VALUES OF ZERO CROSSINGS FOR Λ RANGE $10^{-1} - 10^{2}$.

Figure 4.12 (Concluded).

$$\hat{n}_{co} = 0.053 \left[\frac{\eta_{o\alpha} A_{\alpha}^{3} \overline{W}_{h}^{3}}{\nu C_{\alpha} h} \right]^{1/2} \tag{4.45}$$

where the subscript α denotes the windspeed component of interest. Values of the constants are given in the following listing:

Wind Component	C_{α}	$\eta_{o\alpha}$
w_x	0.056	0.0144
w_y	0.087	0.0265
w_z	0.087	0.0962

Example 4.4: To illustrate the meaning of equation (4.44), consider the following example. A potential WTG site is near Los Angeles, California, where from Table 2.1, Section 2.4, $k = 2.0$, $c = 4.41$ m s^{-1} (9.9 mph), and $\overline{W} = 3.91$ m s^{-1} (8.8 mph). It is desired to estimate how often within the year that the turbulent fluctuation in the longitudinal velocity w_x exceeds prescribed values. This information is contained in Figure 4.11, which is a plot of $G(\hat{w}_x)/G_o$ versus $\hat{w}_x$. The parameter $A(h_{ref}, z_o, L)$ can be computed by assuming $z_o = 0.05$ m (0.16 ft) and $z_o/L = 0$; i.e., neutral stability for the entire year. From equations (4.26), (4.38) and (4.39),

$$A_x(h_{ref}, z_o, L) = \frac{1.3[0.177 + 0.832\, h_{ref}/h_i]^{-0.4}}{\frac{1}{\kappa} \ell n\left(\frac{h_{ref} + z_o}{z_o}\right)} .$$

Hence, $A_x = 1.90 \times 10^{-1}$ for a $h_{ref} = 10$ m (33 ft).

From Figure 4.11 for $k = 2.0$ and converting $\hat{w}_x$ to dimensional form, i.e., $w_{x_p} = cA(h_{ref}, z_o, L)\hat{w}_x$, results

TABLE 4.3 RATIO OF NUMBER OF LONGITUDINAL GUSTS EXCEEDING THE VALUE w_{x_p} PER UNIT TIME TO THE NUMBER CROSSING ZERO WITH POSITIVE SLOPE PER UNIT TIME

w_{x_p} (m/s)	$G(w_{x_p})/G_o$
0	1.00×10^{0}
0.5	6.53×10^{-1}
1.0	3.48×10^{-1}
2.0	7.99×10^{-2}
3.0	1.68×10^{-2}
4.0	3.36×10^{-3}
5.0	6.57×10^{-4}
6.0	1.26×10^{-4}
8.0	4.50×10^{-6}
10.0	1.56×10^{-7}

in Table 4.3. The expression $G(w_{x_p})/G_o$ is the ratio of the number of times the longitudinal fluctuations about the mean exceed w_{x_p} to the number of times $w_x(t)$ crosses the zero mean value.

To convert Table 4.3 to dimensional numbers, G_o is evaluated from equation (4.42) which can be written as

$$G_o = \left[\frac{\int_0^\infty \frac{\hat{n}^3 \phi_{w_x}(\hat{n})}{\sigma_{w_x}^2} \frac{d\,\ell n\,\hat{n}}{\left(1 + \left(\frac{\hat{n}}{\hat{n}_{co}}\right)^2\right)}}{\int_0^\infty \frac{\hat{n}\phi_{w_x}(\hat{n})}{\sigma_{w_x}^2} \frac{d\,\ell n\,\hat{n}}{\left(1 + \left(\frac{\hat{n}}{\hat{n}_{co}}\right)^2\right)}} \right]^{1/2} \tag{4.46}$$

where $\hat{n}_{co}$ is a cutoff frequency and $\hat{n}\phi_{w_x}(\hat{n})/\sigma_{w_x}^2$ is given by equation (4.20). Note integration of equation (4.45) requires filtering of the higher frequency end of the spectrum [4.13]. Numerical integrations of this equation result in Figure 4.12 from which G_o is determined as 0.31 s^{-1}. From this result the number of times w_x exceeds, for example, 6 m s^{-1} within a year, is determined by multiplying G_o by 1.26×10^{-4}, taken from Table 4.3. This gives $G(w_x > 6 \text{ m s}^{-1}) = 3.8 \times 10^{-5} \text{ s}^{-1}$ which, multiplied by the number of seconds per year, gives 1198.

Frequently, equation (4.42) is difficult to integrate, and a discrete approach is used. Consider the lifetime exposure to turbulence of a WTG to be made up of M time periods $t_1, t_2, \ldots, t_M$ where the total time $T = \sum_{i=1}^{M} t_i$. The rms value of the output response for the quantity x due to the ith time period is

$$\sigma_{x_i} = \left(\int_0^\infty |H(\hat{n})|^2 \phi_{w_{\alpha_i}}(\hat{n}) d\hat{n} \right)^{1/2} \tag{4.47}$$

and the approximate number of peaks greater than x per unit time are given by

$$N_i(x) = N_o \exp\left[-\left(x^2/2\sigma_{x_i}^2 \right) \right] \quad . \tag{4.48}$$

Introducing a factor, s, defined as

$$s = \sigma_{x_i}/\sigma_{w_{\alpha_i}} \tag{4.49}$$

the quantity, s, is in the nature of a gust response factor which depends on such WTG parameters as rotor weight, rated speed, air density, etc. The value of

$\sigma_{w_{\alpha_i}}$ is the turbulence intensity for the ith time period of turbulence. The composite discrete-period model will then have approximately $N(x)$ peaks per unit time that exceed the specified value, x, where $N(x)$ is given by

$$N(x) = \frac{N_o}{T}\left(t_1 \exp\left[-\left(\frac{x}{\sqrt{2}\sigma_{w_{\alpha_1}}}\right)^2\right] + t_2 \exp\left[-\left(\frac{x}{\sqrt{2}\sigma_{w_{\alpha_2}}}\right)^2\right] + \ldots + t_M \exp\left[-\left(\frac{x}{\sqrt{2}\sigma_{w_{\alpha_M}}}\right)^2\right]\right) \quad . \tag{4.50}$$

Finally, it should be noted that $N(x)$ refers to the number of exceedances per unit time in the positive values of x, or for negative values of x; for total peaks including positive and negative values of x, the value of $N(x)$ should be multiplied by 2.

The composite model thus allows one to determine the fatigue loading for the lifetime of the WTG based upon the wind speed duration curve, atmospheric stability, and surface roughness at the site. Again, it is pointed out that to carry out an analysis such as described in the preceding example, the frequency response function, $H(\hat{n})$, of the system being analyzed must be known.

4.3.4 Influence of Atmospheric Stability

4.3.4.1 Turbulence Spectra for Varying Stability Conditions

Figure 4.13 shows the longitudinal turbulence spectra for conditions of varying atmospheric stability. Values of the turbulence spectra based on equations (4.20) and (4.22) (neutral case) are plotted as circles on the given figure. The data agree very well for the neutral case. Spectra for the stable case, however, are a function of stability through the dependence of $\eta_{o\alpha}$ on the Richardson's number, Ri.

4.3.4.2 Turbulence Spectra for a Stable Atmosphere

Turbulence spectra in stable atmospheric boundary layers have been developed by Kaimal [4.3]. Kaimal shows that the spectra correlate with

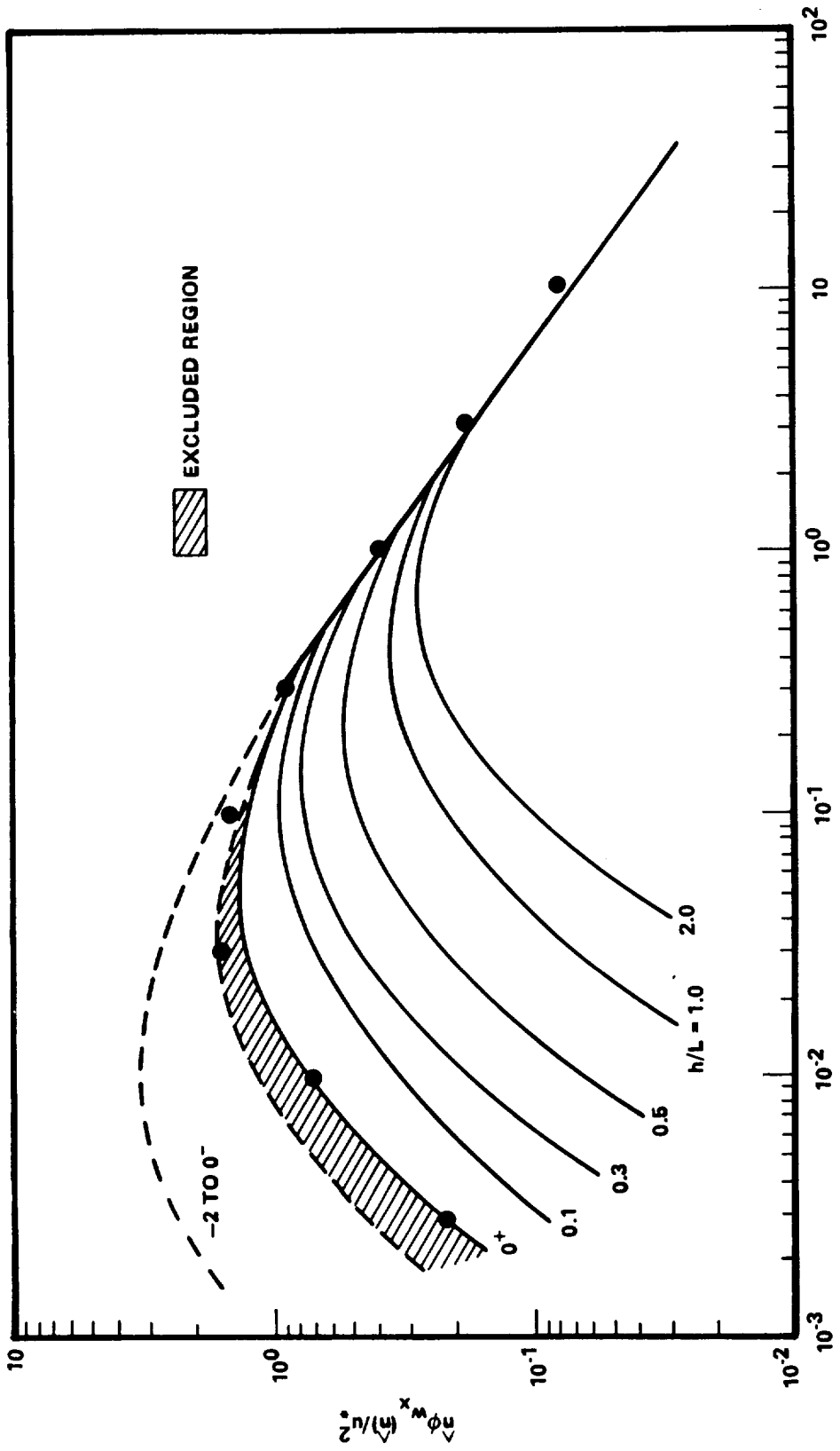

Figure 4.13 Influence of stability on turbulence energy spectrum.

equation (4.20) but where $\eta_{o\alpha}$ is now a function of Ri. Values of $\eta_{o\alpha}$ for the longitudinal, lateral, and vertical wind components are given in Figure 4.14 as a function of the Richardson's number. Also, an equation for $\eta_{o\alpha}$ is given on each of the respective figures.

The computation of turbulence spectra in a stable atmosphere requires as input the value of the variance or turbulence intensity. These values can be determined as described in Section 4.3.2.3.

4.3.4.3 Evaluation of Turbulence Spectra for the Stable Atmosphere

The procedure for evaluating the turbulence energy spectra for stable atmospheres is as follows:

1) Determine the Richardson's number, Ri, for the atmospheric stability condition under investigation.

2) From Figure 4.14, select the η_o corresponding to Ri in Step 1 for the desired longitudinal, lateral, or vertical turbulence component.

3) From Figure 4.6 or equation (4.23), find σ_{w_z}/u_* where h/L is related to Ri by equation (3.1) or Figure 3.1, Section 3.3.

4) Determine u_* from Figures 3.4 and 3.5, Section 3.3, for the surface roughness, z_o, of the site and h/L corresponding to Ri.

5) Determine the longitudinal and lateral turbulence intensities by selecting the ratio $\sigma_{w_x}/\sigma_{w_z}$ and $\sigma_{w_y}/\sigma_{w_z}$ from Figure 4.7 at the appropriate elevation.

The spectrum of the turbulence is then specified by equation (4.20) and can be multiplied by the square of the absolute value of the frequency response function for the system being analyzed. The spectral form of the system output is thus developed as described in Section 4.3.2.5.

4.4 Discrete Gust Model

4.4.1 Discrete Gust Magnitude and Duration

This section describes methods of estimating discrete gust magnitudes and shapes. It is generally recommended that discrete gusts be utilized in maximum load analyses rather than for continuous loading such as encountered

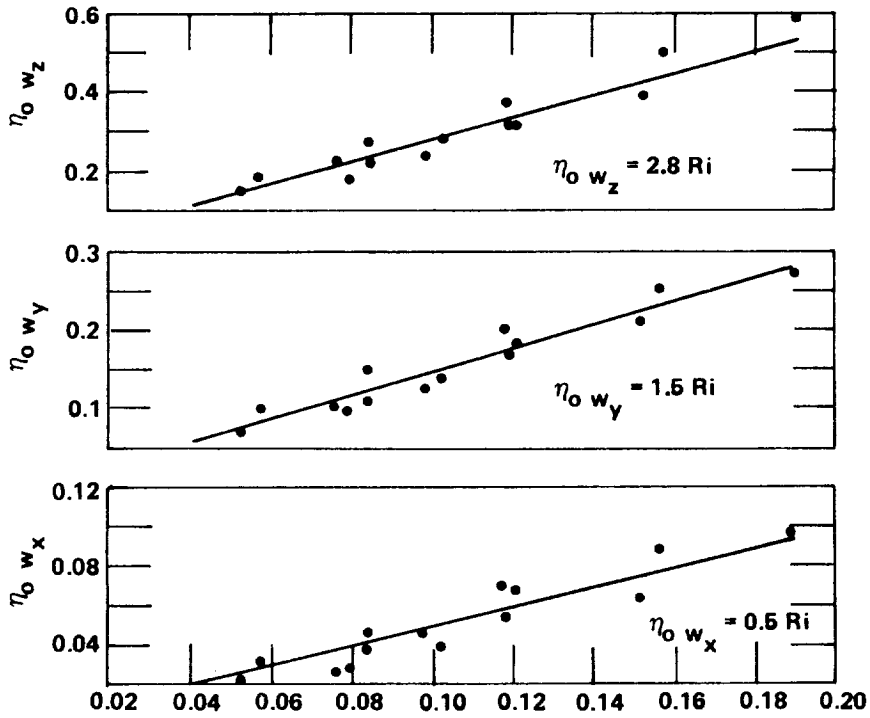

Figure 4.14 Correlation of $\eta_{o\alpha}$ with the Richardson's number for stable boundary layers.

in fatigue analysis. For fatigue analysis the spectral approach described in the preceding sections or the turbulence simulation schemes described in the following sections are recommended. However, when it is impossible to linearize the governing dynamic equations for WTG or too costly to utilize complete turbulence simulation models, the discrete gust approach offers a reasonable approximation. Therefore, this section not only contains methods of estimating discrete gust magnitude and duration extreme gusts, but also methods of estimating average gust magnitudes and shapes along with the number of times each gust may be expected to occur in the lifetime of the structure. The first paragraphs of this section deal primarily with gust properties relative to maximum load analysis; whereas, the latter paragraphs, Section 4.4.3, addresses methods of estimating discrete gust properties for fatigue analysis.

4.4.1.1 Significance of Gust Duration

The prediction of gust magnitude given in this report assumes that the duration, τ, of the required design gust is a known parameter determined from the dynamic analysis of the WTG. If the WTG does not respond to a gust of a given duration, it is immaterial how many gusts of that duration occur in the atmosphere.

Example 4.5: As an example of the preceding argument, consider the response of the simple rotor, described by Frost [4.7], to a gust of triangular shape (see the insert of Figure 4.15). (The triangular shaped gust is used here only for illustrative purposes. More meaningful gust shapes are given later.)

Assuming a linearized system, the response to the specified gust is

$$\Omega(\zeta) = \zeta/\alpha + (e^{-\alpha\zeta}-1)/\alpha^2 \quad ; \quad 0 \leq \zeta \leq 0.5 \tag{4.51}$$

$$\Omega(\zeta) = (2-\zeta)/\alpha + [1-e^{-\alpha\zeta}(1-2e^{\alpha})]/\alpha^2 \quad ; \quad \zeta \geq 0.5 \tag{4.52}$$

where

$$\Omega(\zeta) = \omega'(\zeta)/\beta_2 W_i \tau \quad ; \quad \alpha = \beta_1 \tau \quad ; \quad \zeta = t/\tau \quad . \tag{4.53}$$

β_1 and β_2 are parameters which characterize the properties of the rotor [4.7].

The value of β_1 is essentially a time constant dependent upon the system being analyzed. Figure 4.15 shows that for a fixed gust duration a system with a large value of β_1 is insensitive to a gust of magnitude W_i; whereas a system with a small value of β_1 is highly sensitive.

The magnitude of the gust, W_i, only enters the system linearly. Consider two systems which have a time constant $\alpha = 10$ for system No. 1 and $\alpha = 0.1$ for system No. 2. Then to achieve the same peak response $\omega'(t)/2\beta_2\tau$ for system No. 1, as for system No. 2, a gust approximately 10 times larger is required. That is, the peak response of No. 1 is approximately 0.1 whereas for No. 2 it is approximately 1.0. Hence for the same frequency gust τ and rotor β_2, W_i is different by a factor of 10.

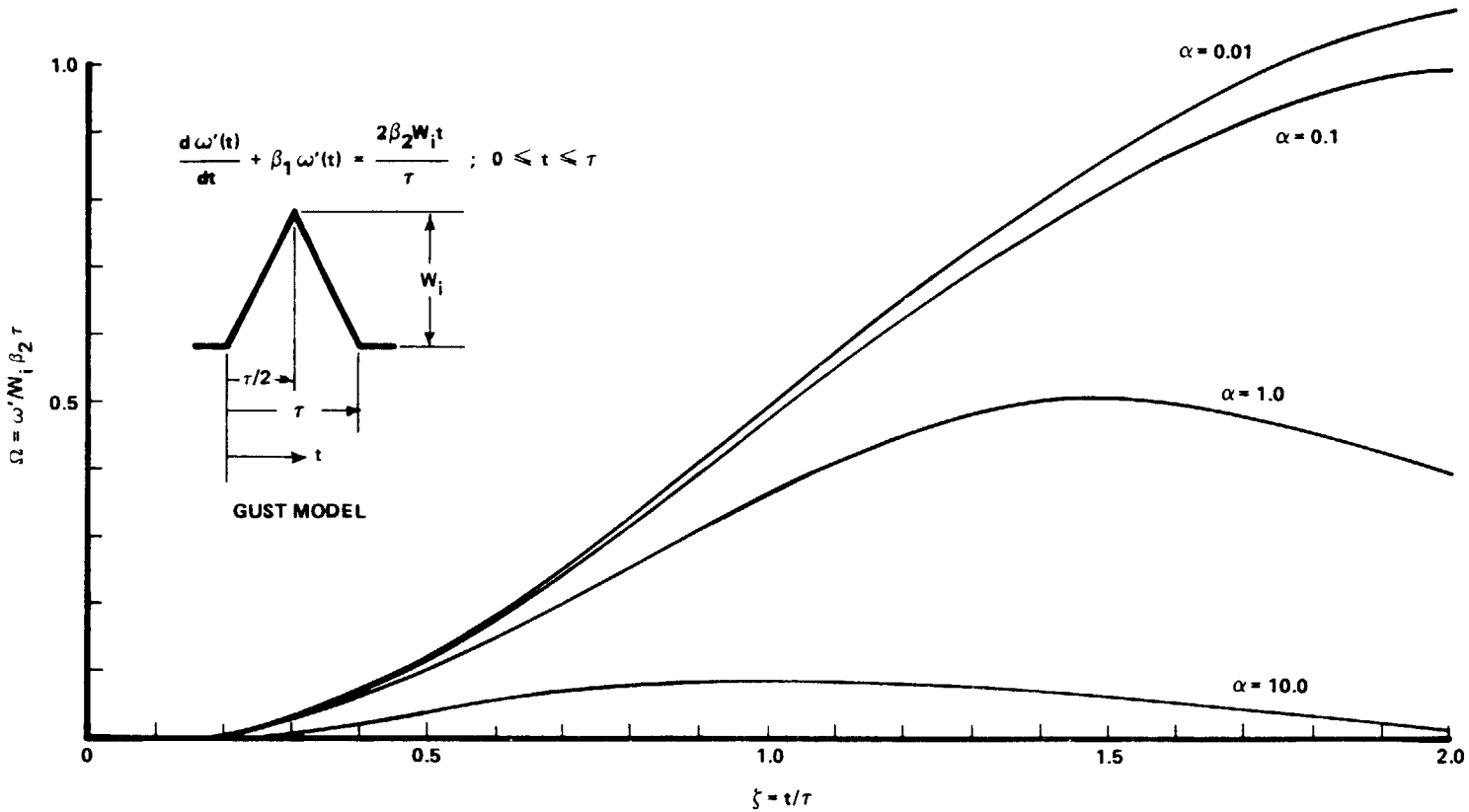

Figure 4.15 Response of a simple rotor to a gust of magnitude, W_i, and duration, τ.

Section 4.4.1.2 describes a procedure for determining design values of gust magnitude and shape assuming the dynamic characteristics of the WTG are known.

4.4.1.2 Longitudinal, Gust Factors

A gust factor $F_G(\overline{W}_{h=10\ m}, h, \tau)$ is defined as the ratio of the wind speed averaged over the period, τ, to the wind speed averaged over a 10-min or longer period. Mean wind speed for longer averaging periods shows little variation from the 10-min average [4.14]. The gust factor is a function of the 10-min averaged wind speed at a reference height of 10 m (30 ft), $\overline{W}_{h=10\ m}$, the height at which it is applied, h, and the duration, τ. Figure 4.16 shows plots of $F_G = \hat{F}_G(\overline{W}_{h=10\ m}, h, \tau) + 1.0$ as a function of height, h, for parametric variation of τ. Curves for $\overline{W}_{h=10\ m} = 2\ m\ s^{-1}$, $5\ m\ s^{-1}$, $10\ m\ s^{-1}$, $15\ m\ s^{-1}$, and greater than $25\ m\ s^{-1}$ are provided. The value of F_G does not change appreciably with values of $\overline{W}_{h=10\ m}$ greater than $25\ m\ s^{-1}$ (56 mph). The function $\hat{F}_G$ is equivalent to $W_i(h,\tau)/\overline{W}_h$, where $W_i(h,\tau)$ is the difference between the wind speed average over τ and the mean wind speed, i.e., $W_i(h,\tau) = W_h(\tau) - \overline{W}_h$.

The gust factors have been evaluated from the results of Reference 4.14 which are based on 17 years of peak wind speed measurements at Cape Kennedy. These data are expected to be representative of other locations having reasonably homogeneous terrain. To select a design value of gust magnitude, W_i, for a given duration, τ, proceed as follows.

4.4.1.3 Basic Design Value

The recommended procedure for selecting a design value of the gust magnitude for the given duration, τ, is as follows:

1) Determine the mean wind speed (i.e., 10-min average or greater) at the height, h, for which the analysis is to be carried out, $\overline{W}_h$.

2) Adjust $\overline{W}_h$ to the reference height $h_{ref} = 10$ m (30 ft) with the relationship

$$\overline{W}_{h=10\ m} = \overline{W}_h(10/h)^n$$

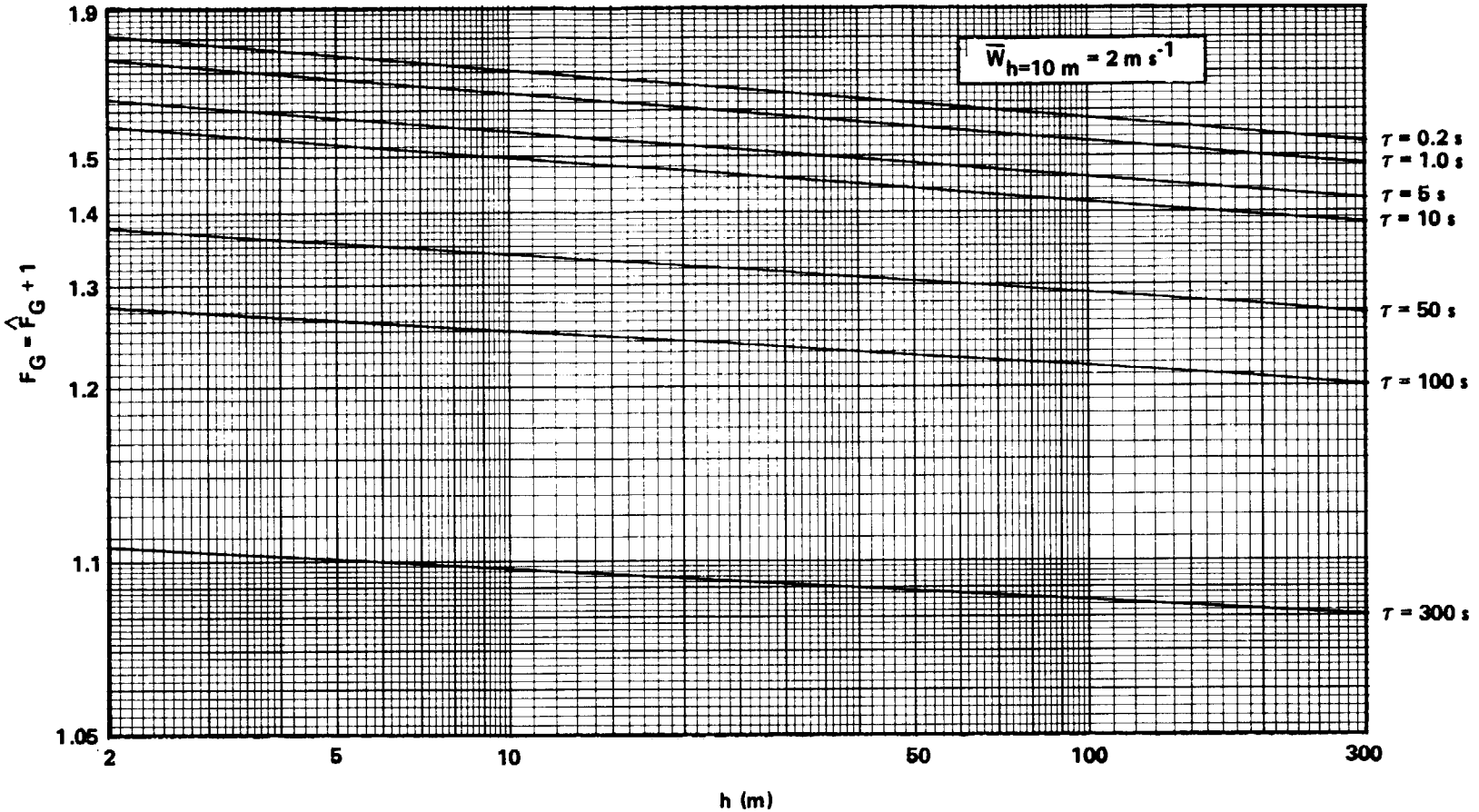

Figure 4.16 Plots of $F_G = \hat{F}_G(\overline{W}_{h=10\ m}, h, \tau) + 1.0$ as a function of height, h, for parametric variation of τ.

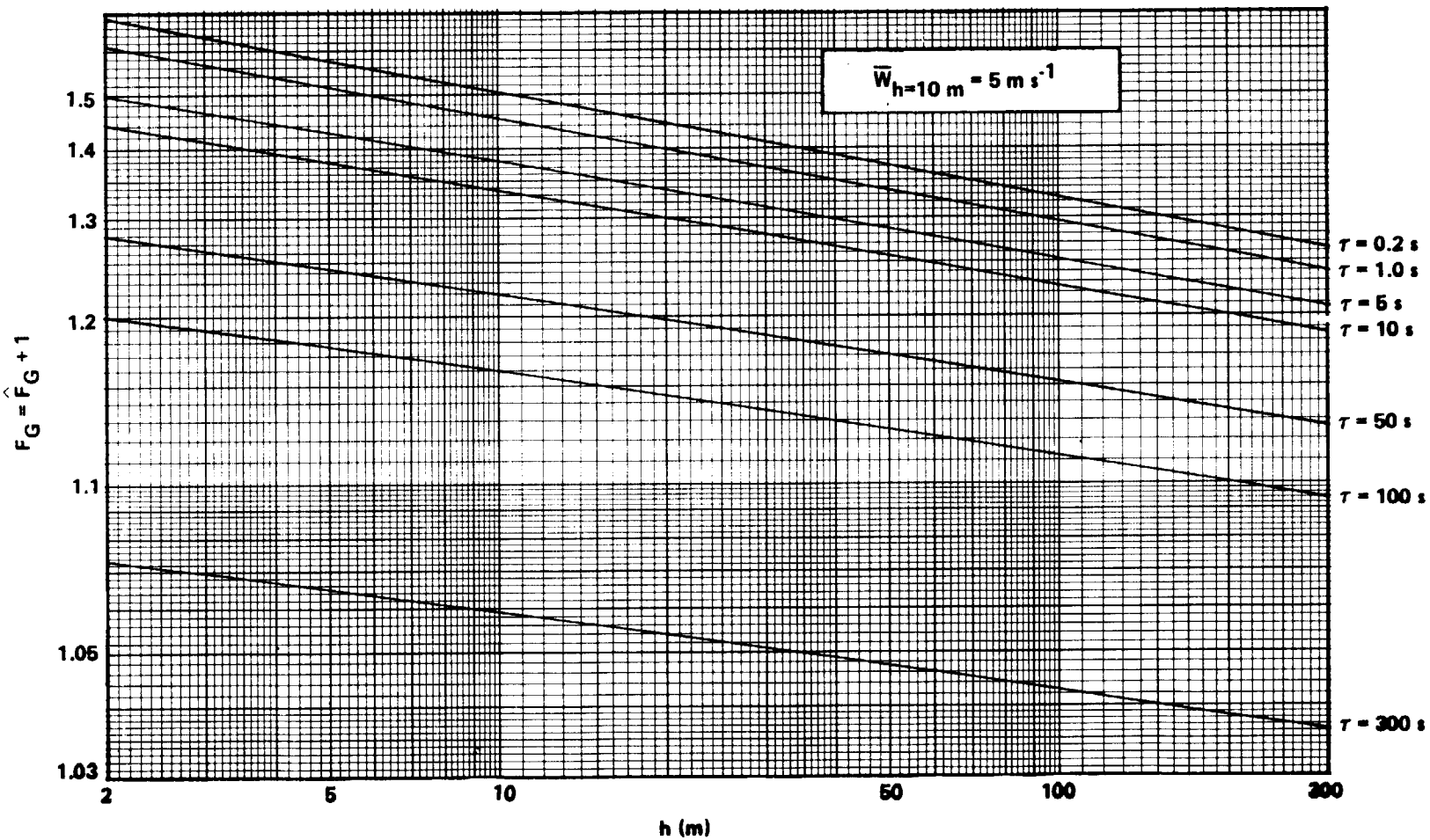

Figure 4.16 (Continued).

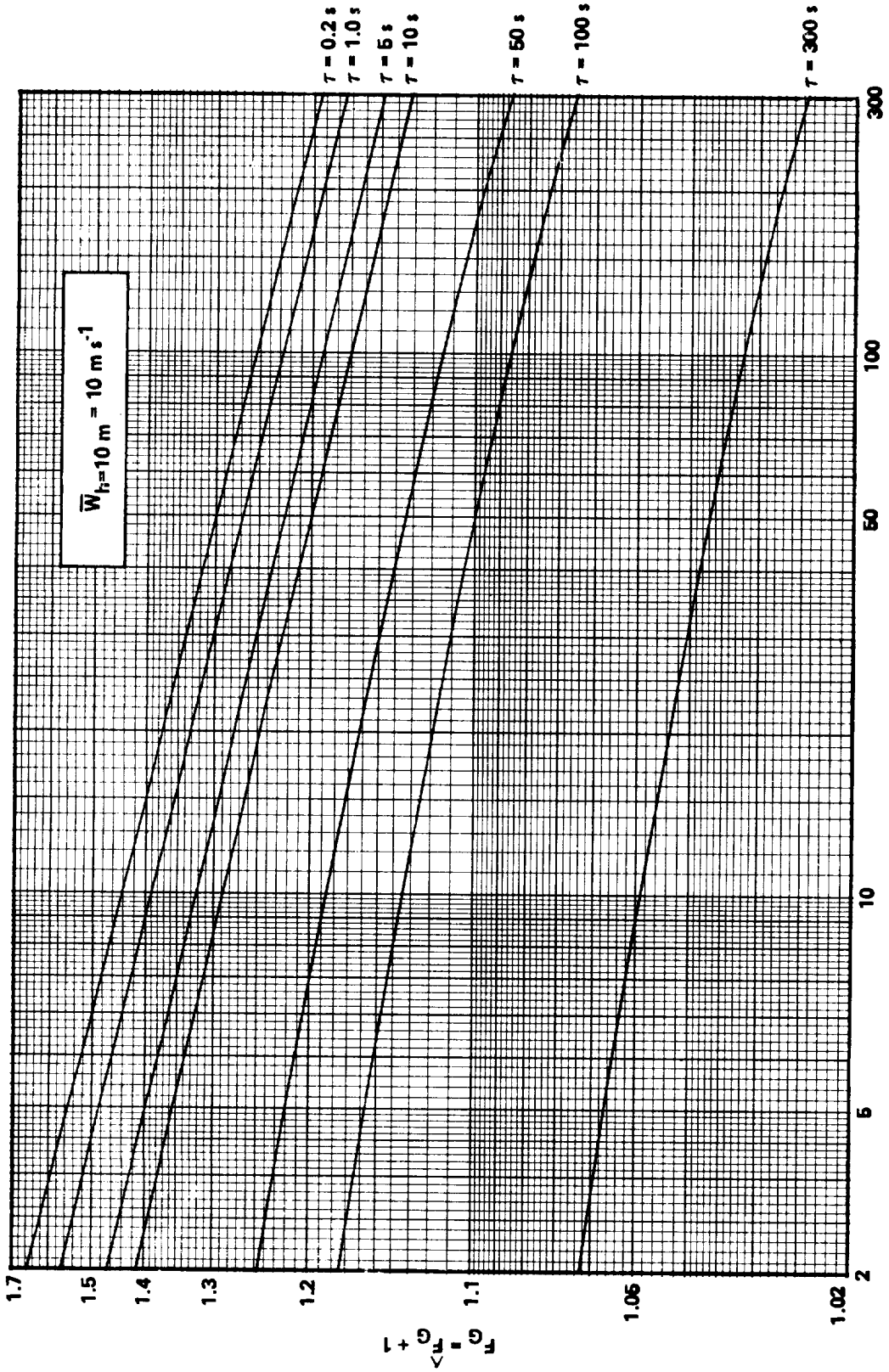

Figure 4.16 (Continued).

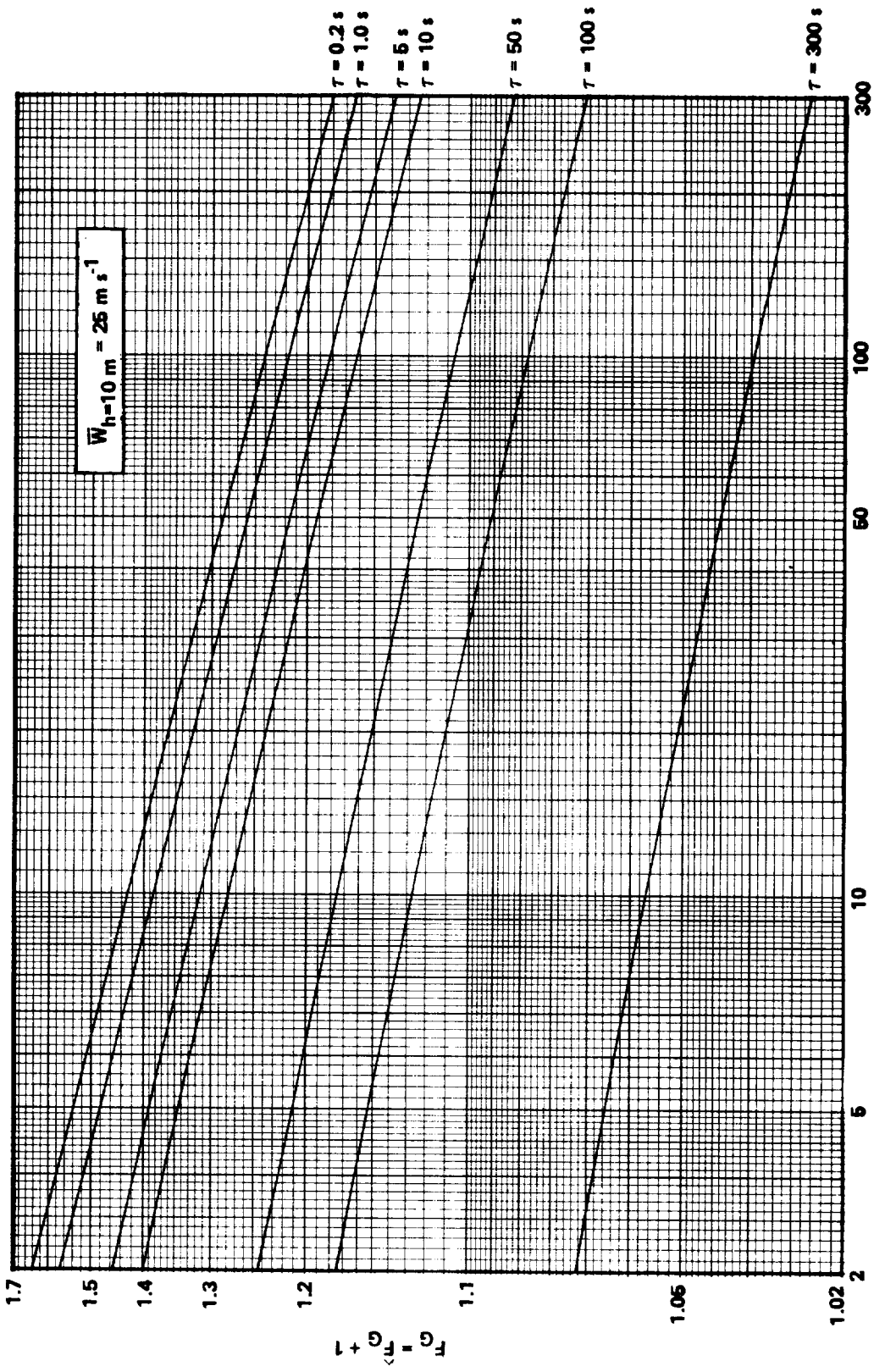

Figure 4.16 (Continued).

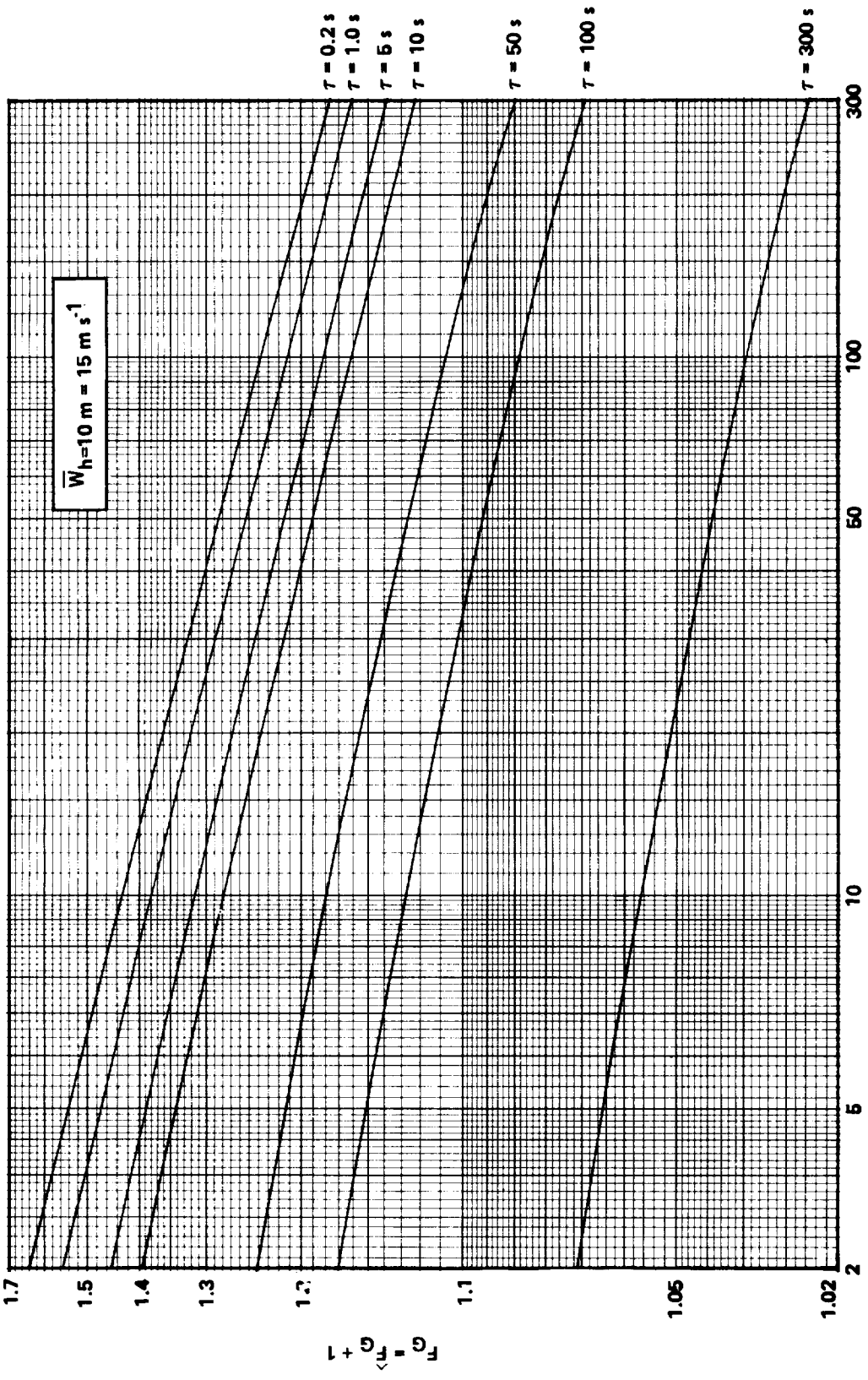

Figure 4.16 (Concluded).

where n is determined as described in Chapter 2 or determine $\overline{W}_h$ from the relationship

$$\overline{W}_{h=10\ m} = \overline{W}_h \, \ell n(10/z_o + 1)/\ell n(h/z_o + 1) \quad .$$

3) Select from the set of figures (Figure 4.16) the figure which corresponds to the value of $\overline{W}_{h=10\ m}$ determined in Step 2; or extrapolate between figures if $\overline{W}_{h=10\ m}$ is not exactly 2, 5, 10, 15, or $\geq$ 25 m s^{-1} (4.5, 11.2, 22.4, 33.6, or $\geq$ 56 mph).

4) Find F_G from the selected figure at the height, h, for the value of τ, or range of values, to which the quantity under design (i.e., rotor bending moment, torque, synchronous speed, etc.) is responsive.

5) The averaged magnitude of the gust $W_i(h,\tau)$ over the duration, τ, is given by

$$W_i(h,\tau) = \hat{F}_G \overline{W}_h \qquad (4.54)$$

or

$$W_h(\tau) = F_G \overline{W}_h \quad . \qquad (4.55)$$

The resulting value of $W_i(h,\tau)$ and $W_h(\tau)$ represents the expected or mean value of the gust magnitude $W_i(h,\tau)$ and $W_h(\tau)$, respectively, of the total population of gusts of duration τ. Random values $W_i'(h,\tau)$ and $W_h'(\tau)$ will be distributed about these mean values. In general, we are interested in the most extreme gust, and a method is required for estimating what is the extreme gust magnitude from the total population. A method of estimating the extreme value is provided in the following section.

4.4.1.4 Estimating the Extremes of the Gust Magnitudes

Figure 4.17 gives a correction factor β by which an estimation of the one, two, and three standard deviation in $W_h(\tau)$ can be made. β is the ratio of the one, two, or three standard deviation gust magnitude to the mean gust magnitude.

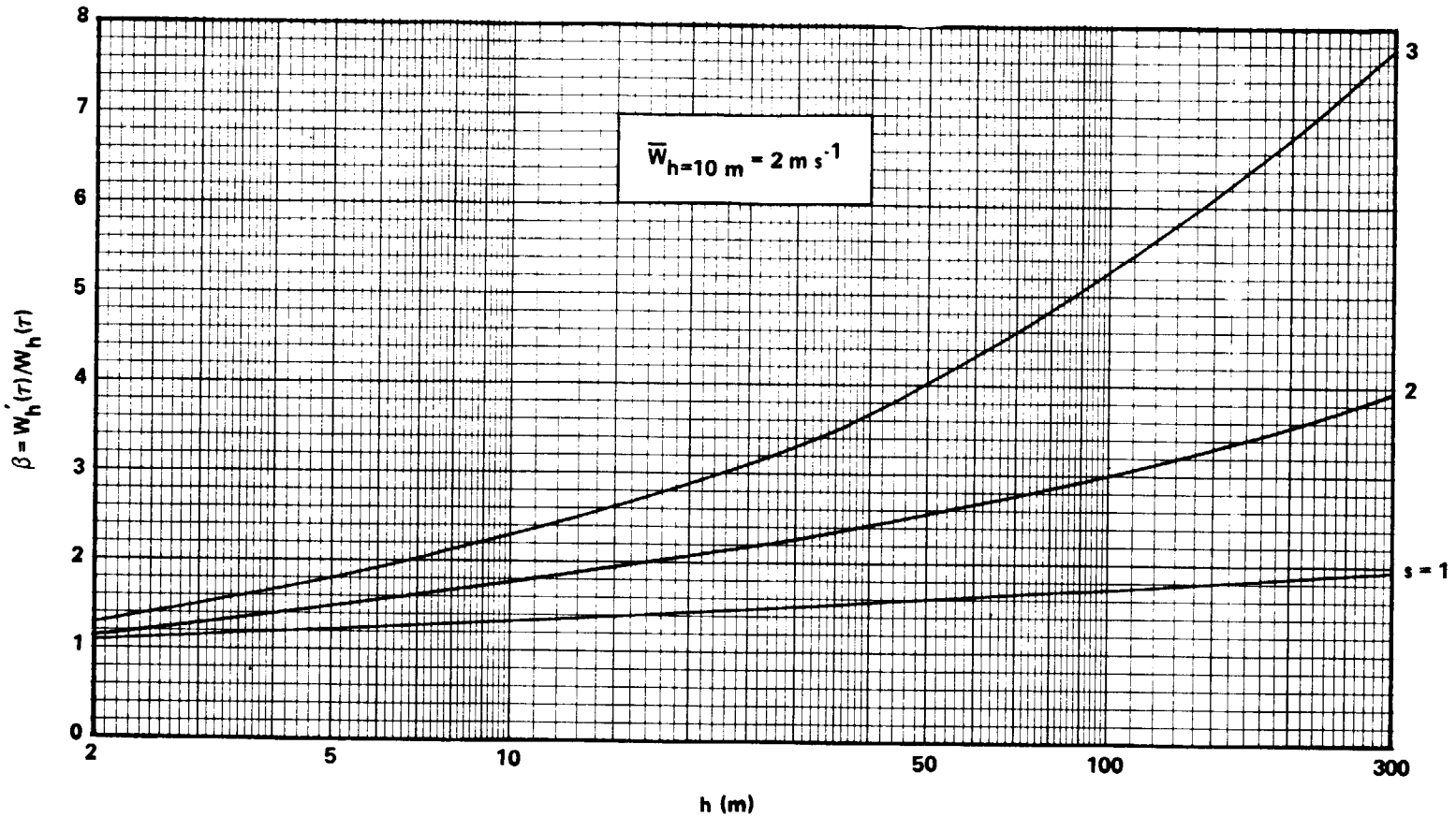

Figure 4.17 Factor for adjusting mean gust magnitude to the one, two, and three standard deviation values.
(S is the number of standard deviations.)

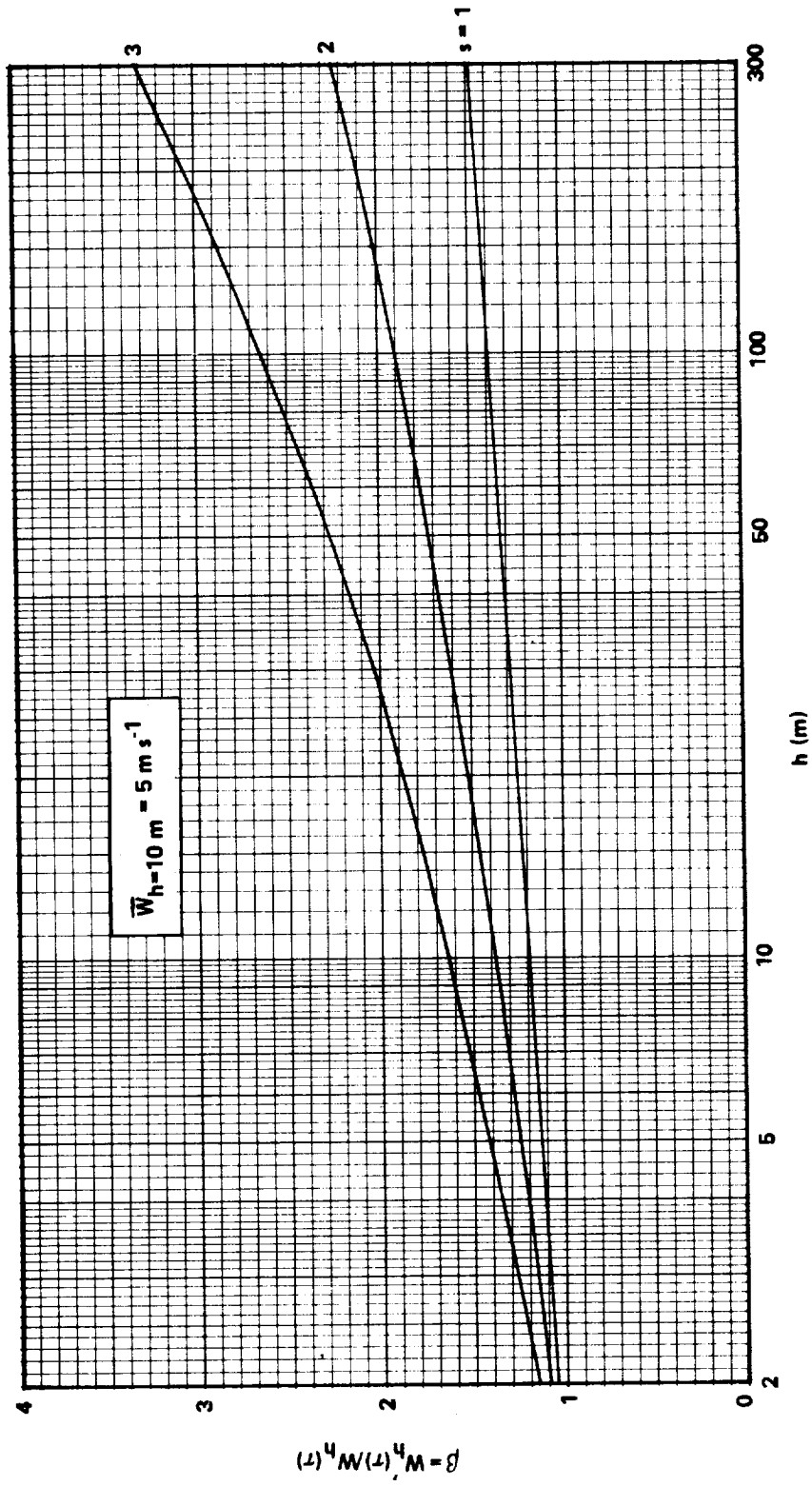

Figure 4.17 (Continued).

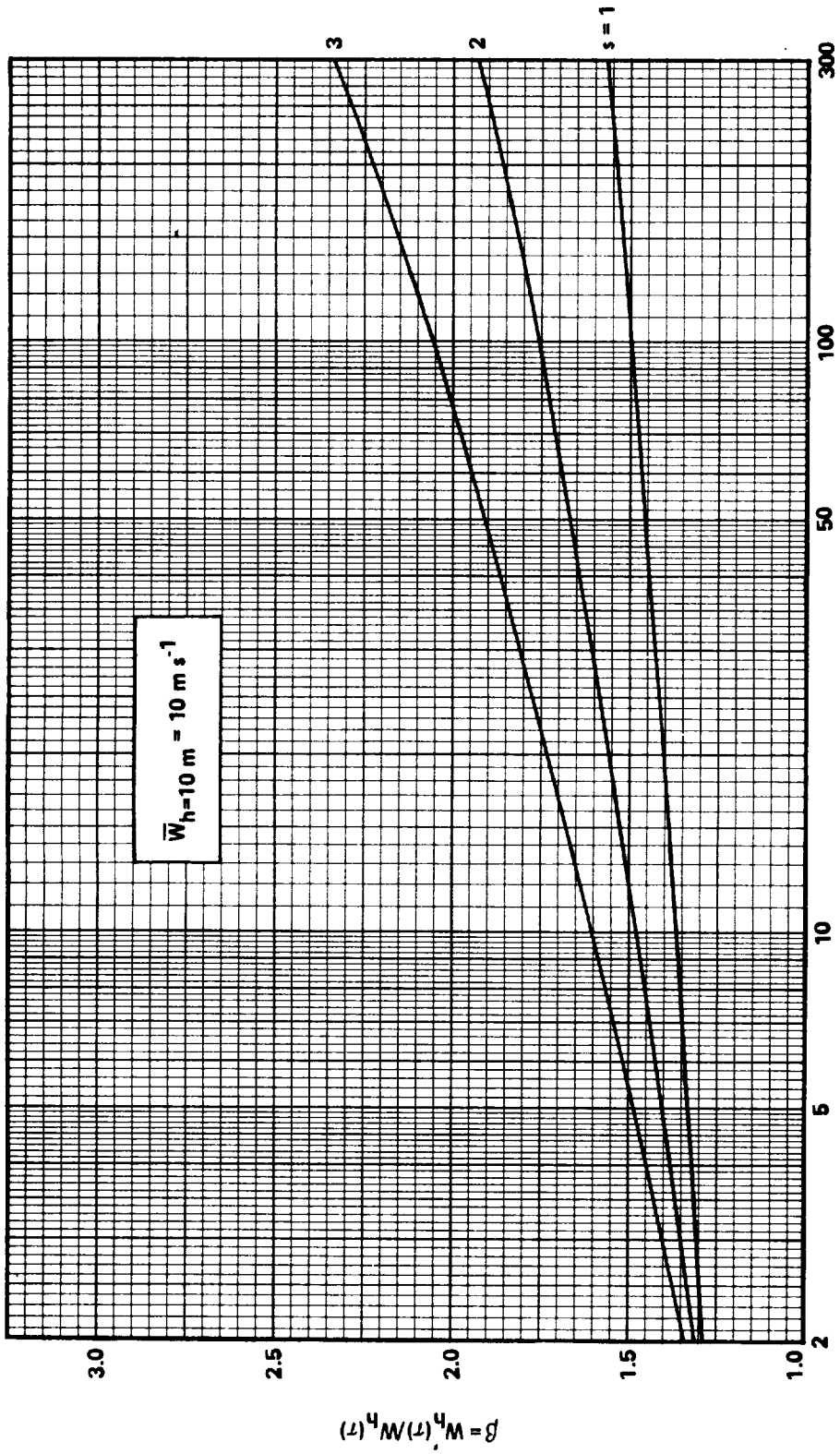

Figure 4.17 (Continued).

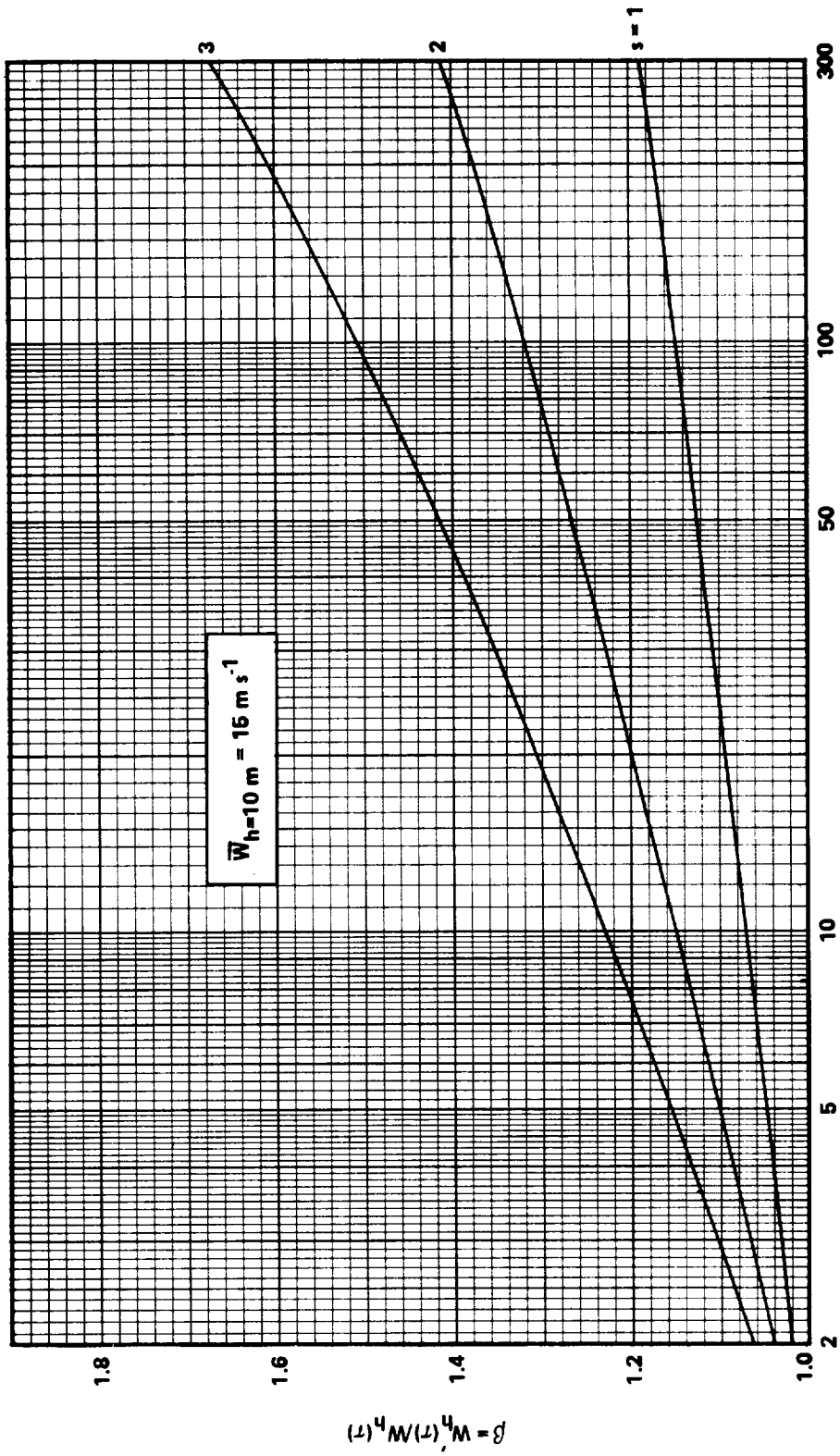

Figure 4.17 (Continued).

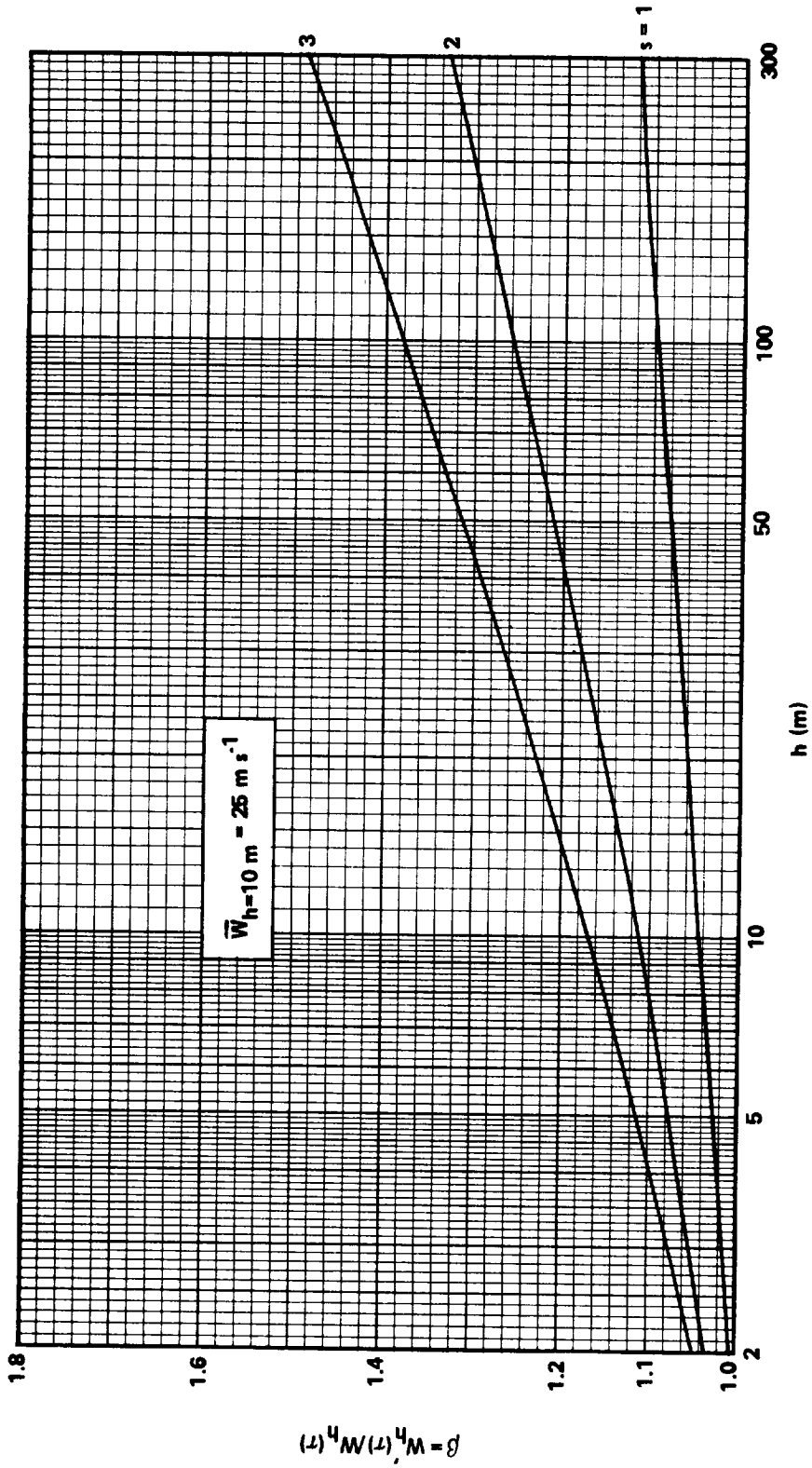

Figure 4.17 (Concluded).

The procedure for adjusting $W_h(\tau)$ determined in Step 5, Section 4.4.1.3, to an extreme value estimate of the gust magnitude is as follows:

1) Select from the set of figures (Fig. 4.17) the figure corresponding to $\overline{W}_{h=10\ m}$ determined in Step 2, Section 4.4.1.3, or extrapolate between figures if $\overline{W}_{h=10\ m}$ is not exactly 2, 5, 10, 15, or $\geq$ 25 m s^{-1} (4.5, 11.2, 22.4, 33.6, or $\geq$ 56 mph).

2) Find $\beta = W_h'(\tau)/W_h(\tau)$ for the height h at which the gust is to be applied, from the curve corresponding to σ, 2σ, or 3σ, depending on the probability of exceeding the gust magnitude desired (i.e., σ corresponds to a 32-percent chance of exceeding $\pm W'(\tau)$, 2σ corresponds to a 5-percent chance, and 3σ corresponds to a 0.3-percent chance).

3) Determine $W'(\tau)$ from

$$W_h'(\tau) = \beta W_h(\tau) \tag{4.56}$$

where $W_h(\tau)$ is the value found from equation (4.55) in Step 5, Section 4.4.1.3.

4.4.2 Discrete Gust Shapes

The rate of gust buildup and decay is a function of the shape of the gust. Very little definitive information on the shape of gusts is available. The most detailed experimental look at gust shapes appears to be given by Camp [4.1]. In this report a gust shape having essentially an exponential rise rate with a long dwell and an exponential decay is suggested by the data. Figure 4.18 illustrates a number of statistical gust shapes proposed by Camp. No mathematical description of these shapes was given in the reference, however. Also, gusts of 2-min or less duration only were considered.

Conventionally, gusts in other fields of research are generally taken as 1-cosine law, i.e., $W_G(t) = W_i(1 - \cos 2\pi t/\tau)/2$. This gust shape is recommended for fatigue analyses and is described in Section 4.4.3.

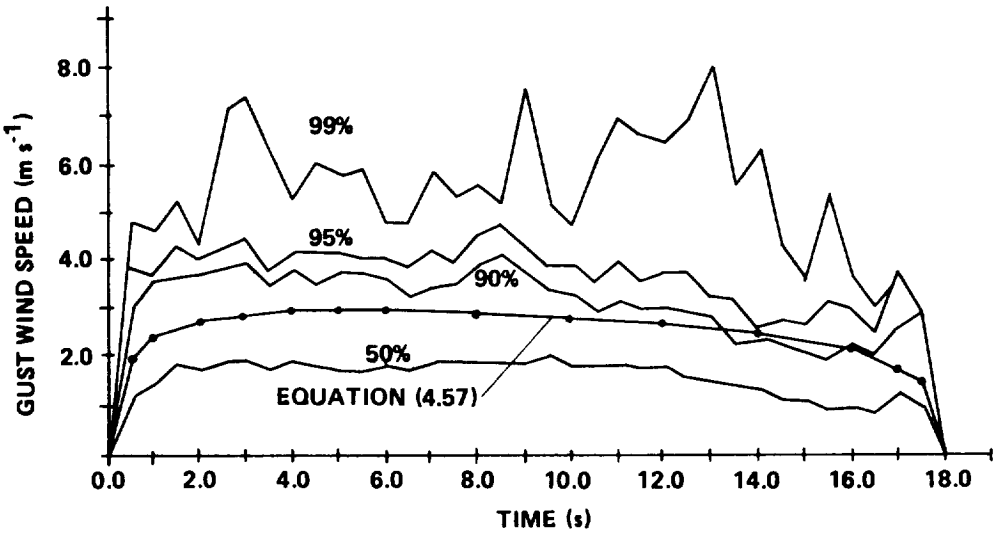

STATISTICAL GUST BASED ON 88 GUSTS HAVING A TIME DURATION OF 14 TO 18 s OCCURRING AT THE 18-m LEVEL

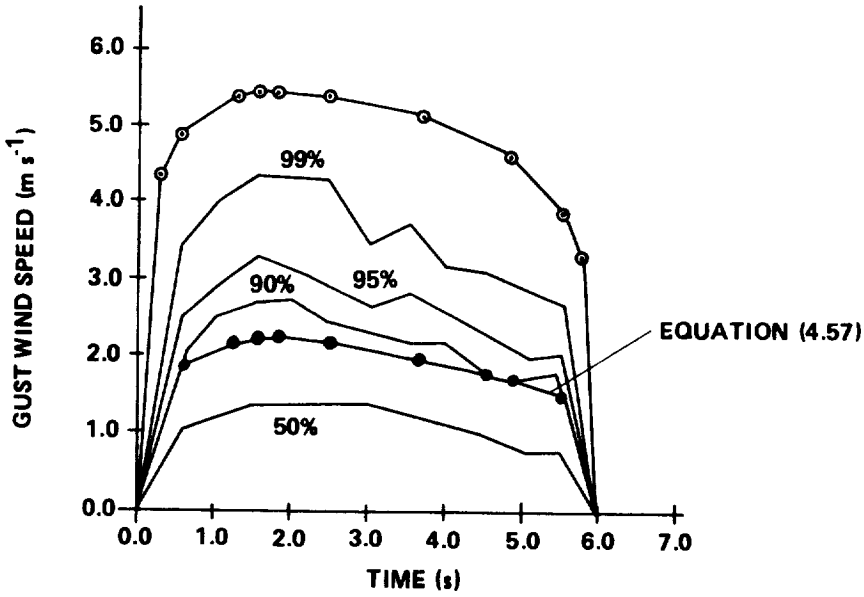

STATISTICAL GUST BASED ON 678 GUSTS HAVING A TIME DURATION OF 4 TO 6 s OCCURRING AT THE 18-m LEVELS

Figure 4.18 Comparison of measured gust shape with curve fit, equation (4.57).

In view of the limited knowledge of gust shapes, it appears optional as to whether a 1-cosine law is used or the gust shape from the results of Camp [4.1] given in the following text.

A suggested approach for developing a workable gust shape is to utilize the gust data proposed in Reference 4.1 and equate the energy of the gust to the energy of a gust of average wind speed, W_i, over the duration of the gust τ. Jones [4.15] suggests that the energy contained within the gust is the important parameter. Based on this approach, the recommended gust shape is:

$$W_G(\zeta) = 1.79\, W_i \left(1 - e^{-\left(\sin \frac{\pi\zeta}{2a}\right)^{1/3}} \right) ; \quad 0 \le \zeta \le a$$

$$W_G(\zeta) = 1.79\, W_i \left(1 - e^{-\left\{\sin \frac{\pi}{2} \frac{1-\zeta}{1-a}\right\}^{1/3}} \right) ; \quad a \le \zeta \le 1 \qquad (4.57)$$

$$a = 0.117 + 0.048\, \ell n\, h \; ; \quad \zeta = t/\tau \; ; \quad h \text{ in meters} \; .$$

Values of W_i for the period τ can be chosen from the procedures outlined in Section 4.4.1.3.

A comparison of equation (4.57) with the experimental results is shown in Figure 4.18. The theoretical results should correspond with the 50-percent curve. The difficulty in comparing the data is that no mean wind speeds are reported in Reference 4.1. For this reason, a comparison of the magnitude of the gust is not actually possible. However, the gust shape compares very well and the magnitude is believed to give a reasonable prediction.

4.4.3 Estimating Discrete Gust Properties for Fatigue Analysis

4.4.3.1 Frequency of Gusts Which Engulf the Entire Structure

If it is desired to utilize a discrete gust design approach for fatigue calculations, it is necessary to estimate the number of gusts of a given size

which occur per unit time. In Section 4.1.2.3, a model was presented for computing the approximate number of gusts of any size per unit time, i.e., $G(\hat{w}_\alpha)$. However, in analyzing a structure such as a large rotor blade [e.g., 100 m (300 ft) in diameter], one is only interested in those gusts which engulf the entire rotor. In Section 4.4.1.5, the concept of a coherence function is defined which is a measure of the coherence of a gust over a given distance in space. The coherence function is usually expressed as

$$\text{coh} = e^{-a\,\Delta x\,\hat{n}/\overline{W}_{h=10\text{ m}}} \quad . \tag{4.58}$$

This equation predicts what degree a gust of frequency $\hat{n}$ is coherent over the distance, Δx, for a mean wind speed at the 10-m level. Selecting a value of the coherence function based on the spatial distance of the structure, Δx, one can estimate the frequency of those gusts which are sufficiently large to extend over the system or system component being analyzed. This frequency, $\hat{n}_G$, is given by

$$\hat{n}_G = -\overline{W}_{h=10\text{ m}}/a\,\Delta x\,\ell n(\text{coh}) \quad . \tag{4.59}$$

The second step in using a discrete gust for fatigue analysis is to determine how many times in the lifetime of the structure gusts of frequency $\hat{n}_G$ impinge upon the rotor. To estimate this number, a similar approach to that taken in Section 4.3.6 for computing the number of cycles of gusts of all frequencies is taken as follows. Rather than integrating equation (4.46) with the cutoff frequency $\hat{n}_{co}$ as given by equation (4.45), the frequency $\hat{n}_G$ is used as the cutoff frequency. This filters out all frequencies higher than $\hat{n}_G$ or gusts of time period less than $1/\hat{n}_G$. Thus, the number of times, G_{o_G}, gusts of frequency $\hat{n}_G$ or less cross the zero axis (or mean wind speed value) with positive slope can be determined directly from Figure 4.12 by introducing $\hat{n}_G$ into Λ; i.e., determine $\hat{G}_o$ at $\Lambda = \eta_{o\alpha}\,\overline{W}_h/h\,\hat{n}_G$. This value of $\hat{G}_o$ must be adjusted by the ratio of $\sigma_{w_\alpha}/\sigma_{w_{\alpha_G}}$ where

$$\frac{\sigma_{w_\alpha}}{\sigma_{w_{\alpha_G}}} = \frac{\int_{-\infty}^{\infty} \phi(\hat{n})\, H(\hat{n}_{co})\, d\hat{n}}{\int_{-\infty}^{\infty} \phi(\hat{n})\, H(\hat{n}_G)\, d\hat{n}} \quad . \tag{4.60}$$

Values of $\sigma_{w_\alpha}/\sigma_{w_{\alpha_G}}$ can be determined from Figure 4.19 which is a plot of the ratio of the rms value calculated from integrating the spectrum with the high frequency filter of $\hat{n}_f$ to the value computed without filtering, i.e., $\sigma_{w_\alpha}(\hat{n}_f)/\sigma_{w_\alpha}(\infty)$, versus the inverse of the dimensionless filter frequency $\eta_{o\alpha}\overline{W}_h/h\hat{n}_f$.

The number of gusts per unit time which exceed a prescribed value w_{α_p} can now be directly determined from Figure 4.11 by introducing w_{x_G} and G_{o_G} into the appropriate dimensionless quantities. Figure 4.11 gives the value of $G(\hat{w}_{\alpha_p})$ integrated over the year for the Wiebull distribution of interest. Thus $G_G(\hat{w}_{\alpha_p})$ is considered to estimate the number of times per unit time the wind speed will exceed values of $\hat{w}_{\alpha_p}$ for gusts of frequency $\hat{n}_G$ or less, averaged over the year.

4.4.3.2 Gust Shape and Magnitude

The gust shapes and magnitudes described in Section 4.4.1 are intended to be extreme values and should be utilized for maximum loading analysis. For fatigue analysis, however, one is interested in an average gust magnitude and shape. It is important, however, in describing a gust to define to what the gust is relative. For example, most of the wind speed data in which gust analyses have been carried out are data that have been averaged over a 1-h period. Discrete gusts formulated from these data must be applied in the context of fluctuations in loads relative to hourly mean wind speeds. Gusts of periods longer than 1 h cannot be considered to represent wind speed excursions from an hourly mean wind speed. Obviously, gusts of greater than 1-h duration must be relative to wind speeds that have been averaged over a much longer period of time. The next unit of time would appear to be a daily averaging period, in

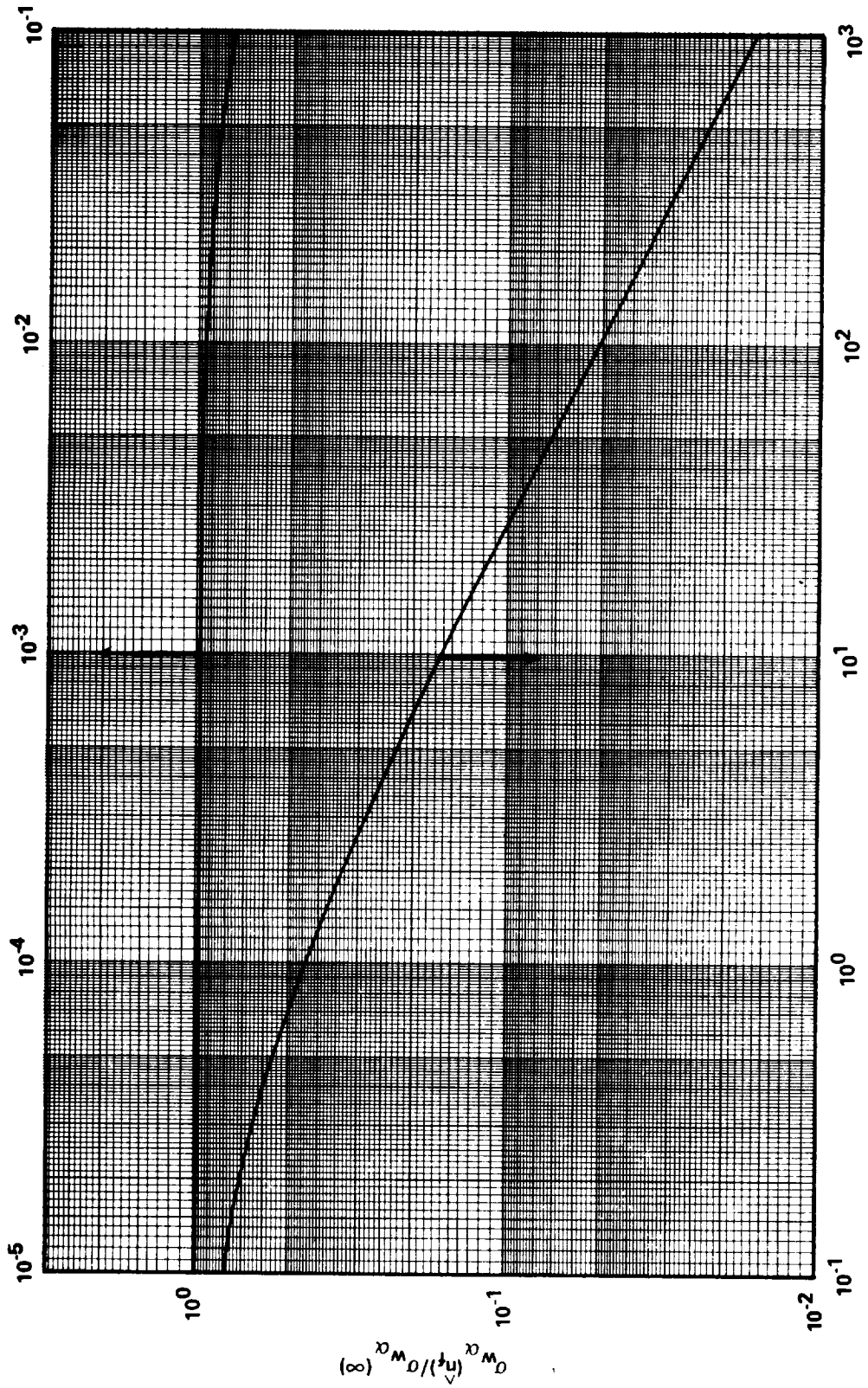

Figure 4.19 Ratio of rms value of $\sigma_{w_\alpha}(\hat{n}_f)/\sigma_{w_\alpha}(\infty)$ for gusts of frequency smaller than $\hat{n}_f$.

which case the fatigue-type gust load would best be treated as a diurnal variation. Gusts relative to an hourly average are discussed in the following text. Gusts relative to a daily average require further study. In this regard one might consider the van der Hoven spectrum and carry out analysis at very low frequencies similar to analyses with conventional spectra. Such information is expected to be of limited use, however, to variable pitch rotors because, in general, pitch responses are on the order of seconds. For fixed pitch rotors, gusts relative to daily averaged wind speeds may be of importance, but they are not considered in this report.

Conventionally, gust shapes utilized for fatigue analysis (e.g., in the aeronautical literature) are assumed to have a 1-cosine distribution. The gust then has the form

$$W_\alpha(t,h,\overline{W}) = W_{A_\alpha}(\tau,h,\overline{W})\,[1 - \cos(\pi t/\tau)] \qquad 0 \le t \le 2\tau \ . \qquad (4.61)$$

The magnitude of the gust amplitude, $W_{A_\alpha}(\tau,h,\overline{W})$, can be related to the rms value of the turbulence fluctuations. The rms turbulence intensities given by equation (4.23) contain gusts of frequencies of all sizes, however; and, as described previously, fatigue analyses for a large structure such as a WTG rotor require knowledge of the amplitude of only those gusts which extend across the entire rotor.

The random amplitude, W_{A_α}, with turbulence intensity $\sigma_{W_{\alpha_G}}$ given by equation (4.60) is assumed to have the distribution

$$p\left(W_{A_\alpha}\right) = 0.44\,|W_{A_\alpha}|\,\exp\left[-\left(W^2_{A_\alpha}/2\sigma^2_{W_{\alpha_G}}\right)^{0.8}\right] \qquad (4.62)$$

where $p\left(W_{A_\alpha}\right)$ is the probability density that a gust of amplitude W_{A_α} will occur. To complete the definition of discrete gusts a set is defined where the period τ is selected according to the following criteria. Let $\tau_o\left(W_{A_\alpha}\right)$ be the most probable period of a gust with amplitude W_{A_α}. Then

$$\tau_o = \begin{cases} \tau_o \ , & \hat{n}_{min} \le 1/\tau_o \le \hat{n}_{max} \\ 1/\hat{n}_{min} \ , & 1/\tau_o < \hat{n}_{min} \\ 1/\hat{n}_{max} \ , & 1/\tau_o > \hat{n}_{max} \end{cases} .$$

The value of $\hat{n}_{max}$ is equivalent to $\hat{n}_G$ defined in the previous section and $\hat{n}_{min}$ corresponds to the minimum frequency response of the WTG system.

4.5 Turbulence Simulation

4.5.1 Introduction

Turbulence simulation is the generation of an analog or digital signal which has the equivalent statistical characteristics to the turbulent atmosphere being simulated. This method is probably the most accurate design tool for analyzing dynamic response of WTG's, although it is the most costly both time-wise and computerwise. Turbulence simulation, however, when properly carried out will provide all three gust components as a function of time. These values can then be input into a dynamic equation of motion for the WTG. Both nonlinear and linear equations can be utilized. The output of the set of equations is the dynamic response of the system as an analog or digital output. From these results the rms response of the system can be determined as well as the extremes or peaks in response, the maximum response time, the energy spectrum of the response, the correlation between the response and the turbulence wind input, and many other such features. Moreover, the turbulence simulation approach to analyzing rotor performance automatically includes directional fluctuations because the w_x, w_y, and w_z components of the wind can be simulated simultaneously. Thus, a complete and reliable turbulence simulation scheme, when applied to a valid and inclusive set of governing equations for the WTG system, allows one to simulate the real life performance of the WTG.

Difficulties associated with the turbulence simulation technique are that computational procedures are generally lengthy and require considerable time on electronic computers. Barring this objection, however, the turbulence simulation analysis of a WTG would provide the most realistic analysis of the effect of turbulence on the turbine generator dynamics, performance, and control systems.

The methodology of turbulence simulation has advanced considerably over the recent years. Section 4.5.2 describes three turbulence simulation techniques from the basic, simple linear filter model to the more elaborate nonlinear models with coherence matching in the vertical direction.

4.5.2 Comparison of Current Simulation Techniques

The degree to which a turbulence simulation is accurate is dependent on the complexity of the filter system used in computing the random signal. The simplest system employs a linear filter with a single Gaussian white noise input, Figure 4.20a. The filter is designed such that the output has the same power spectral density function as the turbulence being simulated. The probability

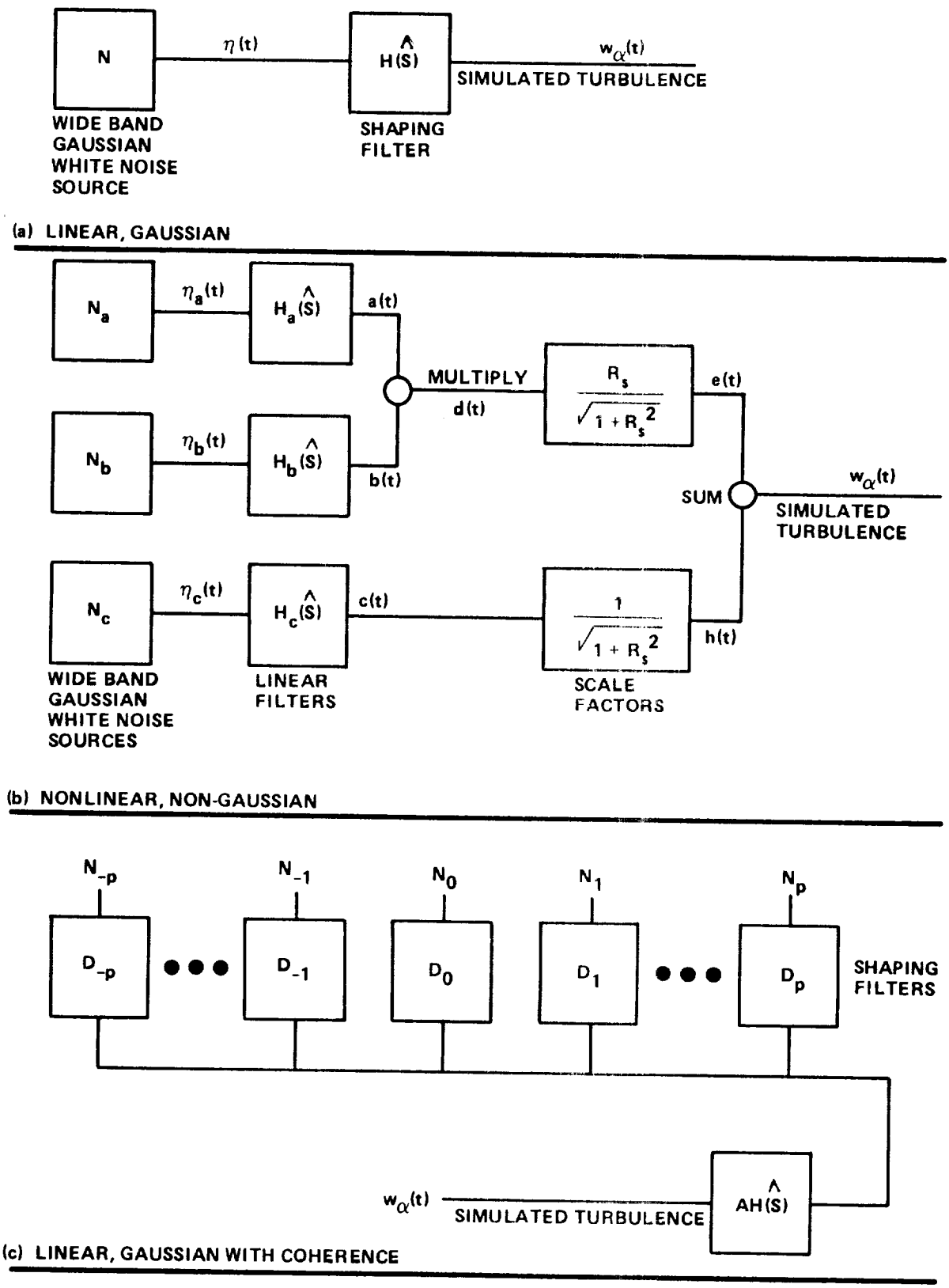

Figure 4.20 Current turbulence simulation models.

distribution of the simulated velocity fluctuations has a Gaussian distribution, however, because a Gaussian input to a linear filter remains Gaussian. Reeves, et al. [4.13] have suggested that atmospheric turbulence is not Gaussian and have developed a nonlinear filter system, as shown in Figure 4.20b. The simulated turbulence by this method has a more realistic probability distribution, as illustrated in Figure 4.21, while at the same time maintaining the correct power spectral density distribution.

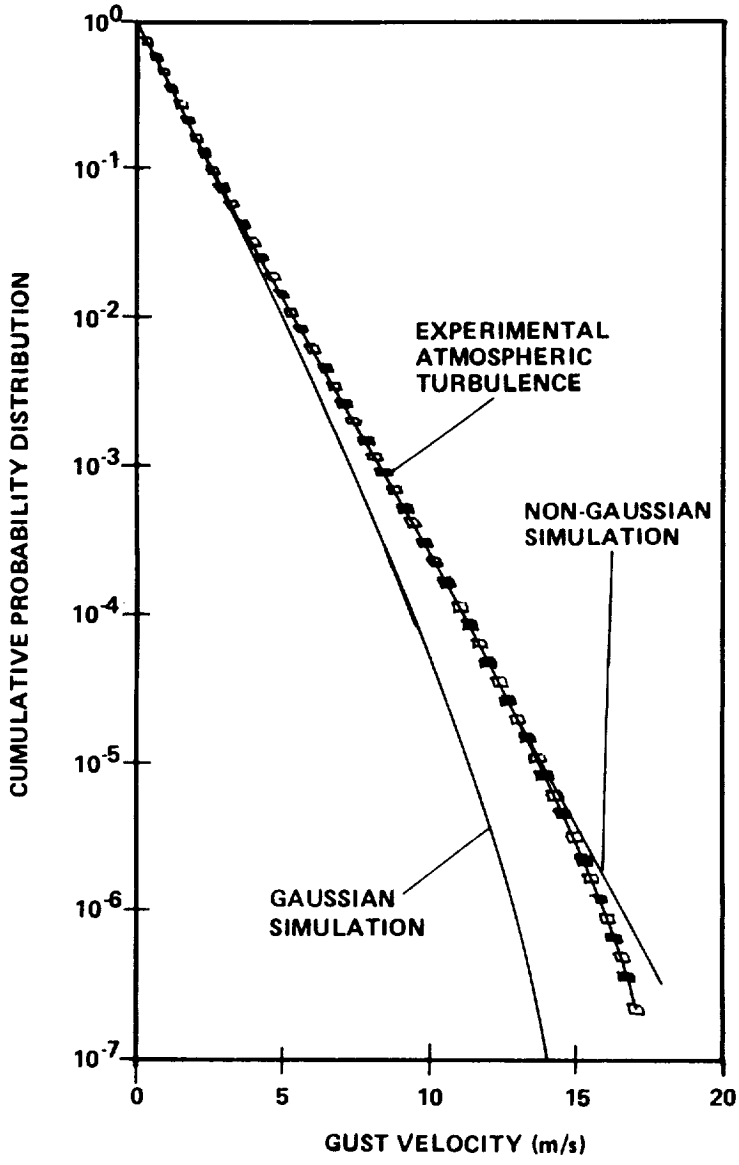

Figure 4.21 Comparison of Gaussian distribution with atmospheric turbulence [4.13].

Fichtl, et al. [4.16] recognized that atmospheric turbulence near the ground has strong coherence between points in the atmosphere separated vertically (Fig. 4.22) and laterally (Fig. 4.23). They have developed a turbulence simulation which accounts for these effects. Figure 4.20c shows the filter system employed, and Figure 4.24 illustrates a simulation by this technique. Other existing models do not take coherence into account and produce turbulence simulation at different levels, as shown in Figure 4.24b. This coherence between vertical layer could possibly become a significant design variable for two-dimensional analysis where fluctuations across the rotor are important.

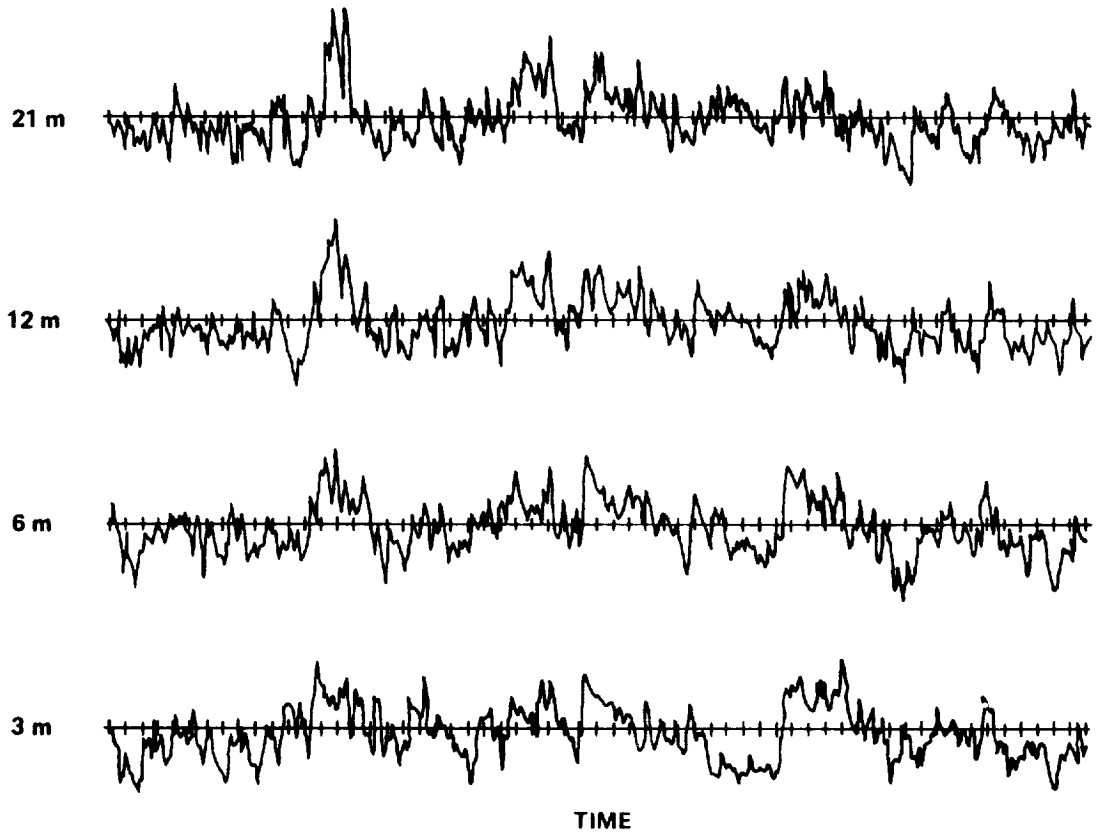

Figure 4.22 Measured time histories of the wind at different evaluations.

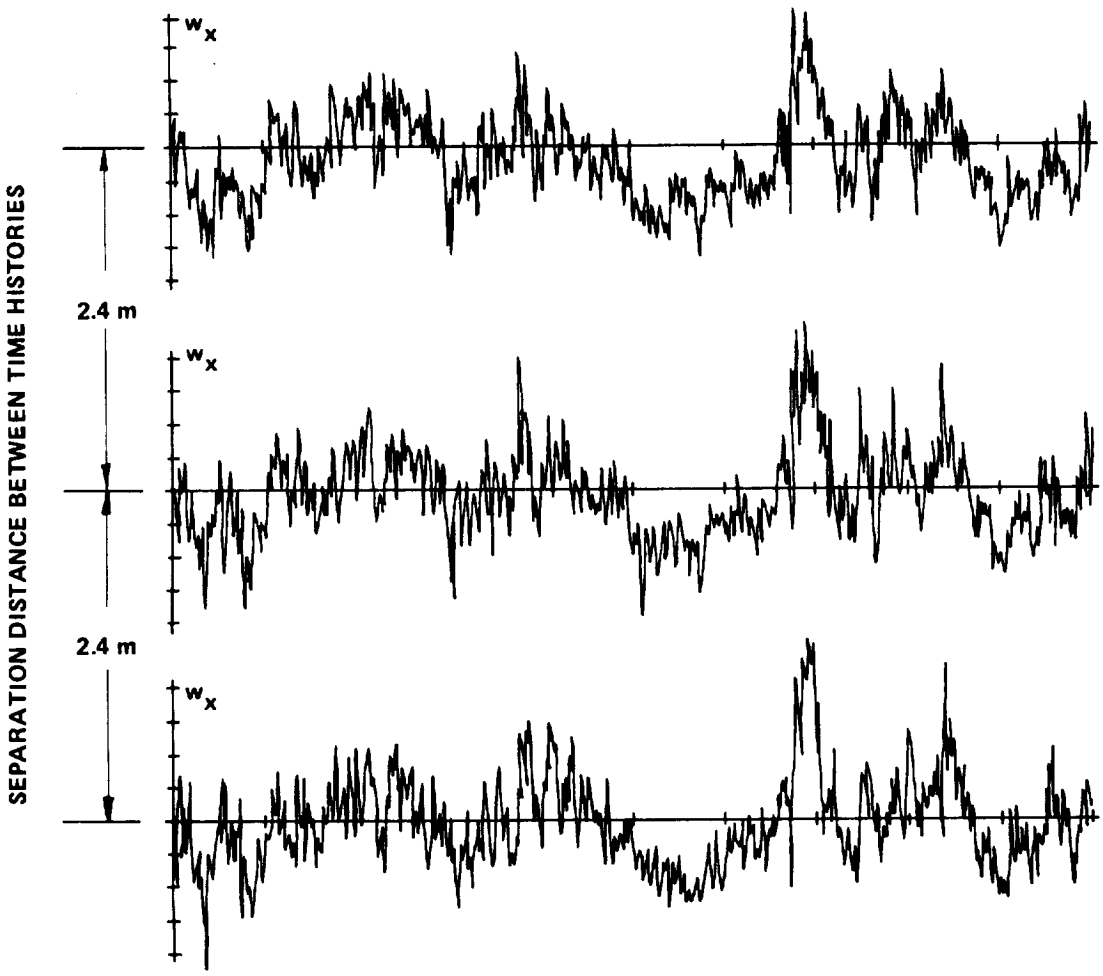

Figure 4.23 Time histories of wind separated in the lateral direction showing strong coherence.

The filter system employed in Reference 4.16 is still linear, however, and therefore the simulated turbulence has a Gaussian probability distribution. Work is required to combine the desirable non-Gaussian features of the Reeves, et al. [4.13] model with the coherence matching of the Fichtl, et al. [4.16] model.

4.5.3 Application to Simple Rotor Solution

Turbulence simulation was applied to the solution of the response of a simplified rotor in Reference 4.7. The one-filter system with Gaussian output is used to generate the random signal. The solution of the nonlinear governing equations of rotor rotation was obtained by a Runge-Kutta integration technique

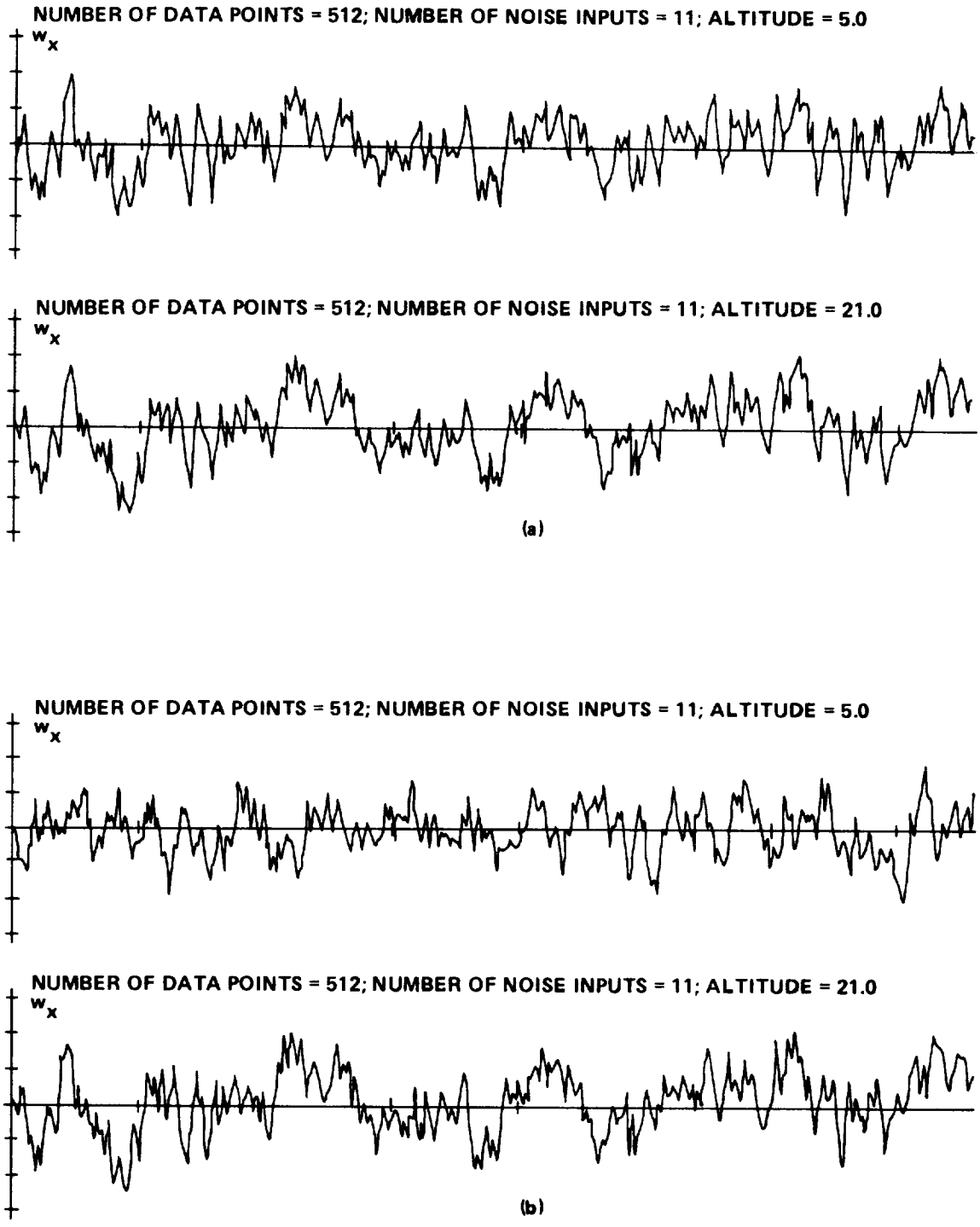

Figure 4.24 Simulated turbulence (a) with coherence and (b) without coherence.

carried out on the IBM 360. A 0.5-s time step was employed with the initial conditions $\bar{\omega} = 0$ at $t = 0$. The mean wind speed was taken as $\overline{W} = 8$ m s^{-1} (18 mph), and the random fluctuation digitized to 0.5-s increments was superimposed on the mean wind. The turbulence simulation incorporated a Dryden spectrum with a length scale of $\hat{L} = 46$ m (150 ft) and a rms value of $\sigma_{w_x} = 0.76$ m s^{-1} (1.7 mph).

Figure 4.25 shows the random response to turbulence of a lightweight, medium weight, and heavy rotor. The lightweight rotor is seen to almost immediately reach quasi-steady-state with rotational fluctuation of standard deviation $\sigma_{\omega'} = 0.80$ s^{-1} around a mean value of $\bar{\omega} = 8.67$ s^{-1}. The heavier concrete rotor reaches quasi-steady-state in approximately 8 min with a mean of $\bar{\omega} = 8.43$ s^{-1} and a rms value of $\sigma_{\omega'} = 0.45$ s^{-1}; whereas for the very heavy rotor the computation was not carried out far enough to establish quasi-steady-state conditions. The total period in real time simulated was approximately 17 min.

Comparison of the wind fluctuations with the response of the lightweight rotor illustrates that this rotor follows the wind very closely. The very heavy rotor, however, is almost insensitive to the turbulence in the wind.

4.6 Two-Dimensional Turbulence

4.6.1 Introduction

Previous analyses contained in earlier chapters have assumed that the gust associated with the turbulence has engulfed the entire rotor or structural component under design. This is the assumption of one-dimensional turbulence. The question as to the validity of this assumption is very important to the design of WTG control systems, to experimental verification of WTG power output, to loading of the rotor resulting from nonuniform gusts over the span of the rotor, etc. These two-dimensional turbulence effects are illustrated schematically in Figure 4.26. Figure 4.26a shows that if the control sensor is located on top of the nacelle, variation in wind speed in a longitudinal direction can result in the sensor monitoring a positive gust, whereas the rotor experiences a negative gust. Therefore, in locating the sensor and computing the appropriate control network, one must have an estimate of how well the wind measured at the sensor location is correlated with the wind which occurs at the rotor. Also, the lag time between the large gusts passing the sensor and impacting upon the rotor is of design interest. Figure 4.26b illustrates the same sort of problem associated with monitoring wind upstream of a wind turbine generator and attempting to correlate

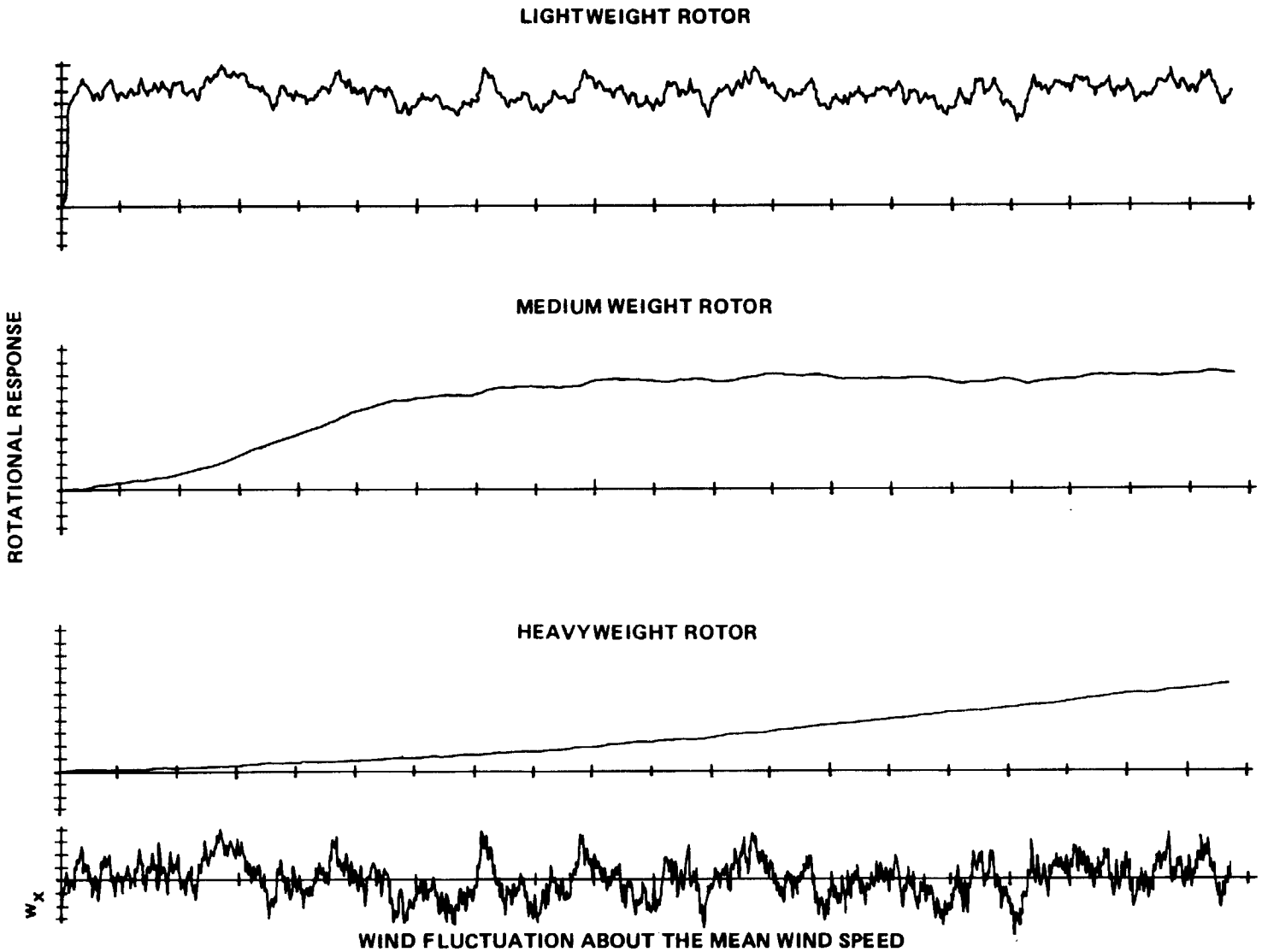

Figure 4.25 Rotational response of wind turbine rotors of different composition starting at rest with a suddenly imposed mean wind of 8 m s^{-1} and simulated turbulence superimposed.

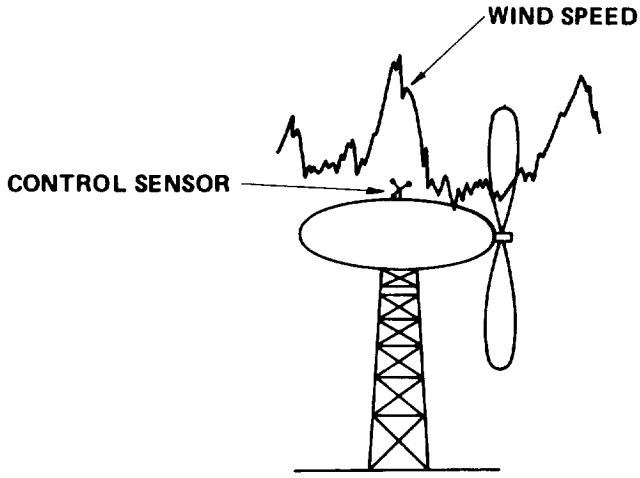

(a) CONTROL SYSTEM REQUIRES CORRELATION BETWEEN WIND SPEED AT SENSOR AND AT ROTOR

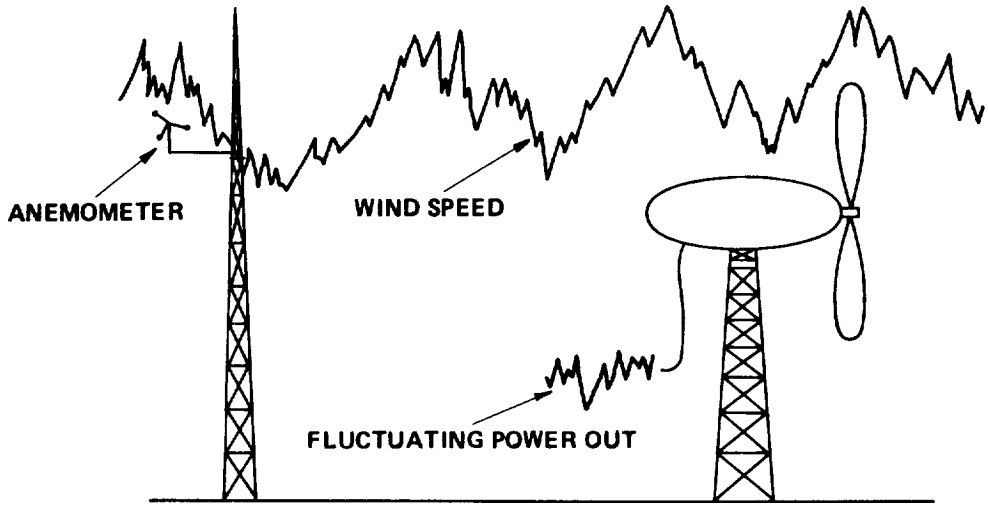

(b) CORRELATION OF WIND SPEED AT MEASURING TOWER WITH WIND SPEED AT ROTOR IS NEEDED FOR EXPERIMENTAL VERIFICATION

Figure 4.26 Schematic illustration of two-dimensional turbulence effects.

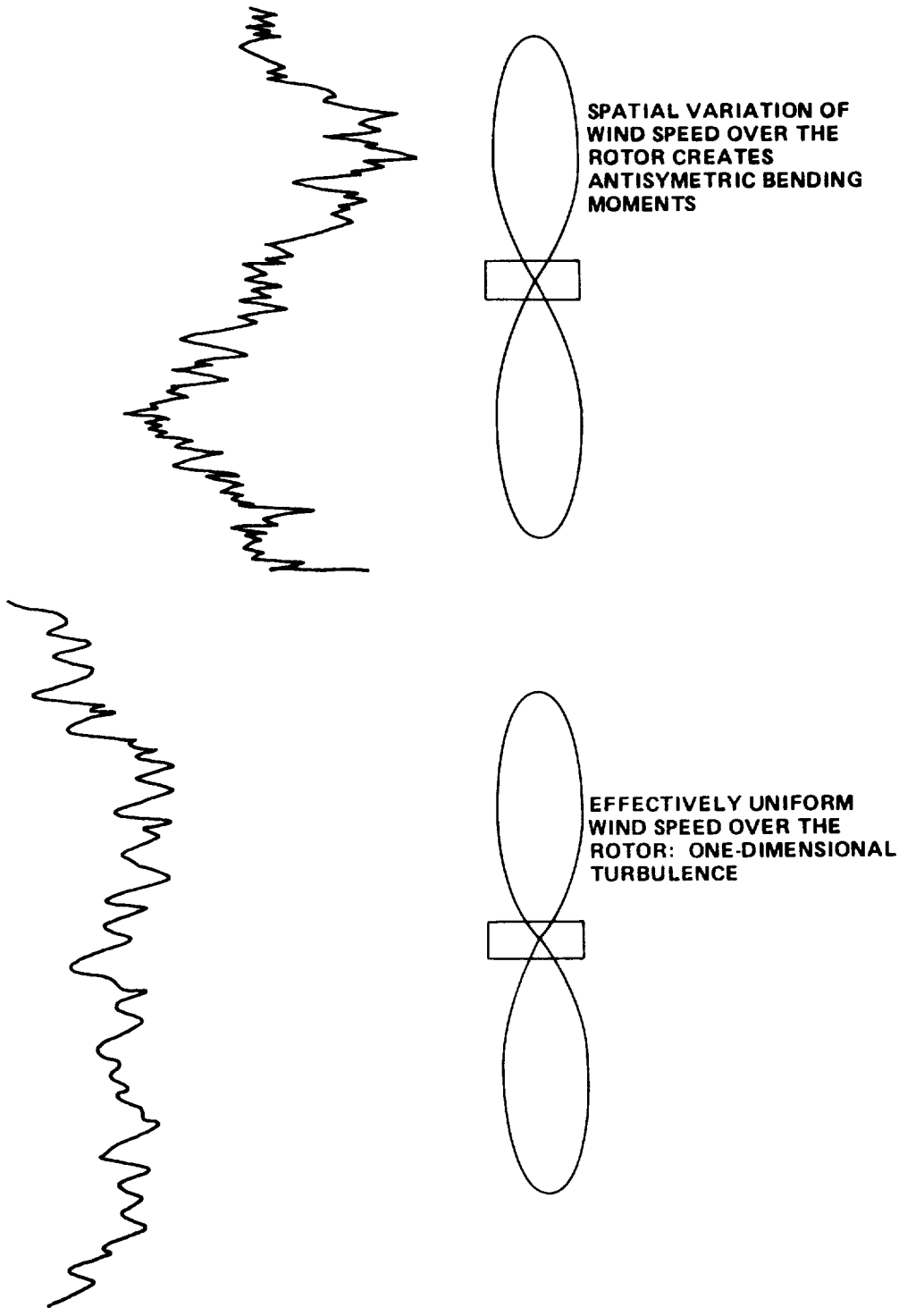

(c) WIND SPEED FLUCTUATION

Figure 4.26 (Concluded).

this with the wind monitored at the rotor and the fluctuating power output. Figure 4.26c schematically illustrates how the spatial variation in wind speed for turbulent gusts across the rotor can create antisymmetric loads and, consequently, large bending moments. These and other problems related to analysis of turbulent effect on WTG's are related specifically to the spatial variation which occurs in gusts making up the turbulent field.

Spatial wind fields are normally determined either by assuming Taylor's hypothesis or by measuring the wind with an array of towers. Since wind speed is normally measured as a time signal at a single point in space, it is generally converted to a spatial distribution with Taylor's hypothesis, i.e.,

$$x = \overline{W}\, t \quad . \tag{4.63}$$

This is also referred to as the frozen turbulence concept. Figure 4.27 shows a time history of wind speed measured at the 24-m level of a tower. The mean wind speed at this level is 6.64 m s^{-1}. The figure illustrates the temporal variation and the spatial variation based on the frozen turbulence concept. Taylor's hypothesis assumes that the velocity profile illustrated would be distributed in space according to the horizontal x-axis.

Spatial variation at two or more points in space can also be measured with one or more towers. The spatial variation in the vertical direction can be measured with a single tower instrumented at different levels and in the horizontal or lateral direction with an array of towers. Figure 4.28 shows the former case of longitudinal wind speed measured at the 24-, 12-, 6-, and 3-m levels. Many interesting features of two-dimensional turbulence are contained in this figure, and these will be discussed in subsequent sections.

Quantitative estimates of the effect of spatial variation in the wind fields are provided by four statistical quantities which are described in Sections 4.6.2 through 4.6.6. These quantities are:

1) Correlation coefficient

2) Cross spectra or cross correlation

3) Coherence function

4) ΔW statistics.

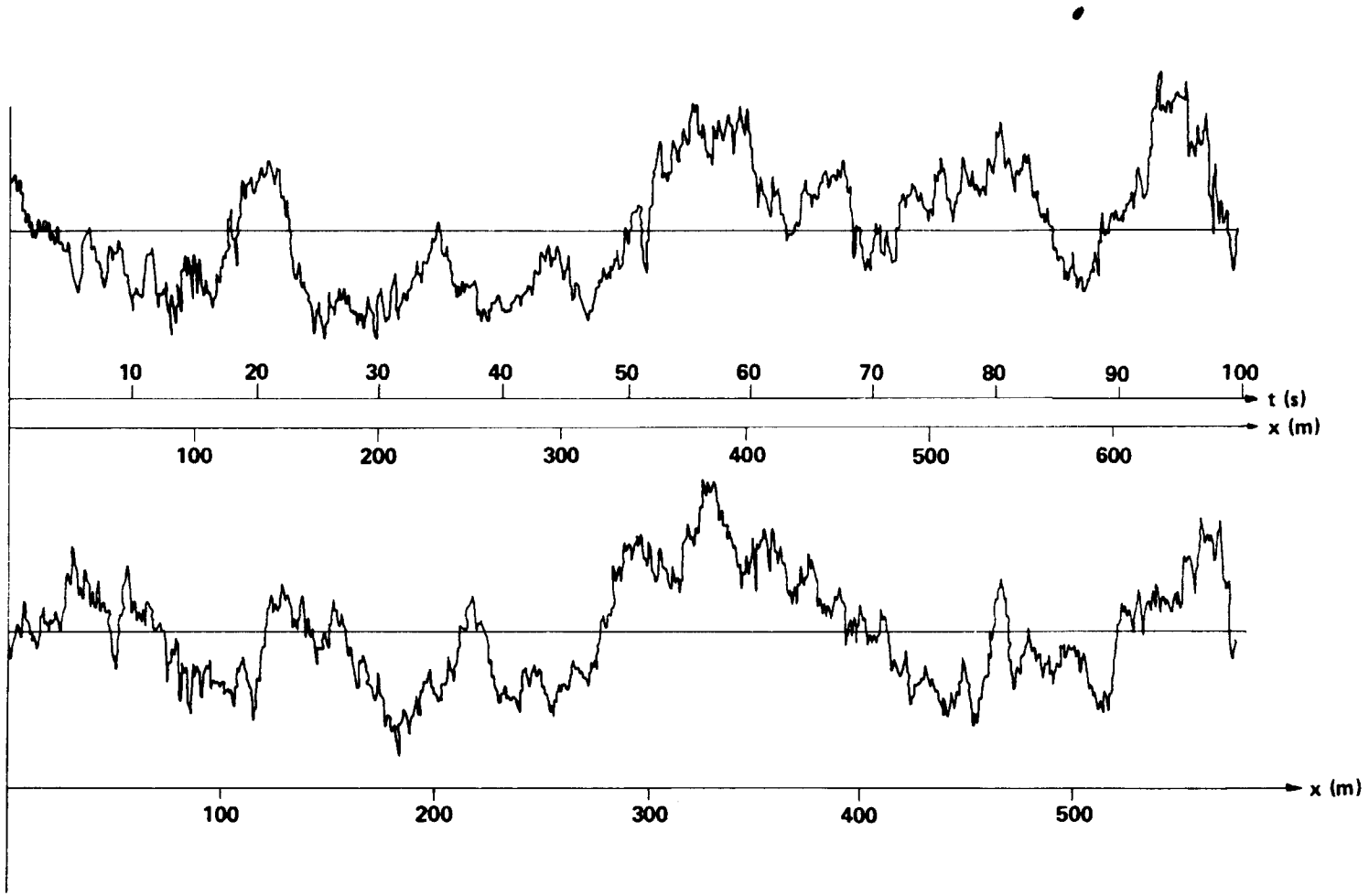

Figure 4.27 Illustrates Taylor's hypothesis (frozen turbulence) with data measured at 24- and 12-m level.

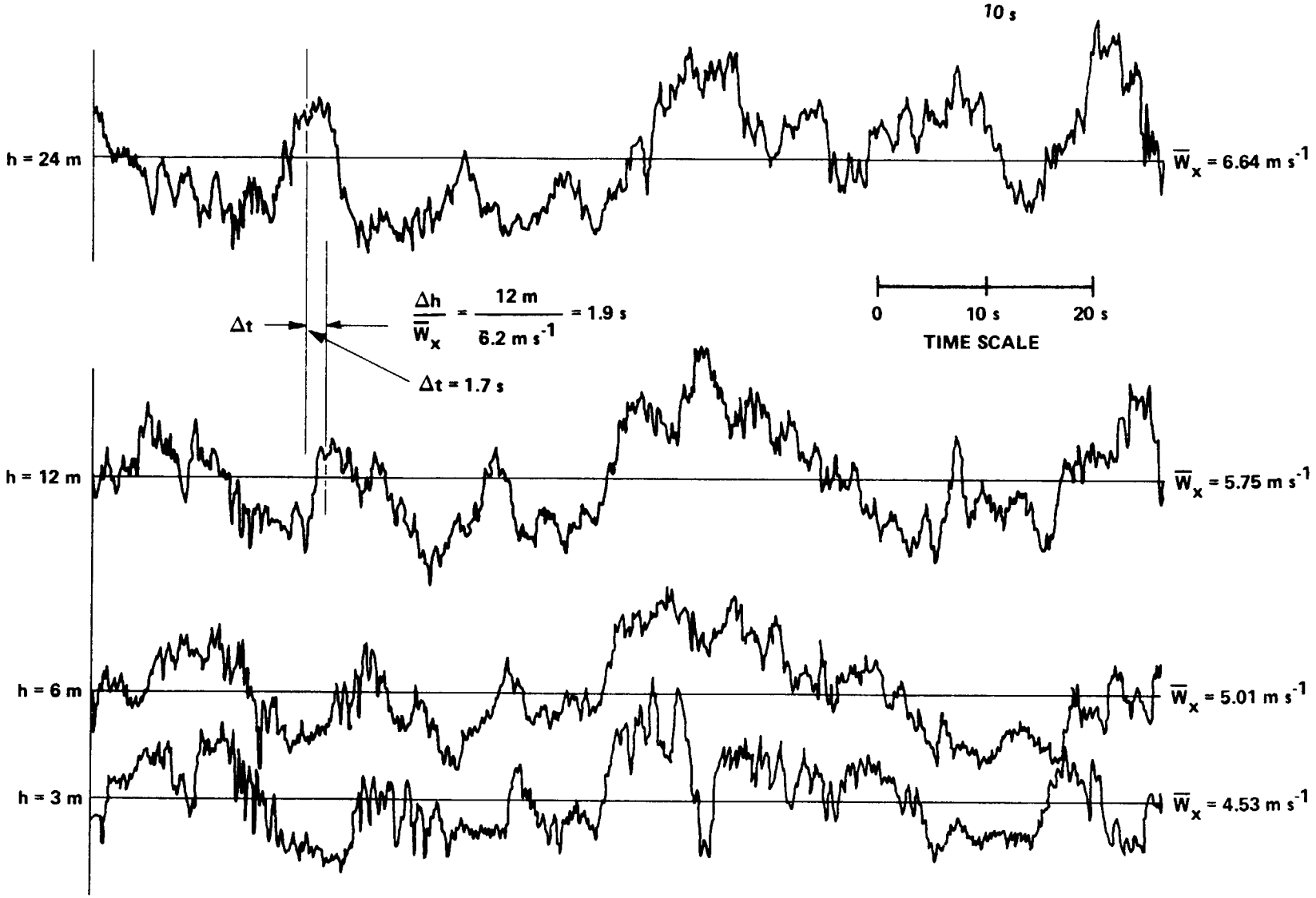

Figure 4.28 Features of two-dimensional turbulence measured with a single tower at 24-, 12-, 6-, and 3-m level.

4.6.2 Correlation Coefficients

The correlation coefficient is defined as

$$R_{ij}(r) = \overline{w_i(x)w_j(x+r)}/\sigma_i\sigma_j \quad . \tag{4.64}$$

This quantity is a measure of how fluctuations in the wind speed component, w_i, measured at the position, x, correspond or correlate with fluctuations in the wind speed component, w_j at $x + r$. Two common mathematical forms of correlation coefficients are the Dryden and the von Karman:

von Karman	Dryden

Longitudinal Correlation Function:

$$f(r) = \frac{2^{2/3}}{\Gamma(1/3)}\left(\frac{r}{aL_p}\right)^{1/3} K_{1/3}\left(\frac{r}{aL_p}\right) \qquad f(r) = e^{-r/L_p} \tag{4.56a}$$

Transverse Correlation Functions:

$$g(r) = \frac{2^{2/3}}{\Gamma(1/3)}\left(\frac{r}{aL_p}\right)^{1/3}\left(K_{1/3}\left(\frac{r}{aL_p}\right) - \left(\frac{r}{2aL_p}\right)K_{2/3}\left(\frac{r}{aL_p}\right)\right) \qquad g(r) = e^{-r/L_p}\left(1 - \frac{r}{2L_p}\right)$$

$$a = 1.339 \tag{4.56b}$$

where K is the modified Bessel function of the second kind, and L_p is the longitudinal isotropic turbulence integral scale. Figure 4.29 defines longitudinal and transverse correlation coefficients and Figure 4.30 gives a plot of both the longitudinal and transverse von Karman correlations. The integral length scale, L_p, appearing in the correlations is discussed in the following section.

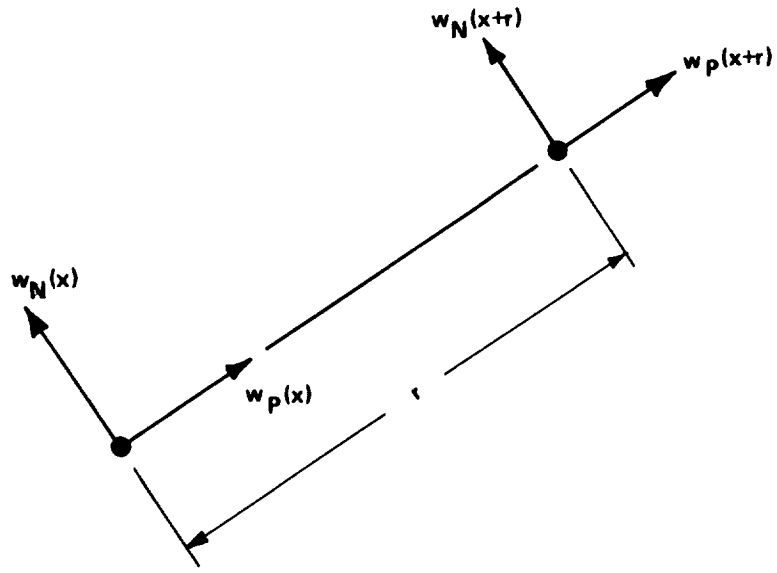

$$f(r) = R_{pp}(r) = \frac{\langle w_p(x) w_p(x+r) \rangle}{\sigma_{pp}^2}$$

$$g(r) = R_{NN}(r) = \frac{\langle w_N(x) w_N(x+r) \rangle}{\sigma_{NN}^2}$$

Figure 4.29 Fundamental correlation function.

4.6.3 Integral Length Scale

Although the preceding correlations are based on the assumption of isotropic turbulence which is a reasonable assumption at high altitudes [h > 300 m (1000 ft)], a technique frequently employed to adapt these isotropic relationships to low altitudes is to permit the integral length scale to vary with height, with surface roughness, and to be different for the longitudinal direction from what they are for the lateral and vertical directions. From the survey by Counihan [4.17] the following relationship for the integral length scales are recommended:

$$L_{w_y}/h_I = L_{w_z}/h_I = \begin{cases} 0.4\, h/h_I & h \leq h_I \\ 1.0 & h \geq h_I \end{cases} \qquad (4.66)$$

h_I = 250 m (820 ft)

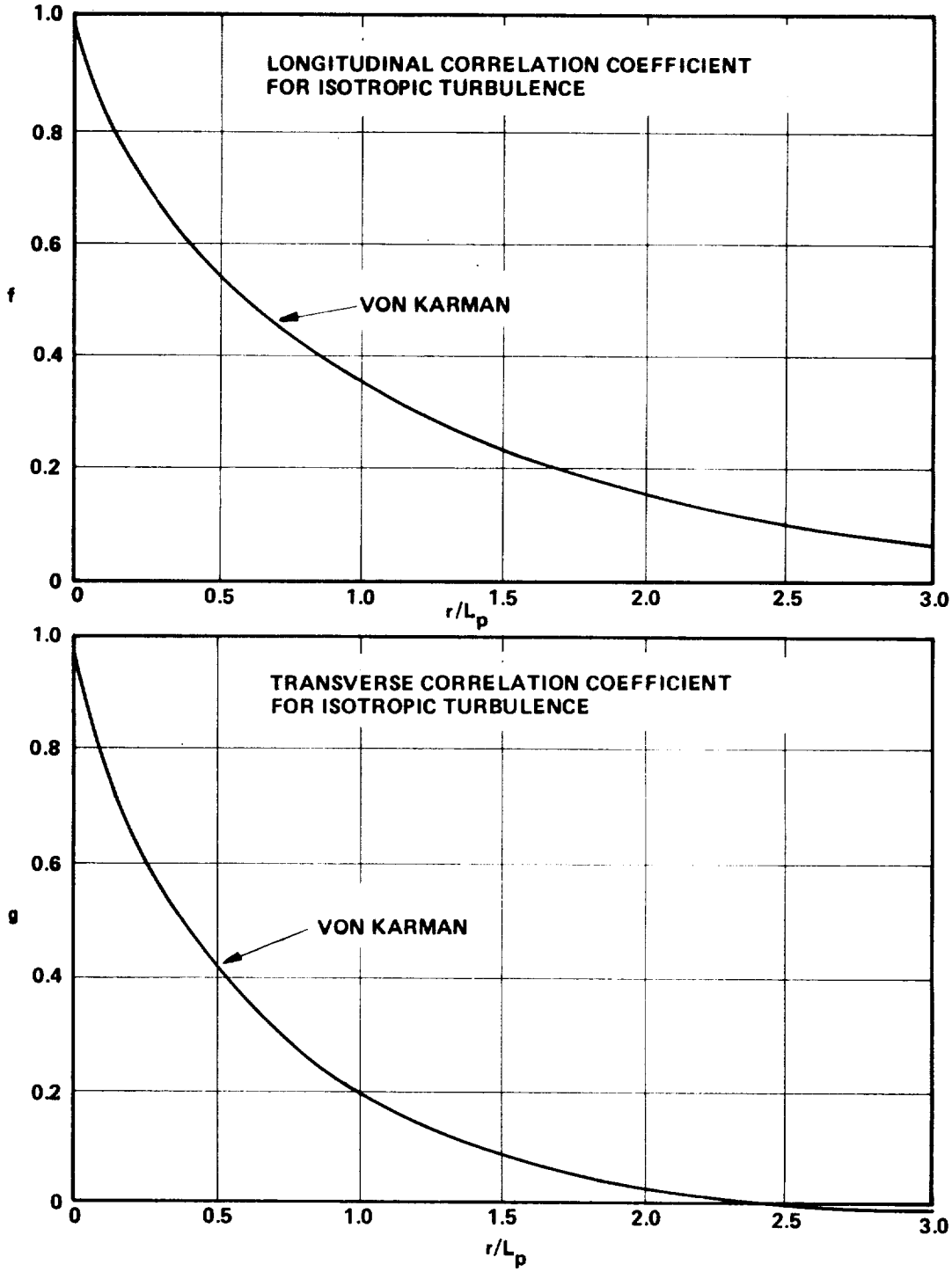

Figure 4.30 Von Karman fundamental correlation function.

$$L_{w_x}/h_I = \begin{cases} 25\, h^c/z_o^{0.4} & h \le h_I \\ 1.0 & h \ge h_I \end{cases}$$

$$h_I = 250 \text{ m } (820 \text{ ft})$$

$$c = e^{-0.025(\ell n\, z_o)^2 + 0.17\, \ell n\, z_o - 0.8} .$$

These relationships are plotted in Figure 4.31. The length scales described are illustrated in Figure 4.32. Two other length scales are also described in the figure. Counihan [4.17] recommends values for these given by

$$\left(L_{w_x}\right)_y = \left(L_{w_x}\right)_z = 0.5\, L_{w_x} .$$

Applications of the correlation coefficients is illustrated by the following example.

Example 4.6: A wind sensor located on top of a nacelle is used to control rotor pitch at the hub (Fig. 4.34a). The question arises as to how far upstream the sensor can be located and have the wind it senses be correlated with that of the hub. Assume a hub height of $h_H = 30$ m (100 ft), a surface roughness of $z_o = 0.1$ m, and a mean wind speed of 3 m s^{-1} (6.7 mph). We will also assume $L_p = L_{w_x}$. From Figure 4.31, the length scale at $h_H = 30$ m is $L_{w_x} = 155$ m (509 ft). If we accept a longitudinal correlation coefficient of 0.8 as being satisfactory, the value of r/L_{w_x} for the longitudinal velocity fluctuations is 0.14. Thus, the sensor should be located within $r = 0.14\, L_{w_x} =$ 21.7 m (71 ft).

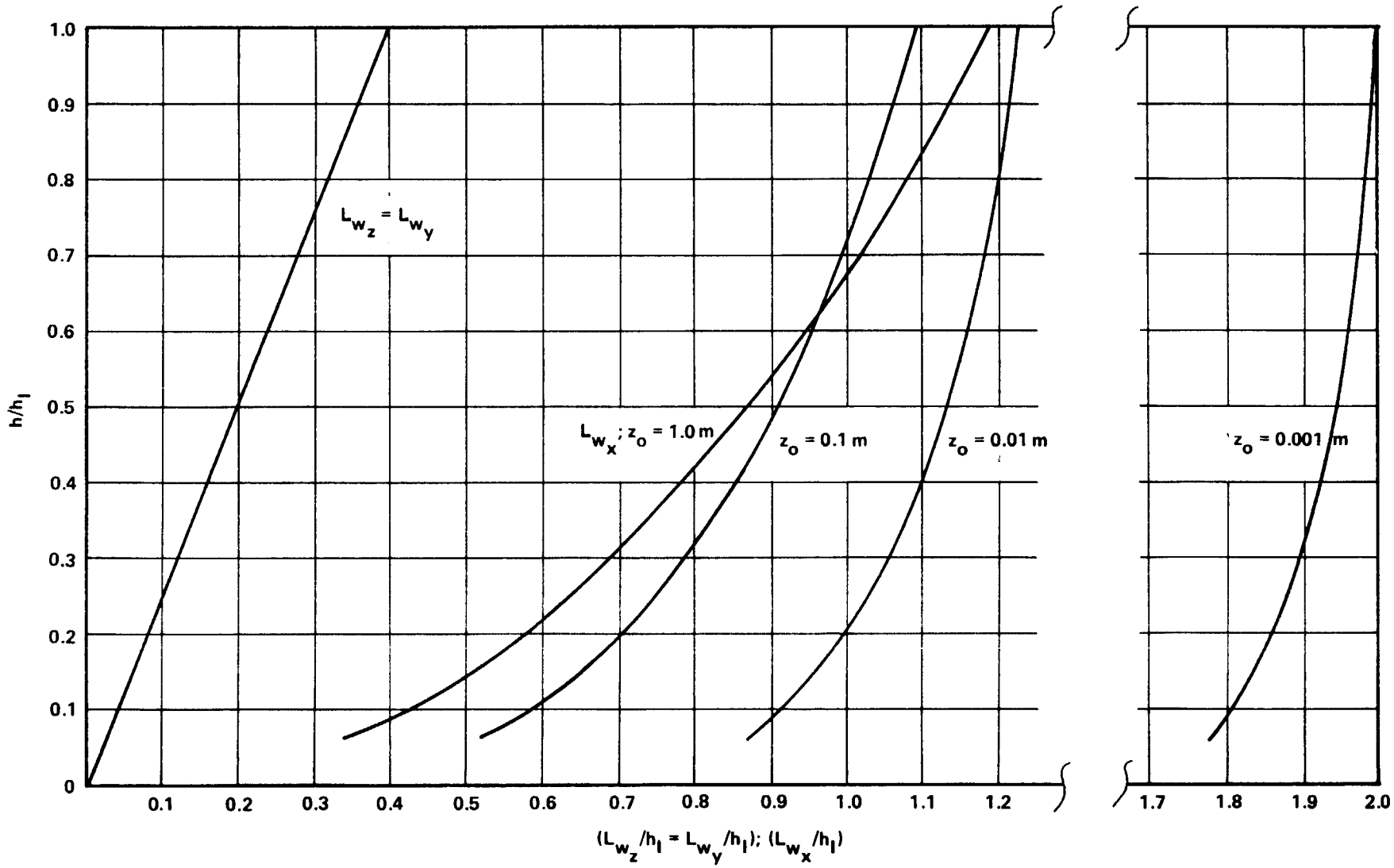

Figure 4.31 Integral scale length h_I = 250 m (820 ft).

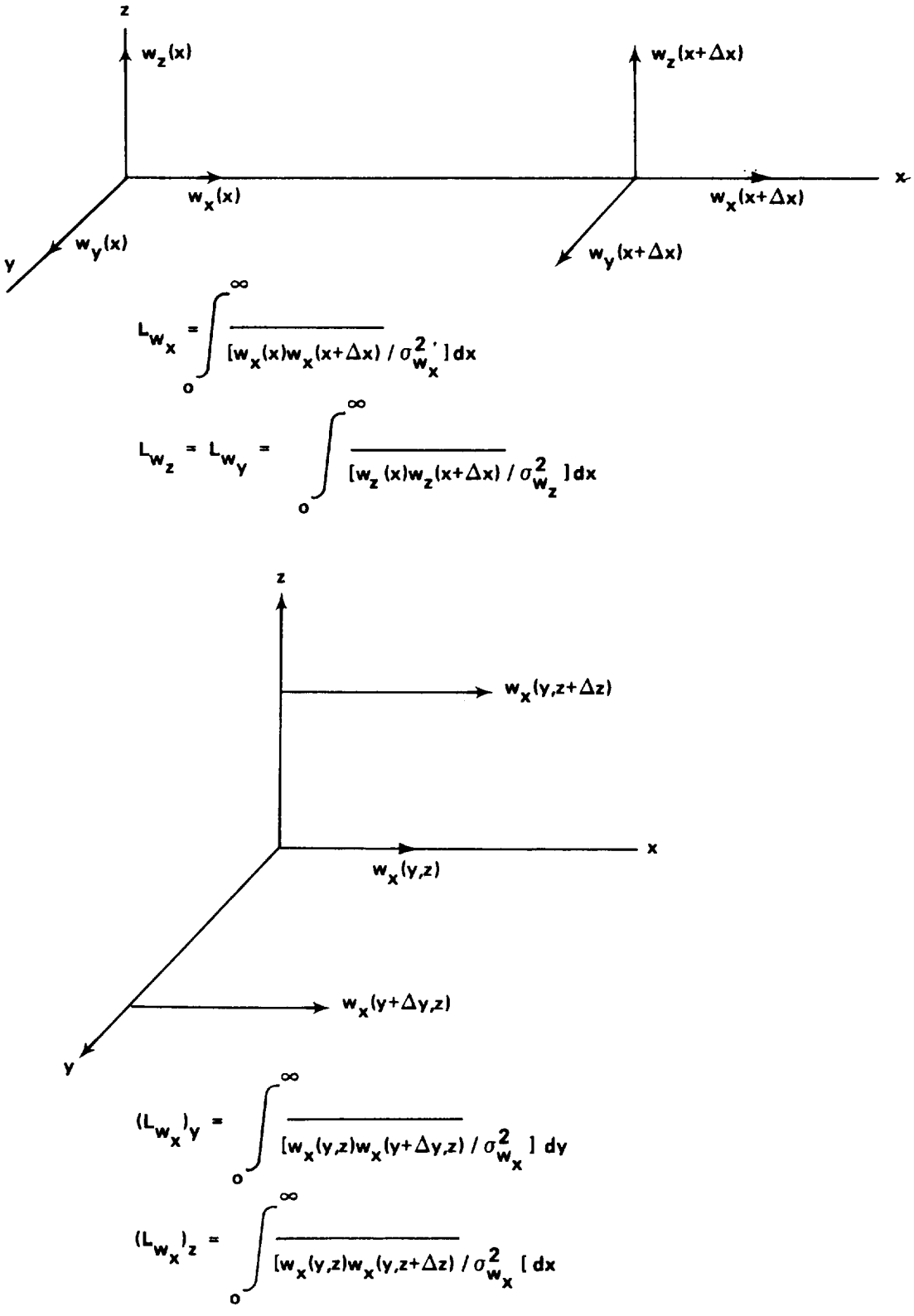

Figure 4.32 Definition of integral length scales.

The correlation coefficient provides us a relationship between the correlation of fluctuations in the wind averaged over all values of gust sizes. In many cases, however, we are interested in the correlation between fluctuation in wind speeds of a prescribed frequency. In this case, we turn to the statistical quantity known as the two-point spectrum or nondimensional two-point spectrum.

4.6.4 Two-Point Spectrum

Correlation of velocity over different spatial separations can be expressed by the two-point spectrum which has two parts — a real part, cospectrum, and an imaginary part, quadrature spectrum. Also, this spatial variation in velocities can be expressed in terms of the dimensionless two-point spectrum. The latter form seems more manageable for wind loading applications and also has real and imaginary components as expressed below:

$$\phi\left(x, x'; \frac{\hat{n}}{\overline{W}}\right) = \frac{Co\left(x; x'; \frac{\hat{n}}{\overline{W}}\right) + iQu\left(x, x'; \frac{\hat{n}}{\overline{W}}\right)}{\left(\phi\left(x; \frac{\hat{n}}{\overline{W}}\right)\ \phi\left(x'; \frac{\hat{n}}{\overline{W}}\right)\right)^{1/2}} \tag{4.67}$$

where $\hat{n}/\overline{W}$ is the wave number, x and $x' = x + r$ are two spatial coordinates, Qu is the quadrature spectrum (out-of-phase component) of the two-point spectrum, Co is the co-spectrum (in-phase component) of the two-point spectrum, and ϕ is the one-point spectrum.

For reasons of symmetry, the quadrature spectrum between similar velocity components is usually zero for points in the same horizontal plane. For vertical separations, however, Qu is nonzero, although usually not as significant as Co. The existence of the quadrature component can be taken to indicate a preferred orientation of eddies and therefore only occurs when there is asymmetry present in the flow. For example, there is no significant quadrature component in the horizontal direction cross wind spectrum between like components of velocity; however, in the vertical direction where there is strong asymmetry, the quadrature component is significant, and the maximum correlation in the horizontal wind speed at two different heights occurs not simultaneously but when the signal from the lower station is delayed by time roughly equal to $\Delta z/\overline{W}$. It is interesting to inspect Figure 4.28 in this regard where it has been

illustrated that the delay time between eddies of the 24- and 12-m level is approximately $\Delta t = 1.7$ s whereas the calculated value of $\Delta z/\overline{W} = 1.9$ s. This means that in the vertical direction a signal hits the top of the tower before it hits the bottom because eddies lean into the wind as a result of wind shear.

Houbolt and Sen [4.18] have computed two-point spectra for vertical gusts in isotropic turbulence based on a von Karman correlation model. They find

$$\phi(\sigma, \eta)_{w_z} = 0.73\sigma_{w_z}^2/\sqrt{2\pi}\,\Gamma(1/3)\left[4.78\,\sigma^{5/3}K_{5/6}(\eta)/\eta^{5/6} - \sigma^{11/3}K_{11/6}(\eta)/\eta^{11/6}\right]$$

while for longitudinal gusts

$$\phi(\sigma,\eta)_{w_x} = 2.61\left(\sigma_{w_x}^2/\sqrt{2\pi}\,\Gamma(1/3)\right)\sigma^{5/3}K_{5/6}(\eta)/\eta^{5/6} \qquad (4.68)$$

where $\sigma = r/L_{w_x}$, $\eta = \hat{n}L_{w_x}/\overline{W}$ and K is the modified Bessel function of the second kind. Equation (4.68) is plotted in Figure 4.33. This figure was developed for two-point spectra of nonuniform spanwise gusts on airfoils but has direct application to nonuniform spanwise gusts on WTG rotors.

Example 4.7: Determine the size of vertical gusts which will be uniform across a 38-m (125-ft) diameter rotor in the horizontal position on a 30-m (100-ft) hub height tower for the same conditions given in Example 4.6.

The length scale from Figure 4.31, Section 4.6.3, is $L_{w_x} = 155$ m (509 ft). The value of $\sigma = r/L_{w_x} = 0.25$. Assume that a value of $\bar{\zeta} = 2\phi(\sigma,\eta)_{w_z}/\sigma_{w_z}^2$ less than 10^{-2} indicates that the velocity fluctuations at one end of the rotor are no longer

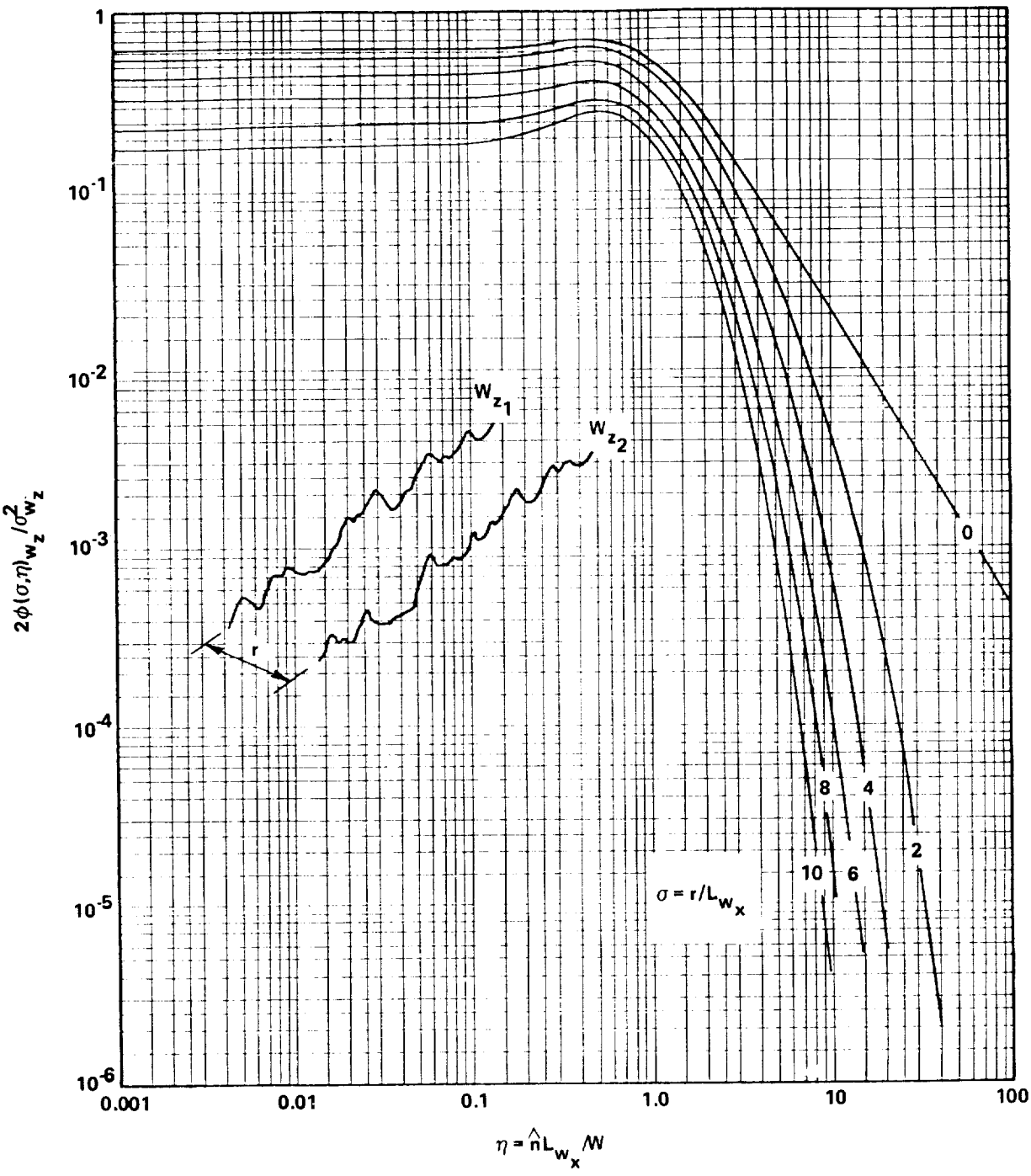

Figure 4.33 Two-point spectra for treatment of nonuniform spanwise gusts [4.18].

correlated with those at the other end. From Figure 4.33 the value of $\eta = \hat{n}L_{w_x}/\overline{W}$ at $\bar{\zeta} = 10^{-2}$ and $\sigma = 0.25$ is approximately 14 from which $\hat{n}$ is computed at $\overline{W}_x = 3.6$ m s^{-1} (8 mph) as 0.33 s^{-1}. This implies that gusts of $\tau = 1/\hat{n} = 3$ s duration or less in the lateral direction will not extend uniformly over the span of the rotor.

4.6.5 Coherence

The coherence is defined as the absolute value of the two-point spectrum

$$\text{coh} = |\phi(x, x'; \hat{n}/\overline{W})| \tag{4.69}$$

and serves as a more useable form of the two-point spectrum.

Coherence is expressed by the relationship:

$$\text{coh} = e^{-a\hat{n}\Delta x/\overline{W}}_{h=10\text{ m}} \tag{4.70}$$

where Δx is the spatial separation between the two points at which the wind speed is measured. The decay coefficient, a, is approximately equal to 7.5 for vertical separation and 4.5 for horizontal separation. These values represent an average of the decay coefficients reported in References 4.19, 4.20, and 4.21. The lateral decay coefficient is approximately equal to the vertical decay coefficient. Hence

$$a_x \approx 4.5 \quad ; \quad a_y = a_z \approx 7.5 \quad . \tag{4.71}$$

The reader is cautioned that the values of a quoted are current state-of-the-art values and much research remains to be done before their value is confirmed. Moreover, it is known that a is dependent on terrain roughness, atmospheric stability, and spatial separation.

The coherence is plotted as a function of reduced frequency $\eta = \hat{n}\Delta x/\overline{W}_{h=10\ m}$ in Figure 4.34.

The coherence function is a measure of the correlation of velocity fluctuations of frequency, $\hat{n}$, between spatial points separated by Δx. Illustrative examples are given as follows:

Example 4.8: Inspection of Figure 4.34 shows that the vertical coherence approaches zero at $\eta \approx 0.5$. This indicates there is negligible correlation when the height separation is approximately one-half of the length scale, $\hat{L} = \overline{W}_{h=10}/\hat{n}$. The eddies are therefore on the average roughly one-half as long as they are high. However, the horizontal coherence approaches zero at $\eta \approx 1$ which confirms the length, $\hat{L} = \overline{W}_{h=10\ m}/\hat{n}$.

Example 4.9: A control sensor is positioned downstream of the wind. How far upstream will it sense a gust of 10-s duration? The gust frequency is $0.1\ s^{-1}$. Assume that the correlation is not significant when the horizontal coherence is less than 0.5. For this case $\Delta x/\overline{W}_{h=10\ m} = 1.54$ s and at a wind speed of $\overline{W}_{h=10\ m} = 4\ m\ s^{-1}$, $\Delta x = 6.2$ m.

4.6.6 $\Delta\overline{W}$ Statistics

Ramsdell [4.22] has established the standard deviation and other statistics of the difference in wind speed at points separated in both the lateral and vertical directions divided by the separation difference. The random variable in this case is

$$\Delta\overline{W}(\Delta x_i, t)/\Delta x_i = [\overline{W}(x_i, t) - \overline{W}(x_i', t)]/\Delta x_i$$

which is called $\Delta\overline{W}$ statistics in this report. The random variable, however, is a measure of the fluctuating wind shear. The terms x_i and x_i' are two positions in the ith direction separated by the distance Δx_i.

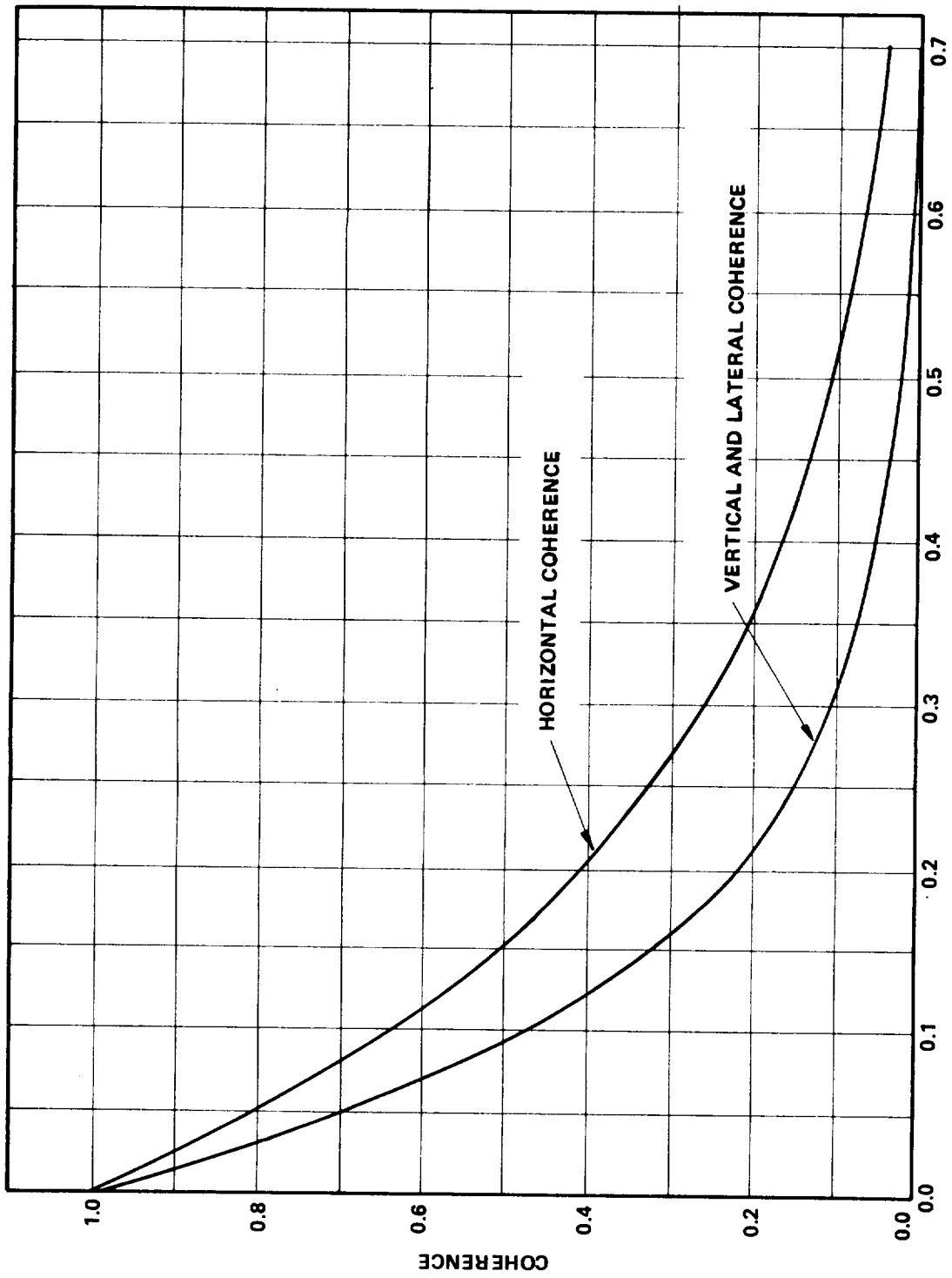

Figure 4.34 Vertical and horizontal coherence.

Figure 4.35 and 4.36 [4.22] are plots of the standard deviation of the wind shear in longitudinal wind speed separated by a vertical distance, Δz, and a lateral distance, Δy, respectively. A correlation of these results is

$$\sigma_{\Delta\overline{W}/\Delta z}/fz_o = 5.44(\overline{W}/f\Delta z)^{0.90}$$

and

$$\sigma_{\Delta\overline{W}/\Delta_y}/fz_o = 12(\overline{W}/f\Delta y)^{0.78}$$

where f is the Coriolis parameter approximately equal to 10^{-4} s^{-1}.

These correlations allow an estimate of the probability of longitudinal wind speed being uniform over the complete rotor. Consider the following example.

Example 4.10: A wind tower having a rotor diameter of 38 m (125 ft) and a hub height of 30 m (100 ft) is located over terrain of roughness, $z_o = 0.1$ m. Estimate the difference in the longitudinal wind speed across the rotor laterally at a wind speed of 4 m s^{-1} (9 mph).

From Figure 4.36 the value of $\sigma_{\Delta W/\Delta y}/fz_o$ at $\overline{W}/f\Delta y = 1053$ is 2732. Thus, $\sigma_{\Delta W/\Delta y} = 0.027$ s^{-1}. The wind speed difference is approximately $\Delta W = 3.38$ m s^{-1} (7.55 mph).

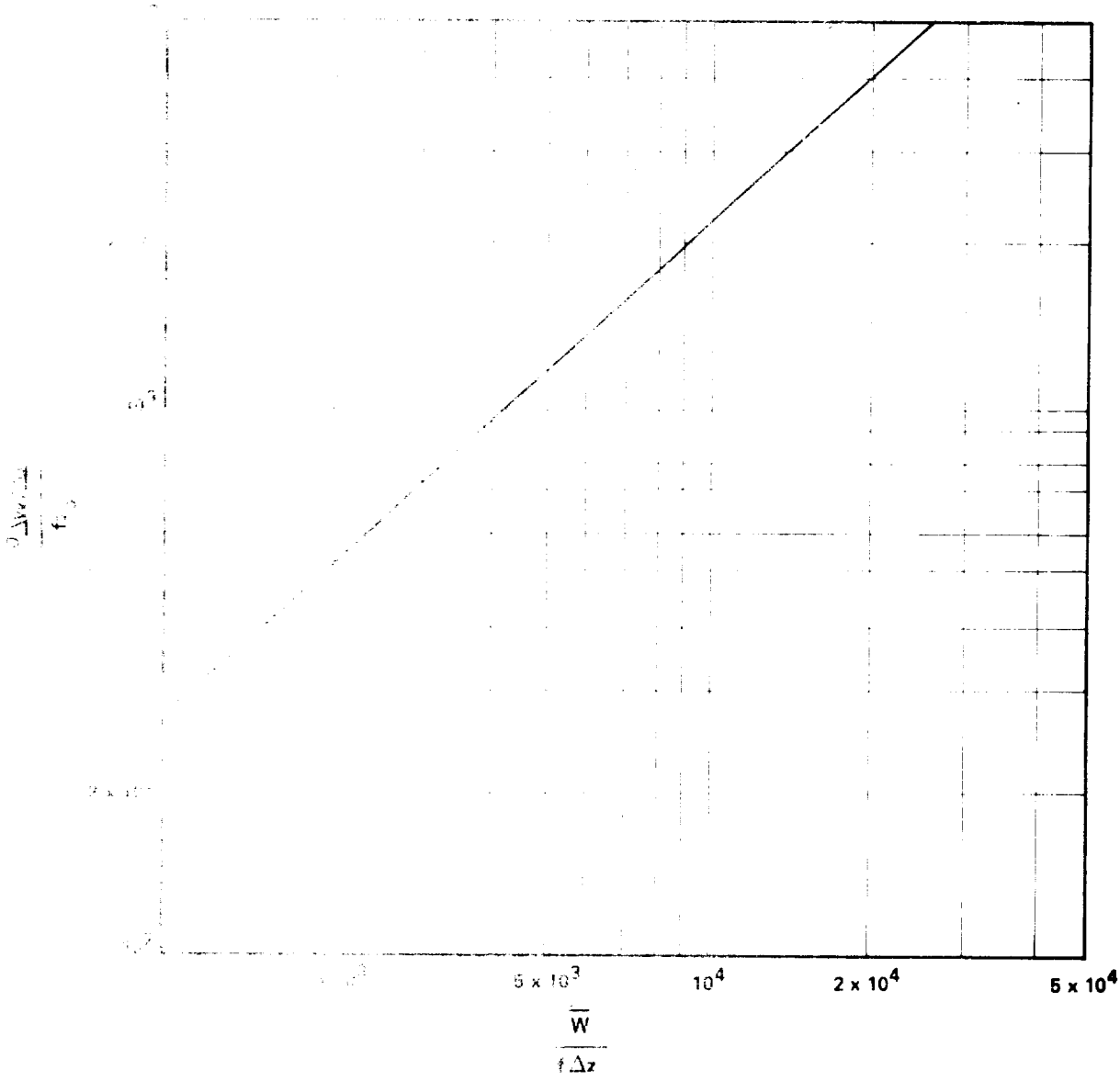

Figure 4.3 Standard deviation of vertical wind shear, $\Delta W/\Delta z$.

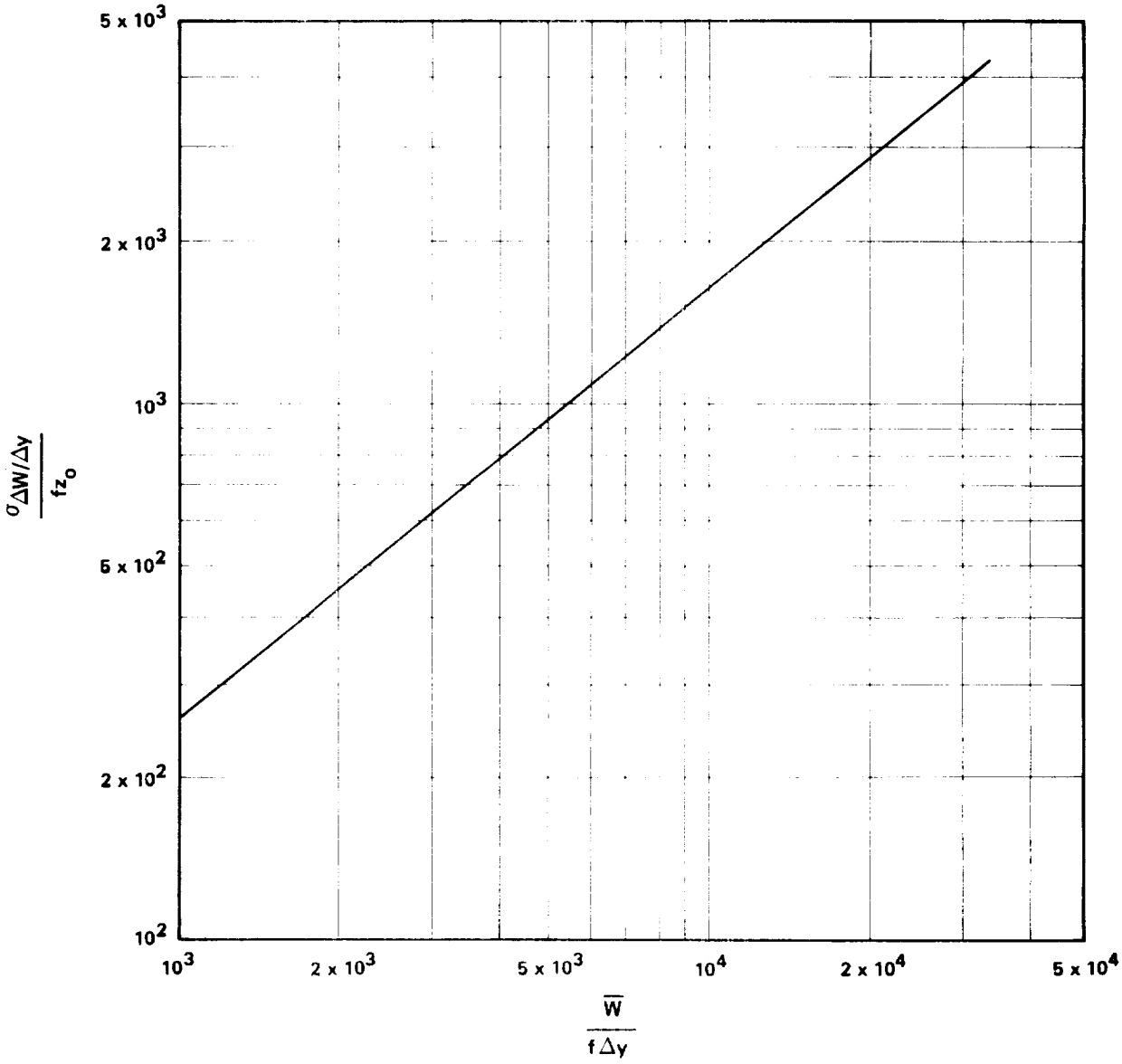

Figure 4.36 Standard deviation of lateral wind shear, $\Delta W/\Delta y$.

REFERENCES

4.1 Camp, D. W.: Low Level Wind Gust Amplitude and Duration Study. NASA TM X-53771, August 1968.

4.2 Busch, Niels E.: The Surface Boundary, Part I. Boundary Layer Meteorology, vol. 4, 1973, pp. 213-240.

4.3 Kaimal, J. C.: Turbulence Spectra, Length Scales and Structure Parameters in the Stable Surface Layer. Boundary Layer Meteorology, vol. 4, 1973, pp. 289-309.

4.4 Cliff, William C., Fichtl, George H., Alexander, Margaret, and Arias, Salvador: Measurements of the Stochastic Nature of Atmospheric Spectral Amplitudes. NASA TM X-73329, August, 1976.

4.5 Duchene-Marullaz, P.: Full-Scale Measurements of Atmospheric Turbulence in a Suburban Area. Centre Scientifique et Technique du Bâtiment.

4.6 Barr, N. M., Dagfinn, Gangas, and Schaeffer, D. R.: Wind Models for Flight Simulator Certification of Landing and Approach Guidance and Control Systems. FAA-RD-74-206, December 1974.

4.7 Frost, Walter.: Analysis of Wind Turbine Generator Rotor Response to One-Dimensional Turbulence. Contract report NAS8-32118, The University of Tennessee Space Institute, February, 1976.

4.8 Panchev, S.: Random Functions and Turbulence. Pergamon Press, Oxford, 1971.

4.9 Houbolt, J. C., Steiner, Roy, and Pratt, K. G.: Dynamic Response of Airplanes to Atmospheric Turbulence Including Flight Data on Input and Response. NASA TR-R-199, June 1964.

4.10 Etkin, Bernard: Dynamics of Atmospheric, Flight. John Wiley and Sons, New York, 1972.

4.11. Frost, W.: Model of Wind Speed Fluctuations. Report in preparation.

4.12 Ramsdell, J. V.: Estimates of the Number of Large Amplitude Gusts. PNL-2508/UC-60, 1978.

4.13 Reeves, Paul M., Joppa, Robert G., and Ganzer, Victor M.: A Non-Gaussian Model of Continuous Atmospheric Turbulence for Use in Aircraft Design. NASA CR-2639, 1976.

4.14 Kaufman, J. W. (editor): Terrestrial Environment (Climatic) Criteria Guidelines for Use in Aerospace Vehicle Development, 1977 Revision. NASA TM X-78118, November 1977.

4.15 Jones, J. G.: A Unified Discrete Gust and Power Spectrum Treatment of Atmospheric Turbulence. RAeS/AIAA/CASI Conf. on Atmospheric Turbulence, London, May 1971.

4.16 Fichtl, G. H., Perlmutter, Morris, and Frost, Walter: Monte Carlo Turbulence Simulation. Handbook of Turbulence, vol. I, Fundamentals and Applications, Walter Frost and Trevor Moulden (editors) Plenum Press, New York, 1977, pp. 433-473.

4.17 Counihan, J.: Adiabatic Atmospheric Boundary Layers: A Review and Analysis of Data From the Period 1880-1972. Atmospheric Environment, vol. 9, Pergamon Press, 1975, pp. 871-905.

4.18 Houbolt, J. C., and Sen, A.: Cross-Spectral Functions Based on von Karman's Spectral Equation. NASA CR-2011, March 1972.

4.19 Brook, R. R.: A Note on Vertical Coherence of Wind Measured in an Urban Boundary Layer. Boundary Layer Meteorology, vol. 9, 1975.

4.20 Ropelewski, C. F., Tennekes, H., and Panofsky, H. A.: Horizontal Coherence of Wind Fluctuations. Boundary Layer Meteorology, vol. 5, 1973.

4.21 Davenport, A. G.: The Spectrum of Horizontal Gustiness Near the Ground in High Wind.

CHAPTER 5. WIND DIRECTION

Summary of Wind Direction

5.1 Summary

Wind direction is not extensively measured in terms of actual directional effects and is generally expressed in terms of the three components of wind speed. Given a probability distribution of the three wind speed components, one can establish an estimate of wind direction and directional fluctuations. The most exact description is a trivariate probability distribution; however, the parameters for this model have not been verified experimentally, and one normally uses a bivariate normal distribution where the correlation between the lateral and longitudinal wind speed components is neglected. This is described in Section 5.3. The parameters appearing in the multivariate probability distribution are dependent upon the mean wind speed which is discussed in Chapter 2 and on the turbulence intensity or variance which is described in Chapter 4. Using the information contained in these chapters and assuming a bivariate normal probability distribution with zero correlation between w_x and w_y, the probability density distribution of the wind vector direction, θ, measured from the mean wind direction $\theta = 0$ is plotted in Figures 5.1 through 5.4. These data assume a neutral atmospheric boundary layer.

Information on vertical and horizontal variation in wind direction in the lower layer of the atmosphere is also limited. Some data are provided in Section 5.4 which are taken from measurements at two specific sites in the United States; although not complete, these data allow the designer some estimate of the magnitude and the probability of the vertical shear in wind direction.

Detailed Computational Procedures and Working Data

5.2 Introduction

Variation in wind direction is a significant parameter in the design of a wind turbine generator from a rotor pitch and nacelle orientation control point of view and from loading considerations. Large variations in wind direction

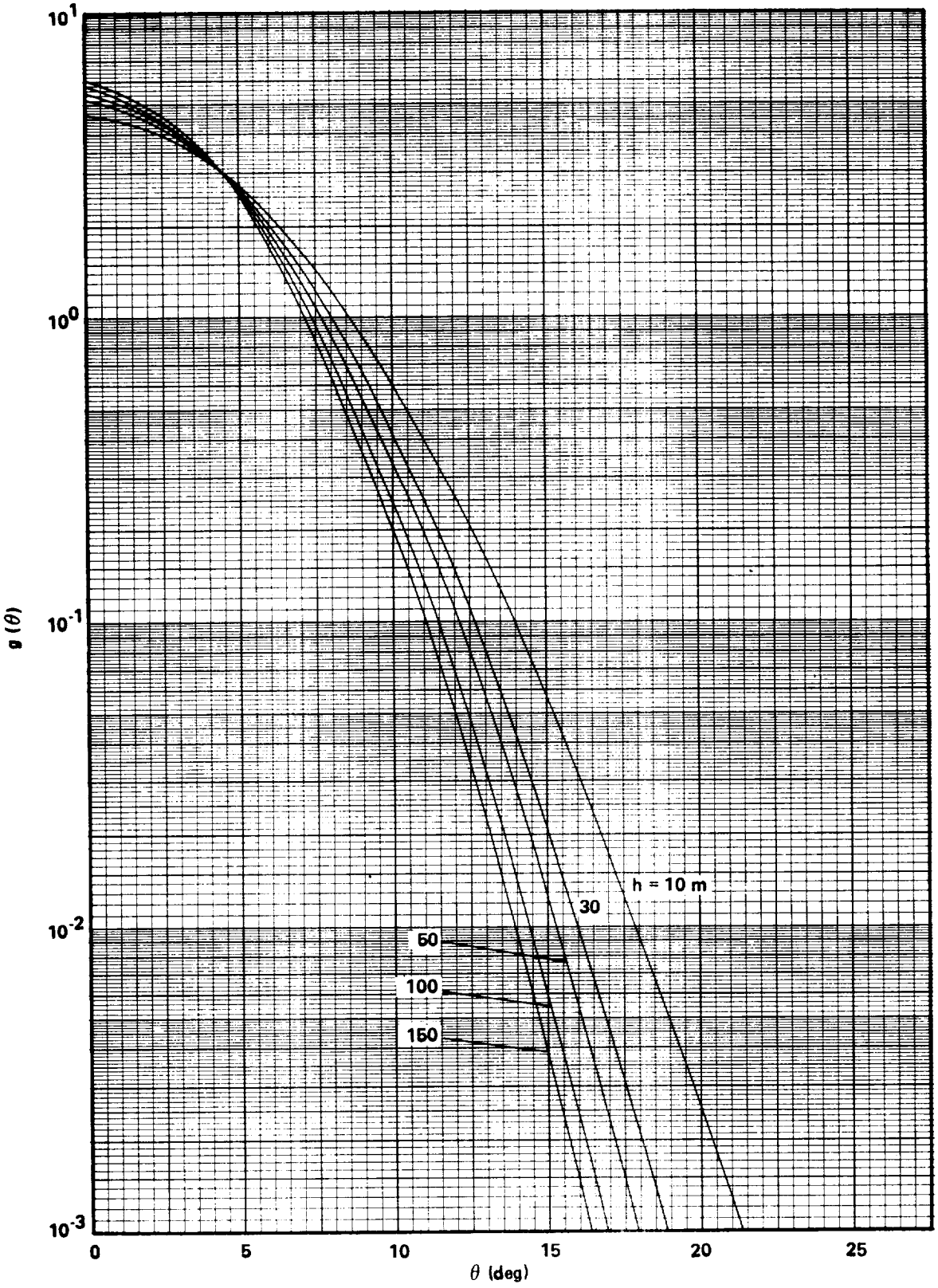

Figure 5.1 Probability density function of wind direction, $z_o = 0.001$.

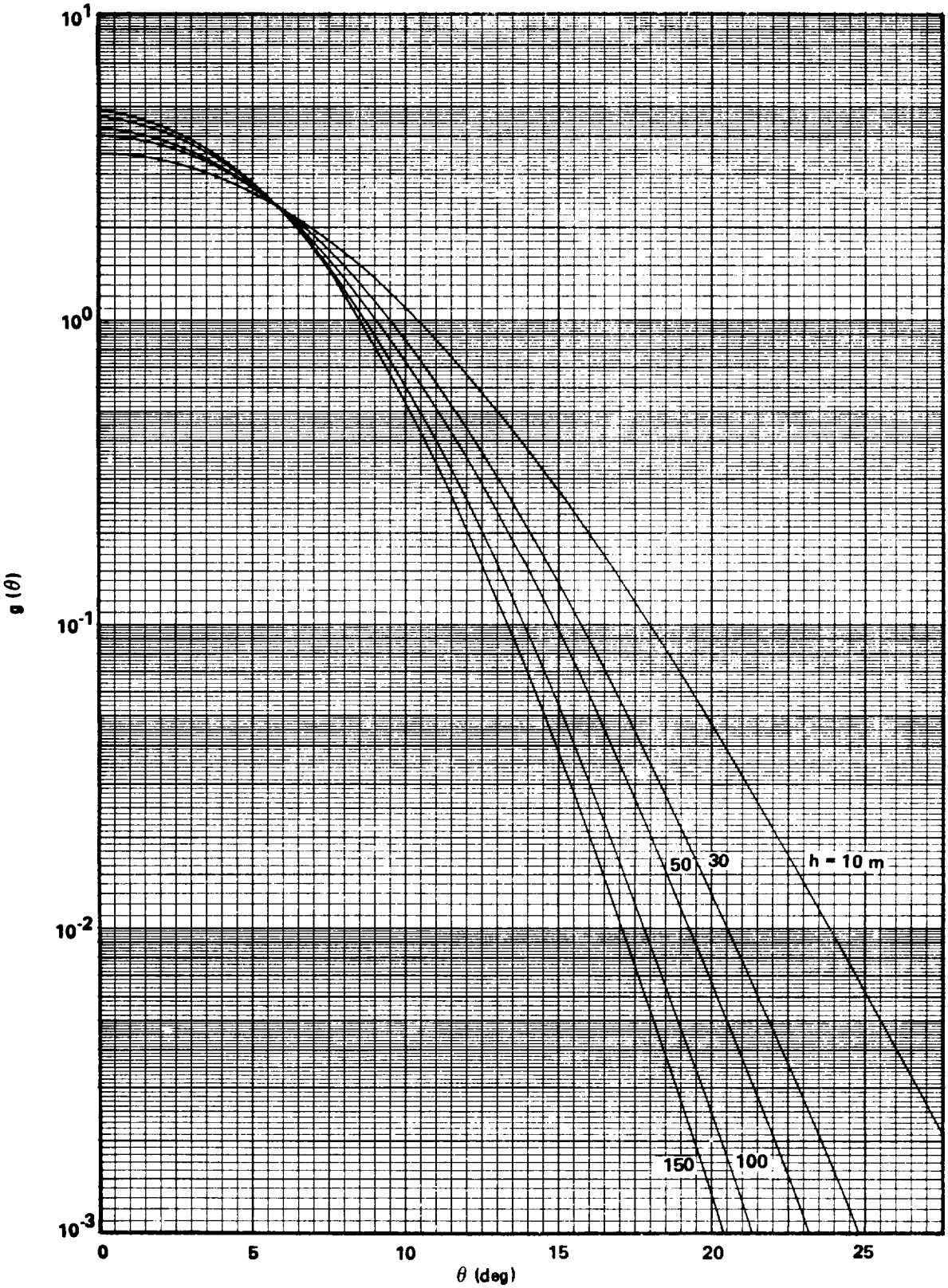

Figure 5.2 Probability density function of wind direction, $z_o = 0.01$.

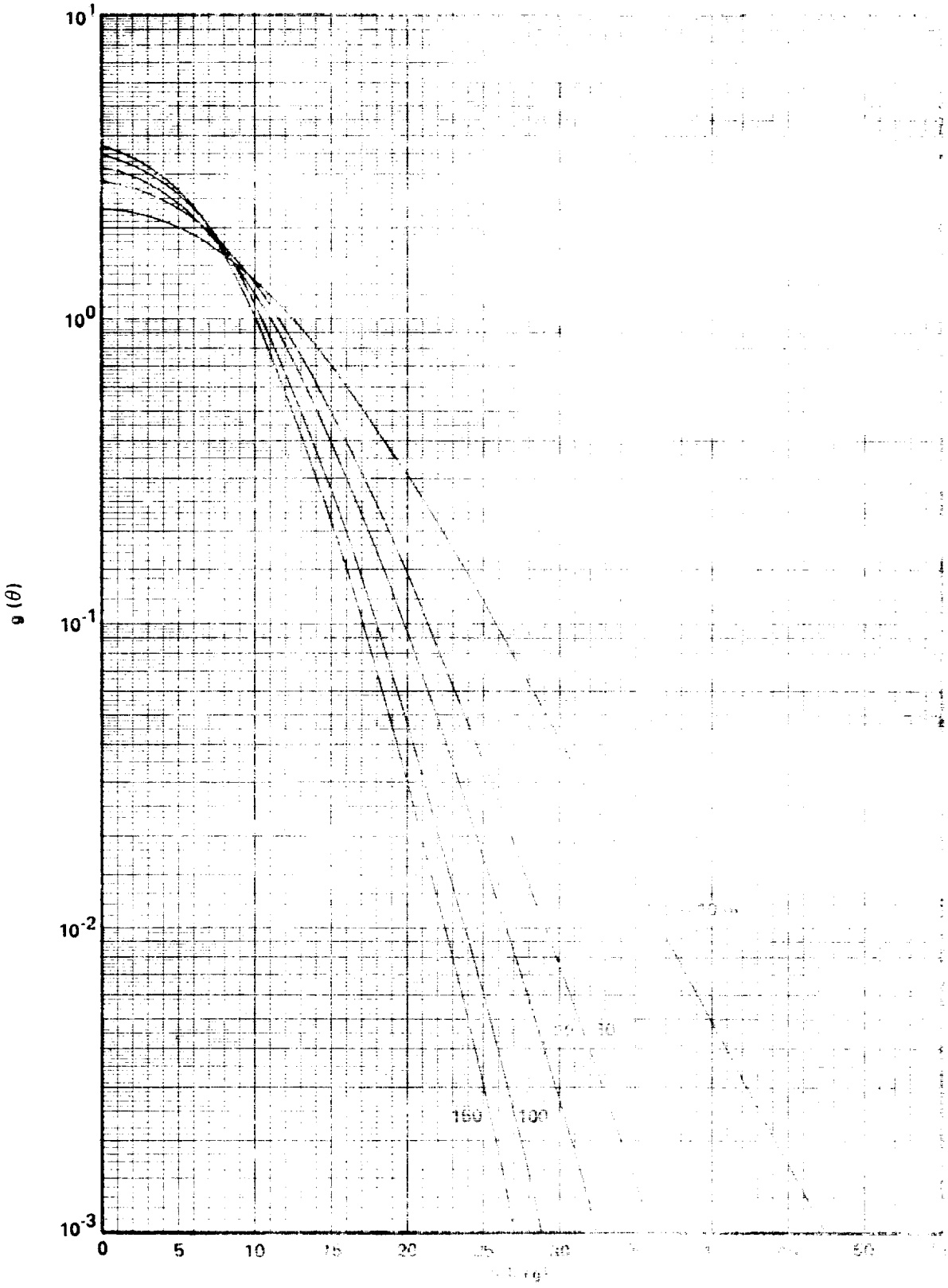

Figure 5.3 Probability densi

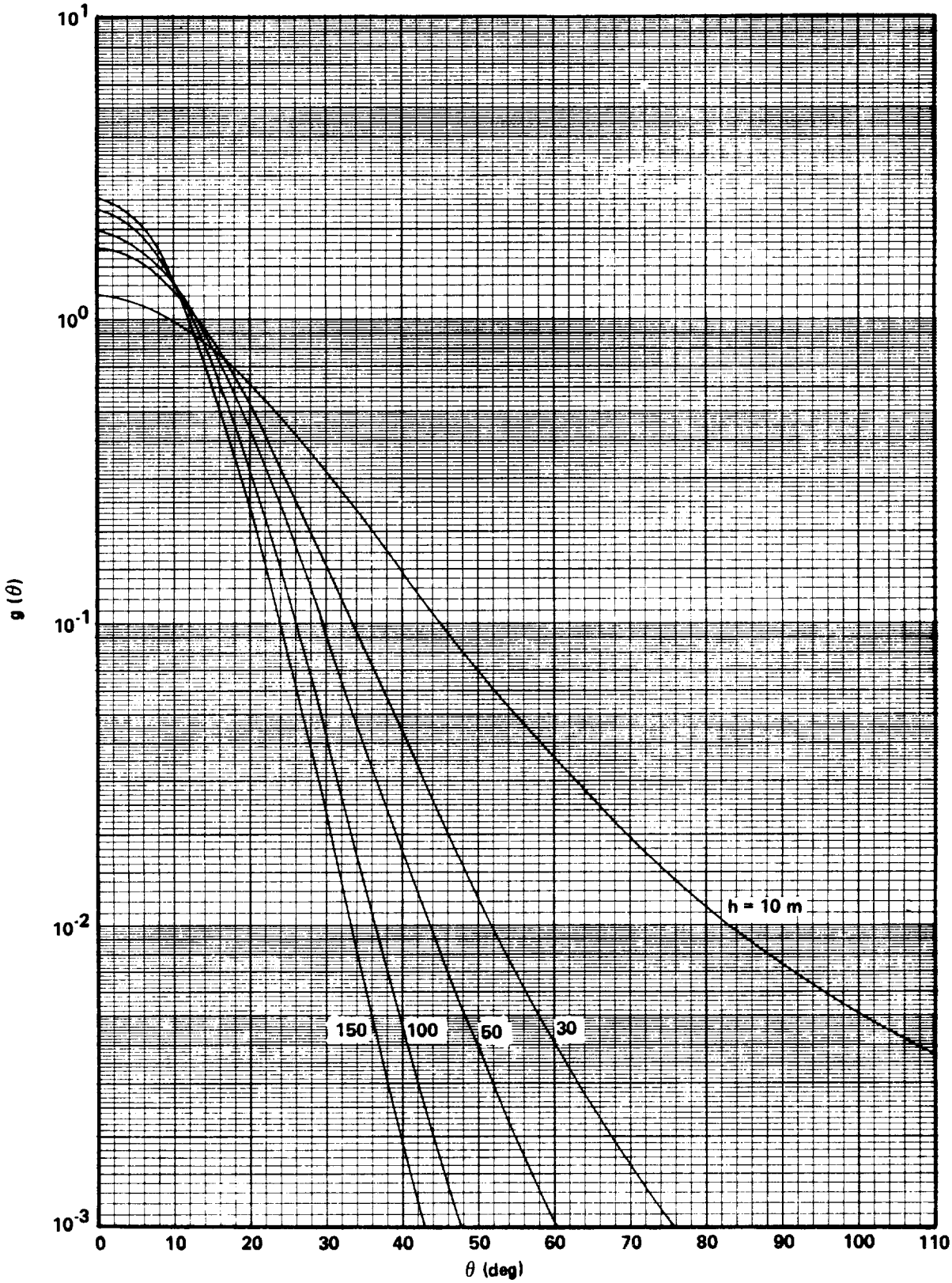

Figure 5.4 Probability density function of wind direction, $z_o = 1.0$.

which cannot be followed by the control system or precession of the mechanical system can result in large variations in the thrust of the rotor, causing it to lose power or to experience extreme fluctuation in the load. To analyze these effects, the engineer must have a model of wind direction and of the fluctuations in direction.

Most experimental data on wind are presented in terms of wind speed components which, in theory, contain the directional information necessary. However, the model with which the wind speed components must be combined for engineering applications is not well developed. Strictly speaking, a trivariant distribution of wind speed which includes the auto- and cross-correlation wind speed terms would provide the most realistic distribution of wind directions [5.1]. The experimental data necessary to utilize this distribution, however, are not well in hand, and it is generally assumed that the wind is bivariate normally distributed [5.2, 5.3]. Also, the correlation between the longitudinal and lateral wind speed components is, in general, neglected, which is possibly a valid assumption for homogeneous flat terrain but is not likely reliable in the vicinity of terrain features which disturb the wind [5.4, 5.5]. However, the bivariate normal distribution gives the engineer a method of estimating directional wind effects based on the current state-of-the-art and is discussed in Section 5.3.

A simple method of estimating the rate of change or fluctuation in wind direction is provided in Section 5.4. This model is not complete but it is consistent with the often used model developed by Rice [5.6] for one normally variable and allows an engineering estimate of the rate of directional fluctuations to be made. Finally, Section 5.5 provides limited information on directional wind shear which is available in the literature. This information has been assembled and, although it pertains only to two specific sites in the United States, it does allow the designer an estimate of the probability and magnitude of vertical variation in wind direction in the lower 300 m of the atmospheric boundary layer.

5.3 Distribution of Wind Direction

Reference 5.3 reports that winds are trivariate, normally distributed. Frost [5.7] discussed the data required to utilize the distribution for practical wind turbine design. References 5.2 and 5.3 propose a bivariate normal distribution which, due to its simpler form, is described here. The bivariate normal distribution is given by

$$p(w_x, w_y) = \frac{1}{2\pi\sigma_{w_x}\sigma_{w_y}\sqrt{1-\rho^2_{w_x w_y}}} e^{-\chi^2/2} \tag{5.1}$$

where

$$\chi^2 = \frac{(W_x - \overline{W}_x)^2}{\sigma^2_{w_x}} - \rho_{w_x w_y} \frac{(W_x - \overline{W}_x)(W_y - \overline{W}_y)}{\sigma_{w_x}\sigma_{w_y}} + \frac{(W_y - \overline{W}_y)^2}{\sigma^2_{w_y}} \quad . \tag{5.2}$$

The parameter $\rho_{w_x w_y}$ is the correlation $\overline{w_x w_y}$ which is normally taken as zero for a homogeneous boundary layer over flat terrain, and the values of σ_{w_x} and σ_{w_y} can be determined from equation (4.23). Thus

$$p(w_x, w_y) = \frac{e^{-\left[(W_x-\overline{W}_x)^2/\sigma^2_{w_x} + (W_y-\overline{W}_y)^2/\sigma^2_{w_y}\right]/2}}{2\pi\sigma_{w_x}\sigma_{w_y}} \quad . \tag{5.3}$$

This expression applies to stationary homogeneous turbulence and is undoubtedly an oversimplification of the actual atmospheric condition. Until further work is carried out to establish a more precise model, it must suffice for engineering purposes.

To derive the probability and the frequency of wind direction, one first changes the variables for the bivariate normal density function to polar coordinates [5.2]; this gives

$$g'(\overline{W}, \theta) = \overline{W} d_1 e^{-(a^2\overline{W}^2 - 2b\overline{W} + c^2)/2}$$

$$a^2 = \frac{\cos^2\theta}{\sigma^2_{w_x}} + \frac{\sin^2\theta}{\sigma^2_{w_y}}$$

$$b = \frac{\overline{W}\cos\theta}{\sigma^2_{w_x}}$$

$$c^2 = \frac{\overline{W}^2}{\sigma^2_{w_x}}$$

$$d_1 = \left(2\pi\sigma_{w_x}\sigma_{w_y}\right)^{-1} \qquad (5.4)$$

where $\overline{W} = \sqrt{\overline{W}_x^{\,2} + \overline{W}_y^{\,2}}$ is the modulus of the instantaneous wind vector and θ is the direction of the vector measured relative to the mean wind speed $\overline{W}$ considered to be in the direction $\theta = 0$. After integrating $g(\overline{W},\theta)$ over $\overline{W} = 0, \infty$, we arrive at the probability density function of θ:

$$g(\theta) = \frac{d_1}{a^2} e^{-c^2/2}\left[1 + \sqrt{2\pi}\frac{b}{a} e^{\frac{1}{2}\left(\frac{b}{a}\right)^2} \Phi\left(\frac{b}{a}\right)\right] \qquad (5.5)$$

where a^2, b, c^2, and d_1 are as previously defined in equation (5.4) and

$$\Phi(b/a) = \frac{1}{\sqrt{2\pi}} \int_{-\infty}^{b/a} e^{-t^2/2}\, dt \qquad (5.6)$$

is taken from tables of normal distribution functions or made available through a computer subroutine. Values of $g(\theta)$ for selected heights, h, and surface roughness, z_o, are plotted in Figures 5.1 through 5.4. Note that the mean wind speed factors out of equation (5.4) making $g(\theta)$ independent of $\overline{W}$.

Equation (5.4) can be integrated numerically over a chosen range of θ to obtain the probability of the wind vector direction lying within the chosen range, i.e.,

$$G(\theta) = \int_{\theta_1}^{\theta^2} g(\theta)\, d\theta \quad . \tag{5.7}$$

Values of the cumulative distribution, i.e.,

$$G(\theta) = \int_{0}^{\theta} g(\theta)\, d\theta \quad , \tag{5.8}$$

are plotted in Figures 5.5 through 5.9. These plots represent an estimate of the probability that the wind vector lies in the angular increment of 0 to θ.

Example 5.1: A 10-m (33-ft) diameter rotor turning at 60 rpm experiences a mean wind $\overline{W}$ = 6.00 m s^{-1} (13.4 mph) at the 10-m (33-ft) level. The surface roughness of the site is 0.1 m (0.3 ft). For a 100-m (328-ft) rotor hub height, determine the influence on rotor lift due to an angular deflection of the wind which occurs 60 percent of the time (Fig. 5.10).

From Figure 5.8, 40 percent of the time fluctuations in θ will be less than ±4 deg and, therefore, 60 percent of the time directional fluctuations will exceed ±4 deg.

Assume that the angle of attach, α, for no wind deflection is 10 deg at the rotor tip. Carrying out the geometry illustrated in Figure 5.10, one determines that due to angular deflections which occur, 60 percent of the time α will exceed values between

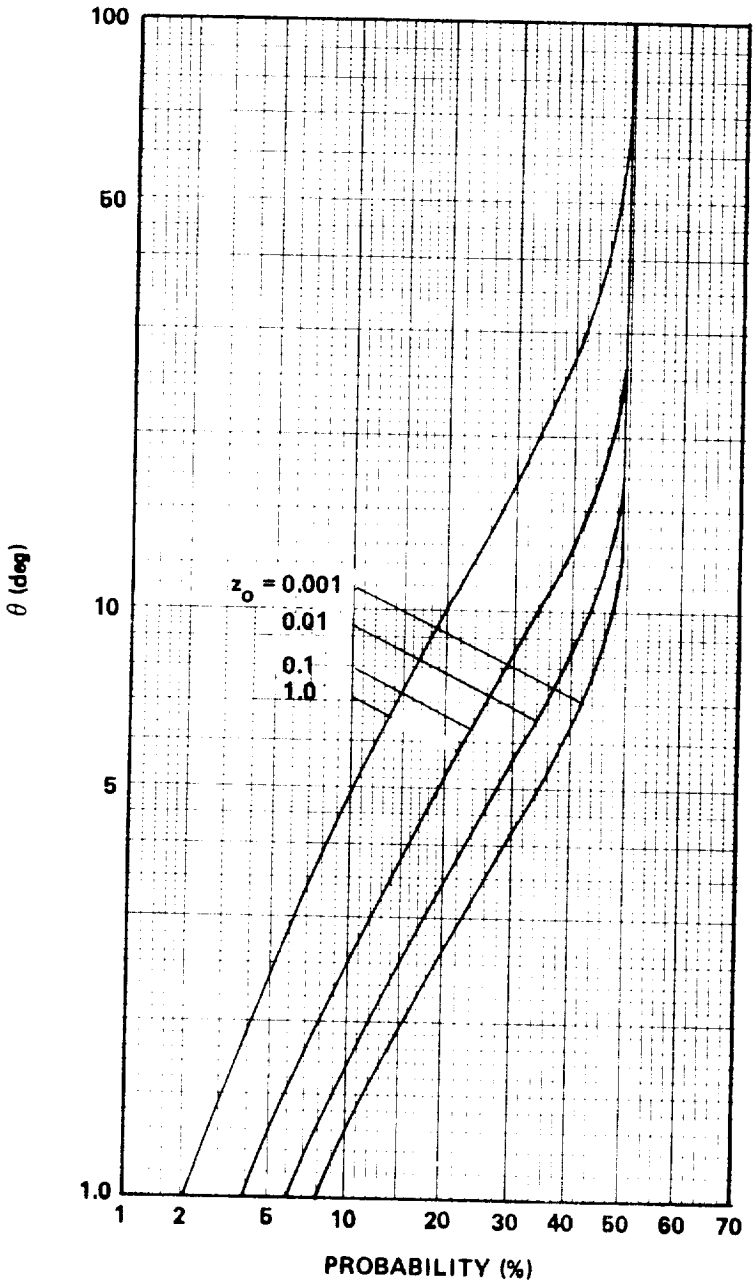

Figure 5.5 Cumulative probability distribution of angular displacement of mean wind for h = 10 m.

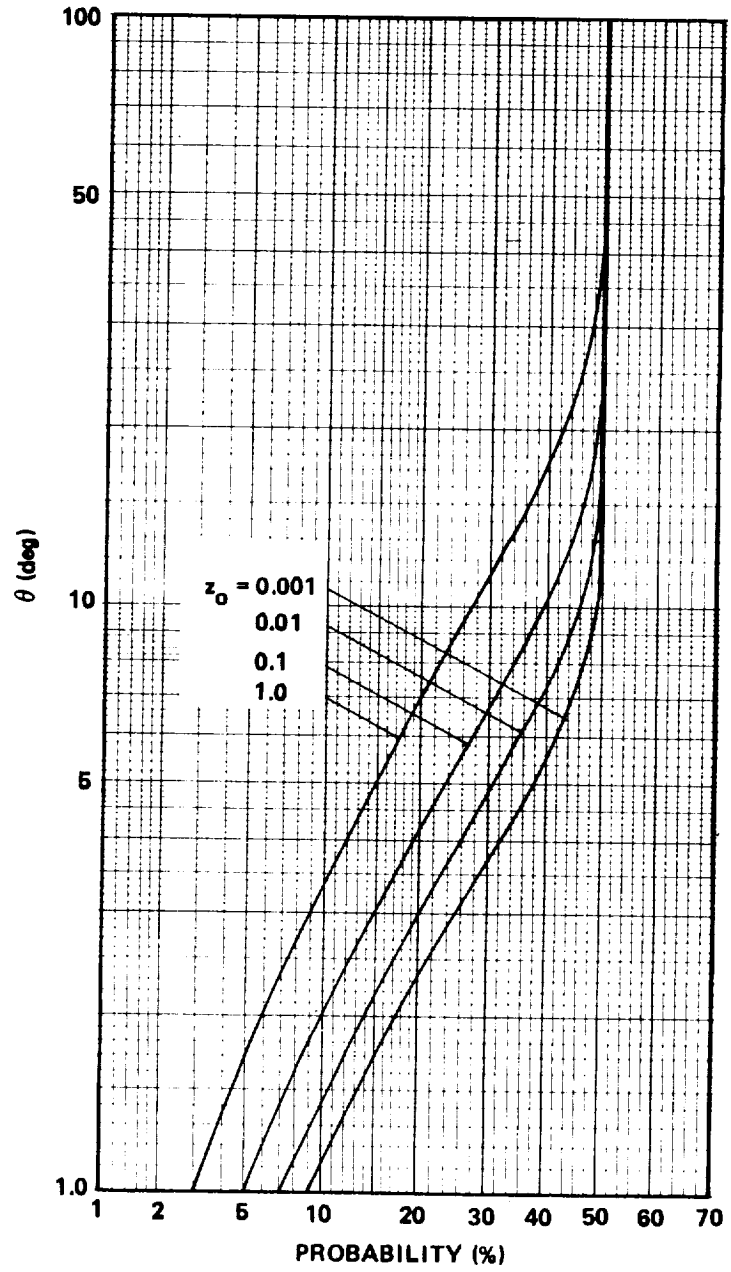

Figure 5.6 Cumulative probability distribution of angular displacement of mean wind for h = 30 m.

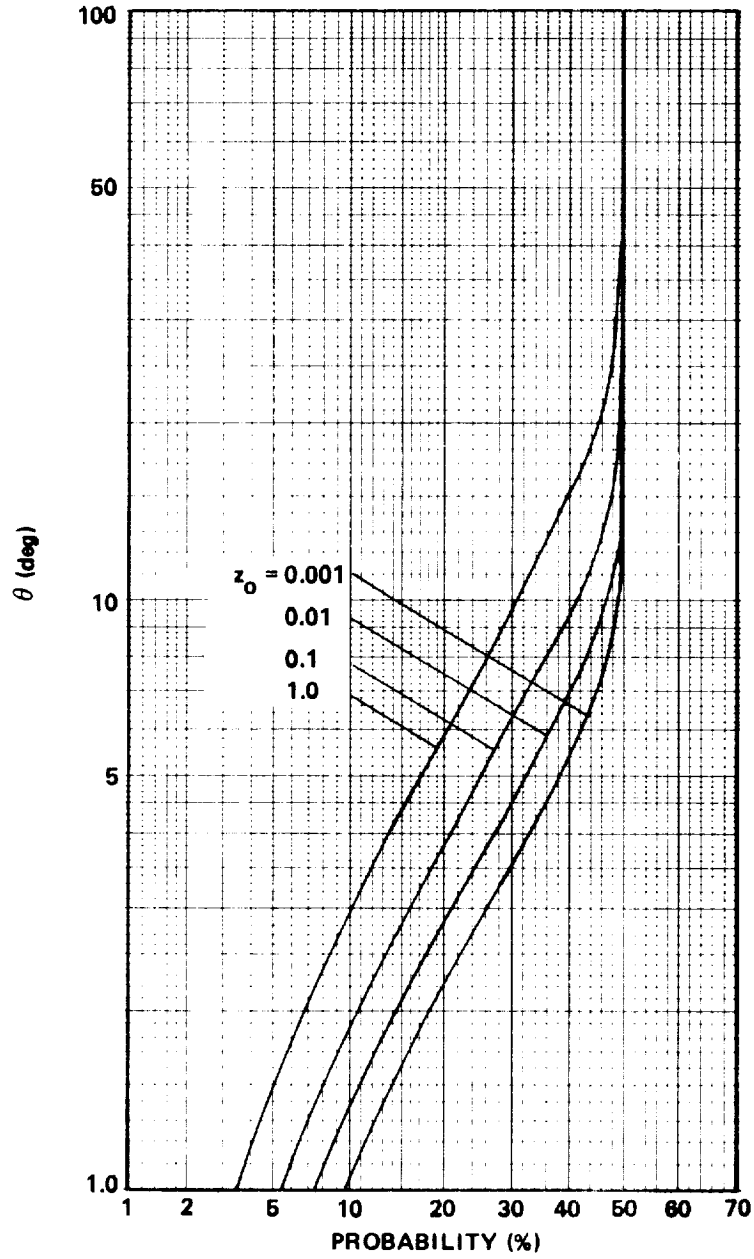

Figure 5.7 Cumulative probability distribution of angular displacement of mean wind for h = 50 m.

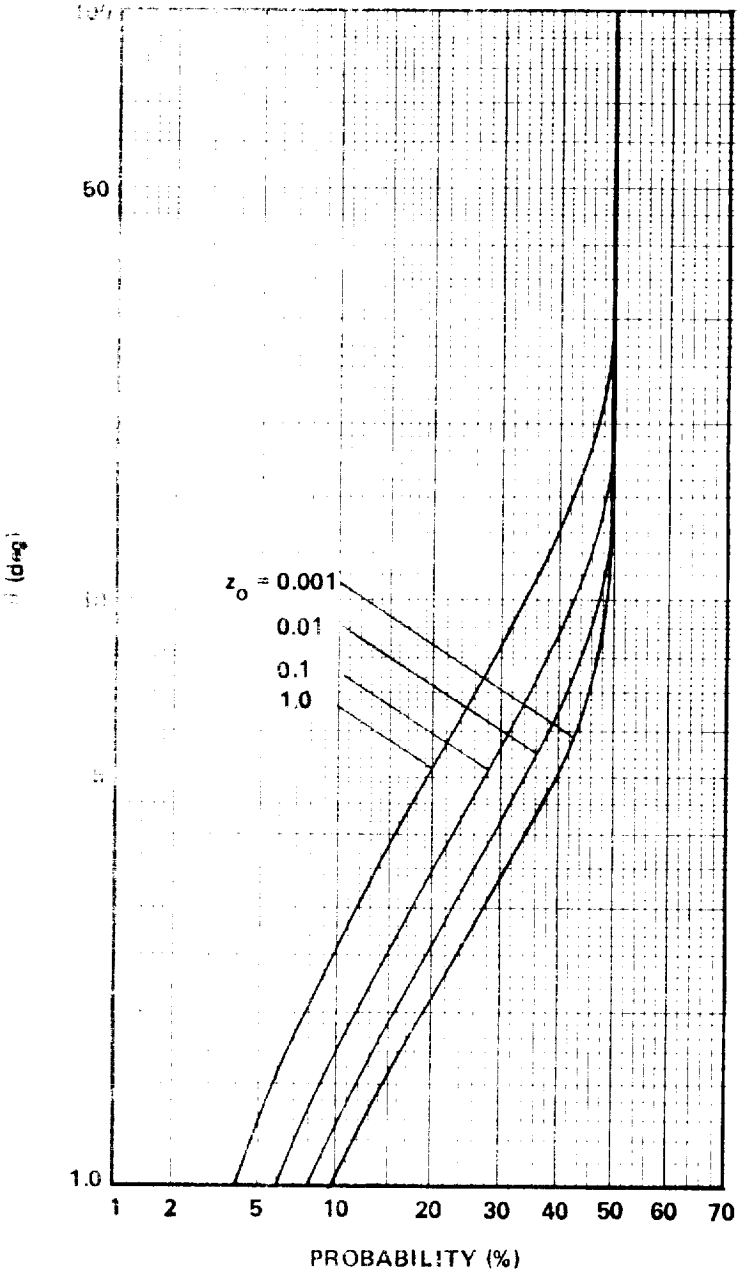

Figure 5.8 Cumulative probability distribution of angular displacement of mean wind for h = 100 m.

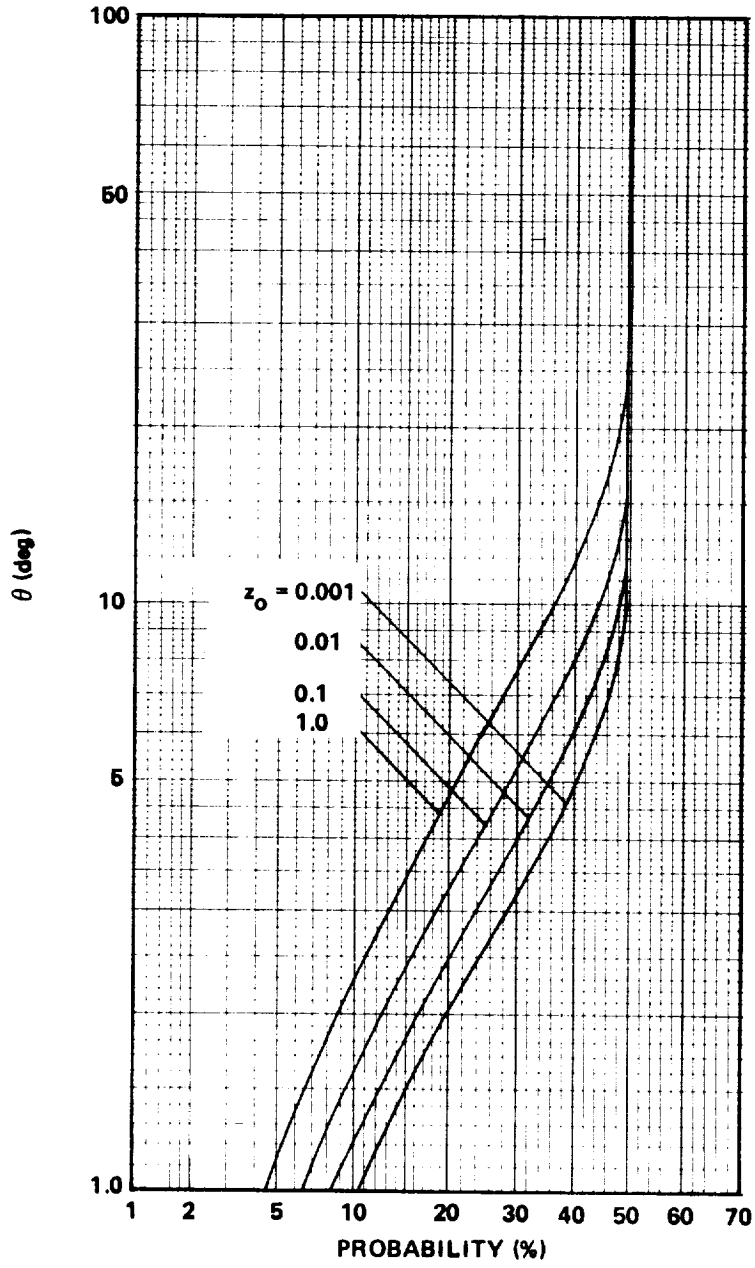

Figure 5.9 Cumulative probability distribution of angular displacement of mean wind for h = 150 m.

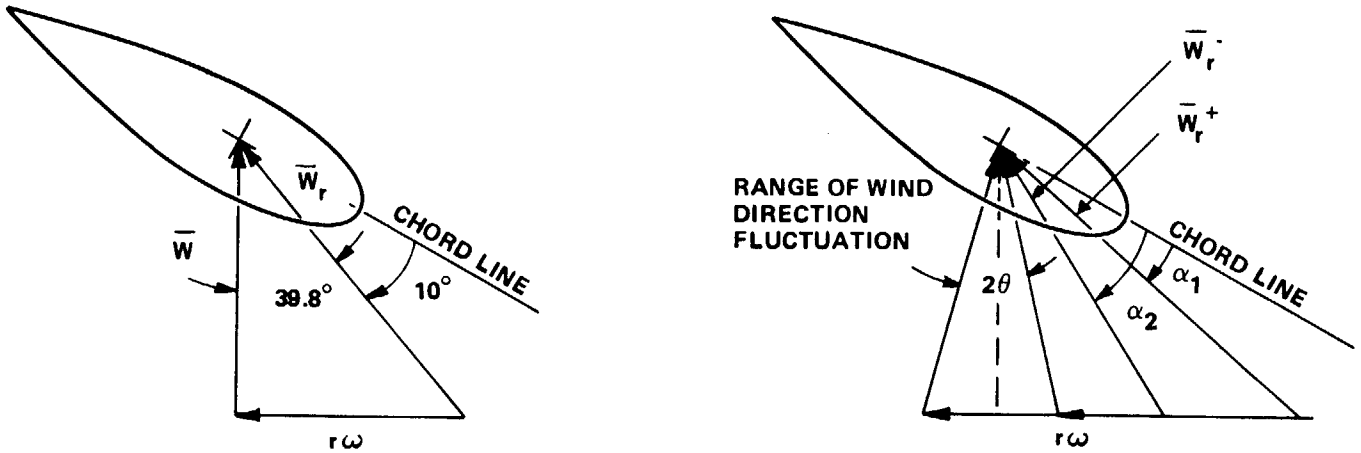

$\bar{W}_r$ – RELATIVE WIND SPEED

$\bar{W}_r^+$ – RELATIVE WIND SPEED WITH POSITIVE FLUCTUATION

$\bar{W}_r^-$ – RELATIVE WIND SPEED WITH NEGATIVE FLUCTUATION

Figure 5.10 Effect of directional change which is exceeded 60 percent of the time on angle of attack.

$$\alpha_1 = (49.8° - 42.2°) = 7.6°$$

or

$$\alpha_2 = (49.8° - 37.4°) = 12.3° \quad .$$

The value of α_1 and α_2 are determined by assuming that during a fluctuation in angle, the rotor speed $r\omega$ and the mean wind speed $\overline{W}$ remain constant. Thus the original angle between $\overline{W}$ and the chord line is 49.8 deg and after a positive fluctuation of 4 deg it becomes 42.2 deg. This reduces the angle between the relative wind vector and the chord line to 7.6 deg. The value of α_2 is found similarly.

Normally, lift is directly proportional to the angle of attack, i.e., $L = a\alpha$. Hence, the lift can experience fluctuations which exceed limits from 0.76 to 1.23 times the value at α = 10 deg, 60 percent of the time, due to angular variations in the wind.

5.4 Exceedance Rate of a Given Direction

Although WTG directional control design requires knowing the number of exceedances of a prescribed angle, a reliable model for predicting these is currently not available.

Reference 5.8 gives a model for estimating the number of outward crossings per unit time of a line segment, ds, in the $w_x - w_y$ plane for a bivariate normal distribution with zero correlation between w_x and w_y as:

$$dN = \frac{1}{(2\pi)^{3/2}} \frac{\sigma_{\dot{w}_n}}{\sigma_{w_x} \sigma_{w_y}} e^{-\chi^2/2} ds \qquad (5.9)$$

where

$$\chi^2 = (W_x - \overline{W}_x)^2/\sigma^2_{w_x} + (W_y - \overline{W}_y)/\sigma^2_{w_y} \qquad (5.10)$$

and $\sigma_{\dot{w}_n}$ is the variance of the acceleration of the wind speed fluctuations perpendicular to the line segment ds, i.e.,

$$\sigma^2_{\dot{w}_n} = \sigma^2_{\dot{w}_x} \cos^2\theta - 2v\sigma_{\dot{w}_x}\sigma_{\dot{w}_y} \cos\theta \sin\theta + \sigma^2_{\dot{w}_y} \sin^2\theta \quad .$$

In this expression, θ is the angle of the line segment and v is the correlation between the random variables $\dot{w}_x$ and $\dot{w}_y$.

To determine the number of times the wind will exceed a prescribed angle, θ, we must determine the number of times the wind fluctuations cross the line,

$$w_y = (\overline{W} + w_x) \tan\theta \quad , \qquad (5.11)$$

as illustrated in Figure 5.11.

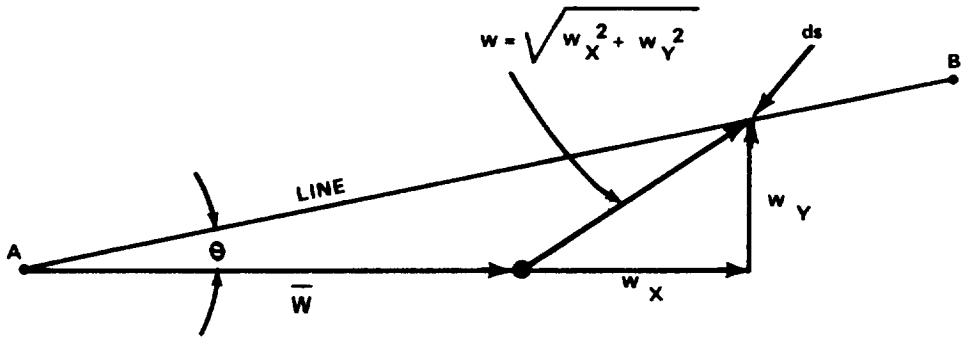

Figure 5.11 The total number of times the vector w crosses the line $\overline{AB}$ is the fluctuation about θ.

This is achieved by integrating equation (5.9) along the line given by equation (5.11). Thus

$$N = \frac{\sigma_{\dot{w}_n}}{(2\pi)^{3/2}\,\sigma_{w_x}\,\sigma_{w_y}} \sqrt{1+a^2} \int_{-W}^{\infty} e^{-(A^2 w_x^{\,2} - 2Bw_x + C^2)/2}\, dw_x \qquad (5.12)$$

where

$$A^2 = \left(1/\sigma^2_{w_x} + a^2/\sigma^2_{w_y}\right)$$

$$B = ab/\sigma^2_{w_y}$$

$$C^2 = b^2/\sigma^2_{w_y}$$

$$a = \tan\theta \quad , \quad b = \bar{W}\tan\theta$$

and

$$\sigma_{\dot{w}_n} = \sqrt{\sigma^2_{\dot{w}_y}\cos^2\theta + \sigma^2_{\dot{w}_x}\sin^2\theta} \quad .$$

Carrying out the integration gives the resulting equation:

$$N(\theta) = \frac{\sigma_{\dot{w}_n}}{2^{3/2}\pi}\, M(\theta) e^{K(\theta)} \left(1 - \Phi\left(L(\theta)\right)\right) \quad ; \quad 0 \le \theta \le \frac{\pi}{2}$$

$$N(\theta) = \frac{\sigma_{\dot{w}_n}}{2^{3/2}\pi}\, M(\theta) e^{K(\theta)} \Phi\left[L(\theta)\right] \quad ; \quad \frac{\pi}{2} \le \theta \le \pi$$

where

$$M(\theta) = \frac{1}{\sigma_{w_y}\sqrt{\left(\frac{2(1+\tan^2\theta)}{1+\sigma^2_{w_x}\tan^2\theta/\sigma^2_{w_y}}\right)}}$$

$$K(\theta) = \frac{1}{2}\left(\frac{\overline{W}\tan\theta}{\sigma_{w_y}}\right)^2\left[\left(\frac{1}{\left[\sigma^2_{w_y}/\sigma^2_{w_x}\tan^2\theta\right]+1}\right)-1\right]$$

and

$$L(\theta) = -\frac{\overline{W}}{\sigma_{w_x}\sqrt{1+\sigma^2_{w_x}\tan^2\theta/\sigma^2_{w_y}}} \quad .$$

Values of $N(\theta)$ are plotted in Figures 5.12 through 5.15 and can be considered representative values of the number of times per unit time the wind vector will fluctuate above a presented value of θ. Doubling the value of $N(\theta)$ provides the number of times the wind vector fluctuates outside a given arc of 2θ per unit time.

Values of $\sigma_{\dot{w}_x}$ and $\sigma_{\dot{w}_y}$ which represent the rms of the wind speed acceleration fluctuation can be determined from the relationship

$$\sigma^2_{\dot{w}_\alpha} = \int_{-\infty}^{\infty} \hat{n}^2 \phi_{w_\alpha}(\hat{n})\, d\hat{n} \quad .$$

Rearranging this expression gives

$$\sigma_{\dot{w}_\alpha} = \frac{\sigma_{w_\alpha}\eta_{o\alpha}\overline{W}\hat{G}_o(\Lambda)}{h}$$

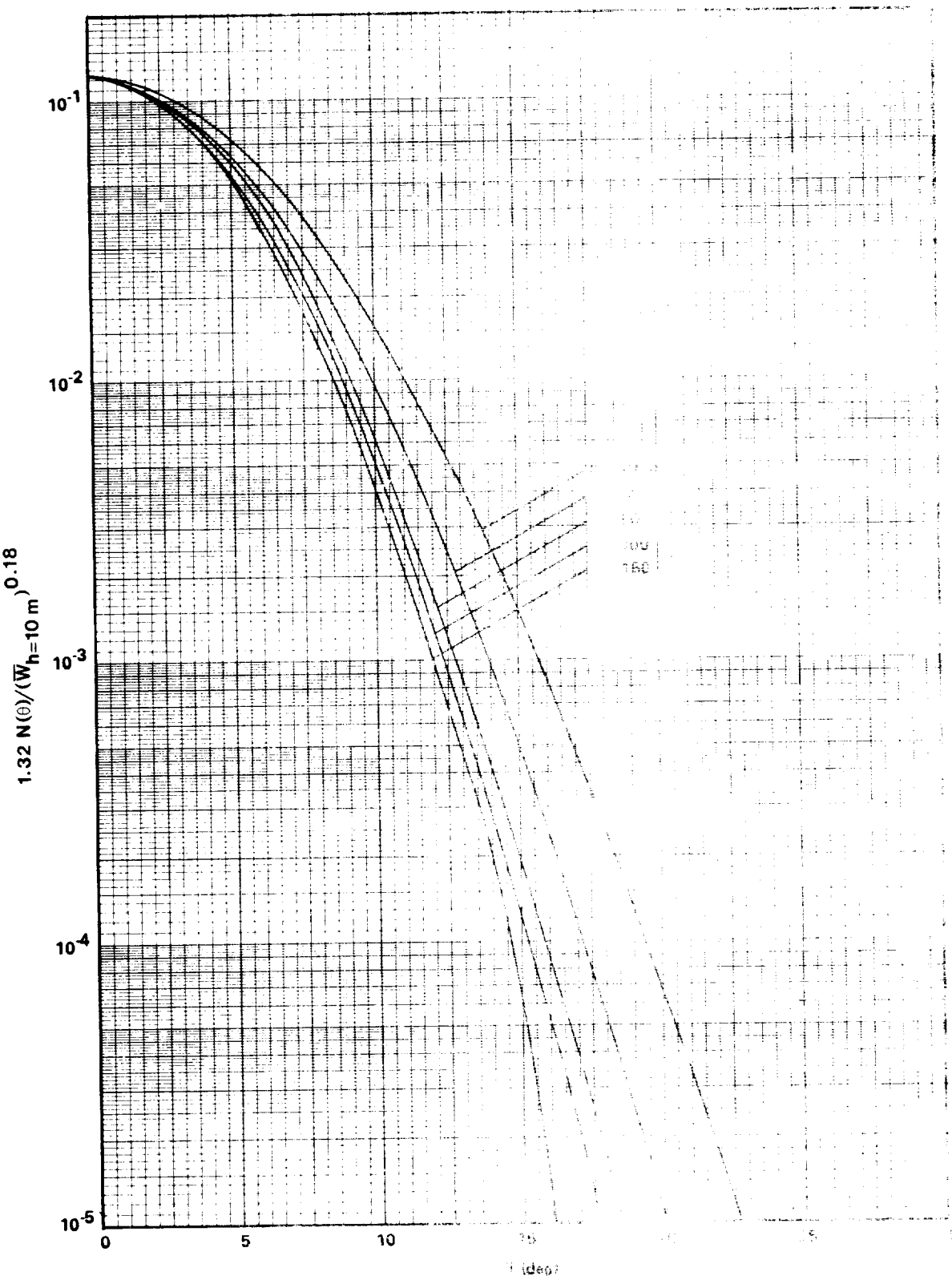

Figure 5.12 Number of ti[illegible] the angle θ centered about the [illegible]

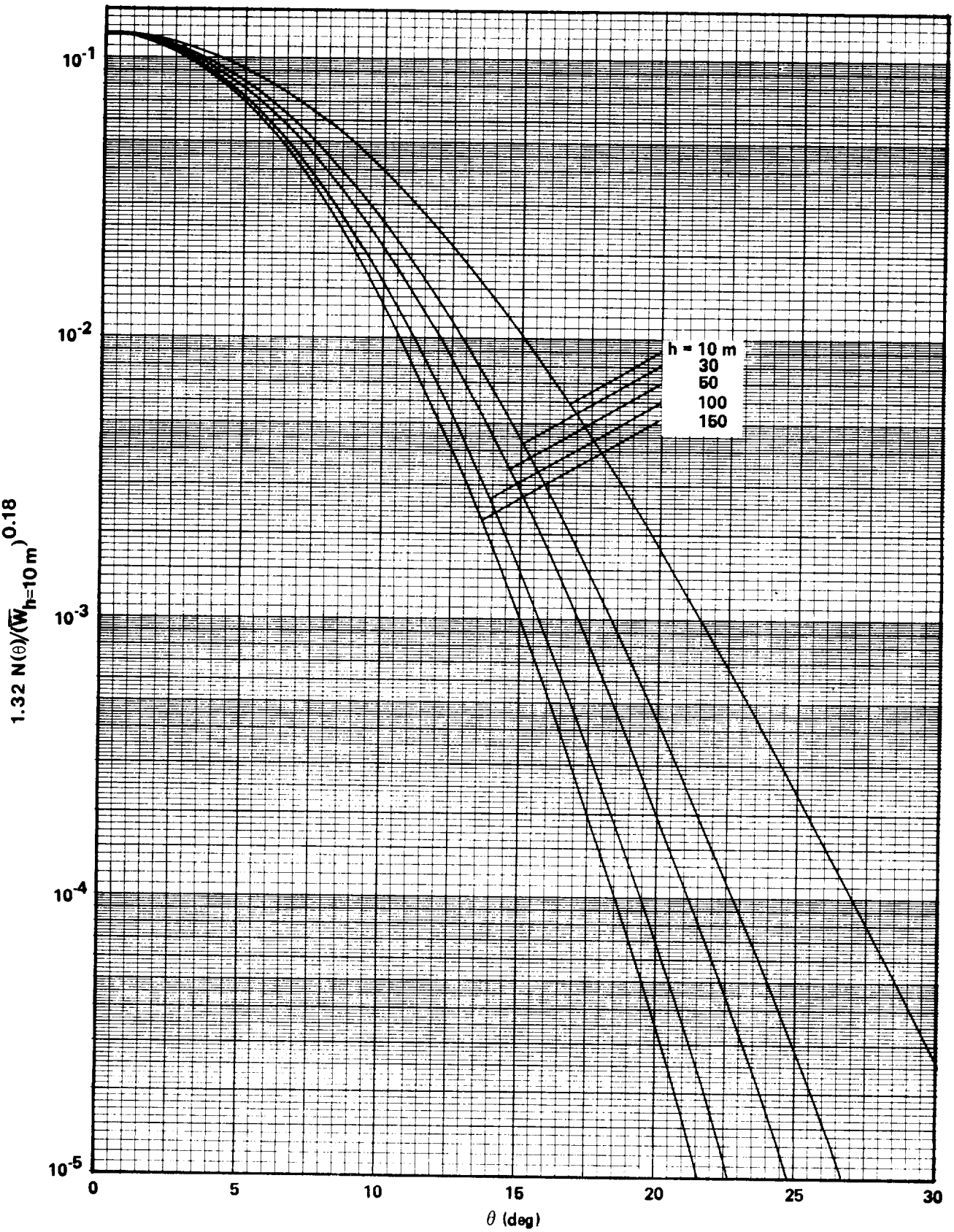

Figure 5.13 Number of times the wind vector fluctuation exceeds the angle θ centered about the mean per unit time for $z_o = 0.01$ m.

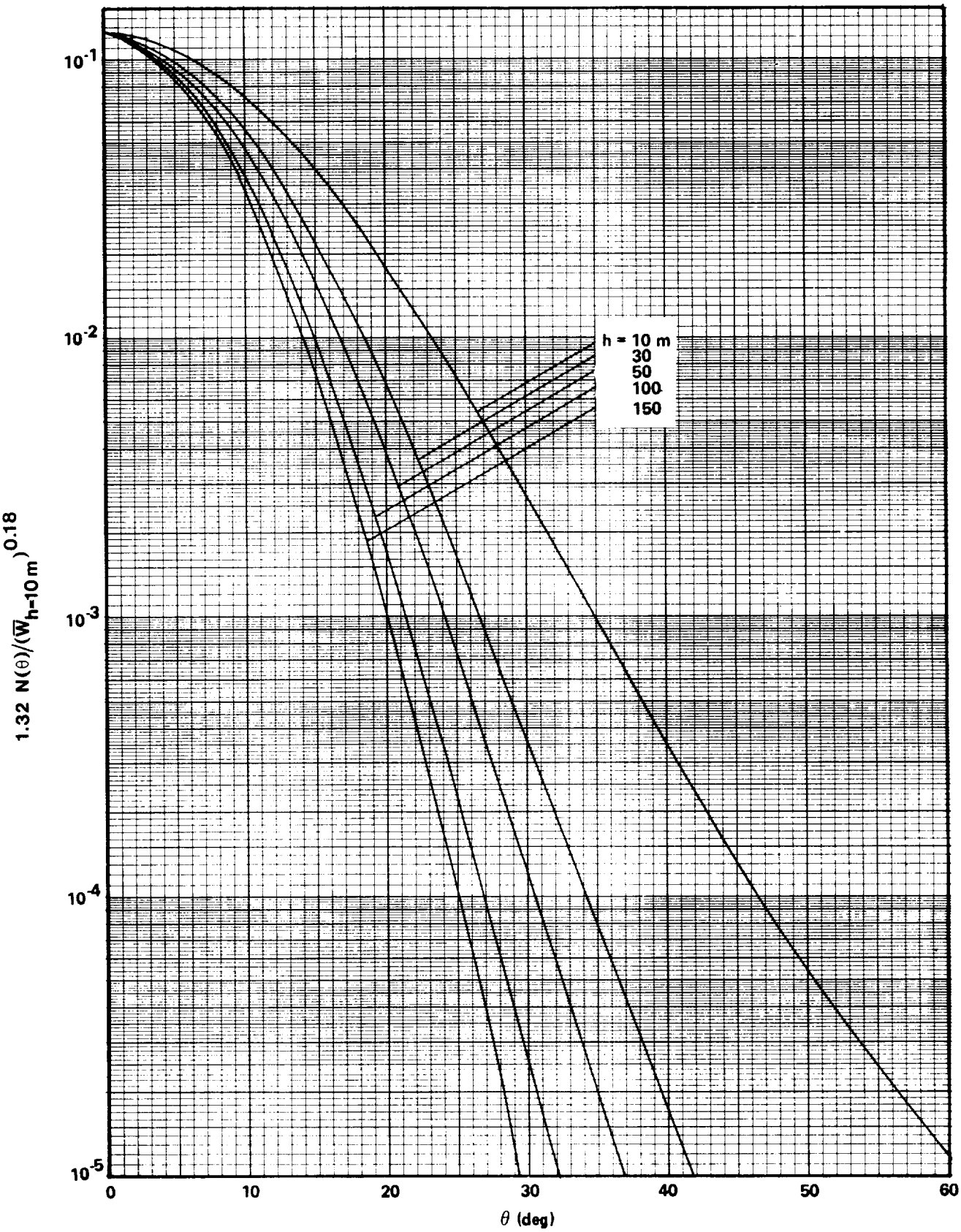

Figure 5.14 Number of times the wind vector fluctuation exceeds the angle θ centered about the mean per unit time for z_o = 0.1 m.

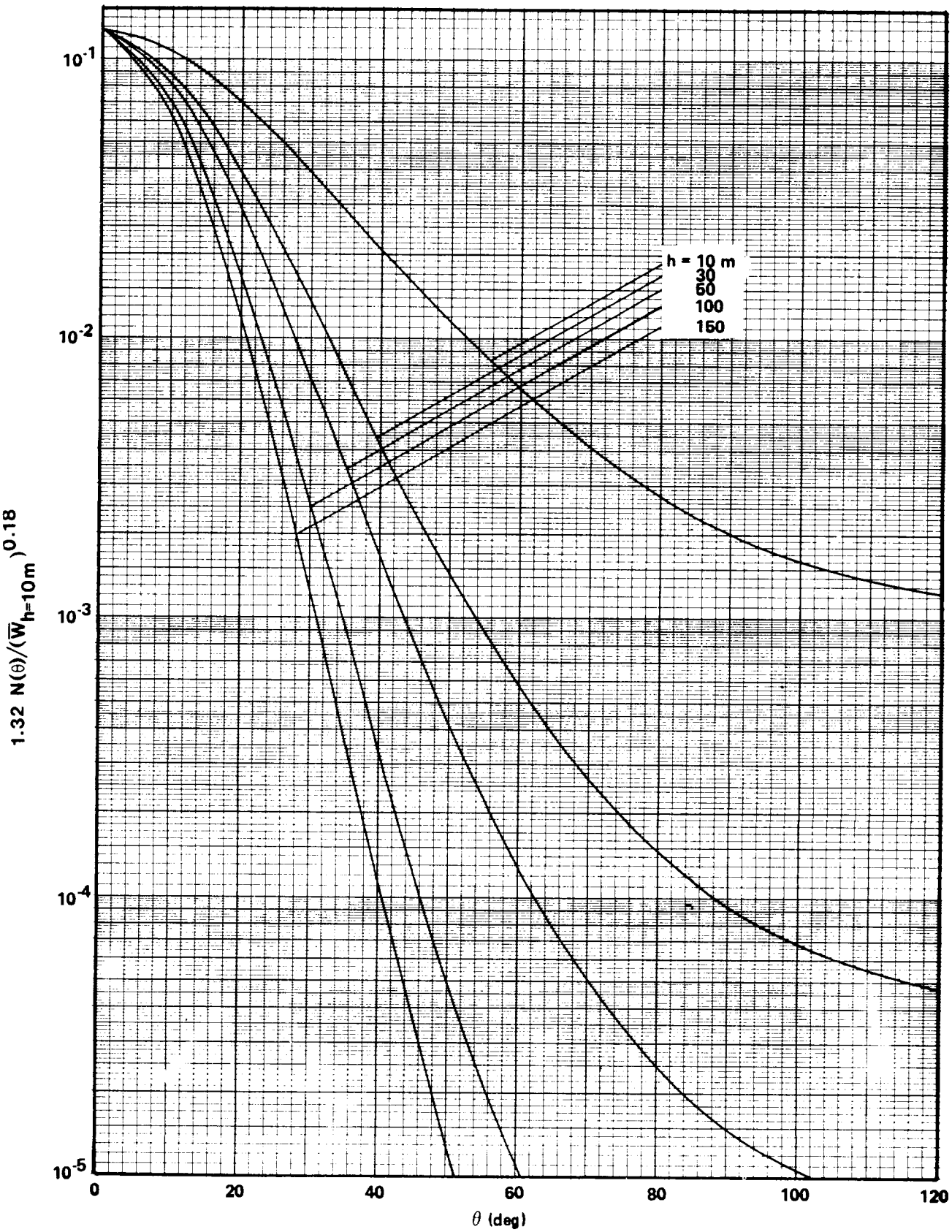

Figure 5.15 Number of times the wind vector fluctuation exceeds the angle θ centered about the mean per unit time for $z_o = 1.0$ m. 5.23

where $\hat{G}_o(\Lambda)$ is as defined in Section 4.3.3.1 and plotted versus Λ in Figure 4.12.

5.5 Wind Direction Shear

Smith [5.2] has developed a "synthetic" vector wind shear profile based on a quadravariate normal probability distribution function which gives good agreement with experimental wind direction shear in the first 28 km of the atmosphere. However, the data in the lower 500 m of the boundary layer are not compiled in the format necessary to allow this model to be employed for WTG design. Additional work in this area would be beneficial.

Wind direction shear from two sets of experimental data taken at Cape Kennedy, Florida, and Cedar Hills, Texas, is reported by Barr, et al. [5.9]. Wind direction shear was determined for each hour of data by subtracting the wind direction at the lowest given level from that at the next lowest given level, assuming this to be equivalent to the directional shear at the geometric height $(h_1, h_2)^{1/2}$ and further assuming that this was a good estimate of the directional shear at 6 m (20 ft). The geometric heights computed for each tower as representative of 6 m (20 ft) are for Cape Kennedy, 5.5 m (18 ft), and for Cedar Hills, 14 m (46 ft). Information from Cape Kennedy indicates that there was not much difference in shear distributions over the interval 5.5 to 14 m (18 to 44 ft) at a given location.

Distribution of directional shear at 6 m (20 ft) in degrees per 30 vertical meters (per hundred vertical feet) for increments of 1 m s^{-1} (2.2 mph) speed intervals at 6 m (20 ft) is shown in Figures 5.16 and 5.17. These figures present the percent probability of that shear not being exceeded. There is apparently small variation with speed except at the extreme probabilities. There is also less directional shear variability at Cedar Hills than at Cape Kennedy. The middle 80 percent of the shears are -10 to +10 deg per 30 meters (per hundred feet), and -30 to +30 deg per 30 meters (per hundred feet), respectively. Figures of the cumulative probability showing directional wind shears at various heights for all wind speeds are also provided by Reference 5.9. These are shown in Figures 5.18 and 5.19. There is a definite decrease in spread of directional shear values with altitude; the smaller range of direction shear variability at Cedar Hills is noticeable in both sets of figures. At Cape Kennedy, 80 percent of the directional wind shears at all but the lower two heights are within ±10 deg per 30 meters (per hundred feet); at the lower two

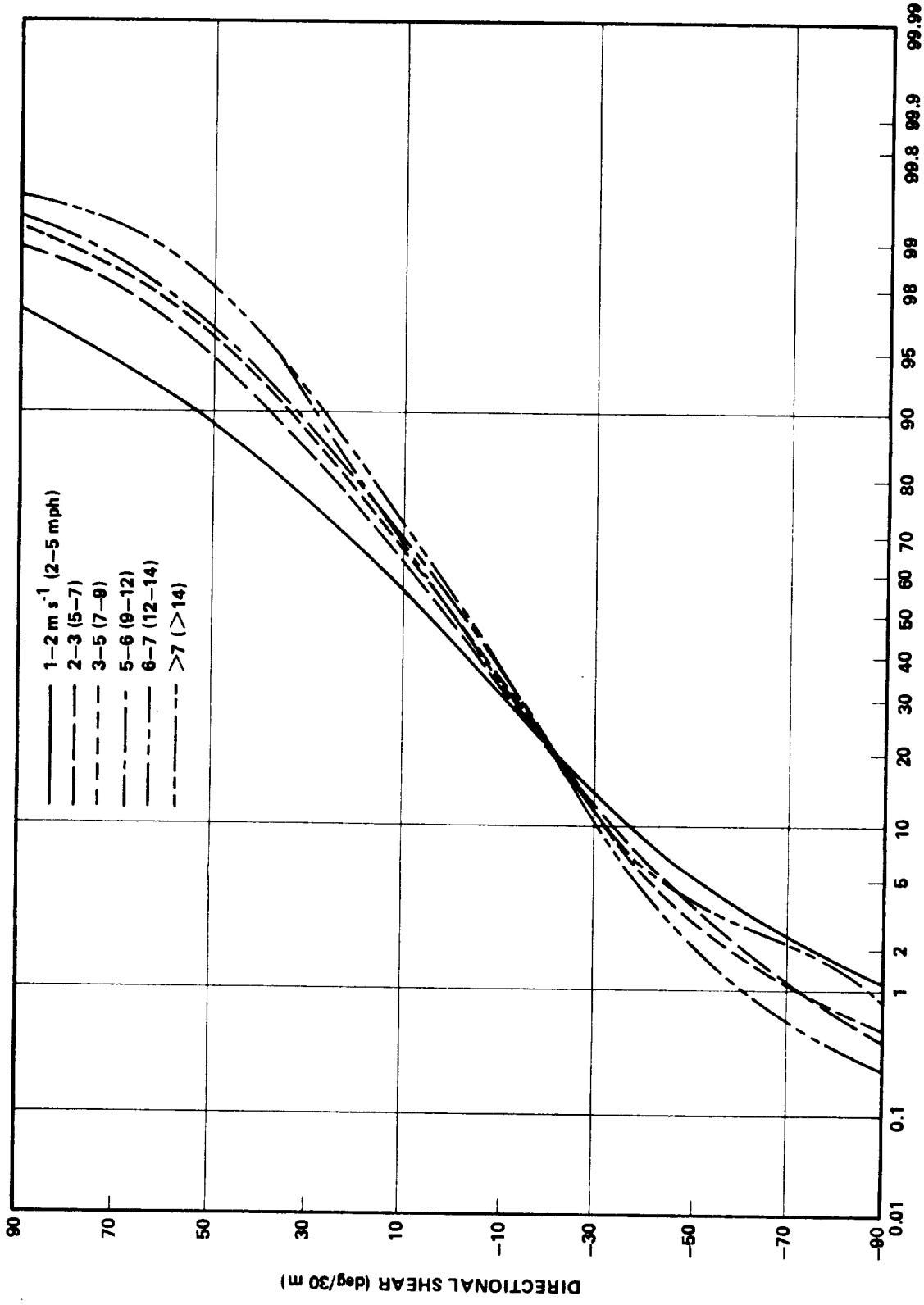

Figure 5.16 Wind direction shear for various wind speeds at 6.1 m (20 ft), 10.06 to 3.05 m (33 to 10 ft), Cape Kennedy, 1966–68 [5.9].

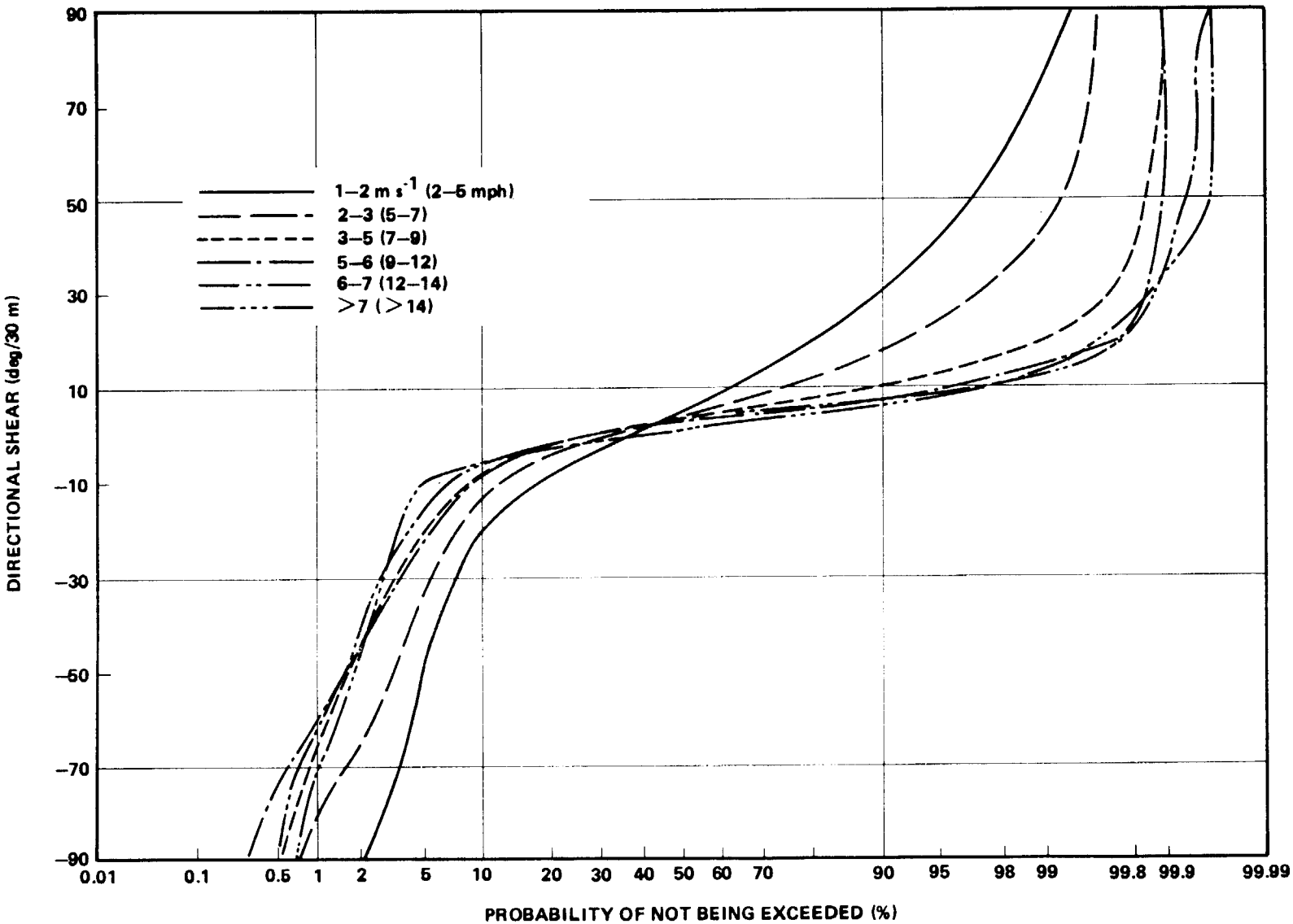

Figure 3.17 Wind direction shear for various wind speeds at 14 m (46 ft), 21 to 9 m (70 to 30 ft), Cedar Hills, Texas, 1960-62 [5.9].

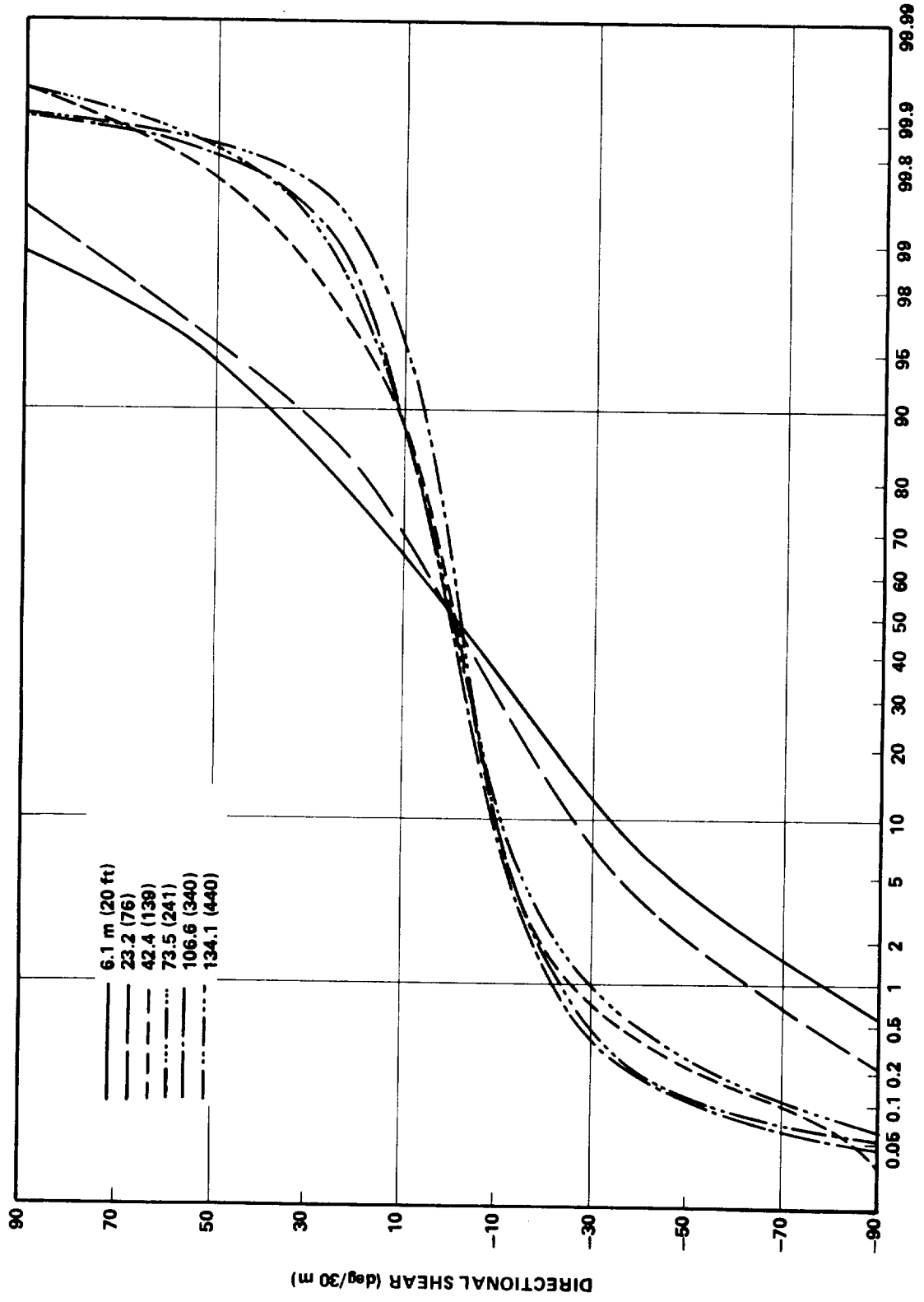

Figure 5.18 Wind direction shear for several heights, all wind speeds, Cape Kennedy, 1966-69 [5.9].

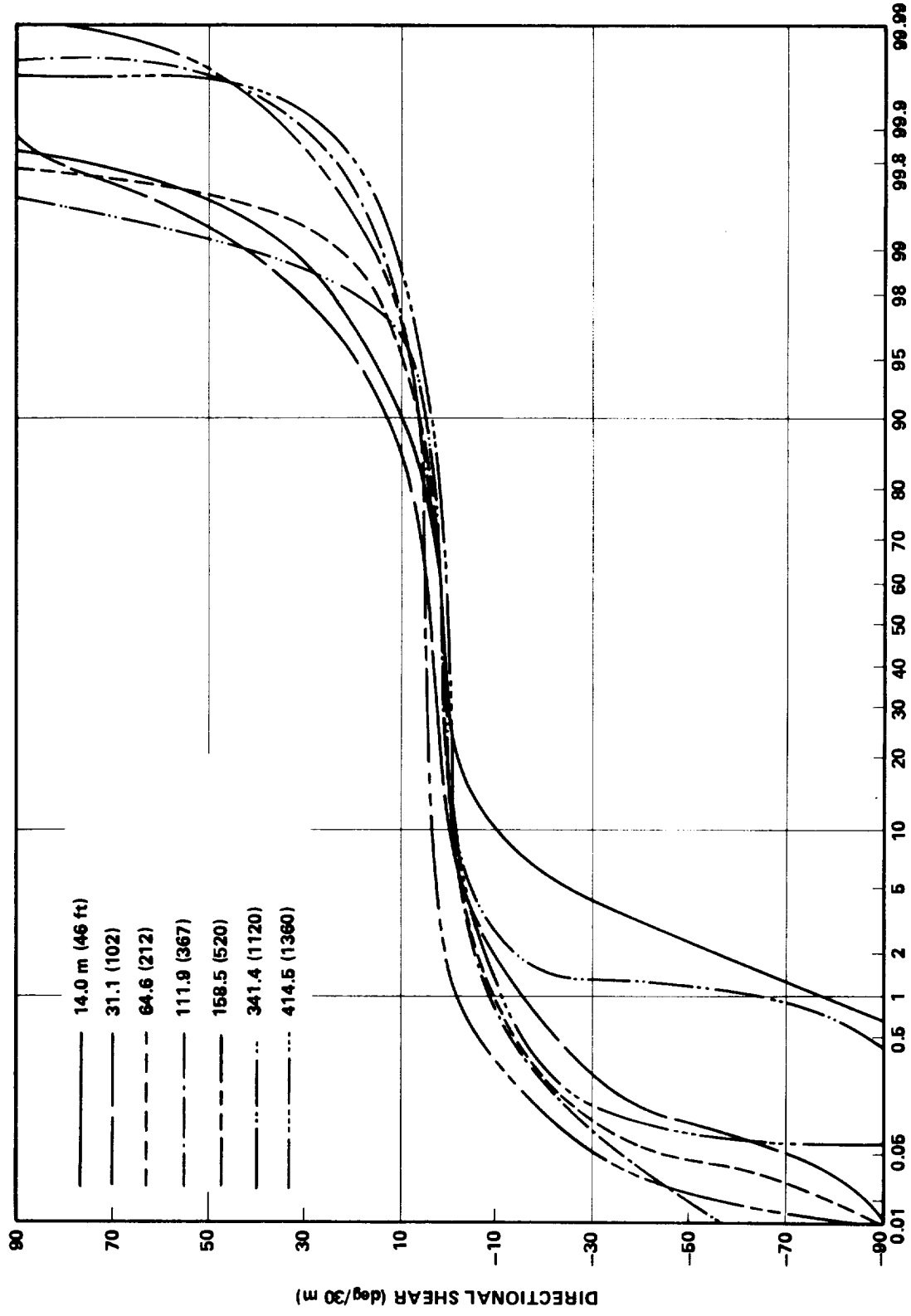

Figure 5.19 Wind direction shear for several heights, all wind speeds, Cedar Hills, Texas, 1960-62 [5.9].

In Reference 5.9, it is pointed out that in addition to the differences noted between locations, there is also a difference in the shape of the distributions from year to year at the same location. Therefore, establishing long period mean curves is difficult.

Several 10-min average profiles were selected at random from the records to provide an indication of the magnitude of directional shear at any time. Four of these are shown in Figure 5.20. In the figure, the $\Delta\theta$ from the lowest level is shown by the curve, and the speed at each height is given numerically. In general, the largest shears occur near the surface and with the lowest wind speeds. In summary, however, the results indicate that in most cases directional shears are low [0 to 20 deg per 30 meters (per hundred feet)] at high speeds. This is especially true when shears are measured over large height differences.

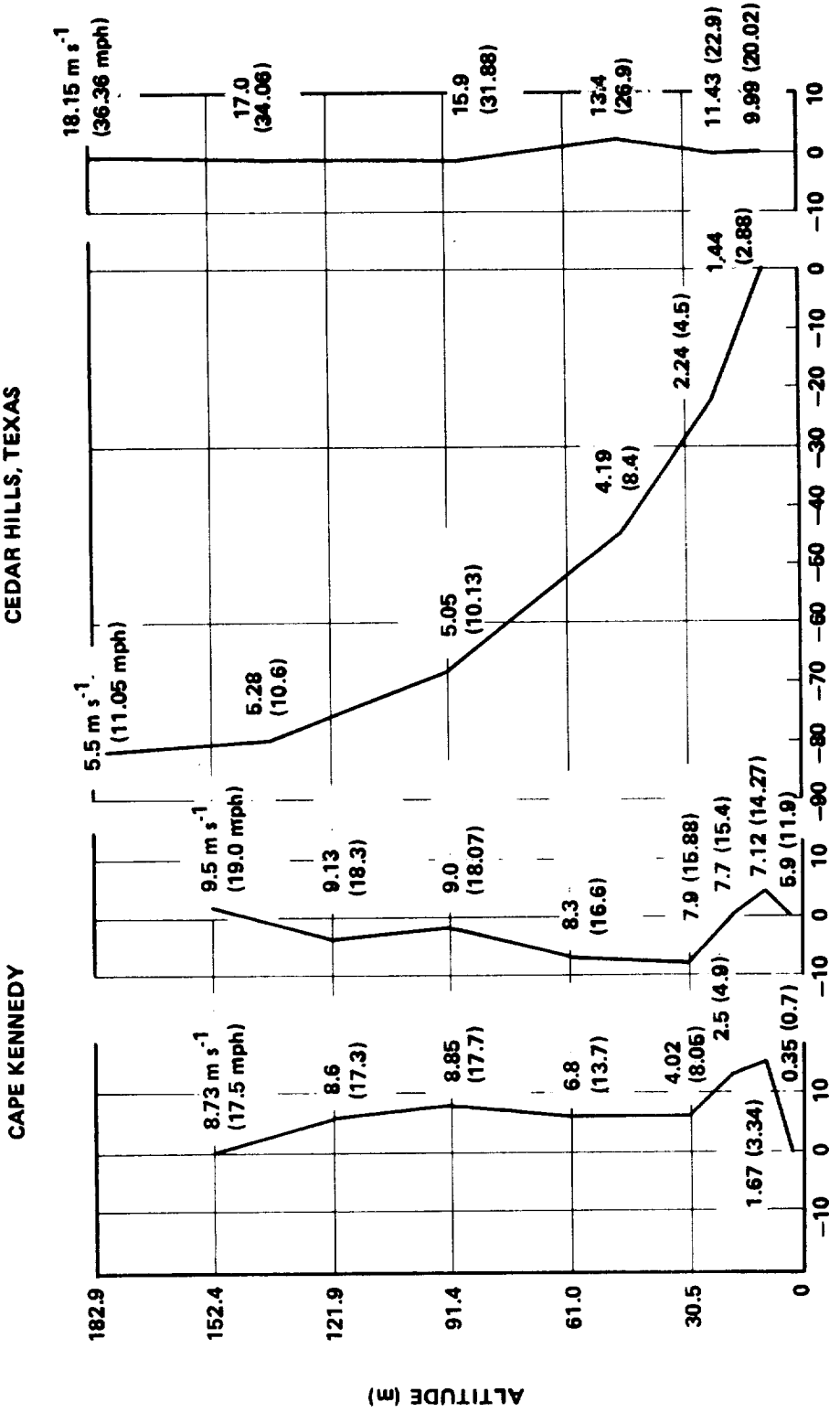

Figure 5.20 Examples of wind direction profiles [5.9].

REFERENCES

5.1 Crutcher, H. L. and Falls, L. W.: Multivariate Normality. NASA TN D-8226, May 1976.

5.2 Smith, O. E.: Vector Wind and Vector Wind Shear Models 0 to 27 km Altitude for Cape Kennedy, Florida, and Vandenberg AFB, California. NASA TM X-73319, George C. Marshall Space Flight Center, Marshall Space Flight Center, Alabama, July 1976.

5.3 Court, Arnold: Wind Shear Extremes (edited by Michael J. Changery). Initial Wind Energy Data Assessment Study. NSF-RA-N-75-020, prepared under Grant AG-517 for the National Science Foundation RANN-Research Applied to National Needs by the National Oceanic and Atmospheric Administration, Environmental Data Service, National Climatic Center, May 1975.

5.4 Fichtl, G. H., Camp, D. W., and Frost, Walter: Sources of Low-Level Wind Shear Around Airports. Survey Paper, Journal of Aircraft, Vol. 14, Number 1, pp. 5-14, January 1977.

5.5 Shieh, C. F., Frost, Walter, and Bitte, Jurgen: Neutrally Stable Atmospheric Flow over a Two-Dimensional Rectangular Block. NASA CR-2926, November 1977.

5.6 Rice, S. O.: Mathematical Analysis of Random Noise. Bell System Technical Journal, Vol. 23, pp. 282-332, 1944 and Vol. 24, pp. 46-156, 1945.

5.7 Frost, Walter and Hutto, M. L.: Trivariate Normal Probability Distribution of Wind Direction. Report in preparation, 1978.

5.8 Houbolt, J. C.: Exceedances of Structural Interaction Boundaries for Random Excitation. AIAA Journal, Vol. 6, No. 11, November 1968.

5.9 Barr, N. M., Gangaas, Dagfinn, and Schaeffer, D. R.: Wind Models for Flight Simulator Certification of Landing and Approach Guidance and Control Systems. Report No . FAA-RD-74-206, December 1974.

CHAPTER 6. ICE AND SNOW LOADING

Summary of Ice and Snow Loading

6.1 Introduction

Section 6.1.1 gives the ice and snow load design values for a general purpose WTG together with correction factors for the effects of elevation and the risk of exceedance. Detailed computational procedures and working data from which these values are selected are given in Sections 6.2 through 6.6. Section 6.1.2 describes the method by which the given design values were determined from the information in Sections 6.2 through 6.6.

6.1.1 Ice and Snow Loading Design Values

6.1.1.1 Extreme Ice Thickness

Suggested design values of ice thickness, T_i, for a general purpose WTG are:

$$T_i = 21 \text{ cm } (8.27 \text{ in.})$$

$$T_i = 10 \text{ cm } (3.94 \text{ in.}) \quad . \tag{6.1}$$

These values are based on the more severe icing conditions reported for the conterminous United States.

The higher value is computed on the basis of aerospace design philosophy which specifies a 10-percent risk of exceedance during the expected life of the structure (a 25-year life expectancy is assumed here). The lower value is computed on the basis of building code design philosophy which specifies a 63-percent risk of exceedance during an expected 50-year life of the proposed structure.

Figure 6.1 (again based on the more extreme icing conditions reported) provides a plot of extreme ice thickness versus risk of exceedance for a 25-year and a 50-year expected life. The WTG design engineer will wish to select his own degree of risk which presumably will be somewhere between aerospace design procedures and standard building code practices.

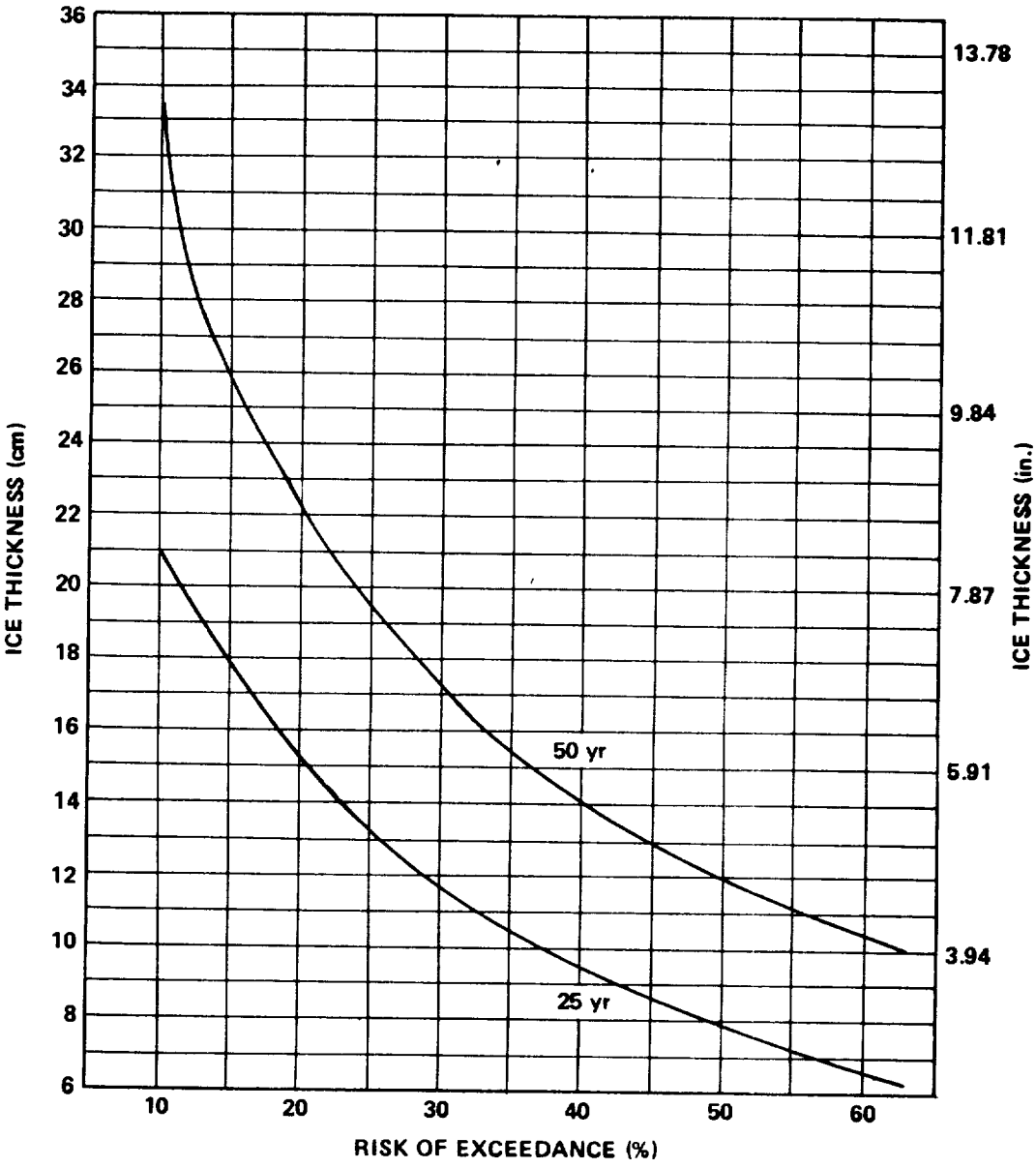

Figure 6.1 Risk of exceeding extreme ice loads.

6.1.1.1.1 Extreme Ice Density

For the purpose of designing a WTG for use in any location, the most severe conditions of ice loading must be considered. To this end, the design engineer must anticipate the formation of glaze ice, which has a specific density, ρ_i, of

$$\rho_i = 0.85 \text{ gm cm}^{-3} \ (53 \text{ lb ft}^{-3}) \quad . \tag{6.2}$$

6.1.1.1.2 Extreme Ice Load

To determine the ice load to which a WTG will be exposed, it is necessary to multiply the ice thickness by the ice density. Using the values previously given, we find the extreme ice loads, L_i, are as follows:

$$L_i = 17.85 \text{ gm cm}^{-2} \ (36.53 \text{ lb ft}^{-2})$$

$$L_i = 8.50 \text{ gm cm}^{-2} \ (17.40 \text{ lb ft}^{-2}) \quad . \tag{6.3}$$

Again, the higher value is based on aerospace design philosophy; whereas, the lower value is based on building code standards.

6.1.1.1.3 Correction of Ice Loading for Elevation

Figure 6.2 provides a plot of scaling factors for ice thickness with respect to elevation. To determine the design ice thickness with respect to elevation, T_{iE}, multiply the ice thickness, T_i, by the scaling factor, S, from Figure 6.2. That is,

$$T_{iE} = ST_i \quad . \tag{6.4}$$

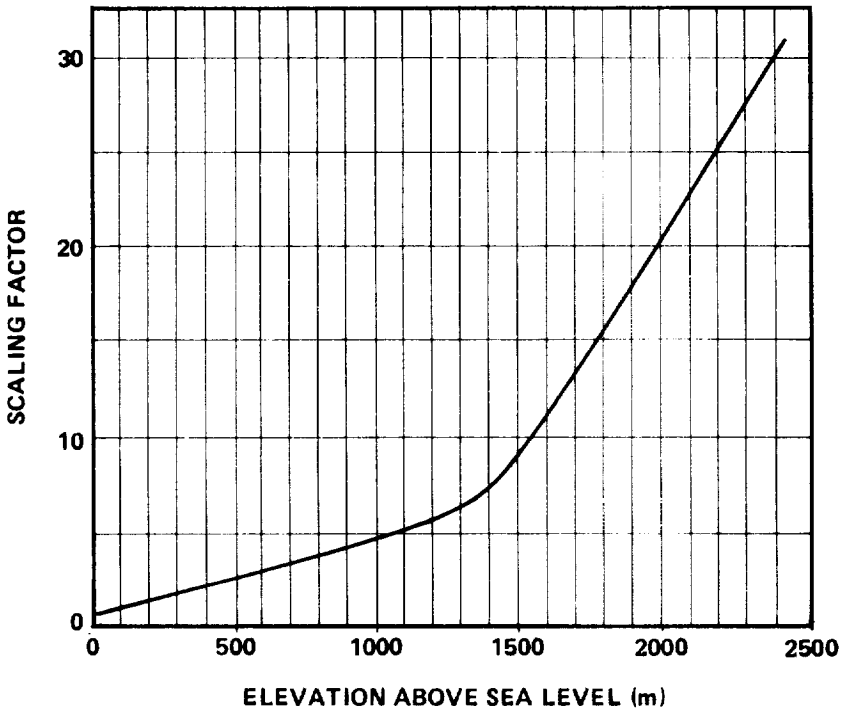

Figure 6.2 Scaling factor for ice thickness as related to elevation (taken from data from a 35-year study of New England icing conditions).

6.1.1.2 Extreme Snow Loading

Two design values of snow loading, L_S, for a general service WTG in the United States are:

$$L_S = 62.5 \text{ gm cm}^{-2} \ (128 \text{ lb ft}^{-2})$$

$$L_S = 36.6 \text{ gm cm}^{-2} \ (73 \text{ lb ft}^{-2}) \quad . \qquad (6.5)$$

The higher value is, again, computed on a 10-percent risk of exceedance during the 25-year expected life of the structure (aerospace design philosophy). The lower value is based on building code design philosophy which specifies a 63-percent risk of exceedance during a 50-year life expectancy.

Figure 6.3 provides a plot of extreme snow loads versus risk of exceedance for a 25-year and 50-year life expectancy. It is assumed that a WTG design engineer will select his own degree of risk which will lie somewhere between the aerospace and building code design practices.

Extreme 24-h snow accumulation is discussed in Section 6.4.3.

6.1.2 Description of Recommended Design Values

The development of the specific design values from information contained in Sections 6.2 and 6.3 of this report is described below.

6.1.2.1 Extreme Ice Loads

The most extreme icing conditions, given in tabular form in Section 6.3.1.3., occur in Region III (Northeast) of the United States [6.1]. This region was therefore selected to represent the most extreme ice load region in which a general service WTG is likely to be sited. A Fisher-Tippett probability distribution for Region III will be given later (for details see Section 6.2). The Fisher-Tippett probability distribution gives the expected mean recurrence interval, T_R, of the extreme ice load. The recurrence interval at which the extreme value is to be selected for design is determined by the application outlined in Section 6.3.1.3.2 in which the recurrence interval associated with a given lifetime of the structure, N, is given for a prescribed risk of exceedance, R. Since ice loading is a statistical quantity, the engineer must accept some risk that his design ice load may be exceeded at least once in the expected useful life of the structure.

Two design philosophies for selecting the basic design value for the extreme ice load conditions were considered. Both values are quoted to establish an estimate of the range of values which may be used by the design engineer. One philosophy is based on aerospace vehicle design principles [6.2] which recommend that a 10-percent risk of exceedance for any given expected life period be used in determining the extreme icing conditions. An alternate design philosophy was taken from the building code standard which accepts a 63-percent risk for an expected life of 50 years [6.3].

The following describes the selection procedure for the basic extreme ice load design value based on both philosophies.

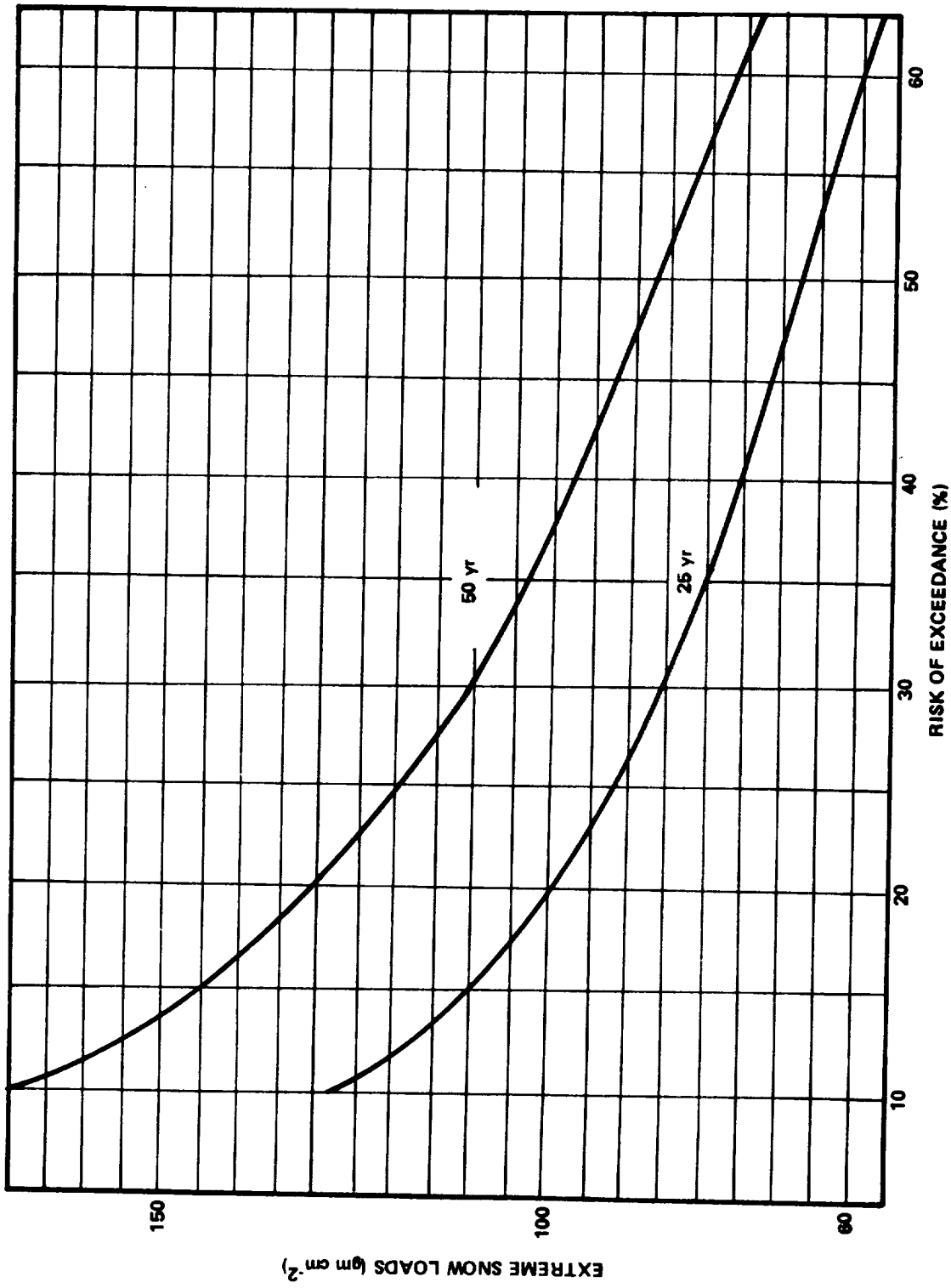

Figure 6.3 Risk of exceeding extreme snow loads.

Since the aerospace vehicle design philosophy gives no specific expected life, assume 25 years as the expected life of the WTG. Employing a 10 percent risk that the design ice load will not be exceeded in the lifetime of the structure, the recurrence interval, T_R, is found to be 238 years, as detailed in Chapter 2, Section 2.1.2.1. A 238-year recurrence interval is associated with an extreme ice load thickness of 21 cm (8.27 in.) (see Section 6.3.1.3.1).

Alternately, utilizing an expected life of 50 years and accepting a 63-percent risk of exceedance, the recurrence interval is found to be 51 years. This indicates a design value for extreme ice thickness of 10 cm (3.94 in.).

The WTG design engineer will probably accept an intermediate value between those previously computed since the WTG does not require the same fail/safe features necessitated in a manned spacecraft. However, the WTG is deliberately exposed to severe environments and therefore requires a greater degree of reliability than that of standard building designs. Figure 6.1 provides a readily useable curve for selection of extreme ice loads based on individual design philosophies.

The extreme ice load design values selected in the preceding paragraphs are measured at approximately sea level. Correction of these values to the elevation at which the WTG might be operating is necessary. The recommended correction of the ice load for height is given by the scaling factor shown in Figure 6.2. To adjust the extreme ice load value, the elevation at which the WTG will be operating is located on the horizontal axis. A vertical line is drawn to intersect the line on the graph. A horizontal line is drawn from this point of intersection to the vertical axis to find the scaling factor. Assume a WTG is to be located in Region III and will be operating on a building with a 100-m (30.5-ft) elevation. From Figure 6.2, the scaling factor is 1.25. Using the value 10 cm (3.94 in.) previously found, the design ice load thickness should be 12.5 cm (4.93 in.) for a WTG operating at this elevation.

6.1.2.2 Extreme Snow Loads

Using isopleth maps showing the snow load conditions in the United States, the most extreme snow loads occur in the northernmost part of Maine. This location was therefore selected to represent the greatest snow load conditions to which a general service WTG is likely to be exposed. Fisher-Tippett probability distribution for these values is shown in Figure 6.4. This figure gives the expected mean recurrence interval, T_R, of the extreme snow load. The

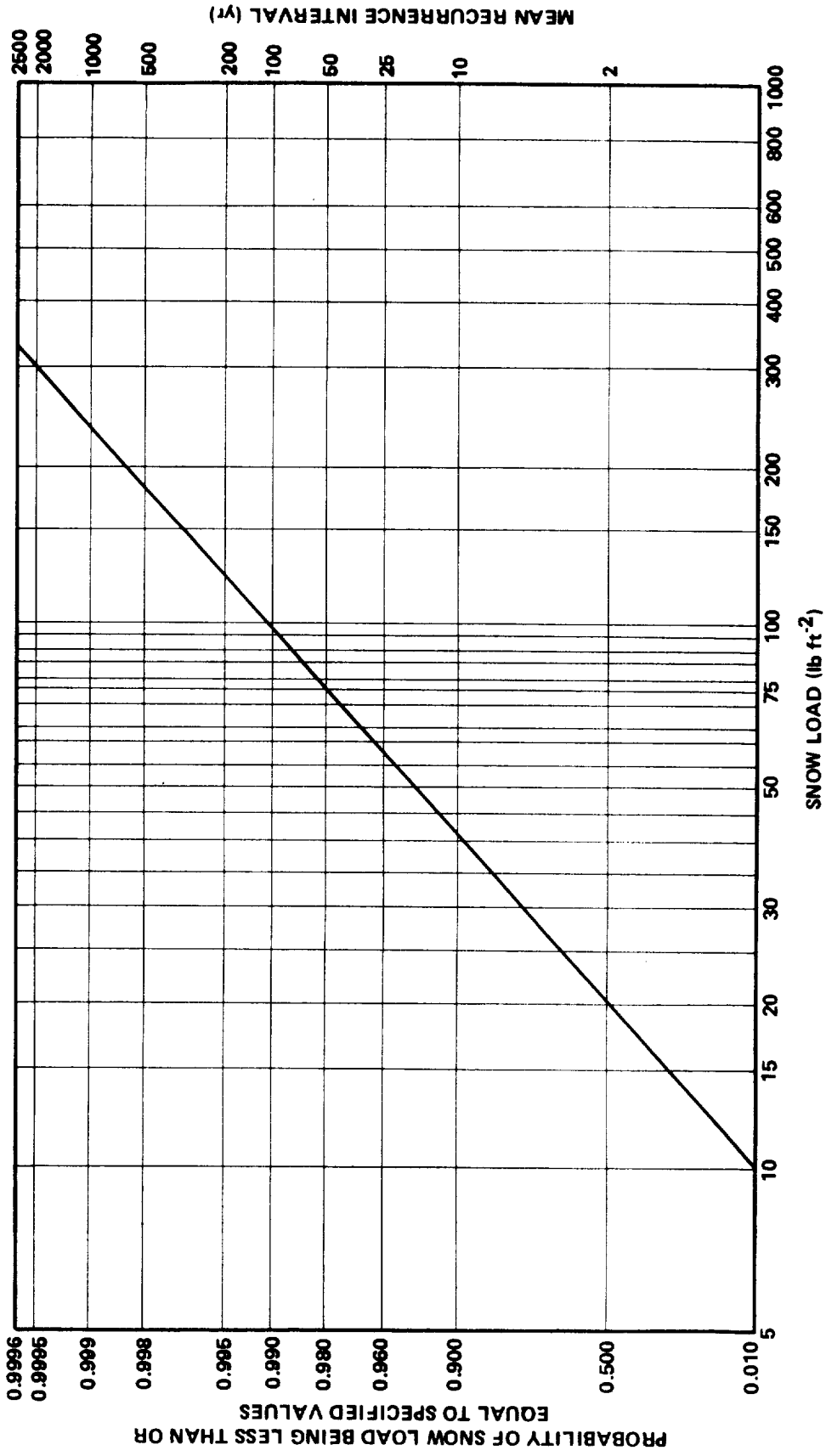

Figure 6.4 Fisher-Tippett Type II distribution for northern Maine which provides the probability of snow load being less than or equal to specified value.

recurrence interval at which the extreme value is to be selected for design is determined as detailed in Section 6.4.2. This gives the recurrence interval associated with a given lifetime of the structure, N, for a prescribed risk of exceedance, R. As before, the design engineer must accept some risk that this extreme snow load value will be exceeded during the expected life of the machine.

The two design philosophies described in Section 6.1.2.1 on icing have also been utilized here. Using the aerospace vehicle design philosophy with an expected life of 25 years and 10-percent risk of exceedance we find the extreme design snow load to be 62.5 gm cm^{-2} (128 lb ft^{-2}). Applying the building code standards, we find the design load to be 36.6 gm cm^{-2} (73 lb ft^{-2}). Figure 6.3 provides a readily useable curve for selection of extreme snow loads based on individual design philosophies.

Detailed Computational Procedures and Working Data

6.2 Introduction

The preceding sections were intended to give a concise overview of characteristic ice and snow loads for general purpose design of a WTG to operate in almost any region of the United States. There will be some areas of the country having unusual climatic conditions for which little or no data are available. The following sections provide detailed information for WTG design for a specific site or region and give data to substantiate the values given in the previous sections.

Ice and snow loading will increase the static loading on the WTG tower and blades, thereby affecting the structural integrity of the machine. (It is assumed the blades will be feathered in cases of severe icing because of rough operation which can occur with icing, as experienced with the Putnam WTG at Grandpa's Knob [6.4].)

There is no information to date on the formation of ice on rotating wind turbine blades. However, there is a large amount of data concerning ice loads forming on airframes, helicopter rotors, etc. Reference 6.5 gives a detailed summary on ice formation on moving airframes which must be interpreted for WTG application.

6.3 Basic Design Ice Loading

6.3.1 Introduction

This section deals with computing ice loads which would be employed in load analyses. The general concept of determining a design ice load is to select the most extreme amount of icing that the structure will experience in a given number of years exposure.

There is, however, a certain probability that the actual ice load will exceed the design value. Hence, the design engineer must select the degree of risk he is willing to accept that this might happen at some time during the useful life expected of the structure.

Icing thicknesses are, therefore, tabulated according to percent probability of occurring at least once in a given recurrence interval. These values must then be corrected for elevation. The procedure for approximately evaluating these factors and the selection of a realistic design ice load is described in the following sections.

6.3.1.1 Types of Ice Deposits and Conditions Causing Them

Freezing rain or icing occurs when there is warm air overrunning a shallow freezing layer near the ground. If the warm air is held stationary by the resistance of the flow of the dense cold air next to the surface, or by stagnation of the latter in a terrain sheltered by mountains, rain which freezes on impact with objects on the ground may continue for many hours. Heavy deposits of glazed ice soon form, doing great damage to electric wires, trees, structures, etc. These conditions are most prevalent in climates near the limit of a continental winter snow cover, with threatened penetration of cyclonic activity developing over a warm ocean. As a rule, icing is most likely to occur at temperatures from -2° to -8°C (28° to 18°F), with an observed maximum frequency at approximately -6°C (21°F).

Hoar frost is produced by direct sublimation of water vapor on a surface of temperature below the freezing point. Its prediction is based on predictions of temperature and humidity. Hoar frost may form on an object on cold, clear nights when radiation cooling has decreased the temperature of the object below the frost point.

Rime ice is caused by freezing of supercooled cloud droplets; it is white, opaque, of granular or crystalline shape, and easily flaked off the object on which it forms. A small supercooled water droplet striking an exposed surface freezes almost at once and takes the form of rime ice. Rime ice usually forms in nonturbulent clouds at all temperatures below freezing; at low temperatures moderate rime ice is more likely than glaze ice.

Glaze ice is hard and glossy and can be broken loose only with difficulty. It is formed on terrestrial objects in two different ways. If dew is cooled slowly [approximately 1°C (1.8°F)/10 h] from just above the freezing point to just below it, clear ice, often in abundant amounts, may form when the objects are distributed, for instance by a sudden but slight surface wind or by falling rain, sleet, or snow. Such ice deposits usually occur around sunrise after a night with overcast, light winds, and no precipitation. On terrestrial objects which are hydrophilic it is possible for glaze ice to form from dew even at temperatures as low as -10°C (14°F), but the usual limiting temperature is approximately -1°C (30°F). Glaze ice deposits on the ground also occur when warm-front rain at temperatures slightly above 0°C (32°F) falls on objects which have previously been cooled well below 0°C (32°F) by the occupying cold air. Table 6.1 gives an example of density of different types of ice.

TABLE 6.1 DENSITY OF DIFFERENT TYPES OF ICE

Temperature of Wall		Type of Ice	Density Range		Remarks
(°F)	(°C)		(lb_m ft^{-3})	(gm cm^{-3})	
23 to 32	-5 to 0	Glaze Ice	60	0.69	Hard Dense Ice
0 to 23	-18 to -5	Milky Ice or Glaze Ice with Air Bubbles	43 to 53	0.69 to 0.85	
Below 15	Below -9	Rime Ice	18 to 25	0.29 to 0.40	Crumbly

6.3.1.2 Geographical Distribution of Icing Conditions

Ice thickness and frequency of occurrence vary from region to region within the United States. If a WTG is to be designed for a particular area of the country, the design engineer will need to know the icing conditions his machine might experience in that location. Figure 6.5 shows the number of times ice thickness greater than 2.5 cm (1 in.) occurred by state. Figure 6.6 shows the number of glaze storms which occurred, without regard to ice thickness, during a 9-year study [6.6].

6.3.1.3 Calculation of Expected Icing Conditions

Figure 6.7 shows the United States divided into regions of similar glaze characteristics. The number of storms affecting Regions I through VII,[1] regardless of how many states within each region were affected, is shown in Tables 6.2 and 6.3. Also shown is the probability of at least one occurrence of thickness ≥ 2.5 cm (1 in.) and ≥ 5 cm (2 in.) somewhere in each region in any year. Probabilities were computed using the Poisson approximation, $\lambda^x e^{-\lambda}/x!$ which, for no occurrences, reduces to $e^{-\lambda}$. Therefore,

$$P(\geq r) = 1 - e^{-\lambda} \quad ,$$

where $P(\geq r)$ is the probability of at least one occurrence of ice $\geq$ the thickness r in any year and λ is the average number of storms in any year (i.e., the number of storms per region divided by the number of years of study).

A stochastic model of the spatial variability of a meteorological element has been developed [6.7] which relates the probability of an event somewhere in a given area to the smaller probability at a single station within the area. To apply the model to the data in Table 6.2, it has to be assumed that the chance, or probability of an ice storm is uniformly the same over the whole region. Point probabilities are shown in Table 6.3. Using data given in Reference 6.6, Tables 6.4 and 6.5 were computed for different intensities and regions [6.1].

1. No data were reported for Region VIII.

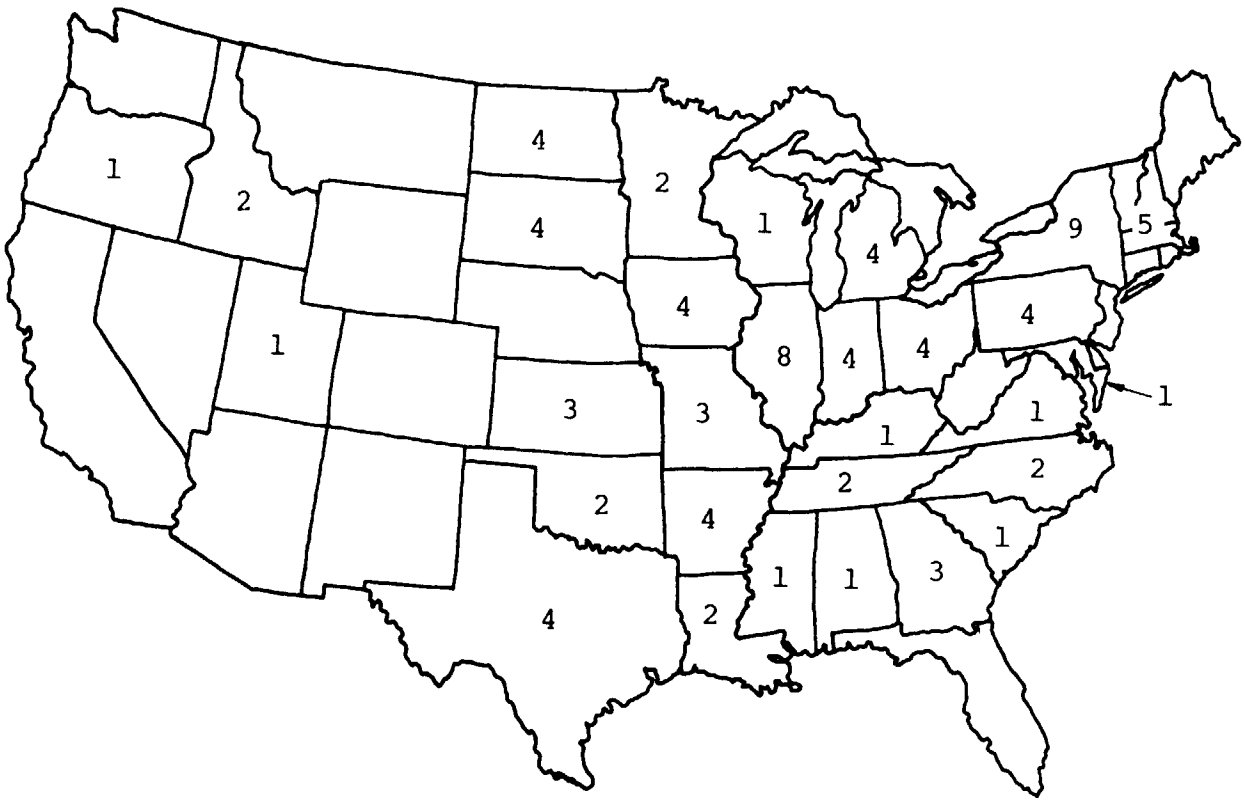

Figure 6.5 Number of times by state that ice thickness greater than 2.5 cm (1 in.) occurred during 50 years (New England and Maryland-Delaware-District of Columbia were treated as single states).

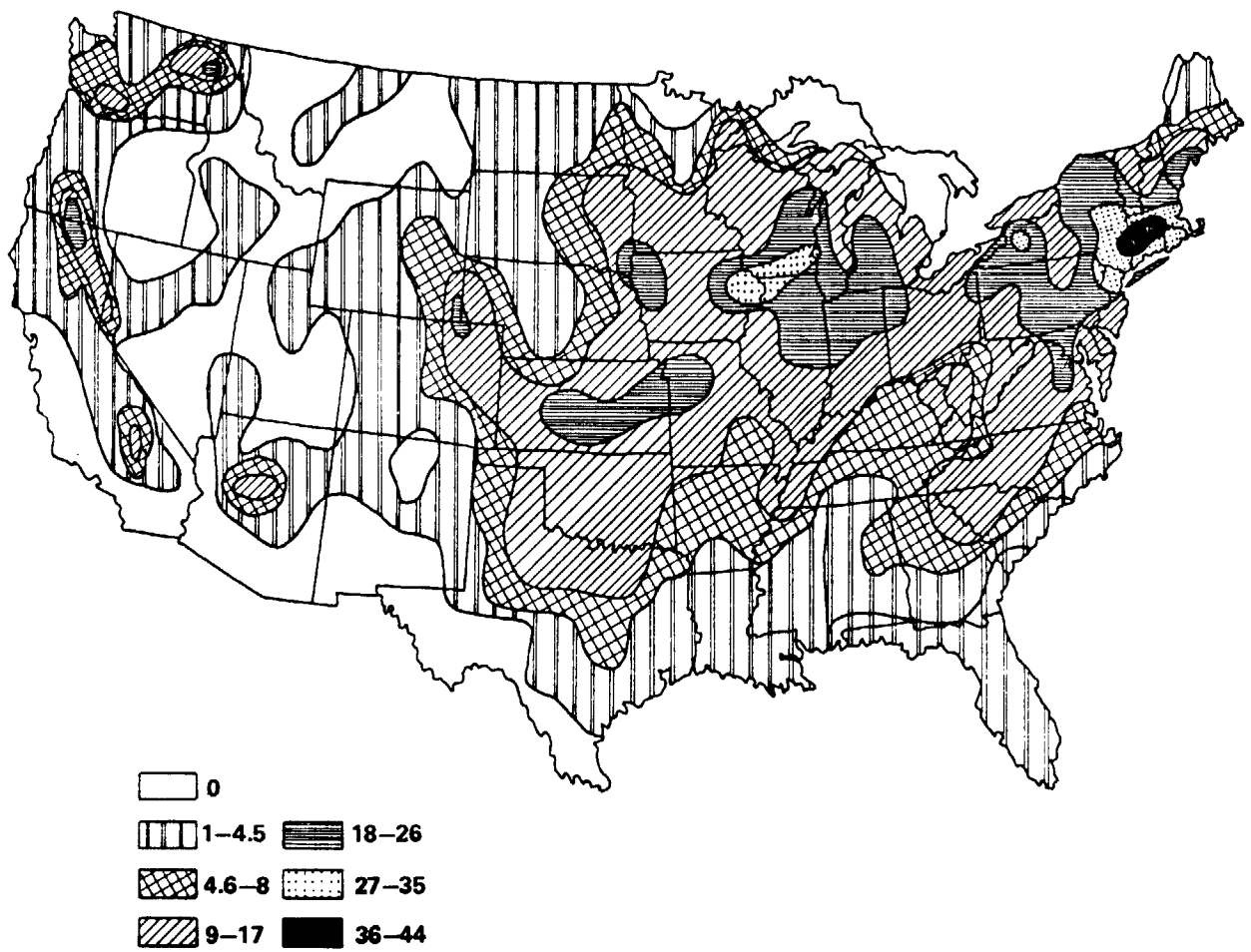

Figure 6.6 Total number of glaze storms, without regard to ice thickness, observed during the 9-year period of the Association of American Railroads Study [6.6].

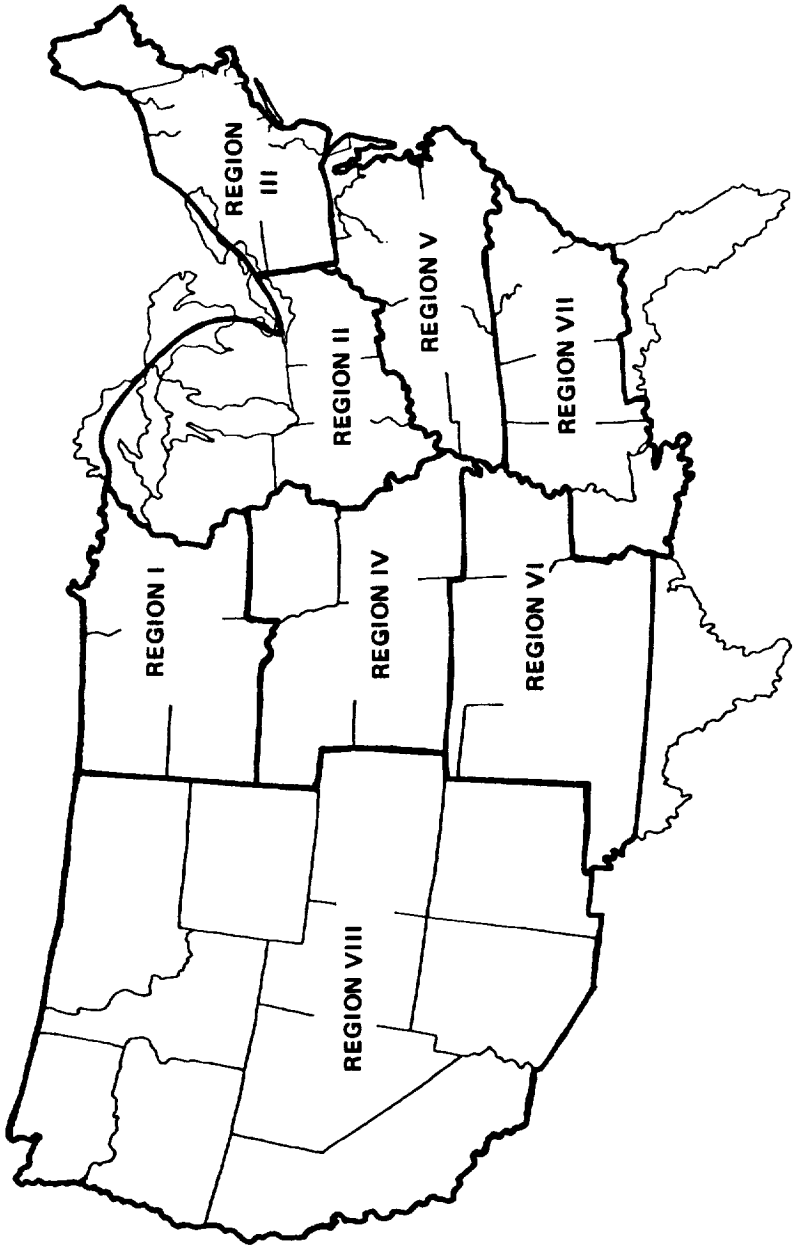

Figure 6.7 Regions of similar glaze ice characteristics.

TABLE 6.2 PROBABILITY OF AT LEAST ONE OCCURRENCE OF AN ICE STORM IN ANY YEAR SOMEWHERE IN THE REGION [6.1]

Region	Land Area (km^2)	Number of Ice Storms in 50 Years ≥ 2.5 cm (1 in.)	Regional Probability of an Ice Storm in 1 Year ≥ 2.5 cm (1 in.)	Number of Ice Storms in 50 Years ≥ 5 cm (2 in.)	Regional Probability of an Ice Storm in 1 Year ≥ 5 cm (2 in.)
I	586,147	8	0.15	3	0.06
II	633,392	15	0.26	3	0.06
III	423,362	14	0.24	4	0.08
IV	734,726	8	0.15	3	0.06
V	534,380	5	0.10	2	0.04
VI	769,457	10	0.18	3	0.06
VII	600,824	5	0.10	1	0.02

TABLE 6.3 PROBABILITY OF AT LEAST ONE OCCURRENCE OF AN ICE STORM IN ANY YEAR AT A REPRESENTATIVE POINT[a] IN THE REGION [6.1] (ESTIMATED FROM SPATIAL VARIABILITY MODEL)

Region	Point Probability of an Ice Storm ≥ 2.5 cm (1 in.) in 1 Year	Point Probability of an Ice Storm ≥ 5 cm (2 in.) in 1 Year
I	0.0006	0.00020
II	0.0060	0.00018
III	0.0020	0.00050
IV	0.0005	0.00016
V	0.0004	0.00012
VI	0.0001	0.00014
VII	0.0004	Negligible

a. Any point in the region.

TABLE 6.4 PROBABILITY OF AT LEAST ONE OCCURRENCE OF AN ICE STORM IN ANY YEAR AT A REPRESENTATIVE POINT IN THE REGION (ESTIMATED FROM BENNETT [6.6])

Region	Regional Average No. Storms in 9-Year Study	Probability of an Ice Storm (Any Thickness) in 1 Year	Regional Average No. Storms ≥0.63 cm in 9-Year Study	Probability of an Ice Storm ≥0.63 cm in 1 Year	Regional Average No. Storms ≥1.25 cm in 9-Year Study	Probability of an Ice Storm ≥1.25 cm in 1 Year
I	8	0.59	5	0.43	3	0.28
II	18	0.86	7	0.54	3	0.28
III	20	0.89	10	0.67	6	0.49
IV	15	0.81	5	0.43	3	0.28
V	8	0.59	4	0.36	2	0.20
VI	6	0.49	4	0.36	2	0.20
VII	4	0.36	2	0.20	0.5	0.05

TABLE 6.5 PROBABILITY OF AT LEAST ONE OCCURRENCE OF AN ICE STORM OF STATED INTENSITY IN ANY YEAR AT A POINT IN THE MOST SEVERE PART OF THE REGION (ESTIMATED FROM BENNETT [6.6])

Region	Regional Maximum No. of Storms in 9-Year Study	Probability of an Ice Storm (Any Thickness) in 1 Year	Regional Maximum No. of Storms ≥ 0.63 cm in 9-Year Study	Probability of an Ice Storm ≥ 0.63 cm in 1 Year	Regional Maximum No. of Storms ≥ 1.25 cm in 9-Year Study	Probability of an Ice Storm ≥ 1.25 cm in 1 Year
I	24	0.93	14	0.79	8	0.59
II	35	0.98	10	0.67	4	0.36
III	44	0.99	19	0.88	9	0.63
IV	35	0.98	11	0.71	8	0.59
V	20	0.89	9	0.63	6	0.49
VI	16	0.83	8	0.59	5	0.43
VII	11	0.71	4	0.36	4	0.36

The probabilities given in Tables 6.3 and 6.4 approximate the probability of an ice storm of given intensity at a representative point in each region (i.e., an average for the region). These data are shown in Figures 6.8a through 6.14a, curves labelled "AVG." Table 6.6 shows the probability of an ice storm in 1 year in the worst state in each region, without regard to where the storms occurred [6.1] in the state. Table 6.6, together with the probabilities in Table 6.5, were used for estimates in the worst location in each region. This is shown in Figures 6.8a through 6.14a, curves labelled "MAX."

It should be noted that the values in Table 6.6 are not directly comparable with those in Table 6.5. The regional maximum number of storms listed in Table 6.5 occurred in the same general location. It is not likely that the same is true for the number of storms listed in Table 6.6. It is believed, however, that these figures provide an approachable maximum for the worst location in each region. The average and maximum frequencies of ice accumulation for each region are shown in Figures 6.8a through 6.14a. Extrapolation between 5- and 7.5-cm ice thickness was accomplished by extending the slope of the 2.5- to 5-cm line (MAX) in these figures. Extrapolation beyond 7.5 cm was considered totally guesswork. Figures 6.8a through 6.14a were used to summarize ice thickness for various return periods. The results of this are shown in Table 6.7.

These figures show the expected ice thickness that may occur for a given recurrence interval. To convert ice thickness into ice load, the thickness of the ice is multiplied by the density of the ice. For WTG design loads, the recommended ice density is that for glaze ice, 0.85 gm cm^{-3} (53 lb_m ft^{-3}). If a WTG is to experience a design ice thickness of 10 cm, the design load is 8.5 gm cm^{-2} (18.8 lb_m ft^{-3}). For the remainder of this section, the emphasis will be on ice thickness, as opposed to load. The engineer may then determine the load in the manner previously demonstrated.

6.3.1.3.1 Extreme Ice Loads for Given Recurrence Intervals

The basic design ice load is determined as follows:

1) The region of the country in which the WTG site is located is found on the map shown in Figure 6.7.

2) The Fisher-Tippett Type II distribution for this region is found in Figures 6.8b through 6.14b.

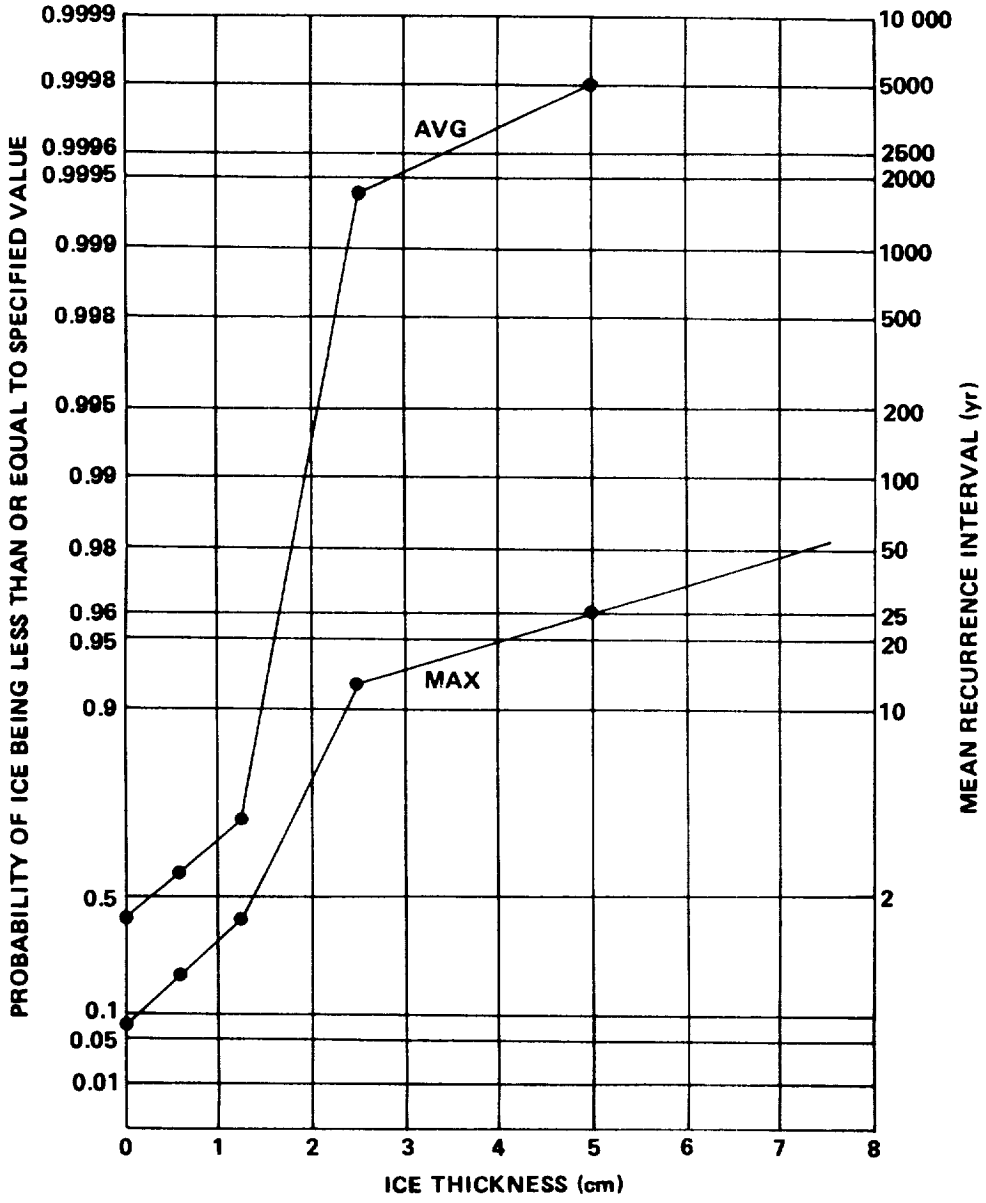

Figure 6.8a Estimated probability of ice thickness occurring at a representative point of Region I (AVG) and in the most severe part of Region I (MAX).

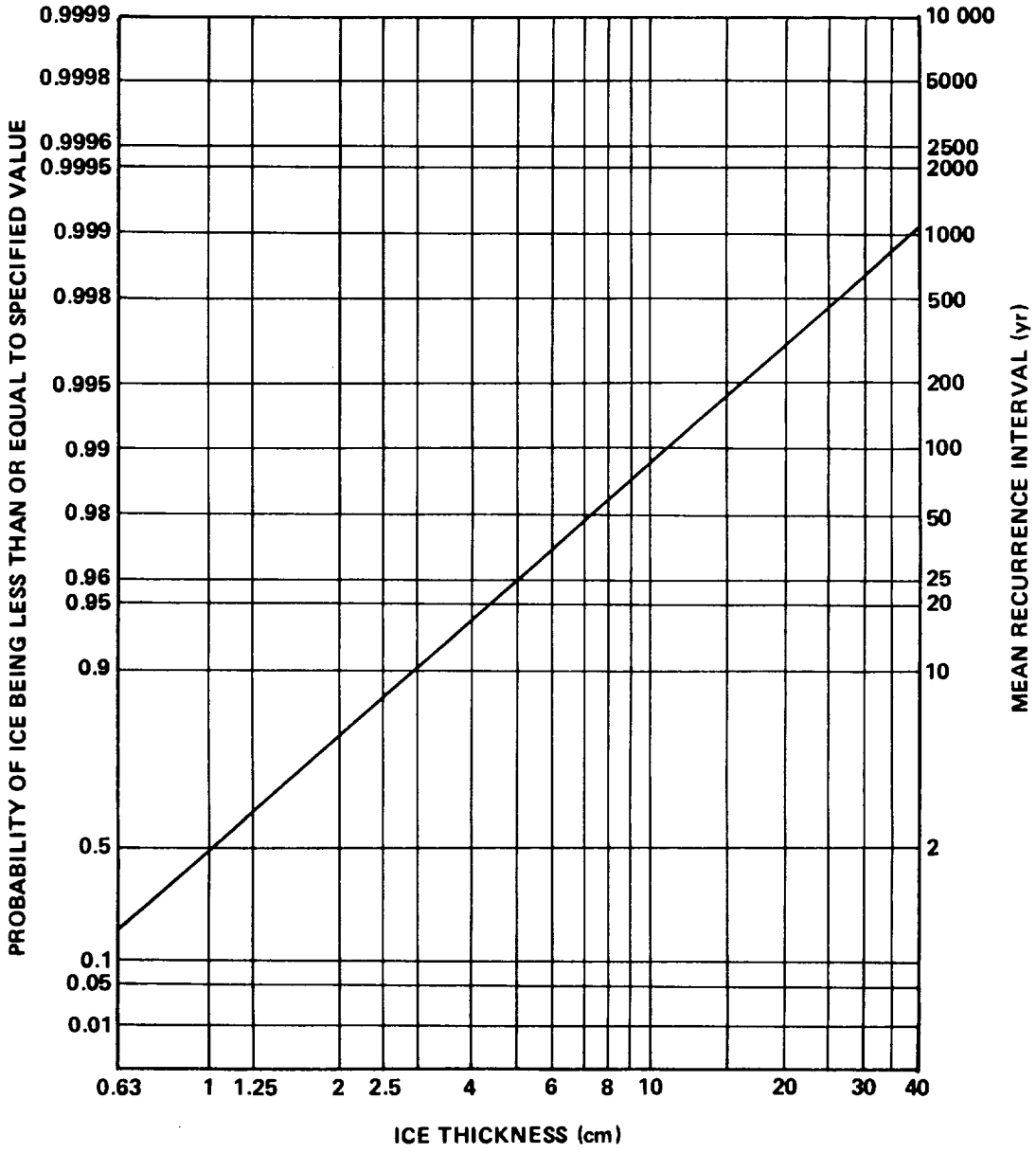

Figure 6.8b Fisher-Tippett Type II distribution for Region I.

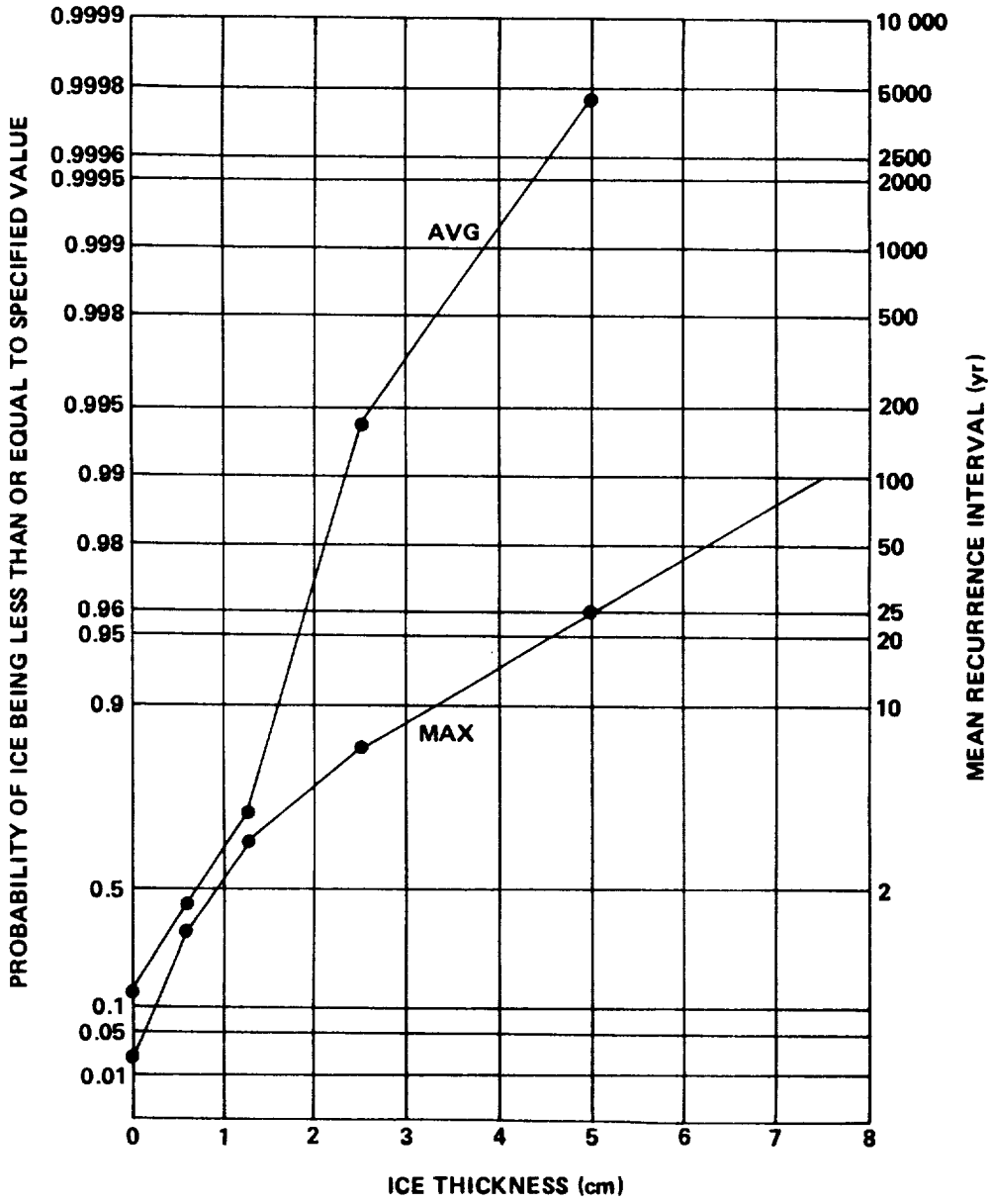

Figure 6.9a Estimated probability of ice thickness occurring at a representative point of Region II (AVG) and in the most severe part of Region II (MAX).

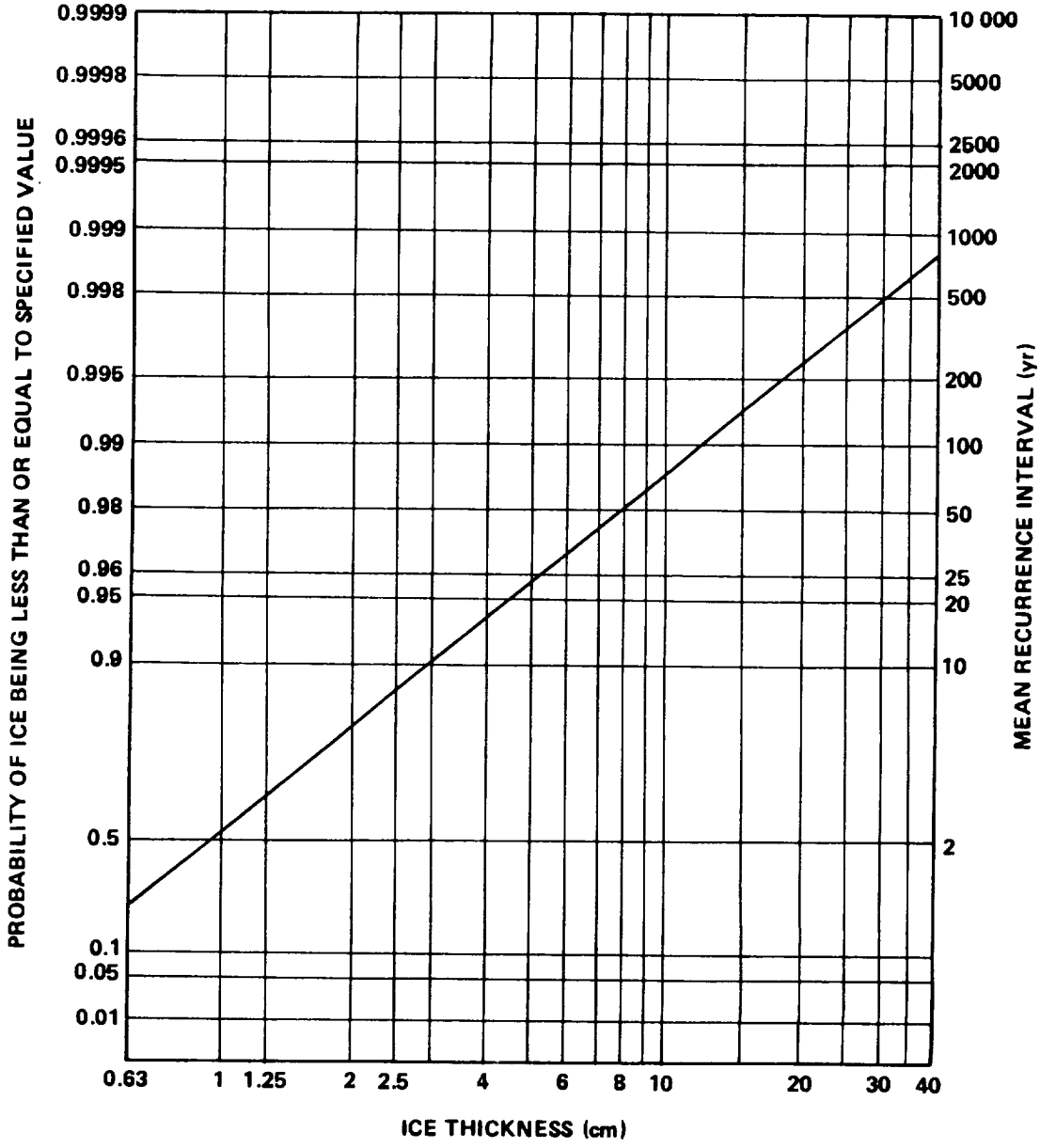

Figure 6.9b Fisher-Tippett Type II distribution for Region II.

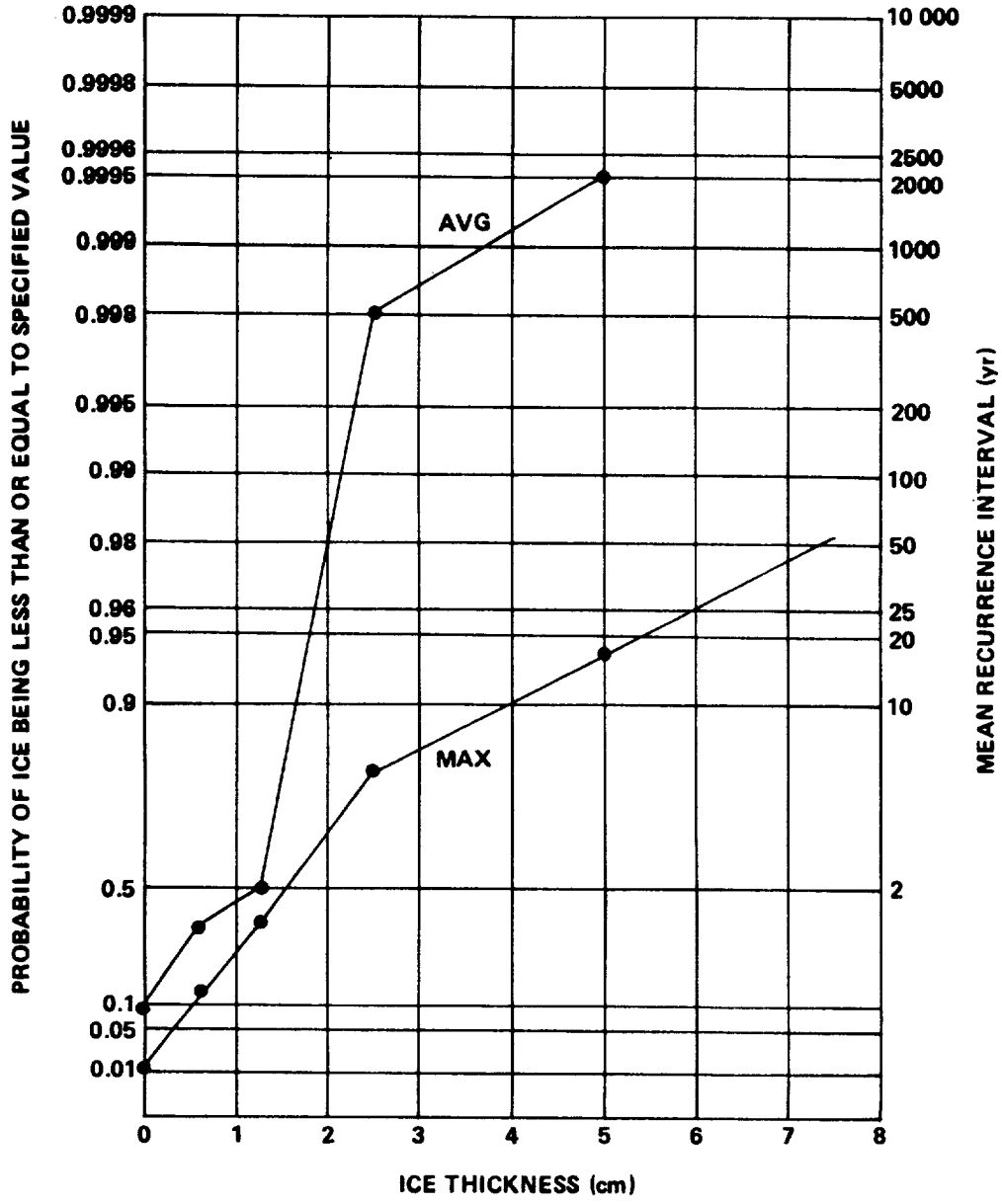

Figure 6.10a Estimated probability of ice thickness occurring at a representative point of Region III (AVG) and in the most severe part of Region III (MAX).

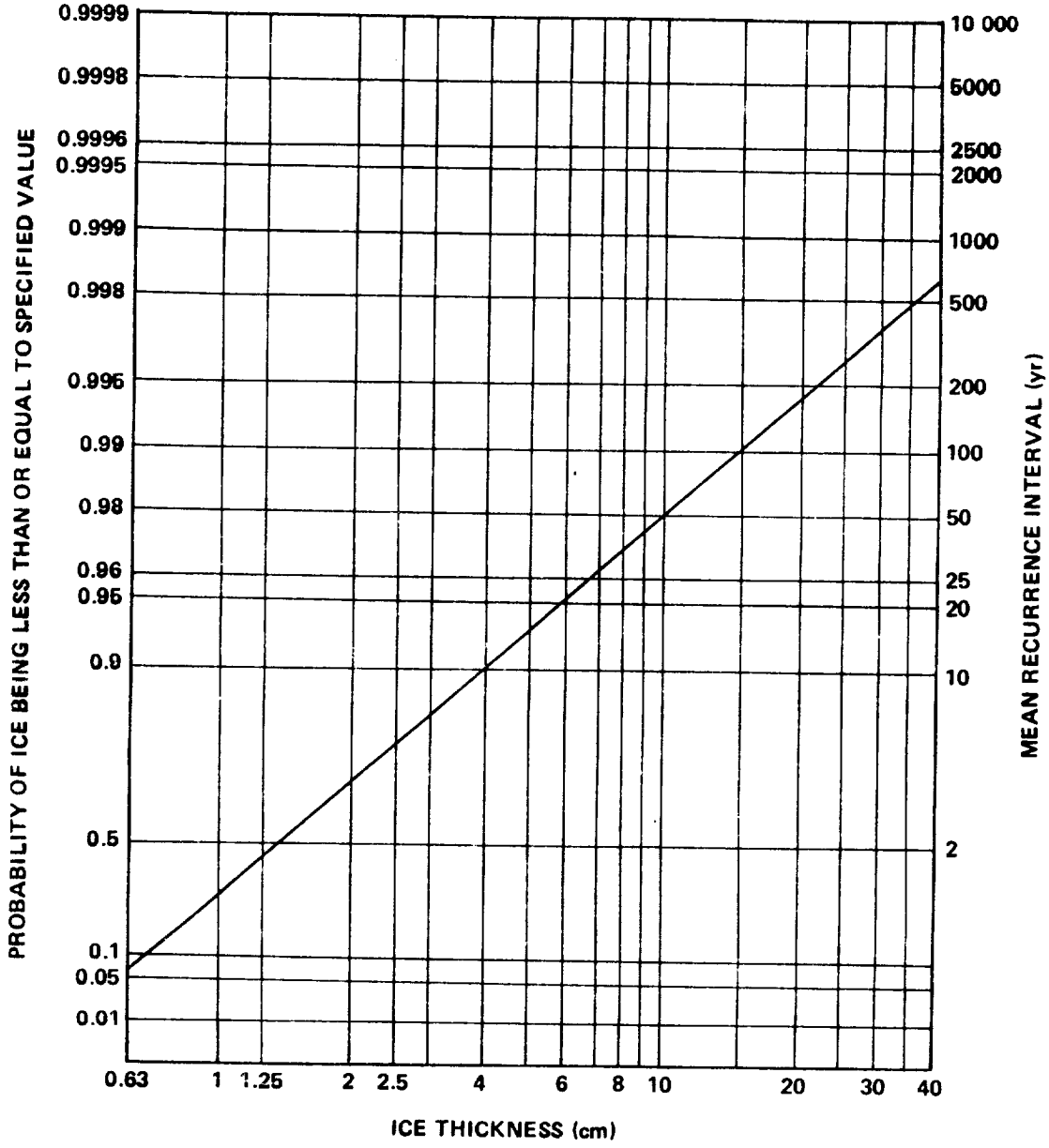

Figure 6.10b Fisher-Tippett Type II distribution for Region III.

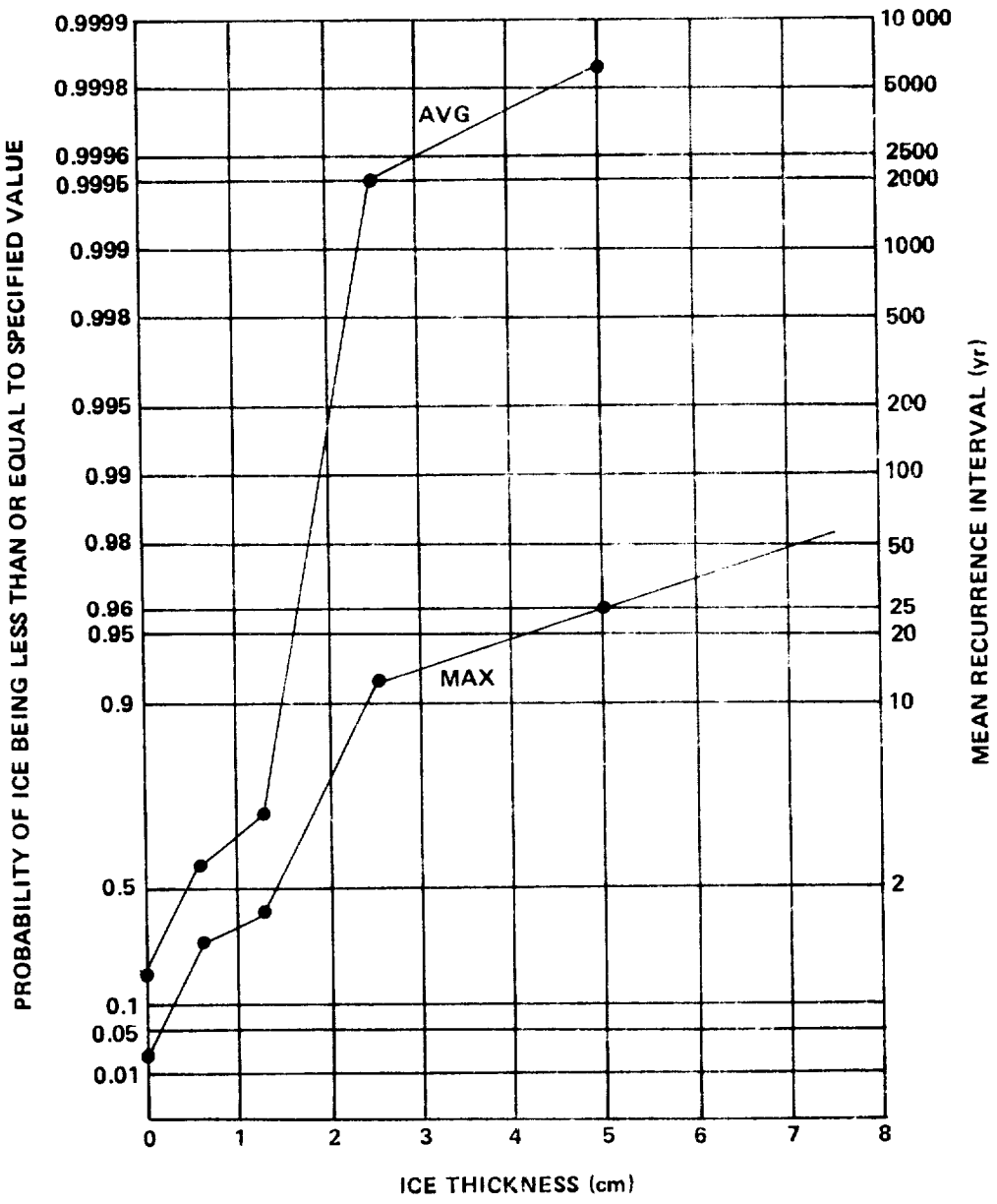

Figure 6.11a Estimated probability of ice thickness occurring at a representative point of Region IV (AVG) and in the most severe part of Region IV (MAX).

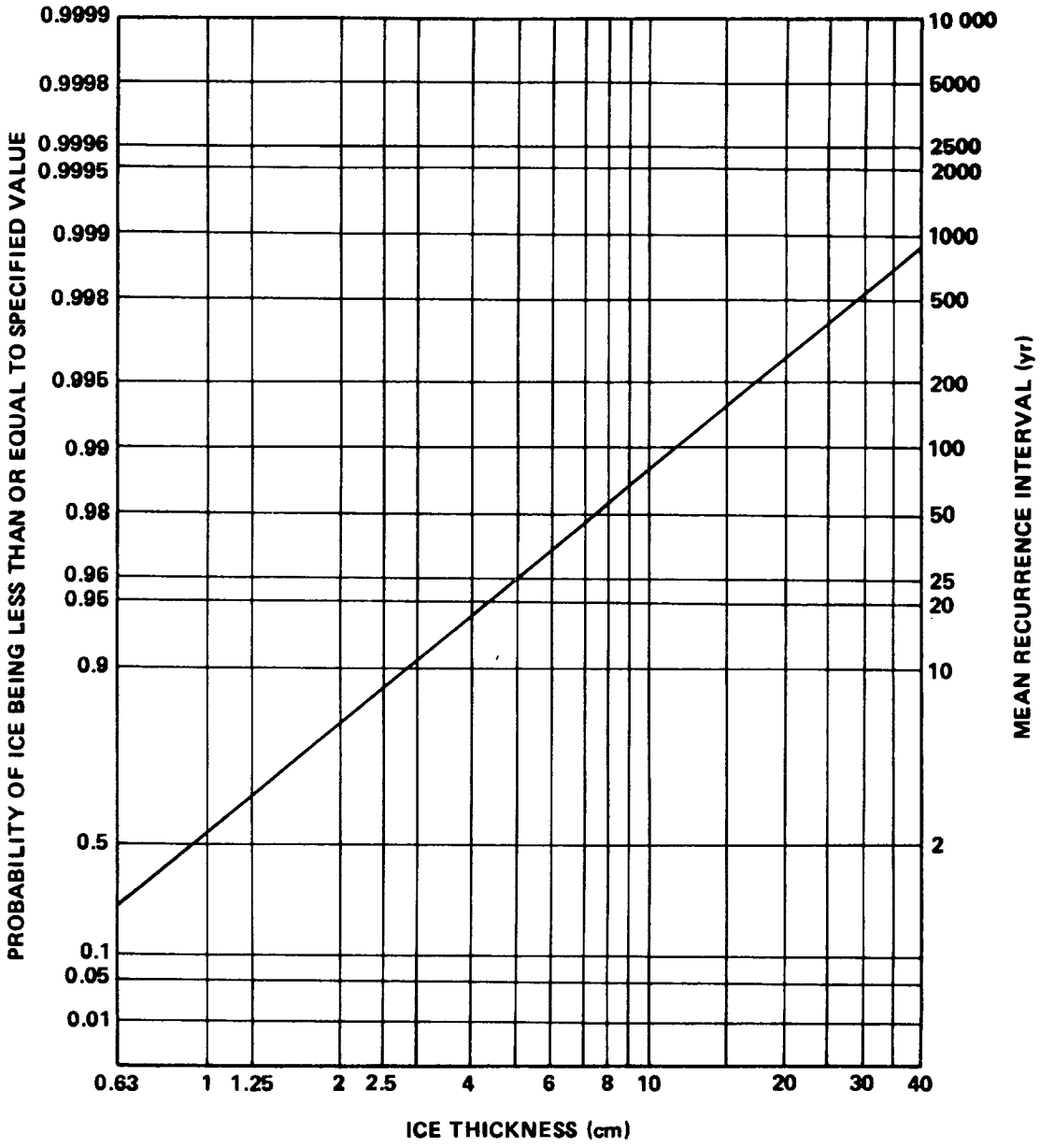

Figure 6.11b Fisher-Tippett Type II distribution for Region IV.

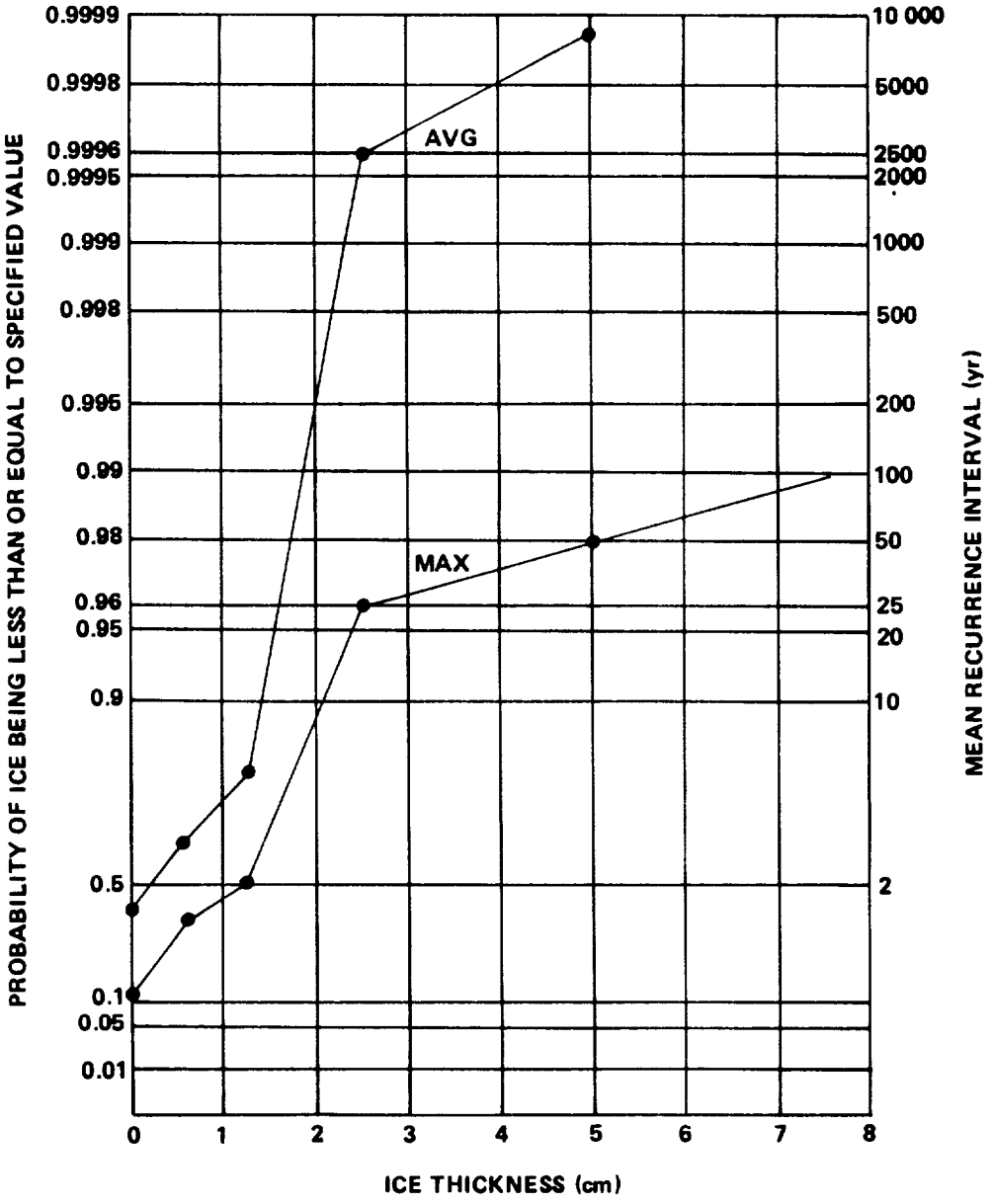

Figure 6.12a Estimated probability of ice thickness occurring at a representative point of Region V (AVG) and in the most severe part of Region V (MAX).

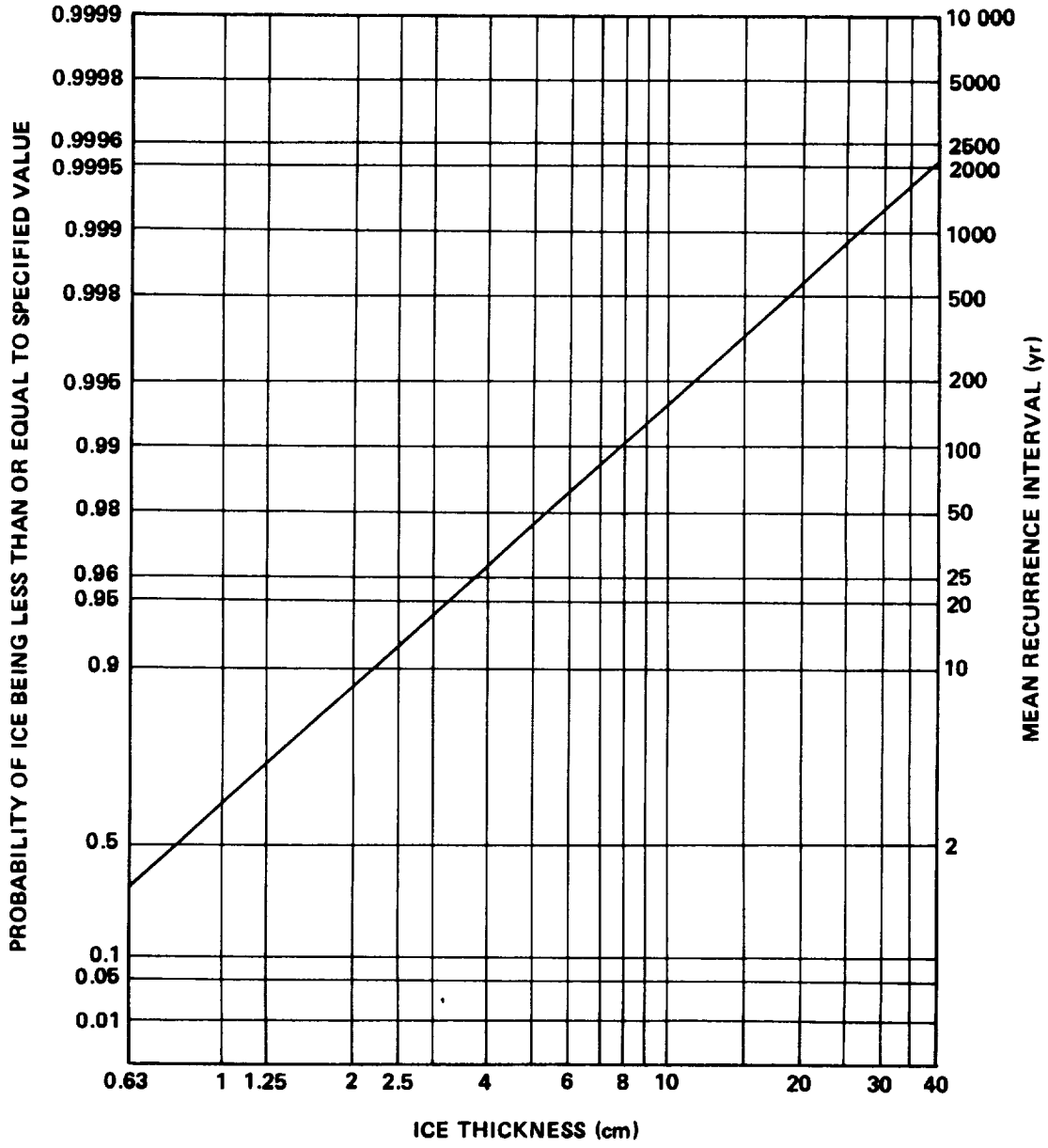

Figure 6.12b Fisher-Tippett Type II distribution for Region V.

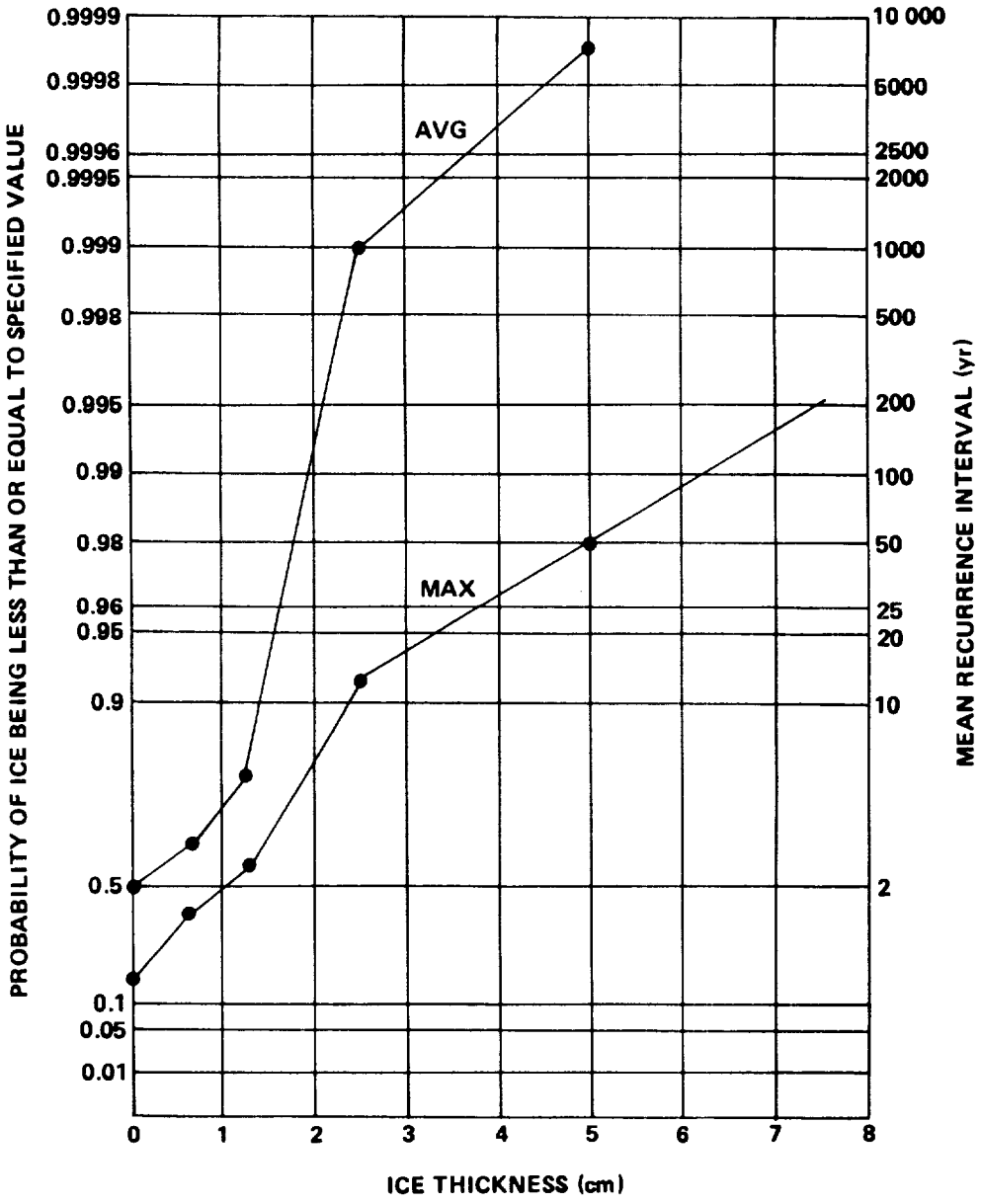

Figure 6.13a Estimated probability of ice thickness occurring at a representative point of Region VI (AVG) and in the most severe part of Region VI (MAX).

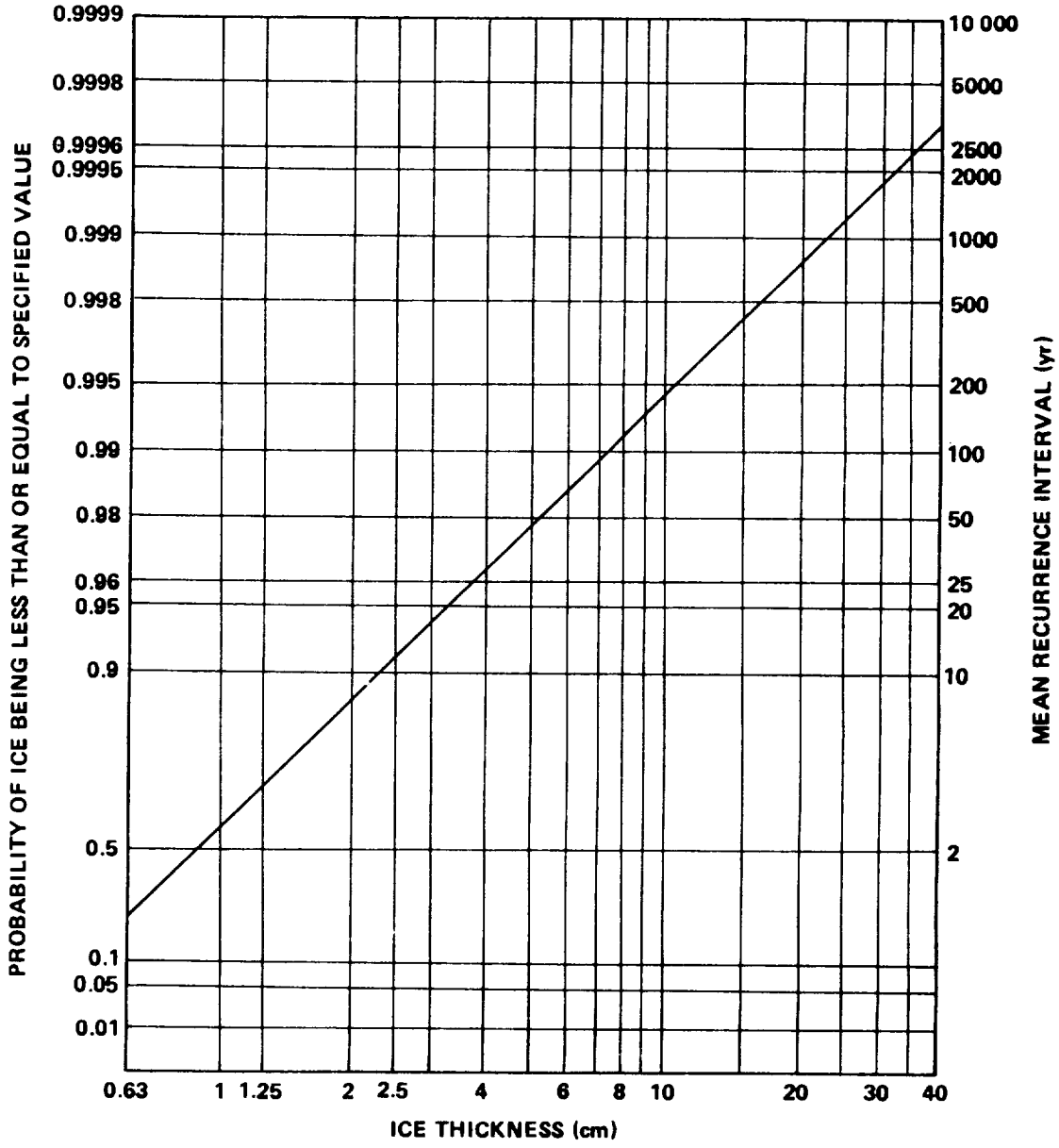

Figure 6.13b Fisher-Tippett Type II distribution for Region VI.

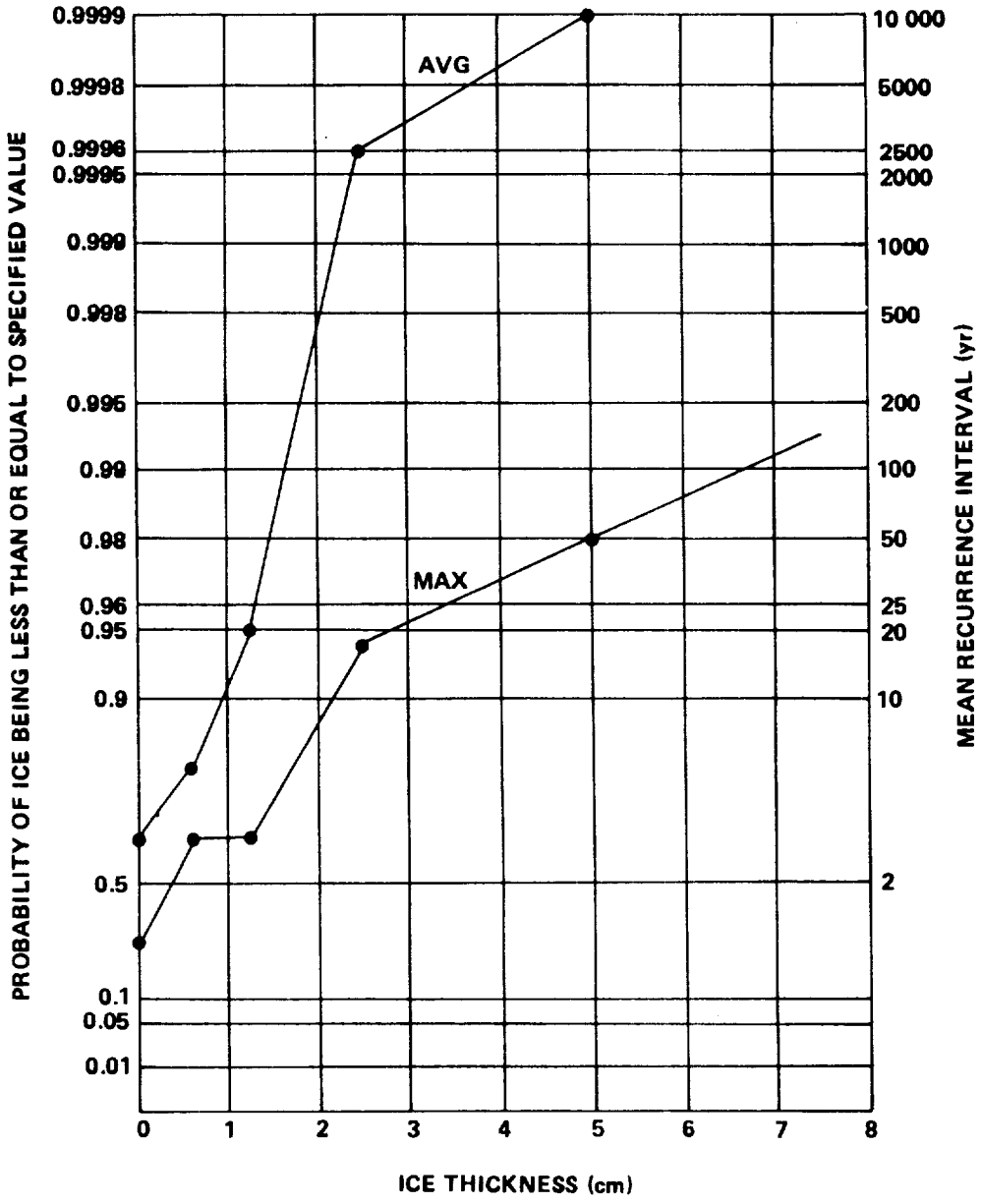

Figure 6.14a Estimated probability of ice thickness occurring at a representative point of Region VII (AVG) and in the most severe part of Region VII (MAX).

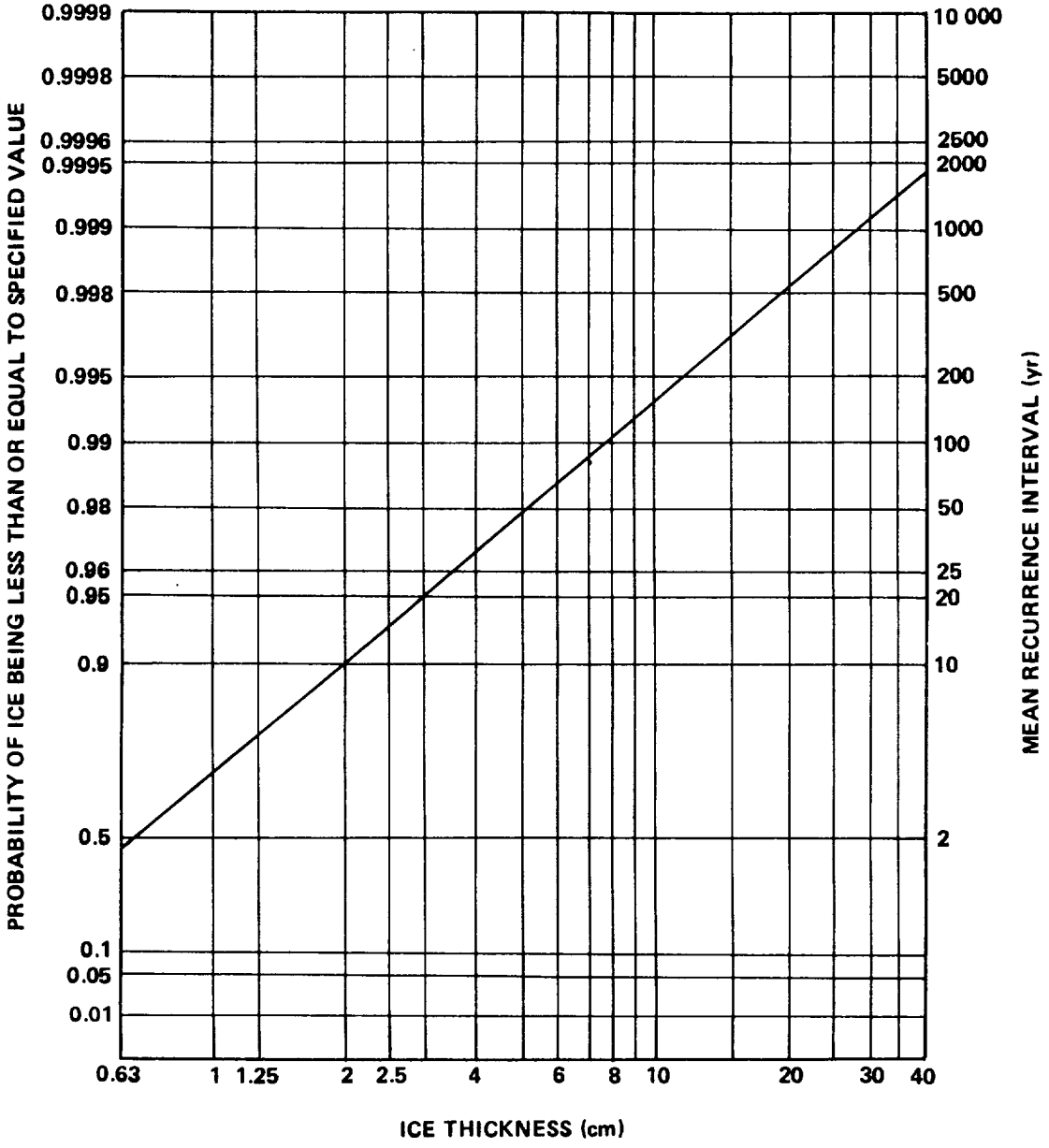

Figure 6.14b Fisher-Tippett Type II distribution for Region VII.

TABLE 6.6 NUMBER OF ICE STORMS ≥ 2.5 cm AND ≥ 5 cm IN 50 YEARS AND THE PROBABILITY OF AT LEAST ONE OCCURRENCE IN 1 YEAR IN THE MOST SEVERE STATE IN EACH REGION

Region	Number of Ice Storms ≥ 2.5 cm in 50 Years	Probability of an Ice Storm ≥ 2.5 cm in 1 Year	Number of Ice Storms ≥ 5 cm in 50 Years	Probability of an Ice Storm ≥ 5 cm in 1 Year
I	4	0.08	2	0.04
II	8	0.15	2	0.04
III	9	0.16	3	0.06
IV	4	0.08	2	0.04
V	2	0.04	1	0.02
VI	4	0.08	1	0.02
VII	3	0.06	1	0.02

The resulting curve gives the ice thickness that may be expected to occur at least once in the given recurrence interval in the region of the United States where the WTG is to be located. If the design engineer prefers to work with probabilities, the curve also provides the probability of ice equal to or less than the given value.

Example 6.1: Assume a WTG is to be located in Tulsa, Oklahoma. From Figure 6.7, we see Tulsa is located in Region VI. The extreme ice load probability for Region VI has been plotted in Figure 6.13b. This plot shows that an extreme ice thickness of 3.7 cm (1.46 in.) may be expected at least once in 25 years and of 10 cm (3.94 in.) at least once in 200 years. In terms of probabilities, the figure shows a 4-percent chance of exceeding 3.7 cm of ice thickness and a 0.5 percent chance of exceeding 10 cm (3.94 in.) of ice thickness.

TABLE 6.7 ICE THICKNESS, ESTIMATED TO THE NEAREST 0.1 cm, FOR DIFFERENT RETURN PERIODS AT A REPRESENTATIVE POINT (AVG) AND AT A POINT IN THE MOST SEVERE LOCATION (MAX) FOR EACH REGION

Region	Return Period (Years)											
	2		5		10		25		50		100	
	AVG	MAX	AVG	MAX	AVG	MAX	AVG	MAX	AVG	MAX	AVG	MAX
I	0.4	1.4	1.4	2.1	1.6	2.4	1.8	5.0	1.9	7.1	2.1	>7.5
II	0.7	1.0	1.4	2.1	1.7	3.3	2.0	5.0	2.2	6.0	2.4	7.0
III	1.2	1.6	1.6	2.4	1.8	3.8	2.0	5.8	2.1	7.2	2.3	>7.5
IV	0.5	1.4	1.4	2.1	1.6	2.4	1.8	5.0	1.9	7.2	2.1	>7.5
V	0.2	1.2	1.2	1.8	1.5	2.2	1.7	2.5	1.8	5.0	2.0	7.0
VI	0	1.0	1.2	1.9	1.5	2.4	1.7	3.8	1.9	5.0	2.1	6.0
VII	0	0.4	0.6	1.8	1.0	2.2	1.3	3.4	1.5	4.0	1.7	6.3

6.3.1.3.2 Risk of Exceeding Design Ice Loads During the Expected Life of the Structure

With a knowledge of the probable recurrence of the extreme ice thickness it is necessary to establish the percent risk of the design ice load being exceeded in the expected life of the structure. Figure 6.15 shows the risk of occurrence of ice loads of various mean recurrence intervals within the expected life of the project.

To use this figure:

1) Select the expected life of the structure under design.

2) Determine the acceptable risk that the ice might exceed the design value. For normal buildings, Reference 6.3 suggests that an acceptable risk for design purposes is a 63-percent chance that in 50 years (expected life period) the ice load will not exceed the 50-year (mean recurrence interval) ice load. When greater than normal safety or operational reliability is required, the acceptable risk should be lower.

3) From Figure 6.15 find the mean recurrence interval corresponding to the values of expected life and risk selected in 1) and 2).

4) From Figure 6.7 the region of the country in which the WTG is located is found.

5) From Figures 6.8b through 6.14b the basic design ice load corresponding to the mean recurrence interval is found for that region.

6) Correct the basic design ice load for elevation as described in Section 6.3.1.4.

> Example 6.2: An example of the procedure involved in steps 1) through 5) is as follows: A structure having a useful life of 25 years is to be designed for the Tulsa area. Since icing data are statistical in nature, it is not possible to categorically state that a given value of ice thickness will not be exceeded. The engineer is willing, however, to take a 10-percent chance that the structure may encounter icing conditions greater than those for which it is designed, and, therefore, it may fail structurally.

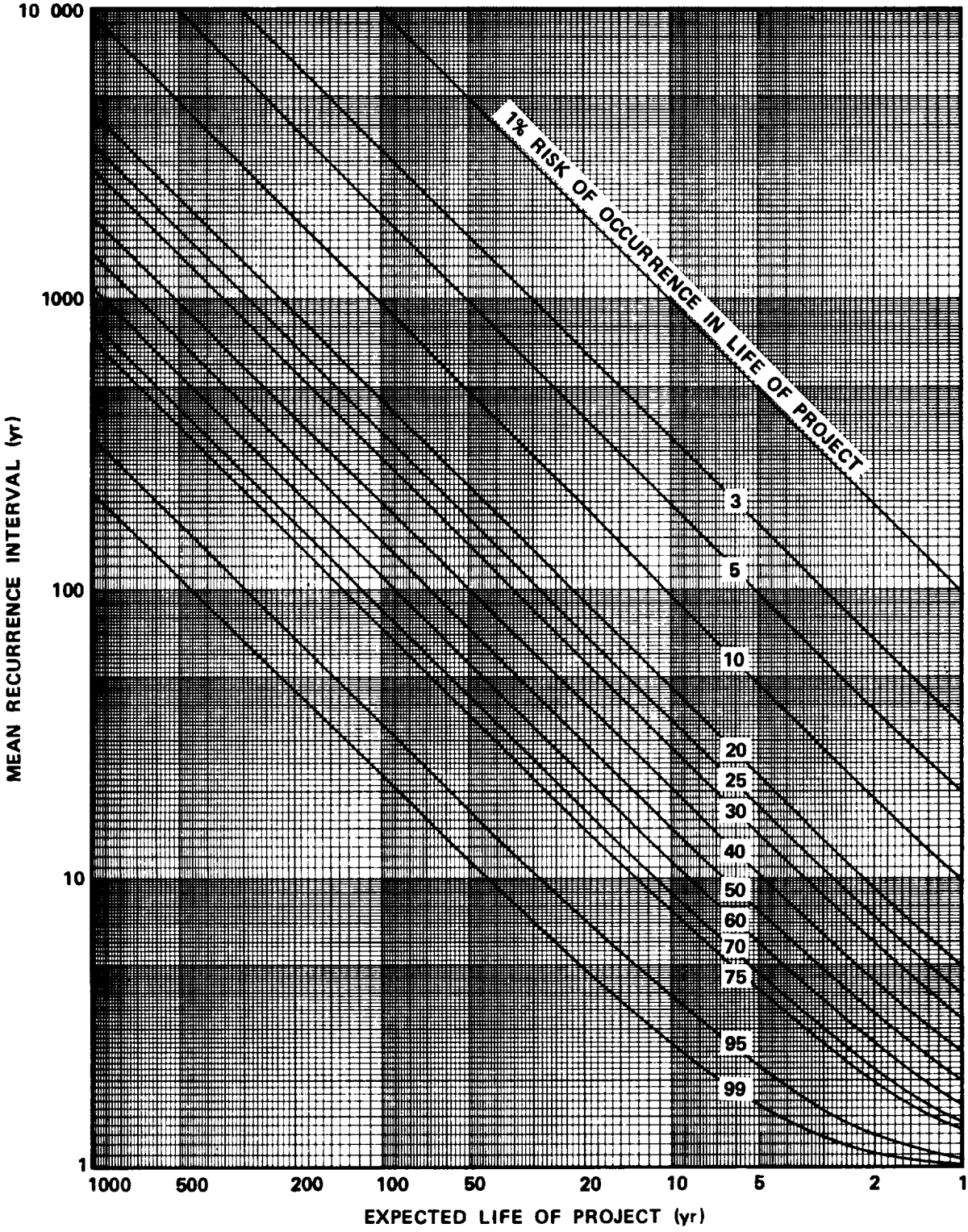

Figure 6.15 Risk of occurrence of ice thickness of various mean recurrence intervals within the expected life of the project.

From Figure 6.15 the mean recurrence interval for a 25-year expected life at a 10-percent risk of exceedance is 240 years. From Figure 6.7, Tulsa is found to be in Region VI, southwest. From Figure 6.13b, for Region VI, the design ice thickness is found to be 10 cm (3.94 in.).

6.3.1.4 Correction of Ice Loading for Elevation

Figure 6.2 [6.8], shows the relationship of ice thickness with elevation above sea level from which the design engineer may adjust the icing conditions determined in the previous section for elevation. The graph has been plotted for conditions occurring in the New England States, Region III. It is felt, however, that these values can be used to approximate values in the remainder of the country.

Example 6.3: An example application of Figure 6.2 is as follows. Assume the ice thickness for a WTG has been determined to be 10 cm (3.94 in.). However, the WTG is to be located upon a 100-m (328-ft) hill. Using Figure 6.2, the correction factor is found to be 1.5. Therefore, the corrected ice thickness is 15 cm (5.9 in.).

6.4 Snow Loading

The ability to be able to predict the amount of snow load a structure may experience is important to the design engineer. These loads are taken into account through a determination of their probability of exceedance. This is done by considering the cumulative frequency of the variable most closely related to the load. For snow load calculation, this variable is the maximum seasonal weight of the snow pack or the largest accumulated seasonal snow mantle. The weight of snow is measured by its water equivalent depth. By using the water equivalent variable, the snow density is automatically taken into account, which makes it unnecessary to determine some average value for this highly variable quantity. The figures used in this section to determine snow loads are based on water equivalent weights. (Water equivalent weight is the weight of water that would result from the melting of the snow pack or a snow sample).

6.4.1 Selection of Basic Design Snow Loading

Thom [6.9] has published isopleth maps of extreme snow load quantities for the 48 states, for quantile values of 0.50, 0.10, 0.04, 0.02, and 0.01 which

have corresponding mean recurrence intervals of 2, 10, 25, 50, and 100 years, respectively. These are given in Figures 6.16 through 6.20 and are based on U.S. Weather Bureau records.

6.4.1.1 Amount of Snow Loading for a Given Recurrence Interval

The basic design snow load is determined as follows:

1) The WTG site is found on the maps in Figures 6.16 through 6.20.

2) The value for the snow loads are read from the isopleth for each mean recurrence interval.

3) These values are then plotted on extreme value probability plotting paper, Fisher-Tippett Type II distribution (Fig. 6.21).

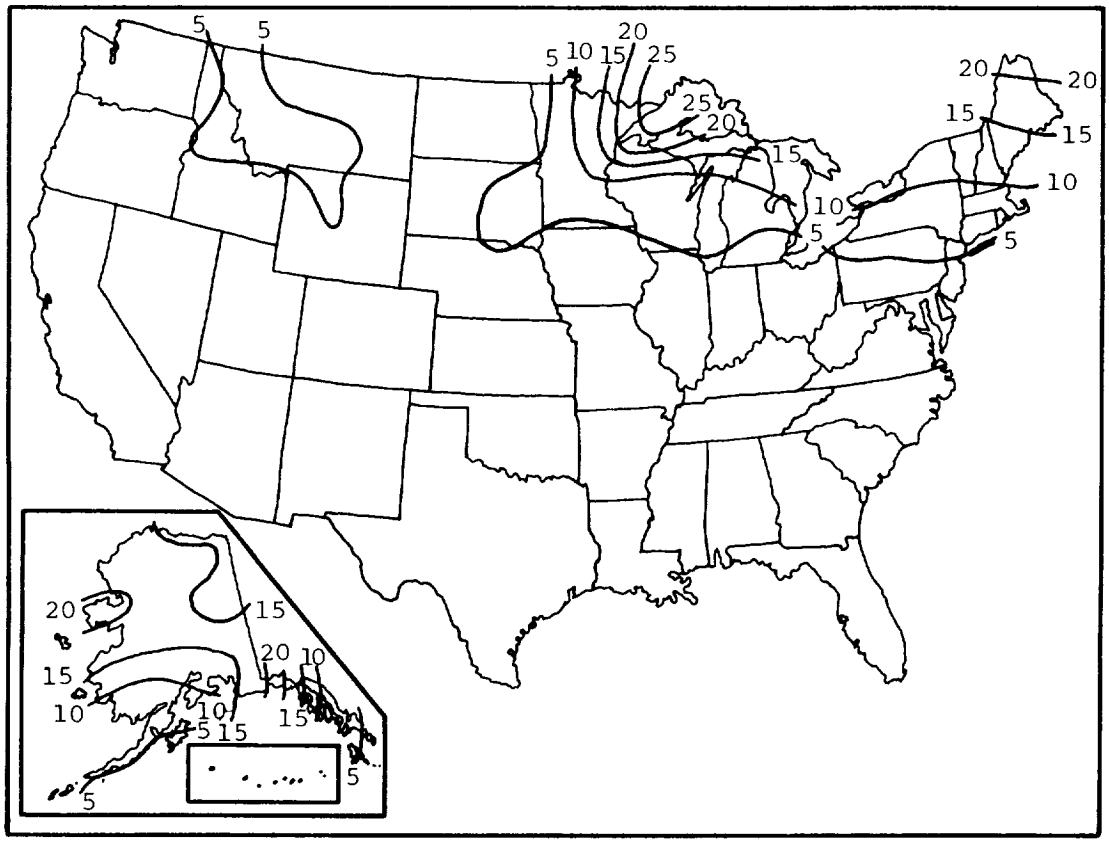

Figure 6.16 Snow load in lb ft^{-2} on the ground, 0.50 quantile, 2-year mean recurrence interval [6.9].

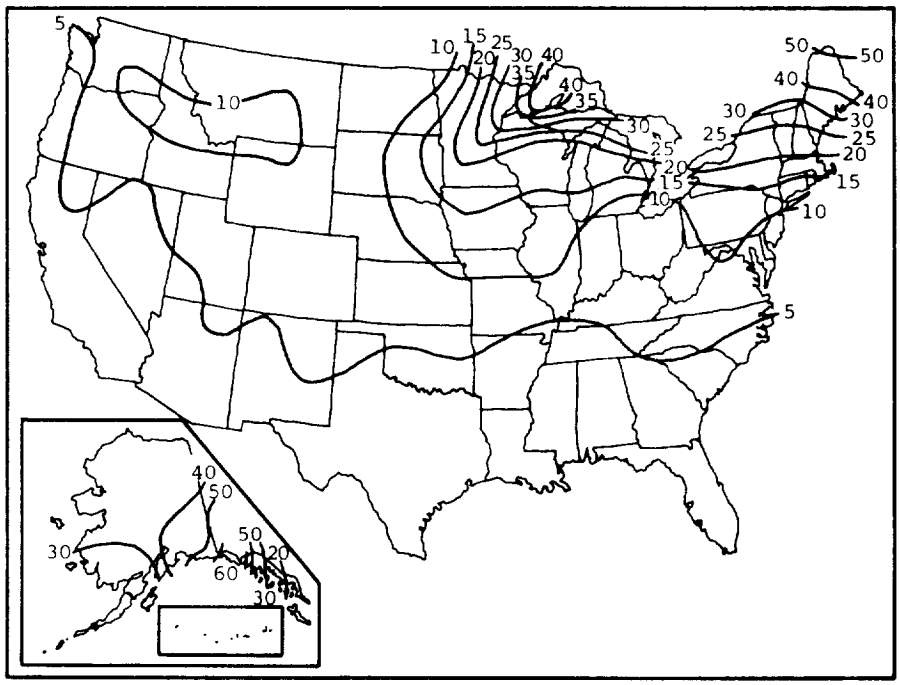

Figure 6.17 Snow load in lb ft^{-2} on the ground, 0.10 quantile, 10-year mean recurrence interval [6.9].

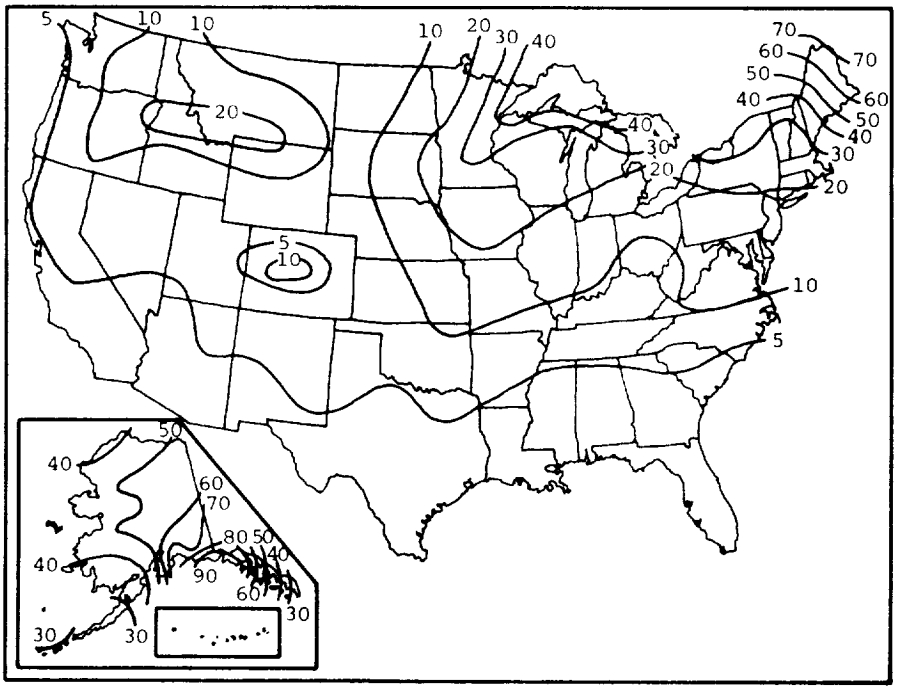

Figure 6.18 Snow load in lb ft^{-2} on the ground, 0.04 quantile, 25-year mean recurrence interval [6.9].

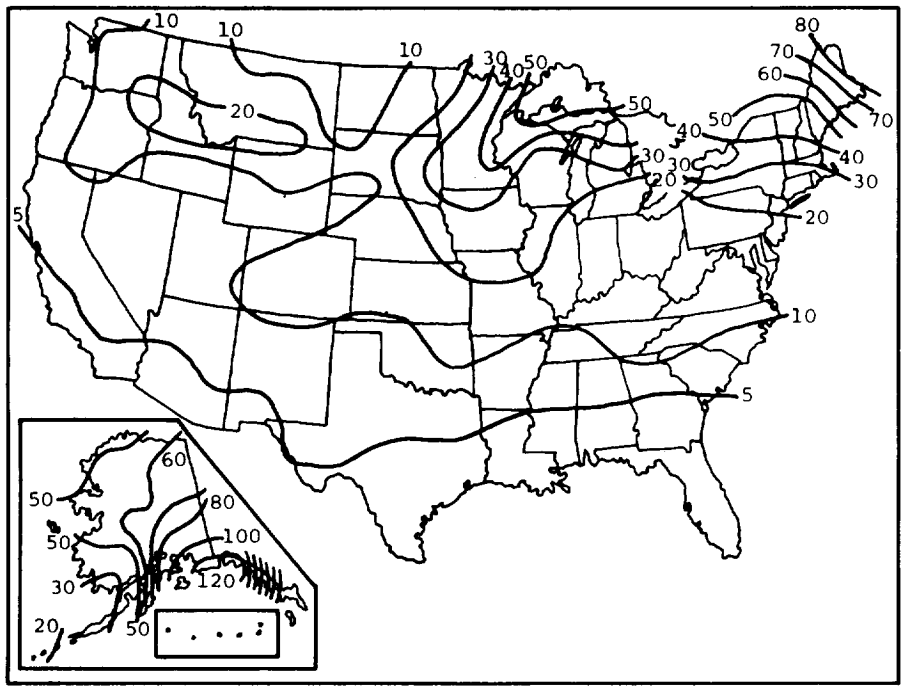

Figure 6.19 Snow load in lb ft^{-2} on the ground, 0.02 quantile, 50-year mean recurrence interval [6.9].

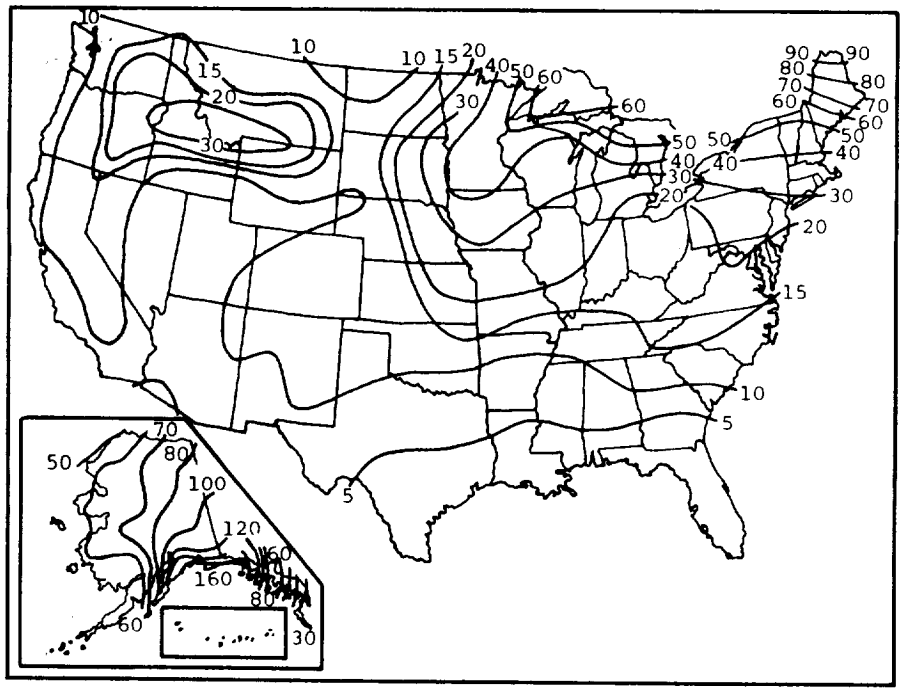

Figure 6.20 Snow load in lb ft^{-2} on the ground, 0.01 quantile, 100-year mean recurrence interval [6.9].

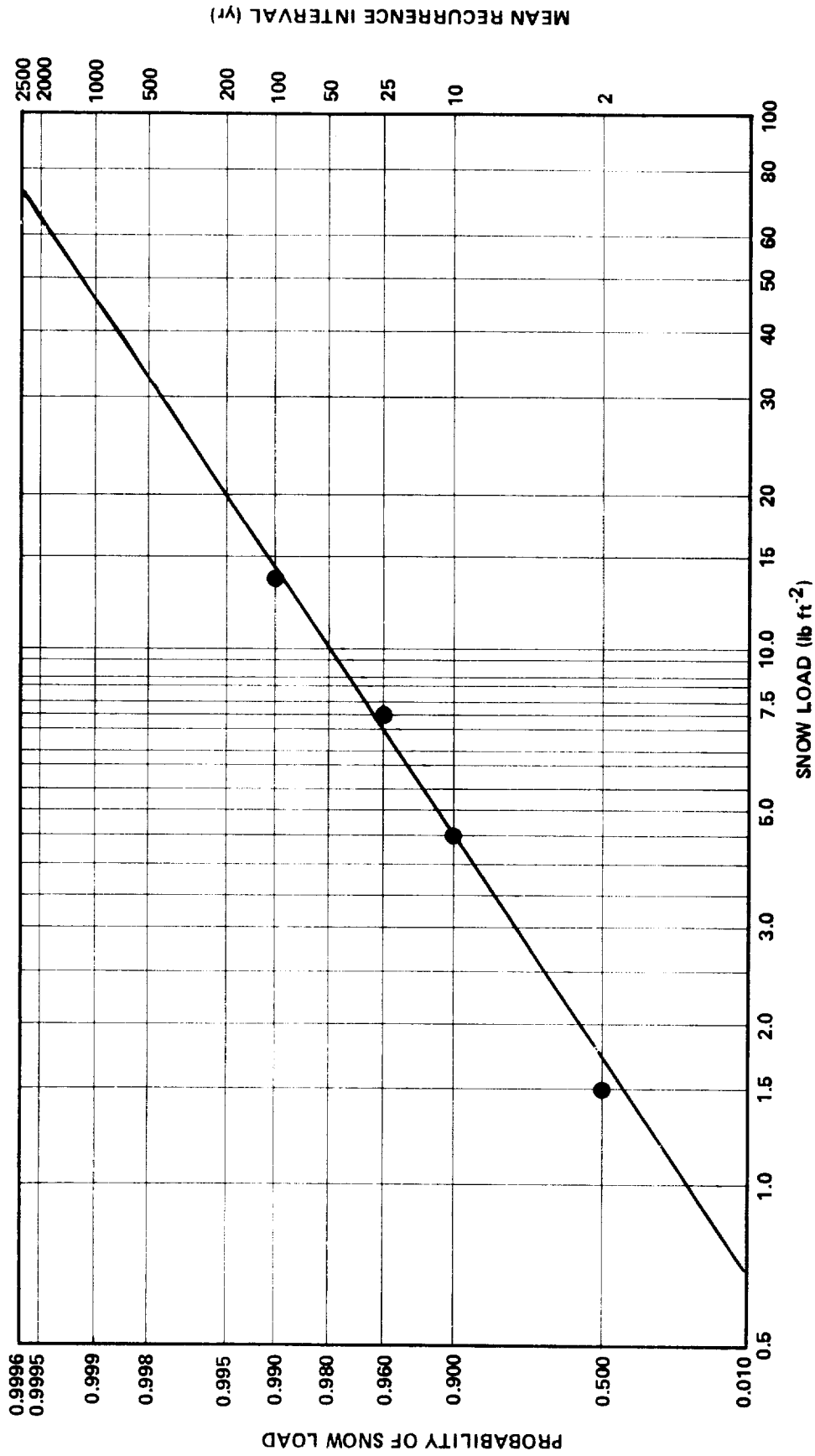

Figure 6.21 Fisher-Tippett Type II distribution for Nashville, Tennessee.

4) A straight line is then drawn through the plotted values. The resulting curve gives the snow load that may be expected to occur at least once in the given recurrence interval for the region of the United States where the data points were taken. If the design engineer prefers to work with probabilities, the curve is also given in the probability of occurrence of the given snow load.

Example 6.4: The extreme value snow load probability for the city of Nashville has been plotted in Figure 6.21. This curve shows that a snow load of 3.8 gm cm^{-2} (8 lb ft^{-2}) may be expected at least once in 25 years and of 21.0 gm cm^{-2} (44 lb ft^{-2}) at least once in 1000 years.

6.4.2 Risk of Exceeding the Design Snow Load During the Expected Life of the Structure

It is now necessary to establish the percent risk that the design snow load will be exceeded during the expected life of the structure. Figure 6.22 shows the risk of occurrence of snow loads of various mean recurrence intervals within the expected life of the structure.

To this figure:

1) Select the expected life of the structure under design.

2) Determine the risk you are willing to accept that the design snow load will be exceeded during the structure's expected life.

3) From Figure 6.22, find the mean recurrence interval corresponding to the values of expected life and percent risk selected in 1) and 2).

4) From figures constructed similarly to Figure 6.21 find the basic design snow load corresponding to the mean recurrence interval.

Example 6.5: The procedure involved in steps 1) through 4) is as follows: A structure having a useful life of 30 years is to be designed for the Nashville area. The engineer is willing to take a 10-percent chance that the structure may be damaged by snow loads greater than those for which he has designed.

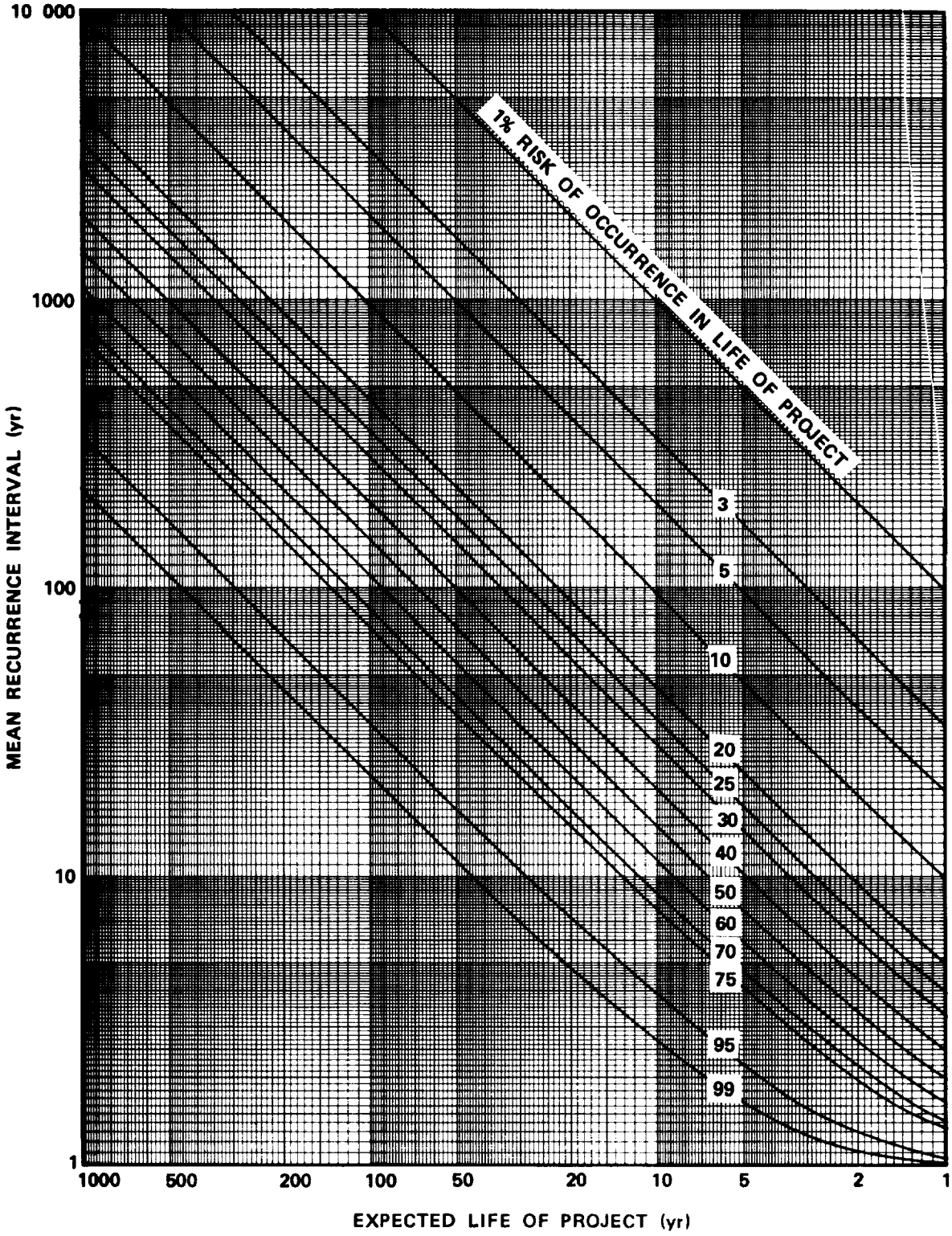

Figure 6.22 Risk of occurrence of snow loads of various mean recurrence intervals within the expected life of the project.

From Figure 6.22 the mean recurrence interval for a 30-year expected life at a 10-percent risk of exceedance is 290 years. From Figure 6.21, the basic design snow load is found to be 12 gm cm^{-2} (25 lb ft^{-2}).

6.4.3 Extreme 24-h Snowfalls

Of the 49 states where snowfall data were recorded (Hawaii was excluded), 23 had snowfalls of 30 in. or more in 24 h (Table 6.8 [6.10]). Of these 23 states where intense snowfalls have occurred, seven were found to have had at least five occurrences from 1951 to 1971 (Table 6.9). From the data in Table 6.9, it can be seen that there are certain areas of intense snowfall in the United States.

6.4.3.1 Areas of Intense Snowfall in the United States

The largest area of intense snowfall in the United States extends approximately 960 km (600 miles) north-south and 480 km (300 miles) east-west in California and Oregon. It includes 18 stations with intense snowfall conditions, which extend southeast to northwest through the San Bernardino, Sierra Nevada, and Cascades mountain ranges. Station elevations range from 814 to 3741 m (2670 to 12 274 ft).

In Washington, the area of intense snowfall covers approximately 112 km (70 miles) north-south and 25 miles east-west, at elevations ranging from 667 to 1665 m (2188 to 5463 ft). One station in this area, the Rainier Paradise Ranger Station, holds the North American record for a snowfall during a season, with 2850 cm (1122 in.) from July 1971 through June 1972.

The Alaskan area is located to the north of the Gulf of Alaska and covers an area approximately 320 km (200 miles) north-south and 224 km (140 miles) east-west. Elevations range from 4.5 to 810 m (15 to 2658 ft). In this area, Thompson Pass reported 32 snowfalls of 76 cm (30 in.) or more in 24 h in the 20 years of the study.

In the Colorado area, Wolf Creek Pass, at 2828 m (9278 ft) and Silver Lake at 3066 m (10 060 ft) are the stations which reported the most intense snowfalls. Silver Lake holds the United States record for a 24-h snowfall, with 192.5 cm (75.8 in.) recorded.

TABLE 6.8 MAXIMUM SNOWFALLS FOR STATES THAT HAVE REPORTED AT LEAST 30 in. IN 24 h [6.10]

State	24 h			Single Storm		
	Snowfall (in.)	Station	Date	Snowfall (in.)	Station	Date
Alaska	62.0	Thompson Pass	29 Dec 55	175.4	Thompson Pass	26-31 Dec 55
Arizona	38.0	Heber R. S.	14 Dec 67	67.0	Heber R. S.	13-16 Dec 67
California	60.0	Giant Forest	18-19 Jan 33	189.0	Mt. Shasta Ski Bowl	13-19 Feb 59[a]
Colorado	75.8	Silver Lake	14-15 Apr 21	141.0	Ruby	23-30 Mar 99
Idaho	38.0	Sun Valley	11 Feb 59[b]	60.0	Roland W. Portal	25-27 Dec 37
Illinois	36.0	Astoria	27-28 Feb 00	37.8	Astoria	27-28 Feb 00
Maine	35.0	Middle Dam	23 Nov 43	56.0	Long Falls Dam	24-28 Feb 69
Maryland	31.0	Clear Spring	29 Mar 42	36.0	Edgemont	29-30 Mar 42
Montana	30.0	Summit	29 Oct 51	46.0	Summit	31 Mar-3 Apr 54
New Hampshire	56.0	Randolph	22-23 Nov 43	77.0	Pinkham Notch	24-28 Feb 69
New Mexico	30.0	Sandia Crest	29 Dec 58	40.0	Corona	14-16 Dec 59
New York	45.0	Watertown	14-15 Nov 00	69.0	Watertown	18-22 Jan 40
North Carolina	31.0	Nashville	2 Mar 27	31.0	Nashville	2 Mar 27
Oregon	37.0	Crater Lake	17 Jan 51 and (27 Jan 37)[a]	95.0	Crater Lake	15-19 Jan 51
Pennsylvania	38.0	Morgantown	20 Mar 58	50.0	Morgantown	19-21 Mar 58
Rhode Island	34.0	Foster	8-9 Feb 45	34.0	Foster	8-9 Feb 45
South Dakota	38.0	Dumont	27 Mar 50	60.0	Dumont	26-28 Mar 50
Utah	35.0	Kanush	9 Feb 53	64.0	Alta	2-7 Dec 51
Vermont	33.0	St. Johnsbury	25 Feb 69	50.0	Readsboro	2-6 Mar 47
Virginia	33.0	Big Meadows	6 Mar 62	42.0	Big Meadows	6-7 Mar 62
Washington	52.0	Winthrop	21 Jan 35	129.0	Laconia	24-26 Feb 10
West Virginia	34.0	Bayard	27-28 Apr 28	57.0	Pickens	23-30 Nov 50
Wyoming	34.0	Bechler River	28 Jan 33	52.0	Bechler River	15-19 Jan 37

Adapted from: D. M. Ludlum, Weather Record Book, United States and Canada, Princeton, N. J., Weatherwise, 1971.

a. R. J. Schmidli, Compiler, Weather Extremes, Salt Lake City, Utah, U.S. Environmental Science Services Administration, Weather Bureau, Dec. 1968. (Weather Bureau Tech Memo WR-28 and Western Region Tech Memo No. 28).

b. Climatological Data, Idaho, Feb. 1959, Asheville, N. C., U.S. Weather Bureau.

TABLE 6.9 SNOWFALLS OF 30 in. OR MORE IN 24 h BY STATIONS FOR THE SEVEN STATES WITH THE MOST FREQUENT OCCURRENCES: 1951 THROUGH 1970[a] [6.10]

State	Station	30 in. < 40 in.		40 in. and Over	
Alaska	1. Cape Hinchinbrook	33.6	Dec 55		
	2. Cordova WB Airport	30.0	Dec 55		
	3. Girdwood			44.0	Dec 59
	4. Mile 47 Camp	30.0	Feb 64	50.0	Mar 62
	5. Moose Pass	31.0	Mar 71		
	6. Seldovia Dock	36.0	Mar 71		
	7. Tanacross	36.0	Dec 55		
	8. Thompson Pass	38.5	Dec 54	62.0	Dec 55
		38.4	Jan 53	58.6	Dec 55
		38.3	Mar 60	49.3	Feb 53
		38.0	Dec 60	48.0	Dec 67
		38.0	Feb 68	46.0	Oct 56
		37.0	Feb 68	44.0	Feb 57
		35.8	Mar 54	42.5	Mar 62
		35.0	Jan 58	42.4	Jan 58
		34.8	Nov 58	42.0	Apr 59
		32.5	Jan 60	42.0	Feb 64
		31.6	Feb 53	41.3	Feb 60
		31.3	Nov 52	40.0	Feb 64
		31.2	Nov 52	40.0	Oct 65
		31.0	Jan 60		
		30.0	Feb 60		

a. Period covered was Jan 51 through Dec 70 for all states except Alaska, for which Jan through Apr 71 data were substituted for unavailable Jan through Apr 51 data.

TABLE 6.9 (Continued)

State	Station	30 in. < 40 in.		40 in. and Over	
Alaska (cont'd)		30.0	Feb 64		
		30.0	Feb 64		
		30.0	Feb 64		
		30.0	Nov 69		
	9. Trims Camp	39.7	Dec 55	43.0	Feb 56
		36.0	Jan 62		
		36.0	Dec 59		
		33.0	Mar 60		
	10. Valdez	35.0	Oct 56		
		30.0	Dec 55		
	11. Whittier			42.0	Dec 60
	12. Yakutat WB Airport	30.0	Mar 60		
California	1. Big Bear Lake Dam	30.5	Apr 67		
	2. Blue Canyon WB Airport	34.5	Jan 52		
		33.7	Apr 55		
		33.0	Feb 59		
		30.0	Mar 52		
	3. Bridgeport	36.0	Feb 69		
	4. Canyon Dam	32.0	Feb 59		
	5. Chester			48.0	Jan 68
	6. De Sabla			45.0	Jan 68
	7. Grant Grove	37.0	Mar 52		
		36.0	Feb 69		

TABLE 6.9 (Continued)

State	Station	30 in. < 40 in.		40 in. and Over	
California (cont'd)		34.0	Feb 59		
		33.0	Mar 52		
	8. Huntington Lake	37.0	Mar 52	42.0	Feb 69
		31.0	Apr 58		
	9. McCloud	33.0	Jan 55		
	10. Manzanita Lake			41.0	Nov 60
	11. Mount Baldy Notch	36.0	Apr 65		
		30.0	Apr 67		
	12. Mount Shasta WB City	37.4	Dec 52		
		30.9	Jan 66		
	13. Mount Shasta Ski Bowl	38.0	Dec 60	54.0	Feb 59
		38.0	Jan 64	49.0	Feb 59
		36.0	Jan 64	48.0	Jan 64
		33.0	Dec 60	44.0	Jan 61
		32.0	Feb 59		
	14. Quincy	34.0	Jan 68		
	15. Sierra City	33.0	Mar 62		
		30.0	Jan 55		
	16. Sierraville Range Sta.	35.1	Jan 52		
	17. Soda Springs	33.9	Mar 62		
		33.0	Jan 54	40.6	Jan 64
		33.0	Jan 68		
		31.0	Mar 58		
		31.0	Jan 69		

TABLE 6.9 (Continued)

State	Station	30 in. < 40 in.		40 in. and Over	
California (cont'd)		30.0	Jan 52		
		30.0	Dec 55		
	18. Snow Laboratory Central Sierra	39.1	Feb 59		
	19. Squaw Valley	38.0	Dec 55	49.0	Apr 58
		33.0	Jan 67	44.0	Feb 59
	20. Squirrel Inn 2	30.0	Mar 52		
	21. Strawberry Valley	39.0	Jan 68		
		36.0	Jan 52		
		30.0	Feb 55		
	22. Table Mountain	30.0	Mar 52		
	23. Tahoe	32.0	Jan 52	42.0	Jan 52
		30.0	Jan 67	42.0	Apr 58
		30.0	Mar 67		
		30.0	Dec 70		
	24. Twin Lakes	38.0	Feb 62	49.0	Mar 62
		37.0	Dec 64		
		37.0	Jan 64		
		34.0	Feb 62		
		34.0	Nov 64		
		33.0	Dec 64		
		33.0	Dec 55		
		32.5	Mar 63		
		32.0	Jan 64		

TABLE 6.9 (Continued)

State	Station	30 in. < 40 in.		40 in. and Over	
California (cont'd)		31.0	Feb 62		
		30.0	Mar 62		
	25. Westwood	30.0	Nov 51		
		32.0	Jan 54		
	26. White Mountain 1	38.0	Dec 66		
		34.0	Jan 69		
	27. White Mountain 2	38.0	Apr 56	44.0	Dec 66
		32.0	Dec 66		
		30.0	Jan 67		
Colorado	1. Idaho Springs	34.0	Apr 57		
	2. Pagosa Springs	30.0	Dec 67		
	3. Salida	38.0	Oct 61		
	4. Wolf Creek Pass 4W	35.0	Dec 59	48.0	Jan 56
		32.0	Jan 65	42.0	Jan 56
		31.0	Dec 68		
		30.0	Mar 52		
		30.0	Dec 55		
		30.0	Jan 63		
New Hampshire	1. Cannon Mountain	30.3	Feb 69		
	2. Lebanon CAA Airport	30.0	Feb 58		
	3. Mount Washington	37.5	Dec 68	49.3	Feb 69
	4. Pinkham Notch	33.5	Feb 52		
		30.0	Feb 69		

TABLE 6.9 (Continued)

State	Station	30 in. < 40 in.		40 in. and Over	
New Hampshire (cont'd)	5. Woodstock	36.0	Feb 69		
New York	1. Bennetts Bridge	30.0	Jan 59		
	2. Derby	32.0	Nov 51		
	3. Oswego Teachers College			40.0	Dec 58
	4. Speculator	32.0	Nov 67		
	5. Watertown	34.0	Dec 51		
Oregon	1. Crater Lake National Park	37.0	Jan 51		
	Service Headquarters	31.5	Oct 56		
		31.0	Jan 54		
		31.0	Jan 64		
	2. Odell Lake Land Pan	30.0	Nov 58		
	3. Sexton Summit WB	34.1	Jan 69		
		32.5	Dec 65		
	4. Timberlane Lodge	32.0	Jan 51		
Washington	1. Cushman Dam	36.0	Jan 54		
	2. Holden	33.0	Jan 54		
	3. Lake Wenatchee	33.0	Jan 67		
	4. Rainier Ohanapecosh	32.0	Dec 68		
	5. Rainier Paradise Ranger Station	34.0	Nov 58		

TABLE 6.9 (Concluded)

State	Station	30 in. < 40 in.	40 in. and Over
Washington (cont'd)	6. Scenic	32.0 Dec 68 30.0 Feb 55 38.0 Mar 55 36.0 Dec 61	
	7. Snoqualmie Pass	34.0 Jan 54 36.0 Jan 69 33.0 Nov 58 32.0 Jan 64 31.0 Jan 54	44.0 Jan 65
	8. Stevens Pass	31.0 Dec 61 36.0 Jan 64 34.0 Jan 69 31.0 Jan 66	45.0 Jan 65

In the eastern United States, a point of intense 24-h snowfall occurs in the White Mountains of New Hampshire. Another point of extreme snowfall is in New York at Oswego Teachers College at 90 m (295 ft) in elevation on the east shore of Lake Ontario.

Snow load quantities for a WTG which is to be located in one of these areas should be determined by taking the maximum snowfall for the area (Table 6.9) and multiplying it by the density of a heavy snow, i.e., between 0.10 g cm^{-3} (6.24 lb ft^{-3}) and 0.15 g cm^{-3} (9.36 lb ft^{-3}). After this load has been determined, it can be compared to the load evaluated by the method described in Section 6.4.1.1. The engineer may then select the higher value, or a value in the interval between the two computed values, for design loads.

6.5 Application of Snow Loading to Structures

In the previous section, the design snow load pertains to snow loads on the ground since loads on the structure can be highly variable. Little information is available on the conversion of ground loads to structural values, but that which is available is presented in the following paragraph.

The conversion of snow loads from ground to roof consists of two factors: (a) the effect of the elevation of the roof above ground level and (b) the effect of the slope of the roof. (Here a roof is to mean any flat or sloping surface on which a snow load may occur.)

Observations made in Canada led to the recommendation that the snow load on roofs of heated structures be reduced to 80 percent of the load on the ground. Observations in the United States led to slightly different conclusions. For snow loads on roofs of heated structures of 9.6 gm cm^{-2} (20 lb ft^{-2}) or less, apply the ground load. For loads under the same conditions greater than 9.6 gm cm^{-2}, add 0.75 of the ground load exceeding 9.6 gm cm^{-2} to 9.6 gm cm^{-2} to obtain the structure load. For unheated roofs apply the ground load directly.

The effect of roof slope in reducing snow loads seems to be well agreed upon. The Canadian practice is given as follows:

Roof Slope Degrees	Reduction Factor
31-40	0.80
41-50	0.60
51-60	0.40
61-70	0.20
>70	0

This is consistent with the British practice. The rule recommended for use in the United States is as follows. The value of the snow load per square foot of horizontal projection is constant up to 25 deg, is reduced by 2 percent per degree of inclination above 25 deg until, on a slope of 75 deg, there remains no load [6.11].

Although these data pertain to the roofs of buildings, they can be applied to snow loads on WTG nacelles and support structures.

6.6 Drifting as Applying to Snow Loads

Drifting is the most uncertain factor in the determination of snow loads. Any projection above the general surface level will cause drifts to form which are believed to have caused many of the structural failures experienced. The engineer should, therefore, double the snow load over areas extending over distances of three times the projection height along a projection as given in Reference 6.11.

REFERENCES

6.1 Tattelman, Paul and Gringorten, I. I.: Estimated Glaze Ice at the Earth's Surface for the Contiguous United States. Air Force Cambridge Research Laboratories, 1973.

6.2 Kaufman, J. W. (editor): Terrestrial Environment (Climatic) Criteria Guidelines for Use in Aerospace Vehicle Development. NASA TM X-78118, November 1977.

6.3 Code of Basic Data for the Design of Buildings. British Standards Institution. Chapter 5, Part 2, 1972.

6.4 Putnam, P. C.: Power From the Wind. Van Nostrand Reinhold, 1948.

6.5 Bowden, D. T., et al.: Engineering Summary of Airframe Icing Data. Federal Aviation Technical Report, FAA ADS-4, 1963.

6.6 Bennett, I.: Glaze, Its Meteorology and Climatology, Geographical Distribution and Economic Effects. Tech. Report EP-105 Quartermaster Research and Engineering Center, 1959.

6.7 Gringorten, I. I.: Stochastic Modelling of the Areal Extent of Weather Conditions. AFCRL, 1973.

6.8 Ackley, S. F. and Itagahi, K.: Distribution of Icing in the North-East's Ice Storm of 26-27 December 1969. Weatherwise, 23, 1970.

6.9 Thom, H. C. S.: Distributions of extreme snow load in the United States. National Oceanic and Atmospheric Administration.

6.10 Riordan, Pauline: Extreme 24-Hour Snowfalls in the United States: Accumulation, Distribution and Frequency. Report No. 6 of Studies of the Army Aviation V/STOL Environment, January 1973.

6.11 National Climatic Data Center, National Oceanic and Atmospheric Administration Report.

CHAPTER 7. OTHER CLIMATOLOGICAL FACTORS

This chapter provides working data for climatological factors other than wind, ice, and snow which may influence the design of a WTG. These are rain, hail, thermal effects, abrasive materials, and humidity. Each of these topics is discussed in a self-contained section. That is, Section 7.1, Rain; Section 7.2, Hail; Section 7.3, Thermal Effects; Section 7.4, Abrasive Materials; and Section 7.5, Humidity.

7.1 Rain

7.1.1 Summary of Rainfall Design Values

Section 7.1.1.1 contains design values of extreme rainfall and duration for a general purpose WTG; whereas, Section 7.1.2 describes the selection of these values from the detailed computational procedures and working data contained in Section 7.1.3.

7.1.1.1 Recommended General Purpose Design Values

Two sets of design values of extreme rainfall, R_e, are as follows:

1) R_e = 11.94 cm (4.7 in.) for a rainfall of 30-min duration
   R_e = 14.22 cm (5.6 in.) for a rainfall of 1-h duration
   R_e = 30.48 cm (12.0 in.) for a rainfall of 6-h duration
   R_e = 40.64 cm (16.0 in.) for a rainfall of 24-h duration

2) R_e = 9.65 cm (3.8 in.) for a rainfall of 30-min duration
   R_e = 11.94 cm (4.7 in.) for a rainfall of 1-h duration
   R_e = 22.86 cm (9.0 in.) for a rainfall of 6-h duration
   R_e = 35.56 cm (14.0 in.) for a rainfall of 24-h duration.

The higher set of values is computed on the basis of aerospace design philosophy which specifies a 10-percent risk of exceedance during the expected life of the structure (in this case assumed to be 25 years). The lower value is computed on the basis of building code design philosophy which specifies a

63-percent risk of exceedance during an expected 50-year life of the proposed structure. Details of the procedure for computing these values are given in Section 7.1.2.

Figures 7.1 and 7.2 provide plots of extreme rainfall for various intervals of duration versus risk of exceedance for a 25-year and a 50-year expected life. It is anticipated that the WTG design engineer will wish to select his own degree of risk which presumably will be somewhere between aerospace design procedures and standard building code practices.

7.1.2 Description of Recommended Design Values

The development of the specific design values given in the preceding sections, from information contained in Section 7.1.3 of this report, is described as follows.

7.1.2.1 Extreme Rainfall

The average annual rainfall for the United States is shown in Figure 7.3. The most extreme rainfall, which has been recorded on isopleth maps of the United States (Figs. 7.4 through 7.15), occurs on the Gulf Coast areas of Louisiana, Mississippi, Alabama, and the Florida Panhandle. These locations were, therefore, selected to represent the highest rainfall region in which a general service WTG is likely to be sited. A Fisher-Tippett probability distribution of the extreme rainfall for this region is shown in Figure 7.16. This figure gives the expected mean recurrence interval, T_R, of the extreme rainfall amounts for various durations of storms. The recurrence interval at which the extreme value is to be selected for design is determined by application of Figure 7.17. This figure gives the recurrence interval associated with a given lifetime of the structure, N, for a prescribed risk of exceedance, R. Since rainfall is a statistical quantity, the engineer must accept some risk that his design rainfall amount may be exceeded at least once in the expected useful life of the structure.

Two design philosophies for selecting the basic design value of extreme rainfall amounts were considered. Both sets of values are quoted to establish an order of magnitude estimate of extreme rainfall amounts for the design engineer. One philosophy is based on aerospace vehicle design principles [7.1] which recommend a 10-percent risk of exceedance for any expected life period to be used in determining the extreme rainfall. An alternate design philosophy was taken from the building code standards [7.2] which accepts a 63-percent risk for an expected life of 50 years.

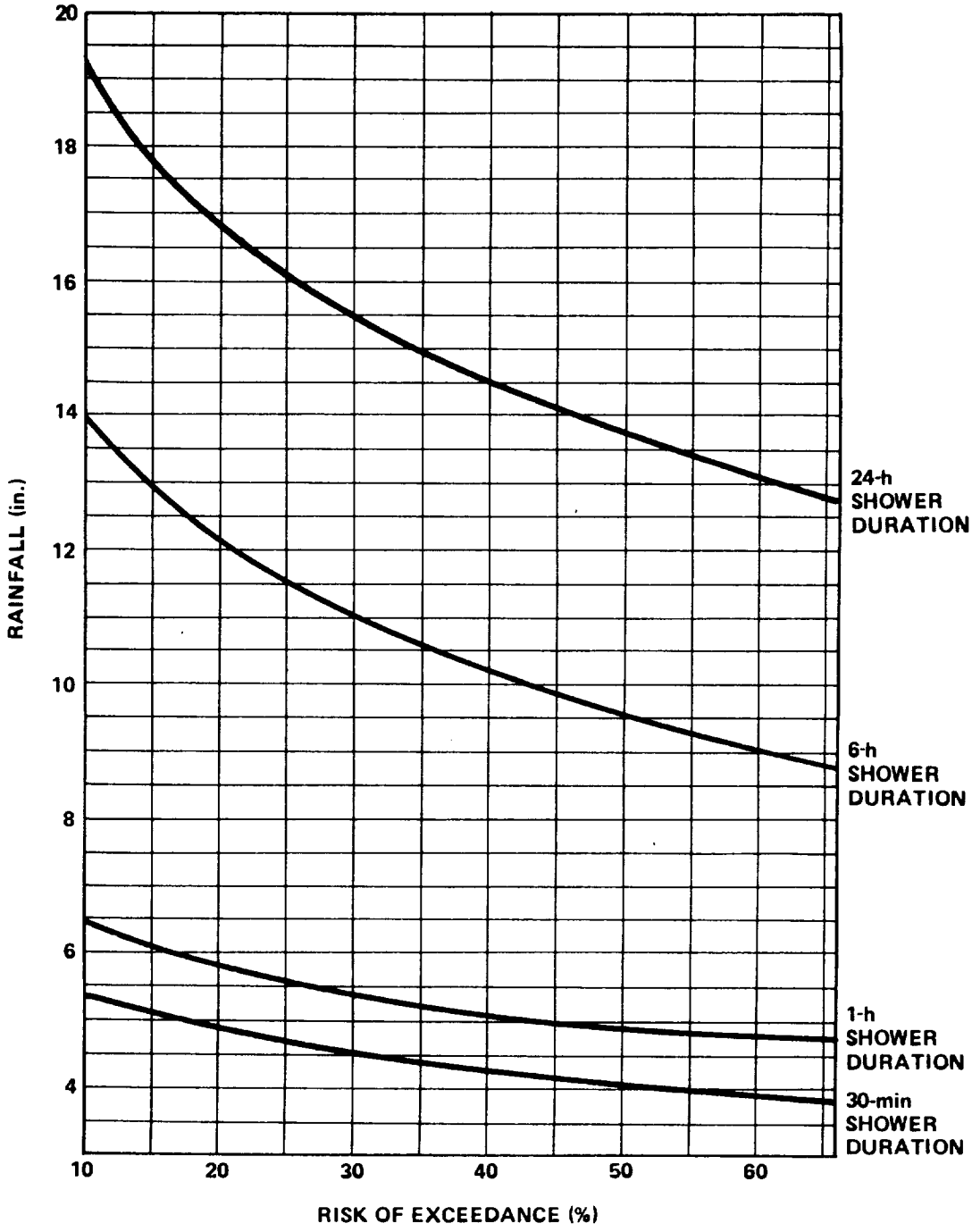

Figure 7.1 Risk of exceeding rainfall, 50-year recurrence interval.

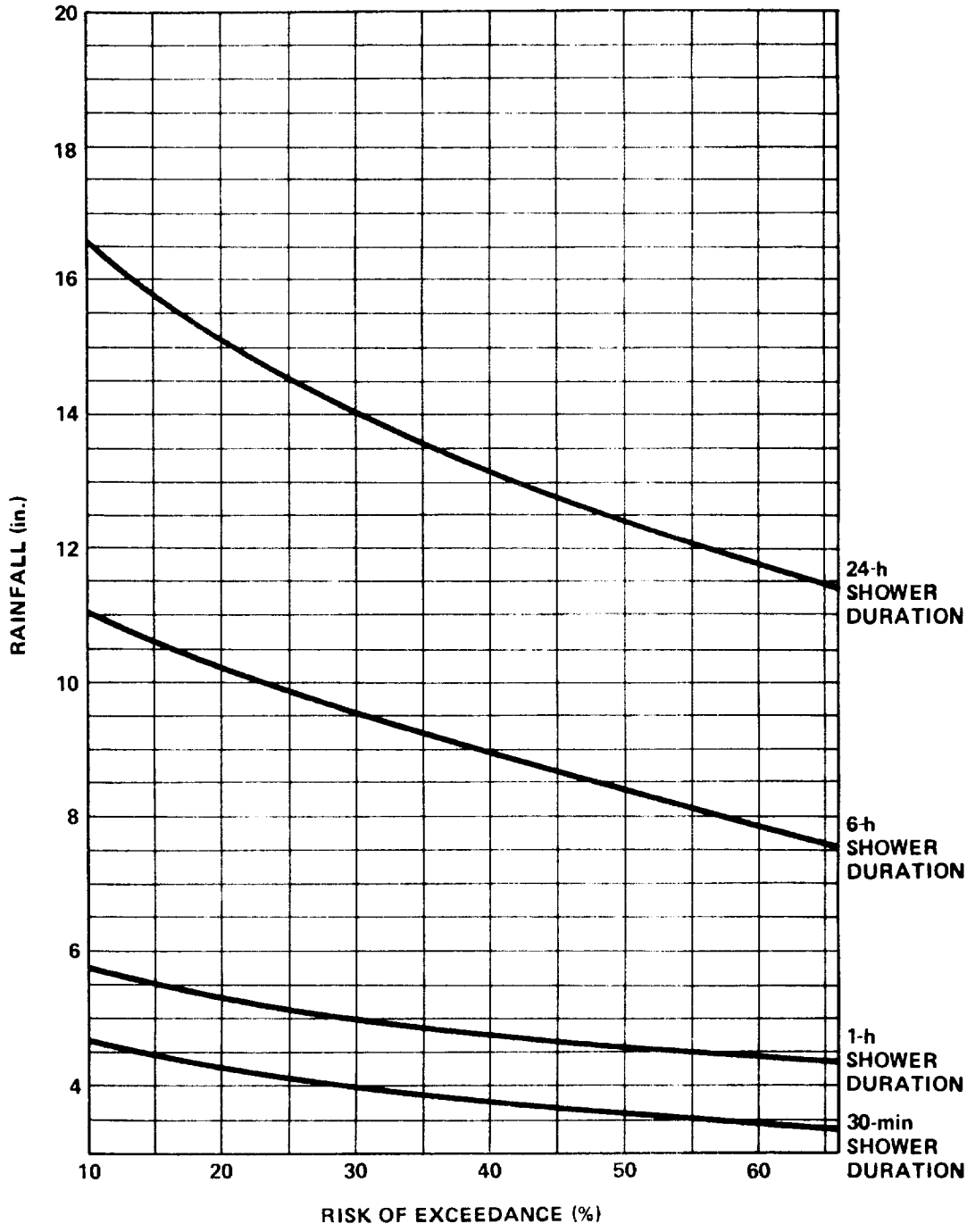

Figure 7.2 Risk of exceeding rainfall 25-year recurrence interval.

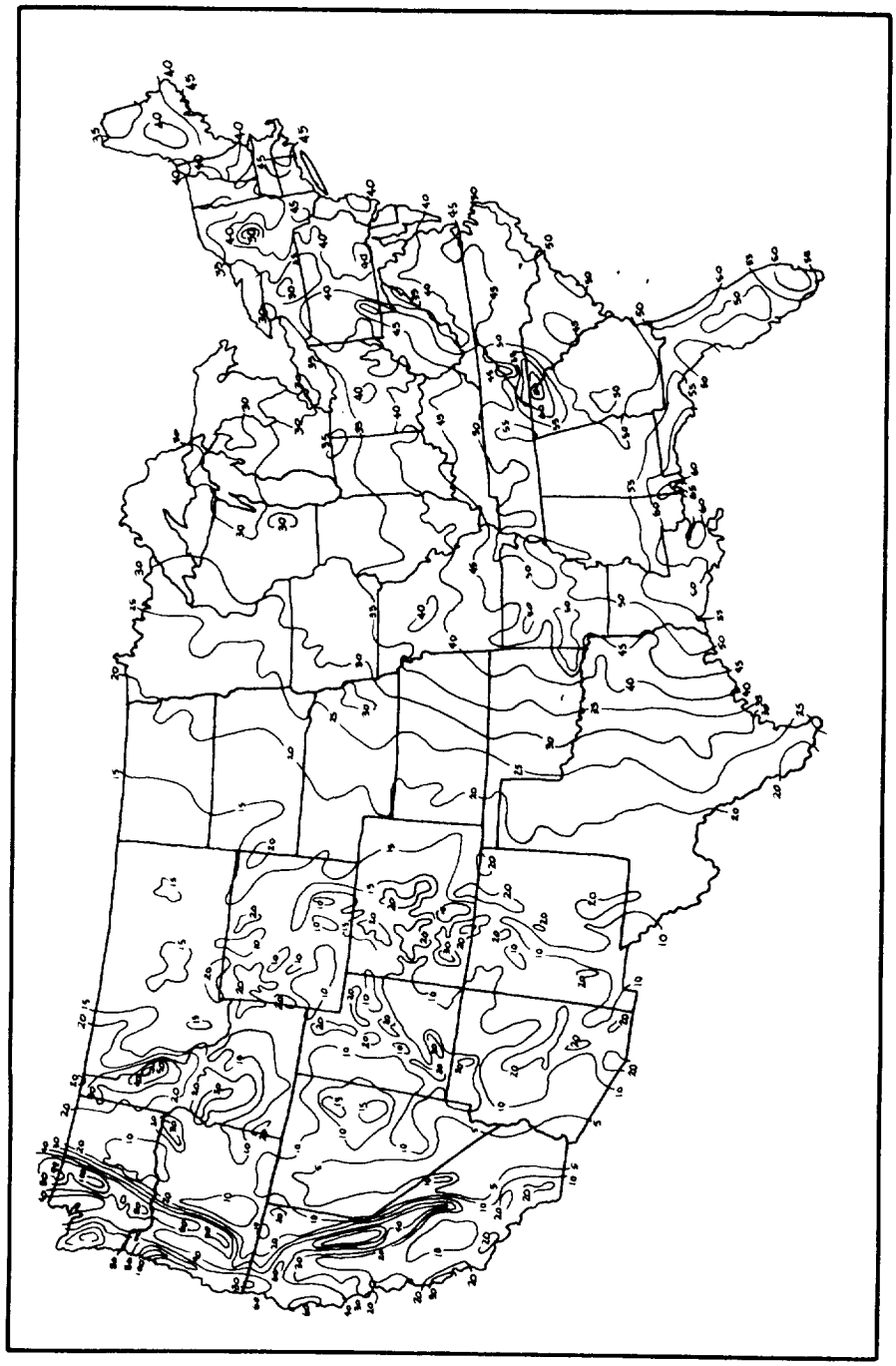

Figure 7.3 Average annual precipitation of the United States in inches.

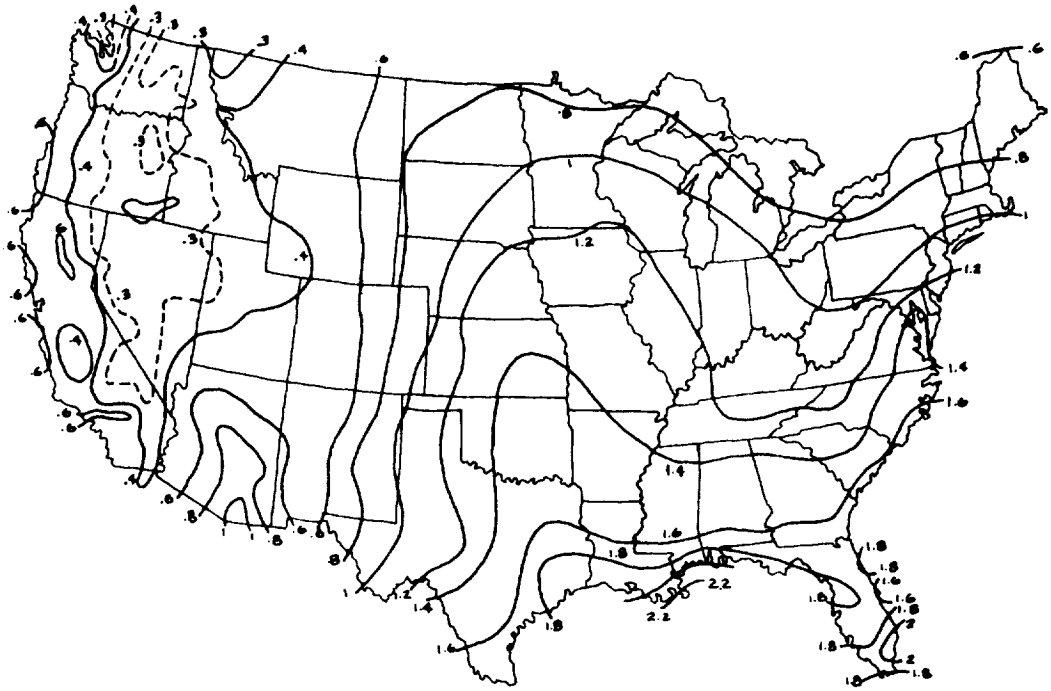

Figure 7.4 Two-year 30-min rainfall in inches [7.3].

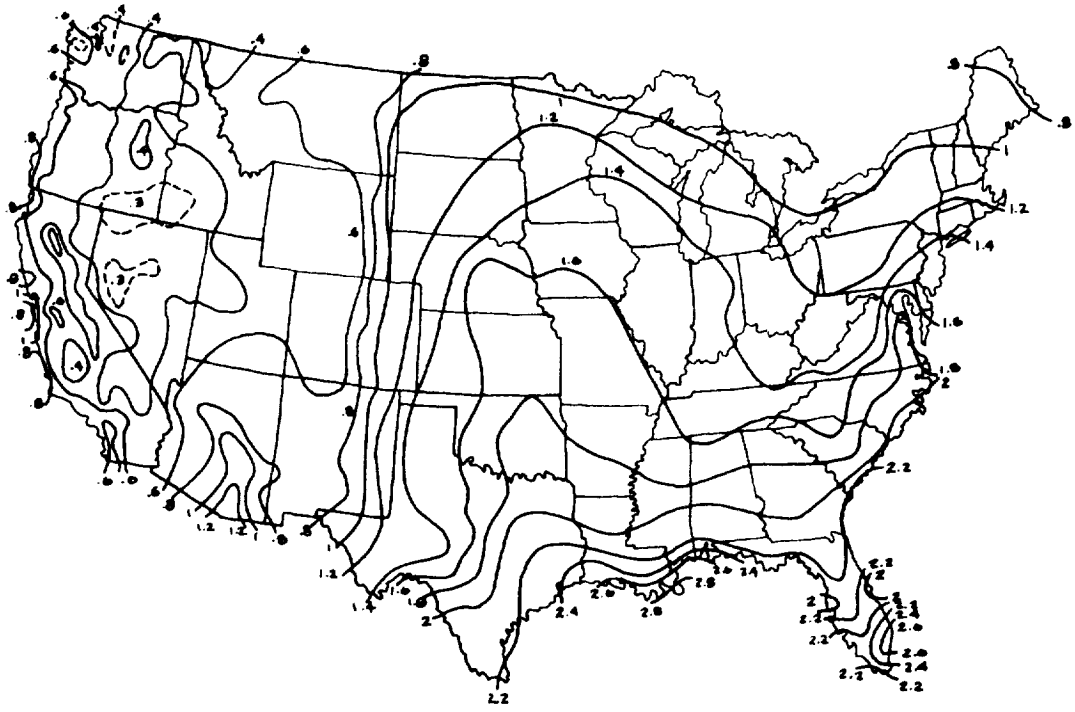

Figure 7.5 Two-year 1-h rainfall in inches [7.3].

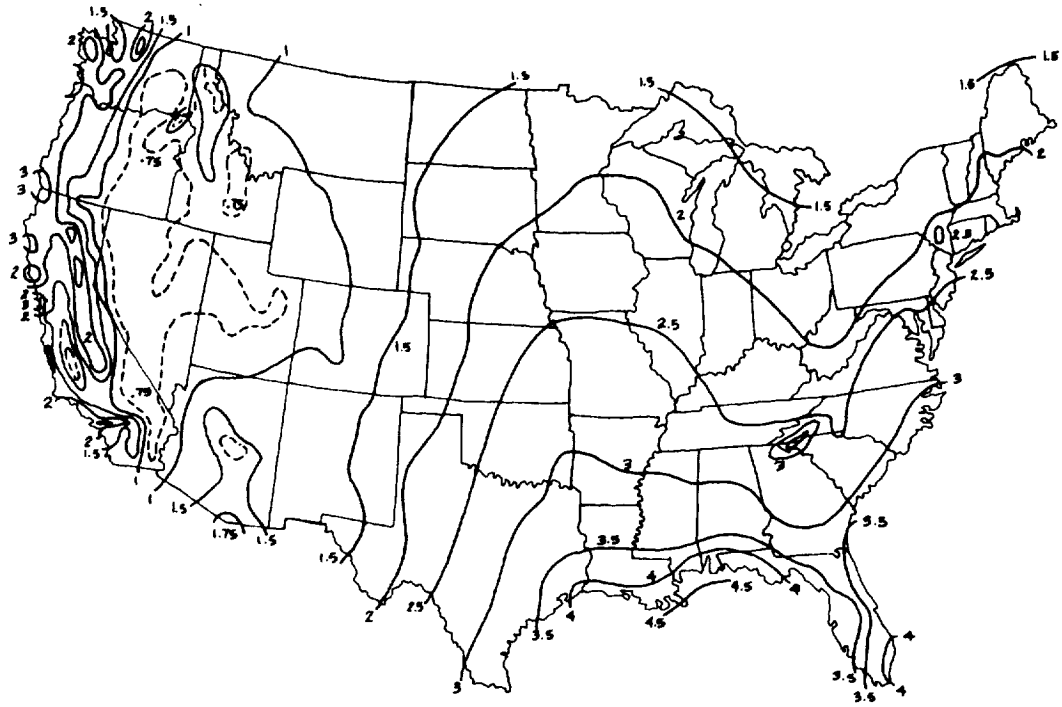

Figure 7.6 Two-year 6-h rainfall in inches [7.3].

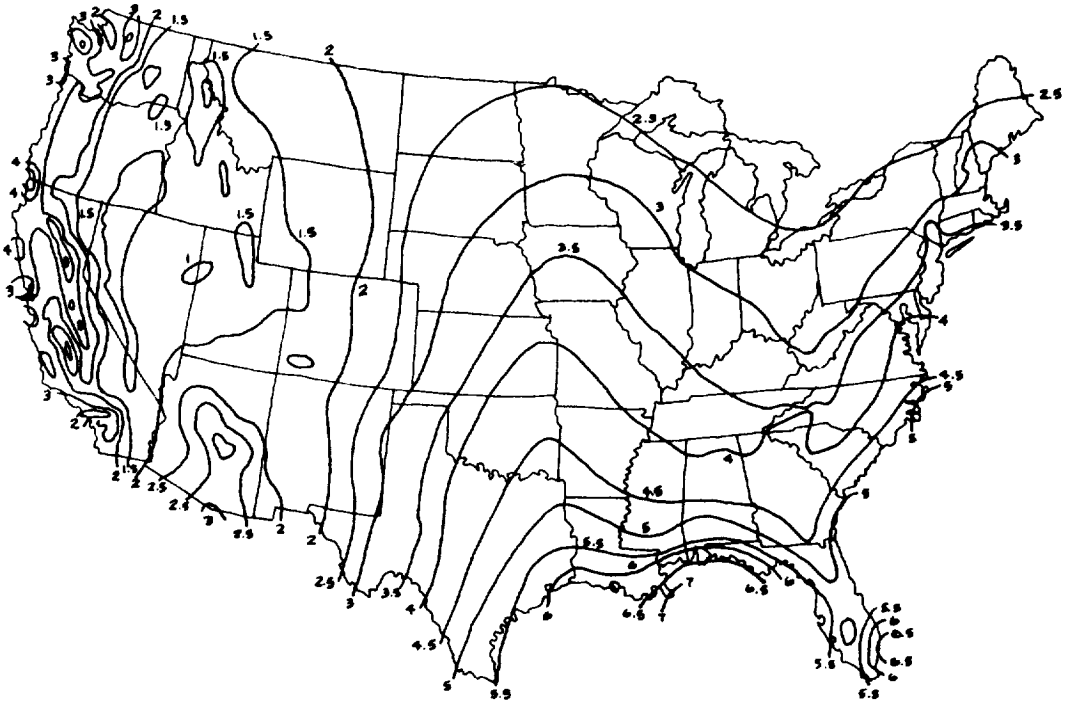

Figure 7.7 Two-year 24-h rainfall in inches [7.3].

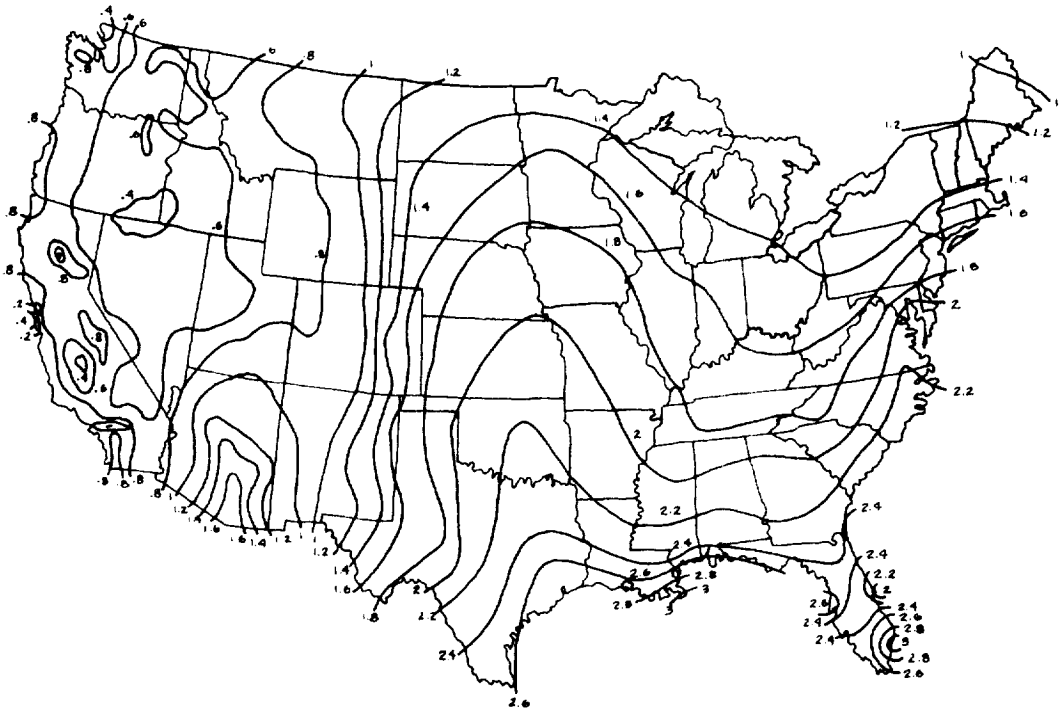

Figure 7.8 Ten-year 30-min rainfall in inches [7.3].

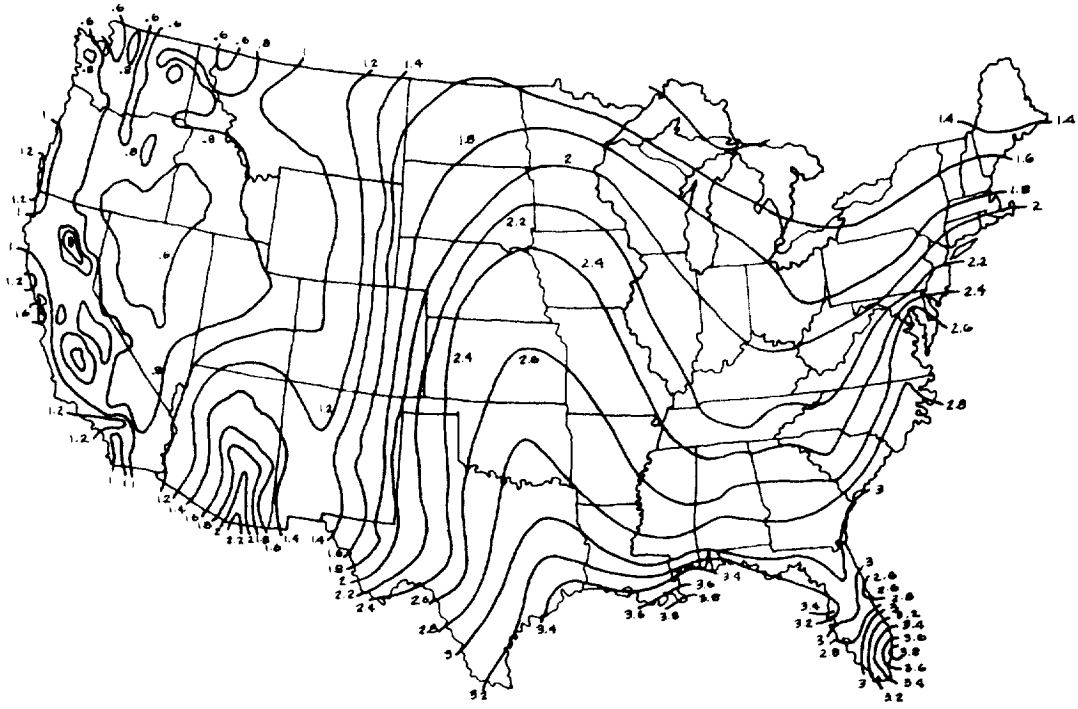

Figure 7.9 Ten-year 1-h rainfall in inches [7.3].

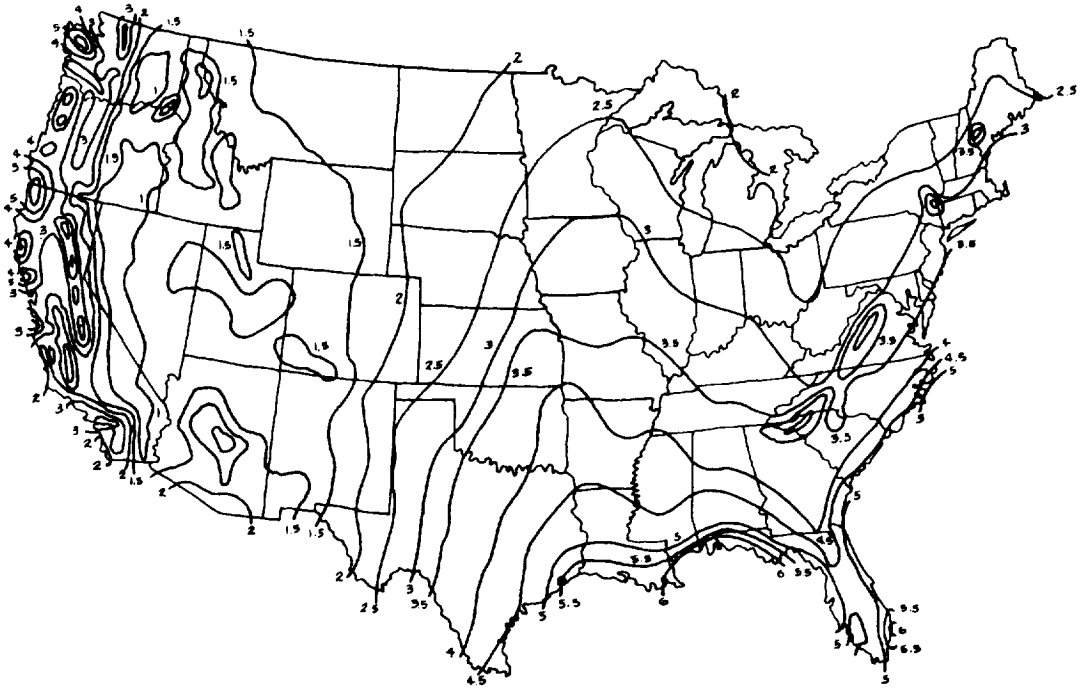

Figure 7.10 Ten-year 6-h rainfall in inches [7.3].

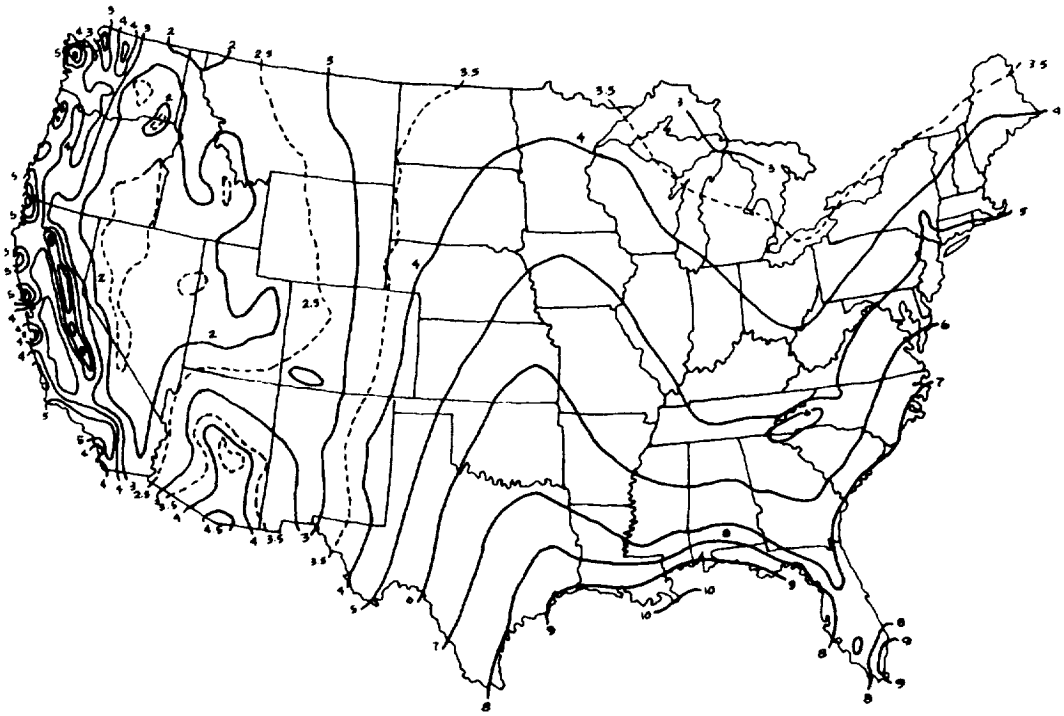

Figure 7.11 Ten-year 24-h rainfall in inches [7.3].

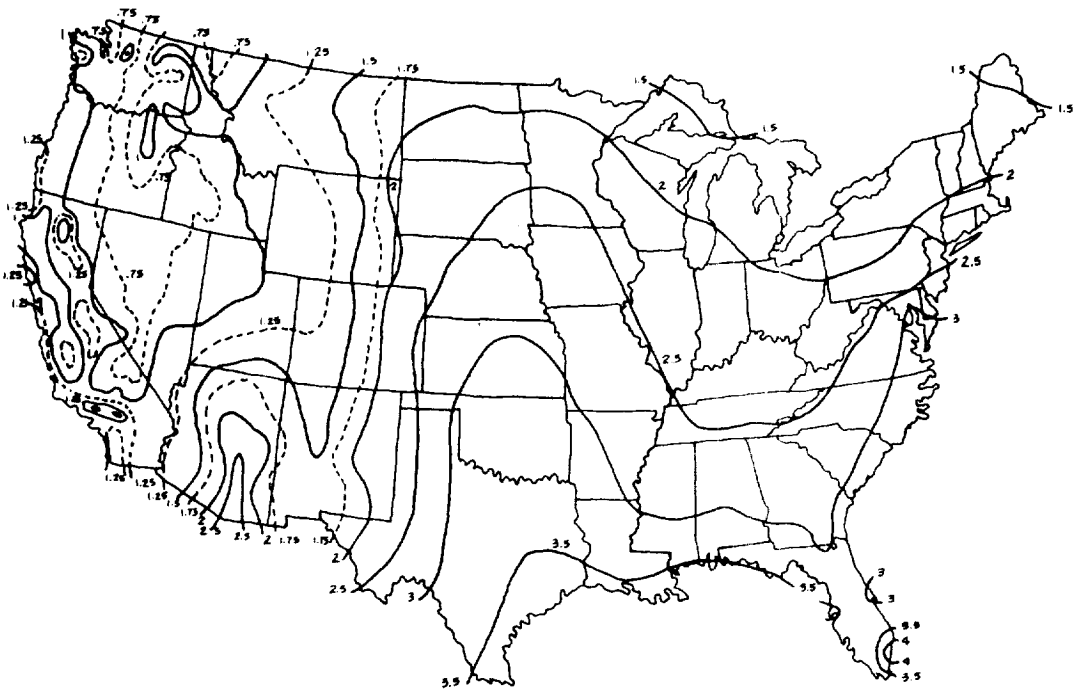

Figure 7.12 One-hundred-year 30-min rainfall in inches [7.3].

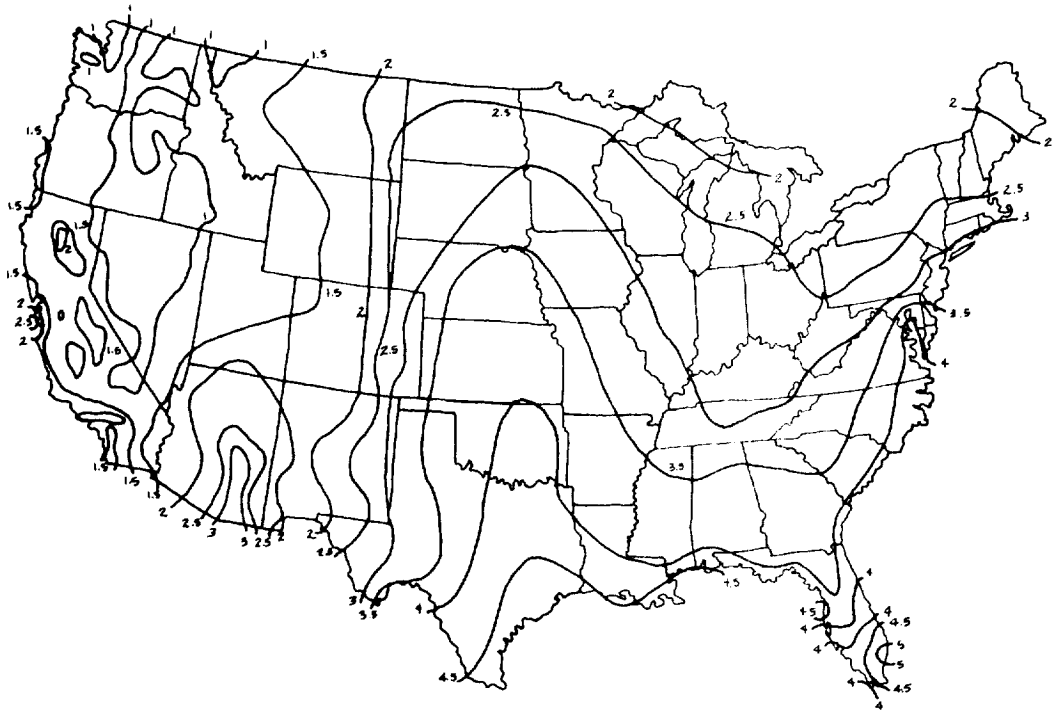

Figure 7.13 One-hundred-year 1-h rainfall in inches [7.3].

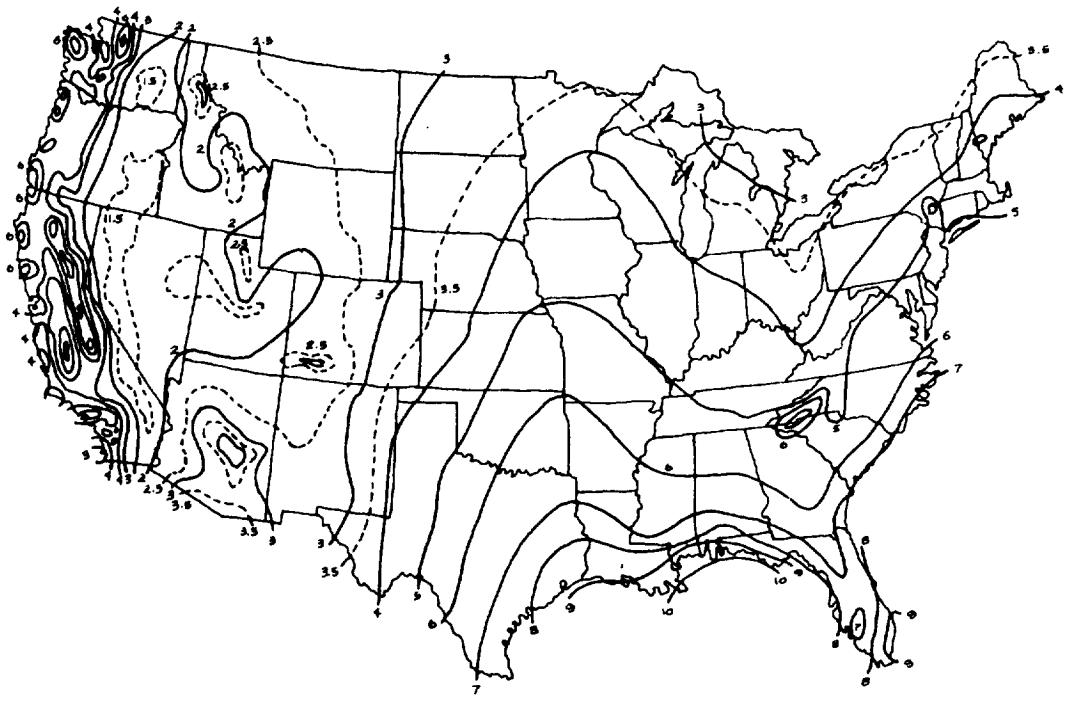

Figure 7.14 One-hundred-year 6-h rainfall in inches [7.3].

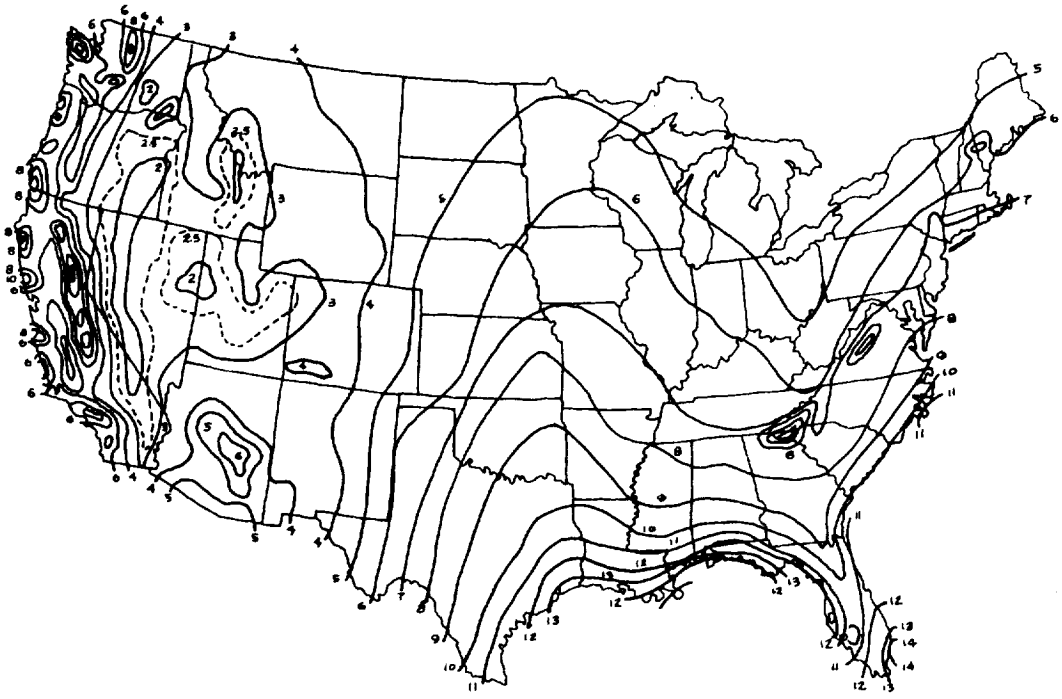

Figure 7.15 One-hundred-year 24-h rainfall in inches [7.3].

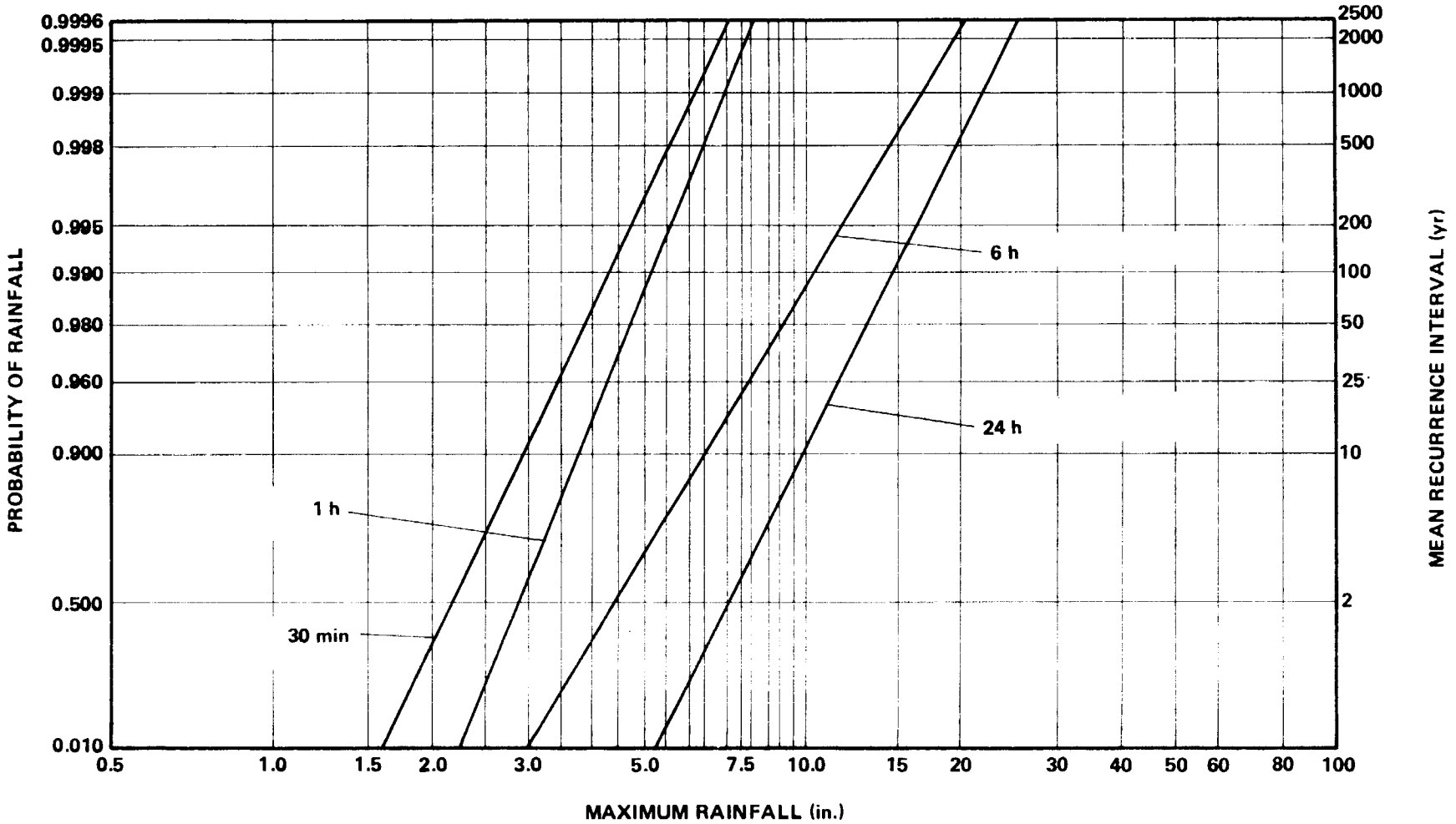

Figure 7.16 Fisher-Tippett Type II distribution for New Orleans, Louisiana.

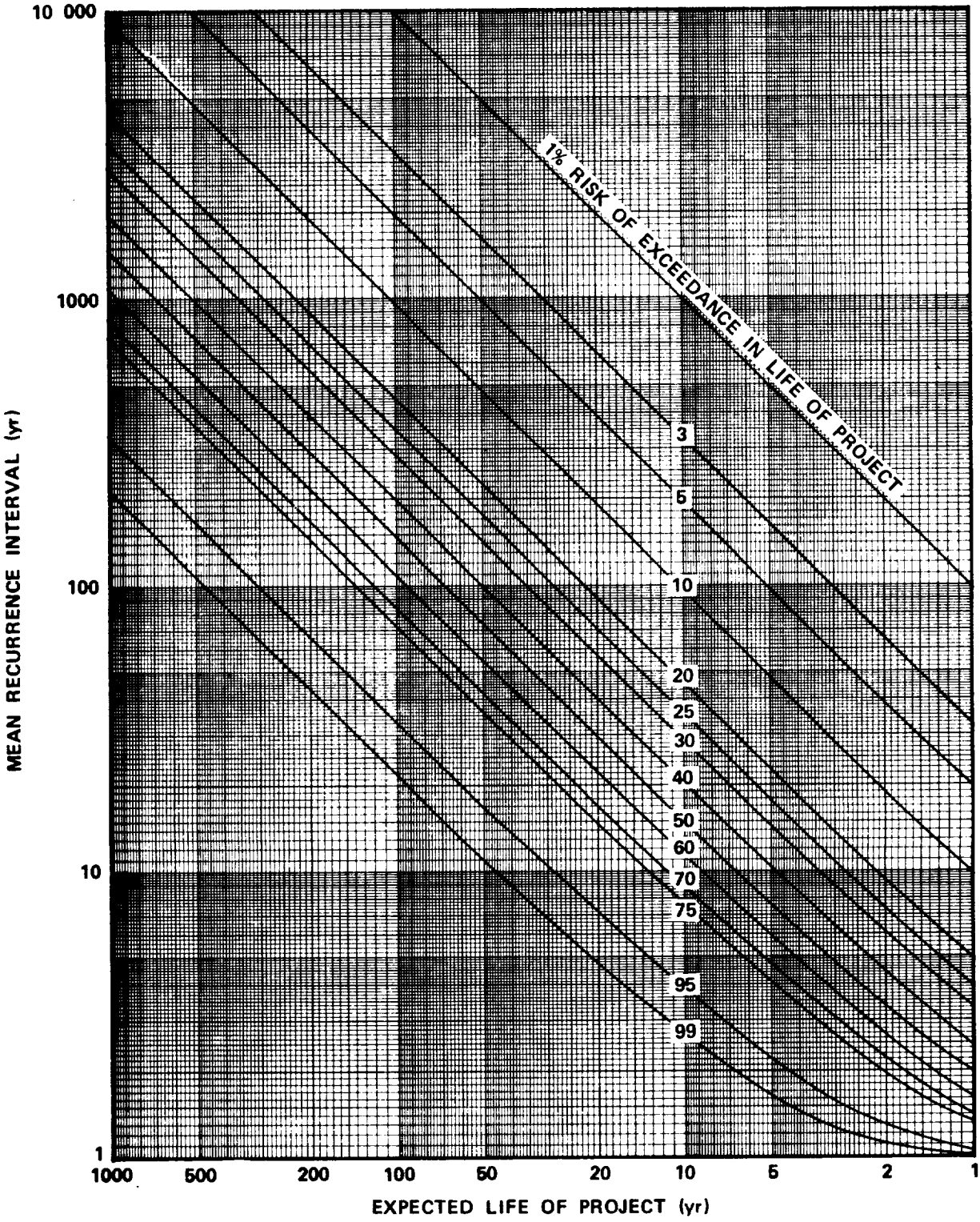

Figure 7.17 Risk of occurrence of rainfall of various mean recurrence intervals within the expected life of the project.

Since the aerospace vehicle design philosophy gives no specific life, assume 25 years as the expected life of the WTG. Employing a 10-percent risk that the design rainfall will be exceeded during the useful life of the structure, the recurrence interval T_R is found in exactly the same manner as described in Chapter 2, Section 2.1.2.1. From Figure 7.17, for a structure with a 25-year life and a 10-percent risk of exceedance, T_R is found to be 238 years. From Figure 7.16, a 238-year recurrence interval is associated with an extreme rainfall amount of 43.2 cm (17.0 in.) for a 24-h duration storm or 14.2 cm (5.6 in.) for a 1-h duration storm. Alternately, using an expected life of 50 years and accepting a 63-percent risk of exceedance, Figure 7.17 indicates a recurrence interval of 51 years. Using this value of 51 years, Figure 7.16 indicates an extreme rainfall of 33.0 cm (13.0 in.) for a 24-h storm or 11.9 cm (4.7 in.) for a 1-h storm.

The WTG designer will probably accept an intermediate value between those previously computed since a WTG does not require the same extreme degree of reliability as a manned spacecraft. However, a WTG will be deliberately exposed to high winds, which requires a higher degree of reliability than a standard building. Figures 7.1 and 7.2 provide readily useable curves for selection of extreme rainfall based on individual design philosophies.

7.1.3 Detailed Computational Procedures

7.1.3.1 Introduction

The preceding sections were intended to give a concise overview of characteristic rainfall for a general purpose WTG designed to operate in any region of the United States. The following sections provide detailed information for a WTG designed for a specific site or region and give data to substantiate the previously quoted values.

Precipitation in the form of rainfall is of importance to the engineer insofar as the amount of water damage that the machine can sustain during severe storms (this is apart from wind damage due to the storm). If the rainfall is intense enough, it can penetrate the WTG housing through seams, around the hub, or any other opening regardless of size. This water penetration may cause damage to internal components.

Precipitation results from condensation of moisture in the atmosphere. Three conditions must be met for condensation to occur and for raindrops to form: (1) the conditions of saturation must be produced (usually through cooling); (2) water vapor must change phase to liquid or solid; and (3) small water droplets or ice crystals must grow to a size which will enable them to fall.

Cooling, as mentioned in step (1), almost always takes place as a result of a lifting process, either convectional, orographic, or cyclonic lifting. Convectional lifting results from localized heating of the Earth's surface. Warm air is lifted in cells, producing thunderstorms. These storms often occur in the afternoons of hot days and, although they are usually of short duration (1 to 2 h), may be quite intense. Orographic lifting occurs when air is forced over mountains. As much as 380 cm (150 in.) of rain falls on the seaward side of Vancouver Island where condensation occurs as air moves inland and is forced over the mountains. Cyclonic lifting results from a warm, light-air mass colliding with a heavier cold-air mass. As the warm air mass rides up over the cold air mass, precipitation forms over a wide area.

7.1.3.2 Calculation of Extreme Rainfall

The average annual rainfall for the United States is shown in Figure 7.3. However, of more importance to the design engineer is the intensity of the rainfall to which the structure will be exposed. Figures 7.4 through 7.15 show intensity-duration maps of the United States for various recurrence intervals [7.3] (as provided by the U.S. Weather Bureau from intensity-duration analysis results). The engineer locates the site of the WTG on these maps. The rainfall values are plotted on extreme value plotting paper, Fisher-Tippett Type II distribution. A straight line is then drawn through these plotted values.

As an example, the rainfall intensity-duration curves have been plotted for New Orleans, Louisiana, as shown in Figure 7.16. As can be seen, a rainfall of 53.3 cm (21 in.) in a 24-h period may be expected at least once in 750 years, and a rainfall of 16.5 cm (6.5 in.) in a 1-h period at least once in 500 years.

7.1.3.3 Risk of Exceedance Design Rainfall During Expected Life of the Structure

With a knowledge of the probable recurrence of extreme rainfall, it is necessary to establish the percent risk that the design rainfall will be exceeded in the expected life of the structure. Figure 7.17 shows the risk of occurrence of rainfall of various mean recurrence intervals, within the expected life of the project.

To use Figure 7.17:

1) Select the expected life of the structure under design.

2) Determine the risk that you are willing to accept that the rainfall intensity will exceed the value for which you have designed.

3) From Figure 7.17 find the mean recurrence interval corresponding to the values of risk and of expected life selected in 1) and 2).

4) From Figure 7.16, find the design rainfall value corresponding to the mean recurrence interval determined in 3).

> Example 7.1: Assume a WTG or other facility is to be constructed in New Orleans with a life expectancy of 25 years. Further, assume that the engineer is willing to take a 10-percent chance that the structure may be damaged by rainfall greater than that for which he designed.
>
> From Figure 7.17, the mean recurrence interval for a 25-year expected life at a 10-percent risk of exceedance is 240 years. From Figure 7.16, the design rainfall is approximately 41 cm (16 in.) of rain in 24 h, or 14 cm (6 in.) of rainfall in 1 h.

7.2 Hail

7.2.1 Summary of Hail Design Value

Hailstorms vary greatly in intensity and duration. Hailstones as large as a grapefruit have been reported as well as hail accumulations on the ground of up to 30 to 46 cm (12 to 18 in.), and a large hail fall could cover 260 km^2 (100 square miles). In general, however, maximum size hailstones during storms are much smaller, approximately 2.5 cm (1 in.) in diameter. More frequently, they are smaller, and accumulations on the ground are a few inches at most. The area extent of hail fall is in tens of square kilometers. Although hail has a higher density than snow, 2.4 kg m^{-2} cm^{-1} (1.25 lb ft^{-2} $in.^{-1}$), the extreme load for hail will not exceed the extreme load for snow. Mean annual frequency of hail can be as high as seven or eight hail days at a station, or as much as 25 or more over an area as large as a section of a state. Roughness

of terrain has a marked influence on the occurrence of hailstorms. In hilly areas, one or two occurrences more than over the adjacent flat land can be expected, while in mountains the expectancy may be two to three times that of the valley floor. The number and severity of hailstorms do vary from year to year.

During the peak season of the year in the region of highest incidence, the risk of encountering a hailstone of near record size 7.6 cm (3 in.) or greater is negligible. However, the probability of occurrence of hail as large as 2.5 to 5.0 cm (1 to 2 in.) in diameter, while small, does exist, particularly in areas between 30°N and 50°N latitudes. The data contained in the following section allow an estimate of the probability of hail of a given size to be made. The data are insufficient for the designer to prescribe a design value and compute the risk of exceeding that particular value as has been described for other environmental factors in previous chapters of this document.

7.2.2 Design Values

The single point location probability of hailstones of a given size and the conditional probability are shown in Table 7.1. This probability is for the region of the United States having the greatest frequency of hail during the most severe month of hailstorms. Other information is:

1) The approximate velocity of fall of a hailstone given in Reference 7.1 is 20 to 30 m s^{-1}.

2) Wind speed occurring during hailstorms is on an average of 10 m s^{-1}.

3) Density of hailstones is 0.8 gm m^{-3} (50 lb_m ft^{-3}).

7.2.3 Hail and Its Distribution

Hail is precipitation in the form of balls or regular lumps of ice. A unit of hail or hailstone may range in size from that of a pea [0.64 cm (0.25 in.)] to that of a grapefruit [12.7 cm (approximately 5 in. diameter)] and has a mean density of approximately 0.8 gm cm^{-3} (50 lb_m ft^{-3}).

7.2.4 Frequency of Hail Occurrences

Hail records are primarily in the form of frequency of occurrence, expressed as number of hail days. A hail day is defined as any day in which

hail was observed or reported, regardless of whether there was a brief shower, prolonged occurrence, large stones, or several occurrences. Figure 7.18 is a map of the United States showing the mean annual hail days taken from Reference 7.4. Although this map is a useful guide to hailstone occurrence, there are several qualifications for interpreting the annual hail day map. The first qualification is that terrain has a marked influence on hail frequency. Reference 7.5 points out that even over areas of small hills, the annual frequency may be one or two occurrences higher than over the neighboring flat areas. In rough and mountainous areas, the annual frequency was found to be 2 1/2 to 3 times that reported in the open valleys. The second qualification concerns use of the term "hail days." Of more importance than whether hail occurred or not is the occurrence of large stones which are most significant to damage of physical property.

7.2.5 Hailstone Size Frequency

The probability of encountering 5 cm (2 in.) or even 2.5 cm (1 in.) hailstones at any one place is small. A probability table based on characteristics of storms over the Midwestern Plains of the United States is given in Table 7.1 [7.5].

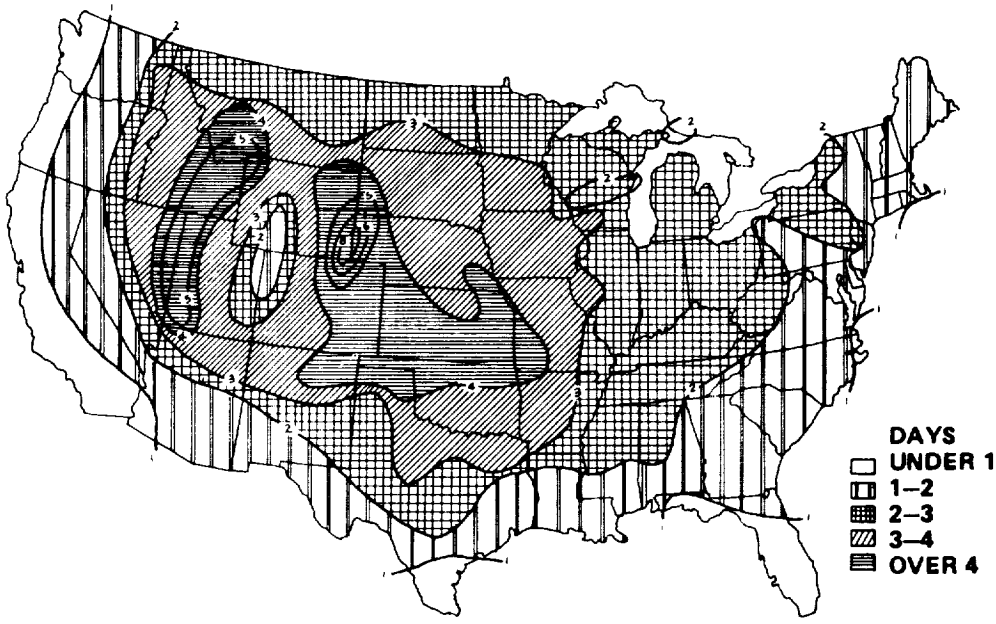

Figure 7.18 Average annual number of days with hail [7.4].

TABLE 7.1 OPERATIONAL HAIL SIZE (PERCENT) EXTREMES-ESTIMATES OF THE PROBABILITY OF ENCOUNTERING HAILSTONES OF GIVEN DIAMETER AT A SINGLE POINT LOCATION [7.5] (THE DATA REFER TO THE MIDWESTERN PLAINS)

Hail Diameter (in.) (h)	Conditional Probability of Size ≥ h	Single-Station Probability	Approximate Percent Extreme
Any size	1.000	0.000448	0.05
≥ 0.25	0.790	0.000354	0.04
≥ 0.5	0.360	0.000161	0.02
≥ 0.75	0.135	0.0000605	0.01
≥ 1.0	0.070	0.0000314	0.003
≥ 2.0	0.019	0.00000851	0.0009
≥ 3.0	0.0038	0.00000170	0.0002
≥ 4.0	0.00055	0.00000025	0.00003

Table 7.1 gives the conditional probability of size which means that should hail of any form occur, the probability of occurrence of hailstones of the prescribed size or greater is as tabulated. The column labeled "Single-Station Probability" represents the probability of hail occurring at a given station in the network utilized in developing the tabulated results. For example, there is a probability of 0.000448 of encountering hail of any size at the location with the greatest frequency given on the distribution map shown earlier. This probability applies from the surface to 1500 m (5000 ft). To convert the point frequency to an areal frequency, a factor of 5 to 8 is usually used. That is, the point frequency is multiplied by the given factor to give the areal frequency estimate. Reference [7.5] does not specify how large an area, but it may be assumed to be on the order of a typical midwestern state.

7.2.6 Hailstone Size Distribution

Histograms of frequency distribution of maximum hailstone size for various locations in the United States and Canada are given in Figure 7.19. As an example, the frequency of stones greater than 3 cm (1.2 in.) is approximately 12 percent in Alberta and 6 percent or less in the other areas. The number of years of data which has gone into establishing the histograms is indicated on the figure.

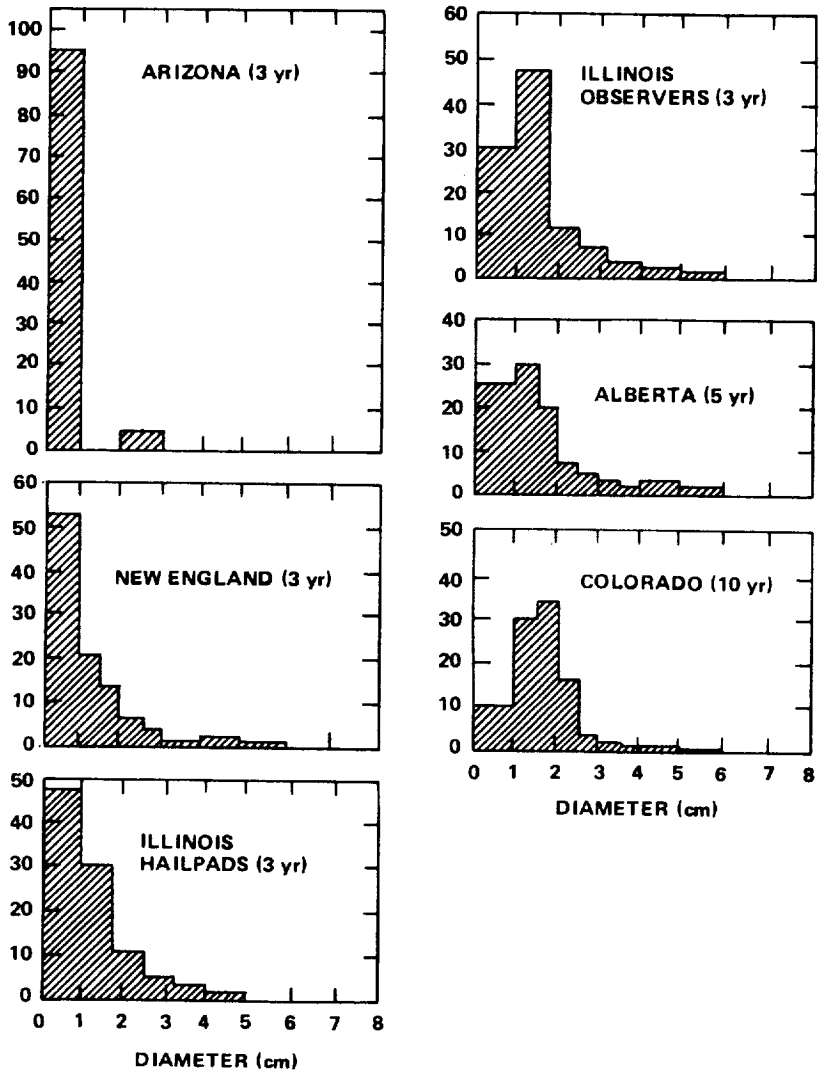

Figure 7.19 Frequency distribution of maximum hailstone sizes for various locations [7.5].

7.2.7 Estimated Fall Velocity of Hailstones

The impact of hailstones on a WTG rotor, housing, support structure, etc., is of importance to the design engineer. Table 7.2 gives a theoretical estimate of the terminal velocity of hailstones with respect to diameter.

TABLE 7.2 ESTIMATED TERMINAL VELOCITY OF HAILSTONES

Diameter (cm)	Terminal Velocity ($m\ s^{-1}$)
0.2	3.1
1.0	13.7
2.0	20.3
10.0	44.3
20.0	61.1

7.2.8 Hail Extremes

Hailstones 43 cm (17 in.) in circumference have been reported in the states of Kansas, Nebraska, and Iowa. The stones weighed in excess of 0.68 kg ($1.5\ lb_m$). Fortunately, hailstones of this size are very rare and are spaced 3.7 to 4.6 m (12 to 15 ft) or more apart, and the storms in which they form are of a short duration. The most recent observation of large hailstones was on September 3, 1970, at Coffeeville, Kansas, where one hailstone was preserved which measured 45 cm (17.5 in.) in circumference and weighed 0.76 kg ($1.7\ lb_m$). Reproductions of the hailstone were made, and free-fall speeds were investigated by dropping the stones from as high as 900 m (2950 ft). The speed of the hailstone as it approached the ground was reported to be 47 $m\ s^{-1}$ (105 mph). If there had been a downdraft at the time of the hail drop, its speed would have been correspondingly higher.

7.3 Thermal

7.3.1 Introduction

One of the more important environmental influences on a metal structure is the thermal environment. Combinations of air temperature, solar radiation, and sky radiation can cause various structural problems. Some examples of potential problems are: (1) differential heating — heating of one side of a structure by the Sun while the other side is not heated — causes stresses since the structure sides will be of different lengths; (2) high temperature may destroy the usefulness of a lubricant. Analyses of the heating or cooling of a surface depend on knowledge of the solar radiation and of the surface air temperature; therefore, methods of determining these parameters are presented in this section.

All objects radiate energy in the electromagnetic spectrum. The amount and frequency of the radiation distribution is a function of temperature. The higher the temperature, the greater the amount of total energy emitted and the higher the frequency (shorter the wavelength) of the peak energy emission. Most of the following information is taken from Reference 7.1.

7.3.1.1 Solar Radiation

The Sun emits energy in the electromagnetic spectrum from 10^{-7} to greater than $10^{5}\ \mu$. This radiation ranges from cosmic rays through the very long radio waves. The total amount of radiation from the Sun is nearly constant in intensity with time.

Of the total electromagnetic spectrum of the Sun, only the radiant energy from that portion of the spectrum between 0.22 and 20.0 μ will be considered in this report since it contains 99.8 percent of the total electromagnetic energy. The spectral distribution of this region closely resembles the emission of a blackbody radiating at 6000 K.

The Earth's atmosphere also absorbs a small part of the solar radiation, so that the major portion of the solar radiation reaching the Earth's surface is between approximately 0.20 and 4.00 μ.

The first detailed information published for use by engineers on the distribution of solar radiation energy (solar irradiation) wavelength was that by Parry Moon in 1940 [7.6]. These data are based on theoretical curves but are still used as the basic solar radiation in design by many engineers.

7.3.1.2 Intensity Distribution

Table 7.3 presents data on the distribution with wavelength of solar radiation at the Earth's surface after 1.0 atmosphere absorption. The values of solar radiation for 1.0 atmosphere absorption are representative of a very clear atmosphere which provides a minimum of atmospheric absorption. This gives a total normal solar radiation value (area under the spectral curve) equal to the highest values that would be measured at the Earth's surface in mid-latitudes. These data are for use in solar radiation design studies when extreme solar radiation effects are desired at the Earth's surface. The same data are shown in graphical form in Figure 7.20.

7.3.1.3 Atmospheric Transmittance of Solar Radiation

The atmosphere of the Earth is composed of a mixture of gases, aerosols, and dust which absorb radiation in different amounts at various wavelengths. If the ratio is taken of the solar spectral irradiance I_o to that of the solar radiation after absorption through one air mass,[1] $I_{1.00}$, an atmospheric transmittance factor M can be found

$$M = \frac{I_o}{I_{1.00}} \quad . \tag{7.1}$$

The atmospheric transmittance constant can be used in the following equation for computations of intensities for any other number of air masses:

$$I_N = I_o(\overline{M}^N) \tag{7.2}$$

1. One air mass is the amount of atmosphere that the solar radiation passes through, considering the vertical path at sea level as unity (i.e., when the Sun is at the zenith).

TABLE 7.3 SOLAR SPECTRAL IRRADIANCE (OUTSIDE ATMOSPHERE) AND SOLAR RADIATION AFTER ABSORPTION BY CLEAR ATMOSPHERE [7.1]

Wavelength (microns) λ	Solar Spectral Irradiance (watts $cm^{-2}\ \mu^{-1}$)	Area Under Solar Spectral Irradiance Curve (watts cm^{-2})	Solar Radiation After One Atmosphere Absorption (watts $cm^{-2}\ \mu^{-1}$)	Area Under One Atmosphere Solar Radiation Curve (watts cm^{-2})	Percentage of Solar Radiation After One Atmosphere Absorption for Wavelengths Shorter than λ (%)
0.120	0.000010	0.00000060	0.000000	0.000000	0.00
0.140	0.000003	0.00000073	0.000000	0.000000	0.00
0.150	0.000007	0.00000078	0.000000	0.000000	0.00
0.160	0.000023	0.00000093	0.000000	0.000000	0.00
0.170	0.000063	0.00000136	0.000000	0.000000	0.00
0.180	0.000125	0.00000230	0.000000	0.000000	0.00
0.190	0.000271	0.00000428	0.000000	0.000000	0.00
0.200	0.00107	0.000010	0.000001	0.000000	0.00
0.210	0.00229	0.000027	0.000003	0.000000	0.00
0.220	0.00575	0.000067	0.000007	0.000000	0.00
0.225	0.00649	0.000098	0.000007	0.000000	0.00
0.230	0.00667	0.000131	0.000008	0.000000	0.00
0.235	0.00593	0.000162	0.000007	0.000000	0.00
0.240	0.00630	0.000193	0.000007	0.000000	0.00
0.245	0.00723	0.000227	0.000008	0.000000	0.00
0.250	0.00704	0.000263	0.000008	0.000000	0.00
0.255	0.0104	0.000306	0.000012	0.000000	0.00
0.260	0.0130	0.000365	0.000015	0.000000	0.00
0.265	0.0185	0.000443	0.000021	0.000000	0.00
0.270	0.0232	0.000548	0.000026	0.000000	0.00
0.275	0.0204	0.000657	0.000023	0.000000	0.00
0.280	0.0222	0.000763	0.000025	0.000000	0.00
0.285	0.0315	0.000897	0.000036	0.000001	0.00
0.290	0.0482	0.001097	0.000055	0.000001	0.00
0.295	0.0584	0.001363	0.000066	0.000001	0.00
0.300	0.0514	0.001638	0.006677	0.000035	0.03
0.305	0.0603	0.001917	0.019830	0.000134	0.12
0.310	0.0689	0.002240	0.029084	0.000279	0.25
0.315	0.0764	0.002603	0.038941	0.000474	0.42
0.320	0.0830	0.003002	0.047684	0.000712	0.64
0.325	0.0975	0.003453	0.062018	0.001022	0.92
0.330	0.1059	0.003961	0.073829	0.001392	1.25
0.335	0.1081	0.004496	0.080896	0.001796	1.61
0.340	0.1074	0.005035	0.084636	0.002219	1.99
0.345	0.1069	0.005571	0.087080	0.002655	2.39
0.350	0.1093	0.006111	0.091327	0.003111	2.80
0.355	0.1083	0.006655	0.092186	0.003572	3.40
0.360	0.1068	0.007193	0.092857	0.004036	3.63
0.365	0.1132	0.007743	0.099873	0.004536	4.08
0.370	0.1181	0.008321	0.105507	0.005063	4.55
0.375	0.1157	0.008906	0.104596	0.005586	5.03
0.380	0.1120	0.009475	0.102971	0.006101	5.49
0.385	0.1098	0.010030	0.102273	0.006613	5.95
0.390	0.1098	0.010579	0.103977	0.007132	6.42
0.395	0.1189	0.011150	0.114309	0.007704	6.93
0.400	0.1429	0.011805	0.137403	0.008391	7.55
0.405	0.1644	0.012573	0.158076	0.009181	8.26
0.410	0.1751	0.013422	0.168365	0.010023	9.02
0.415	0.1774	0.014303	0.170576	0.010876	9.79
0.420	0.1747	0.015183	0.167980	0.011716	10.54
0.425	0.1693	0.016043	0.162788	0.012530	11.28
0.430	0.1639	0.016876	0.157596	0.013318	11.99
0.435	0.1663	0.017702	0.159903	0.014117	12.71
0.440	0.1810	0.018570	0.174038	0.014988	13.40
0.445	0.1922	0.019503	0.184807	0.015912	14.30
0.450	0.2006	0.020485	0.192884	0.016876	15.19
0.455	0.2057	0.021501	0.195904	0.017656	16.07
0.460	0.2066	0.022532	0.196761	0.018839	16.96
0.465	0.2048	0.023560	0.196923	0.019824	17.84
0.470	0.2033	0.024580	0.195480	0.020801	18.72

TABLE 7.3 (Continued)

Wavelength (microns) λ	Solar Spectral Irradiance (watts $cm^{-2} \mu^{-1}$)	Area Under Solar Spectral Irradiance Curve (watts cm^{-2})	Solar Radiation After One Atmosphere Absorption (watts $cm^{-2} \mu^{-1}$)	Area Under One Atmosphere Solar Radiation Curve (watts cm^{-2})	Percentage of Solar Radiation After One Atmosphere Absorption for Wavelengths Shorter than λ (%)
0.475	0.2044	0.025600	0.196538	0.021784	19.61
0.480	0.2074	0.026629	0.197523	0.022772	20.50
0.485	0.1976	0.027642	0.186415	0.023704	21.34
0.490	0.1950	0.028623	0.183962	0.024624	22.17
0.495	0.1960	0.029601	0.183177	0.025539	22.99
0.500	0.1942	0.030576	0.179814	0.026439	23.80
0.505	0.1920	0.031542	0.176146	0.027319	24.60
0.510	0.1882	0.032492	0.172660	0.028183	25.37
0.515	0.1833	0.033421	0.168165	0.029023	26.13
0.520	0.1833	0.034337	0.168165	0.029864	26.88
0.525	0.1852	0.035259	0.169908	0.030714	27.65
0.530	0.1842	0.036182	0.168990	0.031559	28.41
0.535	0.1818	0.037097	0.166788	0.032393	29.16
0.540	0.1783	0.037997	0.163977	0.033211	29.90
0.545	0.1754	0.038882	0.160917	0.034015	30.62
0.550	0.1725	0.039751	0.158256	0.034806	31.33
0.555	0.1720	0.040613	0.157798	0.035595	32.05
0.560	0.1695	0.041466	0.155504	0.036373	32.75
0.565	0.1705	0.042316	0.156422	0.037155	33.45
0.570	0.1712	0.043171	0.157064	0.037940	34.16
0.575	0.1719	0.044028	0.157726	0.038729	34.87
0.580	0.1715	0.044887	0.157339	0.039516	35.57
0.585	0.1712	0.045744	0.157064	0.040301	36.28
0.590	0.1700	0.046597	0.155963	0.041081	36.98
0.595	0.1682	0.047442	0.154311	0.041852	37.68
0.600	0.1666	0.048279	0.152844	0.042616	38.37
0.605	0.1647	0.049107	0.151100	0.043372	39.05
0.610	0.1635	0.049928	0.150000	0.044122	39.72
0.620	0.1602	0.051546	0.146972	0.045592	41.05
0.630	0.1570	0.053132	0.145370	0.047045	42.30
0.640	0.1544	0.054689	0.144299	0.048488	43.66
0.650	0.1511	0.056217	0.142547	0.049914	44.94
0.660	0.1486	0.057715	0.141523	0.051329	46.22
0.670	0.1456	0.059186	0.140000	0.052729	47.48
0.680	0.1427	0.060628	0.137211	0.054101	48.71
0.690	0.1402	0.062042	0.134807	0.055449	49.93
0.700	0.1369	0.063428	0.131634	0.056766	51.11
0.710	0.1344	0.064784	0.129230	0.058058	52.27
0.720	0.1314	0.066113	0.126346	0.059321	53.41
0.730	0.1290	0.067415	0.124038	0.060562	54.53
0.740	0.1260	0.068690	0.121153	0.061773	55.62
0.750	0.1235	0.069938	0.118750	0.062961	56.69
0.800	0.1107	0.075793	0.106442	0.068283	61.48
0.850	0.0988	0.081030	0.095000	0.073033	65.76
0.900	0.0889	0.085723	0.080090	0.077037	69.36
0.950	0.0835	0.090033	0.077314	0.080903	72.84
1.000	0.0746	0.093985	0.071730	0.084490	76.07
1.100	0.0592	0.100675	0.056923	0.090182	81.20
1.200	0.0484	0.106055	0.046538	0.094836	85.39
1.300	0.0396	0.110455	0.036000	0.098436	88.63
1.400	0.0336	0.114115	0.002240	0.098660	88.83
1.500	0.0287	0.117230	0.027333	0.101393	91.29
1.600	0.0244	0.119885	0.023461	0.103739	93.40
1.700	0.0202	0.122115	0.019423	0.105681	95.15
1.800	0.0159	0.123920	0.013826	0.107064	96.40
1.900	0.0126	0.125345	0.000126	0.107077	96.41
2.000	0.0103	0.126490	0.009809	0.108057	97.29
2.100	0.0090	0.127455	0.008653	0.108923	98.07
2.200	0.0079	0.128300	0.007596	0.109682	98.76
2.300	0.0068	0.129035	0.006538	0.110336	99.34

TABLE 7.3 (Concluded)

Wavelength (microns) λ	Solar Spectral Irradiance (watts $cm^{-2} \mu^{-1}$)	Area Under Solar Spectral Irradiance Curve (watts cm^{-2})	Solar Radiation After One Atmosphere Absorption (watts $cm^{-2} \mu^{-1}$)	Area Under One Atmosphere Solar Radiation Curve (watts cm^{-2})	Percentage of Solar Radiation After One Atmosphere Absorption for Wavelengths Shorter than λ (%)
2.4	0.0064	0.129695	0.006153	0.110951	99.90
2.5	0.0054	0.130285	0.001080	0.111059	100.00
2.6	0.0048	0.130795	0.000005	0.111060	100.00
2.7	0.0043	0.131250	0.000004	0.111060	100.00
2.8	0.00390	0.131660	0.000004	0.111061	100.00
2.9	0.00350	0.132030	0.000004	0.111061	100.00
3.0	0.00310	0.132360	0.000003	0.111061	100.00
3.1	0.00260	0.132645	0.000002	0.111062	100.00
3.2	0.00226	0.132888	0.000002	0.111062	100.00
3.3	0.00192	0.133097	0.000002	0.111062	100.00
3.4	0.00166	0.133276	0.000001	0.111062	100.00
3.5	0.00146	0.133432	0.000001	0.111062	100.00
3.6	0.00135	0.133573	0.000001	0.111062	100.00
3.7	0.00123	0.133702	0.000001	0.111062	100.00
3.8	0.00111	0.133819	0.000001	0.111063	100.00
3.9	0.00103	0.133926	0.000001	0.111063	100.00
4.0	0.00095	0.134025	0.000001	0.111063	100.00
4.1	0.00087	0.134116	0.000001	0.111063	100.00
4.2	0.00078	0.134198	0.000000	0.111063	100.00
4.3	0.00071	0.134273	0.000000	0.111063	100.00
4.4	0.00065	0.134341	0.000000	0.111063	100.00
4.5	0.00059	0.134403	0.000000	0.111063	100.00
4.6	0.00053	0.134459	0.000000	0.111063	100.00
4.7	0.00048	0.134509	0.000000	0.111063	100.00
4.8	0.00045	0.134556	0.000000	0.111063	100.00
4.9	0.00041	0.134599	0.000000	0.111063	100.00
5.0	0.0003830	0.13463906	0.000000	0.111063	100.00
6.0	0.0001750	0.13491806	0.000000	0.111063	100.00
7.0	0.0000990	0.13505506	0.000000	0.111063	100.00
8.0	0.0000600	0.13513456	0.000000	0.111063	100.00
9.0	0.0000380	0.13518356	0.000000	0.111063	100.00
10.0	0.0000250	0.13521506	0.000000	0.111063	100.00
11.0	0.0000170	0.13523606	0.000000	0.111063	100.00
12.0	0.0000120	0.13525056	0.000000	0.111063	100.00
13.0	0.0000087	0.13526091	0.000000	0.111063	100.00
14.0	0.0000055	0.13526801	0.000000	0.111063	100.00
15.0	0.0000049	0.13527321	0.000000	0.111063	100.00
16.0	0.0000038	0.13527756	0.000000	0.111063	100.00
17.0	0.0000031	0.13528101	0.000000	0.111063	100.00
18.0	0.0000024	0.13528376	0.000000	0.111063	100.00
19.0	0.0000020	0.13528596	0.000000	0.111063	100.00
20.0	0.0000016	0.13528776	0.000000	0.111063	100.00
25.0	0.000000610	0.13529328	0.000000	0.111063	100.00
30.0	0.000000300	0.13529556	0.000000	0.111063	100.00
35.0	0.000000160	0.13529671	0.000000	0.111063	100.00
40.0	0.000000094	0.13529734	0.000000	0.111063	100.00
50.0	0.000000038	0.13529800	0.000000	0.111063	100.00
60.0	0.000000019	0.13529829	0.000000	0.111063	100.00
80.0	0.000000007	0.13529855	0.000000	0.111063	100.00
100.0	0.000000003	0.13529865	0.000000	0.111063	100.00
1000.0	0.000000000	0.13530000	0.000000	0.111063	100.00

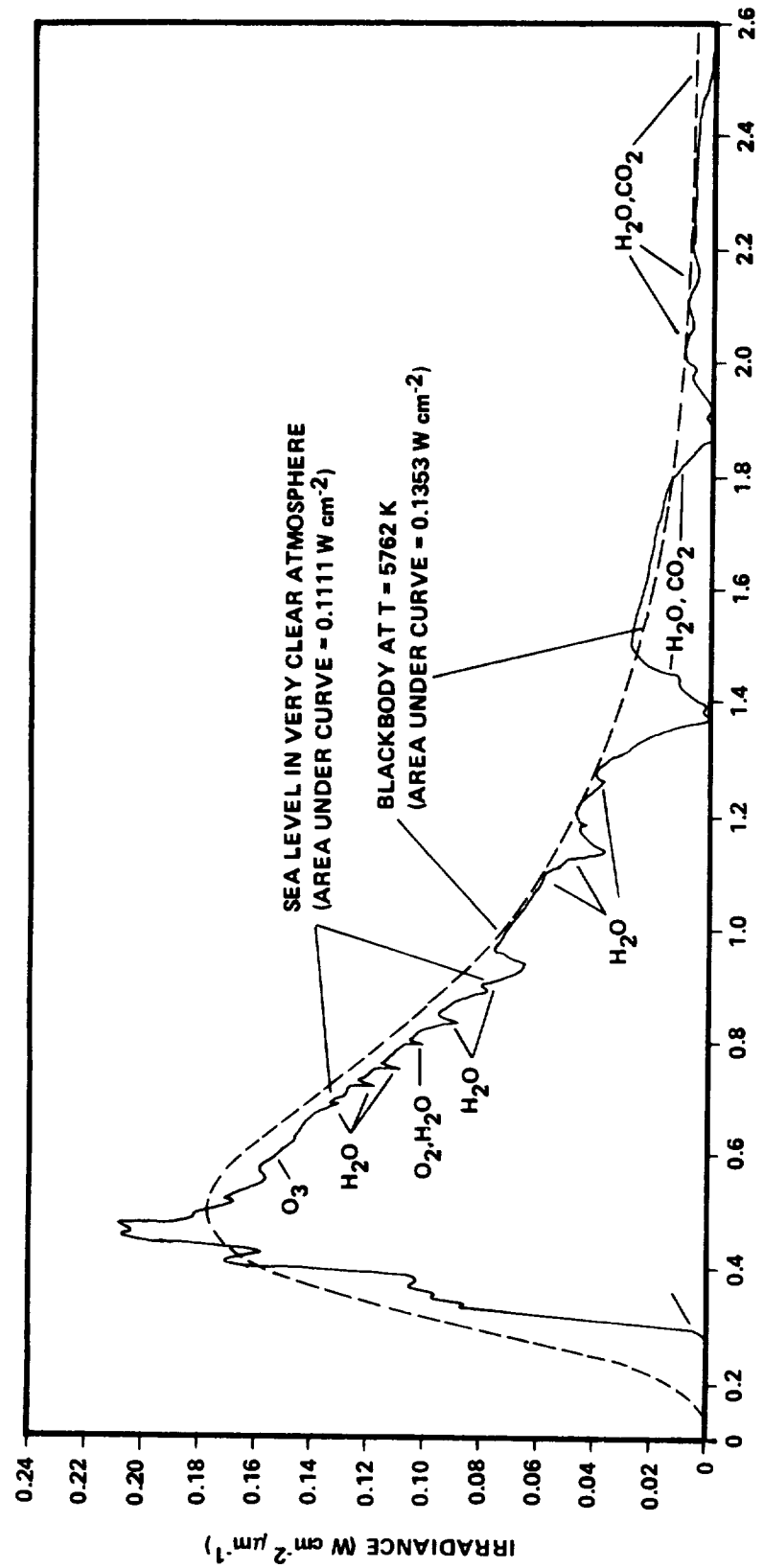

Figure 7.20 Normally incident solar radiation at sea level on very clear days, and blackbody spectral irradiance curve at T = 5762 K (normalized to 1 AU) [7.1].

where

I_N = intensity of solar radiation for N air mass thickness

N = number of air masses.

Equation (7.2) can also be used to obtain solar radiation intensities versus wavelengths for other total normal incident solar radiation intensities (area under curve) by computation of new values of atmospheric transmittance as follows:

$$M_N = M \frac{I_{TN}}{0.1111} \quad , \tag{7.3}$$

where

I_{TN} = new value of total normal incident solar radiation intensity in W cm^{-2}

M = value for atmospheric transmittance given in equation (7.1)

M_N = new value of atmospheric transmittance.

Equations (7.2) and (7.3) are valid only for locations relatively near the Earth' s surface (below 5-km altitude). For higher altitudes, corrections would be needed for the change of the amount of ozone and water vapor in the atmosphere. Also, equation (7.3) should be used only for values of I_{TN} greater than 0.0767 W cm^{-2} (1.10 cal cm^{-2} min^{-1}) since values lower than this would indicate a considerably higher ratio of water vapor to ozone in the atmosphere and require that the curve be adjusted to give more absorption in the infrared water vapor bands at long wavelengths (infrared) and a smaller increase for the ozone at shorter wavelengths.

7.3.1.4 Sky (Diffuse) Radiation

When solar radiation, which is a nearly parallel beam of light, enters the atmosphere of the Earth, molecules of air, dust particles, water vapor droplets, and aerosols either diffuse or absorb a part of the radiation. The diffuse radiation then reaches the Earth as nonparallel light from all directions.

7.3.1.5 Scattered Radiation

The scattered radiation gives the sky its brightness and color. The color is a result of selective scattering at certain wavelengths as a function of the size of the molecules and particles. On a clear day the amount of scattering is very low because there are few particles and water droplets. The clear sky can be as little as 10^{-6} times as bright as the surface of the Sun. The total energy contribution from the diffuse radiation from the entire sky hemisphere to a horizontal surface is only between 0.0007 and 0.014 W cm^{-2} (0.01 and 0.20 cal cm^{-2} min^{-1}).

As a blackbody radiator, the clear sky is considered equivalent to a cold source (Table 7.4). The temperature of the clear sky is the same during the daytime as at nightime. Values of sky radiation for several localities are given in Table 7.4. It is the clear sky at night acting as a cold sink, without the solar radiation heating the surface of the Earth, that causes air temperatures to be lower than the daytime values.

With clouds the amount of diffuse radiation is greater. The total hemisphere during an overcast day may contribute as much as 0.069 W cm^{-2} (1.0 cal cm^{-2} min^{-1}) of radiation to a horizontal surface.

The greater scattering by clouds makes the effective temperature of the clouds warmer than the clear air. At night the clouds act as a barrier to the outgoing radiation. Since they are warmer than the clear sky, the air near the ground will not cool to as low a temperature as will occur when the night is clear.

7.3.1.6 Absorbed Radiation

The various gases in the atmosphere selectively absorb some of the incoming radiation. Absorption changes some of the radiation into heat or radiation at wavelengths different from that received. Absorption by gases is observed in the solar spectrum as bands of various widths. The major gases in the Earth' s atmosphere, which show as absorption bands in the solar spectrum, are water vapor, carbon dioxide, ozone, and molecular oxygen.

TABLE 7.4 SURFACE AIR AND SKY RADIATION TEMPERATURE EXTREMES [7.1]

Area		Surface Air Temperature Extremes[a]				Sky Radiation	
		Maximum		Minimum		Extreme Minimum Equivalent Temperature	Equivalent Radiation ($g\text{-}cal\ cm^{-2}\ min^{-1}$)
		Extreme	95%[b]	Extreme	95%[b]		
Huntsville, Ala.	°C	40.0	36.7	-23.9	-12.8	-30.0	0.28
	°F	104	98	-11	9	-22	
Kennedy Space Center, Fla.	°C	37.2	33.3	-3.9	1.7	-15.0	0.36
	°F	99	92	25	35	5	
Space and Missile Test Center Vandenberg AFB, Calif.	°C	37.8	29.4	-3.3	1.1	-15.0	0.36
	°F	100	85	26	34	5	
Edwards AFB, Calif.	°C	45.0	41.7	-15.6	-7.8	-30.0	0.28
	°F	113	107	4	18	-22	
Honolulu, Oahu — Hickam Field	°C	33.9	32.8	11.1	15.6	-15.0	0.36
	°F	93	91	52	60	5	
Guam — Andersen AFB	°C	34.4	31.1	18.9	22.2	-15.0	0.36
	°F	94	88	66	72	5	
Santa Susana, Calif.	°C	42.2	36.1	-2.2	1.7	-15.0	0.36
	°F	108	97	28	35	5	
Thiokol Wasatch Division, Utah	°C	38.3	35.6	-27.8	-16.1	-30.0	0.28
	°F	101	96	-18	3	-22	
New Orleans, La.	°C	37.8	35.0	-10.0	-3.3	-17.8	0.35
	°F	100	95	14	26	0	
National Space Tech. Lab., Miss.	°C	37.8	35.6	-13.9	-2.2	-17.8	0.35
	°F	100	96	7	28	0	
Continent Transportation (rail, truck, river barge)	°C	47.2	—	-34.4	—	-30.0	0.28
	°F	117	—	-30	—	-22	
Ship Transportation (West Coast, Panama Canal, Gulf of Mexico)	°C	37.8	—	-12.2	—	-15.0	0.36
	°F	100	—	10	—	5	
Johnson Space Center, Tex.	°C	40.0	36.7	-9.4	-2.2	-17.8	0.35
	°F	104	98	15	28	0	
Wallops Flight Center, Va.	°C	37.2	33.3	-20.0	-5.6	-17.8	0.35
	°F	99	92	-4	22	0	
White Sands Missile Range, N.M.	°C	41.7	38.9	-23.9	-10.0	-30.0	0.28
	°F	107	102	-11	14	-22	

a. The extreme maximum and minimum temperatures will be encountered during periods of wind speeds less than about 1 meter per second.

b. Based on daily extreme (maximum or minimum) observations for worst month.

7.3.2 Total Solar Radiation

7.3.2.1 Introduction

The standard solar radiation sensors measure the intensity of direct solar radiation from the Sun falling on a horizontal surface plus the diffuse (sky) radiation from the total sky hemisphere. Diffuse radiation is lowest with dry clear air; it increases with increasing dust and moisture in the air. With extremely dense clouds or fog, the measured horizontal solar radiation (i.e., the solar radiation falling on a horizontal surface) will be nearly all diffuse radiation. The higher (≥ 95 percentile) values of measured horizontal solar radiation occur under clear skies or under conditions of scattered fair weather cumulus clouds which reflect additional solar radiation onto the measuring sensor.

In this report all solar radiation values given are intensities. Solar radiation intensities are measured in calories per square centimeter per minute by stations of the National Oceanic and Atmospheric Administration, National Weather Service; therefore, these units are used in this section. Intensities of solar radiation are numerically equal to solar insolation per minute, i.e., calories per square centimeter per minute.

7.3.2.2 Use of Solar Radiation in Design

When radiation data are used in design studies, the direct solar radiation should be applied from one direction as parallel rays, and, at the same time, the diffuse radiation should be applied as rays from all directions of a hemisphere (Fig. 7.21).

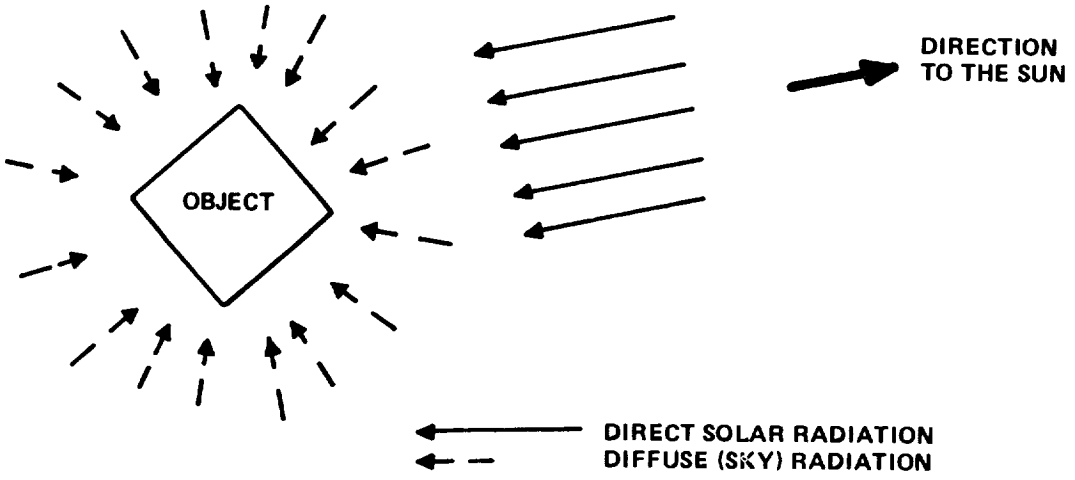

Figure 7.21 Method of applying radiation for design.

Because the Sun provides heat (from radiation) from a specific direction, differential heating of an object occurs; i.e., one part is heated more than another, resulting in stress and deformation.

7.3.2.3 Total Solar Radiation Extremes

Ten years of total horizontal solar and sky radiation data at two stations were analyzed to determine the frequency distribution of solar radiation for use in design in Reference 7.1.

7.3.2.3.1 Basic Data Computations

The basic data used were hourly totals of horizontal solar and sky radiation (I_{TH}) for each hour of the day for 10-year periods at each of two stations: Apalachicola, Florida, and Santa Maria, California. The hourly totals were divided by 60 to obtain the average solar radiation values per minute for each hour. The average values per minute are numerically equal to intensity, and these values were used in the computations of frequency distributions. The diffuse sky radiation intensities I_{DH} were empirically estimated for each value based on the amount of total horizontal solar and sky radiation and solar altitude. After the diffuse sky radiation is subtracted from the total horizontal solar and sky radiation, the resultant horizontal solar radiation I can be used to compute the direct normal incident solar radiation I_{DN} by using the following equation:

$$I_{DN} = \frac{I}{\sin b} \quad , \tag{7.4}$$

where

I_{DN} = direct normal incident solar radiation

I = horizontal solar radiation = $I_{TH} - I_{DH}$

b = Sun's altitude.

The angle b is based on a horizon system of coordinates such as those used by surveyors and astronomers.

The total normal incident solar radiation I_{TN} values were found by adding the direct normal incident solar radiation I_{DN} and the diffuse sky radiation I_{DH} previously estimated. This method of finding the total normal incident solar radiation may result in a slight overestimate of the value for low solar altitudes because the sky hemisphere is intercepted by the ground surface. This error is insignificant, however, when extreme values are used and would be small for values equal to or greater than the mean plus one standard deviation.

Total solar radiation intensities on a south-facing surface, with the normal to the surface at 45 deg to the horizontal, are calculated as follows:

$$I_{D45} = I(\sin 45 \text{ deg} + \cot b \cos a \cos 45 \text{ deg}) \quad , \tag{7.5}$$

where

I_{D45} = intensity of direct solar radiation on a south-facing surface, with normal 45 deg to the horizontal

I = horizontal solar radiation = $I_{TH} - I_{DH}$

a = Sun's azimuth measured from south direction

b = Sun's altitude.

7.3.2.3.2 Solar Radiation Extreme and 95 Percentile

Reference 7.1 presents the solar radiation data in a simplified form; the month of June was selected to represent the summer and the longest period of daylight, and December represents the winter and shortest period of daylight. The June data for normal incident solar radiation from Santa Maria, California, were increased for the period from 1100 to 1900 h to reflect the higher values which occur early in July (first week) during the afternoon. Tables 7.5 and 7.6 give the frequency distributions for the extreme values (highest measured value of record) and the 95 percentile values of solar radiation for hours of the day. The values given for diffuse radiation are the values which occurred associated

TABLE 7.5 EXTREME VALUES OF SOLAR RADIATION FOR THE SPACE AND MISSILE TEST CENTER, WEST COAST TRANSPORTATION, SANTA SUSANA, WHITE SANDS MISSILE RANGE, BRIGHAM CITY, AND EDWARDS AFB [7.1]

TIME OF DAY (Local Standard Time)	Total Horizontal Solar Radiation g-cal cm^{-2} min^{-1}		Diffuse Radiation Associated with Total Horizontal Solar Radiation Extremes g-cal cm^{-2} min^{-1}		Total Normal Incident Solar Radiation g-cal cm^{-2} min^{-1}		Total 45° Surface Solar Radiation g-cal cm^{-2} min^{-1}	
	JUNE							
	EXTREME	95 Percentile	EXTREME	95 Percentile	EXTREME	95 Percentile	EXTREME	95 Percentile
0500	0	0	0	0	0	0	0	0
0600	0.16	0.11	.02	.04	1.14	0.78	0.04	0
0700	0.46	0.40	.05	.08	1.34	1.08	0.19	0.16
0800	0.82	0.76	.06	.09	1.54	1.38	0.34	0.31
0900	1.16	1.11	.04	.08	1.74	1.62	0.84	0.77
1000	1.45	1.42	0	.03	1.79	1.71	1.19	1.12
1100	1.64	1.56	0	.10	1.79	1.69	1.39	1.31
1200	1.69	1.63	0	.08	1.74	1.68	1.49	1.38
1300	1.69	1.64	0	.07	1.74	1.68	1.49	1.40
1400	1.59	1.54	.06	.12	1.74	1.68	1.34	1.29
1500	1.45	1.39	0	.06	1.79	1.70	1.14	1.09
1600	1.21	1.19	0	.02	1.79	1.71	0.89	0.78
1700	0.87	0.83	.03	.05	1.69	1.60	0.34	0.18
1800	0.46	0.42	.05	.08	1.39	1.23	0.19	0.13
1900	0.14	0.12	.02	.04	1.19	0.93	0.04	0
2000	0	0	0	0	0	0	0	0
	DECEMBER							
	EXTREME	95 Percentile	EXTREME	95 Percentile	EXTREME	95 Percentile	EXTREME	95 Percentile
0800	0	0	0	0	0	0	0	0
0900	0.35	0.32	0.04	0.05	1.59	1.39	0.99	0.85
1000	0.65	0.60	0.03	0.05	1.64	1.53	1.29	1.21
1100	0.86	0.80	0	0.04	1.84	1.64	1.64	1.49
1200	0.96	0.89	0.02	0.06	1.79	1.69	1.74	1.63
1300	0.99	0.89	0	0.06	1.84	1.70	1.79	1.64
1400	0.85	0.80	0.01	0.04	1.79	1.64	1.59	1.49
1500	0.66	0.60	0.02	0.05	1.69	1.54	1.34	1.21
1600	0.38	0.31	0.02	0.05	1.64	1.38	1.04	0.87
1700	0	0	0	0	0	0	0	0

TABLE 7.6 EXTREME VALUES OF SOLAR RADIATION FOR EASTERN TEST RANGE, NSTL, JSC, NEW ORLEANS, GULF TRANSPORTATION, AND HUNTSVILLE [7.1]

TIME OF DAY (Local Standard Time)	Total Horizontal Solar Radiation g-cal cm^{-2} min^{-1}		Diffuse Radiation Associated with Total Horizontal Solar Radiation Extremes g-cal cm^{-2} min^{-1}		Total Normal Incident Solar Radiation g-cal cm^{-2} min^{-1}		Total 45° Surface Solar Radiation g-cal cm^{-2} min^{-1}	
	JUNE							
	EXTREME	95 Percentile	EXTREME	95 Percentile	EXTREME	95 Percentile	EXTREME	95 Percentile
0500	0	0	0	0	0	0	0	0
0600	0.12	0.07	0	0	1.09	1.00	0	0
0700	0.42	0.36	0.05	0.07	1.29	1.04	0.19	0.16
0800	0.82	0.71	0.04	0.10	1.59	1.30	0.34	0.27
0900	1.23	1.02	0	0.10	1.59	1.48	0.49	0.41
1000	1.35	1.30	0.02	0.06	1.59	1.54	0.99	0.95
1100	1.52	1.45	0.03	0.09	1.59	1.54	1.19	1.14
1200	1.58	1.53	0.10	0.16	1.64	1.55	1.29	1.24
1300	1.58	1.50	0.10	0.20	1.64	1.53	1.29	1.24
1400	1.50	1.44	0.05	0.12	1.59	1.52	1.19	1.09
1500	1.35	1.30	0.02	0.06	1.59	1.52	1.04	0.95
1600	1.10	1.01	0.05	0.12	1.54	1.44	0.54	0.44
1700	0.77	0.72	0.05	0.09	1.49	1.33	0.34	0.30
1800	0.48	0.40	0.03	0.06	1.44	1.14	0.19	0.18
1900	0.11	0.08	0	0	1.14	1.00	0.14	0.03
2000	0	0	0	0	0	0	0	0
	DECEMBER							
	EXTREME	95 Percentile	EXTREME	95 Percentile	EXTREME	95 Percentile	EXTREME	95 Percentile
0700	0	0	0	0	0	0	0	0
0800	0.16	0.10	0	0	1.34	1.12	0.64	0.50
0900	0.46	0.42	0.04	0.06	1.44	1.36	0.94	0.89
1000	0.79	0.71	0.01	0.07	1.69	1.60	1.39	1.29
1100	0.95	0.92	0.02	0.04	1.79	1.68	1.64	1.56
1200	1.09	1.02	0	0.03	1.79	1.70	1.74	1.66
1300	1.05	1.02	0	0.03	1.79	1.78	1.74	1.66
1400	0.94	0.89	0.02	0.05	1.74	1.67	1.59	1.63
1500	0.79	0.70	0	0.03	1.74	1.57	1.39	1.27
1600	0.46	0.41	0.04	0.06	1.54	1.40	0.99	0.91
1700	0.16	0.10	0	0	1.34	1.12	0.64	0.50
1800	0	0	0	0	0	0	0	0

with the other extreme and 95 percentile values of the other solar radiations given. Since the diffuse radiation decreases with increasing horizontal radiation, the values given in Tables 7.5 and 7.6 are considerably lower than the highest values of diffuse radiation occurring during the period of record. Solar radiation data recommended for use in design are given in Table 7.7 and Figure 7.22 and are valid for all areas.

TABLE 7.7 RECOMMENDED DESIGN SOLAR RADIATION DATA [7.1]

Time of Day (h)	Design High Solar Radiation Btu/ft²/h	(gm-cal/cm²/min)	Design Low Solar Radiation Btu/ft²/h	(gm-cal/cm²/min)
0500	0	0.00	0	0.00
1100	363	1.64	70	0.32
1300			80	0.36
1400	363	1.64		
2000	0	0.00	0	0.00

7.3.2.3.3 Variation with Altitude

Solar radiation intensity on a surface will increase with altitude above the Earth's surface, with clear skies, according to the following equation:

$$I_H = I_{DN} + (1.94 - I_{DN}) \left(1 - \frac{\rho_H}{\rho_S}\right) \quad , \tag{7.6}$$

where

I_H = intensity of solar radiation normal to surface at required height

I_{DN} = intensity of solar radiation normal to surface at the Earth's surface assuming clear skies ($I_{DN} = I_{TN} - I_{DH}$)

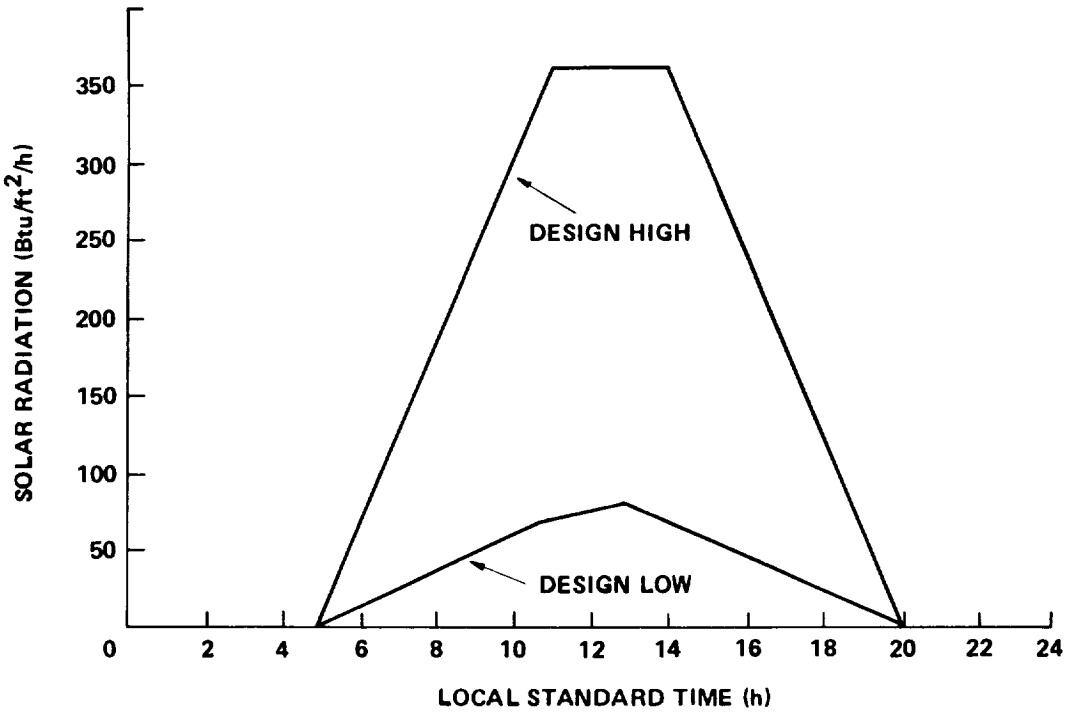

Figure 7.22 Recommended design solar radiation data [7.1].

ρ_H = atmospheric density at required height (from U.S. Standard, U.S. Supplemental Atmospheres) (kg m^{-3})

ρ_S = atmospheric density at sea level (from U.S. Standard, U.S. Supplemental Atmospheres) (kg m^{-3})

1.94 = solar constant (cal cm^{-2} min^{-1}).

The diffuse radiation I_{DH} decreases with altitude above the Earth's surface, with clear skies. A good estimate of the value can be obtained from the following equation based on a cloudless and dust-free atmosphere:

$$I_{DH} = 0.7500 - 0.4076\, I_H \quad , \tag{7.7}$$

where I_{DH} = intensity of diffuse radiation and I_H = intensity of solar radiation normal to surface. Equation (7.7) is valid for values of I_H from equation (7.6) up to 1.84 cal cm^{-2} min^{-1}. For values of I_H greater than 1.84 cal cm^{-2} min^{-1}, $I_{DH} = 0$.

7.3.2.3.4 Solar Radiation during Extreme Conditions

When ground winds occur exceeding the 95, 99, or 99.9 percentile design winds, the associated weather normally is such that clouds, rain, or dust is generally present; therefore, the intensity of the incoming solar radiation will be less than the maximum values given in Tables 7.5 and 7.6. Maximum values of solar radiation intensity to use with corresponding wind speeds are given in Table 7.8.

7.3.3 Temperature

Several types of temperatures at the Earth's boundary layer may be considered in design. These are as follows:

1) Air temperature normally measured at 1.22 m (4 ft) above a grass surface

2) Changes of air temperature (usually the changes which occur in less than 24 h are considered)

3) Surface or skin temperature measured of a surface exposed to radiation

4) Temperatures within a closed compartment.

7.3.3.1 Air Temperature Near the Surface

Surface air temperature extremes (maximum, minimum, and the 95 percentile values) and the extreme minimum sky radiation (equal to the outgoing radiation) are given in Table 7.4 for various geographical areas. Maximum and minimum temperature values should be expected to last only a few hours during a daily period. Generally, the maximum temperature is reached after midday and before sunset, while the minimum temperature is reached just before sunrise.

TABLE 7.8 SOLAR RADIATION MAXIMUM VALUES ASSOCIATED WITH EXTREME WIND VALUES [7.1]

Maximum Solar Radiation (Normal Incident)						
Steady-State Ground Wind Speed at 18-m Height	Huntsville, New Orleans, NSTL, JSC Gulf Transportation, Eastern Test Range, Western Test Range, West Coast Transportation and Wallops Test Range			White Sands Missile Range		
($m\ s^{-1}$)	($kJ\ m^{-2}\ s^{-1}$)	($gm\text{-}cal\ cm^{-2}\ min^{-1}$)	($Btu\ ft^{-2}\ h^{-1}$)	($kJ\ m^{-2}\ s^{-1}$)	($gm\text{-}cal\ cm^{-2}\ min^{-1}$)	($Btu\ ft^{-2}\ h^{-1}$)
10	0.84	1.20	265	1.05	1.50	332
15	0.56	0.80	177	0.70	1.00	221
≥ 20	0.35	0.50	111	0.56	0.80	177

Temperature distribution maps of the United States mainland are given in Figures 7.23 through 7.29 [7.4] for:

1) Average annual

2) Average January

3) Average July

4) Average annual maximum

5) Average annual minimum

6) Highest ever observed

7) Lowest ever observed.

These data were measured over the period 1899 to 1938 at 200 first-order Weather Bureau stations.

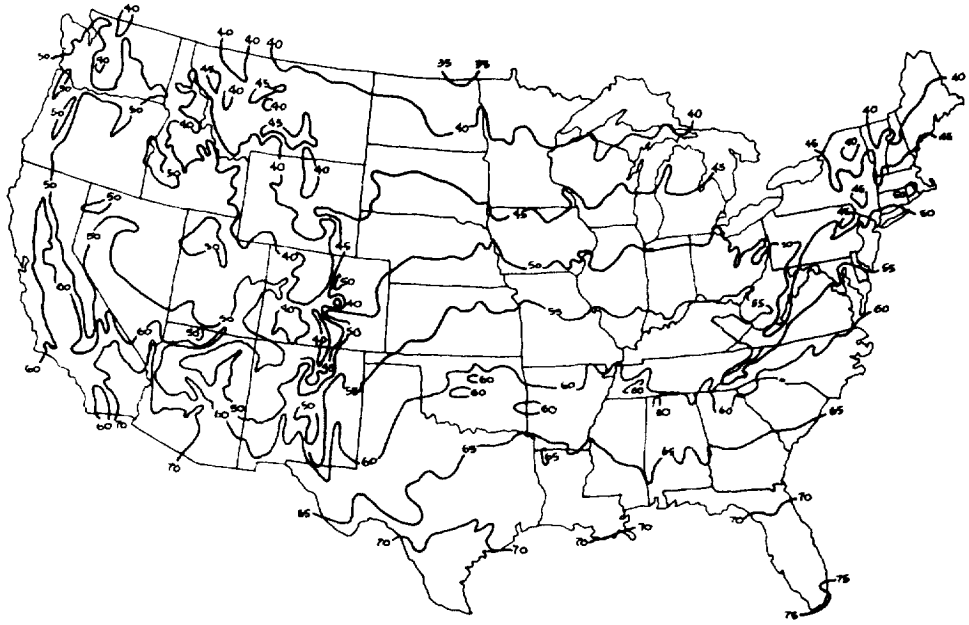

Figure 7.23 Average annual temperature (°F) [7.4].

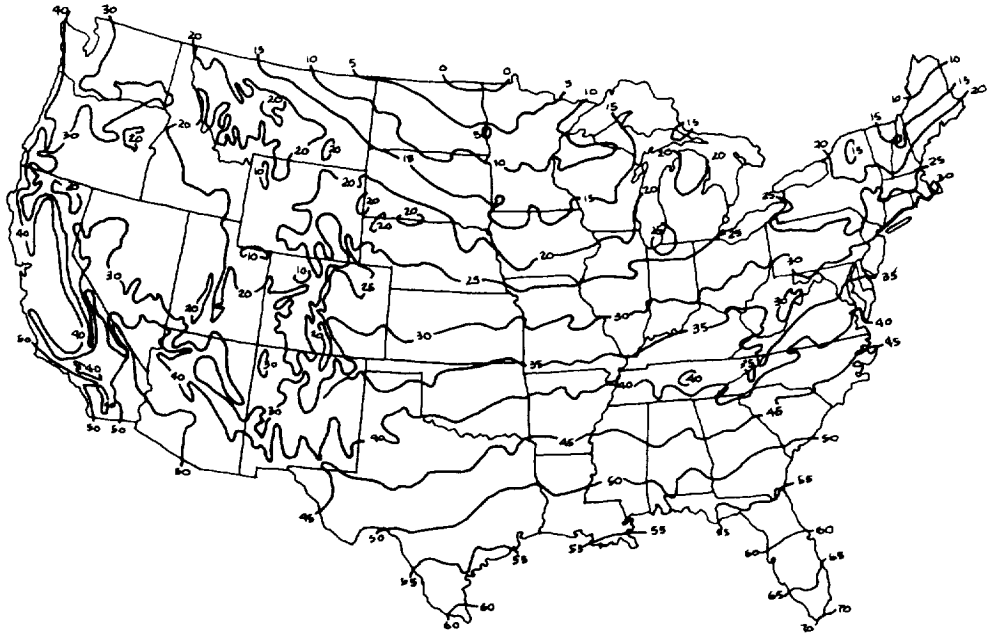

Figure 7.24 Average January temperature (°F) [7.4].

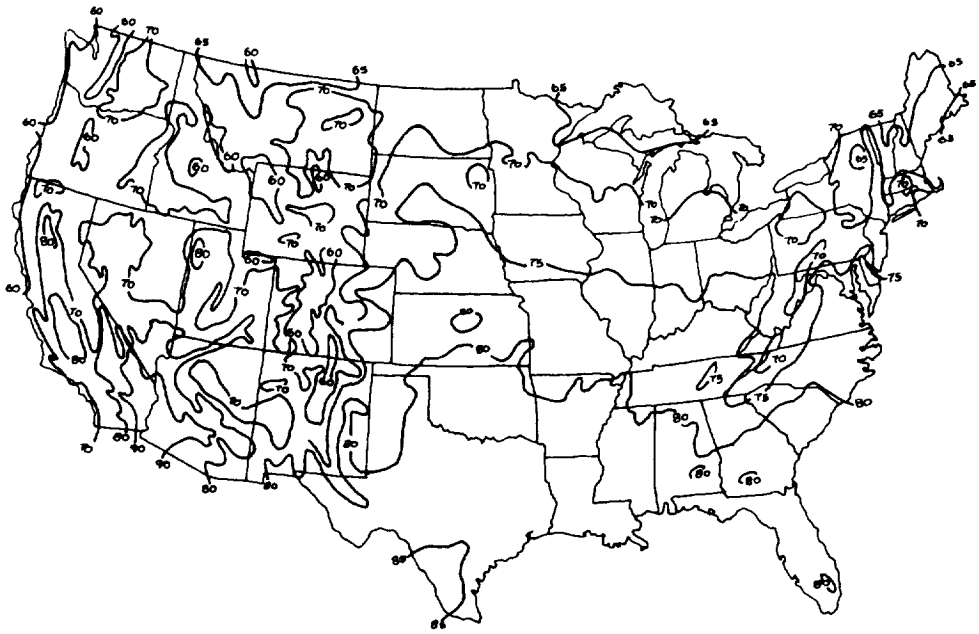

Figure 7.25 Average July temperature (°F) [7.4].

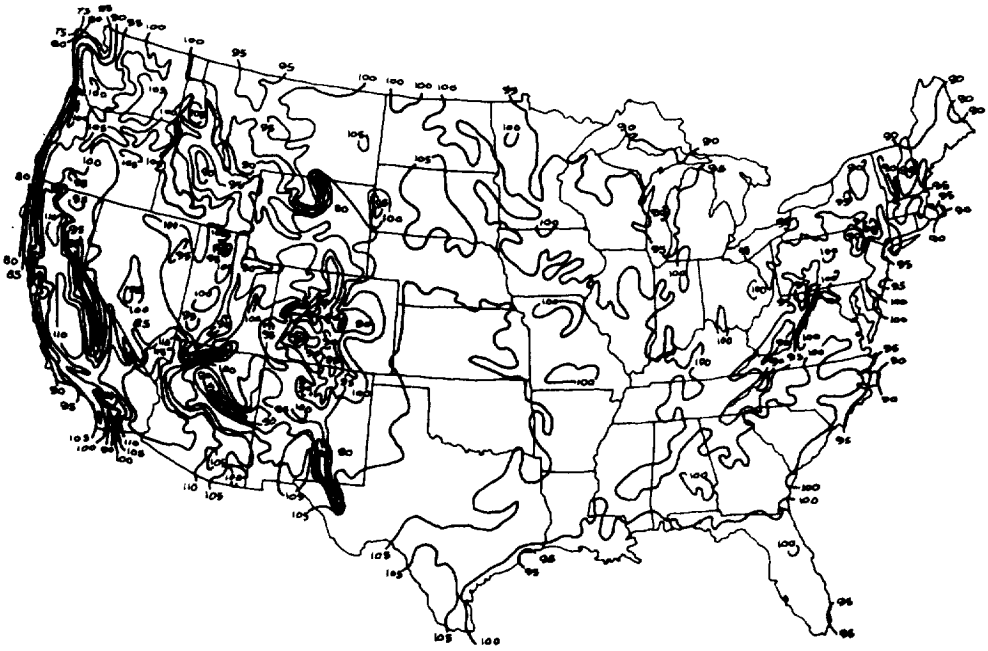

Figure 7.26 Average annual extreme maximum temperature (°F) [7.4].

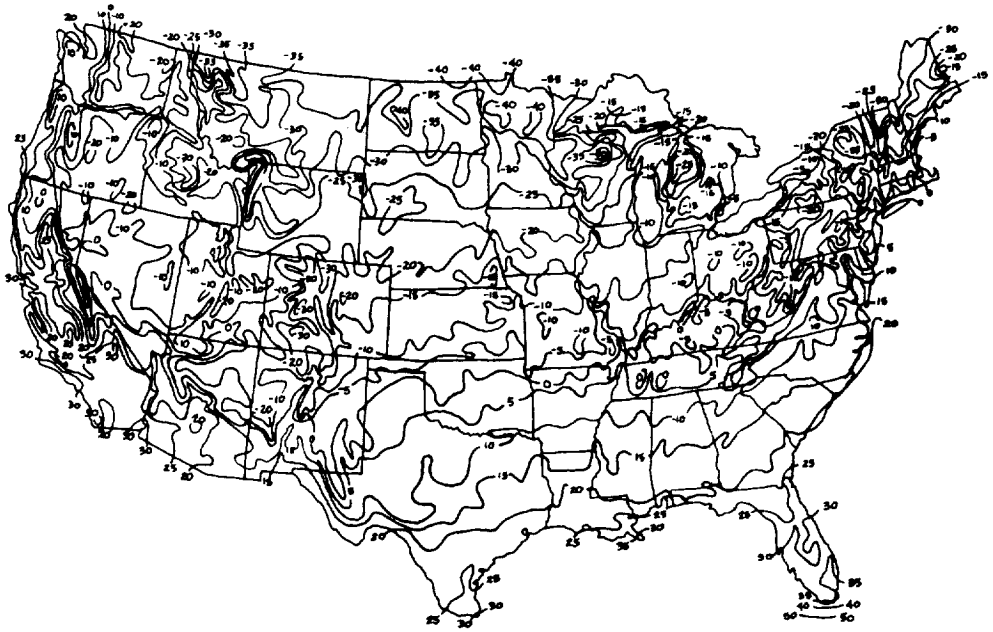

Figure 7.27 Average annual extreme minimum temperature (°F) [7.4].

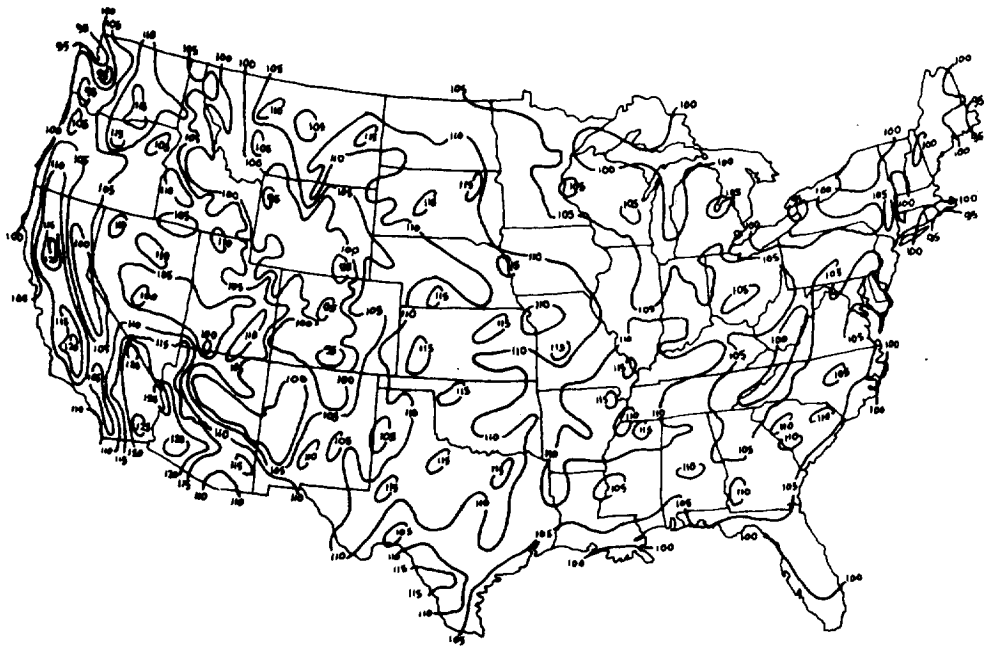

Figure 7.28 Highest temperatures ever observed (°F) [7.4].

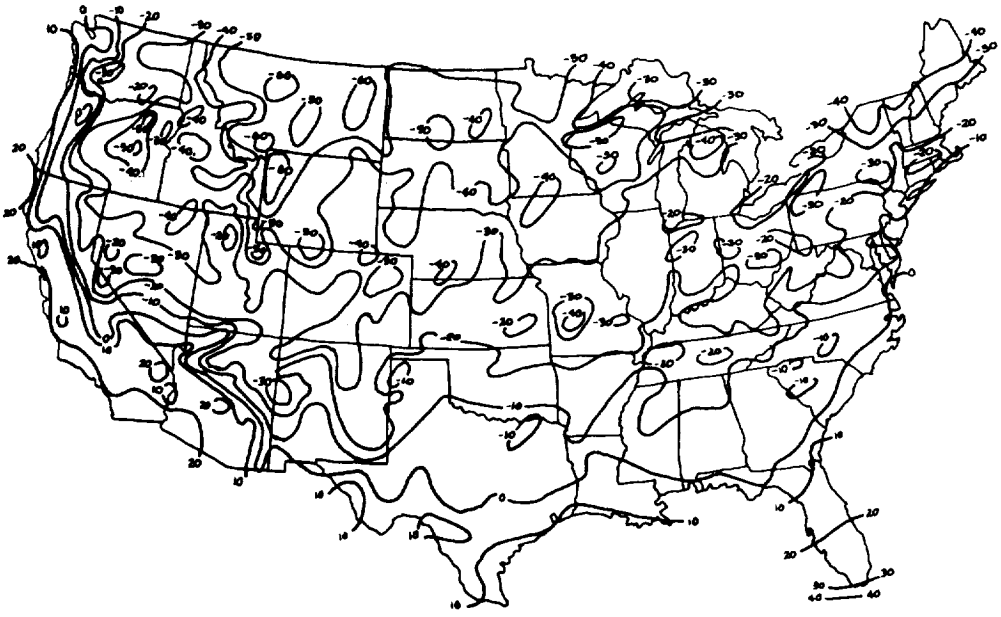

Figure 7.29 Lowest temperatures ever observed (°F) [7.4].

The annual temperature range for WTG design from these maps is 46 to -40°C (115 to -40°F), and the extreme temperature range is 52 to -51°C (125 to -60°F), exclusive of Alaska.

7.3.3.2 Extreme Air Temperature Change

For all areas the design values of extreme air temperature changes (thermal shock) are:

1) An increase of air temperature of 10°C (18°F) with a simultaneous increase of solar radiation (measured on a normal surface) from 0.50 cal cm^{-2} min^{-1} (110 Btu ft^{-2} h^{-1}) to 1.85 cal cm^{-2} min^{-1} (410 Btu ft^{-2} h^{-1}) may occur in a 1-h period. Likewise, the reverse change of the same mangitude may occur for decreasing air temperature and solar radiation.

2) A 24-h change may occur with an increase of 27.7°C (50°F) in air temperature in a 5-h period, followed by 4 h of constant air temperature, then a decrease of 27.7°C (50°F) in a 5-h period, followed by 10 h of constant air temperature.

Although data are not available for the entire United States; for Kennedy Space Center, Florida, the 99.9 percentile air temperature changes are as follows [7.1]:

1) An increase of air temperature of 5.6°C (11°F) with a simultaneous increase of solar radiation (measured on a normal surface) from 0.50 cal cm^{-2} min^{-1} (110 Btu ft^{-2} h^{-1}) to 1.60 cal cm^{-2} min^{-1} (354 Btu ft^{-2} h^{-1}), or a decrease of air temperature of 9.4°C (17°F) with a simultaneous decrease of solar radiation from 1.60 cal cm^{-2} min^{-1} (354 Btu ft^{-2} h^{-1}) to 0.50 cal cm^{-2} min^{-1} (110 Btu ft^{-2} h^{-1}) may occur in a 1-h period.

2) A 24-h temperature change may occur as follows: an increase of 16.1°C (29°F) in air temperature (wind speed under 5 m/s) in an 8-h period, followed by 2 h of constant air temperature (wind speed under 5 m/s), then a decrease of 21.7°C (39°F) in air temperature (wind speed between 7 and 10 m/s) in a 14-h period.

7.3.3.3 Surface (Skin) Temperature

The temperature of the surface of an object exposed to solar, day sky, or night sky radiation is usually different from the air temperature. The amount of the extreme difference in temperature between the object and the surrounding

air temperature is given in Table 7.9 and Figure 7.30(a) for exposure to a clear night (or day) sky or to the Sun on a clear day. Without the Sun's rays striking, the daytime sky is about as cold as the nighttime sky. Since the flow of air across an object changes the balance between the heat transfers from radiation and convection-conduction between the air and the object, the difference in the temperature between the air and the object will decrease with increasing wind speed. Figure 7.30(b) provides information for making the corrections for wind speed. Values are tabulated in Table 7.9 for various wind speeds.

7.4 Atmospheric Corrosion and Abrasion

Corrosion and abrasion are important considerations in the design of WTG since candidate WTG sites are seacoasts or flat, dry, semidesert areas. The former constitutes a corrosive atmosphere due to the salt-laden oceanic air, while the latter creates an abrasive atmosphere due to the wind-driven solid particles of sand, dust, silt, etc. The limited data available to provide design inputs for these environments are summarized from Reference 7.1.

7.4.1 Corrosion

Salt spray or salt fog causes corrosion of many materials. Wind moving over roughened sea surfaces enhances the suspension of small droplets of salt-water in the air. Many droplets are small enough to remain suspended for long periods of time and may be transported significant distances. When these salt droplets and tiny salt particles accumulate on the surface of objects, a film of highly concentrated salt results. When the atmospheric moisture condition becomes saturated, or when light rain or drizzle occurs, these salt films become highly concentrated solutions, causing corrosion of many materials. Salt solutions provide a conductive path between voltage potentials in electrical circuits which alter or completely short out the flow of electricity. Also, corrosion by electrolytic action can result when two dissimilar metals are involved. Numerous other objects, organic or inorganic, are affected by ocean salt as well as other impurities dispersed by the atmosphere.

The amount of corrosion is a function of several factors. Among the most important factors are [7.7]:

1) The distance of the exposed WTG site from the ocean

2) Air temperature

TABLE 7.9 EXTREME SURFACE (SKIN) TEMPERATURE ABOVE OR BELOW AIR TEMPERATURE OF AN OBJECT NEAR THE EARTH'S SURFACE

Air Temperature (°C)	Surface Temperature Differential (°C)									
	Clear Night					Clear Day				
	Wind Speed ($m\ s^{-1}$)					Wind Speed ($m\ s^{-1}$)				
	0	2	4	10	20	0	2	4	10	20
	Correction Factor					Correction Factor				
	1.00	0.25	0.17	0.11	0.08	1.00	0.25	0.17	0.11	0.08
-25	-5.0	-1.2	-0.8	-0.6	-0.4	16.9	4.2	2.9	1.9	1.4
-20	-6.5	-1.6	-1.1	-0.7	-0.5	19.2	4.8	3.3	2.1	1.5
-15	-8.2	-2.0	-1.4	-0.9	-0.6	22.0	5.5	3.7	2.4	1.8
-10	-10.2	-2.6	-1.7	-1.1	-0.8	25.1	6.3	4.3	2.8	2.0
-5	-12.2	-3.0	-2.1	-1.3	-1.0	28.5	7.1	4.8	3.1	2.3
0	-14.5	-3.6	-2.5	-1.6	-1.2	32.0	8.0	5.4	3.5	2.6
5	-16.9	-4.2	-2.9	-1.9	-1.4	36.0	9.0	6.1	4.0	2.9
10	-19.4	-4.8	-3.3	-2.1	-1.6	40.0	10.0	6.8	4.4	3.2
15	-21.9	-5.5	-3.7	-2.4	-1.8	44.0	11.0	7.5	4.8	3.5
20	-24.6	-6.2	-4.2	-2.7	-2.0	48.0	12.0	8.2	5.3	3.8
25	-27.4	-6.8	-4.6	-3.0	-2.2	52.0	13.0	8.8	5.7	4.2
30	-30.5	-7.6	-5.2	-3.4	-2.4	56.0	14.0	9.5	6.2	4.5
35	-34.0	-8.5	-5.8	-3.7	-2.7	60.0	15.0	10.2	6.6	4.8
40	-37.7	-9.4	-6.4	-4.1	-3.0	64.0	16.0	10.9	7.0	5.1
45	-41.7	-10.4	-7.1	-4.6	-3.3	68.0	17.0	11.6	7.5	5.4

Note: Values are given for an emittance value of 1.0. Temperature differences for other emittance can be determined by multiplying tabular value by the appropriate emittance.

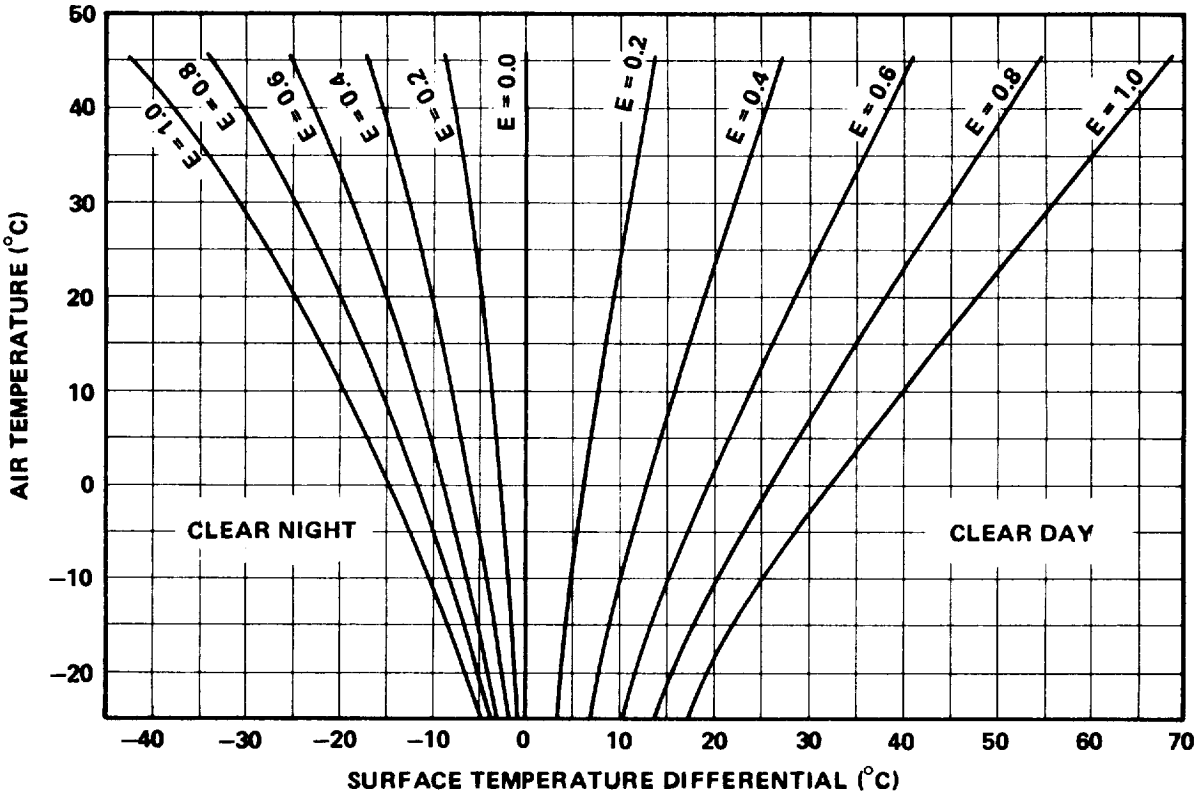

(a) SURFACE TEMPERATURE DIFFERENTIALS WITH RESPECT TO AIR TEMPERATURE FOR SURFACE OF EMITTANCE FROM 0.0 TO 1.0 FOR CALM WIND CONDITIONS. TEMPERATURE DIFFERENCE AFTER CORRECTION FOR WIND IS TO BE ADDED OR SUBTRACTED TO THE AIR TEMPERATURE TO GIVE SURFACE (SKIN) TEMPERATURE

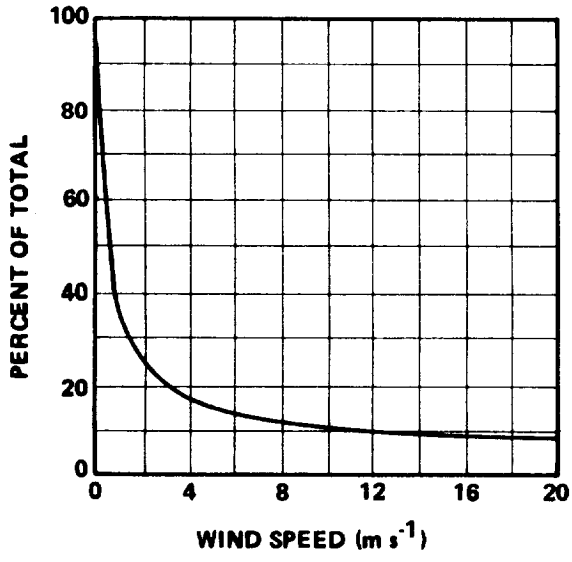

(b) CORRECTION FOR WIND SPEED OBTAINED FROM GRAPH A. VALID ONLY FOR A PRESSURE OF ONE ATMOSPHERE

Figure 7.30 Extreme surface (skin) temperature of an object near the Earth's surface (0 to 300 m) for clear sky.

3) Elevation above sea level

4) Time of high humidity

5) Exposure direction, shelter around or near the material, and the direction and magnitude of the prevailing winds.

The accumulation of salt on exposed surfaces is greatest during onshore winds when many waves are breaking and forming white caps. Extremes expected are as follows [7.8]:

1) Particle size: range from 0.1 to 30 μm, with 98 percent of the total mass greater than 0.8 μm.

2) Fallout of salt particles on eastern coast:

a) Maximum: 5.0×10^{-7} gm cm^{-2} day^{-1}, to produce a coating on an exposed surface of 100 μm day^{-1}. This maximum usually occurs during precipitation.

b) Minimum: 2.5×10^{-8} gm cm^{-2} day^{-1}, to produce a coating on an exposed surface averaging 5 μm day^{-1}. This fallout occurs continuously during periods of no precipitation and is independent of wind direction. This coating will not usually be of uniform thickness but will be spots of salt particles unevenly distributed over the open surfaces.

7.4.2 Atmospheric Abrasion

Solid particles (sand, dust, silt, etc.) carried by the wind can remove protective coatings of objects upon impact. Painted surfaces can become seriously scratched, abraded, and even pitted by the large variety of airborne particles. Under low wind speed conditions, damage results when the hardness of particulates is equal to or greater than exposed surfaces. Particles moved by high wind speeds, even particles with lesser hardness than the surfaces on which they impact, can cause abrasion.

Particle hardness is expressed according to Mohs' hardness scale. It is based on the relative hardness of 10 minerals as shown in Table 7.10 [7.9].

TABLE 7.10 MOHS' SCALE-OF-HARDNESS FOR MINERALS

Mohs' Relative Hardness	Mineral	Mohs' Relative Hardness	Mineral
1	Talc	6	Orthoclase
2	Gypsum	7	Quartz
3	Calcite	8	Topaz
4	Fluorite	9	Corundum
5	Apatite	10	Diamond

More than 50 percent of the sand and dust particles carried by the wind will be composed of angular quartz or harder material, with a hardness of seven to eight.

The presence of sand and dust can be expected in all geographical areas of interest but will occur more frequently in the areas with lower water vapor concentration. The extreme values of particle size and density expected are as follows.

7.4.2.1 Size of Particles

Sand particles will be between 0.080 mm (0.0031 in.) and 1.0 mm (0.039 in.) in diameter. At least 90 percent of the particles will be between 0.080 mm (0.0031 in.) and 0.30 mm (0.012 in.) in diameter.

Dust particles will be between 0.0001 mm (0.0000039 in.) and 0.080 mm (0.0031 in.) in diameter. At least 90 percent of these particles will be between 0.0001 mm (0.0000039 in.) and 0.002 mm (0.000079 in.) in diameter.

7.4.2.2 Number and Distribution of Particles

For a wind speed of 10 m s^{-1} (19.4 knots) at 3 m (9.8 ft) above a surface and relative humidity of 30 percent or less, 0.02 gm cm^{-3} (1.2 lb ft^{-3}) of sand will be suspended in the atmosphere during a sand storm. Under these conditions,

10 percent of the sand grains will be between 0.02 m (0.079 ft) and 1.0 m (3.3 ft) above the ground surface, with the remaining 90 percent below 0.02 m (0.079 ft), unless disturbed by an object moving through the storm. When the wind speed decreases below 10 m s^{-1} (19.4 knots), the sand grains will be distributed over a smaller distance above the ground surface, while a steady state wind speed below 5 m s^{-1} (9.7 knots) will not be sufficient to set the grains of sand in motion. As the wind speed increases above 10 m s^{-1} (19.4 knots), the sand grains will be distributed over higher and higher distances above the ground surface.

For a wind speed of 10 m s^{-1} (19.4 knots) at 3 m (9.8 ft) above surface and relative humidity of 30 percent or less, 6×10^{-9} g cm^{-3} (3.7×10^{-7} lb ft^{-3}) of dust will be suspended in the atmosphere. Distribution will be uniform to approximately 200 m (656 ft) above the ground.

Sharp-edged dust (fine sand) particles up to 150 μ in size may penetrate into cracks, crevices, bearings, and joints in all mechanical, electrical, electronic, electrochemical, and electromechanical devices for which exposure to the effects of a dry dust (fine sand) laden atmosphere is anticipated. The general effects resulting from the penetration of dust can cause a variety of damage such as fouling moving parts, making relays inoperative, forming electrically conductive bridges with resulting shorts, and acting as a nucleus for the collection of water vapor, and hence a source of possible corrosion and malfunction of equipment. Thus, design to avoid dust and sand particles of the indicated size is important for WTG's.

7.5 Humidity

Humidity can play a significant role in the design of WTG's. Minute particulate material suspended in the air tends to settle on any surface. When combined with moisture, such debris can become very corrosive and react with many things on which it is deposited. Water is a dissolving agent and associates with almost everything it comes into contact with. In general, water is the most important single agent affecting the surface of the Earth, and all materials exposed to the substance commonly undergo some chemical or physical change. Degradation of surfaces where dissimilar metals are in contact can take place at a rapid rate in the presence of moisture.

Moreover, atmospheric humidity can impair or alter the performance of electronic equipment. Some of the primary problems are:

1) Dielectric constants of capacitors in tuned networks can change with variations of humidity.

2) Electronic components may deteriorate as a result of metallic corrosion, and electrode chemical reactions with components can take place with the presence of moisture; examples of these are corrosive buildup on inductors and parametric changes of components due to the formation of condensing vapor across contacts.

3) The increase of humidity tends to decrease the breakdown voltage between potentials.

These are a few problems that are identifiable when working with electronic components in a humid environment.

High humidity and warm air temperature accelerate the organic growth of bacteria and fungi; whereas a decrease in the temperature of the air to the dew point will result in the condensation of water vapor from the atmosphere into the liquid or frozen state.

Figure 7-31 gives the average relative humidity distribution for the United States during the months of January, occurring at 8 am (EST), and July at noon (Local Time) [7.4].

More important than the average humidity is the level of the cyclic exposure to humidity during diurnal variation. Temperature cycling provides alternate periods of condensation and evaporation essential to the development of corrosion processes and produces a "breathing" action which tends to force moisture into partially sealed components and containers. Reference 7.1 defines the extreme, high vapor concentration cycle for the southeast coast and Gulf region and the southwest coastal region (Figs. 7.32 and 7.33).

The Space Shuttle Program, Shuttle Master Verification Plan document, also states that the humidity and other environmental parameter tests will use the procedures given in "Military Standards 810B."

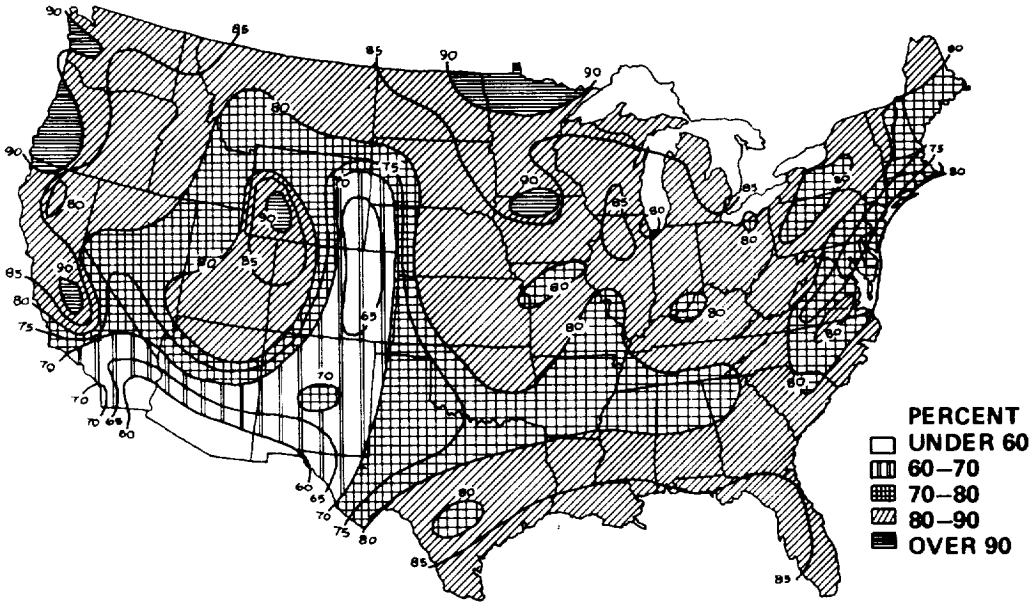

(a) 8 am (EST), JANUARY [7.4].

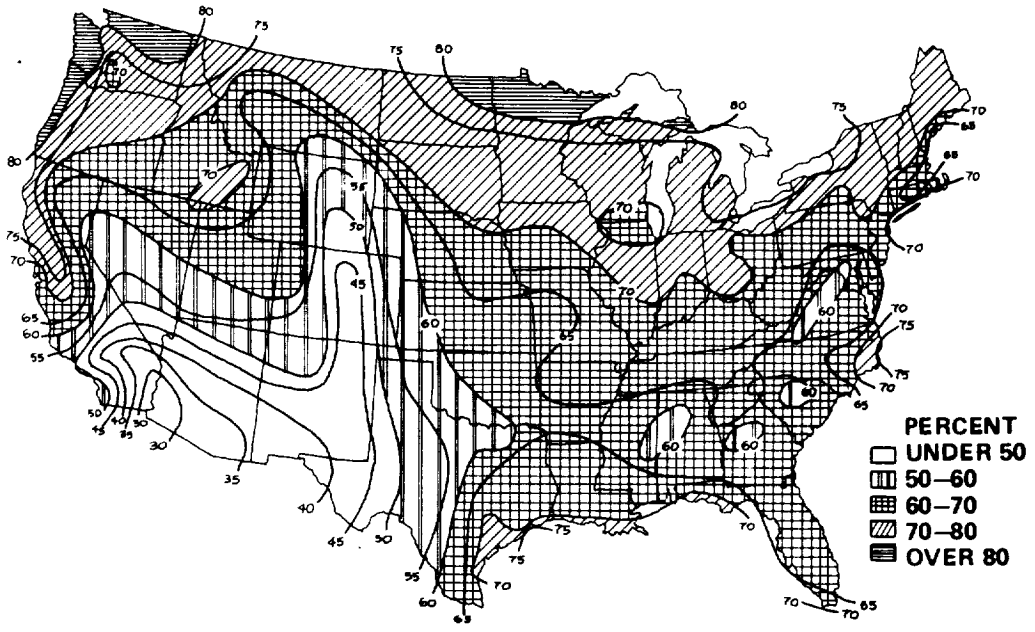

(b) LOCAT NOON, JANUARY [7.4].

Figure 7.31 Average relative humidity distribution for the United States.

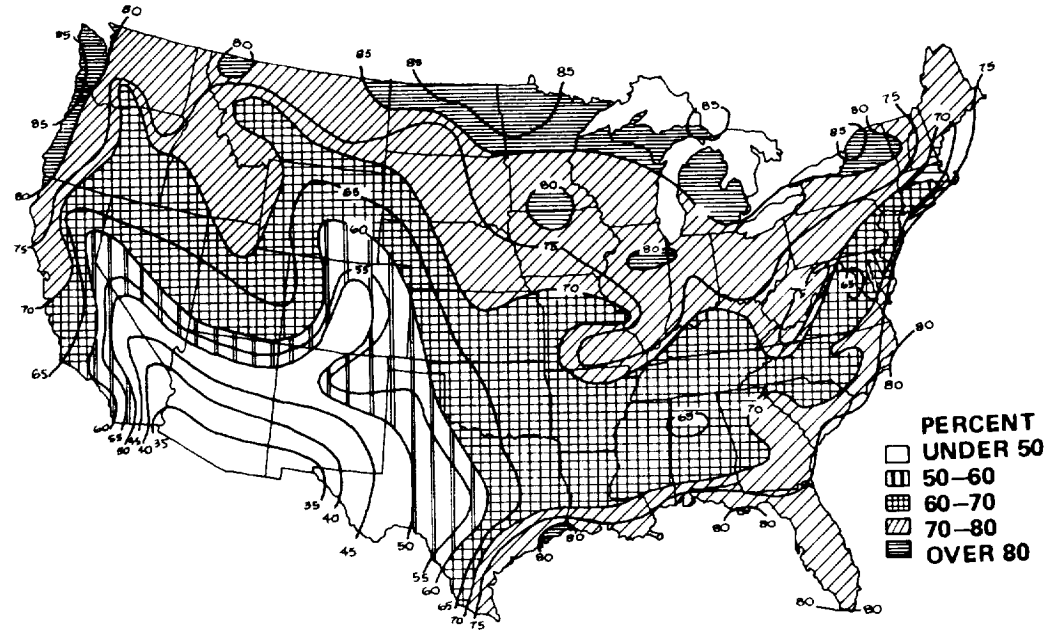

(c) 8 pm (EST), JANUARY [7.4].

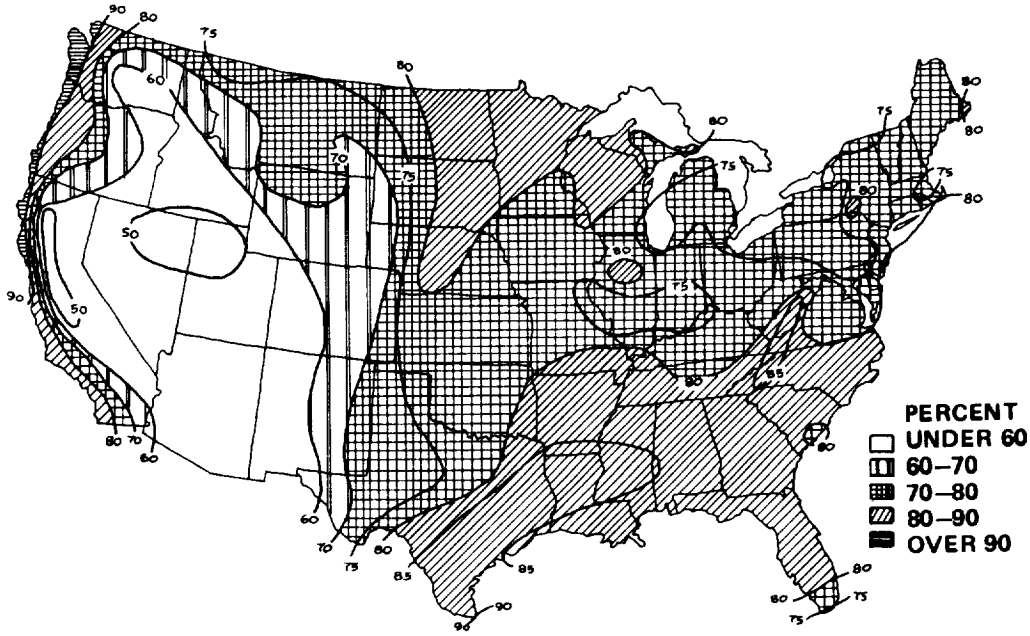

(d) 8 am (EST), JULY [7.4].

Figure 7.31 (Continued).

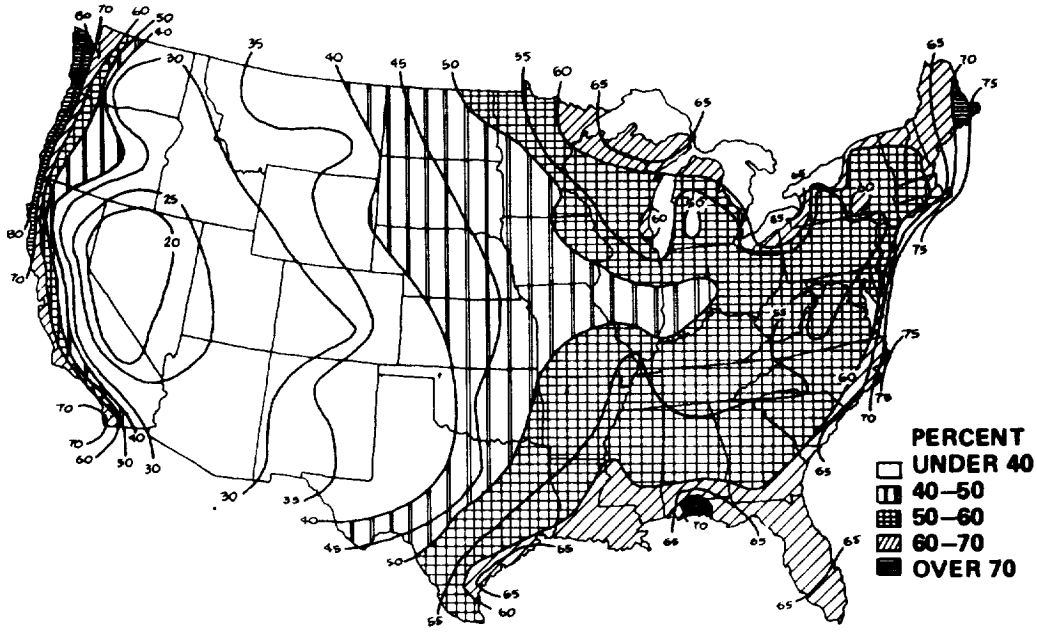

(e) LOCAL NOON, JULY [7.4].

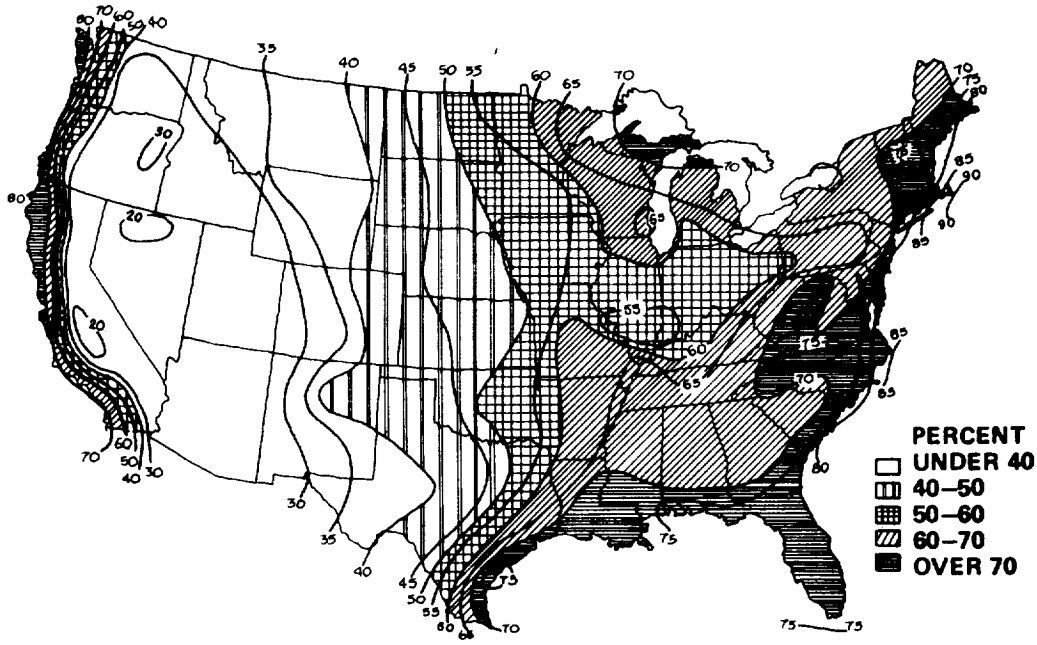

(f) 8 pm (EST), JULY [7.4].

Figure 7-31 (Concluded).

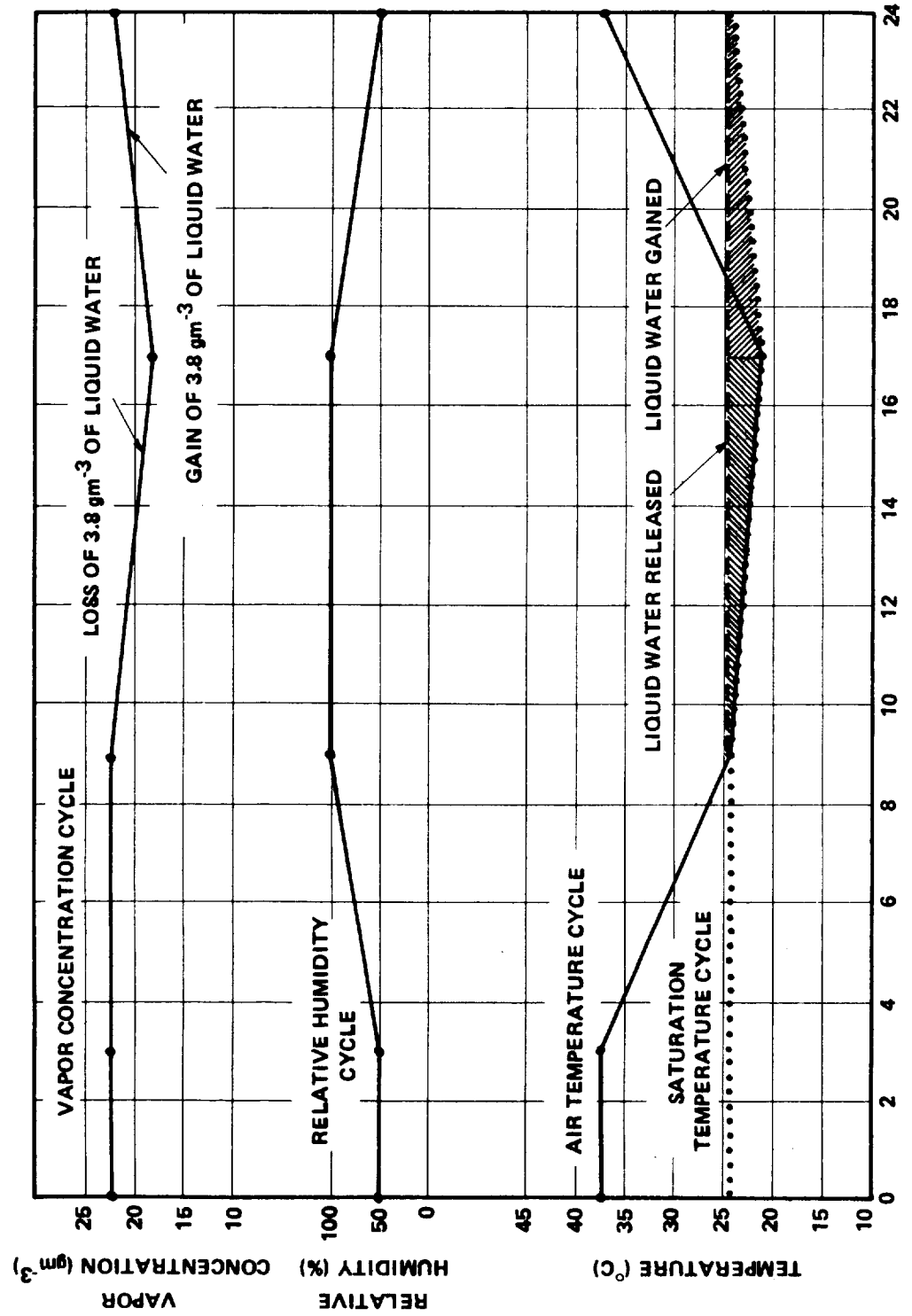

Figure 7.32 Extreme high vapor concentration cycle for southeast Gulf and coastal regions [7.1].

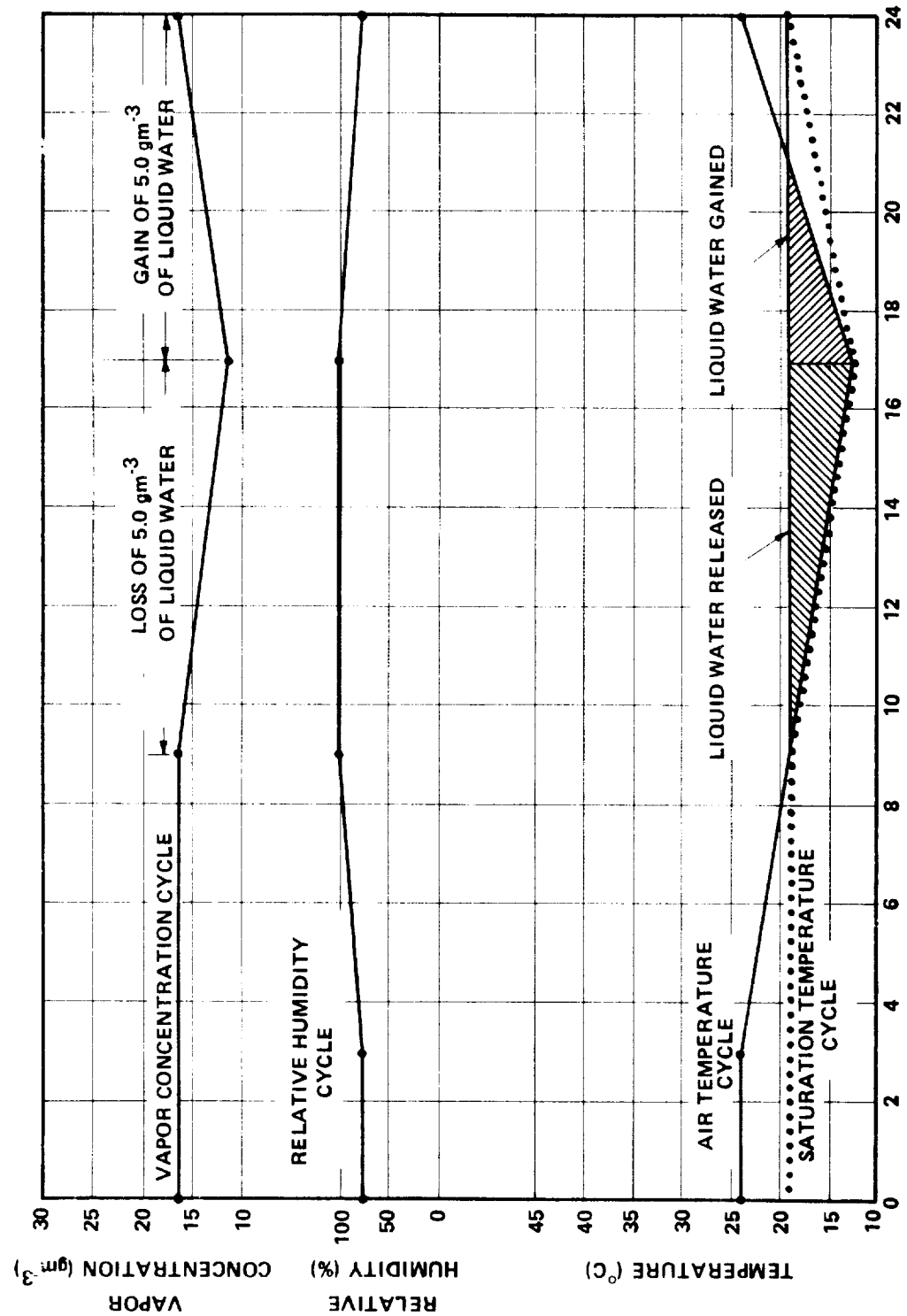

Figure 7.33 Extreme high vapor concentration cycle for southwest coastal region [7.1].

Some information and test procedures have been provided on humidity-temperature chamber test criteria for various systems and their associated electrical-mechanical components. A wide variety of such tests are identified in the various system requirements documents. However, this document has been prepared to emphasize actual environmental criteria, including extreme values, which must be considered in conducting any such tests of components to promote realism about the actual environment.

7.5.1 High Vapor Concentration Cycle for Southeast Gulf and Coastal Region

The following extreme humidity cycle of 24 h with a wind of less than 5 m s^{-1} (9.7 knots) should be considered in design: 3 h of 37.2°C (99°F) air temperature at 50-percent relative humidity and a vapor concentration of 22.2 gm m^{-3} (9.7 gr ft^{-3}); 6 h of decreasing air temperature to 24.4°C (76°F) with relative humidity increasing to 100 percent (saturation); 8 h of decreasing air temperature to 21.1°C (70°F), with a release of 3.8 gm of water as liquid per cubic meter of air (1.7 gr of water per cubic foot of air), humidity remaining at 100 percent; and 7 h of increasing air temperature to 37.2°C (99°F) and a decrease to 50-percent relative humidity (Fig. 7.32).

An extreme relative humidity between 75 and 100 percent and air temperature between 22.8°C (73°F) and 27.8°C (82°F), which would result in corrosion and bacterial and fungal growths, can be expected for a period of 15 days. A humidity of 100 percent occurs one-fourth of the time at the lower temperature in cycles not exceeding 24 h. Any loss of water vapor from the air by condensation is replaced from outside sources to maintain at least 75-percent relative humidity at the higher temperature.

7.5.2 Southwest Coastal Region

The following extreme humidity cycle of 24 h with a wind of less than 5 m s^{-1} (9.7 knots) should be considered in design: 3 h of 23.9°C (75°F) air temperature at 75-percent relative humidity and a vapor concentration of 16.2 gm m^{-3} (7.1 gr ft^{-3}); 6 h or decreasing air temperature to 18.9°C (66°F) with relative humidity increasing to 100 percent; 8 h of decreasing air temperature to 12.8°C (55°F) with a release of 5.0 gm of water as liquid per cubic meter of air (2.2 gr of water per cubic foot of air), humidity at 100 percent; and 7 h of increasing air temperature to 23.9°C (75°F) and the relative humidity decreasing to 75 percent (Fig. 7.33).

Bacterial and fungal growth should present no problem because of the lower temperatures in this area. For corrosion, an extreme humidity of between 75-and 100-percent relative humidity and air temperature between 18.3°C (65°F) and 23.3°C (74°F) can be expected for a period of 15 days. The humidity should be 100 percent during one-fourth of the time at the lower temperature in cycles not exceeding 24 h. Any loss of water vapor from the air condensation is replaced from outside sources to maintain at least 75-percent relative humidity at the higher temperature.

In contrast to high vapor concentrations, low water vapor concentration can occur either at very low or at high temperatures when the air is very dry. In both cases, the dew points are very low. However, in the case of low dew points and high temperatures, the relative humidity is low. If a compartment of a WTG is heated to temperatures well above the ambient air temperature (such as the high temperatures of the nacelle interior of a WTG exposed to the Sun), the relative humidity will be even lower than the relative humidity of the ambient air. These two types of low water vapor concentrations have entirely different environment effects. In the case of low air temperatures, ice or condensation may form on equipment; while in the high temperature-low humidity condition, organic materials may dry and split or otherwise deteriorate. When an enclosed region is considerably warmer than the ambient air (even when the air is cold), the drying increases even more. Low relative humidities may also result in another problem — that of static electricity. The discharge of static electrical charges on equipment may cause shocks to personnel. Because of this danger, two types of low water vapor concentrations (dry extremes) are given. The following extremes of low vapor concentration are given by Reference 7.1:

1) Eastern Coastal and Inland Regions:

a) A vapor concentration of 2.1 gm m^{-3} (0.9 gr ft^{-3}), with an air temperature of -11.7°C (+11°F) and a relative humidity between 98 and 100 percent for a duration of 24 h, must be considered.

b) A vapor concentration of 4.5 gm m^{-3} (2.0 gr ft^{-3}), corresponding to a dew point of -1.1°C (30°F) at an air temperature of 28.9°C (84°F) and a relative humidity of 15 percent occurring for 6 h each 24 h, and a maximum relative humidity of 34 percent at an air temperature of 15.6°C (60°F) for the remaining 18 h of each 24 h for a 10-day period, must be considered.

2) Southeast Gulf Region:

a) A vapor concentration of 4.2 gm m^{-3} (1.8 gr ft^{-3}), with an air temperature of -2.2°C (28°F) and a relative humidity of 98 to 100 percent for a duration of 24 h, must be considered.

b) A vapor concentration of 5.6 gm m^{-3} (2.4 gr ft^{-3}) corresponding to a dew point of 2.2°C (36°F) at an air temperature of 22.2°C (72°F) and a relative humidity of 29 percent occurring for 8 h, and a maximum relative humidity of 42 percent at an air temperature of 15.6°C (60°F) for the remaining 16 h of each 24 h for 10 days, must be considered.

3) Southwest Coastal Region:

a) A vapor concentration of 3.1 gm m^{-3} (1.4 gr ft^{-3}), with an air temperature of -6.1°C (21°F) and a relative humidity of 98 to 100 percent for a duration of 24 h, must be considered.

b) A vapor concentration of 10.1 gm m^{-3} (4.4 gr ft^{-3}), corresponding to a dew point of 11.1°C (52°F) at an air temperature of 37.8°C (100°F) and a relative humidity of 22 percent occurring for 4 h each 24 h, and a maximum relative humidity of 55 percent at an air temperature of 21.1°C (70°F) for the remaining 20 h of each 24 h for 10 days, must be considered.

REFERENCES

7.1 Kaufman, J. W. (editor): Terrestrial Environment (Climatic) Criteria Guidelines for Use in Aerospace Vehicle Development, 1977 Revision. NASA TM X-78118, November 1977.

7.2 Code of Basic Data for the Design of Buildings. British Standards Institution. Chapter 5, Part 2, 1972.

7.3 Hjelmfelt, A. T. and Cassidy, J. J.: Hydrology for Engineers and Planners. Iowa State University Press, 1975.

7.4 Climates of the United States, Yearbook of Agriculture, 1941, pp. 701-747.

7.5 Williams, Llewelyn: Hail and Its Distribution. Special Report ETL-SR-73-3, The Commanding Officer, U.S. Army Engineer Topographic Laboratories, January 1973.

7.6 Moon, Parry: Proposed Standard Solar Radiation Curves for Engineering Use. Journal of the Franklin Institute, Vol. 230, November 1940, pp. 583-617.

7.7 May, T. P. and Taylor, V. G.: Corrosion Testing in Marine Atmosphere. Journal of Environmental Sciences, Vol. 7, No. 7, December 1964, pp. 23-27.

7.8 Doyle, D. P. and Godard, Hugh P.: A Rapid Method for Determining the Corrosivity of the Atmosphere at Any Location. Nature, Vol. 200, No. 4912, December 21, 1963, pp. 1167-1168.

7.9 Brierly, William B.: Atmosphere Sea-Salts Design Criteria Areas. Journal of Environmental Sciences, Vol. 8, No. 5, October 1965, pp. 15-23.

☆U.S. GOVERNMENT PRINTING OFFICE: 1978-635-004/29

TECHNICAL REPORT STANDARD TITLE PAGE

1. REPORT NO.	2. GOVERNMENT ACCESSION NO.	3. RECIPIENT'S CATALOG NO.
NASA TP-1359		

4. TITLE AND SUBTITLE	5. REPORT DATE
Engineering Handbook on the Atmospheric Environmental Guidelines for Use in Wind Turbine Generator Development	December 1978
	6. PERFORMING ORGANIZATION CODE
7. AUTHOR(S) Walter Frost,* B. H. Long,* and R. E. Turner	8. PERFORMING ORGANIZATION REPORT #
9. PERFORMING ORGANIZATION NAME AND ADDRESS	10. WORK UNIT NO. M-267
George C. Marshall Space Flight Center Marshall Space Flight Center, Alabama 35812	11. CONTRACT OR GRANT NO.
	13. TYPE OF REPORT & PERIOD COVERED
12. SPONSORING AGENCY NAME AND ADDRESS National Aeronautics and Space Administration Washington, D.C. 20546	Technical Paper
	14. SPONSORING AGENCY CODE

15. SUPPLEMENTARY NOTES

Prepared by Space Sciences Laboratory, Science and Engineering
*The University of Tennessee Space Institute, Tullahoma, Tennessee 37388.

16. ABSTRACT

Atmospheric environmental guidelines for use in wind turbine generator development are presented. The guidelines are given in the form of design criteria relative to wind speed, wind shear, turbulence, wind direction, ice and snow loading, and other climatological parameters which include rain, hail, thermal effects, abrasive and corrosive effects, and humidity. This report is not a discussion of fundamental concepts or theories, but a presentation of design criteria in an engineering format which can be directly input to wind turbine generator design computations.

A summary section in each chapter provides a range of recommended design values for a general purpose, "off-the-shelf-type" wind turbine generator which could be sited in most any region of the United States. Following these summarized design values, detailed computational procedures and working data are provided which allow the designer to establish his own design values if desired. Thus, guidelines are also provided for developing specialized wind turbine generators or for designing wind turbine generators which are to be used in a specific region of the United States.

17. KEY WORDS	18. DISTRIBUTION STATEMENT
Wind Energy Turbine Wind Environmental criteria Turbulence Climatological	Category 47

19. SECURITY CLASSIF. (of this report)	20. SECURITY CLASSIF. (of this page)	21. NO. OF PAGES	22. PRICE
Unclassified	Unclassified	372	$12.50

*For sale by the National Technical Information Service, Springfield, Virginia 22161